Tofael Ahamed   *Editor*

Remote Sensing Application

Regional Perspectives in Agriculture and Forestry

Springer

New Frontiers in Regional Science: Asian Perspectives

Volume 59

Editor-in-Chief

Yoshiro Higano, University of Tsukuba, Tsukuba, Ibaraki, Japan

This series is a constellation of works by scholars in the field of regional science and in related disciplines specifically focusing on dynamism in Asia.

Asia is the most dynamic part of the world. Japan, Korea, Taiwan, and Singapore experienced rapid and miracle economic growth in the 1970s. Malaysia, Indonesia, and Thailand followed in the 1980s. China, India, and Vietnam are now rising countries in Asia and are even leading the world economy. Due to their rapid economic development and growth, Asian countries continue to face a variety of urgent issues including regional and institutional unbalanced growth, environmental problems, poverty amidst prosperity, an ageing society, the collapse of the bubble economy, and deflation, among others.

Asian countries are diversified as they have their own cultural, historical, and geographical as well as political conditions. Due to this fact, scholars specializing in regional science as an inter- and multi-discipline have taken leading roles in providing mitigating policy proposals based on robust interdisciplinary analysis of multifaceted regional issues and subjects in Asia. This series not only will present unique research results from Asia that are unfamiliar in other parts of the world because of language barriers, but also will publish advanced research results from those regions that have focused on regional and urban issues in Asia from different perspectives.

The series aims to expand the frontiers of regional science through diffusion of intrinsically developed and advanced modern regional science methodologies in Asia and other areas of the world. Readers will be inspired to realize that regional and urban issues in the world are so vast that their established methodologies still have space for development and refinement, and to understand the importance of the interdisciplinary and multidisciplinary approach that is inherent in regional science for analyzing and resolving urgent regional and urban issues in Asia.

Topics under consideration in this series include the theory of social cost and benefit analysis and criteria of public investments, socio-economic vulnerability against disasters, food security and policy, agro-food systems in China, industrial clustering in Asia, comprehensive management of water environment and resources in a river basin, the international trade bloc and food security, migration and labor market in Asia, land policy and local property tax, Information and Communication Technology planning, consumer "shop-around" movements, and regeneration of downtowns, among others.

Researchers who are interested in publishing their books in this Series should obtain a proposal form from Yoshiro Higano (Editor in Chief, higano@jsrsai.jp) and return the completed form to him.

More information about this series at https://link.springer.com/bookseries/13039

Tofael Ahamed
Editor

Remote Sensing Application

Regional Perspectives in Agriculture
and Forestry

 Springer

Editor
Tofael Ahamed
Faculty of Life and Environmental
Sciences
University of Tsukuba
Tsukuba, Ibaraki, Japan

Foreword

I am honored to have the opportunity to provide some insight into the impacts of this volume, *Remote Sensing Application: Regional Perspectives in Agriculture and Forestry*, which is edited by Dr. Tofael Ahamed, my former colleague at the University of Tsukuba. It has been said so long that the method of GIS/Remote Sensing has huge potential to be incorporated into studies in natural science fields as well as engineering and other practical policy-oriented fields. Thanks to miraculous developments in informatics science and technologies and related fields, not only the saying has now become factual but also the methodology has become critically important in interdisciplinary and multidisciplinary studies which focus on policy issues of climate change and global environment. In this sense, the method of GIS/Remote Sensing and its application have a vast frontier with which studies in regional science can be broadened and deepened.

For example, according to the Paris Agreement, which tries to adapt to the IPCC projection and scenario, the goal is to make the peak emission of carbon dioxide in the world at as lower level as possible by the middle of this century as early as possible and after the peak has been attained it must be offset by carbon sinks by drawing upon forest absorption, CCS technology, etc. The most substantial solution in order to achieve the goal is transformation of the current energy system that is critically dependent on fossil fuel into renewable energy system that is mainly dependent on non-fossil energy sources. It is a prerequisite for the construction of the so-called carbon neutral society. Further technology developments must be made targeting the energy transformation in the long run as well as it must be done to improve the efficiency of human activities in terms of GHG emission with a shorter perspective in order to make the GHG emission peak as early as possible.

It is apparent and we do not need to emphasize that the years till 2040 or at latest 2050 are very critical for the existence of human beings on the globe. This means that the construction of carbon neutral society, which can be realized by comprehensively re-organizing not only hardware but also software of the current society relying on developed breakthrough technologies, must be propelled into action being navigated by, e.g., precisely estimated reduction in GHG emission. While each

(marginal) action of human beings must be evaluated and controlled in terms of criteria of carbon offset, carbon sink, sustainability, etc., all actions need to be controlled by being subject to a constraint on the total GHG emission in the world. It is easy to conceptualize the necessity, and difficult to implement it in real settings. In my view, GIS/Remote Sensing combined with advanced technologies of ICT, IoT, AI, etc. is a very powerful and effective method for total control.

Another prosperous application field for GIS/Remote Sensing is adaptation to climate change in order to pursue sustainability by minimizing risk of ecological collapse, disaster, conflicts, etc. In the context of the total control, international collaboration may be taken for granted and we need to know what is really happening elsewhere on the globe and how we should control the subsystem which is cognized in terms of region, country, continent, current generation, future generation, etc. In this sense, GIS/Remote Sensing is also most prosperous and useful architectures.

This book contains many novel and insightful articles which examine practically useful applicability of GIS/Remote Sensing method to real critical issues in agriculture and forest fields by presuming climate change and/or extreme weather. Readers will see how GIS/Remote Sensing is powerful and effective in sustainability management, and they will be incentivized to further expand the frontier of GIS/Remote Sensing in regional science and related fields.

Faculty of Life and Environmental   Yoshiro Higano
Sciences, University of Tsukuba,
Tsukuba, Ibaraki, Japan

Preface

In recent times, remote sensing has become a significant component in policymaking for sustainable development in the agricultural and forestry sectors to establish big data schemes. Big data refers to the volume, variety, velocity, and veracity of data at large scales. In this major component of big data transfer, data structures, data acquisition times, and data authenticity provide for stakeholders' interaction in the action plan. In this regard, this book discusses the application of remote sensing from regional perspectives with vegetation phonologies, water signatures, and socioeconomic criteria to develop decision-making systems related to agricultural land-use planning, land suitability analysis for different crops (rice, maize, cassava) and fruits (grapes), yield forecasting, and damage assessment due to extreme events.

In Chap. 1, introductory notes related to the big data scheme and overall remote sensing application in agriculture and forestry are presented to highlight some recent applications of satellite-derived indices and algorithms to address the scope and application of geographic information systems (GISs). Spatial and temporal resolutions are considered to select the core applications in land-use planning, land suitability analysis, water inundation mapping, change detection, forest productivity, and damage assessment. The review notes along with our team analyses of different regional applications of vegetation and water signature indices are presented together. The high-resolution UAV-based application for yield forecasting of sugarcane is also presented to call attention to obtaining higher flexibility in temporal resolution.

Chapter 2 discusses calorie-based seasonal multicrop land suitability analysis for food and nutrition security with regard to diversified cropland-use planning in Bangladesh. The integrated model proposed here can be implemented for the management of land allocation for diversified crop production, providing more decision-making information for policymakers to ensure regional food and nutrition security. In Chap. 3, agricultural land suitability assessment is discussed based on the soil-vegetation indices using multicriteria decision analysis (MCA) together with weighted linear combinations and fuzzy multicriteria analyses. Furthermore, suitability assessments were evaluated using ground reference yield data through yield

forecasting. Chapter 4 focuses on cassava production and its suitability at regional sites in Indonesia. The study referred to multicriteria analysis, including the analytic hierarchy process (AHP) and the analytical network process (ANP). The AHP method was applied to determine the relative importance of all of the selected criteria and factors. The study will contribute to decision-making processes to increase the production of cassava in suitable regions. In Chap. 5, drought-prone areas were estimated from vegetation phenology analysis of maize in Indonesia using a deep learning algorithm. The deep learning algorithm based on You Only Look Once (YOLO) was applied to monitor the drought condition at different stages of maize production. This research could be used for high computational and real-time monitoring to forecast drought conditions in a simple and quick way. In Chap. 6, the development of a land suitability model for grape cultivation was performed to determine the best location for vineyard cultivation in Afghanistan. It is very important for growers to increase table grape production and reduce the cost of production. The multicriteria technique was used for this purpose. This research could help decision-makers, growers, and other stakeholders conduct precise land assessments for table grape production globally.

In Chap. 7, GIS-based MCA modeling was performed to determine the sustainability of land uses in the suburb areas of Dhaka city in Bangladesh. This study also assessed potential locations for the further growth of industries by land suitability analysis (LSA) to emphasize both agriculture and industries in terms of sustainable growth. In Chap. 8, change detection and land suitability analysis for the extension of potential forest areas in Indonesia was conducted using a two-year series of multispectral datasets. Change detection of forestland is important to understanding the past and current trends of changes and projections for the future. This study could help to create a new policy space for plantation forests and ecosystems in designing national and subnational policies. In Chap. 9, estimating productivity and carbon stock using phenological indices from satellite remote sensing is endeavored to evaluate forest productivity and carbon stock for different types of forests in Indonesia. Different vegetation indices were used to assess the level of forest productivity with different classifications to estimate the carbon stock in six types of forests using gross primary productivity (GPP) approaches. System dynamics modeling was applied to simulate the generated data. The study of the productivity of different types of forests provides justification for the protection and management of forests on different time scales. In Chap. 10, the spatiotemporal evolution of deforestation monitoring in Malaysia was conducted for long-term and continuous forest monitoring on the Google Earth Engine (GEE) platform.

Chapter 11 focuses on climate-resilient agriculture assessment, targeting, and prioritization for the Adaptation and Mitigation Initiative in Agriculture (AMIA), a region of the Philippines. An assessment was carried out to evaluate the climate change variability that increases per use in the agriculture sector. Climate risk vulnerability assessment (CRVA) was performed based on two important climate parameters, rainfall and temperature, across the three main islands. The adaptive capacity was based on the different capitals identified and developed by experts from the Department of Agriculture (DoA). To determine the sensitivity of a crop to

climate change, maximum entropy (MaxEnt) was used. The MaxEnt model is a crop distribution model commonly used to estimate the most suitable areas for a species or crop based on probability in geographic areas where the distribution of crops is scarce. Finally, to determine the vulnerability of each crop for the different municipalities, hazard, sensitivity, and adaptive capacity were summed based on their weights.

In Chap. 12, high-resolution remote sensing technology based on unmanned aerial vehicles (UAVs) for sugarcane production in tropical regions is discussed for sugarcane canopy detection, disease detection, sugar content estimation, and yield predictions. Finally, the harvest schedule and supply chain management are optimized. This remote sensing technology can contribute directly to the increase in profitability for both growers and sugar factories.

The last chapter discusses the conclusion and key findings from all the chapters in this book, which leads to a data-driven concept for big data schemes to serve farmer unions, stakeholders, policy planners, and urban developers. A team effort has been made in this book to align all the applications of remote sensing and GIS in the agriculture and forestry sectors for different countries that contributes to big data schemes from a regional perspective.

Tsukuba, Ibaraki, Japan   Tofael Ahamed

Acknowledgments

I would like to extend my sincere gratitude to Professor Yoshiro Higano, Editor-in-Chief, New Frontiers in Regional Science: Asian Perspectives and Editor-in-Chief of *Asia-Pacific Journal of Regional Science* for his inspiration to accomplish this book. Over time, we published a number of research articles in the *Asia-Pacific Journal of Regional Science* that led us to complete this book along with original contributions from our collaborators and open-access publications. The book was written to align the application of remote sensing-based vegetation and water-related signatures with socioeconomic factors for the regional establishment of big data in policy planning. I envision that this book can serve as a contributing factor on the frontier in regional science series.

I extend my gratitude and thanks to the contributors of this book, who helped me to fulfill the aim of crafting all the chapters together. Appreciation continues to the *Asia-Pacific Journal of Regional Science, Land, and Forests* for their copyright permissions for reusing some of their published articles as chapters in this book. I would also like to thank Professor Tekeshi Mizunoya and Ms. Hatsumi Uchimura from the University of Tsukuba for supporting the copyright process from the Japan Section of the Regional Science Association International (JSRAI).

This time, along with our lab contribution from the University of Tsukuba, contributors from Malaysia, the Philippines, and Thailand spared their time at the different stages of the review process of each chapter. In this regard, I would like to extend my thanks and appreciation to the contributors Dr. Janet E. Pablo, Benguet State University, the Philippines, Professor Mohamed Rashid Sharif, Universiti Putra Malaysia, and Dr. Khwantri Saengprachatanarug, Khon Kaen University, Thailand.

I would like to extend my sincere thanks and appreciation to my PhD students for their tireless assistance and contributions to the book's cross-checking, updating, and figure layout.

In this team, Sara Tokhi Arab, Md. Monirul Islam, Md Shamszzoha, Kazi Faiz Alam, Munirah Hayati Hamidon, R M Rasika D Abeyrathna, Nakaguchi Victor Massaki, and Arkar Minn have outstandingly supported me to develop a unified format requested from Springer. In addition to my team, I would like to extend my

Contents

Chapter 1
A Review of Remote Sensing Applications in Agriculture and Forestry to Establish Big Data Analytics

Sara Tokhi Arab, Md. Monirul Islam, Md. Shamsuzzoha, Kazi Faiz Alam, Nazia Muhsin, Ryozo Noguchi, and Tofael Ahamed

Abstract The advancement of remote sensing provides a new opportunity for a data analytical platform for robust decision-making based on near real-time datasets derived from satellites and unmanned aerial vehicles (UAVs). The spectral signature through passive and active remote sensing has the advantages of providing information on plant responses in low-, medium-, and high-resolution images with temporal variability and enables taking action for sustainable agriculture and forest resource management. Therefore, the aim of this review article is to find a new avenue for generating data management platforms in the field of agriculture and forestry. The advancement of satellite remote sensing technology has already been suggested to open the gateway to establishing big data analytical platforms through decision support systems. Specifically, this review paper highlights some appropriate and important applications of satellite and UAV-derived indices and algorithms

S. T. Arab · K. F. Alam
Graduate School of Life and Environmental Sciences, University of Tsukuba, Tsukuba, Ibaraki, Japan

M. M. Islam
Graduate School of Life and Environmental Sciences, University of Tsukuba, Tsukuba, Ibaraki, Japan

Department of Agricultural Economics, Bangladesh Agricultural University, Mymensingh, Bangladesh

M. Shamsuzzoha
Graduate School of Life and Environmental Sciences, University of Tsukuba, Tsukuba, Ibaraki, Japan

Faculty of Environmental Science and Disaster Management, Patuakhali Science and Technology University, Patuakhali, Bangladesh

N. Muhsin
Faculty of Engineering Studies, BGMEA University of Fashion and Technology, Dhaka, Bangladesh

R. Noguchi · T. Ahamed (✉)
Faculty of Life and Environmental Sciences, University of Tsukuba, Tsukuba, Ibaraki, Japan
e-mail: tofael.ahamed.gp@u.tsukuba.ac.jp

to address the scope and application of geographic information systems (GISs) in the field of agriculture and forestry research. The analytical signatures of changes in vegetation and water storage in leaves and water bodies were analyzed and presented using different phenological properties, land use land cover (LULC) changes, and natural disaster damage assessments to support policy formations and the livelihoods of farmers. The remote sensing and GIS-based analytical datasets cover crop calendars and phenological changes from forest canopies that refer to productivity according to seasons. Seasonal variations in the productivity of crops and forests can ensure appropriate actions with resilience for the sustainable management of bioresources.

Keywords Satellite remote sensing · GIS · Agriculture and forestry · Vegetation indices · Water signatures · LULC · Land suitability · Change detection · Disaster damage assessment

1.1   Introduction

Agriculture and forestry are the leading sectors in the world, especially in developing countries. These sectors ensure food, feed, and nonfood products to meet the demands of the world's rising population and a wide range of industries. The productivity of agriculture and forestry has increased remarkably in recent decades due to the use of advanced technologies. For example, between 1948 and 2011, the yield of soybeans and corn and labor productivity increased almost 16-fold in the United States (US) (Wang et al. 2015). Furthermore, between 1960 and 2015, agricultural productivity increased more than three times due to green revolution technologies and a considerable increase in the usage of natural resources (such as water, land, and other resources) (Foley et al. 2011). At the same time, the world was witnessing the industrialization and globalization of industrial food and agricultural products. Moreover, in recent years, due to the usage of production technologies, the production of major crops has increased by 53% between 2000 and 2019, to a higher record of 9.4 billion tons in 2019 (FAO 2021). This indicated that the 3.2-billion-ton excess was more than the production of 2000. In addition, advanced cutting-edge technologies, namely, satellite remote sensing, geographic information system (GIS), unmanned aerial vehicle (UAV), big data analytics, global positioning system (GPS), precision agriculture (PA), the internet of things (IoT), and artificial intelligence (AI) technologies, have also been used in this sector to optimize agricultural operations and input management, reduce input and yield losses and support growers, interveners, policymakers, and governments in decision-making (Harrower et al. 2002; Eli-Chukwu 2019). Remote sensing datasets provide the soil-water-vegetation indices for policy implementation (Fig. 1.1). These big data, which come from the combination of technology and advanced analytical processes, provide effective and timely information about farms and forest areas. The big data processes start from the collection of data, data management, and data use, mostly on a farm or on a large scale (region), to enable decision support systems. To meet the growing
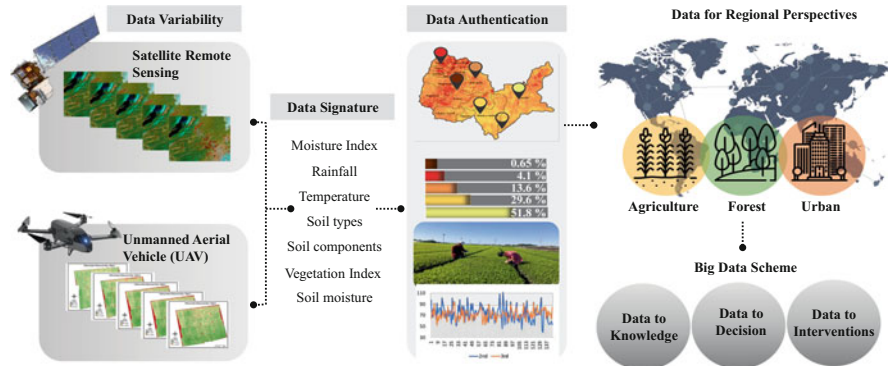
Fig. 1.1 Big data scheme for soil-water-vegetation indices for core policy planning from a regional perspective

needs of food and feed in the agriculture and forestry sectors, site-specific management and the applications of remote sensing methods with big data analytical platforms are inevitable (Stubb 2016; Kamilaris et al. 2017).

Among advanced methods, remote sensing technologies (active or passive) play a significant role at different scales and platforms. Based on spatial resolution, there are three main platforms that are generally used: ground-based, airborne, and satellite platforms. Ground-based small-scale remote sensing instruments are very helpful for field-level monitoring, such as temperature, humidity, plant water requirements, and plant growth (Jackson 1986). This ground-based method has better spatial resolution and accuracy in farm-level experiments than satellite remote sensing and aerial imagery (Jackson 1986). Airborne remote sensing was mainly controlled by piloted aircraft. However, recently, they have been replaced by UAVs, which are unmanned, remote-controlled aircraft. Drones are a cost-effective technology able to easily transport to the farm and are more flexible in terms of flight schedule and length. However, the only problem is a limited battery capacity. With this UAV technology, researchers can easily obtain very high-resolution images of agricultural fields (Franklin et al. 2006; Laliberte et al. 2006). Recently, there have been more than 7000 satellites (space objects) orbiting the planet with different spatial and temporal resolutions (high, medium, and low resolutions). These various satellites are responsible for continuously collecting photos and data regarding Earth's surface (land, water, and atmosphere). As a result, a vast amount of remotely accessible information is globally available for many countries, regions, and areas on an annual, quarterly, daily, and hourly basis (Ruiz-Luna and Berlanga-Robles 2003; Anderson 2001).

The application of remote sensing techniques is broader. They can be used for land suitability assessments of different crops, fruits, and vegetables. In addition, yield estimation, crop status analysis and drought detection, land use change, forest change detection, urban land use planning, and climate resilience assessment can be performed through remotely sensed technologies. Usually, these applications are

used over large areas at the regional level. However, satellite remote sensing has recently enabled within-field monitoring, such as water stress, flood and cyclone damage assessment, and the estimation of yield losses and damages. Remote sensing tools and satellite remote sensing can provide timely and accurate information. Information regarding the agriculture and forestry sectors can be provided in a large platform (Huang et al. 2018). In this context, this review article discusses the application of remote sensing through different phenological indices to find the best land use opportunities, prevent natural disaster effects and losses in agriculture and forest areas, and evaluate its potential to establish a big data analytics platform for policy formulation.

1.2 Satellite Data Attribution

Satellite remote sensing is considered a primary source for acquiring spatial and temporal datasets for the agriculture and forestry sectors. It measures the electromagnetic radiation that interacts with the atmosphere and objects. Each satellite has a specific band, which is the portion of the electromagnetic spectrum sensed by the satellite (Duveiller and Defourny 2010). The bands consist of visible light, infrared, and invisible light to human eyes. Interactions of electromagnetic radiation with the surface of the Earth can provide information about objects regarding the characteristics of surface materials (Zhu et al. 2018). To detect the objects and the characteristics of material in the ground, the spatial resolution of a sensor is critical. These resolution categories include spatial, spectral, temporal, and radiometric (Fig. 1.2).

Medium spatial resolutions are Landsat (Landsat 1, Landsat 2, Landsat 4–5, Landsat 7, and Landsat 8–9), Sentinel (Sentinel-1, Sentinel-2, and Sentinel-3), SPOT (SPOT-1, SPOT-2, SPOT-3, SPOT-4, SPOT-5, SPOT-6, and SPOT-7), and the Advanced Land Observing Satellite (ALOS-2), and the low spatial resolutions are moderate resolution imaging spectroradiometer (MODIS Atmosphere products, MODIS land products, MODIS cryosphere products, and MODIS ocean products), Sentinel-3 A, and HJ-1A (NASA 2021; ALOS-PASCO 2021; USGS 2021). A satellite spectral resolution indicates the wavelengths captured by the satellite. According to the spatial resolution, remote sensing has been divided into three parts: high, medium, and low. A high spatial resolution has been used in UAVs, Quickbrid, IKONOS, ASTER, orthophotos, and others.

1.3 Phenological Assessment

Vegetation phenology assessment is a process of collecting data about vegetation or plants in a particular area. Mapping and classifying vegetation are essential technical tasks for managing natural resources and providing information about natural and man-made environments through quantifying vegetation on a local to global scale in
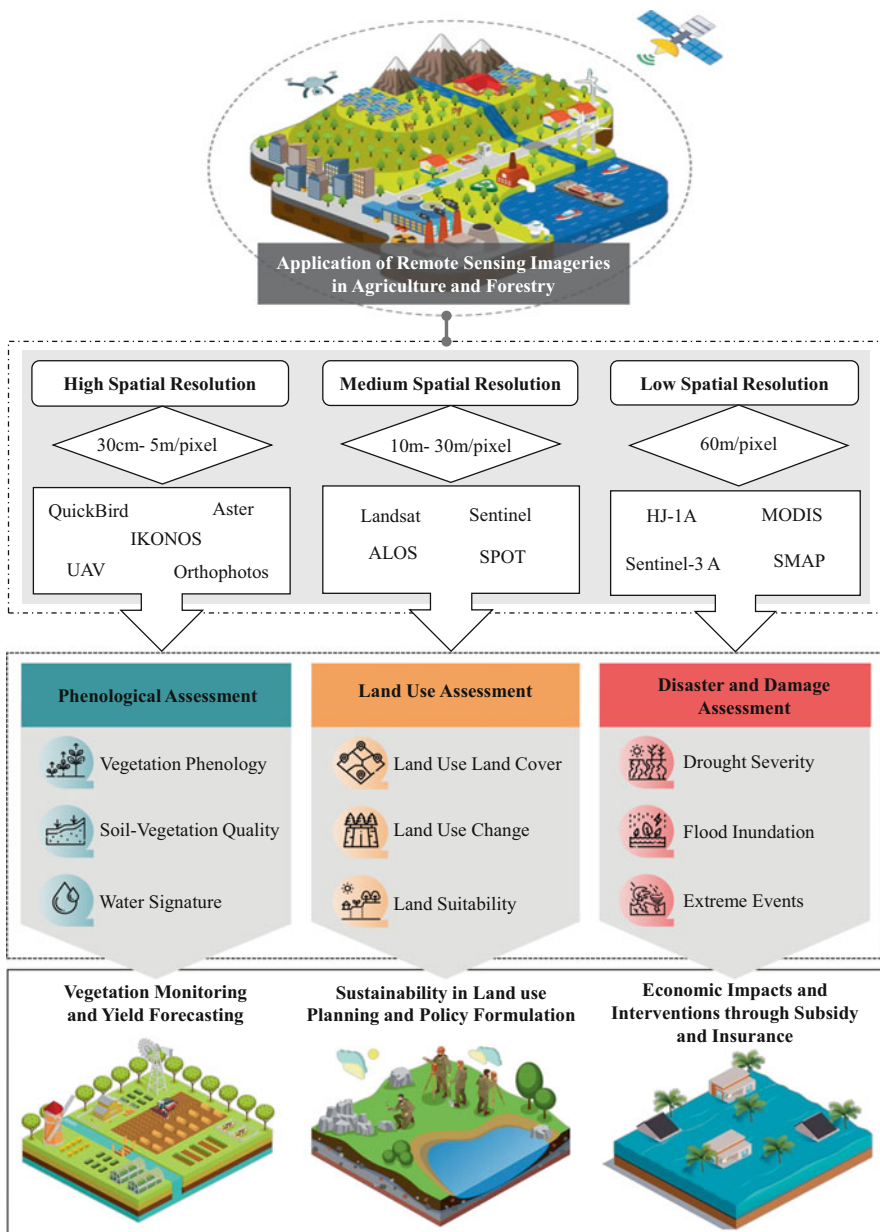
Fig. 1.2 Remote sensing imagery application and opportunities for big data analytical processes in agriculture and forestry research to support field operational management

a particular time period or through continuous time periods (He et al. 2005). Pervious methods for vegetation phenology assessment included field surveys, literature reviews, map interpretation, and collateral and ancillary data analysis. All these methods were expensive, lagged data, and were time-consuming. In this regard, remote sensing technology offers a practical and economical approach to studying plant coverage changes, growth, and regular observations at various scales (farm level, regional, and global scales) that can be assessed against time series data from the present to several years ago (Langley et al. 2001).

1.3.1   Vegetation Indices

Several spectral vegetation indices have been developed from multiband to single band indices to show the biophysical properties of vegetation in the agriculture sector (Rouse et al. 1973; Bannari et al. 1995; Merrick et al. 2020). Most of these indices are derived from the visible bands (ultraviolet, blue, green, and red) and the near- and mid-infrared bands (wavelengths) (Rahim et al. 2016). Plants absorb the red and blue wavelengths, reflect the green wavelength, and strongly reflect the near-infrared (NIR) wavelength. Further variations in the biophysical and biochemical properties of a plant, such as water content, pigment, carbon content, nitrogen content, and other properties, cause further variation across the spectrum. Measuring these variations and their relation to one another can provide information regarding plant health, biomass, vegetation characteristics, and other biophysical and biochemical prosperities of plants. Two main methods have been used for vegetation extraction: image preprocessing and image classification through satellite remote sensing datasets. One of the most common implantations of vegetation indices calculated from multiband information is the normalized ratio between the red and the near-infrared bands or other bands. The normalized vegetation index values range from −1 to 1. For example, in the Normalized Difference Vegetation Index (NDVI), zero and below correspond to nonplant surfaces; thus, values above 1 correspond to vegetation areas. In Fig. 1.3, the UAV NDVI map indicates that the higher the NDVI value is, the greater the plant density and healthy vegetation. As noted, the NDVI palette not only quantifies green vegetation but also helps to recognize and mitigate any issues with plant health and vigor, thus boosting crop yields and making agricultural businesses more profitable (Lenney et al. 1996; Arab et al. 2021). The following satellite-derived vegetation indices have recently been used in agricultural and forestry research (Tables 1.1).

1.3.2   Soil-Vegetation Quality Indices

The soil-vegetation index was proposed by Huete in 1988 at the University of Arizona, USA. This index is often used in arid regions where vegetative coverage
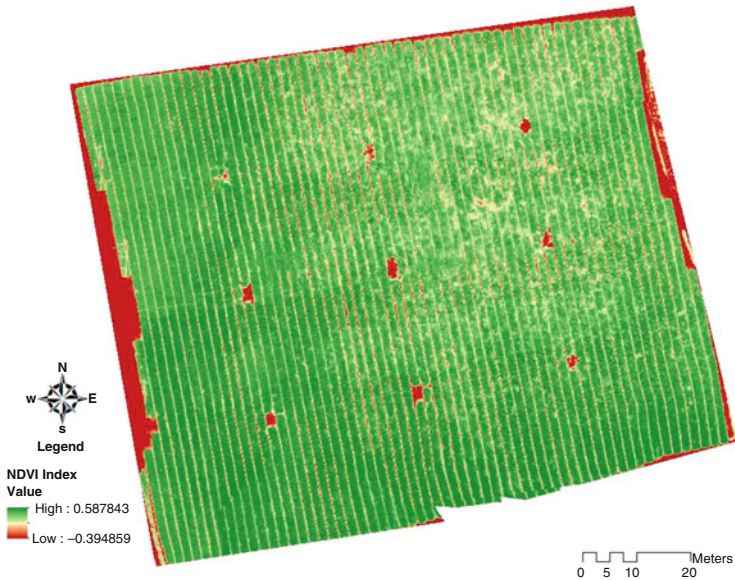
Fig. 1.3 Distribution of NDVI derived from Parrot Sequoia attached to the Parrot Bluegrass UAV, mid-March 2019 first harvest in Ichibancha, Tsukuba city, Ibaraki Prefecture, Japan

is low (Huete 1988). The spectral reflectance of a plant's canopy is a combination of plant and soil particles, which are regulated by the optical characteristics of these elements and the photon exchange within the canopy. When plants grow, the effect of soil decreases, but it may still remain in the satellite imagery (Fig. 1.4). Various soil and vegetation quality indices are used to analyze soil lines in agricultural fields and forests (Table 1.2). The soil-vegetation index is basically developed from NDVI and orthogonal indices (PVI). These indices have a variety of applications in agriculture and forestry, including aboveground biomass estimation, leaf nitrogen content, chlorophyll content, soil condition analysis, plant growth, desertification research, and grassland yield estimation (Major et al. 1990; Baret et al. 1993; Xue and Su 2017; Islam et al. 2021a, b).

1.3.3 Water Signature or Water Spectral Indices

Water spectral indices were developed in the late 1970s, and they show the presence of spectral signatures of liquid water in soil or vegetation (Lyzenga 1978). These water indices (WIs) are broadly used in agricultural, ecological, and forestry research, including surface water body characterization, vegetation water status estimation (crops, fruits, vegetables, and forest trees), soil water content assessment, and wetland (e.g., paddy rice) monitoring (Colwell 1974). Several water-related

Table 1.1 Lists of vegetation indices used in agriculture and forestry research

Vegetation indices	Equation	References
Normalized difference vegetation index (NDVI)	$\frac{R_{NIR} - R_{red}}{R_{NIR} + R_{red}}$	Rouse et al. (1973)
Green NDVI (GNDVI)	$\frac{R_{NIR} - R_{green}}{R_{NIR} + R_{green}}$	Zhou et al. (2016)
Renormalized difference vegetation index (RDVI)	$\frac{R_{NIR} - R_{red}}{\sqrt{R_{NIR} + R_{red}}}$	Rondeaux et al. (1996)
Simple ratio (SR)	$\frac{R_{NIR}}{R_{red}}$	Baret et al. (1993)
Modified SR (MSR)	$[R_{700} - R_{670} - 0.2\,(R_{700} - R_{550})] \times (R_{700} + R_{670})$	Chen (1996)
Difference vegetation index (DVI)	$R_{NIR} - R_{red}$	Ranjan et al. (2019)
Ratio vegetation index (RVI)	$R_{NIR} - R_{red\ edge}$	Gitelson and Merzlyak (1997), Vogelmann (1993)
Chlorophyll-/pigment-related indices MCARI (modified CARI)	$[R_{700} - R_{670} - 0.2\,(R_{700} - R_{550}) \times (R_{700} + R_{670})]$	Duveiller and Defourny (2010)
Normalized difference moisture index (NDMI)	$\frac{R_{NIR} - SWIR2}{R_{NIR} + SWIR}$	Gao (1996)
Rice growth vegetation index (RGVI)	$\frac{(Red + NIR + SWIR) - (Blue + Green)}{Red + NIR + SWIR1}$	Lillesand and Kiefer (1994)

Table 1.2 Lists of important soil-vegetation indices used in agriculture and forestry research

Vegetation indices	Equation	References
Soil-adjusted vegetation index (SAVI)	$\frac{(R_{NIR} - R_{red})(1 + L)}{(R_{NIR} + R_{red} + L)}$	Huete (1988)
Modified soil-adjusted vegetation index (MSAVI)	$0.5 \times \{2R_{800} + 1 - \text{SQRT})[2R_{800} + 1)^2 - 8\,(R_{800} - R_{670})]\}$	Qi et al. (1994)
Modified secondary soil-adjusted vegetation index (MSAVI2)	$0.5 \times (2NIR + 1) - \sqrt{(2NIR + 1)^2 + 8\,(NIR - R)}$	Chen (1996)
Optimized soil-adjusted vegetation index (OSAVI)	$\frac{(NIR - R)}{(NRI + R + 0.16)}$	Rondeaux et al. (1996)

indices have been developed from visible, NIR, and shortwave infrared (SWIR) bands (Hardisky et al. 1983; Gao 1996). Two main water indices and other water indices developed from these two are presented in Table 1.3. However, an example of NDWI as a measure of water indices is highlighted in Fig. 1.5.
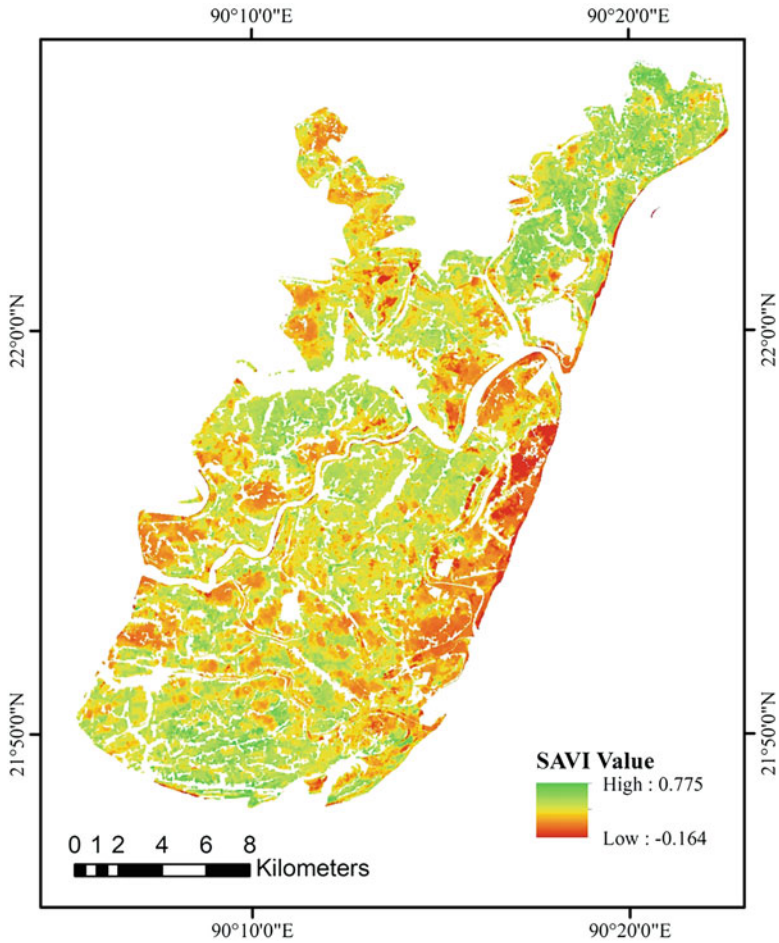
Fig. 1.4 Distribution of SAVI derived from Landsat 8 OLI during June 2020 from the Kalapara subdistrict in Bangladesh

Table 1.3 List of water-related indices used in agriculture and forestry research

Vegetation indices	Equation	References
Normalized difference water index (NDWI*Gao*) based on plant water content	$\frac{NIR-SWIR}{NIR+SWIR}$	Gao (1996)
Normalized difference water index (NDWI*McFeeters*) based on water body	$\frac{Green-NIR}{Green+NIR}$	Xu (2006)
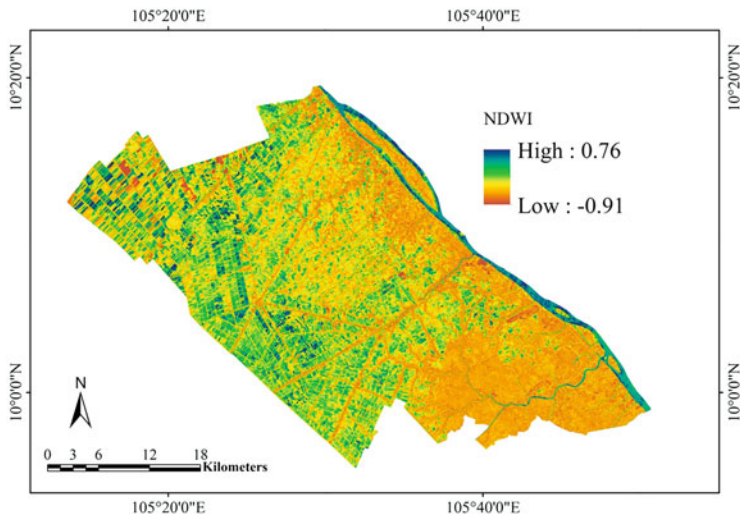
Fig. 1.5 Distribution of normalized difference water index based on a water body during August 2021 in the Can Tho province of Vietnam

1.4 Land Use Assessment

The assessment of land in the agriculture and forestry sectors is very important to driving sustainable development in developing nations. Population growth, industrialization, and rapid urbanization constantly cause agricultural land use changes, which have an influence on the ecological balance and food security around the world. Land use assessments have mainly focused on resource production and the influence on climate change (Lambin et al. 2001), soil erosion (Yang et al. 2003), biodiversity, food security (Lambin et al. 2003), and even threats to public health (Shi et al. 2018) while also concentrating on determining the drivers of LULC.

1.4.1 Land Use Land Cover (LULC) Analysis

Within a timeframe, the categorization or classification of human activities and natural elements (such as agricultural land, forest, urban area, water body, etc.) on the landscape based on established scientific and statistical methods from appropriate source materials refers to the land use land cover (LULC) classification. Data on vegetation, water, natural surfaces, and cultural features are described in the LULC classification (Akinci et al. 2013). Information about LULC is a very important requirement for administrative purposes, business development, and policymaking. The LULC data with their spatial details can also serve for environmental protection and planning. LULC data are vital because they can be used as input for modeling,

especially those related to climate change and policy-oriented data (Disperati and Virdis 2015).

LULC has two separate technologies that are interchangeably used (Dimyati et al. 1996). LULC classification can be performed from the available satellite images (such as Landsat and Sentinel) using GIS and machine learning approaches through image classification algorithms. For example, a composite natural color (RGB) image is produced from the seven bands (bands 1–7) of a satellite image, and then classification (supervised or unsupervised) is performed depending on the interest of the study and the attributes required for that research. According to the purposes, the spatial resolution can be fixed to develop an LULC map and to calculate the covered area. The accuracy of LULC classification depends on the resolution of the image and the ground reference information.

An LULC map with five land use classes (water body, wetland, vegetation, agricultural land, and urban) of five districts adjacent to the Jamuna River, Bangladesh, is shown in Fig. 1.6. The map was produced from Landsat 8 Operational Land Imager (OLI) satellite imagery acquired in 2020. The map was prepared to identify the effect of riverbank erosion in the five districts near the riverbank.

1.4.2   Land Use Change

The process by which the transformation of the natural landscape occurs through human and natural activities is referred to as land use change. The driving forces responsible for land use changes are population and climate. The demands of increasing populations put pressure on land resources, and climate change affects the supply or constraints of lands. These processes are very widespread, are accelerating, and impact natural ecosystems (Ruiz-Luna and Berlanga-Robles 2003; Turner and Ruscher 1988).

The land use change can be determined from the LULC classification, which is performed using satellite imagery through different remote sensing approaches, including change detection. To understand the dynamics of landscapes during a certain period, it is essential to identify land use change scenarios for sustainable land use management. For example, it is possible to calculate the increment of urban area in a certain place for a certain period or how much agricultural land or forest area has been reduced in a certain area within a certain period, which may be short term or long term. A land use change map from 2010 to 2017 in the suburban areas of Bangladesh shows rapid land use changes within a short period of time in Bangladesh (Fig. 1.7).
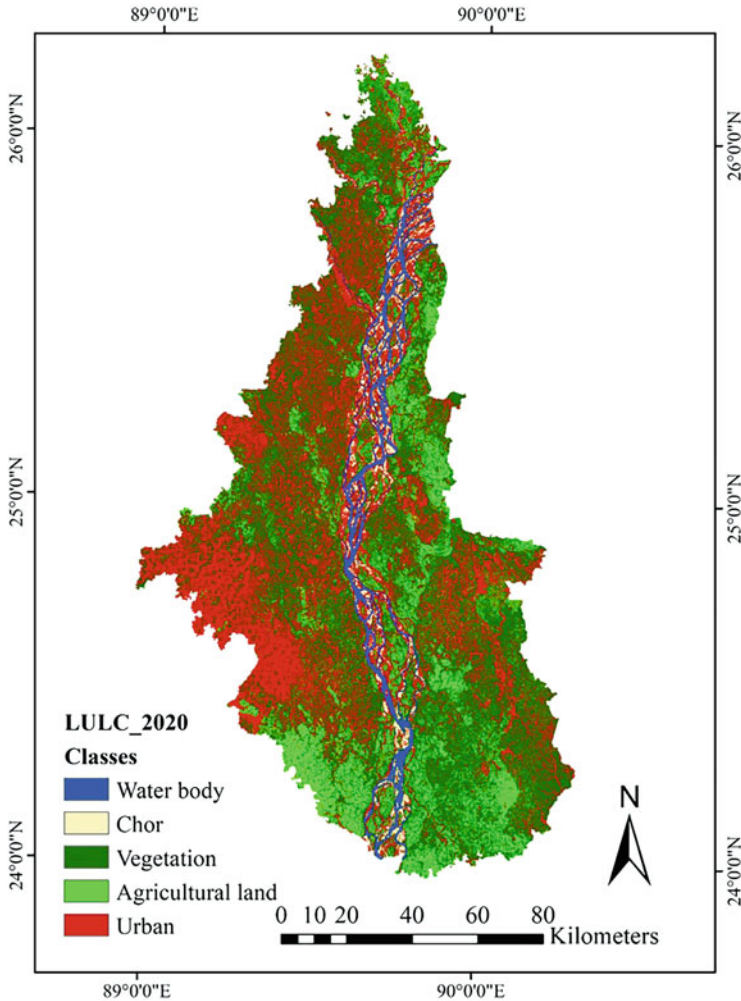
Fig. 1.6 Distribution of LULC classes (water body, wetland, vegetation, agricultural land, and urban) of five districts adjacent to the Jamuna River in Bangladesh

1.4.3 Land Suitability Analysis

Land suitability analysis (LSA) is a GIS-based approach used to establish the suitability of a given region based on land and environmental parameters to discover the best possible area for agriculture, urbanization, and socioeconomic analysis. In land suitability analysis, each criterion is overlaid based on the obtained weight through three methods: the analytical hierarchy process (AHP), the analytical network process (ANP), and fuzzy methods. The AHP was introduced by Saaty in 1980 and is still a powerful tool. This method can be used in two distinct procedures, such
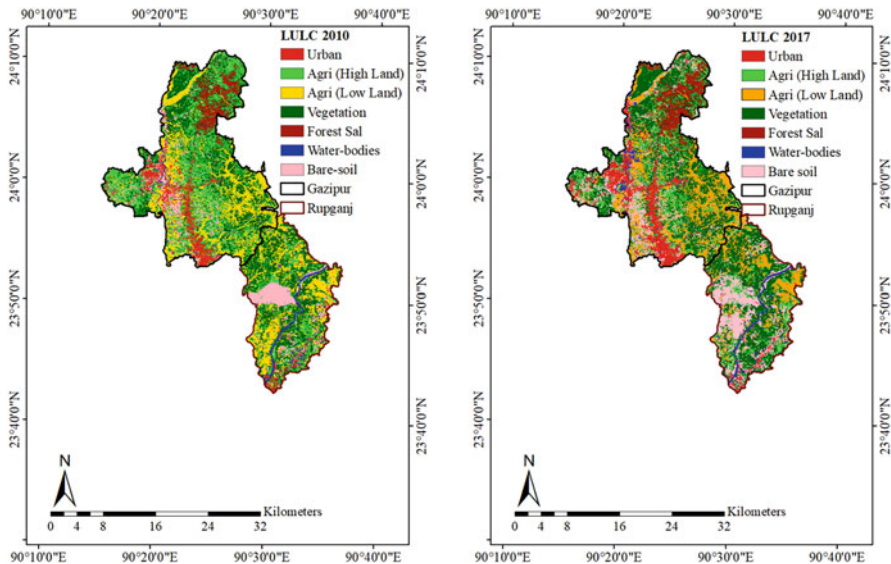
Fig. 1.7 Land use changes from 2010 to 2017 in suburban areas of the Gazipur and Rupganj in Bangladesh
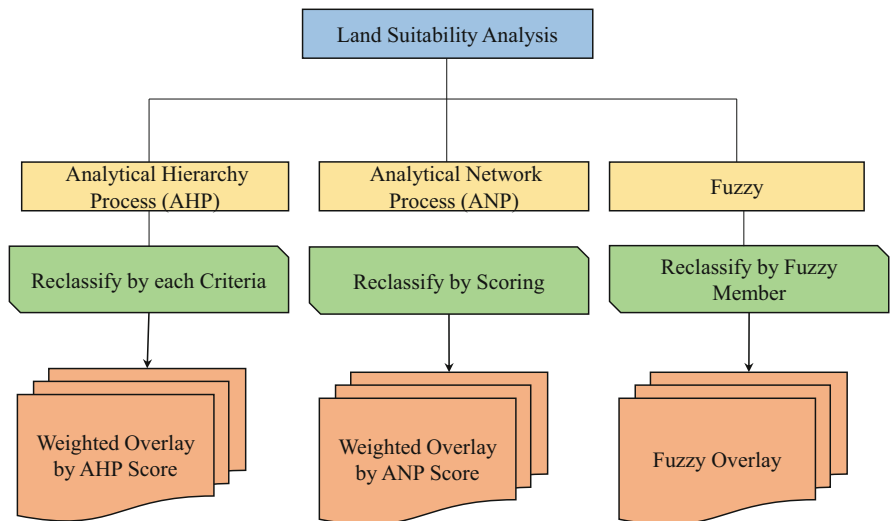
Fig. 1.8 Flowchart of land suitability analysis based on overlay methods

as weighting vector layers and raster layers. After obtaining the weight for each layer (vector or raster), the weight can be combined with other vector layers or raster layers to develop the final suitability map (Richard 1994) (Figs. 1.8 and 1.9).
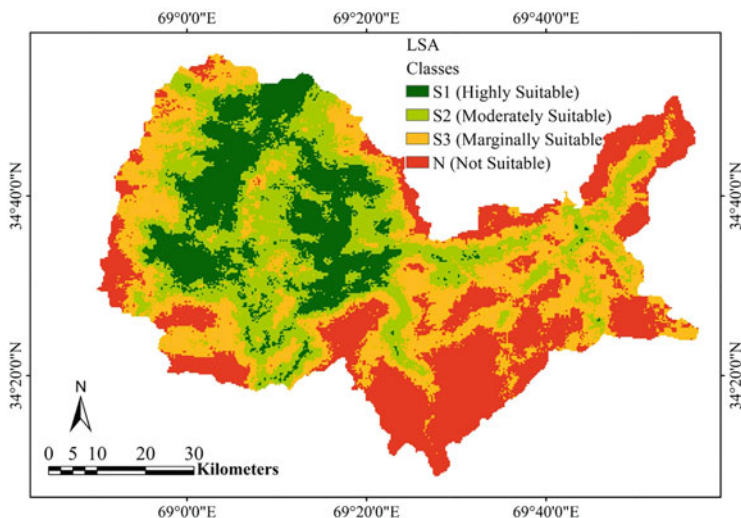
Fig. 1.9 The map shows the vineyard land suitability in Kabul Province of Afghanistan during 2020

On the other hand, ANP is more common than AHP for multicriteria decision-making procedures. This method was also developed by Saaty (1980) and is used for land suitability parameter (criteria) weight calculation. After obtaining the criterion weight by ANP, the map layers overlay in the ArcGIS interface. The fuzzy method has been used for multicriteria overlay analysis to investigate the relationship between the memberships of the various fuzzy sets (Azizi et al. 2014; Burrough et al. 1992).

Land suitability has many applications in agricultural crops (rice, tea, sugarcane, oil palm, grapes, maizes, and so on) and the forestry sector (prospective forest area) to ensure a better future. An example of a land suitability map is presented in Fig. 1.8, which shows four suitability classes, S_1 (highly suitable), S_2 (moderately suitable), S_3 (marginally suitable), and N (not suitable), for vineyards in Kabul Province of Afghanistan.

1.5 Disaster and Damage Assessment

Climate resilience assessment is vital in our period due to global climate change since it aids in adapting to climate change impacts and provides a better knowledge of present and long-term weather patterns. Drought, floods, flash floods, excessive rainfall, soil erosion, cyclones, wildfires, and other natural disasters are the most prevalent natural catastrophes, all of which have a direct impact on agricultural productivity and forestry. Water, wastewater, and stormwater utilities, as well as the

communities they serve, face issues as a result of climate change, including excessive temperatures and more powerful storms. Since 1880, the total land and ocean temperature has risen at an average pace of 0.13 °F (0.08 °C) every decade, according to NOAA's 2020 Annual Climate Report; however, the average rate of increase since 1981 (0.18 °C/0.32 °F) has been more than double that pace. How much carbon dioxide and other greenhouse gases we emit in the next decades will determine how much warming the Earth will experience in the future. Human activities now, such as burning fossil fuels and cutting forests, contribute approximately 11 billion metric tons of carbon to the atmosphere each year. In both the air and the sea, trends showing increasingly severe temperatures have been seen.

1.5.1   Drought Severity

Drought is a widespread natural disaster that refers to a period of time with declining soil moisture that consequently causes biomass and crop yield failure. Plant water requirements are affected by the weather, biological features of the individual plant and phases of growth, and physical and biological properties of the soil. Consequently, agricultural drought causes agricultural product loss, food shortages, famines, migration, and natural resource degradation in an area (Malmgren-Hansen et al. 2020). Many countries have suffered as a result of global warming and climate change, particularly developing countries where the majority of the population lives in rural areas and whose livelihoods are dependent on natural resources. Drought assessment using traditional methods requires time and budget, which is expensive. Therefore, traditional techniques are extremely challenging in most developing countries due to a lack of trustworthy data, limited information networks, and a lack of technological and institutional skills. To overcome these issues, it is preferable to use satellite sensor data, which are continuously accessible and cost-effective and may be used to detect the start of a drought, as well as its length and extent with a high efficacy level. In this regard, different types of satellite sensors, such as MODIS, Landsat, AVHRR, and Sentinel, have been used for drought monitoring (Rojas et al. 2011). A series of drought indices calculated based on a satellite remote sensing dataset was used to detect regional drought, which is presented in Table 1.4.

To cope with drought and to minimize agricultural product losses, it is important to analyze the drought impact on agricultural production at the early stages of plant growth using satellite remote sensing (Fig. 1.10). Moreover, providing support via agricultural organizations based on the drought conditions of each field could be an effective intervention for different drought-affected farms.

Table 1.4 Major drought monitoring indices used in agriculture

Indicators	Equation	References
Normalized difference vegetation index (NDVI)	$\frac{R_{NIR} - R_{red}}{R_{NIR} + R_{red}}$	Turner and Ruscher (1988)
Normalized difference water index (NDWI)	$\frac{NIR - SWIR}{NIR + SWIR}$	Gao (1996)
Vegetation condition index (VCI)	$\frac{NDVI_J - NDVI_{min}}{NDVI_{max} - NDVI_{min}} * 100$	Kogan (1990)
Temperature condition index (TCI)	$\frac{BT_{max} - BT_J}{BTI_{max} - BT_{min}} * 100$	Kogan (1995)
Vegetation health index (VHI)	$_a VCI + (1 + a) TCI$	Kogan (1997)
Standard precipitation index (SPI)	$\frac{P_{ijk} - \overline{P_{ij}}}{\delta_{ij}}$	Bonaccorso et al. (2003)
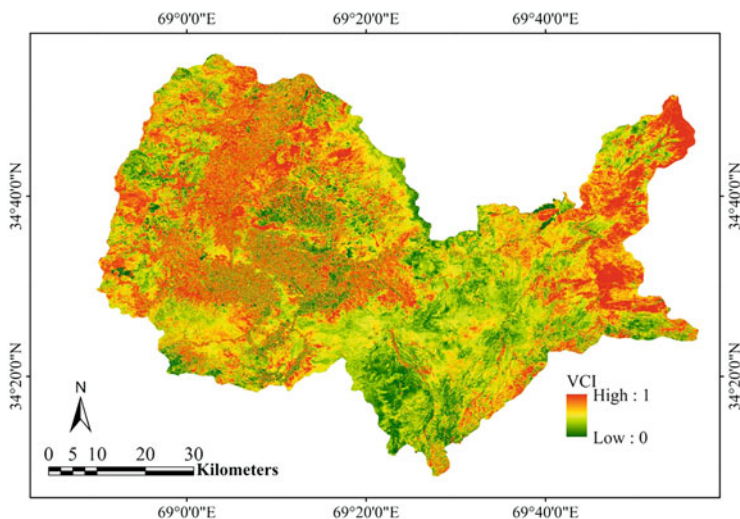
Fig. 1.10 The map shows the vegetation condition index (VCI) during the drought period in August 2021 in Kabul Province of Afghanistan

1.5.2 Flood Inundation

Flash flooding is defined as flooding that occurs within 6 h and commonly within 3 h of severe rainfall (or other sources). Flash floods can be caused by several scenarios but are most often due to extremely heavy rainfall, which are the main causes of damaging crops and livestock in this region. The consequences of these losses are very adverse for wetland farmers. However, the progress in minimizing or preventing this catastrophe has been inadequate, and hurdles continue to increase. Therefore, it is essential to develop an integrated approach to estimate damage proportions and sustainable and effective intervention strategies for vulnerable communities globally. Therefore, to improve and ensure sustainable livelihoods, it

is time to develop site-specific economic models by leveraging cutting-edge technology to optimize insurance premium rates based on different damage levels.

Application of Remote Sensing in Damage Assessment Through Inundation Analysis

Heavy rainfall, storms, and cyclones will become more frequent and intense because of global climate change, resulting in more floods and disasters (Seneviratne et al. 2012). In this regard, damage mapping is essential for enabling rapid crisis response, such as to help rescue, humanitarian, and reconstruction efforts in a disaster region. However, advanced technologies, particularly remote sensing and GIS, have become essential new instruments in disaster management in this area (Du et al. 2014). Furthermore, multiple approaches for classifying water pixels have been created by analyzing the surface reflectance collected by distinct spectral bands of optical sensors (Feyisa et al. 2014). Furthermore, numerous studies have revealed that NDWI is an important index for inundation modeling and analysis around the world in regard to removing surface water bodies and creating inundation maps (Du et al. 2014; Islam et al. 2021a, b). An example of flash flood inundation mapping based on a havoc flash flood on 28 March 2017 in Bangladesh is presented in Fig. 1.11.
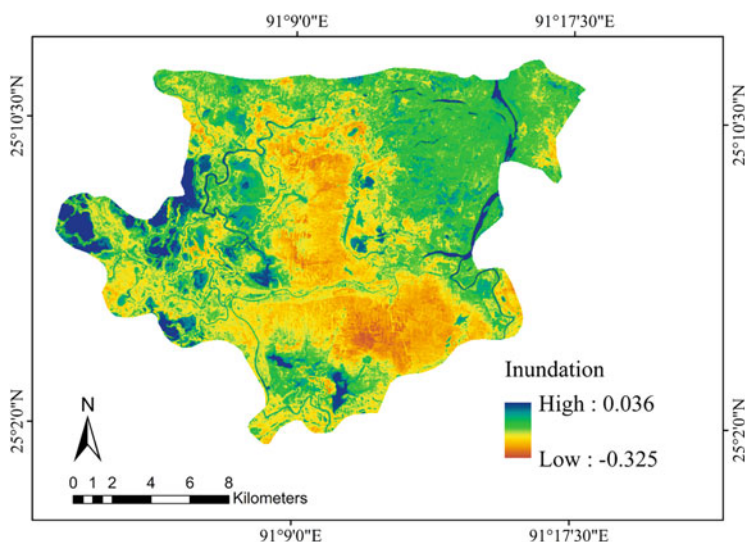
Fig. 1.11 Inundation map for damage assessment of Tahirpur subdistrict under Sunamganj district from Bangladesh

Intervention for Flash Flood-Affected Farmers Through Crop Insurance

Agricultural insurance has been studied and used extensively, but how much farmers prefer it over other safeguards is still unknown (Jensen et al. 2018). Given the magnitude and high exposure to various risks, mainly in developing nations, as well as issues with risk premiums with index insurance (Clement et al. 2018), large-scale, subsidized multiperil indemnity-based crop insurance programs have been an important aspect of government countermeasures (Hazell and Varangis 2020). However, without the explicit assistance of huge government subsidies, these programs have seldom experienced significant take-up rates, and in many countries, demand has been meager even at costs well below actuarially reasonable rates (Feng et al. 2020). Conventional indemnity-based insurance programs face a slew of well-documented issues, such as knowledge asymmetry in the form of adverse selection and moral hazard. They are also vulnerable to additional issues, such as high administrative costs and covariate risks, resulting in increased bankruptcy risks or higher reinsurance prices. These worries are amplified in developing countries, where information and knowledge shortages, as well as other structural and functional challenges, are more common (Anderson 2001). A damage-based crop insurance scheme for flash flood-affected wetland areas could be a viable and fruitful solution to assist all these challenges (Islam et al. 2021a, b).

1.5.3   Extreme Events

Extreme events enforce damage to crop yields and result in production losses in agricultural lands. Tropical cyclones are one of the most recurrent extreme events that cause extreme agricultural crop damage in South and Southeast Asian countries (Shamsuzzoha and Al-Maruf 2012; Hoque et al. 2018; Sattar and Cheung 2019; Malmgren-Hansen et al. 2020). In recent years, the tropical cyclone Amphan entered the coastal region of Bangladesh on 20 May 2020 (NAWG 2020), and the area was severely damaged. In this regard, a damaged area assessment (DAA) method was used to calculate the damage type in agricultural land areas (total 309.08 km^2) using Landsat 8 OLI and TIRS datasets due to cyclone Amphan in the Kalapara subdistrict in Bangladesh (Shamsuzzoha et al. 2021). The damaged area assessment was measured as (1) not damaged (10.96 km^2, 3.54%); (2) slightly damaged (51.99 km^2); (3) moderately damaged (102.41 km^2); (4) very damaged (89.76 km^2); and (5) extremely damaged (53.97 km^2) at the Kalapara subdistrict affected by cyclone Amphan (Fig. 1.12). In addition, 420 ground reference points were used to validate the damaged areas and further validate the assessment due to cyclones (Shamsuzzoha et al. 2021).
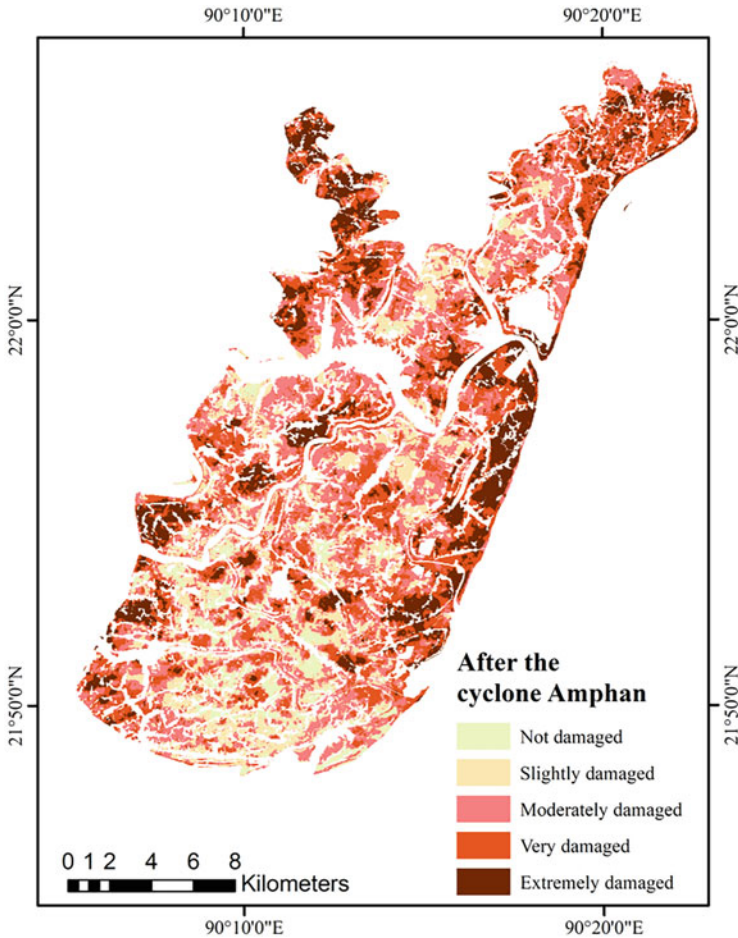
Fig. 1.12 The affected agricultural land in the Kalapara subdistrict in Bangladesh in the aftermath of cyclone *Amphan*

1.6 Conclusion

The sustainable management of bioresources from agriculture and forests is very important for food and environmental security. Agriculture and forestry are the primary sources of nourishment for present and future generations. It is essential to monitor these two domains in cost-effective ways. In this regard, satellite remote sensing and other advanced technologies provide many opportunities in agriculture and forestry for analyzing vegetation conditions; identifying and estimating crop growth; providing surveillance of forests, forest tree decline, and temporal soil changes in forests; evaluating desertification; and so on. In addition to vegetation

monitoring, it is also utilized for agricultural production forecasts with accurate, accessible, effective, and timely evaluations. Furthermore, another use of remote sensing in agriculture and forestry is the examination of land-based suitability and change detection. These two techniques can quickly determine the best locations for finding future land uses and changes that have occurred to land in the long run. Both analyses are beneficial to land resource management and monitoring. To rescue agricultural and forestry fields from natural catastrophes and to assist farmers' livelihoods during calamities, damage-based crop insurance can be an important risk management tool for poor farmers in emerging nations who face weather-related output concerns. Identifying the danger of a flash flood or severe drought and giving farmers precise information via inundation mapping or severity mapping might lead to a solution via the implementation of a damage-based crop insurance system. In addition to establishing advanced risk management methods and providing agricultural financing, subsidies, and service supply, policymakers and research institutions may benefit from damage estimation and assessing livelihood vulnerability on a single platform in a farm base or regional base. Therefore, remote sensing and GIS-based analytical datasets establish big data analytical platforms for sustainable agriculture and forest resource management.

References

Akinci H, Özalp AY, Turgut B (2013) Agricultural land use suitability analysis using GIS and AHP technique. Comput Electron Agric 97:71–82. https://doi.org/10.1016/j.compag.2013.07.006

ALOS-PASCO (2021) December 16. Retrieved from https://alos-pasco.com/

Anderson J (2001) Risk management in rural development: a review rural strategy, Background Paper 7. The World Bank, Washington

Arab ST, Noguchi R, Matsushita S, Ahamed T (2021) Prediction of grape yields from time-series vegetation indices using satellite remote sensing and a machine-learning approach. Remote Sens Appl Soc Environ 22:100485. https://doi.org/10.1016/j.rsase.2021.100485

Azizi A, Malekmohammadi B, Jafari HR, Nasiri H, Parsa VA (2014) Land suitability assessment for wind power plant site selection using ANP-DEMATEL in a GIS environment: case study of Ardabil province, Iran. Environ Monit Assess 186(10):669. https://doi.org/10.1007/s10661-014-3883-6

Bannari A, Morin D, Bonn F, Huete A (1995) A review of vegetation indices. Remote Sens Rev 13(1-2):95–120. https://doi.org/10.1080/02757259509532298

Baret F, Jacquemoud S, Hanocq JF (1993) The soil line concept in remote sensing. Remote Sens Rev 7(1):65–82. https://doi.org/10.1080/02757259309532166

Bonaccorso B, Bordi I, Cancelliere A, Rossi G, Sutera A (2003) Spatial variability of drought: an analysis of the SPI in Sicily. Water Resour Manag 17(4):273–296. https://doi.org/10.1023/A:1024716530289

Burrough PA, MacMillan RA, Van Deursen W (1992) Fuzzy classification methods for determining land suitability from soil profile observations and topography. J Soil Sci 43(2):193–210. https://doi.org/10.1111/j.1365-2389.1992.tb00129.x

Chen JM (1996) Evaluation of vegetation indices and a modified simple ratio for boreal applications. Can J Remote Sens 22(3):229–242. https://doi.org/10.1080/07038992.1996.10855178

Clement KY, Botzen WW, Brouwer R, Aerts JC (2018) 'A global review of the impact of basis risk on the functioning of and demand for index insurance. Int J Disaster Risk Reduc\t 28:845–853. https://doi.org/10.1016/j.ijdrr.2018.01.001

Colwell JE (1974) Vegetation canopy reflectance. Remote Sens Environ 3(3):175–183

Dimyati MUH, Mizuno K, Kobayashi S, Kitamura T (1996) An analysis of land use/cover change in Indonesia. Int J Remote Sens 17(5):931–944. https://doi.org/10.1080/01431169608949056

Disperati L, Virdis SGP (2015) Assessment of land-use and land-cover changes from 1965 to 2014 in Tam Giang-Cau Hai Lagoon, central Vietnam. Appl Geogr 58:48–64. https://doi.org/10.1016/j.apgeog.2014.12.012

Du Z, Li W, Zhou D, Tian L, Ling F, Wang H, Sun B (2014) Analysis of landsat-8 OLI imagery for land surface water mapping. Remote Sens Lett 5:672–681. https://doi.org/10.1080/2150704X.2014.960606

Duveiller G, Defourny P (2010) A conceptual framework to define the spatial resolution requirements for agricultural monitoring using remote sensing. Remote Sens Environ 114(11):2637–2650. https://doi.org/10.1016/j.rse.2010.06.001

Eli-Chukwu NC (2019) Applications of artificial intelligence in agriculture: a review. Eng Technol Appl Sci Res 9(4):4377–4383

FAO (2021) World food and agriculture statistical yearbook 2021. FAO, Rome. https://doi.org/10.4060/cb4477en

Feng H, Du X, Hennessy DA (2020) Depressed demand for crop insurance contracts, and a rationale based on third generation prospect theory. Agric Econ 51:59–73. https://doi.org/10.1111/agec.12541

Feyisa GL, Meilby H, Fensholt R, Proud SR (2014) Automated water extraction index: a new technique for surface water mapping using Landsat imagery. Remote Sens Environ 140:23–35. https://doi.org/10.1016/j.rse.2013.08.029

Foley JA, Ramankutty N, Brauman KA, Cassidy ES, Gerber JS, Johnston M, Mueller ND, O'Connell C, Ray DK, West PC et al (2011) Solutions of a cultivated planet. Nature 478:337–342. https://doi.org/10.1038/nature10452

Franklin P, Pearlstine L, Dewitt B, Smith S, Watts A, Ifju P (2006) Autonomus unmanned aerial vehicle (UAV) for ecological research. http://www.wec.ufl.edu/coop/print/posters/2006watts.pdf

Gao BC (1996) NDWI—A normalized difference water index for remote sensing of vegetation liquid water from space. Remote Sens Environ 58(3):257–266

Gitelson A, Merzlyak MN (1997) Remote estimation of chlorophyll content in higher plant leaves. Int J Remote Sens 18:291–298. https://doi.org/10.1080/014311697217558

Hardisky M, Klemas V, Smart M (1983) The influence of soil salinity, growth form, and leaf moisture on the spectral radiance of. Spartina Alterniflora 49:77–83

Harrower M, McCorriston J, Oches EA (2002) Mapping the roots of agriculture in Southern Arabia: the application of satellite remote sensing, global positioning system and geographic information system technologies. Archaeol Prospect 9(1):35–42. https://doi.org/10.1002/arp.182

Hazell P, Varangis P (2020) Best practices for subsidizing agricultural insurance. Glob Food Sec 25:100326. https://doi.org/10.1016/j.gfs.2019.100326

He C, Zhang Q, Li Y, Li X, Shi P (2005) Zoning grassland protection area using remote sensing and cellular automata modeling—a case study in Xilingol steppe grassland in northern China. J Arid Environ 63(4):814–826. https://doi.org/10.1016/j.jaridenv.2005.03.028

Hoque MA, Phinn S, Roelfsema C, Childs I (2018) Assessing tropical cyclone risks using geospatial techniques. Appl Geogr 98:22–33. https://doi.org/10.1016/j.apgeog.2018.07.004

Huang Y, Chen ZX, Tao YU, Huang XZ, Gu XF (2018) Agricultural remote sensing big data: management and applications. J Integr Agric 17(9):1915–1931

Huete AR (1988) A soil-adjusted vegetation index (SAVI). Remote Sens Environ 25(3):295–309. https://doi.org/10.1016/0034-4257(88)90106-X

Islam MM, Matsushita S, Noguchi R, Ahamed T (2021a) Development of remote sensing-based yield prediction models at the maturity stage of boro rice using parametric and nonparametric approaches. Remote Sens Appl 22:100494. https://doi.org/10.1016/j.rsase.2021.100494

Islam MM, Matsushita S, Noguchi R, Ahamed T (2021b) A damage-based crop insurance system for flash flooding: a satellite remote sensing and econometric approach. Asia-Pac J Reg Sci. https://doi.org/10.1007/s41685-021-00220-9

Jackson RD (1986) Remote sensing of biotic and abiotic plant stress. Annu Rev Phytopathol 24: 265–286

Jensen ND, Mude AG, Barrett CB (2018) How basis risk and spatiotemporal adverse selection influence demand for index insurance: evidence from northern Kenya. Food Policy 74:172–198. https://doi.org/10.1016/j.foodpol.2018.01.002

Kamilaris A, Kartakoullis A, Prenafeta-Boldú FX (2017) A review on the practice of big data analysis in agriculture. Comput Electron Agric 143:23–37. https://doi.org/10.1016/j.compag.2017.09.037

Kogan FN (1990) Remote sensing of weather impacts on vegetation in non-homogeneous areas. Int J Remote Sens 11:1405–1419

Kogan FN (1995) Application of vegetation index and brightness temperature for drought detection. Adv Space Res 15:91–100. https://doi.org/10.1016/0273-1177(95)00079-T

Kogan FN (1997) Global drought watch from space. Bull Am Meteorol Soc 78(4):621–636. https://doi.org/10.1175/1520-0477(1997)078<0621:GDWFS>2.0.CO;2

Laliberte A, Rango A, Slaughter A (2006) Unmanned aerial vehicle (UAVs) for rangeland remote sensing. In Proc. 3rd annual symposium research insights in semiarid ecosystems RISE. USDA-ARS Walnut Experimental Watershed

Lambin EF, Turner BL, Geist HJ, Agbola SB, Angelsen A, Bruce JW, Coomes OT, Dirzo R, Fischer G, Folke C, George P (2001) The causes of land-use and land-cover change: moving beyond the myths. Glob Environ Chang 11(4):261–269. https://doi.org/10.1016/S0959-3780(01)00007-3

Lambin EF, Geist HJ, Lepers E (2003) Dynamics of land-use and land-cover change in tropical regions. Annu Rev Environ Resour 28(1):205–241

Langley SK, Cheshire HM, Humes KS (2001) A comparison of single date and multitemporal satellite image classifications in a semi-arid grassland. J Arid Environ 49(2):401–411. https://doi.org/10.1006/jare.2000.0771

Lenney MP, Woodcock CE, Collins JB, Hamdi H (1996) The status of agricultural lands in Egypt: the use of multitemporal NDVI features derived from Landsat. Remote Sens Environ 56(1): 8–20. https://doi.org/10.1016/0034-4257(95)00152-2

Lillesand TM, Kiefer RW (1994) Remote sensing and image interpretation, 3rd edn. Wiley, New York

Lyzenga DR (1978) Passive remote sensing techniques for mapping water depth and bottom features. Appl Opt 17(3):379–383. https://doi.org/10.1364/AO.17.000379

Major DJ, Baret F, Guyot G (1990) A ratio vegetation index adjusted for soil brightness. Int J Remote Sens 11(5):727–740. https://doi.org/10.1080/01431169008955053

Malmgren-Hansen D, Sohnesen T, Fisker P, Baez J (2020) Sentinel-1 change detection analysis for cyclone damage assessment in urban environments. Remote Sens 12(15):2409. https://doi.org/10.3390/rs12152409

Merrick T, Jorge MLS, Silva TS, Pau S, Rausch J, Broadbent EN, Bennartz R (2020) Characterization of chlorophyll fluorescence absorbed photosynthetically active radiation, and reflectance-based vegetation index spectroradiometer measurements. Int J Remote Sens 41(17):6755–6782. https://doi.org/10.1080/01431161.2020.1750731

NASA (2021) December 16. Retrieved from https://modis.gsfc.nasa.gov/data/dataprod/

NAWG (2020) Cyclone amphan: joint rapid assessment report. Needs Assessment Working Group (NAWG) of Bangladesh, Dhaka

Qi J, Chehbouni A, Huete AR, Kerr YH, Sorooshian S (1994) A modified soil adjusted vegetation index. Remote Sens Environ 48(2):119–126

Rahim HRBA, Lokman MQB, Harun SW, Hornyak GL, Sterckx K, Mohammed WS, Dutta J (2016) Applied light-side coupling with optimized spiral-patterned zinc oxide nanorod coatings for multiple optical channel alcohol vapor sensing. J Nanophoton 10(3):036009. https://doi.org/10.1117/1.JNP.10.036009

Ranjan R, Chandel AK, Khot LR, Bahlol HY, Zhou J, Boydston RA, Miklas PN (2019) Irrigated pinto bean crop stress and yield assessment using ground based low altitude remote sensing technology. Inf Process Agric 6(4):502–514. https://doi.org/10.1016/j.inpa.2019.01.005

Richard JL (1994) Detection of zones of abnormal strains in structures using Gaussian curvature analysis. AAPG Bull 78(12):1811–1819. https://doi.org/10.1306/A25FF305-171B-11D7-8645000102C1865D

Rojas O, Vrieling A, Rembold F (2011) Assessing drought probability for agricultural areas in Africa with coarse resolution remote sensing imagery. Remote Sens Environ 115(2):343–352. https://doi.org/10.1016/j.rse.2010.09.006

Rondeaux G, Steven M, Baret F (1996) Optimization of soil-adjusted vegetation indices. Remote Sens Environ 55(2):95–107. https://doi.org/10.1016/0034-4257(95)00186-7

Rouse JW, Haas RH, Schell JA, Deering DW (1973) Monitoring vegetation systems in the great plains with ERTS. In Third ERTS Symp., NASA SP-351, U.S. Gov. Printing Office, Washington, DC, vol I, pp 309–317

Ruiz-Luna A, Berlanga-Robles CA (2003) Land use, land cover changes and coastal Lagoon surface reduction associated with urban growth in northwest Mexico. Landsc Ecol 18(2):159–171. https://doi.org/10.1023/A:1024461215456

Saaty TL (1980) The analytic hierarchy process. McGraw-Hill, New York

Sattar AM, Cheung KKW (2019) Comparison between the active tropical cyclone seasons over the Arabian Sea and Bay of Bengal. Int J Climatol 39(14):5486–5502. https://doi.org/10.1002/joc.6167

Seneviratne SI, Nicholls N, Easterling D, Goodess CM, Kanae S, Kossin J, Luo Y, Marengo J, McInnes K, Rahimi M et al (2012) Changes in climate extremes and their impacts on the natural physical environment. In: Field CB, Barros V, Stocker TF, Qin D, Dokken DJ, Ebi KL, Mastrandrea MD, Mach KJ, Plattner G-K, Allen SK et al (eds) Managing the risks of extreme events and disasters to advance climate change adaptation; a special report of working groups I and II of the Intergovernmental Panel on Climate Change (IPCC). Cambridge University Press, Cambridge, pp 109–230

Shamsuzzoha M, Al-Maruf A (2012) Post SIDR life strategy: adaptation scenario of settlements of the south. Inst Bangladesh Stud J 19:207–222

Shamsuzzoha M, Noguchi R, Ahamed T (2021) Damaged area assessment of cultivated agricultural lands affected by cyclone bulbul in coastal region of Bangladesh using Landsat 8 OLI and TIRS datasets. Remote Sens Appl 23:100523. https://doi.org/10.1016/j.rsase.2021.100523

Shi G, Jiang N, Yao L (2018) Land use and cover change during the rapid economic growth period from 1990 to 2010: a case study of shanghai. Sustain For 10(2):426. https://doi.org/10.3390/su10020426

Stubb M (2016) Big data in US agriculture. Congressional Research Service, Washington, DC

Turner MG, Ruscher CL (1988) Changes in landscape patterns in Georgia, USA. Landsc Ecol 1(4):241–251. https://doi.org/10.1007/BF00157696

USGS (2021) December 16. Retrieved from https://earthexplorer.usgs.gov/

Vogelmann TC (1993) Plant tissue optics. Annu Rev Plant Physiol Plant Mol Biol 44:231–251. https://doi.org/10.1146/annurev.pp.44.060193.001311

Wang SL, Heisey P, Schimmelpfennig D, Ball E (2015) US agricultural productivity growth: the past, challenges, and the future (No. 1490-2016-128351)

Xu H (2006) Modification of normalised difference water index (NDWI) to enhance open water features in remotely sensed imagery. Int J Remote Sens 27(14):3025–3033. https://doi.org/10.1080/01431160600589179

Xue J, Su B (2017) Significant remote sensing vegetation indices: a review of developments and applications. J Sens 2017:1353691. https://doi.org/10.1155/2017/1353691

Yang D, Kanae S, Oki T, Koike T, Musiake K (2003) Global potential soil erosion with reference to land use and climate changes. Hydrol Process 17(14):2913–2928. https://doi.org/10.1002/hyp.1441

Zhou L, Chen N, Chen Z, Xing C (2016) ROSCC: an efficient remote sensing observation-sharing method based on cloud computing for soil moisture mapping in precision agriculture. IEEE J Select Top 9(12):5588–5598. https://doi.org/10.1109/JSTARS.2016.2574810

Zhu L, Suomalainen J, Liu J, Hyyppä J, Kaartinen H, Haggren H (2018) A review: remote sensing sensors. In: Multi-purposeful application of geospatial data. Intech Open, London, pp 19–42. https://doi.org/10.5772/intechopen.71049

Chapter 2
Calorie-Based Seasonal Multicrop Land Suitability Analysis Using GIS and Remote Sensing for Regional Food Nutrition Security in Bangladesh

Rubaiya Binte Mustafiz, Ryozo Noguchi, and Tofael Ahamed

Abstract Cereal-based food consumption and agricultural practices contribute to food nutritional insecurity, which has become a threatening issue in South Asian countries. The purpose of this research is to develop a seasonal land use planning model incorporating diversified crops for regional self-sufficiency based on land suitability and a balanced calorie demand. A multicriteria decision-making analysis was undertaken, and multicrop land planning maps were developed with the help of a geographical information system (GIS) and fuzzy membership functions. The vegetation index data were collected according to the crop calendar. The factors and constraints were generated in ArcGIS 10.4$^{®}$ to perform spatial analysis. Fuzzy overlay analysis was performed to determine the suitable areas for crop production. The seasonal cropland suitability assessment results were validated with data from the Survey of Bangladesh (SoB). Among the three individual cropping seasons in Bangladesh, the analysis determined that, in the Kharif-1 season, 42% (3469 km^2) of the total area was suitable for vegetable growing and, in the Kharif-2 season, the area of suitability was 55% (4543 km^2). However, in the present practices, only 12% and 18% of the land are used for vegetable cultivation in the Kharif-1 and Kharif-2 seasons, respectively, which are less than the regional requirements. In addition, in the Rabi season, the most suitable zones for cereals, vegetables, pulses, oilseeds, and potatoes were reported as 35% (2891 km^2), 19% (1569 km^2), 15% (1239 km^2), 10% (826 km^2), and 21% (1734 km^2) of the total land area, respectively. Moreover, the land areas suitable for farming pulses and oilseeds were found to be 15% (1239 km^2) and 10% (826 km^2), respectively. The integrated model proposed herein could be implemented for the management of land allocation for diversified crop production,

R. B. Mustafiz
Graduate School of Life and Environmental Sciences, University of Tsukuba, Tsukuba, Ibaraki, Japan

R. Noguchi · T. Ahamed (✉)
Faculty of Life and Environmental Sciences, University of Tsukuba, Tsukuba, Ibaraki, Japan
e-mail: tofael.ahamed.gp@u.tsukuba.ac.jp

providing more decision-making information for policymakers to ensure regional food nutrition security in the target area as well as in other South Asian countries.

Keywords Calorie demand · Food nutrition · Fuzzy membership · Fuzzy multicriteria decision-making · GIS · Land suitability · Seasonal crop mapping · Regional self-sufficiency

2.1 Introduction

Diet, nutrition, and health are closely interrelated. The availability of foods does not ensure the intake of a well-balanced diet; a well-balanced diet depends on optimum food consumption, purchasing capacity, and local food habits (World Health Organization 2019). The food nutrition security concept refers to increasing food availability, improving food accessibility, enhancing crisis prevention and management, and improving the nutritional adequacy of food intake (El Bilali et al. 2019). Dietary intake patterns are especially related to energy, protein, and micronutrient-rich foods and the diversity of food items. The Food and Agriculture Organization (FAO) of the United Nations evaluated in 2001 that 53% of the world's average daily calorie intake was provided by cereals and starch-based staples in overall food consumption. Cereals and starch-based staples also compose approximately 26% of the daily calories consumed in the United States (US); however, in Bangladesh, these staples compose 83% of the daily calories consumed. In Bangladesh, the major food groups have been limited and dominated by cereals. As a result, dietary patterns have been relatively stable over time for this region where rice dominates as the major cereal.

In addition, rice is a staple food for over half of the world's population (Food and Agriculture Organization of the United Nations (FAO) 2004a, b). Rice accounts for over 20% of the global calorie intake. Around 90% of the world's rice is produced and consumed in Asia by six countries (China, India, Indonesia, Bangladesh, Vietnam, and Japan) (Abdullah et al. 2006). Rice feeds more than two billion people in the developing countries of Asia (Food and Agriculture Organization of the United Nations (FAO) 1995). In Asia, Africa, and Latin America, the demand trend for rice consumption is increasing (Wang and Li 2005).

Therefore, monotonous dietary practices create a new hazard that can preclude a healthy life. Specifically, South Asian food consumption is dominated by cereals (Mottaleb et al. 2018); 25% of the world (Food and Agriculture Organization of the United Nations (FAO) 2014a, b), almost 23% of the population, does not have access to adequate calorie intake (WDI 2014). Bangladesh is vulnerable to inadequate nutritional security and has a tendency to increase cereal crop production. One-third of households in Bangladesh are affected by food insecurity with significant inequalities regarding access to food (Bangladesh Institute of Research and Rehabilitation in Diabetes, Endocrine and Metabolic Disorders (BIRDEM) 2013; HIES 2016). Rice accounts for over 50% by weight and 70% by calories of the total food (Food and Agriculture Organization of the United Nations (FAO) 2014a, b). Food habits are a natural practice for each region. However, imbalanced food

consumption creates a new issue in terms of food nutritional inadequacy globally. This inadequacy in food nutrition is observed more acutely in developing countries where cereals dominate food consumption. Imbalanced food consumption practices influence these countries to produce more cereals to ensure their social and political stability. Most of the agricultural lands in developing countries are occupied by cereal crop production throughout the year, which also creates another issue: water resource depletion. Rice is mostly grown under irrigated conditions, and maize is usually limited to irrigated areas or regions where precipitation is both adequate and dependable (Koohafkan and Stewart 2008). Wheat is the most widely grown cereal crop and is extensively grown in dryland regions under both nonirrigated and irrigated conditions (Koohafkan and Stewart 2008). On a consumptive use basis, 80–90% of the water is consumed in agriculture (Hamdy et al. 2003). Using water for irrigation expansion not only is a costly approach but also threatens conditions because of soil degradation, particularly the buildup of salts and the depletion of water resources (Cosgrove et al. 2000). Food and Agriculture Organization of the United Nations (FAO) (2003) estimated that irrigated land, which currently covers 197 million ha in developing countries, will increase by 45 million ha by 2030. Bangladesh is a developing country where food consumption is dominated more by carbohydrates (rice and wheat-based food items) than by vegetables, oilseeds, and pulses. Land use plans considering climatic factors would be a potential solution for this region. The climatic requirements in different seasons are characterized by different climatic atmospheres that normally affect crop germination, growth, flowering, and ultimately yield (Todmal et al. 2018).

Following this concern, climatic smart agriculture and multicriteria decisions for land use plans are required. Land suitability analysis (LSA) can be performed using the multicriteria decision method (MCDM). Several approaches of MCDM using fuzzy membership systems have been used to conduct land suitability evaluations (Ostovari et al. 2019; Elsheikh et al. 2013; Kazemi and Akinci 2018). The MCDM becomes more appropriate with geospatial references. In recent years, computing technologies combined with GIS have enabled geospatial references using land suitability evaluation based on FAO classes (Food and Agriculture Organization of the United Nations (FAO) 1976). In MCDM, fuzzy set membership has the capability to standardize the criteria (Aydi et al. 2016; Feizizadeh et al. 2013; Romano et al. 2015). The fuzzy set theory allows for continuous factors to be modeled for suitability assessment within GIS analysis. However, most of those studies used either the MCDM technique or the fuzzy set overlay alone, resulting in an inadequately handled weight of each factor or an inappropriate calculation of the suitability index. Furthermore, the MCDM with fuzzy set theory has the potential to reduce the subjectivity in the assessment of the results. An integrated approach combining GIS with fuzzy set theory and land use planning using the proportion of calories has substantial potential to design and allocate multicrop seasonal land use planning. In addition, the fuzzy overlay technique in the GIS platform has the opportunity to overcome the above limitations by applying the required (FAO-recommended) calorie ratio to prepare seasonal multicrop land suitability maps for regional self-sufficiency.

Therefore, the purpose of this research is to develop a seasonal multicrop land suitability analysis model based on land use planning to determine the optimal land distribution according to dietary intake to ensure nutritional food security using fuzzy-based multicriteria decision analysis. A methodology has been proposed to be adopted in other countries to reduce the dependency on cereal production to achieve nutritional food security.

2.2   Materials and Methods

The proposed method using GIS-based multicriteria analysis to develop a seasonal map for land use planning consists of three major steps (Fig. 2.1): the calculation of calorie demand of the target area, the creation of suitability maps of diversified crops,
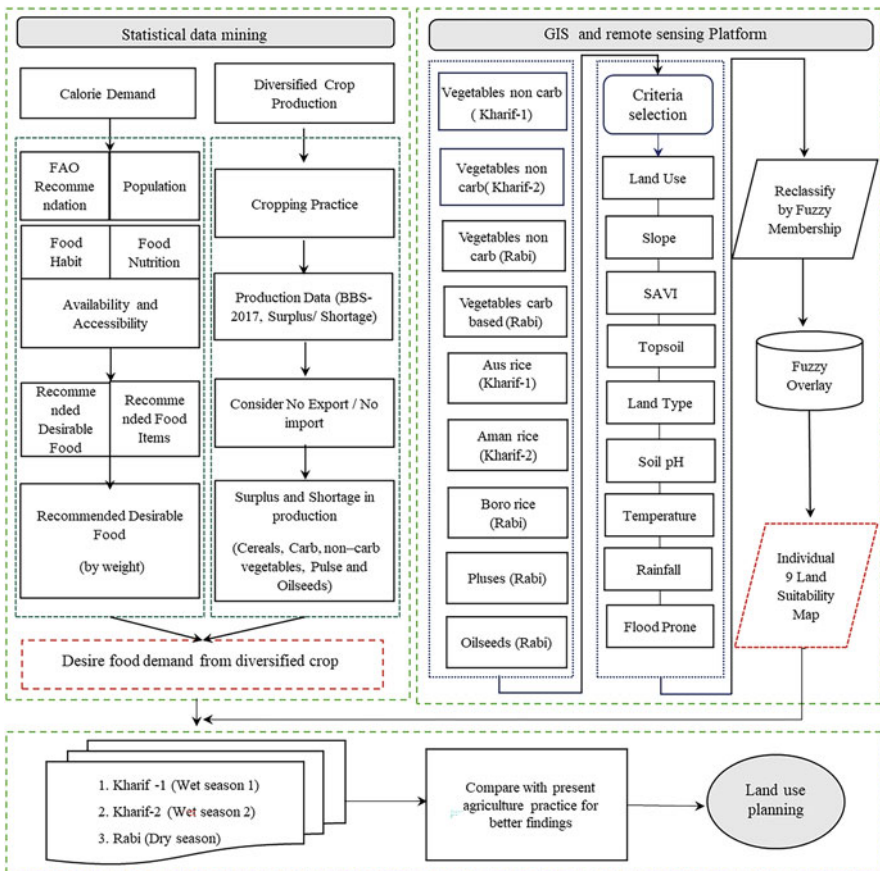
Fig. 2.1 Research framework for multicrop land use plan

and the proposal of seasonal maps. ArcGIS 10.4® (ESRI, Boston, CA) software was used for criteria aggregation, data preprocessing and calculation standardization, weight determination by a fuzzy membership function, fuzzy overlay, and raster calculation.

2.2.1 Study Area

The study was conducted in the Dinajpur, Rangpur, Kurigram, and Gaibandha districts of the Rangpur Division (Fig. 2.2b), a region that is highly vulnerable to food nutrition insecurity. The area consists of 37 administrative units with an overall population of 11,498,000 (Bangladesh Bureau of Statistics (BBS) 2011). In this region, the unhealthy or borderline food consumption pattern rate is higher than in other regions (Fig. 2.2a). Agriculture is the main source of income in the study area; nevertheless, agronomic land use is highly inconsistent due to climatic factors, soil property issues, water infiltration, environmental resources, and local socioeconomic conditions. Based on weather data, the minimum and maximum mean annual
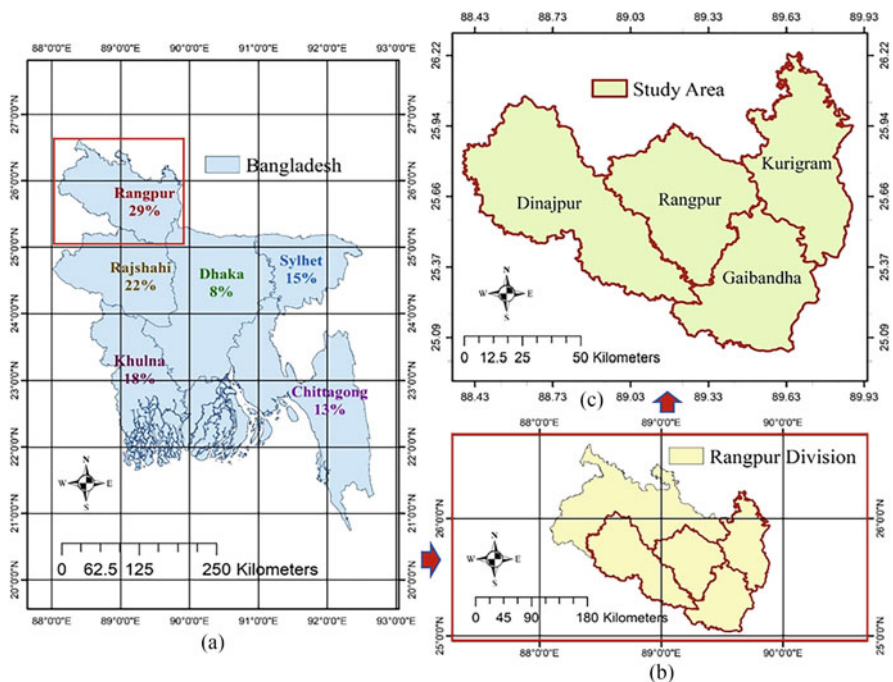
Fig. 2.2 (**a**) High prevalence of undernutrition throughout Bangladesh. (**b**) Northern part of Bangladesh (Rangpur Division), (**c**) study area: four districts of Rangpur Division, Dinajpur, Rangpur, Gaibandha, and Kurigram

temperatures vary between 8.47 °C and 36.3 °C. The annual average rainfall recorded is 765–1233 mm with high humidity at 41–77% (Bangladesh Bureau of Statistics (BBS) 2018a, b). The elevation ranges from 5 to 30 m above sea level.

2.2.2 Desirable Calorie Demand

Bangladesh Institute of Research and Rehabilitation in Diabetes, Endocrine and Metabolic Disorders (BIRDEM) has published a report of desirable dietary pattern for Bangladesh in 2013. The suggested food formation was formed by varieties item considering balanced nutrition (Table 2.1). This recommended food plan was followed by FAO/WHO (World Health Organization) recommendations for requirements of macro- and micronutrients. Besides, food items were chosen according to population, local people food habit, cropping practice, accessibility, and availability (Fig. 2.1). This assessment was developed for a single year. In the same way, the procedure was used for the following years.

The recommended desirable food items were calculated based on energy requirement, nutrient requirement, food intake pattern following the reference, household dietary diversity score (HDDS), key food identification, and crop calendar. Besides, the proposed result was adapted with the updated FAO/WHO recommendations for requirements of macro- and micronutrients. A minor modified chart was assisted in the current research. Desirable calorie demand was calculated as g/person/day. The production of different crops was converted into calorie equivalents by assuming that all crop production was consumed without any being exported or wasted. Food items applied for energy requirements were calculated by weight. First, daily food consumption was computed in g/day. After that, desirable food intake was calculated (in metric tons per year).

Table 2.1 Recommended desirable food items

Food		Desirable intake (g)		Energy (%)
Cereal	Major	350	400	56.0
	Minor	50		
Pulses		50		6.5
Vegetables items	Carb-based	100	400	8.0
	Non-carb-based	300		
Oil seed		30		11.0
Sugar/molasses		20		3.0
Animal foods		260		10.5
Fruits		100		3.0
Spices		20		2.0
Total		1280		100.0

Source: Bangladesh Institute of Research and Rehabilitation in Diabetes, Endocrine and Metabolic Disorders (BIRDEM) (2013)

(a) Step 1:

Desirable net calorie intake (g) or total requirement of each food items:

$$\text{TF} = \sum_{i=1}^{n} R_i \times P \times 365 \tag{2.1}$$

P is the total population of target area. Annual based (365 days) calculation was done. R_i is the daily requirement of major food items ($n = 8$) by metric ton (Table 2.1).

(b) Step 2:

In the second phase, potential diversified food crops were selected to estimate the required production annually. In the analysis, the annual production information of selected crops was collected from the Bangladesh Bureau of Statistics (BBS) (2016). There were 78 varieties of food items locally grown, and they were divided into 8 groups of recommended food classes (Appendix). The total production of crops can be expressed as:

$$\text{TP} = \sum_{j=1}^{n1} \text{CL}_j + \sum_{k=1}^{n2} \text{VN}_k + \sum_{l=1}^{n3} \text{VC}_l + \sum_{m=1}^{n4} \text{OS}_m + \sum_{p=1}^{n5} \text{PL}_p$$
$$+ \sum_{q=1}^{n6} \text{FR}_q + \sum_{r=1}^{n7} \text{SP}_r + \sum_{s=1}^{n8} \text{MS}_s \tag{2.2}$$

where CLj refers to cereals (vector variable), in which ith element is the intake of nutrient of type i through the cereal of type j ($j = 1,2, \ldots, n1$) and $n1$ is the number of cereals, $n_1 = 5$, which can be produced in the study area. Similarly, VN_k refers to noncarbohydrate vegetables, in which ith element is the intake of nutrient of type i through noncarbohydrate vegetables of type k ($j = 1,2, \ldots, n2$); $n2$ is the number of noncarbohydrate vegetables ($n_2 = 31$). In the same way, VC_l refers to carbohydrate vegetables ($n_3 = 2$); OS_m refers to oilseeds ($n_4 = 4$); PL_p refers to pulses ($n_5 = 7$); FR_q refers to fruits ($n_6 = 18$); SP_r refers to spices ($n_7 = 8$); and MS_s refers to molasses/sugars ($n_8 = 3$) (Table 2.1, Appendix). n ($n_1 \ldots \ldots n_8$) refers to the variation of each food group. For example, CL is denoted as a cereal food that is usually grown in the study area. In ($n_1 = 5$), there are five varieties of cereal: Aus rice, Aman rice, Boro rice, wheat, and maize. Following this way, the next item is VN that denoted noncarbohydrate vegetables, and here, $n_2 = 31$. In this group, there are 31 varieties of vegetables, such as cauliflower, tomato, radish, bean, eggplant, cabbage, bitter gourd, pumpkin, and other listed crops (Appendix).

(c) Step 3:

The specific crops that required further production to meet the calorie or nutritional requirements were identified. Food items produced more than required regionally were also identified (from Eqs. (2.1) and (2.2)) and can be expressed as:

Fig. 2.3 Recommended energy percentage from diversified food items per person/day
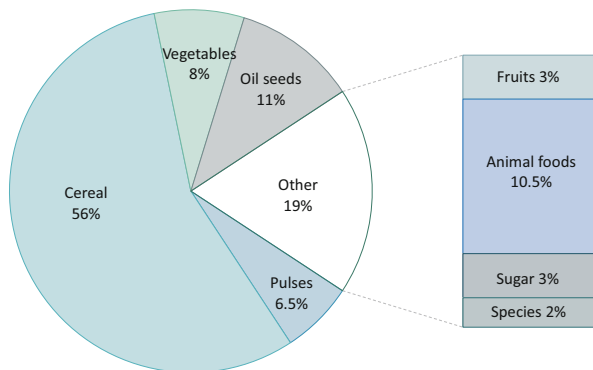
$$TP \geq T\text{F}, G = \text{TP} - \text{TF} \qquad (2.3)$$

where G is a vector variable, in which element showed surplus (if positive) or shortage (if negative) in intakes of nutrient. In this research, a primary land use plan was proposed for cereal food items, vegetables, oilseeds, and pulses. Fruits, spices, and molasses/sugars were not considered for current land use planning (Fig. 2.3). Therefore, land use planning was designed based on 81.5% of the total calorie consumption. Therefore, Eq. (2.2) is given by the following expression that was used for this research (for Eq. (2.4), indices were as like as Eq. (2.2)):

$$\text{TP} = \sum_{j=1}^{n1} \text{CL}_j + \sum_{k=1}^{n2} \text{VN}_k + \sum_{l=1}^{n3} \text{VC}_l + \sum_{m=1}^{n4} \text{OS}_m + \sum_{p=1}^{n5} \text{PL}_p \qquad (2.4)$$

2.2.3   Seasonal Cropping Strategies/Crop Calendar

In Bangladesh, diversified crops are grown by rotation usually three times on the same piece of land in a year. There are three main cropping seasons: (1) pre-Kharif or pre-monsoon (also called Kharif-1) from March/April to June/July, (2) Rabi or winter from October/November to February/March, and (3) Kharif or monsoon (also called Kharif-2) from June/July to September/October. In Kharif-2, rice is mostly under rainfed conditions. During the Rabi season, a wide range of crops, including rice (called Boro), wheat, maize, pulses (chickpea, lentil, and field peas), potatoes, and oilseeds, are grown. In Kharif-1, short-duration cultivars and rice (called Aus) are grown. Thus, rice-rice (R-R), rice-wheat (R-W), and rice-maize (R-M) are the dominant systems; besides, other vegetables, pulses, and oilseeds are grown. In Bangladesh, cropping practices are especially rice-based (Timsina et al. 2018). However, established landowners decide everything, and people's intake of nutrients must be constrained by the cropping pattern that is decided by landowners
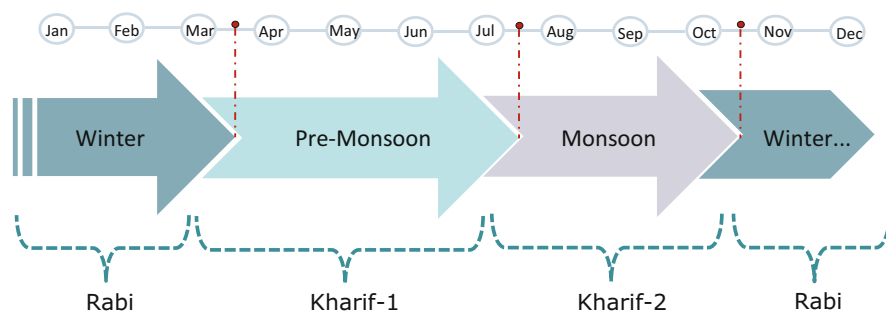
Fig. 2.4 Crop practice calendar in the northern part of Bangladesh

because tenant farmers are paid by with spot goods. Even if there can be several established landowners and even if their dynamic cropping system may be different, tenant farmers' intake of nutrients must be restricted to what they produce as they have almost no cash earnings and no access to the market. In addition, cropping practices influence food consumption patterns regionally. The crops in each sequence were selected from major cereals, minor cereals, pulses, oilseeds, carbohydrate-based vegetables, and noncarbohydrate-based vegetables that are locally grown in the study area. Usually, the triple-cropping strategy in a year is the most popular and extensively applicable method in Bangladesh (Fig. 2.4) (Nasim et al. 2017; Alam et al. 2010; Sarker et al. 1997; Hassan et al. 1985).

2.2.4 Land Suitability with Multicriteria Decision Analysis

LSA is a challenging task consisting of different domains; climatic conditions, environmental aspects, and topography are involved and influential in the production process. Moreover, the suitability of land is also affected by local regulations and the availability of land. The complexity of LSA increases when areas with mixed land uses and densely populated areas are considered. Multicriteria decision-making is a process that combines and transforms many types of geographical data (Table 2.2) into a resulting decision output (Malczewski 2006). The decision problems consist of a large set of reasonable alternatives and multiple conflicting and disproportionate criteria. As a result, many real-world spatial problems give rise to MCDM based on GIS. According to the research objectives in this study, nine criteria were selected to conduct MCDM with several steps in the spatial environment (Beinat and Nijkamp 1998). In MCDM, each criterion for a different crop was given a weight to represent its importance in the phenomenon (Chow and Sadler 2010). Multicriteria evaluation (MCE) approach (assessed by fuzzy membership function in ArcGIS® platform) was used in the current study because various production variables can be evaluated and

Table 2.2 Inputs for criteria of crop suitability

No	Data	Description	Source
1	Land use map	Scale 1:25,000	2019, SoB, Bangladesh
2	SAVI	Derived from 30-m resolution	Landsat 8, USGS
3	Slope map	Derived from 30-m resolution	2019, DEM, STRM
4	Land type	Scale 1:50,000	2018, BCA, Bangladesh
5	Topsoil map	Scale 1:50,000	2018, BCA, Bangladesh
6	Soil pH map	Scale 1:50,000	2018, BCA, Bangladesh
7	Flood-prone map	Scale 1:50,000	2018, BCA, Bangladesh
8	Temperature map	Scale 1:50,000	2018, BCA, Bangladesh
9	Rainfall map	Scale 1:50,000	2018, BCA, Bangladesh
10	Recommended desirable food items	Listed in Table 2.1	Bangladesh Institute of Research and Rehabilitation in Diabetes, Endocrine and Metabolic Disorders (BIRDEM) (2013)
11	Crop production data	Locally grown 78 varieties of crops	Bangladesh Bureau of Statistics (BBS) (2016), Bangladesh

weighted separately according to their relative importance in the optimal growth conditions for crops.

Criteria Aggregation and Preprocessing

The criteria used (Table 2.2) in this study are (a) land use, (b) SAVI, (c) slope, (d) land type, (e) topsoil, (f) soil pH, (g) flood prone, (h) temperature, and (i) rainfall. These criteria were further classified into constraints and factors for analysis (Fig. 2.5). According to Beinat and Nijkamp (1998), a factor is a criterion that enhances or detracts from suitable alternatives for the activity under consideration, and a constraint serves to limit any alternative.

Land Type

Considering seasonal flooding, the Government of Bangladesh (GoB) has divided the land into five categories: highland, medium highland, medium lowland, lowland, and very lowland (Bangladesh Bureau of Statistics (BBS) 2016). The study area comprised highland (29.5%), medium highland (17.5%), medium lowland (47%), and lowland and very lowland (<6%) (Fig. 2.5a). Medium highland and lowland were considered highly suitable, highland was considered moderately suitable, lowland was considered marginally suitable, and very lowland was considered unsuitable for crop growth.
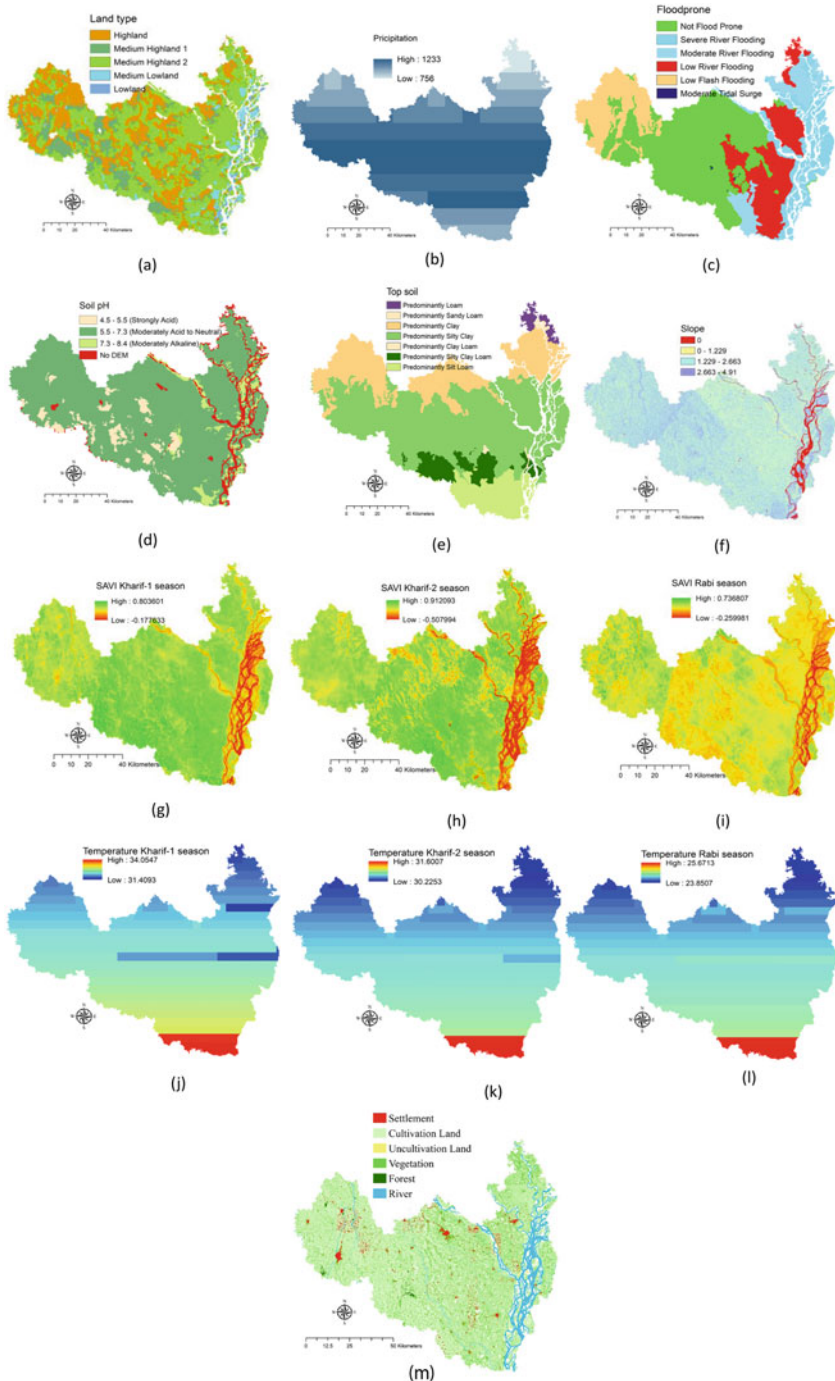
Fig. 2.5 Criteria for land suitability analysis: (**a**) land type, (**b**) precipitation, (**c**) flood prone, (**d**) soil pH, (**e**) topsoil, (**f**) slope, (**g**) SAVI of the Kharif-1 season, (**h**) SAVI of the Kharif-2 season, (**i**) SAVI of the Rabi season, (**j**) temperature of the Rabi season, (**k**) temperature of the Kharif-1 season, (**l**) temperature of the Kharif 2 season, and (**m**) land use map (SoB) for 2019

Rainfall

Rainfall in the critical stages of paddies increases crop yield through the rapid dissolution of nutrients for uptake by plants (Amin et al. 2015). According to Bangladesh Meteorological Department (BMD), the four districts in the study area receive 1250–2000 mm of annual rainfall. The annual average rainfall was recorded between 756 and 1233 mm (Fig. 2.5b).

Flood Prone

Bangladesh ranks as the sixth most flood-prone country in the world (United Nations Development Program (UNDP) 2004). Flood-prone environments include deepwater areas submerged under more than 100 cm of water from 10 days to a few months and areas that are affected by flash floods of longer than 10 days (Bangladesh Bureau of Statistics (BBS) 2014; Chauhan et al. 2017). The area was divided into five categories depending on the flood-prone data; not flood prone (45%), severe river flooding (13%), moderate river flooding (8%), low river flooding (19%), low flash flooding (14%), and moderate tidal surge (>1%) (Fig. 2.5c). According to the depth and duration of water stagnation, not flood-prone areas were considered highly suitable, areas susceptible to low river flooding were considered moderately suitable, areas susceptible to moderate river flooding were considered marginally suitable, and areas susceptible to moderate tidal surge and severe river flooding were considered unsuitable for field crop farming (Ministry of Environment and Forests (MoEF) 2008).

Soil pH

The pH of the soil is defined as the negative logarithm of the hydrogen ion concentration of the soil solution. pH is an important factor in quality assessment (Guo et al. 2018). However, it has been found that major cereals can grow in a wide range of pH values, varying from 4 to 8 (Samanta et al. 2011; Ayehu and Besufekad 2015; Kihoro et al. 2013; Amin et al. 2015). Additionally, the suitable pH condition for growing vegetables is usually considered to be the neutral pH level ($6.5 < pH < 7.5$) (Hu et al. 2018). Considering the availability of data, the study ranked pH values of 5.5–7.3 as highly suitable conditions, covering 83% of the study area (Fig. 2.5d. Moreover, areas with pH values of 7.3–8.4 and 4.5–5.5 each covered 5% of the land.

Topsoil

Vegetable cropping systems are highly influenced by seasonal variations and soil texture properties. Within a season, crop growing profiles are influenced by soil type (Schutter et al. 2001). Additionally, the major cereal grain yield in clay soil was 46%

higher than that in sandy loam soil averaged across cultivar and water areas (Dou et al. 2016). The effective soil depth is defined as the thickness of soil above a layer restricting root growth (e.g., consolidated rock or cemented materials, such as gravel) (Zolekar and Bhagat 2018). The chemical relationships influencing soil fertility are complex and affected by the soil development and the type of clay present; the proportions of the components and sizes of sand, silt, and clay have important properties on soil structure (Dexter 2004). There were seven categories of topsoil formats available in the area: predominant loam (1.6%), predominant sandy loam (0.38%), predominant clay (26.4%), predominant silty clay (54.5%), predominant clay loam (0.27%), predominant silty clay loam (6.8%), and predominant silt loam (9.9%) (Fig. 2.5e). These categories were converted into a land suitability class according to their seasonal crop cultivation characteristics based on the United States Department of Agriculture (USDA) soil texture suitability rating for diversified crops and were observed as sands, loamy sands, sandy loams, sandy clay loams, and silts.

Slope

The slope is a vital topographic element for cropland suitability analysis. Slope affects many landscape processes, such as soil water content, erosion potential, runoff, and surface and subsurface flow velocity. The thickness of the soil layer decreases with increasing slope (Ashford et al. 1997). This layer was developed by using the original Shuttle Radar Topography Mission (SRTM) and digital elevation model (DEM) for the study area. The Universal Transverse Mercator (UTM) projection and WGS84 datum were used as rectifying agents in ArcGIS®. The slope was calculated from the maximum rate of change between each cell and its neighbors. Every cell in the output raster had a slope value. Seasonal plants generally require flat land; only a slight slope between 0% to 8% is protected from the danger of erosion (Zolekar and Bhagat 2015). In the study area, the slope range was mostly under 40% (Fig. 2.5f), which was a suitable condition for most of the field crops (Nahusenay and Kibebew 2015; Novara et al. 2019; Basche et al. 2016).

Soil-Adjusted Vegetation Index (SAVI)

Soil has a spectral signature that varies from that of other types of land cover. In the visible and near-infrared zones, reflectance increases in proportion to an increase in the wavelength. However, the rate of increase is affected by various factors. Soil moisture and organic matter may lower the soil reflectance. The relationship between red and near-infrared reflectance remains constant for different soil type physiognomies. When the moisture content changes, the two values are associated and have a linear relationship. This relationship is very specific for each type of soil. SAVI is therefore useful for monitoring soils and vegetation. Furthermore, SAVI is a modification of Normalized Difference Vegetation Index (NDVI), which corrects for the

influence of soil brightness when the vegetation cover is low (Jiang et al. 2006). SAVI was extracted from Landsat 8 Operational Land Imager (OLI) imagery and extracted by a mask for the study area. Datasets were acquired from 2015 to 2019. These datasets were used to build the triple raster for three seasons. Each raster represented a specific period of multiple years (Fig. 2.5g–i). For each of the seasons, a single raster was created.

To reduce the soil background effect, modified indices were proposed using the soil adjustment factor L to account for first-order soil background variations and obtain SAVI (Huete 1988). SAVI can be expressed as follows:

$$\text{SAVI} = \frac{\rho_{\text{NIR}} - \rho_{\text{RED}}}{\rho_{\text{NIR}} + \rho_{\text{RED}} + L} \; (1 + L) \tag{2.5}$$

where ρ_{NIR} is the reflectance value in the near-infrared band, ρ_{RED} is the reflectance value in the red band, and L is the soil brightness correction factor. An L value of 0.5 in reflectance space was found to minimize soil brightness variations and eliminate the need for additional calibration for different soils.

Temperature

Temperature was the most important criterion of this research. Seasonal conditions and crop yield are greatly affected by land surface temperature (Kawasaki and Uchida 2016). In this study, three different temperature layers were considered for three distinct seasons: Kharif-1, Kharif-2, and Rabi. Using cell statistical tools, the average temperature was calculated. In the Kharif-1 and Kharif-2 seasons, temperatures fluctuated between 34 °C and 31 °C and between 32 °C and 30 °C, respectively (Fig. 2.5j, k). However, in the Rabi season, the temperature ranged from 23 °C to 25 °C (Fig. 2.5l). Temperature and rainfall are two climatic factors that have favorable influences and, in some cases, unfavorable influences on the development, growth, and yield of different crops.

Land Use

Land use data allow the evaluation of an area for vegetation, settlement, forest, and waterbodies. Land use data were collected from the SoB, which was split into 92 blocks. After aggregation in the ArcGIS® platform, the data were used to develop a more accurate land use/land cover (LULC) map for the land suitability analysis. In this study, rivers, forests, waterbodies, and settlements were considered restrictions in the analysis. Subsequently, excluding the constraints, only agricultural land was contemplated for land suitability analysis. Agricultural land was subclassified into cultivated land (80%), uncultivated land (0.5%), and vegetation land (19%) (Fig. 2.5m).

2.2.5 Fuzzy Membership Function

After aggregating all the criteria, fuzzy membership functions were used for the further analytical procedure. Firstly, the value of each criterion was given to the system for decision-making. The second step was fuzzification. In this process, input values from the domain were transformed into fuzzy inputs with the help of the membership function. Thirdly, the fuzzy-based inference used the rules to input map explanations to outputs. The next step was defuzzification; it was a process of transposing the fuzzy outputs to input formatted outputs, from the given fuzzy sets and corresponding membership functions. The system refers a decision to the final output value (Thaker and Nagori 2018). The fuzzification process has no sharply defined boundaries that characterize the imprecision of classes. Fuzzification converts the primal values of each phenomenon to the likelihood that the phenomenon belongs to a defined set. The defined set can be considered suitable, within an acceptable distance, or having the possibility of finding a specified condition. The original values were reclassified on this membership continuum through predetermined fuzzy membership functions. In the fuzzification process, each value of the phenomenon central to the core of the definition of the set was set to 1. Those values that were not part of the set were set to 0. Those values that fell between these two extremes were in the transitional zone of the set, the boundary. As the values moved away from the ideal or the center of the set, they were assigned a decreasing value on a continuous scale from 1 to 0; the assigned values decreased, and the original phenomenon value had a lower probability of being a member of that set (Zadeh 1965; Olivero et al. 2011; Mitchell and Cohen 2014; Barbosa 2015).

2.2.6 Fuzzy Reclassification

Fuzzy set theory was used to standardize factors using different fuzzy membership functions. The membership was within the 0–1 range. Fuzzy set theory allowed the concept of these continuous factors to be modeled in a suitability assessment within GIS or a spatial domain. In a standard approach, membership within a class was clearly and crisply defined as either in the class or not in the class (Bellman and Zadeh 1970). In the present study, fuzzy membership classification was used to accommodate the high uncertainty of scoring methods in assigning the suitability classes; several fuzzy membership functions were used in ArcGIS 10.4® for normalization. For this research, fuzzy functions were determined based on references and a literature review (Tables 2.3, 2.4, 2.5, 2.6, and 2.7).

Out of seven varieties of fuzzy membership functions in ArcGIS 10.4®, four fuzzy functions were used in this study considering ecological criteria: the large, small, Gaussian, and linear functions. These functions generate continuous fuzzy classifications of standardized criteria. The reclassification tool in ArcGIS® allows the transformation of categorical data to the range from 0 to 10 and then divides the

Table 2.3 Suitability class by fuzzy membership function for cereal crops (different varieties of rice)

Criteria	Most suitable condition	Maximum acceptable condition	Minimum acceptable condition	Not fuzzy member	Reference	Fuzzy membership function
Slope	$x < 4°$	20°	0°	$20° < x$	Ayehu and Besufekad (2015)	Fuzzy small
Land type	Medium High-/lowland	Highland	Lowland	Very lowland	Paul and Rashid (2016) Bangladesh Bureau of Statistics (BBS) (2016)	Fuzzy Gaussian
Topsoil	Predominant clay Predominant silt clay Predominant silt Clay loam	Predominant silt loam Predominant clay loam	Predominant loam	Predominant sandy loam	Dou et al. (2016) Asai et al. (2009)	Fuzzy small
Soil pH	$5.6 < x < 7.3$	8.4	4	$x < 4$ or $x > 8$	Ayehu and Besufekad (2015) Kihoro et al. (2013)	Fuzzy Gaussian
Flood prone	Not flood prone	Moderate river flooding	Moderate tidal surge	Low river flooding, severe river flooding	Datta et al. (2017) Bangladesh Bureau of Statistics (BBS) (2016)	Fuzzy small
Temperature	$20\ °C < x < 30\ °C$ (Aus, Aman) $10\ °C < x < 20\ °C$ (Boro)	Aus and Aman up to 45 °C Boro rice up to 35 °C	10 °C	$x > 35\ °C$ or $x < 20\ °C$	Samanta et al. (2011) Kihoro et al. (2013)	Fuzzy Gaussian
Rainfall	$x > 1400$ mm	2000 mm	800 mm	<800	Ayehu and Besufekad (2015)	Fuzzy large
SAVI	0.80301 (Aus) 0.912093 (Aman) 0.736807 (Boro)	+1	−1	$-0.178 < x < 0.803$ (Aus) $-0.508 < x < 0.912$ (Aman) $-0.26 < x < 0.737$ (Boro)	Purnamasari et al. (2019) Habibie et al. (2019) Venancio et al. (2019) Rondeaux et al. (1996)	Fuzzy linear
Land use	Agriculture land	Vacant land	Used land	Settlements, rivers, waterbodies, forests	Bahrani et al. (2016) Zhu et al. (2020)	Fuzzy Gaussian

Table 2.4 Suitability class by fuzzy membership for carbohydrate-based vegetables (potatoes)

Criteria	Most suitable condition	Maximum acceptable condition	Minimum acceptable condition	Not fuzzy member	Reference	Fuzzy membership function
Slope	$x < 3°$	$3° < x < 5°$	$5° < x < 8°$	$x > 8$	Gitari et al. (2019) Shimoda et al. (2018)	Fuzzy small
Land type	Medium high-/lowland	High land	Lowland	Very lowland	Bangladesh Bureau of Statistics (BBS) (2016)	Fuzzy Gaussian
Topsoil	Loam Sandy loam Sandy clay loam Silt loam	Predominant sandy loam	Sandy clay	Gravel Sand Silty clay loam Clay loam Silty clay Silt Clay	Shimoda et al. (2018)	Fuzzy small
Soil pH	$5 < x < 6.5$	$6.6 < x < 8.2$	$5.0 < x < 5.4$	$x > 8.2$ or $x < 5.0$	Saini and Grant (1980)	Fuzzy Gaussian
Flood prone	Not flood prone	Moderate tidal surge	Moderate river flooding	Low river flooding, severe river flooding	Bangladesh Bureau of Statistics (BBS) (2016)	Fuzzy small
Temperature	$15\ °C < x < 18\ °C$	$30\ °C$	$10\ °C$	$x > 35\ °C$ $x < 2.5\ °C$	Zhao et al. (2012)	Fuzzy Gaussian
Rainfall	$700 < x < 1000$ mm	2000 mm	Less than 700 mm	$x < 300$	Xing et al. (2011) Qin et al. (2013)	Fuzzy large
SAVI	0.736807	+1	−1	$x < 0.736680$ or $x > -0.29981$	Purnamasari et al. (2019) Habibie et al. (2019) Venancio et al. (2019) Rondeaux et al. (1996)	Fuzzy linear
Land use	Agriculture land	Vacant land	Used land	Settlements, rivers, waterbodies, forests	Bahrani et al. (2016) Zhu et al. (2020)	Fuzzy Gaussian

Table 2.5 Suitability class by fuzzy membership for noncarbohydrate-based vegetables

Criteria	Most suitable condition	Maximum acceptable condition	Minimum acceptable condition	Not fuzzy member	Reference	Fuzzy membership function
Slope	$0° < x < 7°$	$15° < x < 25°$	$7° < x < 15°$	$x < 25°$	Yalew et al. (2016)	Fuzzy small
Land type	Medium high-/lowland	Highland	Lowland	Very lowland	Bangladesh Bureau of Statistics (BBS) (2016)	Fuzzy Gaussian
Topsoil	Loam soils with moderate to gentle slope	Clay loam, loam soils on steep slope (also acceptable condition)	Clay loam, loam soils on steep slope		Zolekar and Bhagat (2015)	Fuzzy small
Soil pH	$5.3 < x < 6.6$	8.2	5	$x > 8.3, x < 5$	Mapanda et al. (2005) Yang et al. (2014)	Fuzzy Gaussian
Flood prone	Not flood prone	Moderate tidal surge	Moderate river flooding	Low river flooding Severe river flooding	Bangladesh Bureau of Statistics (BBS) (2016)	Fuzzy small
Temperature	$14\,°C < x < 15\,°C$	$30\,°C < x < 32\,°C$ (summer) $26\,°C < x < 28\,°C$ (winter)	$13\,°C < x < 15\,°C$ (summer) $4\,°C < x < 7\,°C$ (winter)	$x > 38\,°C$ $x < 3\,°C$	Meng et al. (1997) Marklein et al. (2020) Ngoy and Shebitz (2020)	Fuzzy Gaussian
Rainfall	$1000 < x < 2000$ mm	$700 < x < 1000$ mm	Less than 700 mm		Richards et al. (2014)	Fuzzy large
SAVI	0.80301 (Kharif-1) 0.912093 (Kharif-2) 0.736807 (Rabi)	$+1$	-1	(Kharif-1) $-0.178 < x < 0.803$ $-0.508 < x < 0.912$ (Kharif-2) $-0.26 < x < 0.737$ (Rabi)	Purnamasari et al. (2019) Habibie et al. (2019) Venancio et al. (2019) Rondeaux et al. (1996)	Fuzzy linear
Land use	Agriculture and fallow land	Sparse forest, scrubland, barren land, dense forest (also acceptable condition)		Waterbody, settlement	Zolekar and Bhagat (2015) Akinci et al. (2013)	Fuzzy Gaussian

Table 2.6 Suitability class by fuzzy membership for pulses

Criteria	Most suitable condition	Maximum acceptable condition	Minimum acceptable condition	Not fuzzy member	Reference	Fuzzy membership function
Slope	<2°	8°	3° < x < 5°	>8	Kladivko et al. (1986)	Fuzzy small
Land type	Medium high-/lowland	Highland	Lowland	Very lowland	Bangladesh Bureau of Statistics (BBS) (2016)	Fuzzy Gaussian
Topsoil	Loam Sandy loam Sandy clay loam Silt loam	Predominant sandy loam	Sandy clay	Gravel Sand	Nguyen et al. (2015)	Fuzzy small
Soil pH	5.8 < x < 6	8.5	x > 5.5	x > 8.5 and x < 5.5	Food and Agriculture Organization of the United Nations (FAO) (2016) Egamberdieva et al. (2016)	Fuzzy Gaussian
Flood prone	Not flood prone	Moderate tidal surge	Moderate river flooding	Low river flooding, severe river flooding	Bangladesh Bureau of Statistics (BBS) (2016)	Fuzzy small
Temperature	17 °C < x < 20 °C	26 °C < x < 30 °C	10 °C < x < 12 °C	x > 32 °C x < 10 °C	Yalew et al. (2016) Kladivko et al. (1986)	Fuzzy Gaussian
Rainfall	700 < x < 1000 mm	1000 < x < 2000 mm	Less than 360 mm		Miller et al. (2002)	Fuzzy large
SAVI	0.736807	+1	−1	x < −0.0259981 or x > 0.736807	Purnamasari et al. (2019) Habibie et al. (2019) Venancio et al. (2019) Rondeaux et al. (1996)	Fuzzy linear
Land use	Agriculture land	Vacant land	Used land	Settlements, rivers, waterbodies, forests	Bahrani et al. (2016) Zhu et al. (2020)	Fuzzy Gaussian

Table 2.7 Suitability class by fuzzy membership for oilseeds

Criteria	Most suitable condition	Maximum acceptable condition	Minimum acceptable condition	Not fuzzy member	Reference	Fuzzy membership function
Slope	$0° < x < 4.5°$	$0°$	$16.7°$	$x > 16.7°$	Arief and Nafi (2018)	Fuzzy small
Land type	Medium high-/lowland	Highland	Lowland	Very lowland	Bangladesh Bureau of Statistics (BBS) (2016) Kamkar et al. (2014)	Fuzzy Gaussian
Topsoil	Silty loam, silty clay loam				Pelosi et al. (2020)	Fuzzy small
Soil pH	$5.8 < x < 7.3$	8.7	4.3	$x < 4.3, x > 9$	Pelosi et al. (2020) Chaignon et al. (2002)	Fuzzy Gaussian
Flood prone	Not flood prone	Moderate tidal surge	Moderate river flooding	Low river flooding, severe river flooding	Bangladesh Bureau of Statistics (BBS) (2016)	Fuzzy small
Temperature	20 °C	35 °C	$10 °C < x < 15 °C$	$x > 35 °C, <10 °C$	Pelosi et al. (2020) Johnston et al. (2002)	Fuzzy Gaussian
Rainfall	$400 < x < 600$ mm	3500 mm	325 mm	$x > 500$ mm	Arief and Nafi (2018) McCormick et al. (2012) Kamkar et al. (2014)	Fuzzy large
SAVI	0.736807	+1	−1	$x < −0.0259981$ or $x >$ 0.736807	Purnamasari et al. (2019) Habibie et al. (2019) Venancio et al. (2019) Rondeaux et al. (1996)	Fuzzy linear
Land use	Agriculture land	Vacant land	Used land	Settlements, rivers, waterbodies, forests	Salman et al. (2010) Bahrani et al. (2016) Zhu et al. (2020)	Fuzzy Gaussian

resulting transformed data by 10 to derive a 0 to 1 scale. The equations for the fuzzy large (Eq. (2.6)), small (Eq. (2.7)), linear (Eq. (2.8)), and Gaussian functions (Eq. (2.9)) are found below.

$$\mu(x) = \frac{1}{1 + \left(\frac{x}{f2}\right)^{-f1}} \tag{2.6}$$

The fuzzy large transformation function was used when large input values were more likely to be members of the set. For example, the rainfall layer was followed by a fuzzy large membership function; the higher yield of rice can be obtained with a greater amount of water supplied to the area.

$$\mu(x) = \frac{1}{1 + \left(\frac{x}{f_2}\right)^{f_1}} \tag{2.7}$$

The fuzzy small transformation function was used when small input values were more likely to be members of the set. The criteria slope, topsoil, and flood-prone layers were each followed by a fuzzy small function in this research, e.g., the slope was followed by the fuzzy small function for rice cultivation. Here, the most suitable slope condition was 0° to 4° for rice. If the slope increases, the condition becomes more unsuitable following the study area.

$$\mu(x) = e^{\left(-f1*(x-f2)^2\right)} \tag{2.8}$$

The SAVI criterion followed a fuzzy linear transformation function that related a linear function between the user-specified minimum and maximum values for reclassification.

$$\mu(x) = f(x) = \begin{cases} 0 & x \le a \\ \frac{x-a}{b-a} & a < x < b \\ 1 & x \ge b \end{cases} \tag{2.9}$$

The fuzzy Gaussian function converts primal values into a normal distribution. If the input values decrease in membership, they move away from the midpoint. The midpoint of the fuzzy Gaussian function was set to 1 (Purnamasari et al. 2019). The land type, soil pH, temperature, and land use layers were analyzed under the fuzzy Gaussian membership function. For example, both extreme high and low temperature are unsuitable for rice growth. According to the analysis, the most suitable rice growing temperature is 10–20 °C. These values are different for each nine criterion and each crop item following the references.

In the fuzzy large, small, and Gaussian membership functions, the control point included a midpoint (f2) and a spread (f1). A midpoint was a specific point that had a

0.5 value of membership in the large and small functions. Gaussian functions were determined by the user based on references (ESRI, CA, USA). The spread was generally allocated a number between 1 and 10. The fuzzy membership curve became steeper for a higher spread value. The fuzzy linear transformation function applied a linear function between the minimum and maximum values. Any value below the minimum was determined to be 0 (not a member), and any value above the maximum was 1 (a member) (Barbosa 2015; Bahrani et al. 2016). For this research, fuzzy functions were determined based on references and a literature review (Tables 2.3, 2.4, 2.5, 2.6, and 2.7).

2.2.7 Overlay

Fuzzy Overlay

In ArcGIS®, the fuzzy overlay analysis consents to the possibility of a phenomenon belonging to multiple sets in multicriteria overlay analysis and analyzes the relationship among the memberships of the multiple sets. Each fuzzy overlay method permits the exploration of the membership of each cell belonging to various input criteria. To analyze the relationships and interactions between all the sets for the nine criteria in the overlay model, fuzzy overlay techniques were used. Since the fuzzification process is based on the degree of membership to a set, the overlay techniques describe the interaction of the inaccuracies in the small, large, linear, and Gaussian memberships of the sets. The fuzzy overlay technique was used based on set theory (ESRI, CA, USA). Set theory is the mathematical discipline quantifying the relationship of each membership to specific sets.

The available fuzzy set overlay techniques in ArcGIS® are fuzzy And, fuzzy Or, fuzzy Product, fuzzy Sum, and fuzzy Gamma. Each of these techniques describes the cell's membership related to the input sets. In this study, fuzzy Gamma overlay assisted in developing nine varieties of cropland suitability maps for three identical seasons, which were determined based on references and a literature review (ESRI, Boston, CA).

Scoring for Individual Suitability Map Preparation

After conducting fuzzy overlay, the resulting map was shown as stretched values that required scoring for visual understanding and significant justification. The land suitability analysis for the diversified crops was conducted using different classification categories proposed by the FAO. In the FAO's framework for land evaluation, the first class was designated as suitable (S) or not suitable (N). The suitability classification aimed to show the suitability of each land unit for crop production. In practice, three classes—S1, S2, and S3—are usually used to identify land that is highly suitable, moderately suitable, and marginally suitable, respectively (Fig. 2.6).
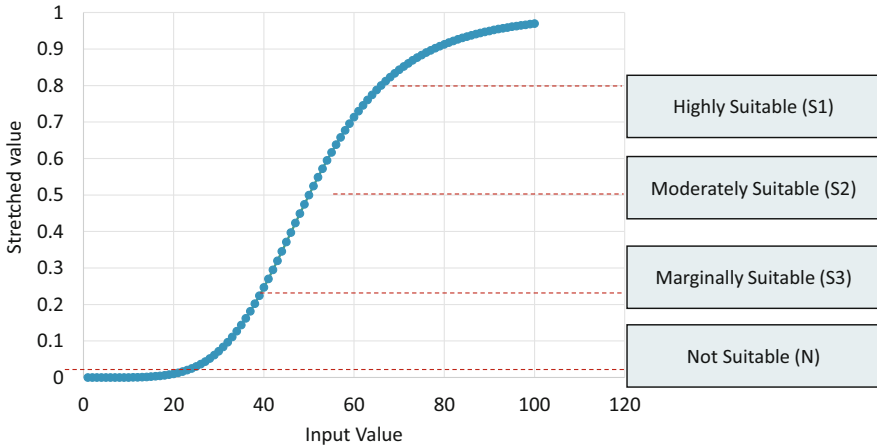
Fig. 2.6 Suitability range of classification by scoring based on fuzzy overlay

2.2.8 Seasonal Land Suitability Map Preparation

The seasonal suitability maps were prepared considering regional diversified food demand. In addition, land suitability analysis helped to identify the suitable zone for each type of crop. After that, seasonal suitability maps (Kharif-1, Kharif-2, and Rabi season) were prepared following the crop calendar. In this stage, ArcGIS$^{®}$ was used for spatial and statistical analyses to develop seasonal crop suitability maps according to regional required food demand. Then, the proposed results were compared with the present farming practices of the study area.

2.3 Results

2.3.1 Regional Crop Production for Balanced Nutrition

Crop production data showed that some crops produced more than required and some crops cultivated less than required in the study area considering the nutritional balance (Fig. 2.7). Major cereal rice, minor cereals, and carbohydrate-based vegetables were cultivated 2,396,992 metric tons, 750,366 metric tons, and 3,104,403 metric tons higher, respectively. On the other hand, production was lower than the requirement for noncarbohydrate-based vegetables, pulses, and oilseeds: 1,009,120 metric tons, 204,293 metric tons, and 89,550 metric tons, respectively.

Production Gap (metric tons-per year)

	Rice	Wheat,Maize	Pulses	Oil Seeds	Spices	Fruits	Vegetables-non-carb	Potatoes	Molassess
metric-tons/ year	2396992	750366	-204293	-89550	1945	-271813	-1009120	3104403	19289
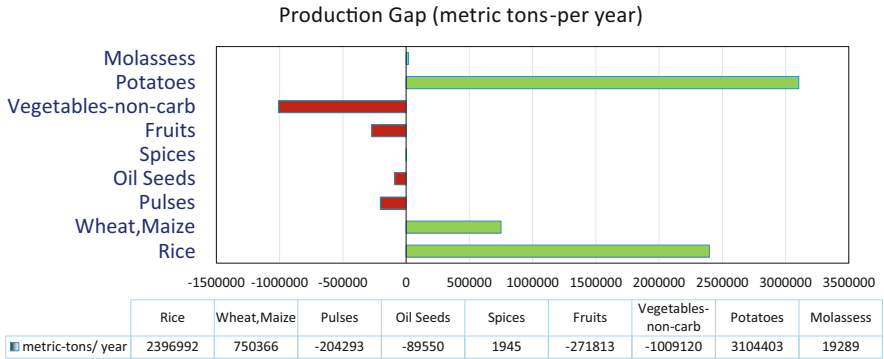
Fig. 2.7 Crop production status (surplus and shortage) per year regarding balanced nutritional requirement

2.3.2 Land Suitability for Diversified Crops

The F-MCDM model indicated the suitable areas for different crops in the Kharif-1, Kharif-2, and Rabi seasons in different localities (Fig. 2.8a–r). In the Kharif-1 season, the highly suitable area was found to be 30.9% for Aus rice (Fig. 2.8d), and the suitable area for vegetables was 50% (Fig. 2.8b). The not suitable area was found to be 25.5% and 17% for rice and vegetables, respectively (Table 2.8). The results of the Kharif-2 season showed that the highly suitable area for the local variety of Aman rice (Fig. 2.8h) was approximately 5% smaller than the highly suitable area for vegetables (Fig. 2.8f). A moderately suitable area was detected as 34.6% for rice and 22% for vegetables in the Kharif-2 season. The not suitable area appeared to be 46.5% for Aman rice (Table 2.8).

Furthermore, highly (S1), moderately (S2), marginally (S3), and not suitable (N) areas showed diversified results for the five types of crops grown in the Rabi season. The highly suitable area was 47% for Boro rice (Fig. 2.8r). The highly suitable zone for winter vegetables was found to be 40% (Fig. 2.8j), and the not suitable area was found to be 16.5% in the Rabi cropping season. Basically, the northeastern part of the study area appeared to be a suitable zone for pulse (Fig. 2.8n) cultivation; in this region, the highly suitable area covered 43%. In addition, marginal and not suitable areas were detected altogether at 20%. Highly suitable areas for growing carbohydrate-based vegetables (potatoes) (Fig. 2.8l) were found to reach 19% and were mostly located in the northern part of the study area. Moreover, scattered suitable area was found for oilseed cultivation, which covered some of the northern and western regions; highly, moderately, marginally, and not suitable areas for growing oilseeds were detected at 16%, 17%, 9%, and 58%, respectively (Fig. 2.8p).
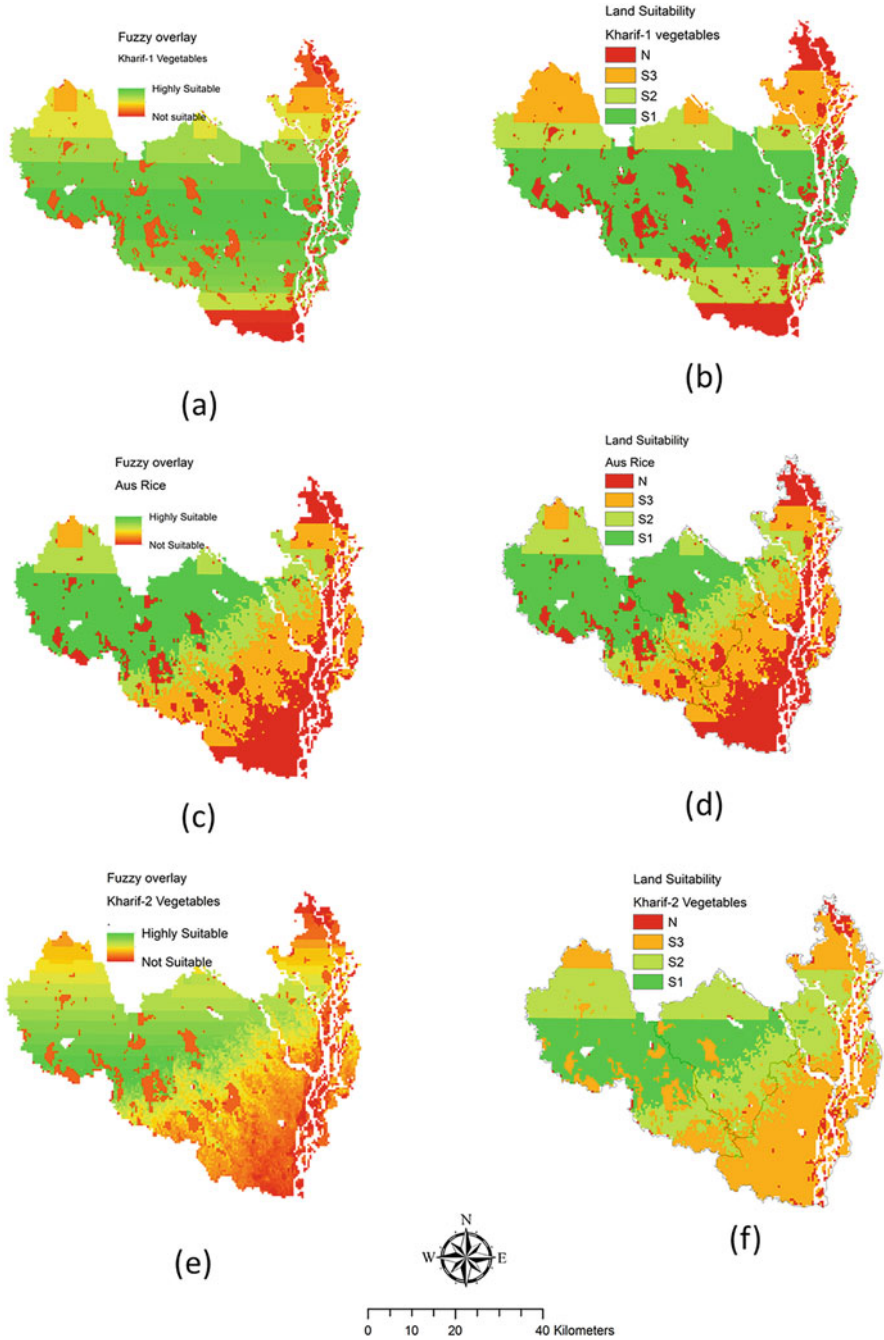
Fig. 2.8 Land suitability map: (**a**, **b**) Kharif-1 vegetables, (**c**, **d**) Kharif-1 Aus rice, (**e**, **f**) Kharif-2 vegetables, (**g**, **h**) Kharif-2 Aman rice, (**i**, **j**) Rabi vegetables, (**k**, **l**) potatoes, (**m**, **n**) pulses, (**o**, **p**) oilseeds, (**q**, **r**) Boro rice
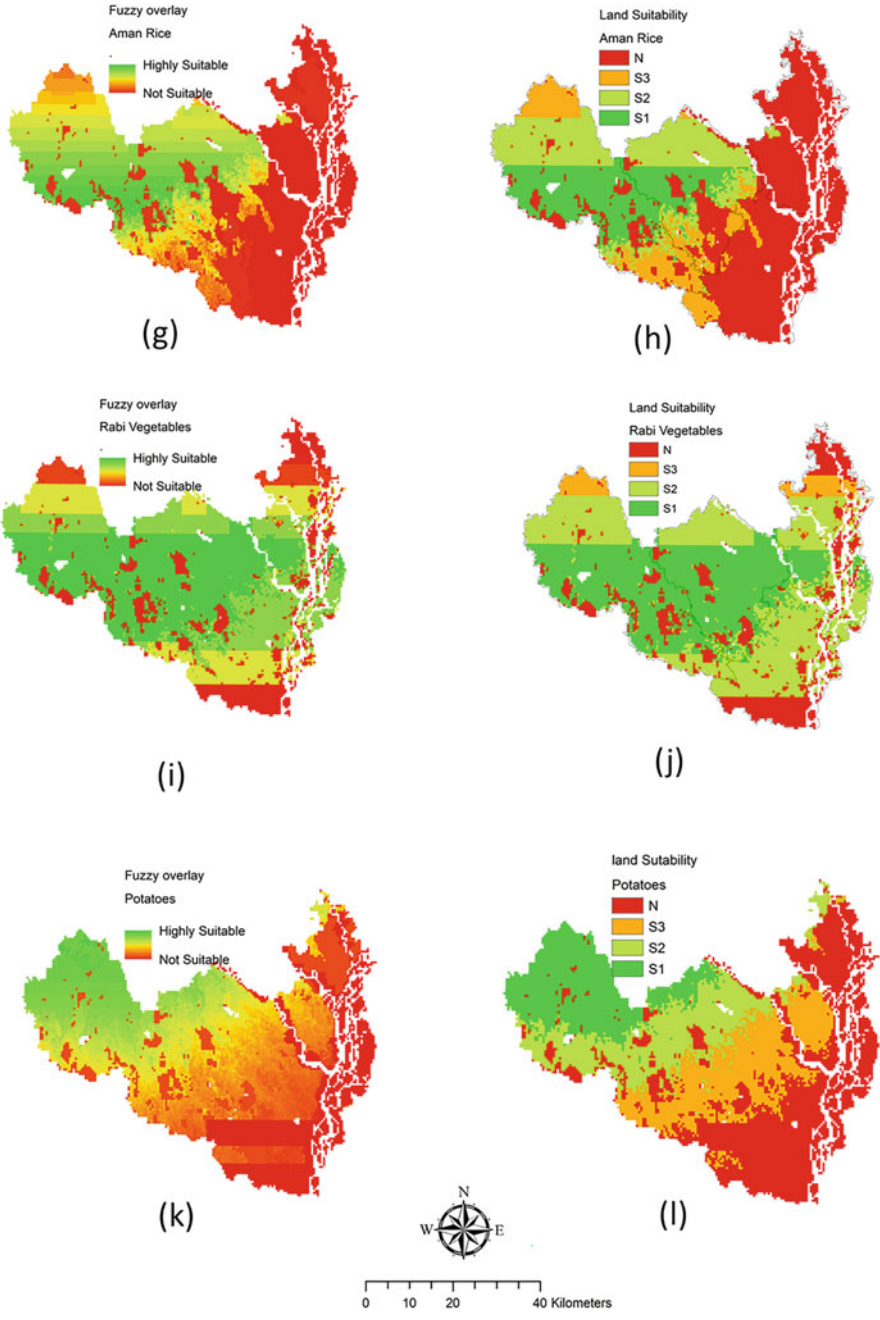
Fig. 2.8 (continued)
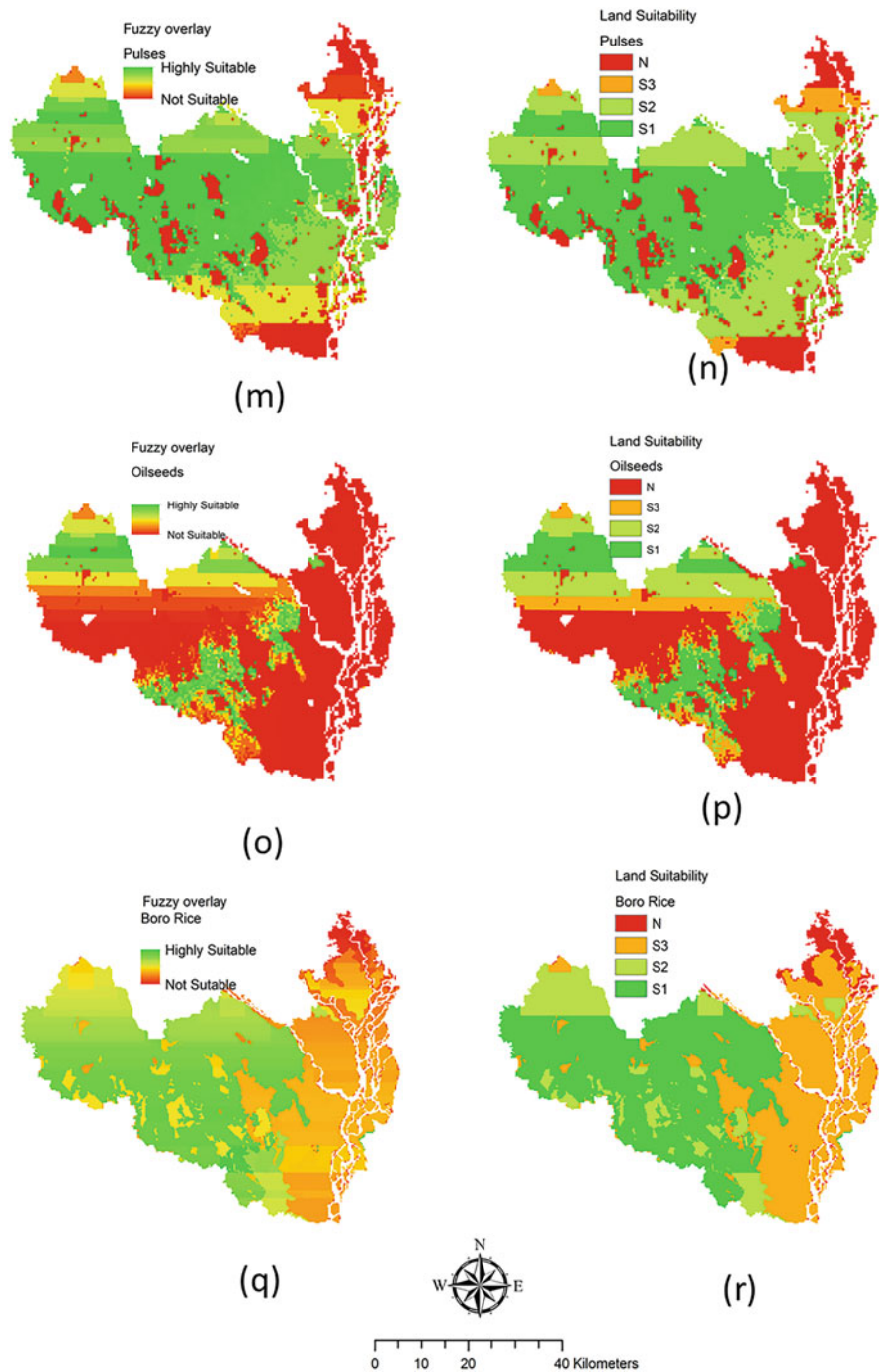
Fig. 2.8 (continued)

Table 2.8 Results of land suitability analysis of diversified crops

Suitability classes	K1 rice areas (km²)	K1 vegetables areas (km²)	K2 rice areas (km²)	K2 vegetables areas (km²)	Rabi rice areas (km²)	Rabi vegetables areas (km²)	Pulses areas (km²)	Potatoes areas (km²)	Oilseeds areas (km²)
Highly suitable (S1)	3745 (30.9%)	4130 (50%)	1569 (19%)	1999 (24.2%)	3887.9 (47%)	3304 (40%)	3551 (43%)	3279 (19%)	1321 (16%)
Moderately suitable (S2)	2298 (19%)	1555 (20.6 %)	1817 (22%)	2458 (34.6%)	11564 (14%)	3221 (39%)	3056 (37%)	1784.2 (19.7%)	1404 (17%)
Marginally suitable (S3)	2979 (24.6%)	1024 (12.4%)	1032 (12.5%)	3138 (38%)	2849.7 (34.5%)	371 (4.5%)	330 (4%)	1627.2 (21.6%)	743 (9%)
Not suitable (N)	3094 (25.5%)	1404 (17%)	3840 (46.5%)	264 (3.2%)	364.3 (4.5%)	1362 (16.5%)	1321 (16%)	15694 (39.7%)	4790 (58%)

2.3.3   Seasonal Land Suitability for Multicrop

Combining the specific crops of each season, triple-cropping suitability maps were prepared showing distinct suitable zones. The calorie ratio was integrated with seasonal suitability analysis to produce three specific suitable maps of the Kharif-1, Kharif-2, and Rabi seasons. The study area was masked by the land use maps from the SoB, where three seasonal maps were developed using the land practices for agriculture. Restricted areas, such as rivers, settlements, and forests, were not aggregated for the final output or area calculation and appeared as a white color in the resulting maps (Fig. 2.9).

The result from the Kharif-1 calorie-based distribution map shows that 42% (3469 km^2) of the land area consists of the most suitable area for vegetable production (Fig. 2.9a). Considering rice, 20% (1652 km^2) of the land area was most suitable. In addition, 21% of the land was recognized as suitable for growing both crops. Suitable areas for growing rice were mostly located in the northern part of Dinajpur and Rangpur districts and some western parts of Kurigram district. Suitable areas for growing vegetables were identified mostly in the middle part of the study area, covered by Gaibandha and Kurigram districts. Moreover, the southern regions of two districts, Dinajpur and Rangpur, were also recommended for summer vegetable production. This common suitable area can be used for growing both rice and vegetables. However, according to the balanced calorie recommendation, this area can be used for rice and some cereal crop cultivation. The local agricultural practices of the Kharif-1 season map also showed that the rice cultivation zone was mostly the northern parts and some discrete areas of the four districts. However, a very stimulating result was found in so much that only 12% (991 km^2) of the area was suitable for growing vegetables (Fig. 2.9b). Fallow land accounted for 45% of the land used in the Kharif-1 season (Table 2.9).

Mainly two types of crops, Aman rice and vegetables, are usually grown in the subsequent season, Kharif-2. The results of the Kharif-2 map indicated that 55% of the area and 35% of the area were the most suitable for vegetables and rice, respectively (Fig. 2.9c). The moderately suitable area for rice and vegetables was 6% (495 km^2). The not suitable area for rice and vegetables was 4% of the total land area. The area suitable for vegetables was mostly located in Kurigram and Gaibandha districts. Areas suitable for rice cultivation were found mainly in Dinajpur and Rangpur districts. The current cultivation method practices showed that 57% of the area was used for rice and 18% of the area was used for vegetable farming (Fig. 2.9d). In the Kharif-2 season, 21% of the area was noted as fallow land (Table 2.10).

In the Rabi season, land was occupied by five varieties of crops (Fig. 2.9e): Boro rice and cereals, winter vegetables, carbohydrate-based vegetables (potatoes), pulses, and oilseeds. The results of the seasonal suitability map showed that 35% (2891 km^2), 19% (1569 km^2), 15% (1239 km^2), 10% (826 km^2), and 21% (1734 km^2) of the land were reported as the most suitable areas for cereal crops, vegetables, pulses, oilseeds, and potatoes, respectively. Areas suitable for carbohydrate-based
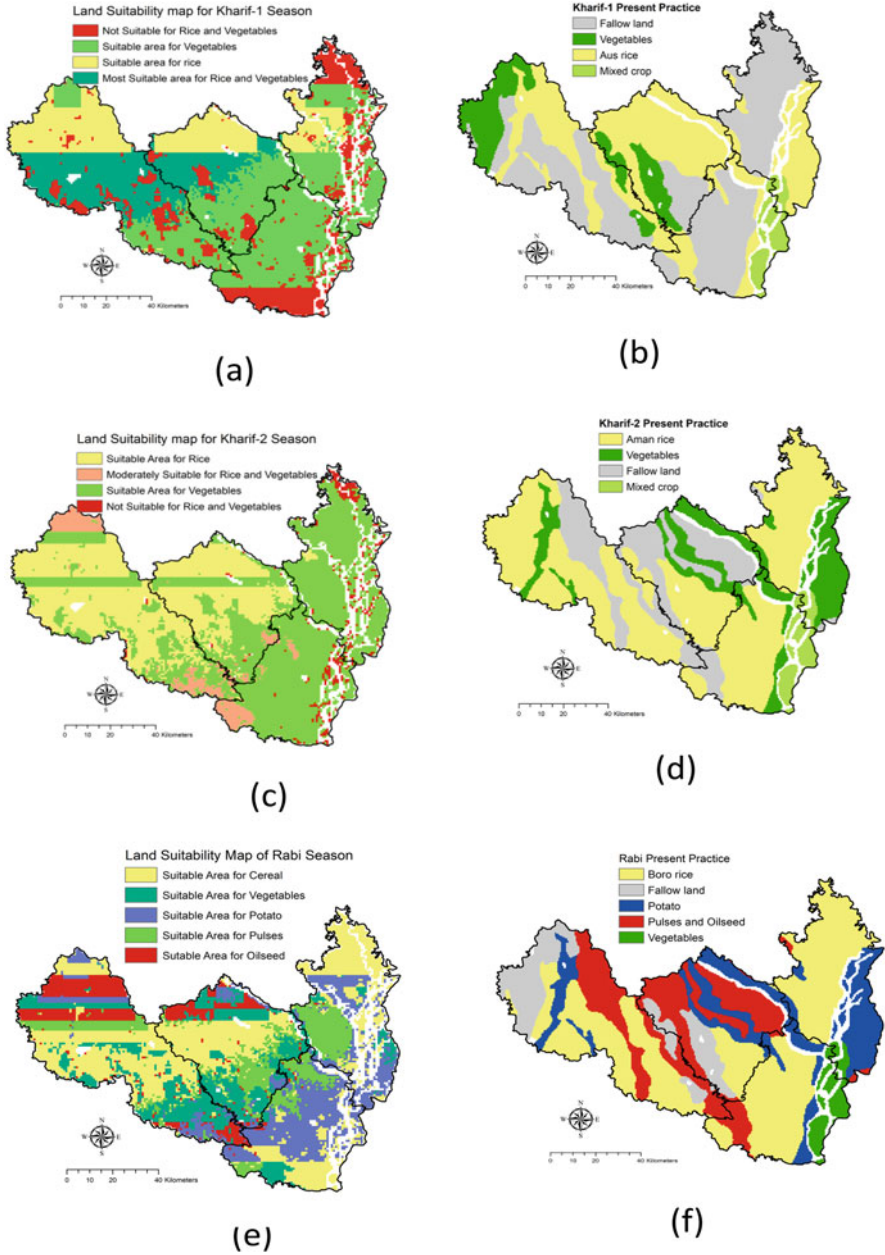
Fig. 2.9 Seasonal crop growing suitable zoning: (**a**) Kharif-1 season land suitability map, (**b**) Kharif-1 present practice map, (**c**) Kharif-2 land suitability map, (**d**) Kharif-2 present practice map, (**e**) Rabi season land suitability map, and (**f**) Rabi present practice map

Table 2.9 Comparison between the present practice and the suitable area of the Kharif-1 season

Criteria	Present practice		Suitability zoning	
	Area (%)	Area (km^2)	Area (%)	Areas (km^2)
Cereal	39	3221	20	1652
Vegetables	12	991	42	3469
Mixed crops	4	330	21	1734

Table 2.10 Comparison between the present practice and the suitable area of the Kharif-2 season

Criteria	Present practice		Suitability zoning	
	Area (%)	Areas (km^2)	Area (%)	Areas (km^2)
Cereal	57	4708	35	2891
Vegetables	18	1487	55	4543
Mixed crops	4	330	6	495

Table 2.11 Comparison between the present practice and the suitable area of the Rabi season

Criteria	Present practice		Suitable zoning	
	Area (%)	Area (km^2)	Area (%)	Area (km^2)
Cereal	45	3717	35	2891
Vegetables	4	330	19	1569
Pulses and oilseed	21	1735	15+10	1239 + 826
Potatoes	18	1486	21	1734

vegetables and noncarbohydrate-based vegetables were mainly located in Kurigram and Gaibandha districts. Land suitable for cereal crops was distinctly observed in the four districts of the study area. The oilseed cultivation area predominantly appeared in the northern parts of Dinajpur and Rangpur districts. The farming practice of the Rabi season showed that 45% (3717 km^2) of the area was used for cereal crops (Fig. 2.9f). In addition, 21% of the area was used for pulses and oilseeds. Only 4% (330 km^2) of the area was used for noncarbohydrate-based vegetable growing, and 18% of the land was used for potato cultivation (Table 2.11).

2.4 Discussion

This research has provided a comprehensive strategy to create agricultural land use plans for diversified seasonal crops considering calorie demand. Previously, much of the research conducted only reported land suitability for site-specific plans or single-cropping plans (Noorollahi et al. 2016; Sulaiman et al. 2019). However, this research attempted to develop season-based multicrop land suitability maps. Preparing a seasonal map using balanced, calorie-rich crops was another concern that required a new dimension of land suitability analysis. In this study, regional calorie demand

and balanced nutrition conditions were checked by statistical data mining, and the results were used as a weight for the land use map preparation, which will ensure better performance in land use planning. This result provided another aspect that confirmed the recommendation to improve food nutrition security.

Usually, either the AHP-based weighted overlay or the equal-overlay technique is used in most studies (Salman et al. 2010; Seyedmohammadi et al. 2019; Pilevar et al. 2020; Tashayo et al. 2020); few studies conducted with fuzzy membership methods employed in the GIS platform incorporate the AHP technique (Pilevar et al. 2020; Ustaoglu and Aydınoglu 2020; Amini et al. 2019), but considering the preparation of seasonal, diversified crop suitability maps using the F-MCDM approach is an innovation of this research. However, individual suitability maps were also constructed to check the identical suitable zones of diversified crops. A multicriteria decision-making system was applied to reduce the biases for land suitability assessment. Variation in the seasonal temperature was one of the most dominant factors in this area and influenced the locations most suitable for crop cultivation. Remote sensing data have a vital role in land suitability analysis as they aid in categorizing the growing locations of each crop as suitable or not suitable.

Crop production data represented the rice-based dominant cultivation practice in the study area compared to nutritional requirement (Fig. 2.7). Such deviations from "ideal crop production patterns" were observed with the currently produced patterns. Besides, rice is the staple food in this region and ensures social stability for the country. Therefore, the common belief of the people of the country is if they can grow plenty of rice, the country will not face food insecurity; this concept created a new issue in sense of food nutritional adequacy. Now, the main concern of this study is not only the food security but also to ensure the food nutrition security of Bangladesh.

Regarding seasonal land planning, a diversified production plan was developed including present practices following the locally grown crop calendar (Fig. 2.9a–f). Three seasons were considered: Kharif-1, Kharif-2, and Rabi. In the Kharif-1 season, 42% (3469 km^2) of land was recommended for growing vegetables, but previously, this value was 12% (991 km^2). In the Kharif-2 season, the vegetable-growing area was detected to be 55% (4543 km^2); before, it was 18%. In the following season, the land area suitable for growing vegetables was 4%, but this study identified 19% (1569 km^2) of land as suitable for cultivating vegetables. Moreover, this recommendation was also shown in the Rabi season; 25% (2065 km^2) of suitable land was detected for pulse and oilseed cultivation, although this area was only 21% previously. Only agricultural land was considered in this study, which is a limitation for developing a planning model. Moreover, spices, fruits, and molasses/sugars were not studied in the proposed seasonal maps. In addition, dairy products were not considered in this research. This planning model helps to ensure 81.5% food nutrition security.

Furthermore, the aim of this research was to develop diversified crop production based on nutritional consideration of cereals, vegetables, pulses, and oilseeds. The study area was vulnerable because of poor food consumption practice. Therefore, the hypothesis of this research was to find a way to increase diversified food (nutritive)

cultivation along with consumption. In this regard, the suitable area was noted by land suitability analysis for recommendation to the locally adapted grown crops. However, the limitation of this research was economic analysis, which was insubstantial considering food nutrition security. Further research is necessary to allocate economic analysis. Additionally, in the study area, the chain shops are not introduced and not familiar to the farmers and inhabitants. Usually, most of the agriculture products are sold in the local market. Moreover, postharvest losses were also higher due to lack of transportation. Therefore, closed economic condition was considered to introduce diversified cropping practice in the local region. In this respect, the production values of different crops were converted into similar units by presuming that all crop productions were consumed without being exported or misused to ensure regional self-sufficiency of the present planning model.

2.5 Conclusion

This research not only concerned food security but also emphasized ensuring food nutrition security in Southeast Asia. Throughout all Southeast Asian countries, nutritional diets are the most imbalanced in Bangladesh. Therefore, the goal of this research was to conduct a land suitability analysis for land use planning considering nutritional proportions using the required calorie intake ratio from cereals, vegetables, and pulses. The geographical extent was considered with high-resolution vector and satellite remote sensing datasets to develop land suitability maps for the Kharif-1, Kharif-2, and Rabi seasons. In addition, the development of seasonal land suitability maps with a balanced food demand ratio in GIS platform provided better findings. This study clearly revealed the spatial distributions of different crops from remote sensing data in conjunction with the evaluation of biophysical variables of soil. Topographic information in the context of GIS could be helpful for crop management decisions regarding intensification or diversified foods. The findings in this study were compared with the present cropping practices: in the Kharif-1 (42%), Kharif-2 (55%), and Rabi (19%) seasons, suitable land was found for vegetable cultivation. Regarding calorie-based land use planning, it is recommended that an additional 30% of land can be used in the Kharif-1 season, an additional 37% of land can be used in the Kharif-2 season, and an additional 15% of land can be used in the Rabi season; vegetable crops have the potential for further agricultural land use compared to the present practices. Moreover, 25% of suitable land was recognized for pulses and oilseeds, which could be used for cultivation considering the local demands of the study area. The land use layer from the SoB was applied to unmask the agricultural land to help with the accuracy assessment. The recommended seasonal land suitability maps based on the nutrition demand and the F-MCDM approaches confirmed the satisfactory results of land use planning. Finally, a nutrition assessment will help to recommend policy for the planning of land use in the coming years, which is the key issue concerning food nutrition security in the developing countries.

Appendix: Diversified Crop Practices in the Northern Part of Bangladesh

Category (number)	No	Crop name	Category (number)	No	Crop name	Category (number)	No	Crop name
Cereal (CL) ($n_1 = 5$)	1	Aus rice		22	Water gourd	Fruits (FR) ($n_6 = 18$)	1	Mango
	2	Aman rice		23	Wax gourd		2	Banana
	3	Boro rice		24	Tomato		3	Pineapple
	4	Maize		25	Radish		4	Jackfruit
	5	Wheat		26	Bean		5	Papaya ripe
Noncarbohydrate vegetables (VN) ($n_2 = 31$)	1	Pumpkin		27	Carrot		6	Watermelon
	2	Brinjal		28	Spinach		7	Litchi
	3	Patal		29	Bengal spinach		8	Guava
	4	Okra		30	Red amaranth		9	Lime lemon
	5	Ridge gourd		31	Amaranth		10	Pomelo
	6	Bitter gourd	Carb-veg (VC) ($n_3 = 2$)	1	Potato		11	Melon
	7	Arum		2	Sweet potato		12	Star apple
	8	Ash gourd	Pulses (PL) ($n_5 = 7$)	1	Lentil		13	Kirai
	9	Cucumber		2	Pea (motor)		14	Blackberry
	10	Long bean		3	Green gran		15	Carambola apple
	11	Snake gourd		4	Black gram		16	Wood apple (bell)
	12	Amaranth		5	Arhar		17	Green coconut
	13	Cucurbitaceae		6	Khesari		18	Ripe palmyra
	14	Sponge gourd		7	Gram		1	Chili
	15	*Colocasia*		1	Sesame		2	Onion

(continued)

Category (number)	No	Crop name	Category (number)	No	Crop name	Category (number)	No	Crop name
	16	Green papaya	Oilseed (OS) ($n_4 = 4$)	2	Mustard	Spices (SP) ($n_7 = 8$)	3	Garlic
	17	Green banana		3	Groundnut		4	Turmeric
	18	Rabi brinjal		4	Coconut		5	Ginger
	19	Cauliflower	Molasses (MS) ($n_8 = 3$)	1	Sugarcane		6	Coriander seed
	20	Cabbage		2	Date palm		7	Fennel seed
	21	*Cucurbita*		3	Palmyra palm		8	Fenugreek

References

Abdullah AB, Ito S, Adhana K (2006) Estimate of rice consumption in Asian countries and the world towards 2050. In Proceedings for workshop and conference on rice in the world at stake, vol. 2, pp 28–43

Akinci H, Özalp AY, Turgut B (2013) Agricultural land use suitability analysis using GIS and AHP technique. Comput Electron Agric 97:71–82. https://doi.org/10.1016/j.compag.2013.07.006

Alam MS, Quayum MA, Islam MA (2010) Crop production in the Haor areas of Bangladesh: insights from farm level survey. Agriculturists 8(2):88–97

Amin M, Zhang J, Yang M (2015) Effects of climate change on the yield and cropping area of major food crops: a case of Bangladesh. Sustain For 7(1):898–915. https://doi.org/10.3390/su7010898

Amini S, Rohani A, Aghkhani MH, Abbaspour-Fard MH, Asgharipour MR (2019) Assessment of land suitability and agricultural production sustainability using a combined approach (Fuzzy-AHP-GIS): a case study of Mazandaran province, Iran. Inf Process Agric. https://doi.org/10.1016/j.inpa.2019.10.001

Arief UM, Nafi AY (2018) An accurate assessment tool based on intelligent technique for suitability of soybean cropland: case study in Kebumen Regency, Indonesia. Heliyon 4(7): e00684. https://doi.org/10.1016/j.heliyon.2018.e00684

Asai H, Samson BK, Stephan HM, Songyikhangsuthor K, Homma K, Kiyono Y, Horie T (2009) Biochar amendment techniques for upland rice production in Northern Laos: 1. Soil physical properties, leaf SPAD and grain yield. Field Crop Res 111(1-2):81–84. https://doi.org/10.1016/j.fcr.2008.10.008

Ashford SA, Sitar N, Lysmer J, Deng N (1997) Topographic effects on the seismic response of steep slopes. Bull Seismol Soc Am 87(3):701–709

Aydi A, Abichou T, Nasr IH, Louati M, Zairi M (2016) Assessment of land suitability for olive mill wastewater disposal site selection by integrating fuzzy logic, AHP, and WLC in a GIS. Environ Monit Assess 188(1):59. https://doi.org/10.1007/s10661015-5076-3

Ayehu GT, Besufekad SA (2015) Land suitability analysis for rice production: a GIS based multi-criteria decision approach. Am J Geogr Inf Syst 4(3):95–104. https://doi.org/10.5923/j.ajgis.20150403.02

Bahrani S, Ebadi T, Ehsani H, Yousefi H, Maknoon R (2016) Modeling landfill site selection by multi-criteria decision making and fuzzy functions in GIS, case study: Shabestar, Iran. Environ Earth Sci 75(4):337. https://doi.org/10.1007/s12665-015-5146-4

Bangladesh Bureau of Statistics (BBS) (2011) Statistics and informatics division (SID). Ministry of Planning, Dhaka

Bangladesh Bureau of Statistics (BBS) (2014) Small area atlas of Bangladesh. Ministry of Planning, Dhaka

Bangladesh Bureau of Statistics (BBS) (2016) Yearbook of agricultural statistics-2015. Ministry of Planning, Dhaka

Bangladesh Bureau of Statistics (BBS) (2018a) Statistical pocket book Bangladesh 2016. Ministry of Planning, Dhaka

Bangladesh Bureau of Statistics (BBS) (2018b) Bangladesh agricultural statistics yearbook 2017. Ministry of Planning, Dhaka

Bangladesh Institute of Research and Rehabilitation in Diabetes, Endocrine and Metabolic Disorders (BIRDEM) (2013) Desirable dietary pattern for Bangladesh. National Food Policy Capacity Strengthening Programme, Dhaka

Barbosa AM (2015) fuzzySim: applying fuzzy logic to binary similarity indices in ecology. Methods Ecol Evol 6(7):853–858. https://doi.org/10.1111/2041-210X.12372

Basche AD, Archontoulis SV, Kaspar TC, Jaynes DB, Parkin TB, Miguez FE (2016) Simulating long-term impacts of cover crops and climate change on crop production and environmental outcomes in the Midwestern United States. Agric Ecosyst Environ 218:95–106. https://doi.org/10.1016/j.agee.2015.11.011

Beinat E, Nijkamp P (eds) (1998) Multicriteria analysis for land-use management, vol 9. Springer, New York

Bellman RE, Zadeh LA (1970) Decision-making in a fuzzy environment. Manag Sci 17(4):141. https://doi.org/10.1287/mnsc.17.4.B141

Chaignon V, Bedin F, Hinsinger P (2002) Copper bioavailability and rhizosphere pH changes as affected by nitrogen supply for tomato and oilseed rape cropped on an acidic and a calcareous soil. Plant Soil 243:219–228. https://doi.org/10.1023/A:1019942924985

Chauhan BS, Jabran K, Mahajan G (2017) Rice production worldwide, vol 247. Springer, Basel, pp 255–277. https://doi.org/10.1007/978-3-319-47516-5

Chow TE, Sadler R (2010) The consensus of local stakeholders and outside experts in suitability modeling for future camp development. Landsc Urban Plan 94(1):9–19. https://doi.org/10.1016/j.landurbplan.2009.07.013

Cosgrove WJ, Rijsberman FR, Rijsberman F (2000) World water vision: making water everybody's business. World Water Council, Publications, London

Datta A, Ullah H, Ferdous Z (2017) Water management in rice. In: Chauhan B, Jabran K, Mahajan G (eds) Rice production worldwide. Springer, Cham, pp 255–277

Dexter AR (2004) Soil physical quality: part I. Theory, effects of soil texture, density, and organic matter, and effects on root growth. Geoderma 120(3-4):201–214. https://doi.org/10.1016/j.geoderma.2003.09.004

Dou F, Soriano J, Tabien RE, Chen K (2016) Soil texture and cultivar effects on rice (Oryza Sativa, L.) grain yield, yield components and water productivity in three water regimes. PLoS ONE 11: e0150549. https://doi.org/10.1007/978-3-319-47516-5_11

Egamberdieva D, Jabborova D, Berg G (2016) Synergistic interactions between Bradyrhizobium japonicum and the endophyte Stenotrophomonas rhizophila and their effects on growth, and nodulation of soybean under salt stress. Plant Soil 405:35–45. https://doi.org/10.1007/s11104-015-2661-8

El Bilali H, Callenius C, Strassner C, Probst L (2019) Food and nutrition security and sustainability transitions in food systems. Food Energy Secur 8(2):e00154. https://doi.org/10.1002/fes3.154

Elsheikh R, Shariff ARBM, Amiri F, Ahmad NB, Balasundram SK, Soom MAM (2013) Agriculture land suitability evaluator (ALSE): a decision and planning support tool for tropical and subtropical crops. Comput Electron Agric 93:98–110. https://doi.org/10.1016/j.compag.2013.02.003

Feizizadeh B, Blaschke T, Nazmfar H, Rezaei Moghaddam MH (2013) Landslide susceptibility mapping for the Urmia Lake basin, Iran: a multi-criteria evaluation approach using GIS. Int J Environ Res 7(2):319–336. https://doi.org/10.1007/s11069-012-0463-3

Food and Agriculture Organization of the United Nations (FAO) (1976) A framework for land evaluation. Food and Agriculture Organization of the United Nations, Soils Bulletin 32. FAO, Rome

Food and Agriculture Organization of the United Nations (FAO) (1995) FAO quarterly bulletin of statistics, vol 18. FAO, Rome, pp 1–2

Food and Agriculture Organization of the United Nations (FAO) (2003) World agriculture: towards 2015/2030: an FAO perspective. Earthscan, London

Food and Agriculture Organization of the United Nations (FAO) (2004a). Cereals and other starch-based staples: are consumption patterns changing? FAO 2004 Rome, Italy, 10-11 February 2004. Joint meeting of the intergovernmental group on grains (30th session) and the intergovernmental group on rice (41st session) Rome, Italy, 10–11 February 2004

Food and Agriculture Organization of the United Nations (FAO) (2004b) The state of food security in the world. FAO, Rome, pp 30–31

Food and Agriculture Organization of the United Nations (FAO) (2014a) Country nutrition paper: Bangladesh. FAO, Rome

Food and Agriculture Organization of the United Nations (FAO) (2014b) Country nutrition paper Bangladesh. In: Joint FAO/WHO International Conference on nutrition, vol 21. FAO, Rome, p 47

Food and Agriculture Organization of the United Nations (FAO) (2016) Soils and pulses: symbiosis for life. FAO, Rome

Gitari HI, Gachene CKK, Karanja NN et al (2019) Potato-legume intercropping on a sloping terrain and its effects on soil physico-chemical properties. Plant Soil 438:447–460. https://doi.org/10.1007/s11104-019-04036-7

Guo X, Li H, Huimin Y, Li W, Ye Y, Biswas A (2018) Drivers of spatio-temporal changes in paddy soil pH in Jiangxi Province, China from 1980 to 2010. Sci Rep 8(1):1–11. https://doi.org/10.1038/s41598-018-20873-5

Habibie MI, Noguchi R, Shusuke M, Ahamed T (2019) Land suitability analysis for maize production in Indonesia using satellite remote sensing and GIS-based multicriteria decision support system. GeoJournal 2019:1–31. https://doi.org/10.1007/s10708-019-10091-5

Hamdy A, Ragab R, Scarascia-Mugnozza E (2003) Coping with water scarcity: water saving and increasing water productivity. Irrig Drain 52(1):3–20. https://doi.org/10.1002/ird.73

Hassan N, Huda N, Ahmad K (1985) Seasonal patterns of food intake in rural Bangladesh: its impact on nutritional status. Ecol Food Nutr 17(2):175–186. https://doi.org/10.1080/03670244.1985.9990891

HIES (2016) Preliminary report on household income and expenditure survey 2016. Ministry of Planning, Dhaka. https://doi.org/10.5897/AJAR2014.9248

Hu W, Huang B, Borggaard OK, Ye M, Tian K, Zhang H, Holm PE (2018) Soil threshold values for cadmium based on paired soil-vegetable content analyses of greenhouse vegetable production systems in China: implications for safe food production. Environ Pollut 241:922–929. https://doi.org/10.1016/j.envpol.2018.06.034

Huete A (1988) A soil-adjusted vegetation index (SAVI). Remote Sensing of Environment. Remote Sens Environ 25:295–309. https://doi.org/10.1016/0034-4257(88)90106-X

Jiang Z, Huete AR, Chen J, Chen Y, Li J, Yan G, Zhang X (2006) Analysis of NDVI and scaled difference vegetation index retrievals of vegetation fraction. Remote Sens Environ 101(3):366–378. https://doi.org/10.1016/j.rse.2006.01.003

Johnston AM, Tanaka DL, Miller PR, Brandt SA, Nielsen DC, Lafond GP, Riveland NR (2002) Oilseed crops for semiarid cropping systems in the northern Great Plains. Agron J 94(2):231–240. https://doi.org/10.2134/agronj2002.2310

Kamkar B, Dorri MA, da Silva JAT (2014) Assessment of land suitability and the possibility and performance of a canola (Brassica napus L.)–soybean (Glycine max L.) rotation in four basins of Golestan province, Iran. Egypt J Remote Sens Space Sci 17(1):95–104. https://doi.org/10.1016/j.ejrs.2013.12.001

Kawasaki K, Uchida S (2016) Quality matters more than quantity: asymmetric temperature effects on crop yield and quality grade. Am J Agric Econ 98(4):1195–1209. https://doi.org/10.1093/ajae/aaw036

Kazemi H, Akinci H (2018) A land use suitability model for rainfed farming by multi-criteria decision-making analysis (MCDA) and geographic information system (GIS). Ecol Eng 116:1–6. https://doi.org/10.1016/j.ecoleng.2018.02.021

Kihoro J, Bosco NJ, Murage H (2013) Suitability analysis for rice growing sites using a multicriteria evaluation and GIS approach in great Mwea region, Kenya. Springerplus 2(1):265. https://doi.org/10.1186/2193-1801-2-265

Kladivko EJ, Griffith DR, Mannering JV (1986) Conservation tillage effects on soil properties and yield of corn and soya beans in Indiana. Soil Tillage Res 8:277–287. https://doi.org/10.1016/0167-1987(86)90340-5

Koohafkan P, Stewart BA (2008) Water and cereals in drylands. Chapter 2 - cereal production in drylands. Earthscan, London

Malczewski J (2006) GIS-based multicriteria decision analysis: a survey of the literature. Int J Geogr Inf Sci 20(7):703–726. https://doi.org/10.1080/13658810600661508

Mapanda F, Mangwayana EN, Nyamangara J, Giller KE (2005) The effect of long-term irrigation using wastewater on heavy metal contents of soils under vegetables in Harare, Zimbabwe. Agric Ecosyst Environ 107(2-3):151–165. https://doi.org/10.1016/j.agee.2004.11.005

Marklein A, Elias E, Nico P, Steenwerth K (2020) Projected temperature increases may require shifts in the growing season of cool-season crops and the growing locations of warm-season crops. Sci Total Environ 746:140918. https://doi.org/10.1016/j.scitotenv.2020.140918

McCormick JI, Virgona JM, Kirkegaard JA (2012) Growth, recovery, and yield of dual-purpose canola (Brassica napus) in the medium-rainfall zone of south-eastern Australia. Crop Pasture Sci 63(7):635–646. https://doi.org/10.1071/CP12078

Meng XD, Ma H, Wei M, Xing YX (1997) Breeding of vegetable crops for protected growing conditions. Acta Hortic 481:695–700. https://doi.org/10.17660/ActaHortic.1999.481.83

Miller PR, McConkey BG, Clayton GW, Brandt SA, Staricka JA, Johnston AM et al (2002) Pulse crop adaptation in the northern great plains. Agron J 94(2):261–272. https://doi.org/10.2134/agronj2002.2610

Ministry of Environment and Forests (MoEF) (2008) Bangladesh climate change strategy and action plan 2008. Government of the People's Republic of Bangladesh, Dhaka

Mitchell S, Cohen K (2014) Fuzzy logic decision making for autonomous robotic applications. In: 2014 IEEE 6th international conference on awareness science and technology (iCAST). IEEE, Piscataway, pp 1–6. https://doi.org/10.1109/ICAwST.2014.6981843

Mottaleb KA, Rahut DB, Kruseman G, Erenstein O (2018) Evolving food consumption patterns of rural and urban households in developing countries: a Bangladesh case. Br Food J 120(2):392–408. https://doi.org/10.1108/BFJ-12-2016-0620

Nahusenay A, Kibebew K (2015) Land suitability evaluation in Wadla Delanta Massif of north central highlands of Ethiopia for rainfed crop production. Afr J Agric Res 10(13):1595–1611. https://doi.org/10.5897/AJAR2014.9248

Nasim M, Shahidullah SM, Saha A, Muttaleb MA, Aditya TL, Ali MA, Kabir MS (2017) Distribution of crops and cropping patterns in Bangladesh. Bangladesh Rice J 21(2):1–55. https://doi.org/10.3329/brj.v21i2.38195

Ngoy KI, Shebitz D (2020) Potential impacts of climate change on areas suitable to grow some key crops in New Jersey, USA. Environments 7(10):76. https://doi.org/10.3390/environments7100076

Nguyen TT, Verdoodt A, Van Y, Delbecque N, Tran TC, Van Ranst E (2015) Design of a GIS and multi-criteria based land evaluation procedure for sustainable land-use planning at the regional level. Agric Ecosyst Environ 200:1–11. https://doi.org/10.1016/j.agee.2014.10.015

Noorollahi E, Fadai D, Akbarpour Shirazi M, Ghodsipour SH (2016) Land suitability analysis for solar farms exploitation using GIS and fuzzy analytic hierarchy process (FAHP)—a case study of Iran. Energies 9(8):643. https://doi.org/10.3390/en9080643

Novara A, Minacapilli M, Santoro A, Rodrigo-Comino J, Carrubba A, Sarno M, Gristina L (2019) Real cover crops contribution to soil organic carbon sequestration in sloping vineyard. Sci Total Environ 652:300–306. https://doi.org/10.1016/j.scitotenv.2018.10.247

Olivero J, Real R, Marquez AL (2011) Fuzzy chorotypes as a conceptual tool to improve insight into biogeographic patterns. Syst Biol 60(5):645–660. https://doi.org/10.1093/sysbio/syr026

Ostovari Y, Honarbakhsh A, Sangoony H, Zolfaghari F, Maleki K, Ingram B (2019) GIS and multi-criteria decision-making analysis assessment of land suitability for rapeseed farming in calcareous soils of semi-arid regions. Ecol Indic 103:479–487. https://doi.org/10.1016/j.ecolind.2019.04.051

Paul B, Rashid H (2016) Climatic hazards in Coastal Bangladesh: non-structural and structural solution. Butterworth-Heinemann, Oxford, pp 121–152

Pelosi C, Baudry E, Schmidt O (2020) Comparison of the mustard oil and electrical methods for sampling earthworm communities in rural and urban soils. Urban Ecosyst. https://doi.org/10.1007/s11252-020-01023-0

Pilevar AR, Matinfar HR, Sohrabi A, Sarmadian F (2020) Integrated fuzzy, AHP and GIS techniques for land suitability assessment in semi-arid regions for wheat and maize farming. Ecol Indic 110:105887. https://doi.org/10.1016/j.ecolind.2019.105887

Purnamasari RA, Noguchi R, Ahamed T (2019) Land suitability assessments for yield prediction of cassava using geospatial fuzzy expert systems and remote sensing. Comput Electron Agric 166:105018. https://doi.org/10.1016/j.compag.2019.105018

Qin S, Li L, Wang D, Zhang J, Pu Y (2013) Effects of limited supplemental irrigation with catchment rainfall on rain-fed potato in semi-arid areas on the Western Loess Plateau. Am J Potato Res 90(1):33–42. https://doi.org/10.1007/s12230-012-9267-y

Richards J, Madramootoo CA, Goyal MK (2014) Determining irrigation requirements for vegetables and sugarcane in Jamaica. Irrig Drain 63(3):340–348. https://doi.org/10.1002/ird.1811

Romano G, Dal Sasso P, Liuzzi GT, Gentile F (2015) Multi-criteria decision analysis for land suitability mapping in a rural area of Southern Italy. Land Use Policy 48:131–143. https://doi.org/10.1016/j.landusepol.2015.05.013

Rondeaux G, Steven M, Baret F (1996) Optimization of soil-adjusted vegetation indices. Remote Sens Environ 55(2):95–107. https://doi.org/10.1016/0034-4257(95)00186-7

Saini GR, Grant WJ (1980) Long-term effects of intensive cultivation on soil quality in the potato-growing areas of New Brunswick (Canada) and Maine (USA). Can J Soil Sci 60(3):421–428. https://doi.org/10.4141/cjss80-047

Salman SM, Mahul O, Bagazonzya HK (2010) Agricultural insurance in Bangladesh: promoting access to small and marginal farmers. The World Bank, Washington, DC, pp 1–146

Samanta S, Pal B, Pal DK (2011) Land suitability analysis for rice cultivation based on multi-criteria decision approach through GIS. Data Base 2011:12–20

Sarker RA, Talukdar S, Haque AA (1997) Determination of optimum crop mix for crop cultivation in Bangladesh. Appl Math Model 21(10):621–632. https://doi.org/10.1016/S0307-904X(97)00083-8

Schutter M, Sandeno J, Dick R (2001) Seasonal, soil type, and alternative management influences on microbial communities of vegetable cropping systems. Biol Fertil Soils 34(6):397–410. https://doi.org/10.1007/s00374-001-0423-7

Seyedmohammadi J, Sarmadian F, Jafarzadeh AA, McDowell RW (2019) Development of a model using matter element, AHP and GIS techniques to assess the suitability of land for agriculture. Geoderma 352:80–95. https://doi.org/10.1016/j.geoderma.2019.05.046

Shimoda S, Kanno H, Hirota T (2018) Time series analysis of temperature and rainfall-based weather aggregation reveals significant correlations between climate turning points and potato (Solanum tuberosum L) yield trends in Japan. Agric For Meteorol 263:147–155. https://doi.org/10.1016/j.agrformet.2018.08.005

Sulaiman AA, Sulaeman Y, Mustikasari N, Nursyamsi D, Syakir AM (2019) Increasing sugar production in Indonesia through land suitability analysis and sugar mill restructuring. Landscape 8(4):61. https://doi.org/10.3390/land8040061

Tashayo B, Honarbakhsh A, Akbari M, Eftekhari M (2020) Land suitability assessment for maize farming using a GIS-AHP method for a semi-arid region, Iran. J Saudi Soc Agric Sci 19(5):332–338. https://doi.org/10.1016/j.jssas.2020.03.003

Thaker S, Nagori V (2018) Analysis of fuzzification process in fuzzy expert system. Proc Comput Sci 132:1308–1316. https://doi.org/10.1016/j.procs.2018.05.047

Timsina J, Wolf J, Guilpart N, Van Bussel LGJ, Grassini P, Van Wart J, Van Ittersum MK (2018) Can Bangladesh produce enough cereals to meet future demand? Agric Syst 163:36–44. https://doi.org/10.1016/j.agsy.2016.11.003

Todmal RS, Korade MS, Dhorde AG, Zolekar RB (2018) Hydro-meteorological and agricultural trends in water-scarce Karha Basin, western India: current and future scenario. Arab J Geosci. https://doi.org/10.1007/s12517-018-3655-7

United Nations Development Program (UNDP) (2004) Reducing disaster risk: a challenge for development-a global report. New York, UNDP

Ustaoglu E, Aydınoglu AC (2020) Suitability evaluation of urban construction land in Pendik district of Istanbul, Turkey. Land Use Policy 99:104783. https://doi.org/10.3390/rs12091463

Venancio LP, Mantovani EC, do Amaral CH, Neale CM, Gonçalves IZ, Filgueiras R, Campos I (2019) Forecasting corn yield at the farm level in Brazil based on the FAO-66 approach and soil-adjusted vegetation index (SAVI). Agric Water Manag 225:105779. https://doi.org/10.1016/j.agwat.2019.105779

Wang YH, Li JY (2005) The plant architecture of rice (Oryza sativa). Plant Mol Biol 59:75–84

WDI (2014) World development indicators. World Bank, Washington DC. https://doi.org/10.1596/978-1-4648-0163-1

World Health Organization (2019) Healthy diet (No. WHO-EM/NUT/282/E). World Health Organization. Regional Office for the Eastern Mediterranean. https://apps.who.int/iris/handle/10665/325828

Xing Z, Chow L, Rees W, H., Meng, F., Monteith, J., & Stevens, L. (2011) A comparison of effects of one-pass and conventional potato hilling on water runoff and soil erosion under simulated rainfall. Can J Soil Sci 91(2):279–290. https://doi.org/10.4141/cjss10099

Yalew SG, van Griensven A, Mul ML, van der Zaag P (2016) Land suitability analysis for agriculture in the Abbay basin using remote sensing, GIS and AHP techniques. Model Earth Syst Environ 2(2):101.101. https://doi.org/10.1007/s40808-016-0167-x

Yang L, Huang B, Hu W, Chen Y, Mao M, Yao L (2014) The impact of greenhouse vegetable farming duration and soil types on phytoavailability of heavy metals and their health risk in eastern China. Chemosphere 103:121–130. https://doi.org/10.1016/j.chemosphere.2013.11.047

Zadeh LA (1965) Fuzzy sets. Inf Control 8(3):338–353. https://doi.org/10.1016/S0019-9958(65)90241-X

Zhao H, Xiong YC, Li FM, Wang RY, Qiang SC, Yao TF, Mo F (2012) Plastic film mulch for half growing-season maximized WUE and yield of potato via moisture-temperature improvement in a semi-arid agroecosystem. Agric Water Manag 104:68–78. https://doi.org/10.1016/j.agwat.2011.11.016

Zhu KW, Chen YC, Zhang S, Yang ZM, Huang L, Li L et al (2020) Output risk evolution analysis of agricultural non-point source pollution under different scenarios based on multi-model. Glob Ecol Conserv 2020:e01144. https://doi.org/10.1016/j.gecco.2020.e01144

Zolekar RB, Bhagat VS (2015) Multi-criteria land suitability analysis for agriculture in hilly zone: remote sensing and GIS approach. Comput Electron Agric 118:300–321. https://doi.org/10.1016/j.compag.2015.09.016

Zolekar RB, Bhagat VS (2018) Multi-criteria land suitability analysis for plantation in Upper Mula and Pravara basin: remote sensing and GIS approach. J Geogr Stud 2(1):12–20

Chapter 3
Agricultural Land Suitability Assessment Using Satellite Remote Sensing-Derived Soil-Vegetation Indices

Rubaiya Binte Mustafiz, Ryozo Noguchi, and Tofael Ahamed

Abstract Satellite remote sensing technologies have a high potential in applications for evaluating land conditions and can facilitate optimized planning for agricultural sectors. However, misinformed land selection decisions limit crop yields and increase production-related costs to farmers. Therefore, the purpose of this research was to develop a land suitability assessment system using satellite remote sensing-derived soil-vegetation indicators. A multicriteria decision analysis was conducted by integrating weighted linear combinations and fuzzy multicriteria analyses in a GIS platform for suitability assessment using the following eight criteria: elevation, slope, LST, and vegetation indices (SAVI, ARVI, SARVI, MSAVI, and OSAVI). The relative priorities of the indicators were identified using a fuzzy expert system. Furthermore, the results of the land suitability assessment were evaluated by ground truth yield data. In addition, a yield estimation method was developed using indices representing influential factors. The analysis utilizing equal weights showed that 43% of the land (1832 km^2) was highly suitable, 41% of the land (1747 km^2) was moderately suitable, and 10% of the land (426 km^2) was marginally suitable for improved yield productions. Alternatively, expert knowledge was also considered, along with references, when using the fuzzy membership function; as a result, 48% of the land (2045 km^2) was identified as being highly suitable; 39% of the land (2045 km^2) was identified as being moderately suitable, and 7% of the land (298 km^2) was identified as being marginally suitable. Additionally, 6% (256 km^2) of the land was described as not suitable by both methods. Moreover, the yield estimation using SAVI ($R^2 = 0.773$), ARVI ($R^2 = 0.689$), SARVI ($R^2 = 0.711$), MSAVI ($R^2 = 0.745$), and OSAVI ($R^2 = 0.812$) showed a good predictive ability. Furthermore, the combined model using these five indices reported the highest accuracy ($R^2 = 0.839$); this model was then applied to develop yield prediction maps for the corresponding

R. B. Mustafiz
Graduate School of Life and Environmental Sciences, University of Tsukuba, Tsukuba, Ibaraki, Japan

R. Noguchi · T. Ahamed (✉)
Faculty of Life and Environmental Sciences, University of Tsukuba, Tsukuba, Ibaraki, Japan
e-mail: tofael.ahamed.gp@u.tsukuba.ac.jp

years (2017–2020). This research suggests that satellite remote sensing methods in GIS platforms are an effective and convenient way for agricultural land use planners and land policy makers to select suitable cultivable land areas with potential for increased agricultural production.

Keywords Satellite · Remote sensing · Soil-vegetation indices · Fuzzy membership function · Yield prediction · Agricultural land suitability

3.1 Introduction

Proper land use planning is essential for enhancing agricultural production and ecological conservation and for the protection of biodiversity (Kennedy et al. 2016). Inappropriate land management practices lead to a higher rate of soil erosion, a diminished crop production, a hindered productivity, and a deteriorated soil quality (Pimentel and Burgess 2013). Therefore, land management focusing on suitability should be a key issue of research and policy development mainly due to its influence on crop production. The knowledge of local land conditions has become increasingly recognized for its importance in sustainable land management (Jyoti et al. 2015). Farmers of local communities assess their farmland using consistent observations and collective experiences (Niemeijer and Mazzucato 2003). However, for rural communities, this knowledge is usually insufficient to understand the adequacy of suitable condition, management strategies, and land use decisions.

In addition, many conventional techniques for Earth monitoring applications require specific spectral features that are defined only for multispectral data such as deep learning, exploiting both temporal and cross-sensor dependencies, and deep neural networks achieve much better performance than traditional methods (Mazza et al. 2018; Li et al. 2020). Furthermore, innovative farming technologies incorporate biology with computers, and device exchange-based smart agriculture becomes achieved in a structured farm management system. The high spatial imagery from remote sensing datasets may provide an aid to systematically consider issues associated with smart farming technology. Remote sensing methods support the formation of growth profiles of plants and temporal evolution scheme of soils over their developmental phases (Ennouri and Kallel 2019). Remote sensing indices that incorporate environmental recovery factors are useful for tracing the development of crops, their interrelatedness, and the consequences of the variables of interest for crop development. Following this concern, the application of smart agriculture and satellite remote sensing-based soil-vegetation indices evaluations for agricultural land condition assessments is the key target of this research. Therefore, land suitability assessments can be performed using the multicriteria decision method (MCDM). Such evaluation provides information about specific land use potentials and constraints. The MCDM becomes more suitable when incorporating geospatial references. In recent years, computing technologies combined with GIS have

enabled geospatial references using MCDM-land suitability evaluations. Furthermore, the MCDM, combined with linear combination and fuzzy set theory, has the potential to reduce subjectivity in the assessment of results. Several approaches to the MCDM that utilize equal-weighted linear combinations or fuzzy membership systems have been applied to conduct land suitability evaluations (Olivero et al. 2011; Elsheikh et al. 2013; Kazemi and Akinci 2018; Habibie et al. 2019). In addition, for sustainable land resource management, the Food and Agriculture Organization (FAO) has proposed guidelines for land evaluation (Food and Agriculture Organization 1976). According to the guidelines, land is classified into four categories: highly suitable, moderately suitable, marginally suitable, and not suitable. Additionally, the equal-weighted linear combination-fuzzy overlay technique in the GIS platform has the capabilities needed to overcome these limitations by applying the required calorie ratio (FAO recommended) to prepare land suitability assessments for smart agricultural practices. However, there is a lack of datasets in some areas of developing regions where assessments of land suitability are really challenging. In addition, recent datasets of geographic information system (GIS) have limitation, especially land uses, drainage, and lack of soil sampling information for soil nutrients in a distant time period.

It is worth mentioning that quick and accurate land suitability assessments can aid in the improvement of yield prediction models. Regarding the judgment of the prediction of yield using vegetation indices (VIs), it is the most straightforward approach to establishing empirical relationships between ground-based yield measures and VIs (Tucker 1979; Das et al. 2020; Romano et al. 2015). In this regard, satellite remote sensing technologies and GIS applications for monitoring crops have the potential to establish timely assessments of changes in the growth and development of crops on regional scales (Campos et al. 2018). The yield prediction is also helpful for making decisions on regional food security policies and production inventories to understand the availability of field crop.

Additionally, local farmer's perceptions and their assessment of land suitability can differ from scientific approaches due to the much broader contextual implications of the former and how they are often framed. This often results in differences in perceived problems and the required solutions (Essougong et al. 2020). In most cases, developing location-specific descriptions by soil sampling and analysis is expensive and challenging. Following this concern, advanced and affordable smart satellite remote sensing multicriteria technologies that consider climate factors are required for land suitability and accuracy assessments.

Therefore, the purpose of this research was to develop a soil-vegetation intent land suitability assessment model based on multicriteria decision-making analysis to determine optimal land distributions according to soil-vegetation indices to ensure elevated productivity, and a yield prediction method was developed using vegetation indices. A methodology that can be applied across various countries is proposed to reduce the complexities of farmland evaluation practices.

3.2 Materials and Methods

The proposed method utilizes a GIS-based multicriteria analysis to develop a soil-vegetation index-associated suitability analysis by exploiting satellite remote sensing for land suitability assessment and consists of three major steps (Fig. 3.1): the calculation of soil-vegetation indices for land suitability mapping of diversified crops, regression analysis using ground truth yield data for validation, and the utilization of a yield prediction model to develop a yield map. ArcGIS 10.4® (ESRI, Boston, CA) software was used for criteria aggregation, data preprocessing and calculation standardization, weight determination by an equal-weighted overlay, fuzzy membership function, fuzzy overlay, and raster calculation.
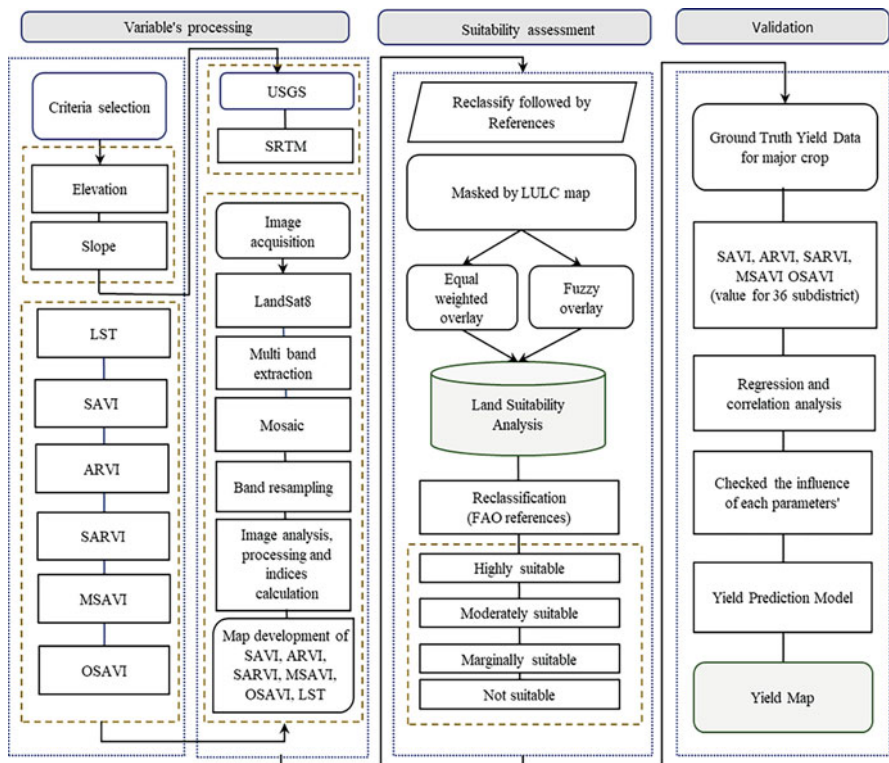
Fig. 3.1 Framework for land suitability assessment using satellite remote sensing-derived soil-vegetation indices

3.2.1 Study Area

The study area is located between 25°14′ and 26°02′ N latitudes and 88°22′ and 89°54′ E longitudes in the northern part of Bangladesh and has a total area of 8260 km². The study was conducted in the Dinajpur, Rangpur, Kurigram, and Gaibandha districts of the Rangpur division where the inhabitants derive their livelihoods from agriculture (Fig. 3.2). The area consists of 36 administrative units with an overall population of 11,498,000 (Bangladesh Bureau of Statistics (BBS) 2011). The population is economically active in agriculture; nevertheless, agronomic land use is highly inconsistent due to climatic factors, soil property issues, water infiltration, environmental resources, and local socioeconomic conditions. Based on weather
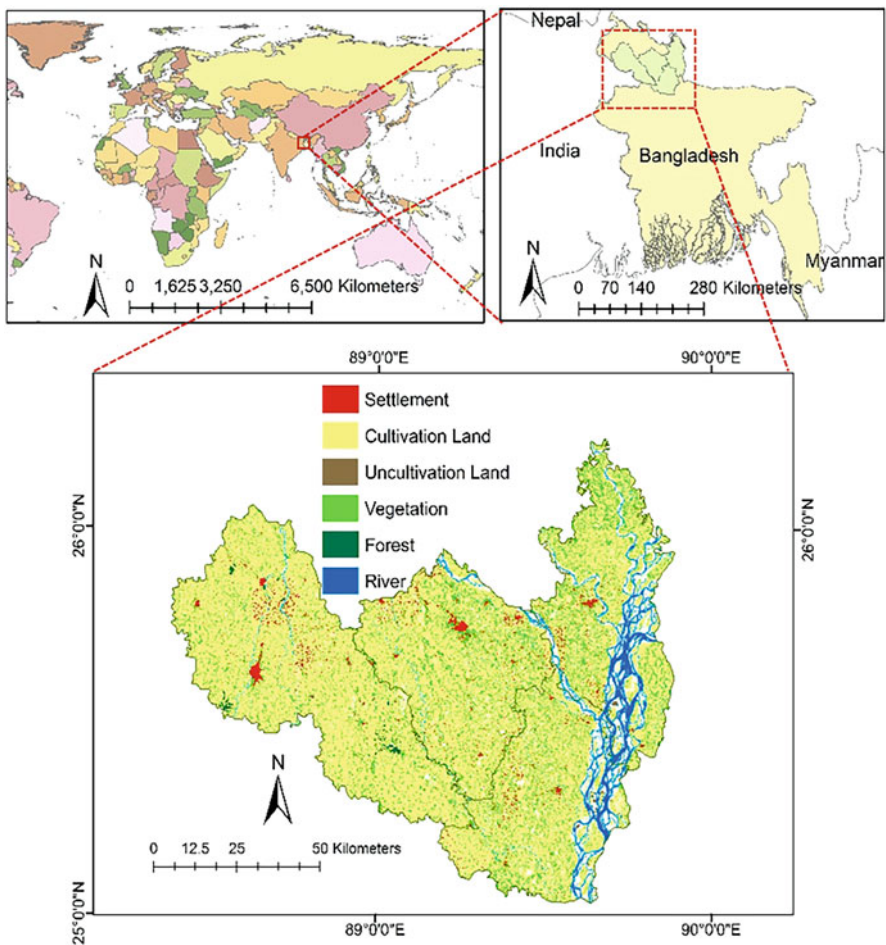
Fig. 3.2 Study area: northern part of Bangladesh, four districts: Dinajpur, Rangpur, Gaibandha, and Kurigram

data, the minimum and maximum mean annual temperature varies between 8.47 °C and 36.3 °C. The annual average rainfall recorded is 765–1233 mm, with a high humidity in the range of 41–77% (Bangladesh Bureau of Statistics (BBS) 2018). The elevation ranges from 5 to 30 m above sea level.

3.2.2   Image Acquisition

Landsat 8 is the most recently launched Landsat satellite and carries the Operational Land Imager (OLI) and Thermal Infrared Sensor (TIRS) instruments. OLI collects data in the visible, near-infrared (NIR), and shortwave infrared (SWIR) spectral bands and in a panchromatic band. These two sensors provide seasonal coverage of the global landmass at a spatial resolution of 30 m (visible, NIR, and SWIR), 100 m (thermal), and 15 m (panchromatic). The 100 m TIRS data are registered to the OLI dataset to create radiometrically, geometrically, and terrain-corrected 12-bit data products. Images were acquired from 2017 to 2020. In this study, all satellite data were downloaded from the United States Geological Survey (USGS). The image was acquired (less than 10% cloud cover) in growing stage of the specific crop cycle (dry season irrigated rice).

3.2.3   Digital Image Preprocessing

All satellite images were first processed by resampling the band resolution at 30 m and then mosaicked and masked. Subsequently, an algebraic raster operation and a radiometric calibration as well as geometric and atmospheric corrections were applied to the remote sensing images using ArcGIS 10.4®. Image acquisition was performed for each band. After that, all selected bands were converted to a 30 m resolution using a resampling technique to ensure a similar cell size and data uniformity. The average reflectance values were calculated for the study area in each band using the raster calculator tool to compensate for the spatial variability to minimize the bias. Three different blocks collected during related time periods were mosaicked to cover the large study area.

3.2.4   Criteria Aggregation for Land Fertility Assessment

Three vital layers were developed by satellite data, and five vegetation indices were used as the input parameters to develop the land suitability analysis (Fig. 3.3). The most important land and soil affiliated indices, SAVI, SARVI, ARVI, MSAVI, and OSAVI, were utilized to describe land conditions (Table 3.1). In addition, the slope and elevation layers were used as representative land conditions. The land surface
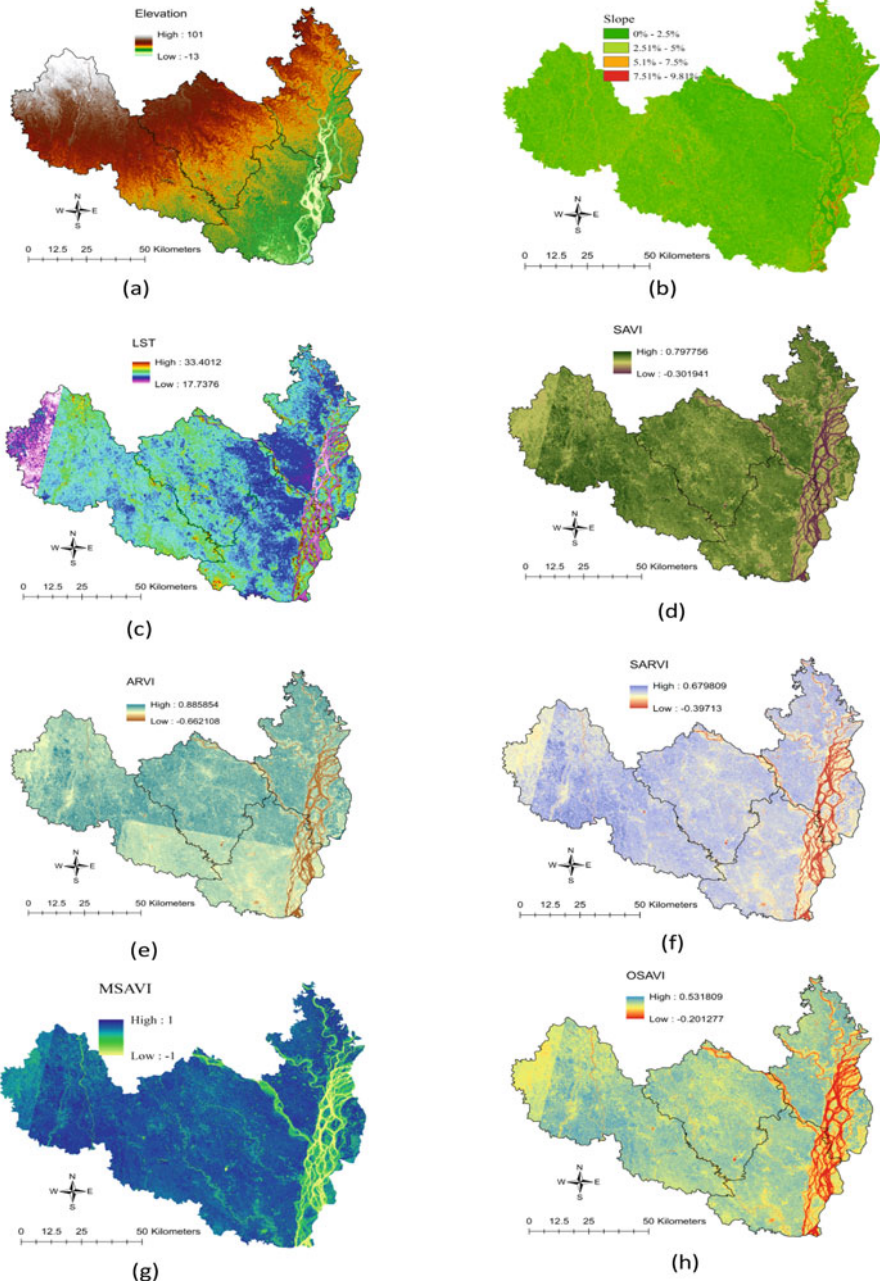
Fig. 3.3 Criteria: (**a**) elevation, (**b**) slope, (**c**) LST, (**d**) SAVI, (**e**) ARVI, (**f**) SARVI, (**g**) MSAVI, (**h**) OSAVI

Table 3.1 List of data and original data sources for land suitability analysis

No	Data	Native format	Description	Source
1	Land use map	92 small vectors Blocks (point, line, polygon, and tabular)	Scale at 1:25,000 m	2019, SoB, Bangladesh
2	Elevation map	Raster	Extracted from 30 m resolution	2020, STRM
3	Slope map	Raster	Derived from 30 m resolution	2020, STRM
4	Land surface temperature (LST)	Raster	Derived from 30 m resolution	2020, Landsat 8
5	SAVI map	Raster	Derived from 30 m resolution	2020, Landsat 8, USGS
6	ARVI map	Raster	Derived from 30 m resolution	2020, Landsat 8, USGS
7	SARVI map	Raster	Derived from 30 m resolution	2020, Landsat 8, USGS
8	MSAVI map	Raster	Derived from 30 m resolution	2020, Landsat 8, USGS
9	OSAVI map	Raster	Derived from 30 m resolution	2020, Landsat 8, USGS

temperature (LST) was taken as another influential criterion of agriculture land suitability assessment.

Elevation

Elevation is an important factor that plays a vital role in the variability of plant cover and causes temperature changes, particularly in highland areas. Areas with higher topographic elevations are more affected by rainfall and soil erosion (Bozdağ et al. 2016). Soil erosion is the alarming condition of agriculture field crop. Also, it is the main problems of agricultural development, such as landslides and flood events; these disasters have been severely influenced by the soil erosion process (Senanayake et al. 2020). Most of the study area is plains land, and the elevation is less than 131 m (Fig. 3.3a). The elevation data were extracted using a digital elevation model (DEM) and were downscaled to a 30 m resolution.

Slope

Slope is a vital topographic element for indicating suitable farmland in assessments. Slope indicates many landscape processes, such as soil water content, erosion potential, runoff, and surface and subsurface flow velocity. The thickness of the soil layer decreases with the increasing slope (Ashford et al. 1997). The slope gradient has an impact on the runoff and soil loss: the greater the slope gradient,

the higher the potential for runoff and soil loss (El Kateb et al. 2013). The slope was developed by using data from the original Shuttle Radar Topography Mission (SRTM) and the DEM. The DEM was downscaled to a 30 m resolution. The Universal Transverse Mercator (UTM) projection system and WGS84 datum were used as rectifying agents in ArcGIS. The slope was calculated from the maximum rate of change between each cell and its neighbors. Every cell in the output raster had a slope value. Field crops generally require flat land; only a slight slope between 0% and 8% is resistant to erosion (Zolekar and Bhagat 2015). When the slope gradient is very steep (40%), soil sediment losses remain at the same high levels after cultivation abandonment because slope gradient is the main factor controlling soil erosion (Koulouri and Giourga 2007). In the study area, the slope range was under 10% (Fig. 3.3b), which is a suitable condition for most farming practices (Nahusenay and Kibebew 2015; Novara et al. 2017).

Land Surface Temperature (LST)

The LST (Fig. 3.3c) was calculated for selected land areas using temporal information from Landsat 8 OLI images when less cloud coverage was present (Jeevalakshmi et al. 2017). From 2017 to 2020, the LST data received from the obtained images ranged between 17 °C and 33 °C. The LST calculation was based on the moving average method. A single raster was formed from multiple years of raster datasets as the multiple predictions' raster.

LST was calculated for the cropland using temporal information from Landsat 8 OLI that was selected during period of less cloud coverage. Two steps were required to calculate the LST; first, the *NDVI* was calculated for the given time period.

$$\text{NDVI} = \frac{\rho_{\text{NIR}} - \rho_{\text{RED}}}{\rho_{\text{NIR}} + \rho_{\text{RED}}} \tag{3.1}$$

After that, the resulting *NDVI* value was used to analyze the proportion vegetation (*PV*), which can be expressed as follows:

$$\text{PV} = \left(\frac{\text{NDVI} - \text{NDVI}_{\text{min}}}{\text{NDVI}_{\text{max}} - \text{NDVI}_{\text{min}}} \right)^2 \tag{3.2}$$

After calculating the *PV*, the land surface emissivity (ε_λ) could be expressed as follows:

$$\varepsilon_\lambda = 0.004 * \text{PV} + 0.986 \tag{3.3}$$

Second, the thermal bands are included in band 10 and band 11 from the Landsat 8 imagery. The thermal bands were converted to digital numbers (DN) to estimate the radiance. The spectral radiance could be expressed as follows:

$$L\lambda = \mathrm{ML} + Q_{\mathrm{CAL}} + \mathrm{AL}$$

$$L\lambda = 0.0003342 * \mathrm{Band}10 + 0.1 \text{ and } L\lambda = 0.0003342 * \mathrm{Band}11 + 0.1$$

$$L\lambda = 0.0003342 * \mathrm{Band}10 + 0.1 \text{ and } L\lambda = 0.0003342 * \mathrm{Band}11 + 0.1 \quad (3.4)$$

where $L\lambda$ is the TOA spectral radiance at the sensor aperture, ML is the band-specific multiplicative rescaling factor from the metadata, Q_{CAL} is the quantized and calibrated standard product pixel value (DN), and AL is the band-specific additive rescaling factor from the metadata. Then, the brightness temperature (BT) could be expressed as follows (Jeevalakshmi et al. 2017):

$$BT = \frac{K2}{\ln\left[\left(K1/_{L\lambda}\right) + 1\right]} - 273.15 \quad (3.5)$$

where BT is the satellite brightness temperature (°C); $K2$ is the calibration constant 2 (K), where the band-specific thermal conversion constant is taken from the metadata; and $K1$ is the calibration constant 1 (K), where the band-specific thermal conversion constant is taken from the metadata. Finally, LST was calculated and expressed as follows (Jeevalakshmi et al. 2017):

$$LST = \frac{BT}{1 + \left(\frac{\lambda * BT}{\rho}\right) * \ln \varepsilon\lambda} \quad (3.6)$$

where λ is the average wavelength of band 10; $\varepsilon\lambda$ is the emissivity calculated from Eq. (3.6); and ρ is ($h * \frac{c}{\sigma}$), which is equal to 1.438×10^{-2} mK, where σ is the Boltzmann constant (1.38×10^{-23} J/K), h is Planck's constant (6.626×10^{-34} J s), and c is the velocity of light (3×10^{8} m/s).

Soil-Adjusted Vegetation Index (SAVI)

Soil has a unique spectral signature that differs from that of other types of land cover. In the visible and near-infrared zones, reflectance increases in proportion to increases in wavelength. However, the rate of increase is affected by various factors. Soil moisture and organic matter may lower the soil reflectance. The association between red and near-infrared reflectance remains constant for different soil type physiognomies. When the moisture content changes, the two values are related and have a linear relationship. This relationship is very specific for each type of soil. SAVI is therefore useful for monitoring soils. Furthermore, SAVI is a modification of the Normalized Difference Vegetation Index (NDVI), which corrects for the influence of

soil brightness when the vegetation cover is low (Jiang et al. 2006). SAVI (Fig. 3.3d) was extracted from Landsat 8 OLI imagery by a mask for the study area. Datasets were acquired from 2017 to 2020. These datasets were used to build a single raster using map algebra in the ArcGIS platform.

To reduce the soil background effect, modified indices were proposed using the soil adjustment factor L to account for first-order soil background variations and obtain the SAVI (Huete 1988). *SAVI* can be expressed as follows:

$$ \text{SAVI} = \frac{\rho_{\text{NIR}} - \rho_{\text{RED}}}{\rho_{\text{NIR}} + \rho_{\text{RED}} + L} \ (1 + L) \tag{3.7} $$

where ρ_{NIR} is the reflectance value in the near-infrared band, ρ_{RED} is the reflectance value in the red band, and L is the soil brightness correction factor. An L value of 0.5 in the reflectance space was found to minimize soil brightness variations and eliminate the need for additional calibration for different soils. The described SAVI value was 0.798 to −0.302 for the study area (Fig. 3.3d).

Atmospherically Resistant Vegetation Index (ARVI)

The ARVI (Fig. 3.3e) is obtained using a self-correction process for the atmospheric effect on the red channel, using the difference in the radiance between the blue and red channels to correct the radiance in the red channel due to the excellent atmospheric resistance of the *ARVI* (Somvanshi and Kumari 2020).

$$ \text{ARVI} = \frac{\rho_{\text{NIR}} - (\rho_{\text{RED}} - \gamma \, (\rho_{\text{BlUE}} - \rho_{\text{RED}}))}{\rho_{NIR} + (\, \rho_{\text{RED}} - \gamma \, (\rho_{\text{BlUE}} - \rho_{\text{RED}})} \tag{3.8} $$

where γ depends on the aerosol type. A good default value is $\gamma = 1$ when the aerosol model is not available. *ARVI* is resistant to atmospheric effects due to its self-correction process. This index uses the difference in the radiance between the blue and red bands to correct the radiance in the red band. Simulations show that *ARVI* has a similar dynamic range as SAVI, but on average, its sensitivity to atmospheric effects is four times less than that of NDVI. The ARVI value fluctuated between 0.886 and −0.662 (Fig. 3.3e).

Soil-Adjusted and Atmospherically Resistant Vegetation Index (SARVI)

SARVI has a similar dynamic range to NDVI but is four times less sensitive to atmospheric effects than NDVI. SARVI performs much better for moderate- to small-sized aerosol particles (e.g., continental, urban, or smoke aerosol) than for large particles. Consequently, a single combination of blue and red channels in ARVI calculations may be used in all or most remote sensing applications (Kaufman and Tanre 1992).

$$\text{SARVI} = (1 + L)(\rho_{\text{NIR}} - (\rho_{\text{RED}} - \gamma(\rho_{\text{BlUE}} - \rho_{\text{RED}})))/$$

$$(\rho_{\text{NIR}} + (\rho_{\text{RED}} - \gamma(\rho_{\text{BlUE}} - \rho_{\text{RED}})) + L) \tag{3.9}$$

where L is a correction factor similar to that in the SAVI calculation and γ is similar to that in the ARVI calculation. SARVI can minimize both canopy background and atmospheric effects (Haboudane et al. 2004; Kim et al. 1994). In this research, the SARVI value was found to range from 0.679 to -0.397 (Fig. 3.3f).

Modified Soil-Adjusted Vegetation Index (MSAVI)

Richardson and Wiegand (1977) proposed a modified secondary Soil-Adjusted Vegetation Index (MSAVI), which can be expressed as follows:

$$\text{MSAVI} = 0.5 * \left[(2\rho_{\text{NIR}} + 1) - \sqrt{(2\rho_{\text{NIR}} + 1)^2 - 8\rho_{\text{NIR}} - \rho_{\text{RED}}} \right] \tag{3.10}$$

MSAVI does not rely on the soil line principle and has a simpler algorithm; it is mainly used in soil organic matter analysis, drought monitoring, and soil erosion analysis. In addition, it is useful for plant growth analyses, desertification studies, grassland yield estimations, and leaf area index (LAI) assessments. In the study area, the MSAVI value was observed to be between +1 and -1 (Fig. 3.3g).

Optimized Soil-Adjusted Vegetation Index (OSAVI)

The Optimized Soil-Adjusted Vegetation Index (OSAVI) is a newly developed alternative that can accommodate greater variability due to high soil background values (Mao et al. 2020). OSAVI does not depend on the soil line and can eliminate the influence of the soil background effectively. However, the applications of OSAVI are not extensive; it is mainly used for the calculation of aboveground biomass, leaf nitrogen content, and chlorophyll content (Gitari et al. 2019).

$$\text{OSAVI} = \frac{\rho_{\text{NIR}} - \rho_{\text{RED}}}{\rho_{\text{NIR}} + \rho_{\text{RED}} + X} \tag{3.11}$$

where $X = 1.6$. OSAVI is mainly used for the calculation of aboveground biomass, leaf nitrogen content, chlorophyll content, etc. The observed value was between 0.531 and -0.201 (Fig. 3.3h).

3.2.5   Data Aggregation

Pattern Analysis

Several criteria were used for pattern analysis, which required pattern analyses from multiple years or months of data to form a predicted raster for reclassification. The single raster-based calculation was not reliable, nor did it provide enough datasets. This section shows several criteria from multiple years of data (2017–2020) for building a predicted raster for LST, SAVI, ARVI, SARVI, MSAVI, and OSAVI. The following section introduces the pattern analysis for multitemporal datasets into a single raster.

Moving Average

The moving average was processed after completing the digital image processing steps. The moving average was calculated in each year and can be expressed as follows:

$$\mathrm{MA}_n = \frac{\sum_{i=1}^{n} Di}{n} \tag{3.12}$$

where D is the number of data points in the raster cell and n is the amount of data to average.

Multiple Predicted Raster

As a part of the point pattern analysis, a single predicted raster was made. After that, LST, SAVI, ARVI, SARVI, MSAVI, and OSAVI were computed from 2017 to 2020. The basic extent encompassed the overall density pattern. This is basically the ratio of the observed number of single predicted rasters of points (r) to the study region area (a) and referred to as the multiple predicted raster (MPR). The MPR was applied as a criterion for land suitability analysis. *MPR* can be expressed as follows:

$$\mathrm{MPR} = \frac{r}{a} \tag{3.13}$$

where r is the ratio of the observed number of single predicted raster points and a is the area of the study region.

Land Use/Land Cover

Land use data enable the estimation of an area's coverage with vegetated areas, settlements, forests, and water bodies. Land use data were collected from the Survey of Bangladesh (SoB), which was split into 92 blocks. After aggregation in the ArcGIS platform, the data were used to develop a more accurate land use/land cover (LULC) map for the land fertility assessment. In this study, rivers, forests, water bodies, and settlements were considered restrictions in the analysis. Subsequently, after excluding the constraints, only agricultural land was considered for land evaluation. Agricultural land was subclassified into cultivated land (80%), uncultivated land (0.5%), and vegetated land (19%) (Fig. 3.2).

3.2.6   Land Fertility Assessment

The weighted overlay was used to prioritize the weights of each criterion to generate a land fertility assessment map. The reclassified raster data layers were combined with the weighted overlay in ArcGIS®. First, the combination criteria were input as equally weighted linear combinations. Second, the land suitability analysis was carried out by a fuzzy membership function, fuzzy reclassification, and fuzzy overlay to evaluate the consistency of the two outcomes.

Map Development by Weighted Linear Combination

First, reclassification was conducted to interpret the raster data by substituting a single value as the new value or by categorizing the ranges of values into a single value. Each criteria source map was reclassified into four classifications (Table 3.2). Land suitability analysis was conducted using different classification categories proposed by the FAO. As suggested by the FAO's framework for land evaluation, the first class was designated as suitable (S) or not suitable (N). The suitability classification aimed to show the suitability of each land unit for crop production. In practice, three classes, namely, S1, S2, and S3, are typically used to identify land that is highly suitable, moderately suitable, and marginally suitable, respectively. The analysis was built using the aforementioned criteria and reclassified into four classes. Finally, the classes were found based on their weighted linear combination.

$$\text{Weighted Overlay} = \sum_{i=1}^{n} C_i * W_n \qquad (3.14)$$

where C_i is each criterion (i) that has been reclassified and W_n is the number of data (n) that were weighted.

Table 3.2 Criteria reclassification for weighted linear combination

Criteria	Suitability class	Subcriteria	Reference
Slope	S1	0–8%	Zolekar and Bhagat (2015), Gitari et al. (2019), Shimoda et al. (2018)
	S2	8–15%	
	S3	15–25%	
	N	>25%	
Elevation	S1	0–25	Bozdağ et al. (2016), GRiSP (2013), Yalew et al. (2016)
	S2	25–125	
	S3	125–250	
	N	>250	
LST	S1	20–25	Jeevalakshmi et al. (2017), Ceglar et al. (2018), Samanta et al. (2011)
	S2	18–20	
	S3	15–18	
	N	9–15, >25	
SAVI	S1	0.372483–0.797756	Huete (1988), Ren and Feng (2014), Venancio et al. (2019)
	S2	0.217838–0.372483	
	S3	0–0.217838	
	N	−0.301941–0	
ARVI	S1	0.293275–0.885854	Somvanshi and Kumari (2020), Kaufman and Tanre (1992), Sonobe et al. (2018)
	S2	0.1542–0.293275	
	S3	0–0.1542	
	N	−0.662108–0	
SARVI	S1	0.301197–0.671395	Kaufman and Tanre (1992), Svinurai et al. (2018), Cho and Skidmore (2008)
	S2	0.301197–0.16658	
	S3	0.16658–0	
	N	−0.39713–0	
MSAVI	S1	0.752112–1	Richardson and Wiegand (1977), Ren and Feng (2014), Ren et al. (2018)
	S2	0.752112–0.443157	
	S3	0.443157–0	
	N	−1–0	
OSAVI	S1	0.245221–0.526082	Mao et al. (2020), Ren and Feng (2014), Gilabert et al. (2002)
	S2	0.145221–0.248311	
	S3	0–0.145221	
	N	−0.201272–0	

Map Development by the Fuzzy Membership Function

The fuzzification process had no sharply defined boundaries that characterized the imprecision of the classes. In this process, each value of the phenomenon central to the core of the definition of the set was set to 1. Those values that were not part of the set were set to 0. Those values that fell between these two extremes were within the transitional zone of the set, which was defined as the boundary (Olivero et al. 2011; Zadeh 1965; Bellman and Zadeh 1970; Mitchell and Cohen 2014). In the present

study, fuzzy membership classification was used to accommodate the high uncertainty of the scoring methods in assigning the suitability classes; several fuzzy membership functions were used for normalization. For this research, fuzzy functions were determined based on references and a literature review (Table 3.3).

Out of the seven varieties of fuzzy membership functions available, three fuzzy functions were used in this study considering ecological criteria: the fuzzy small, Gaussian, and fuzzy linear functions. These functions generate continuous fuzzy classifications under standardized criteria. The reclassification tool in ArcGIS enables the transformation of categorical data to range from 0 to 10 and then divides the resulting transformed data by 10 to derive a 0 to 1 scale. The equations for the fuzzy small (Eq. (3.15)), fuzzy linear (Eq. (3.16)), and fuzzy Gaussian functions (Eq. (3.17)) are as follows:

$$\mu(x) = \frac{1}{1 + \left(\frac{x}{f_2}\right)^{f_1}} \tag{3.15}$$

The fuzzy small transformation function was used when small input values were more likely to be members of the set. The criterion slope was followed by a fuzzy small function in this research.

$$\mu(x) = e^{\left(-f1(x-f2)^2\right)} \tag{3.16}$$

The layers of SAVI, ARVI, SARVI, MSAVI, and OSAVI were each followed by a fuzzy linear transformation function that related to a linear function between the user-specified minimum and maximum values for reclassification.

$$\mu(x) = f(x) = \begin{cases} 0 & x \leq a \\ \frac{x-a}{b-a} & a < x < b \\ 1 & x \geq b \end{cases} \tag{3.17}$$

The fuzzy Gaussian function converts the primal values into a normal distribution. If the input values decrease in membership, they move away from the midpoint. The midpoint of the fuzzy Gaussian function was set to 1 (Purnamasari et al. 2019). The elevation and LST layers were analyzed under the fuzzy Gaussian membership function.

In the fuzzy small and fuzzy linear membership functions, the control point included a midpoint (f2) and a spread (f1). The midpoint was a specific point that had a 0.5 value of membership in the large and small functions. Gaussian functions are determined by the user based in the references (ESRI, Boston, CA). The spread was generally allocated a number between 1 and 10. The fuzzy membership curve became steeper for higher spread values. The fuzzy linear transformation function applied a linear function between the minimum and maximum values. Any value below the minimum was determined to be 0 (not a member), and any value above the

Table 3.3 Criteria reclassification for fuzzy membership function

Criteria	Most suitable condition	Maximum acceptable condition	Minimum acceptable condition	Not fuzzy member	Reference	Fuzzy membership function
Slope	<4°	20°	0°	<20	Yalew et al. (2016), Ayehu and Besufekad (2015)	F small
Elevation	0	0–25	250	>250	Bozdağ et al. (2016), Gerpacio and Pingali (2007)	F Gaussian
LST	10 °C–20 °C	Up to 35 °C	10 °C	>35 °C or <20 °C	Samanta et al. (2011), Kihoro et al. (2013)	F Gaussian
SAVI	0.7978	+1	−1	−0.3019 < SAVI < 0.7978	Habibie et al. (2019), Venancio et al. (2019), Purnamasari et al. (2019)	F linear
ARVI	0.8859	+1	−1	−0.3971 < ARVI < 0.8859	Somvanshi and Kumari (2020), Kaufman and Tanre (1992), Sonobe et al. (2018)	F linear
SARVI	0.6713	+1	−1	−0.3971< SARVI <0.6713	Kaufman and Tanre (1992), Cho and Skidmore (2008), Svinurai et al. (2018)	F linear
MSAVI	1	+1	−1	−0.1 < MSAVI < 1	Ren and Feng (2014), Ren et al. (2018), Richardson and Wiegand (1977)	F linear
OSAVI	0.5261	+1	−1	−0.2013< OSAVI <0.5261	Mao et al. (2020), Fern et al. (2018), Gilabert et al. (2002)	F linear

maximum was 1 (a member) (Fern et al. 2018). To analyze the relationships and interactions between all the sets for the eight criteria in the overlay model, fuzzy overlay techniques were used. The available fuzzy set overlay techniques in ArcGIS are fuzzy And, fuzzy Or, fuzzy Product, fuzzy Sum, and fuzzy Gamma. Each of these techniques described the cell's membership related to the input sets. In this study, the fuzzy Gamma overlay assisted in developing suitability maps for three identical seasons, which were determined based on references and a literature review (ESRI, Redlands, CA).

3.2.7 Validation Using Ground Truth Data

The detected fertile zone was verified by ground reference data. The time series datasets played a vital role in developing and validating the yield prediction models. In Bangladesh, nearly 80% of the total land is allocated solely to rice cultivation (Mottaleb et al. 2018). Additionally, in the northwestern part of the country, approximately 70% (Acharjee et al. 2017; Alamgir et al. 2020; Zinat et al. 2020) of the land is cultivated with dry season irrigated rice (boro rice). To facilitate further analysis, the major rice crop was carefully chosen for approval. The suitable area was verified by ground truth yield data. The yield data of dry season irrigated rice were collected from the Department of Agricultural Extension (DAE), Ministry of Agriculture, Bangladesh, for the 36 subdistricts in 2017–2020 to evaluate the accuracy of the land suitability analysis (Figs. 3.4 and 3.5). After preparing the data in Microsoft Excel®, the correlations among the five selected indices were evaluated.

3.2.8 Yield Prediction and Analysis

The performances of the yield prediction models were examined by field data. After the correlations among the five selected vegetation indices were established, the yield map was developed. Simple and multiple regression analyses were carried out between the mean values of the vegetation indices and the ground reference data of the dry season irrigated rice to determine the best-fitted models for rice production. These data were classified to evaluate the production that occurred between 2017 and 2020. The SAVI, ARVI, SARVI, MSAVI, and OSAVI values were aggregated into a time series pattern (Appendix). The yield data were compared through regression. The 5 vegetation indices values were collected from reference points in the 36 subdistricts. Ground truth data information was obtained from the 36 subdistricts, and the yield was reported in metric tons per hectare (MT/ha).
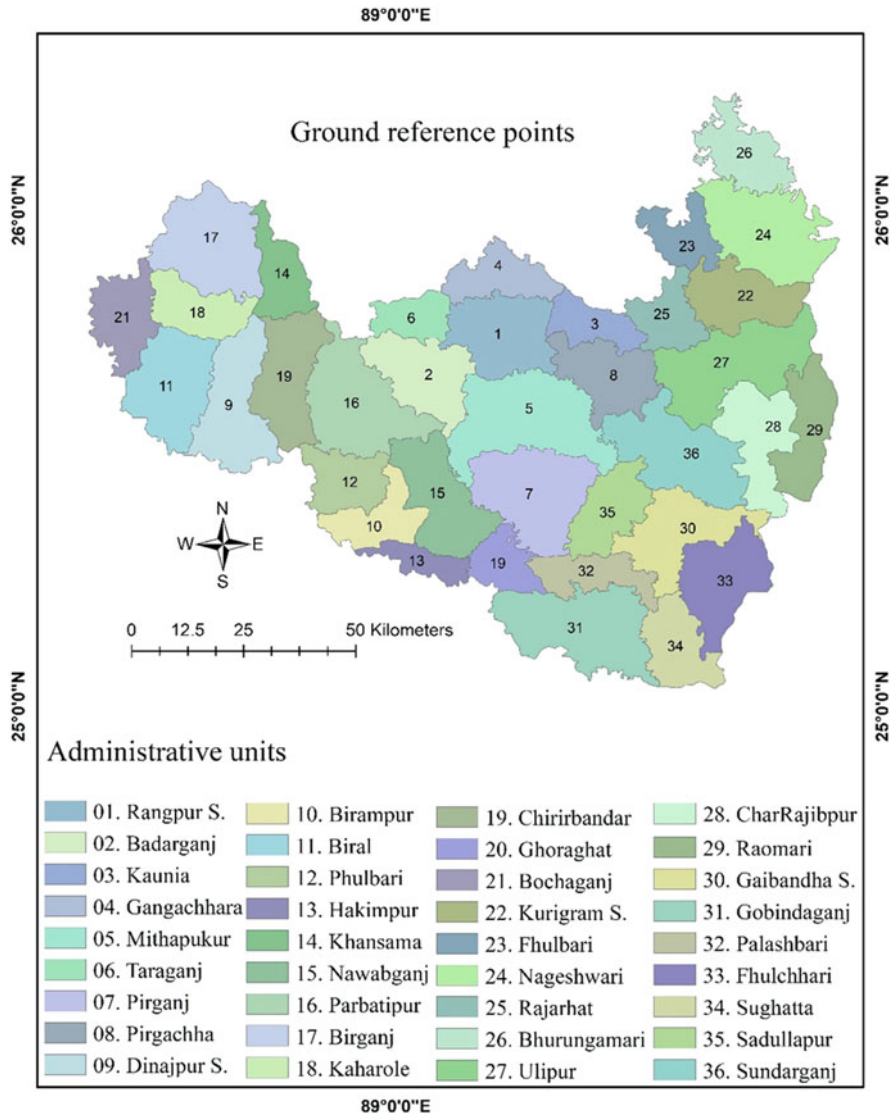
Fig. 3.4 Ground reference information points in 36 subunits

3.3   Results

3.3.1   Land Suitability Analysis

The weighted linear model was used to prioritize the weights of each criterion to generate the land suitability assessment. First, the variables were analyzed as equally weighted linear combinations. Second, the suitability assessment was carried out by
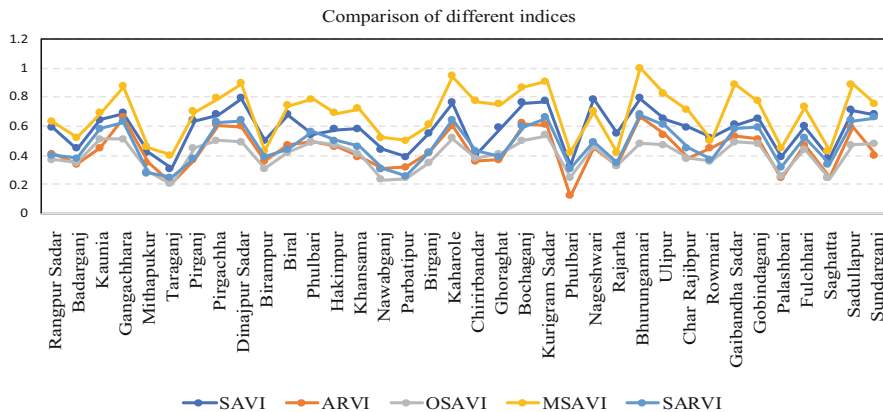
Fig. 3.5 Comparison of different indices and ground reference information points in 36 subunits

Table 3.4 Percentage and area of each land suitability analysis

Classification	Suitability assessment by equal-weighted linear combination		Suitability assessment by fuzzy membership function	
	Percentage (%)	Area (km²)	Percentage (%)	Area (km²)
Highly suitable (S1)	43	1832	48	2045
Moderately suitable (S2)	41	1747	39	1661
Marginally suitable (S3)	10	426	7	298
Not suitable (N)	6	256	6	256

a fuzzy membership function to verify the consistency of the two procedure results (Table 3.4). The land fertility analysis (Fig. 3.6a) with equal weights showed that 43% of the land (1832 km²) was highly suitable, 41% of the land (1747 km²) was moderately suitable, and 10% of the land (426 km²) was marginally suitable. In addition, the restricted zone was defined as an unsuitable area. In this research, the unsuitable area was found to cover 6% (256 km²). However, the land suitability analysis using the fuzzy membership function (Fig. 3.6b) showed that 48% (2045 km²) of the land area consisted of the most suitable area, 39% of the land (1661 km²) was moderately suitable, and 7% of the land (298 km²) was marginally suitable. In addition, restricted areas accounted for 6% of the land area. In fuzzy overlay analysis, 256 km² of the area was classified as fallow land that is not suitable for cultivation.

3.3.2 Yield Estimation

The predictors derived from the satellite imagery in the form of spectral bands or vegetation indices (SAVI, ARVI, SARVI, MSAVI, and OSAVI) were the most
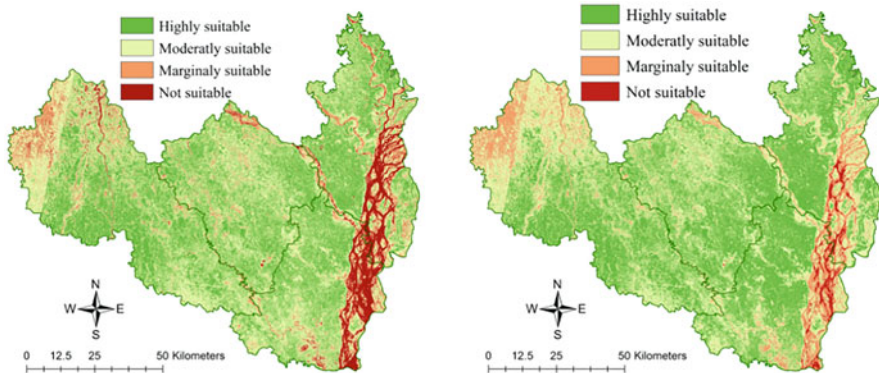
Fig. 3.6 Suitable classes of land suitability analysis using soil specified remote sensing data. (**a**) Equal-weighted overlay. (**b**) Fuzzy overlay

effective spectral parameters for predicting rice yield (Fig. 3.7). In addition, the individual index values were extracted from the ground truth information (Figs. 3.4 and 3.5) for the subdistricts that were located in the highly suitable areas. A trend line approach was used to verify the index influences at different study points (Fig. 3.8). Regression analysis was performed between the vegetation indices and the observed yield. The SAVI, SARVI, ARVI, MSAVI, and OSAVI values were obtained from satellite imagery from 2017 to 2020 (Table 3.5). The results showed good accuracy in the regression analysis using SAVI ($R^2 = 0.773$), ARVI ($R^2 = 0.689$), SARVI ($R^2 = 0.711$), MSAVI ($R^2 = 0.745$), and OSAVI ($R^2 = 0.812$) (Fig. 3.9). From the multiple regression model, it was observed that using more than one variable for the yield prediction increased the model accuracy by enhancing the R^2 value. However, the best-fitted models were obtained using the SAVI-ARVI-SARVI-MSAVI-OSAVI composite vegetation index. The yield prediction model with the composite index had a goodness of fit of $R^2 = 0.839$. The model was used to estimate the yield in the time series dataset (Table 3.6).

The developed yield map indicated that in 2017, the maximum yield was 4.59 MT/ha (Fig. 3.10). Furthermore, in 2018 and in 2019, it was 4.9 MT/ha and 5.08 MT/ha, respectively. For 2020, the predicted yield range appeared to be between 0.269 MT/ha and 4.537 MT/ha.

3.4   Discussion

This research provided a comprehensive strategy to create agricultural land use plans for cultivation considering suitable conditions, which were derived from satellite remote sensing data. Previously, much of the research conducted only reported land suitability for site-specific plans or single-cropping plans (Noorollahi et al. 2016; Sulaiman et al. 2019). However, this research attempted to develop an overall land

(a)

(b)

(c)

(d)

(e)
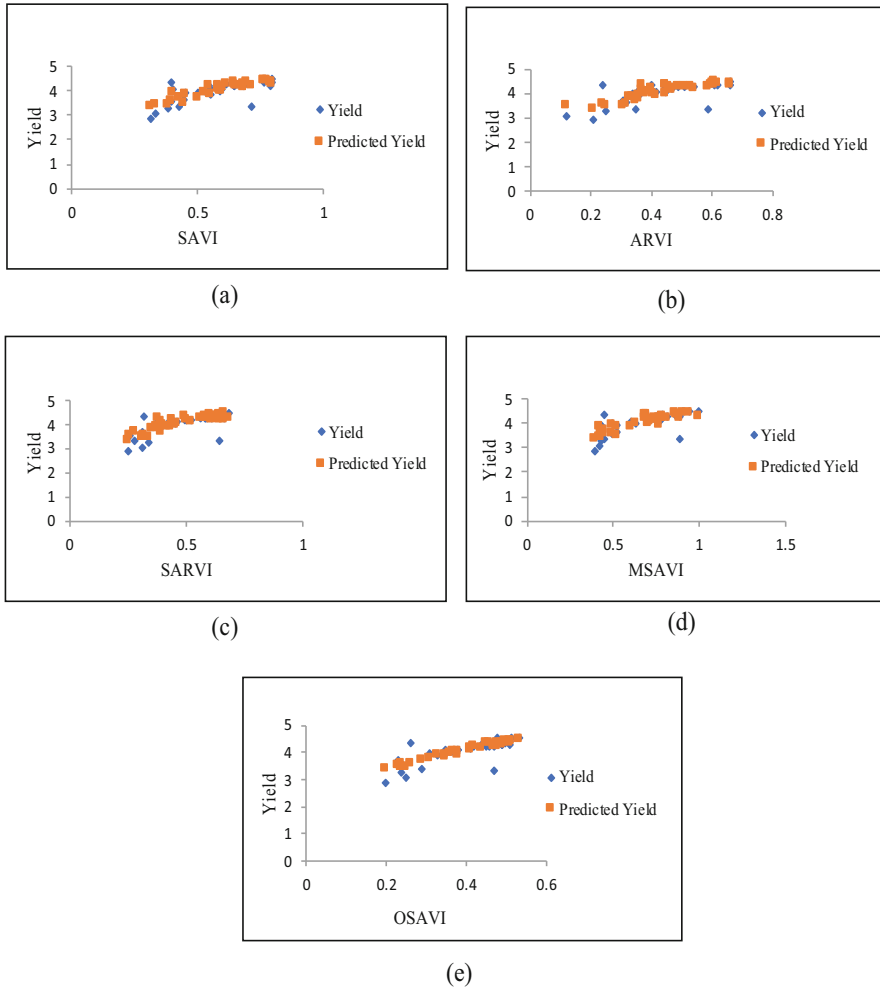
Fig. 3.7 Comparison of actual yield and predicted yield for different indices: (**a**) SAVI (**b**) ARVI, (**c**) SARVI, (**d**) MSAVI, (**e**) OSAVI

suitability assessment using soil-vegetation representative variables that extracted only satellite remote sensing data from the GIS platform when field soil sampling is inconvenient and expensive. Applying only remote satellite datasets to assess suitable land conditions was a source of concern that added a new feature to MCDM-land suitability analyses. In this study, the reliability of five vegetation indices was verified by a regression analysis that incorporated ground truth yield data, and the results were used for yield map preparation. Vegetation phenology analyses have potential (Habibie et al. 2019; Das et al. 2020) in estimating yield prediction with good accuracy in highly suitable areas. In addition, two topological
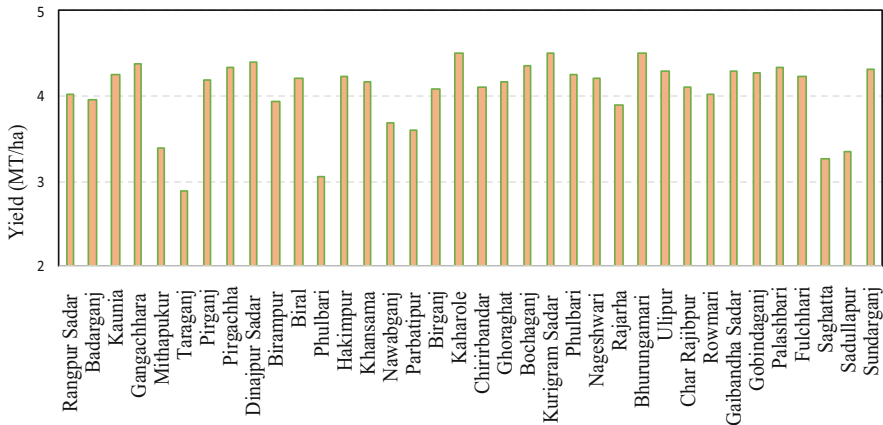
Fig. 3.8 Ground reference rice yield distributions in the 36 subunits

factors (slope and elevation) and another environmental parameter, LST, were extracted from the USGS, which ensured better performance of the results in land use planning.

Either the AHP-based weighted overlay or equal-overlay technique is typically applied in most studies (Seyedmohammadi et al. 2019; Pilevar et al. 2020; Tashayo et al. 2020); few studies have conducted fuzzy membership methods employed in the GIS platform by incorporating with the AHP technique (Radočaj et al. 2020; Amin et al. 2015; Pilevar et al. 2020). Some studies have conducted farmland assessments based on soil testing (De Lima et al. 2019; Buthelezi et al. 2013); however, considering the preparation of a suitable map for agricultural land using soil-represented remote sensing data for the linear combination of the F-MCDM approach is a new dimension of this research. A multicriteria decision-making system was applied to reduce the biases in the analysis. Variation in the land surface temperature was an important factor in this area and influenced the locations considered most suitable for crop cultivation. Moreover, atmospherically restricted vegetation indices (ARVI) and soil-adjusted atmospherically restricted vegetation indices (SARVI) were used to reduce the biases associated with atmospheric effects.

Most of the suitable lands were located in the northern part, and marginally suitable lands were mostly located in the northwestern part; this result was likely due to the influence of high elevation. In addition, unsuitable zones were found mostly in the eastern part due to the presence of water bodies that are not arable for cultivation along with other adverse edaphic factors. Previous studies had the limitation of obtaining inappropriate validation results due to inadequate ground reference information. In this research, the validation of the results was accomplished by physical verification with the corresponding time series yield data of the most cultivated crop, dry season irrigated rice, which usually grows over 70% (Pilevar et al. 2020) of the agricultural land area. The suitable conditions were not verified by the other crop yield data, which was the main limitation of this research.

Table 3.5 Yield estimation based on satellite remote sensing-derived soil-vegetation indices for the 36 subunits

No	Name	Longitude	Latitude	SAVI	ARVI	SARVI	MSAVI	OSAVI	Yield (MT/ha)
1	Rangpur Sadar	89°12′38.681″ E	25°45′19.004″ N	0.588	0.41	0.37	0.63	0.40	4.03
2	Badarganj	89°3′3.041″ E	25°40′31.185″ N	0.445	0.34	0.35	0.52	0.38	3.96
3	Kaunia	89°23′36.554″ E	25°46′41.239″ N	0.644	0.45	0.51	0.69	0.58	4.26
4	Gangachhara	89°12′52.386″ E	25°51′42.764″ N	0.69	0.66	0.51	0.87	0.63	4.37
5	Mithapukur	89°15′9.443″ E	25°35′2.248″ N	0.42	0.35	0.29	0.45	0.28	3.38
6	Taraganj	89°1′54.513″ E	25°46′54.944″ N	0.31	0.21	0.20	0.40	0.25	2.89
7	Pirganj	89°16′17.972″ E	25°25′40.315″ N	0.64	0.37	0.45	0.701	0.38	4.19
8	Pirgachha	89°24′58.788″ E	25°40′31.185″ N	0.681	0.61	0.50	0.79	0.63	4.34
9	Dinajpur Sadar	88°40′39.883″ E	25°36′38.188″ N	0.79	0.60	0.49	0.89	0.64	4.40
10	Birampur	88°58′15.222″ E	25°22′55.846″ N	0.50	0.36	0.31	0.43	0.39	3.94
11	Biral	88°32′53.89″ E	25°38′55.245″ N	0.68	0.47	0.42	0.74	0.44	4.20
12	Phulbari	88°53′27.402″ E	25°27′2.549″ N	0.54	0.49	0.49	0.78	0.56	4.25
13	Hakimpur	89°2′49.336″ E	25°17′13.204″ N	0.579	0.46	0.47	0.69	0.50	4.23
14	Khansama	88°45′55.114″ E	25°52′51.292″ N	0.58	0.39	0.41	0.72	0.46	4.16
15	Nawabganj	89°5′33.804″ E	25°25′12.903″ N	0.44	0.31	0.23	0.52	0.31	3.69
16	Parbatipur	88°55′44.459″ E	25°37′19.305″ N	0.39	0.32	0.24	0.50	0.26	3.60
17	Birganj	88°37′28.004″ E	25°56′3.172″ N	0.55	0.42	0.35	0.61	0.42	4.08
18	Kaharole	88°35′38.358″ E	25°48′17.178″ N	0.76	0.60	0.51	0.94	0.64	4.50
19	Chirirbandar	88°47′3.643″ E	25°40′31.185″ N	0.40	0.36	0.38	0.77	0.43	4.10
20	Ghoraghat	89°12′52.386″ E	25°17′26.91″ N	0.59	0.37	0.41	0.75	0.39	4.16
21	Bochaganj	88°26′43.836″ E	25°47′22.356″ N	0.761	0.62	0.50	0.86	0.60	4.35
22	Kurigram Sadar	89°41′39.304″ E	25°49′39.413″ N	0.77	0.61	0.54	0.91	0.66	4.50
23	Phulbari	88°53′27.402″ E	25°27′2.549″ N	0.33	0.12	0.25	0.42	0.31	3.06
24	Nageshwari	89°44′37.478″ E	25°58′6.523″ N	0.79	0.45	0.46	0.70	0.49	4.20
25	Rajarha	89°32′44.782″ E	25°47′8.65″ N	0.55	0.33	0.33	0.42	0.35	3.90
26	Bhurungamari	89°41′39.304″ E	26°7′1.045″ N	0.79	0.66	0.48	0.99	0.67	4.50

27	Ulipur	89°40′3.364″ E	25°40′58.596″ N	0.65	0.54	0.47	0.82	0.61	4.30
28	Char Rajibpur	89°45′4.889″ E	25°30′55.546″ N	0.59	0.38	0.38	0.71	0.45	4.10
29	Rowmari	89°49′11.592″ E	25°33′53.72″ N	0.52	0.45	0.36	0.50	0.37	4.02
30	Gaibandha Sadar	89°34′48.133″ E	25°57′11.701″ N	0.61	0.53	0.49	0.88	0.58	4.30
31	Gobindaganj	89°22′0.614″ E	25°10′8.327″ N	0.65	0.51	0.48	0.77	0.59	4.28
32	Palashbari	89°23′22.848″ E	25°16′18.381″ N	0.39	0.24	0.26	0.45	0.32	4.34
33	Fulchhari	89°39′35.953″ E	25°15′37.264″ N	0.60	0.47	0.44	0.73	0.52	4.24
34	Saghatta	89°34′34.427″ E	25°7′37.565″ N	0.38	0.25	0.24	0.43	0.34	3.27
35	Sadullapur	89°25′12.494″ E	25°24′4.375″ N	0.71	0.59	0.47	0.88	0.64	3.34
36	Sundarganj	89°33′39.605″ E	25°30′28.134″ N	0.68	0.4	0.48	0.75	0.66	4.31
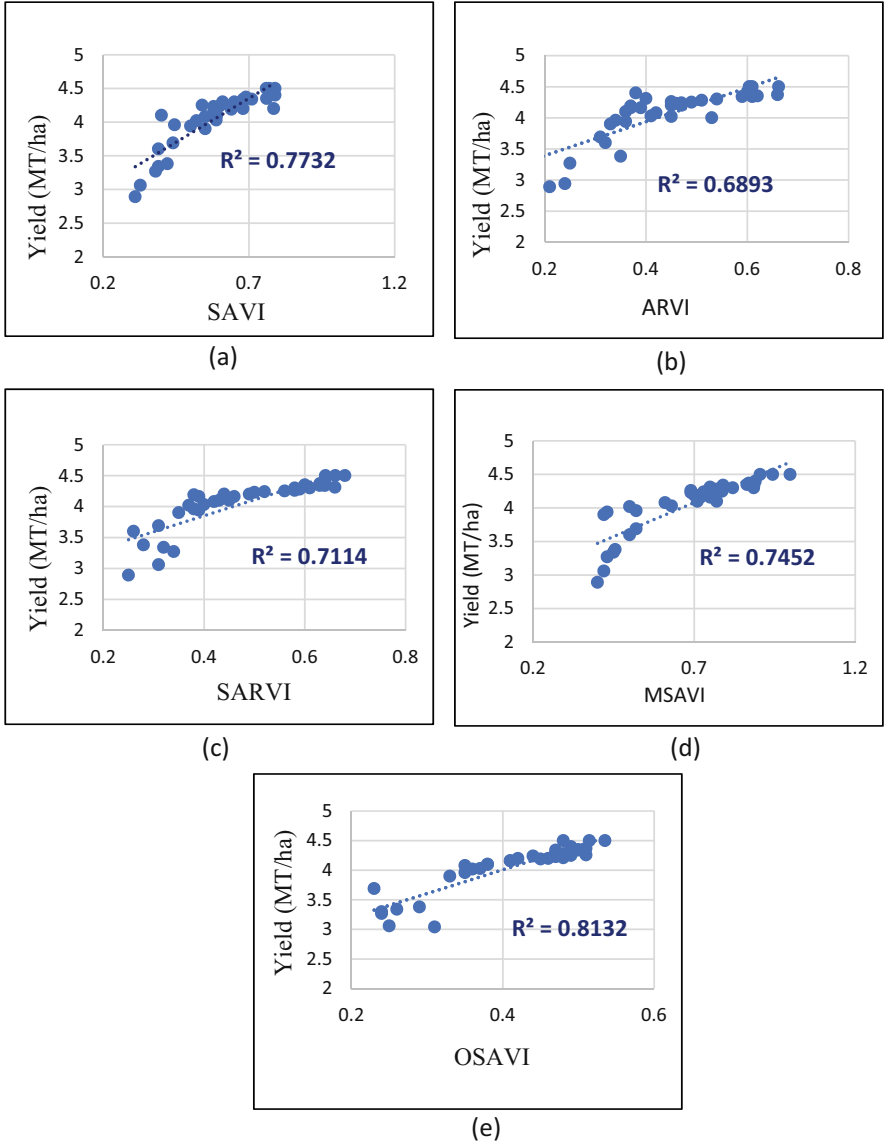
Fig. 3.9 Regression analysis for vegetation indices and ground reference time series yield information. (**a**) SAVI, (**b**) ARVI, (**c**) SARVI, (**d**) MSAVI, (**e**) OSAVI

Table 3.6 Yield prediction models based on satellite remote sensing-derived soil-vegetation indices

Soil-adjusted vegetation indices	R^2	Simple regression
SAVI	0.773	Y = 2.6021* SAVI + 2.5319
ARVI	0.689	Y = 2.726 *ARVI + 2.8479
SARVI	0.711	Y = 2.5832* SARVI + 2.8184
MSAVI	0.745	Y = 2.024* MSAVI + 2.6627
OSAVI	0.812	Y = 4.0094 *OSAVI + 2.4039
All combination	0.839	Y = 0.534* SAVI + 0.226 *ARVI − 0.907 *SARVI + 0.0922 * MSAVI + 3.264 * OSAVI
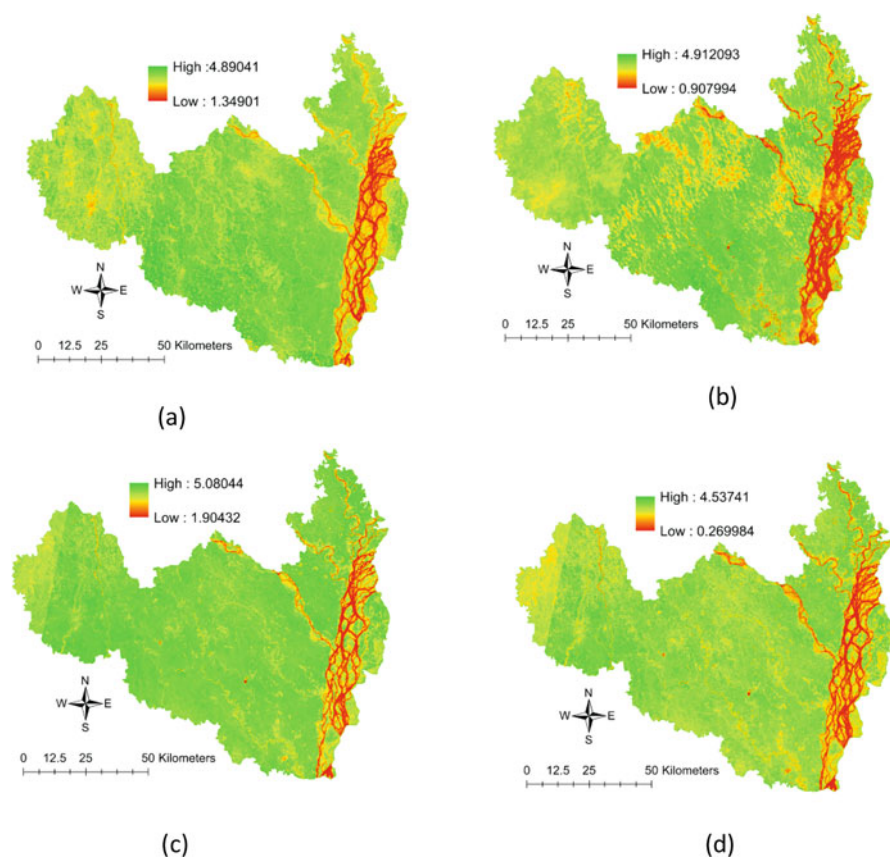
Fig. 3.10 Yield prediction map (MT/ha) (**a**) 2017, (**b**) 2018, (**c**) 2019, (**d**) 2020

3.5 Conclusions

This research established a method to identify the most suitable agricultural land by using the potentiality of satellite remote sensing data integrated with weighted linear combinations and fuzzy multicriteria analyses in a GIS platform. The multicriteria decision analysis was performed for suitability assessment using eight criteria: elevation, slope, LST, and vegetation indices (SAVI, ARVI, SARVI, MSAVI, and OSAVI). To derive a more accurate result, a land use/land cover layer was also used to mask restricted zones. The land suitability analysis with equal weights showed that 43% of the land (1832 km^2) was highly suitable, 41% of the land (1747 km^2) was moderately suitable, and 10% of the land (426 km^2) was marginally suitable. Conversely, expert knowledge was also considered, along with consistent assessments when using the fuzzy membership function; 48% of the land (2045 km^2) was highly suitable, 39% of the land (2045 km^2) was moderately suitable, and 7% of the land (298 km^2) was marginally suitable. The yield estimation using SAVI ($R^2 = 77.3\%$), ARVI ($R^2 = 68.9\%$), SARVI ($R^2 = 71.1\%$), MSAVI ($R^2 = 74.5\%$), and OSAVI ($R^2 = 81.2\%$) showed a good accuracy. In addition, every combination of these five indices represented the best accuracy ($R^2 = 0.839$), which was used to develop the yield maps for the corresponding years (2017–2020). The results of the land suitability evaluation for field crops will be very useful in the decision-making process to increase production as well as for the sustainable management of agricultural lands. Thus, the influence of vegetation index evaluations, suitable condition assessments, and yield prediction models is essential for understanding future land use and production trends in the agricultural crop sector in Bangladesh, as well as other applications.

Appendix: SAVI, ARVI, SARVI, MSAVI, and OSAVI from 2017 to 2020 for 36 Subunits

Ground points	SAVI				ARVI				SARVI				MSAVI				OSAVI			
	2017	2018	2019	2020	2017	2018	2019	2020	2017	2018	2019	2020	2017	2018	2019	2020	2017	2018	2019	2020
1	0.501	0.557	0.698	0.593	0.388	0.42	0.398	0.43	0.388	0.42	0.418	0.303	0.688	0.582	0.668	0.602	0.388	0.402	0.458	0.401
2	0.445	0.54	0.35	0.42	0.405	0.303	0.355	0.32	0.345	0.34	0.385	0.32	0.545	0.54	0.55	0.452	0.415	0.394	0.435	0.302
3	0.534	0.65	0.71	0.69	0.414	0.525	0.501	0.39	0.544	0.475	0.531	0.49	0.684	0.785	0.739	0.59	0.544	0.595	0.591	0.589
4	0.643	0.67	0.682	0.77	0.69	0.66	0.71	0.57	0.539	0.506	0.51	0.47	0.869	0.866	0.919	0.827	0.69	0.66	0.61	0.57
5	0.408	0.519	0.417	0.375	0.42	0.35	0.29	0.355	0.282	0.285	0.309	0.2655	0.442	0.475	0.4729	0.3949	0.292	0.295	0.329	0.195
6	0.321	0.401	0.315	0.227	0.251	0.201	0.224	0.19	0.221	0.21	0.235	0.2	0.31	0.41	0.501	0.4	0.631	0.621	0.6827	0.62
7	0.472	0.597	0.698	0.784	0.394	0.397	0.385	0.301	0.448	0.447	0.47	0.421	0.674	0.707	0.745	0.681	0.364	0.397	0.377	0.5501
8	0.595	0.671	0.772	0.689	0.681	0.661	0.5	0.59	0.4801	0.51	0.54	0.439	0.7981	0.7981	0.829	0.739	0.681	0.61	0.5	0.79
9	0.799	0.797	0.779	0.769	0.669	0.577	0.67	0.539	0.479	0.508	0.529	0.449	0.799	0.896	0.99	0.859	0.379	0.386	0.49	0.289
10	0.479	0.621	0.631	0.303	0.33	0.366	0.431	0.31	0.33	0.32	0.31	0.303	0.415	0.436	0.4831	0.423	0.5	0.436	0.431	0.383
11	0.748	0.699	0.692	0.598	0.48	0.487	0.49	0.44	0.48	0.39	0.42	0.404	0.68	0.747	0.842	0.724	0.608	0.547	0.642	0.474
12	0.584	0.394	0.733	0.4387	0.54	0.49	0.539	0.387	0.454	0.49	0.49	0.487	0.754	0.749	0.89	0.707	0.54	0.49	0.49	0.487
13	0.519	0.603	0.645	0.538	0.479	0.46	0.47	0.439	0.479	0.46	0.507	0.45	0.679	0.686	0.747	0.669	0.479	0.46	0.497	0.4069
14	0.688	0.789	0.667	0.582	0.38	0.439	0.41	0.312	0.408	0.415	0.478	0.37	0.718	0.739	0.741	0.702	0.358	0.309	0.371	0.252
15	0.484	0.411	0.583	0.292	0.312	0.301	0.391	0.282	0.22	0.291	0.23	0.212	0.44	0.31	0.623	0.52	0.24	0.31	0.33	0.182
16	0.419	0.372	0.44	0.36	0.35	0.312	0.34	0.30	0.29	0.22	0.254	0.22	0.39	0.32	0.24	0.5	0.39	0.432	0.424	0.405
17	0.45	0.562	0.685	0.541	0.43	0.502	0.425	0.341	0.35	0.373	0.385	0.31	0.655	0.642	0.635	0.5601	0.645	0.622	0.735	0.621
18	0.786	0.699	0.794	0.744	0.676	0.604	0.6144	0.544	0.56	0.504	0.5144	0.4944	0.976	0.904	0.991	0.904	0.476	0.404	0.4744	0.384
19	0.401	0.36	0.548	0.297	0.4	0.36	0.38	0.307	0.349	0.395	0.418	0.3279	0.74	0.736	0.858	0.77	0.34	0.426	0.434	0.377
20	0.487	0.601	0.751	0.475	0.387	0.397	0.441	0.25	0.487	0.37	0.431	0.375	0.787	0.797	0.794	0.695	0.587	0.607	0.641	0.595
21	0.788	0.692	0.789	0.774	0.696	0.652	0.66	0.501	0.531	0.502	0.53	0.464	0.761	0.862	0.85	0.824	0.661	0.692	0.695	0.584
22	0.787	0.793	0.8013	0.699	0.617	0.771	0.535	0.505	0.507	0.56	0.575	0.505	0.977	0.9161	0.8535	0.905	0.337	0.301	0.335	0.29
23	0.4027	0.212	0.45	0.222	0.127	0.102	0.165	0.102	0.2277	0.262	0.275	0.222	0.4377	0.432	0.425	0.382	0.477	0.462	0.5495	0.442

(continued)

(continued)

Ground points	SAVI				ARVI				SARVI				MSAVI				OSAVI			
	2017	2018	2019	2020	2017	2018	2019	2020	2017	2018	2019	2020	2017	2018	2019	2020	2017	2018	2019	2020
24	0.795	0.806	0.799	0.708	0.415	0.45	0.506	0.427	0.485	0.45	0.476	0.44	0.6725	0.65	0.816	0.697	0.385	0.385	0.346	0.27
25	0.65	0.393	0.693	0.492	0.35	0.343	0.33	0.302	0.325	0.33	0.373	0.302	0.35	0.533	0.493	0.342	0.55	0.733	0.783	0.642
26	0.79	0.762	0.818	0.799	0.69	0.662	0.68	0.598	0.479	0.469	0.498	0.4998	0.979	0.9662	0.998	0.998	0.609	0.622	0.648	0.591
27	0.75	0.54	0.77	0.55	0.45	0.54	0.67	0.52	0.475	0.488	0.479	0.4022	0.795	0.854	0.847	0.782	0.465	0.454	0.497	0.382
28	0.693	0.487	0.688	0.491	0.39	0.418	0.418	0.281	0.39	0.408	0.408	0.321	0.709	0.718	0.738	0.701	0.39	0.398	0.398	0.2971
29	0.512	0.605	0.586	0.36	0.491	0.425	0.56	0.35	0.32	0.35	0.36	0.395	0.45	0.52	0.603	0.495	0.52	0.55	0.66	0.5
30	0.701	0.503	0.629	0.635	0.51	0.523	0.619	0.485	0.497	0.453	0.509	0.4785	0.761	0.853	0.849	0.785	0.61	0.53	0.649	0.585
31	0.622	0.731	0.687	0.547	0.512	0.501	0.591	0.47	0.492	0.501	0.489	0.437	0.7652	0.751	0.848	0.697	0.552	0.591	0.648	0.547
32	0.339	0.44	0.486	0.295	0.27	0.224	0.256	0.235	0.249	0.247	0.299	0.225	0.439	0.474	0.486	0.385	0.37	0.324	0.326	0.295
33	0.568	0.647	0.704	0.503	0.48	0.47	0.49	0.43	0.46	0.44	0.44	0.43	0.6	0.747	0.844	0.73	0.56	0.47	0.644	0.43
34	0.392	0.45	0.44	0.23	0.28	0.235	0.314	0.193	0.28	0.205	0.294	0.213	0.438	0.445	0.424	0.403	0.32	0.35	0.324	0.33
35	0.791	0.59	0.787	0.686	0.57	0.59	0.607	0.586	0.471	0.593	0.457	0.389	0.871	0.859	0.947	0.786	0.51	0.79	0.6747	0.586
36	0.598	0.697	0.778	0.609	0.38	0.403	0.458	0.395	0.488	0.447	0.549	0.435	0.688	0.582	0.668	0.602	0.68	0.694	0.6948	0.575

References

Acharjee TK, Van Halsema G, Ludwig F, Hellegers P (2017) Declining trends of water requirements of dry season Boro rice in the north-west Bangladesh. Agric Water Manag 180:148–159. https://doi.org/10.1016/j.agwat.2016.11.014

Alamgir S, Furuya J, Kobayashi S, Mostafiz RB, Ahmed R (2020) Farm income, inequality, and poverty among farm families of a flood-prone area in Bangladesh: climate change vulnerability assessment. GeoJournal 86:2861–2885. https://doi.org/10.1007/s10708-020-10231-2

Amin SR, Zhang J, Yang M (2015) Effects of climate change on the yield and cropping area of major food crops: a case of Bangladesh. Sustain For 7:898–915. https://doi.org/10.3390/su7010898

Ashford SA, Sitar N, Lysmer J, Deng N (1997) Topographic effects on the seismic response of steep slopes. Bull Seismol Soc Am 87:701–709

Ayehu GT, Besufekad SA (2015) Land suitability analysis for rice production: a GIS based multi-criteria decision approach. Am J Geogr Inf Syst 4:95–104. https://doi.org/10.5923/j.ajgis.20150403.02

Bangladesh Bureau of Statistics (BBS) (2011) Statistics and Informatics Division (SID) Ministry of Planning: Population and housing census 2011. Bangladesh Bureau of Statistics, Dhaka

Bangladesh Bureau of Statistics (BBS) (2018) Statistical pocket book Bangladesh 2016. Ministry of Planning, Dhaka

Bellman RE, Zadeh LA (1970) Decision-making in a fuzzy environment. Manag Sci 17:141. https://doi.org/10.1287/mnsc.17.4.b141

Bozdağ A, Yavuz F, Günay AS (2016) AHP and GIS based land suitability analysis for Cihanbeyli (Turkey) county. Environ Earth Sci 75:813. https://doi.org/10.1007/s12665-016-5558-9

Buthelezi NN, Hughes JC, Modi A (2013) The use of scientific and indigenous knowledge in agricultural land evaluation and soil fertility studies of two villages in KwaZulu-Natal, South Africa. Afr J Agric Res 8:507–518

Campos I, González-Gómez L, Villodre J, González-Piqueras J, Suyker AE, Calera A (2018) Remote sensing-based crop biomass with water or light-driven crop growth models in wheat commercial fields. Field Crop Res 216:175–188. https://doi.org/10.1016/j.fcr.2017.11.025

Ceglar A, Toreti A, Prodhomme C, Zampieri M, Turco M, Doblas-Reyes FJ (2018) Land-surface initialisation improves seasonal climate prediction skill for maize yield forecast. Sci Rep 8:1–9. https://doi.org/10.1038/s41598-018-19586-6

Cho MA, Skidmore AK (2008) Hyperspectral predictors for monitoring biomass production in Mediterranean mountain grasslands: Majella National Park, Italy. Int J Remote Sens 30:499–515. https://doi.org/10.1080/01431160802392596

Das AC, Noguchi R, Ahamed T (2020) Integrating an expert system, GIS, and satellite remote sensing to evaluate land suitability for sustainable tea production in Bangladesh. Remote Sens 12:4136. https://doi.org/10.3390/rs12244136

De Lima TM, Weindorf DC, Curi N, Guilherme LR, Lana RM, Ribeiro BT (2019) Elemental analysis of Cerrado agricultural soils via portable X-ray fluorescence spectrometry: inferences for soil fertility assessment. Geoderma 353:264–272. https://doi.org/10.1016/j.geoderma.2019.06.045

El Kateb H, Zhang H, Zhang P, Mosandl R (2013) Soil erosion and surface runoff on different vegetation covers and slope gradients: a field experiment in Southern Shaanxi Province, China. Catena 105:1–10. https://doi.org/10.1016/j.catena.2012.12.012

Elsheikh R, Shariff ARBM, Amiri F, Ahmad NB, Balasundram SK, Soom MAM (2013) Agriculture land suitability evaluator (ALSE): a decision and planning support tool for tropical and subtropical crops. Comput Electron Agric 93:98–110. https://doi.org/10.1016/j.compag.2013.02.003

Ennouri K, Kallel A (2019) Remote sensing: an advanced technique for crop condition assessment. Math Probl Eng 2019:1–8. https://doi.org/10.1155/2019/9404565

Essougong UPK, Slingerland M, Mathé S, Vanhove W, Ngome PIT, Boudes P, Giller KE, Woittiez LS, Leeuwis C (2020) Farmers' perceptions as a driver of agricultural practices: understanding soil fertility management practices in cocoa agroforestry systems in Cameroon. Hum Ecol 48: 709–720. https://doi.org/10.1007/s10745-020-00190-0

Fern RR, Foxley EA, Bruno A, Morrison ML (2018) Suitability of NDVI and OSAVI as estimators of green biomass and coverage in a semi-arid rangeland. Ecol Indic 94:16–21. https://doi.org/10.1016/j.ecolind.2018.06.029

Food and Agriculture Organization (1976) A framework for land evaluation. Food and Agriculture Organization, Rome

Gerpacio RV, Pingali PL (2007) Tropical and subtropical maize in Asia: production systems, constraints, and research priorities. CIMMYT, Texcoco

Gilabert M, González-Piqueras J, Garcia-Haro F, Melia J (2002) A generalized soil-adjusted vegetation index. Remote Sens Environ 82:303–310. https://doi.org/10.1016/s0034-4257(02)00048-2

Gitari HI, Gachene CKK, Karanja NN, Kamau S, Nyawade S, Schulte-Geldermann E (2019) Potato-legume intercropping on a sloping terrain and its effects on soil physico-chemical properties. Plant Soil 438:447–460. https://doi.org/10.1007/s11104-019-04036-7

GRiSP (2013) Rice almanac, 4th edn. Global Rice Science Partnership, Los Baños

Habibie MI, Noguchi R, Shusuke M, Ahamed T (2019) Land suitability analysis for maize production in Indonesia using satellite remote sensing and GIS-based multicriteria decision support system. GeoJournal 86:777–807. https://doi.org/10.1007/s10708-019-10091-5

Haboudane D, Miller JR, Pattey E, Zarco-Tejada PJ, Strachan IB (2004) Hyperspectral vegetation indices and novel algorithms for predicting green LAI of crop canopies: modeling and validation in the context of precision agriculture. Remote Sens Environ 90:337–352. https://doi.org/10.1016/j.rse.2003.12.013

Huete A (1988) A soil-adjusted vegetation index (SAVI). Remote Sens Environ 25:295–309. https://doi.org/10.1016/0034-4257(88)90106-x

Jeevalakshmi D, Narayana Reddy S, Manikiam B (2017) Land surface temperature retrieval from LANDSAT data using emissivity estimation. Int J Appl Eng Res 12:9679–9687

Jiang Z, Huete AR, Chen J, Chen Y, Li J, Yan G, Zhang X (2006) Analysis of NDVI and scaled difference vegetation index retrievals of vegetation fraction. Remote Sens Environ 101:366–378. https://doi.org/10.1016/j.rse.2006.01.003

Jyoti NA, Lal R, Das AK (2015) Ethnopedology and soil quality of bamboo (Bambusa sp.) based agroforestry system. Sci Total Environ 521:372–379. https://doi.org/10.1016/j.scitotenv.2015.03.059

Kaufman YJ, Tanre D (1992) Atmospherically resistant vegetation index (ARVI) for EOS-MODIS. IEEE Trans Geosci Remote Sens 30:261–270. https://doi.org/10.1109/36.134076

Kazemi H, Akinci H (2018) A land use suitability model for rainfed farming by multi-criteria decision-making analysis (MCDA) and geographic information system (GIS). Ecol Eng 116:1–6. https://doi.org/10.1016/j.ecoleng.2018.02.021

Kennedy CM, Hawthorne PL, Miteva DA, Baumgarten L, Sochi K, Matsumoto M, Evans JS, Polasky S, Hamel P, Vieira EM et al (2016) Optimizing land use decision-making to sustain Brazilian agricultural profits, biodiversity and ecosystem services. Biol Conserv 204:221–230. https://doi.org/10.1016/j.biocon.2016.10.039

Kihoro J, Bosco NJ, Murage H (2013) Suitability analysis for rice growing sites using a multicriteria evaluation and GIS approach in great Mwea region, Kenya. Springerplus 2:265. https://doi.org/10.1186/2193-1801-2-265

Kim MS, Daughtry CST, Chappelle EW, McMurtrey JE, Walthall CL (1994) The use of high spectral resolution bands for estimating absorbed photosynthetically active radiation. In Proceedings of the 6th symposium on physical measurements and signatures in remote sensing, pp 299–306

Koulouri M, Giourga C (2007) Land abandonment and slope gradient as key factors of soil erosion in Mediterranean terraced lands. Catena 69:274–281. https://doi.org/10.1016/j.catena.2006.07.001

Li Y, Chen W, Zhang Y, Tao C, Xiao R, Tan Y (2020) Accurate cloud detection in high-resolution remote sensing imagery by weakly supervised deep learning. Remote Sens Environ 250: 112045. https://doi.org/10.1016/j.rse.2020.112045

Mao Z-H, Deng L, Duan F-Z, Li X-J, Qiao D-Y (2020) Angle effects of vegetation indices and the influence on prediction of SPAD values in soybean and maize. Int J Appl Earth Obs Geoinf 93: 102198. https://doi.org/10.1016/j.jag.2020.102198

Mazza A, Gargiulo M, Scarpa G, Gaetano R (2018) Estimating the NDVI from SAR by convolutional neural networks. In: Proceedings of the IGARSS 2018 IEEE international geoscience and remote sensing symposium. IEEE, New York, pp 1954–1957

Mitchell S, Cohen K (2014) Fuzzy logic decision making for autonomous robotic applications. In: Proceedings of the 2014 IEEE 6th international conference on awareness science and technology (iCAST). IEEE, New York, pp 1–6

Mottaleb KA, Kruseman G, Erenstein O (2018) Determinants of maize cultivation in a land-scarce rice-based economy: the case of Bangladesh. J Crop Improv 32:453–476. https://doi.org/10.1080/15427528.2018.1446375

Nahusenay A, Kibebew K (2015) Land suitability evaluation in Wadla Delanta Massif of north central highlands of Ethiopia for rainfed crop production. Afr J Agric Res 10:1595–1611. https://doi.org/10.5897/ajar2014.9248

Niemeijer D, Mazzucato V (2003) Moving beyond indigenous soil taxonomies: local theories of soils for sustainable development. Geoderma 111:403–424. https://doi.org/10.1016/S0016-7061(02)00274-4

Noorollahi E, Fadai D, Shirazi MA, Ghodsipour SH (2016) Land suitability analysis for solar farms exploitation using GIS and fuzzy analytic hierarchy process (FAHP)—a case study of Iran. Energies 9:643. https://doi.org/10.3390/en9080643

Novara A, Gristina L, Sala G, Galati A, Crescimanno M, Cerdà A, Badalamenti E, La Mantia T (2017) Agricultural land abandonment in Mediterranean environment provides ecosystem services via soil carbon sequestration. Sci Total Environ 576:420–429. https://doi.org/10.1016/j.scitotenv.2016.10.123

Olivero J, Real R, Márquez AL (2011) Fuzzy chorotypes as a conceptual tool to improve insight into biogeographic patterns. Syst Biol 60:645–660. https://doi.org/10.1093/sysbio/syr026

Pilevar AR, Matinfar HR, Sohrabi A, Sarmadian F (2020) Integrated fuzzy, AHP and GIS techniques for land suitability assessment in semi-arid regions for wheat and maize farming. Ecol Indic 110:105887. https://doi.org/10.1016/j.ecolind.2019.105887

Pimentel D, Burgess M (2013) Soil erosion threatens food production. Agriculture 3:443–463. https://doi.org/10.3390/agriculture3030443

Purnamasari RA, Noguchi R, Ahamed T (2019) Land suitability assessments for yield prediction of cassava using geospatial fuzzy expert systems and remote sensing. Comput Electron Agric 166: 105018. https://doi.org/10.1016/j.compag.2019.105018

Radočaj D, Jurišić M, Gašparović M, Plaščak I (2020) Optimal soybean (Glycine max L.) land suitability using GIS-based multicriteria analysis and sentinel-2 multitemporal images. Remote Sens 12:1463. https://doi.org/10.3390/rs12091463

Ren H, Feng G (2014) Are soil-adjusted vegetation indices better than soil-unadjusted vegetation indices for above-ground green biomass estimation in arid and semi-arid grasslands? Grass Forage Sci 70:611–619. https://doi.org/10.1111/gfs.12152

Ren H, Zhou G, Zhang F (2018) Using negative soil adjustment factor in soil-adjusted vegetation index (SAVI) for aboveground living biomass estimation in arid grasslands. Remote Sens Environ 209:439–445. https://doi.org/10.1016/j.rse.2018.02.068

Richardson AJ, Wiegand CL (1977) Distinguishing vegetation from soil background information. Photogramm Eng Remote Sens 43:1541–1552

Romano G, Sasso PD, Liuzzi GT, Gentile F (2015) Multi-criteria decision analysis for land suitability mapping in a rural area of Southern Italy. Land Use Policy 48:131–143. https://doi.org/10.1016/j.landusepol.2015.05.013

Samanta S, Pal B, Pal DK (2011) Land suitability analysis for rice cultivation based on multi-criteria decision approach through GIS. Data Base Int J Sci Emerg Technol 2:12–20

Senanayake S, Pradhan B, Huete A, Brennan J (2020) Assessing soil erosion hazards using land-use change and landslide frequency ratio method: a case study of Sabaragamuwa Province, Sri Lanka. Remote Sens 12:1483. https://doi.org/10.3390/rs12091483

Seyedmohammadi J, Sarmadian F, Jafarzadeh AA, McDowell RW (2019) Development of a model using matter element, AHP and GIS techniques to assess the suitability of land for agriculture. Geoderma 352:80–95. https://doi.org/10.1016/j.geoderma.2019.05.046

Shimoda S, Kanno H, Hirota T (2018) Time series analysis of temperature and rainfall-based weather aggregation reveals significant correlations between climate turning points and potato (Solanum tuberosum L) yield trends in Japan. Agric For Meteorol 263:147–155. https://doi.org/10.1016/j.agrformet.2018.08.005

Somvanshi SS, Kumari M (2020) Comparative analysis of different vegetation indices with respect to atmospheric particulate pollution using sentinel data. Appl Comput Geosci 7:100032. https://doi.org/10.1016/j.acags.2020.100032

Sonobe R, Yamaya Y, Tani H, Wang X, Kobayashi N, Mochizuki K-I (2018) Crop classification from Sentinel-2-derived vegetation indices using ensemble learning. J Appl Remote Sens 12:026019. https://doi.org/10.1117/1.jrs.12.026019

Sulaiman AA, Sulaeman Y, Mustikasari N, Nursyamsi D, Syakir AM (2019) Increasing sugar production in Indonesia through land suitability analysis and sugar mill restructuring. Landscape 8:61. https://doi.org/10.3390/land8040061

Svinurai W, Hassen A, Tesfamariam E, Ramoelo A (2018) Performance of ratio-based, soil-adjusted and atmospherically corrected multispectral vegetation indices in predicting herbaceous aboveground biomass in a Colophospermum mopane tree-shrub savanna. Grass Forage Sci 73:727–739. https://doi.org/10.1111/gfs.12367

Tashayo B, Honarbakhsh A, Akbari M, Eftekhari M (2020) Land suitability assessment for maize farming using a GIS-AHP method for a semi-arid region, Iran. J Saudi Soc Agric Sci 19:332–338. https://doi.org/10.1016/j.jssas.2020.03.003

Tucker CJ (1979) Red and photographic infrared linear combinations for monitoring vegetation. Remote Sens Environ 8:127–150. https://doi.org/10.1016/0034-4257(79)90013-0

Venancio LP, Mantovani EC, Amaral CHD, Neale CMU, Gonçalves IZ, Filgueiras R, Campos I (2019) Forecasting corn yield at the farm level in Brazil based on the FAO-66 approach and soil-adjusted vegetation index (SAVI). Agric Water Manag 225:105779. https://doi.org/10.1016/j.agwat.2019.105779

Yalew SG, Van Griensven A, Mul ML, Van Der Zaag P (2016) Land suitability analysis for agriculture in the Abbay basin using remote sensing, GIS and AHP techniques. Model Earth Syst Environ 2:1–14. https://doi.org/10.1007/s40808-016-0167-x

Zadeh LA (1965) Fuzzy sets. Inf Control 8:338–353. https://doi.org/10.1016/s0019-9958(65)90241-x

Zinat MRM, Salam R, Badhan MA, Islam ARMT (2020) Appraising drought hazard during Boro rice growing period in western Bangladesh. Int J Biometeorol 64:1687–1697. https://doi.org/10.1007/s00484-020-01949-2

Zolekar RB, Bhagat VS (2015) Multi-criteria land suitability analysis for agriculture in hilly zone: remote sensing and GIS approach. Comput Electron Agric 118:300–321. https://doi.org/10.1016/j.compag.2015.09.016

Chapter 4
Land Suitability Assessment for Cassava Production in Indonesia Using GIS, Remote Sensing, and Multi-Criteria Analysis

Riska Ayu Purnamasari, Ryozo Noguchi, and Tofael Ahamed

Abstract Sustainable land use is essential for increasing the production of cassava as a diversified crop for ensuring food security in Indonesia. Understanding the spatial factors and criteria is required for locating suitable production areas to increase cassava production. In this study, a spatial model was developed to assess the suitability of land for supporting sustainable cassava production. The model was divided into three stages considering different criteria. First, satellite digital images were processed from Landsat-4 Thematic Mapper (TM), Landsat-8 Operational Land Imager (OLI), and Sentinel-2 satellites to create vector data layers and a normalized difference vegetation index (NDVI) database. Second, a spatial analysis was performed to identify highly suitable areas for cassava production using a geographical information system (GIS) and the multi-criteria analysis including the analytical hierarchy process (AHP) and the analytical network process (ANP). Third, a sustainability evaluation was conducted based on land suitability information for a study period of 5 years. Land suitability assessment was performed to increase cassava production. We found that 43.11% (11,094 ha) of the study area was highly suitable for cassava production, whereas 30.87% (8233 ha) was moderately suitable and 9.83% (2623 ha) was marginally suitable with incorporating AHP analysis. Moreover, 17.69% (4718 ha) of the land was occupied by residents and settlements. On the other hand, ANP analysis also conducted to confirm the AHP results. Although many decision problems are studied through the AHP, however as the novelty in this study, ANP have added the better decision judgment based on the expert opinions. This research recommended that the integrated approach of GIS based on multi-criteria can be extended with satellite remote sensing vegetation datasets to assess the regional production and site-specific management of cassava crops.

R. A. Purnamasari
Mu, Innovation Center for Tropical Science, A Non-Government Organization with Innovation Center for Tropical Science (ICTS), Bogor City, Indonesia

R. Noguchi · T. Ahamed (✉)
Faculty of Life and Environmental Sciences, University of Tsukuba, Tsukuba, Ibaraki, Japan
e-mail: tofael.ahamed.gp@u.tsukuba.ac.jp

© The Author(s), under exclusive license to Springer Nature Singapore Pte Ltd. 2022

4.1 Introduction

Land suitability assessments are important for sustainable land use and for the selection of potential crops in the changing climates of Indonesia. Indonesia is a developing country with the fifth largest population in the world (Statistik 2014). The dependence on rice of increased population as a staple food can create the threat of food insecurity (Elsheikh et al. 2013). To mitigate this dependency, diversification through the consumption of local foods, such as cassava, is desirable. Cassava is a good alternative of rice that poses fewer risks as a root crop and plays an important role in Indonesia, which is one of the Asian countries to support sustainable local food (Noerwijati and Budiono 2015) production (Campo et al. 2011; Noerwijati and Budiono 2015; Feenstra 1997; Ariningsih 2018). Cassava can be easily grown, cultivated, and distributed to local communities (Kolawole et al. 2010). The benefits of cassava as a local food could strengthen the food security of developing countries (Kolawole et al. 2010). In the future, cassava has the potential to become a promising crop that can adapt to changing climatic patterns due to its low water and soil acidity requirement compared to rice (FAO 2013; Khumaida et al. 2016). Therefore, sustainable cassava production in Indonesia must ensure maximum benefits for growers. While considering the sustainability of cassava production, criteria related to environment, ecological, economic, and social indicators must be addressed (Sydorovych and Wossink 2008; Tiwari et al. 1991). Furthermore, food security is one of the major concern in the context of agricultural sustainability and the sustainable supply of food for the increasing population (Ahamed et al. 2015). Sustainable land use for cassava production significantly drives maximizing the production of cassava to contribute to the food security of Indonesia.

To increase cassava production, suitable areas and ecological conditions must be identified (Heumann et al. 2011). Such important tasks associated with increasing the production of cassava can be addressed through spatial analyses of land suitability. Suitability classification reflects the suitability of each land unit for cassava production. In the Food and Agriculture Organization's (FAO 1976) framework for land evaluation, land was divided into four classes: highly suitable (S1), moderately suitable (S2), marginally suitable (S3), and not suitable (N). Spatial assessments of land suitable for cassava production could serve as a starting point for sustainability evaluations. Additionally, interactions between suitability and sustainability have been reported in the FAO's international framework for evaluating sustainable land management. Environmental factors deemed the suitability which can reflect the level of sustainability for the same land use over a period of time.

As a spatial tool, geographic information systems (GIS) have been used to conduct spatial analyses of suitability for various purposes, especially land suitability (Ferretti and Pomarico 2013; Malczewski 2006; Smyth and Dumanski 1993). In addition, applications of remote sensing in agriculture include several aspects such

as plant phenology, economic features, and land use management (Ceballos-Silva and Lopez-Blanco 2003). These applications have played an important role and suggest that remote sensing technology is suitable for monitoring agricultural activities (Lobell et al. 2015; Purnamasari et al. 2019; Misra et al. 2020). In regional scales of land suitability assessment, satellite remote sensing provides the opportunity to include phenological information of vegetation. The vegetation information can help determine the growth information of cassava plantations and help to inform the decision-making process of land suitability (Vrieling et al. 2011).

Therefore, investigating land suitability depends on multiple criteria and factors in the decision-making process that can largely be assessed using geospatial datasets (Ceballos-Silva and Lopez-Blanco 2003). A key step of land suitability assessment for cassava production is to determine the weight of each factor that influences the land suitability. The presence of various and multiple criteria makes land suitability assessment complicated because factors that influence land suitability have unequal levels of significance (Elsheikh et al. 2013). This inequality of weight also varies by location, land use, and productivity. The criteria for evaluation is largely dependent on geographical aspects and the socio-economic status of the country. A common rule for choosing a weight is very challenging, as growers have perceptions of weight that match their experiences.

A number of multi-criteria decision rules have been implemented to solve the land use suitability problems. The decision rules can be classified into multi-objective and multi-attribute decision-making methods (Malczewski 1999, 2004). The multi-objective approaches are mathematical programming model-oriented methods such as linear programming. The single-objective multi-criteria evaluation has a "goal" and is computed using multi-attribute analysis. The methodology has several ways to weight the criteria such as ordered weighted averaging (OWA) using weighted linear combination (WLC), AHP, and analytical network process (ANP). AHP method introduced by Saaty (1990) has incorporated into the GIS for land use suitability analysis. As an extension of the criterion importance weighting in WLC, the OWA allows the decision-maker to specify a degree of risk in their approach to decision-making (Rinner and Voss 2013; Feizizadeh and Blaschke 2014). AHP method uses pairwise comparison of each criterion, while WLC directly assigns the weights of relative importance to each attribute map layer and OWA involves two-step weighting (criterion and order of weights) (Ahmed 2015).

The AHP is a multiple criteria decision-making process that uses analytical hierarchies to determine the importance of criteria and their associated relationships in complex problems (Brandt et al. 2015; Qureshi et al. 2017; Saaty 1990). The AHP has the advantage of assigning the weights based on the preferences of experts for the regional concepts. For this reason, the AHP-modeling framework is widely accepted and has been extensively applied for multi-criteria decision analysis (MCDA) purposes and utilized in many decision-making problems regarding land suitability evaluation at a regional level (Zabihi et al. 2015; Akıncı et al. 2013; Zolekar and Bhagat 2015; Malczewski 2004).

Furthermore, GIS and AHP tools have recently been used for land suitability assessment and planning for suitable sites of agricultural land use, major crops, and

local foods (Pramanik 2016; Akıncı et al. 2013; Bunruamkaew and Murayam 2011; Elsheikh et al. 2013; Zolekar and Bhagat 2015; Zabihi et al. 2015; and Widiatmaka 2016). In land suitability analysis, criteria associated with topographic features, vegetation, and weather parameters are included. The extension and evaluation of suitability analysis methods can help to assess and improve the sustainability of crop production over time. Selecting the most appropriate model for land suitability assessment is important for current and future land use planning. Several approaches have been used to conduct land suitability assessments. The FAO land evaluation framework (1976) was the first procedure to assess local, regional, and national land use planning. In recent years, computing technologies combined with GIS have included geospatial criteria to help find solutions for land suitability at the regional scale. Therefore, GIS, remote sensing, and AHP would be used in land suitability analysis for various criteria related to ecological conditions or maximizing cassava production at the regional scale in Indonesia. Thus, the aim of this study was to develop a spatial model to assess land suitability levels for cassava production by integrating GIS, remote sensing, and AHP.

4.2 Methodology

The model was built in three stages. First, Landsat-4 Thematic Mapper (TM), Landsat-8 Operational Land Imager (OLI), and Sentinel-2 Multispectral Instrument (MSI) satellite digital images and vector data layers were processed to establish criteria for the suitability analysis. Such criteria included land cover type, topographical features, and the normalized difference vegetation index (NDVI). Second, we obtained highly suitable sites for increasing cassava production using GIS and AHP techniques. Third, we evaluated the sustainability levels of cassava production using four categories and images from the satellite database (Fig. 4.1). Primary data were collected through fieldwork involving questionnaires, interviews, and surveys. Additionally, secondary data from Statistics Indonesia and the Geospatial Information Agency of Indonesia were used. A global positioning system (GPS) receiver was used in our field survey to determine the locations of cassava fields in the city of Serang and to provide ground truth information (Table 4.1).

4.2.1 Study Area

Geographically, the city of Serang is located at 5990–6220 south and 106,070–106,250 east. The city is bordered by the Java Sea to the north and is surrounded by the Serang Regency to the east, south, and west. The city of Serang holds a position as the central government of the Banten Province and is an alternative area for Indonesia's state capital, Jakarta, which is located approximately 70 km away. The city includes 6 districts and 46 villages and covers a total area of
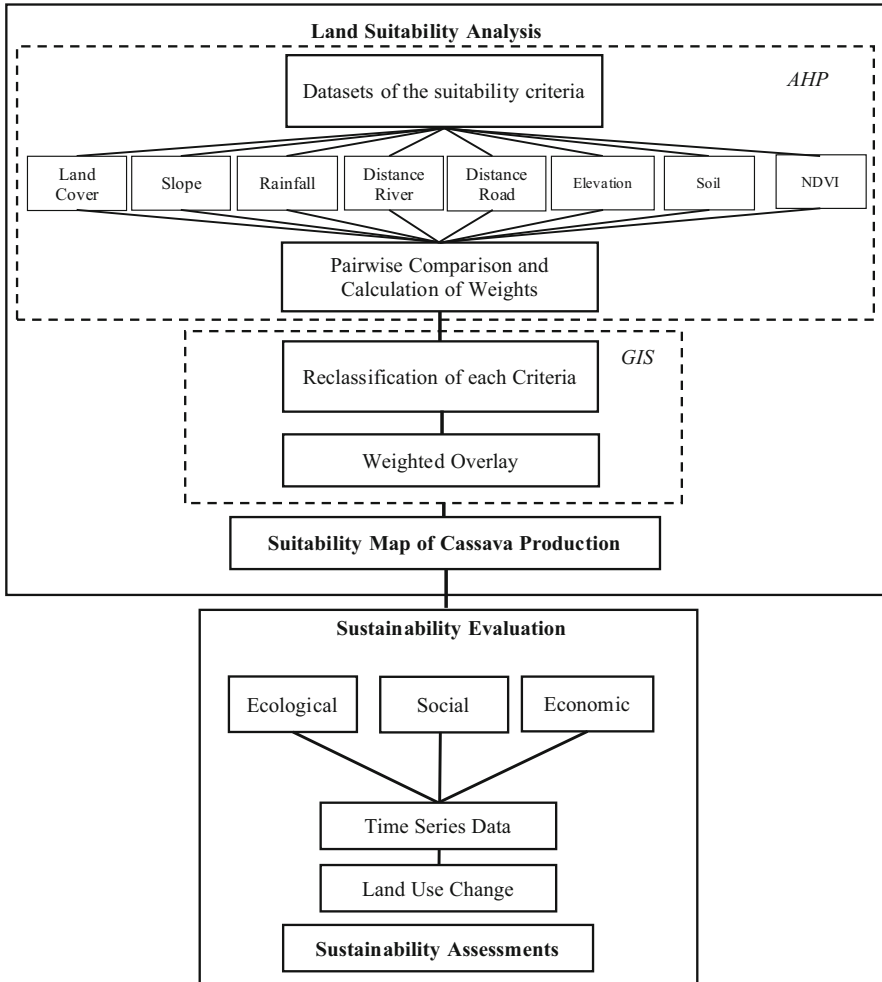
Fig. 4.1 The framework of site suitability for cassava production

266.7 sq. km. Most of the area is flat land with an elevation of less than 500 m and is characterized by a tropical climate (Fig. 4.2a–c). The city includes coastal land to the north, rural areas to the south and north, and an urban area in the middle of the region. The urban area includes infrastructural facilities that support socio-economic development.

Residences are also concentrated in the central part of the region. Rice cultivation constitutes the main land use in the northern area, whereas fields and dry land are found in the southern area. Cassava is an important alternative source of food, especially for traditional cuisine that is prepared for traditional events. In the city of Serang, cassava has historically been grown by poor farmers with minimal input on poorly managed land. When land is managed poorly, cassava can cause severe erosion on steep slopes (Howeler 1991).

Table 4.1 List of data used and their original sources of land suitability assessment for cassava production

No	Data	Description	Source
1	Land use map	Scale at 1:50,000	2011, Ministry of Environment and Forestry
2	NDVI map	Extracted from 10-m resolution	2016, Sentinel-2 MSI
3	Slope map	Derived from 30-m resolution	2015, DEM STRM
4	Elevation map	Derived from 30-m resolution	2015, DEM STRM
5	Road map	Scale 1:50,000	2005, Indonesia Geospatial Agency
6	River map	Scale 1:50,000	2005, Indonesia Geospatial Agency
7	Rainfall map	Scale 1:50,000	2010, Indonesia Geospatial Agency
8	Location of market	GPS data	2014, Survey
9	Cassava field location	GPS data	2014, Survey
10 11 12	Cassava production Land use/land cover map 2010 Land use/land cover map 2016	Statistics data Derived from 30-m resolution Derived from 30-m resolution	2014, Indonesian Statistics 2016, Landsat-4 TM 2016, Landsat-8 OLI

4.2.2 Criteria for Suitability Analysis

The criteria for the suitability analysis were land cover, slope angles, elevation levels, soil types, rainfall, distance from rivers, distance from roads, and the vegetation index (Fig. 4.3a–h). The details of criteria's characteristics focusing on Serang city are given in the following sections.

Land Use/Land Cover

Land use/land cover (LULC) data files describe the vegetation, water, natural surfaces, and cultural features of a land surface (Akıncı et al. 2013). Most land in the city of Serang is covered by rice fields. Other areas include fields, settlements, forests, plantations, and water bodies. The LULC database was divided into four classes. Class I referred to fields with fertile soils that were easily cultivated for cassava. Class II land was used for rice cultivation with cassava intercropping. Class III referred to plantation and forested land on steep slopes, and class IV land was unsuitable for cassava cultivation due to the presence of settlements, residents, water bodies, or mangrove forests.
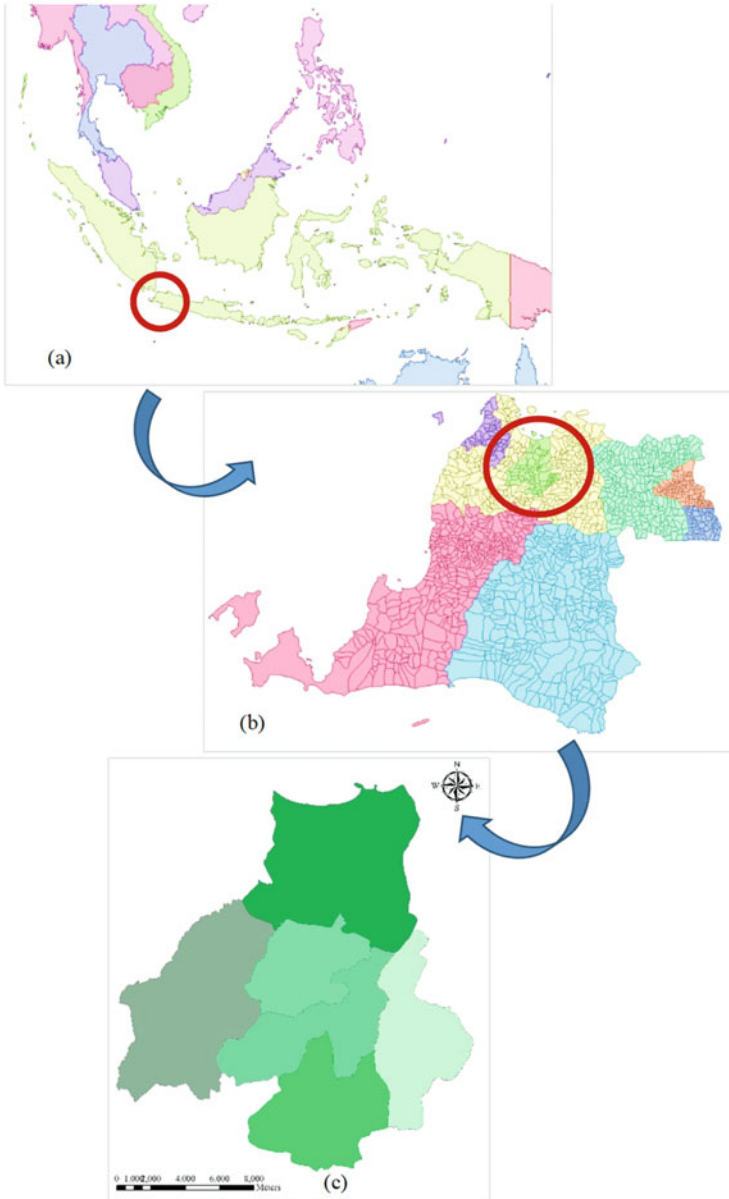
Fig. 4.2 (**a–c**) Geographical extent of the study area

Slope

In the city of Serang, most topography was classified as slopes between 0% and 45% in steepness. On slopes between 0% and 15%, most crops were easily cultivated. For cassava cultivation, slope angles were considered when determining cassava land management. Steep-sloped areas generally undergo soil erosion (Heumann et al. 2011), and soil steepness levels can affect soil formation. Additionally, a slope of 15% is optimal for livestock production and crop planting including the cassava (FAO 2000). Land variety, in terms of slope angles, constitutes an important factor in determining the suitability of cassava production areas.
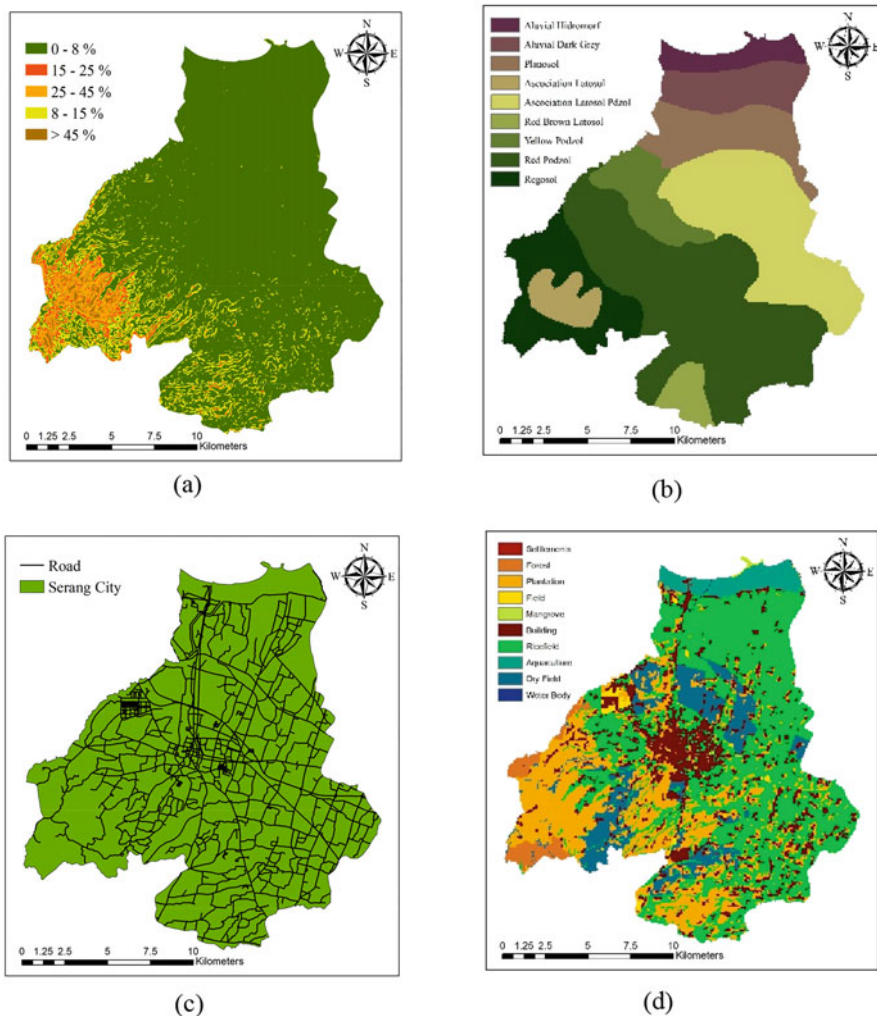
Fig. 4.3 (**a–h**) Criteria for land suitability analysis for cassava production
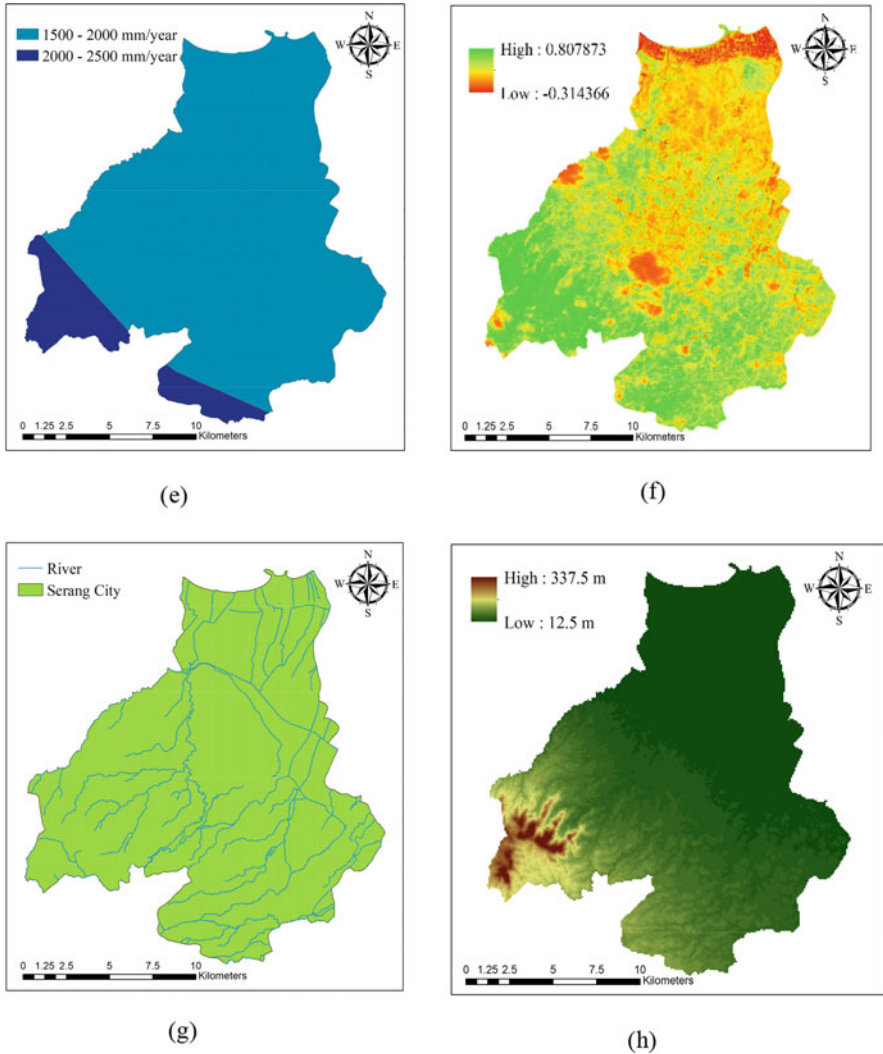
Fig. 4.3 (continued)

Distance from Rivers

The Cibanten River, the main river in Serang, supplies irrigation water. Other rivers in the area include the Cilandak, Cikaduan, Cikarang, Cipari, and Pelamunan rivers. The physical factors associated with water supply, such as the distance from water bodies, streams, rivers, and irrigation zones, were used to determine suitability levels for cassava production (Noerwijati and Budiono 2015). Rice fields were found in plains areas located close to major water resources, such as large rivers and water bodies, whereas cassava can be planted on sloped areas located farther from water resources (Statistik 2014).

Rainfall

Serang is characterized by a tropical climate, and significant periods of rainfall occur throughout the year. The precipitation amount is 1500–2000 mm per year, respectively (Statistik 2014). Cassava can also be intercropped with maize, legumes, or rain-fed crops in areas of high and well-distributed rainfall (Devendra and Thomas 2002). Cassava can grow in areas that receive as little as 400 mm of average annual rainfall. However, higher yields have been obtained in the presence of greater water supplies (FAO 2013). Moisture stress on cassava roots can result in low yields, especially in years characterized by low rainfall (Devendra and Thomas 2002). Therefore, irrigation management should be practiced effectively.

Soil Types

The major soil types found in Serang are alluvial, red regosol, red yellow podzolic, and latosol soils (Wargiono and Sudaryanto 2000). Alluvial soils are mostly used in rice-based cropping systems, and regosol soils are used for upland rice and dryland crop cultivation (Wargiono and Sudaryanto 2000). Regosol soils are found in hilly areas and in the center of mountain slopes. In Java, cassava-growing areas are generally located where soils classified as Mediterranean, alluvial, podzolic, latosols, or regosols are found. According to Wargiono, latosol areas are optimal for cultivating cassava. Latosol soils have good physical properties and are deep and tolerant to erosion. However, podzols include low levels of organic matter and tend to erode easily. Wargiono and Sudaryanto (2000) divided soil types for cassava cultivation into four classes. Class I includes latosol, gray hydromorphic, and planosol soils. Class II includes yellow podzolic soils. Class III refers to yellow regosol and red podzolic soils. Class IV refers to unsuitable soils that consist of gray alluvial hydromorphic soils with high water contents.

Elevation

In Asia, practically no cassava is grown at an elevation of 1000 m above sea level. In Indonesia, most cassava-growing areas are located in the lowland humid and subhumid tropics (Heumann et al. 2011). In some areas, cassava can be grown in hilly or mountainous areas, but the sustainability of these systems is compromised when sustained inputs are introduced for maintaining soil fertility and reducing erosion. Additionally, elevation has a strong effect on temperatures in some areas. In the city of Serang, elevation ranges from 12.5 m to 375 m. Most of the area is suitable for cassava production, although the optimal elevation for cassava production is approximately 62.5–137.5 m.

Distance from Roads

The number of vehicles in the city has increased due to economic growth, but road networks have not been expanded at the same rate. Therefore, traffic congestion in the city has increased. Regarding socio-economic factors, main roads are needed to sell fresh cassava at any distance from areas of cultivation. In selecting areas suitable for cassava production, the distance from roads must be considered because such distances affect transportation costs for supply processes. Shorter distances between fields and roads facilitate access to the transportation infrastructure and link farmers and farming activities to marketing channels (Statistik 2014).

Normalized Difference Vegetation Index (NDVI)

To avoid soil erosion during cassava production, land covered by low vegetation can reduce the rate of surface runoff. Vegetation index variations were assessed using a satellite-based measure: the NDVI. The NDVI is a vegetation index that is correlated with several important biophysical properties and that generates different crop indices (Ahamed et al. 2013; Elhag 2014). The proportion of vegetative biomass in the area being sensed or captured in satellite data is important for crop monitoring. Additionally, crop stages can be determined from NDVI data. In Indonesia, cassava production begins with planting at various times, but most field harvests occur during June or July. In this study, the NDVI was calculated for each cassava field using temporal information from Sentinel-2 MSI images acquired at the end of the growing period and before the harvest in January or February, because cassava needs about 7 until 8 months to grow.

4.2.3 Digital Image Processing

We used image data for each criterion. A 1:50,000 scale map of land cover types, rainfall levels, distances from rivers, soil types, elevations, distances from roads, and NDVI data was used for the analysis. Basic vector data layers were collected from the Geospatial Information Agency of Indonesia. Landsat-4 TM, Landsat-8 OLI, and Sentinel-2 MSI vegetation index (VI) datasets were used for field-level area crop monitoring in conjunction with NDVI data.

NDVI Computation Technique

The NDVI was proposed by Rouse et al. (1973), and it has become the most popular indicator for studying vegetation health and crop production. The NDVI is developed from two important wave bands: the red and near-infrared (NIR) bands. It has

been widely used for agricultural mapping and yield monitoring. The NDVI is calculated as follows:

$$\text{NDVI} = \frac{\text{RNIR} - \text{Rred}}{\text{RNIR} + \text{Rred}} \tag{4.1}$$

We acquired all available cloud-free Sentinel-2 scenes and calculated the NDVI from band combinations corresponding to the red and NIR reflections using Band 4 and Band 8. The Sentinel-2 mission combines 2 satellites—Sentinel-2A and Sentinel-2B—equipped with identical multispectral instruments capable of acquiring data in 13 bands at different spatial resolutions (between 10 m and 60 m). These satellites provide continuity for the Satellite Pour l'Observation de la Terre (SPOT) missions of the European Space Agency (ESA).

4.2.4 Reclassification of Criteria

Reclassification technique was used to simplify or change our interpretation of raster data by changing a single value to a new value or by grouping ranges of values into single values. Each criteria source map was reclassified into four classifications. The reclassification used the following suitability classes: highly suitable (S1), moderately suitable (S2), marginally suitable (S3), and not suitable (N) (Fig. 4.4a–h). Spatial data were converted into raster layers and then processed in ArcGIS® (ESRI, USA). They were then classified into four classes as integer raster that represented different suitability levels based on assigned threshold values (Table 4.2) (Tienwong et al. 2009).

For each of the suitability levels, we chose a suitability score. The suitability score is a way of computing values across the source layers so that there is a common standard. All source layer values are placed on the same scale with the same units. The same scale is used for all individual suitability layers and for the final overall suitability layer. In this study, we used a score of 9 for highly suitable areas, a score of 6 for moderately suitable areas, a score of 3 for marginally suitable areas, and a score of 1 and a restricted value for unsuitable areas.

4.2.5 Land Suitability Assessments

The land suitability assessment for the cassava production model was developed using the classification categories of land suitability proposed by the FAO (1976). The suitability classification is designed to determine the suitability of each land unit for a particular use. In the FAO's framework for land evaluation, land, the first class, is designated as suitable (S) or not suitable (N). These suitability classes can then be further subdivided as needed. In practice, three classes (S1, S2, and S3) are often

used to identify land that is highly suitable, moderately suitable, or marginally suitable for cassava production. The AHP application was used to support our weighted overlay calculations in the GIS environment. The AHP results were obtained from experts in related fields and from literature reviews. Through this process, the consistency ratio (CR) was calculated and was used in the land suitability analysis. The AHP method was applied to determine the relative importance of all of the selected criteria and factors (Ahamed et al. 2013).

A set of questionnaires within the AHP framework were developed. In the questionnaire, respondents can determine the relative importance of each criterion
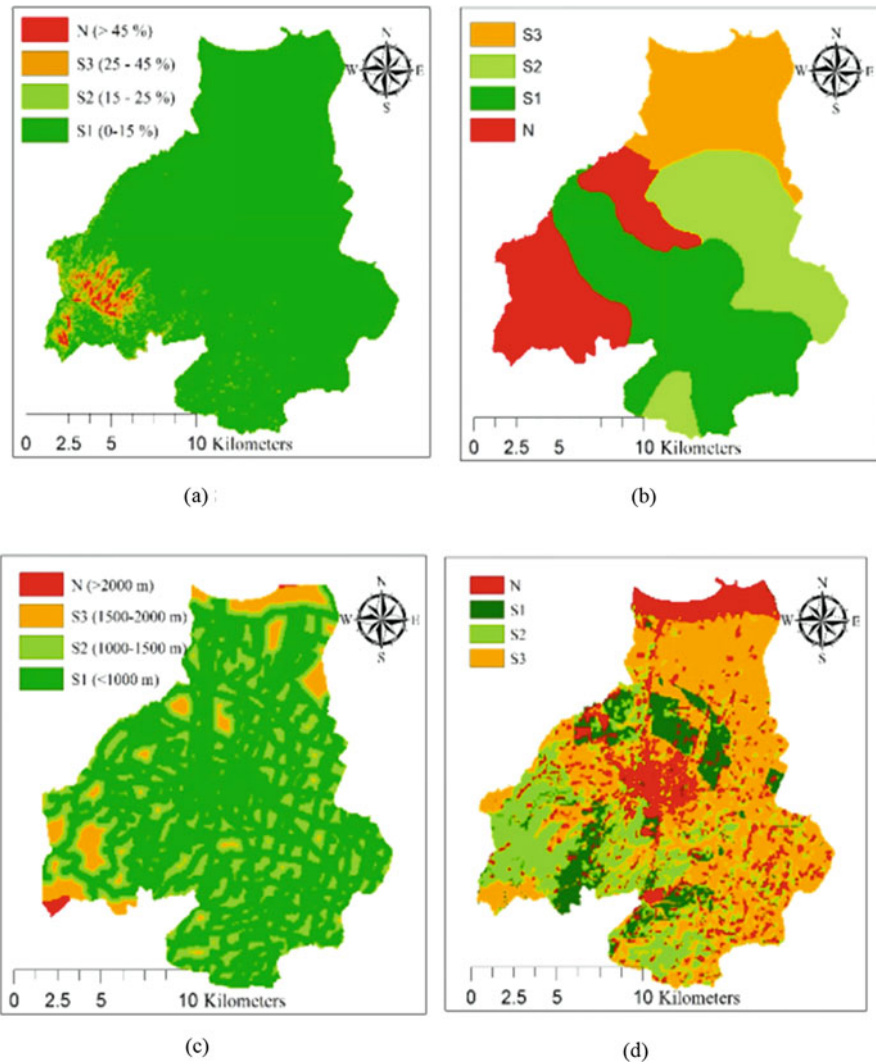
Fig. 4.4 (**a–h**) Reclassification of criteria

(e)   (f)

(g)   (h)
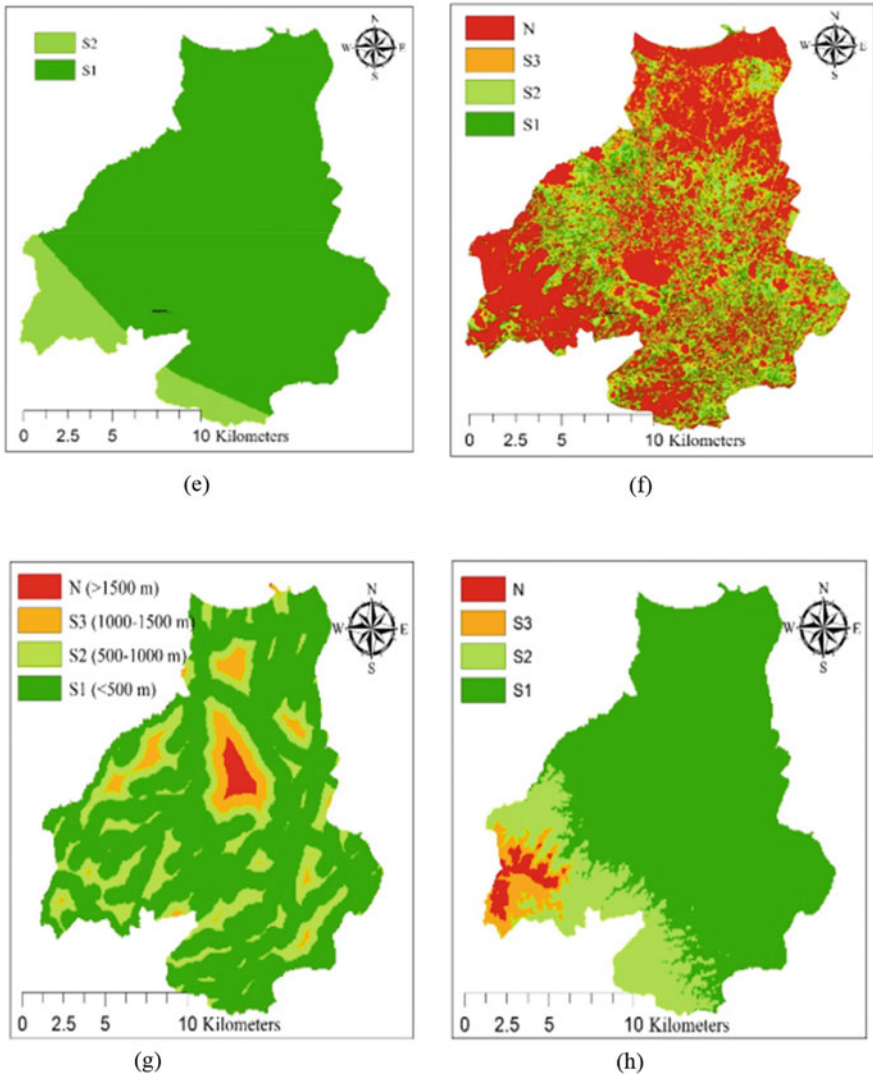
Fig. 4.4 (continued)

with respect to others, for example, the importance of soil with respect to land use, water, roads, and markets, and vice versa. Sets of questionnaires were disseminated to five key people in the province with various backgrounds (cassava experts, agriculture experts, and agriculture planners) during the field survey. The AHP is widely used by decision-makers and researchers. Calculation of criteria weights is central in the AHP method and depends on experts' opinions and determination for each criterion.

Table 4.2 Reclassification of criteria of land suitability assessment for cassava production

Criteria	Suitability class	Sub-criteria	Percentage area (%)	Area (ha)
LULC	S1	Class I	11.38	3059
	S2	Class II	43.27	11,631
	S3	Class III	27.61	7422
	N	Class IV	17.74	4767
Slope (%)	S1	0–8%	83.81	22.352
	S2	8–15%	10.25	2.734
	S3	15–25%	3.07	818
	N	> 25%	2.87	765
Rainfall (mm)	S1	1000–1500	89.22%	23.794
	S2	1500–2000	10.78%	2.875
Distance from roads (m)	S1	<1000	88.31	23.794
	S2	1000–2000	10.51	2.803
	S3	2000–3000	1.11	296
	N	>3000	0.07	18
Distance from rivers (m)	S1	<500	72.4	19.309
	S2	500–1000	20.76	5536
	S3	1000–1500	4.66	1.242
	N	>1500	2.18	581
Elevation (meters)	S1	12.5–62.5	76.93	20,517
	S2	62.5–137.5	17.14	4571
	S3	137.5–212.5	4.14	1104
	N	212.5–337.5	1.79	477
Soil type	S1	Latosol	37.93	10,115
	S2	Podzolic	21.36	5698
	S3	Regosol	20.48	5462
	N	Alluvial hydromorphic	20.23	5395
NDVI	S1	Vegetation	10.06	1829
	S2	Rice field	13.83	2514
	S3	Forest	43.94	7986
	N	Water body settlements	32.16	5845

The study results are fully dependent on the applied AHP evaluation, how the criteria were defined, and how the criteria were measured. The structured interviews were performed with relevant professionals who were working for the cassava production in Indonesia for more than 10 years. Through this process, the CR was calculated and used in the land suitability analysis. The total suitability score (S_i) of each land unit was calculated using the following expression:

$$S_i = \sum_{i=1}^{n} W_i \times R_i \tag{4.2}$$

Analytical Hierarchy Process (AHP)

Weights were used to determine the priorities of criteria (land cover, distance from rivers, rainfall levels, distance from roads, slope angles, elevation levels, soil types, and vegetation index data) and to identify the suitability of different land uses for cassava production. The resultant AHP weights were used to determine the priority of each criterion for weighted overlay applications using GIS.

In the first stage of the analysis, we organized elements of the decision model into a hierarchy that included first level (goal), second level (criteria), and third level (alternative) elements. The first level involved selecting the best goal. The second level of the hierarchy considered rules or criteria associated with the goal. The lowest level considered alternative decisions (Fig. 4.5).

The second phase involved scoring the criteria via pairwise comparisons and scoring scales of relative importance (Table 4.3). Questionnaires were used to gather expert opinions on the relative importance of the considered criteria and factors. Comparative results (for each factor pair) were described as integer values of 1 (equal value) to 9 (extremely different), where a higher number denotes that the
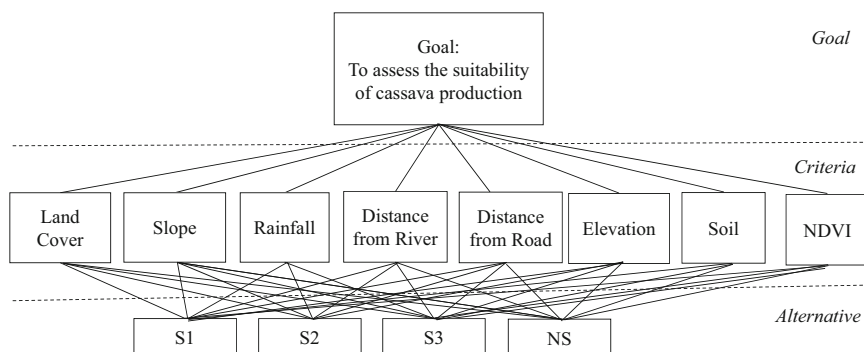
Fig. 4.5 The AHP framework to select suitable areas for cassava production

Table 4.3 Preference scale for AHP pairwise comparison (Saaty 1989)

Scale	Degree of preference	Explanation
1	Equal importance	Two activities contribute equally to the objective
3	Moderate importance	Experience and judgments slightly favor one activity over another
5	Strong or essential importance	Experience and judgments strongly favor one activity over another
7	Very strong importance	An activity is favored very strongly over another
9	Extreme importance	The evidence favoring one activity over another is the highest possible order of affirmation
2, 4, 6, 8	Intermediate values between two adjacent judgments	When compromise is needed
Reciprocals	Opposites	Used for inverse comparisons

Table 4.4 Pairwise comparison for the AHP model among the criteria selected for cassava production

	Soil	Land cover	Elevation	Slope	Rainfall	Distances from roads	River	NDVI
Soil	1	3	5	5	7	9	9	3
Land cover	0.33	1	3	3	7	7	9	1
Elevation	0.2	0.3	1	1	3	5	7	0.3
Slope	0.2	0.3	1	1	3	3	5	0.3
Rainfall	0.14	0.14	0.33	0.33	1	3	3	0.14
Distance from roads	0.11	0.14	0.2	0.33	0.33	1	1	0.14
Distance from rivers	0.11	0.11	0.14	0.2	0.33	1	1	0.11
NDVI	0.33	1	3	3	7	7	9	1

chosen factor was considered to be more important than other factors to which it was compared. For example, when comparing land cover and slope angle criteria, a score of 1 indicates that both were equally relevant to evaluating suitability, and a score of 9 indicates that land cover is more important than the slope angle. All scores were assembled in a pairwise comparison matrix with diagonal and reciprocal scores located in the lower left-hand triangle. Reciprocal values (1/3, 1/5, 1/7, and 1/9) were used where the row criterion was found to be less important than the column criterion (Table 4.4).

Third, we calculated the matrix and ensured the consistency of the pairwise comparison criteria. The AHP also provided measurements for calculating normalized values of each criterion and alternatives and for determining the normalized principal Eigenfactors and priority vectors. The pairwise matrix was calculated and is given by the following expression:

$$
\begin{bmatrix}
C_{11} & C_{12} & \cdots & C_{1n} \\
C_{21} & C_{22} & \cdots & C_{2n} \\
\cdot & \cdot & \cdot & \cdot \\
\cdot & \cdot & \cdot & \cdot \\
C_{n1} & C_{n2} & \cdot & C_{nn}
\end{bmatrix}
\tag{4.3}
$$

The sum of each column of the pairwise matrix was denoted as follows:

$$
C_{ij} = \sum_{i=1}^{n} C_{ij}
\tag{4.4}
$$

We then divided each element of the matrix by its column total to generate a normalized pairwise matrix:

$$X_{ij} = \frac{C_{ij}}{\sum\limits_{i=1}^{n} C_{ij}} = \begin{bmatrix} X_{11} & X_{12} & \ldots & X_{1n} \\ X_{21} & X_{22} & \ldots & X_{2n} \\ \cdot & \cdot & \cdot & \cdot \\ \cdot & \cdot & \cdot & \cdot \\ X_{n1} & X_{n2} & \cdot & X_{nn} \end{bmatrix} \tag{4.5}$$

Finally, we divided the sum of the normalized matrix column by the number of criteria used (n) to generate the weighted matrix of priority criteria:

$$W_{ij} = \frac{\sum\limits_{j=1}^{n} X_{ij}}{n} = \begin{bmatrix} W_{11} \\ W_{12} \\ \cdot \\ \cdot \\ W_{1n} \end{bmatrix} \tag{4.6}$$

The initial consistency vectors were derived by multiplying the pairwise matrix by the vector of weights:

$$\begin{bmatrix} C_{11} & C_{12} & \cdots & C_{1n} \\ C_{21} & C_{22} & \cdots & C_{2n} \\ \cdot & \cdot & \cdot & \cdot \\ \cdot & \cdot & \cdot & \cdot \\ C_{n1} & C_{n2} & \cdot & C_{nn} \end{bmatrix} \times \begin{bmatrix} W_{11} \\ W_{12} \\ \cdot \\ \cdot \\ W_{1n} \end{bmatrix} = \begin{bmatrix} C_{11}W_{11}+ & C_{12}W_{11}+ & \cdots & +C_{13}W_{11} \\ C_{21}W_{12}+ & C_{22}W_{12}+ & \cdots & +C_{23}W_{12} \\ \cdot & \cdot & \cdot & \cdot \\ \cdot & \cdot & \cdot & \cdot \\ C_{n1}W_{1n} & C_{n1}W_{1n} & \cdot & C_{n1}W_{1n} \end{bmatrix}$$

$$= \begin{bmatrix} V_{11} \\ V_{12} \\ \cdot \\ \cdot \\ V_{1n} \end{bmatrix} \tag{4.7}$$

The principal eigenvector ($\lambda_{\max}$) was then calculated by averaging the values of the consistency vector:

$$\lambda_{\max} = \sum_{i}^{n} \mathrm{CV}_{ij} \tag{4.8}$$

Eigenvalues were calculated by averaging the rows of each matrix. Eigenvalues were also referred to as relative weights. The largest eigenvalue was equal to the number of criteria, and when $\lambda_{\max} = n$, judgments were consistent. Normalized eigenvalues were generated as weights of priority criteria. The principal value

suggests that eight criteria were consistent, as the calculation results reveal a maximum value of 8.34 (Table 4.5). The judgments were also checked to determine the consistency index (CI), which was calculated as:

$$CI = \frac{\lambda_{\max} - n}{n - 1} \qquad (4.9)$$

Here, n is the total number of criteria. Saaty (1989) also introduced the *consistency ratio (CR)* and compared it to the consistency index and the random index (RI) value, which is the calculated value for matrices of different sizes (Table 4.6). The consistency ratio was calculated as:

$$CR = \frac{CI}{RI} \qquad (4.10)$$

A lower CR ratio indicates a higher degree of consistency. For further confirmation and understanding about weight and influence among the criteria, ANP is also employed in this research.

Analytical Network Process (ANP)

ANP is an extension of the AHP and proposed by Saaty (1990). ANP is a nonlinear structure with bilateral relationships (Azizi et al. 2014). In this research, ANP was used to obtain the weight of the criteria to compare with the weight from AHP. In the ANP analysis, first, the construction of a conceptual model was developed to determine relationships among the criteria and alternatives. If no relationship exists among the criteria, then there is influence among the criteria and alternatives. The criteria were compared pairwise by Super Decisions® software to form an unweighted super matrix. Then, the priorities derived from pairwise comparison matrices were entered as parts of the columns referred as the evaluation matrix U for criteria (C1, C2, C3, C4, C5, C6, C7, C8) and alternatives (A1, A2, A3, A4). The evaluation matrix for the criteria can be expressed as follows:

$$U = \begin{bmatrix} U_{11} & U_{12} & \cdots & U_{18} \\ U_{21} & U_{22} & \cdots & U_{28} \\ \cdot & \cdot & \cdot & \cdot \\ \cdot & \cdot & \cdot & \cdot \\ U_{41} & U_{42} & \cdot & U_{48} \end{bmatrix} \qquad (4.11)$$

In contrast, the evaluation matrix V in which alternatives (A1, A2, A3, A4) are evaluating according to the criteria (C1, C1, C3, C4, C5, C6, C7, C8) is expressed as follows:

Table 4.5 Normalized matrix for the criteria selected for cassava production

	Soil	Land cover	Elevation	Slope	Rainfall	Distance from roads	Distance from rivers	NDVI	Total	Average	Consistency measure
Soil	0.413	0.500	0.365	0.360	0.244	0.25	0.204	0.500	2.840	0.355	8.649
Land cover	0.136	0.166	0.219	0.216	0.244	0.194	0.204	0.166	1.549	0.193	8.621
Elevation	0.082	0.050	0.073	0.072	0.104	0.138	0.159	0.050	0.730	0.091	8.238
Slope	0.082	0.050	0.073	0.072	0.104	0.083	0.113	0.050	0.629	0.078	8.411
Rainfall	0.057	0.023	0.024	0.023	0.034	0.083	0.068	0.023	0.338	0.042	7.977
Distance from roads	0.045	0.023	0.014	0.023	0.011	0.027	0.022	0.023	0.192	0.024	8.167
Distance from rivers	0.045	0.018	0.010	0.014	0.011	0.027	0.022	0.018	0.168	0.021	8.023
NDVI	0.136	0.166	0.219	0.216	0.244	0.194	0.204	0.166	1.549	0.193	8.621

Table 4.6 Random Consistency Index (RI) to determine consistency ratio (CR) (Saaty 1989)

N	1	2	3	4	5	6	7	8	9	10
RI	0	0	0.58	0.9	1.12	1.24	1.32	1.41	1.45	1.49

$$V = \begin{matrix} V_{11} & V_{12} & V_{13} & V_{14} \\ V_{21} & V_{22} & V_{23} & V_{24} \\ \cdot & \cdot & \cdot & \cdot \\ \cdot & \cdot & \cdot & \cdot \\ V_{81} & V_{82} & V_{83} & V_{81} \end{matrix} \tag{4.12}$$

Then, the weighted super matrix is expressed as a function of the evaluation matrices U and V. The super matrix S should be a probability matrix and irreducible. The weighted super matrix can be expressed as follows:

$$S_{\text{weighted}} \begin{bmatrix} 0 & U \\ V & 0 \end{bmatrix} = \begin{bmatrix} A_1 \\ \vdots \\ A_4 \\ C_1 \\ \vdots \\ C_8 \end{bmatrix} \begin{bmatrix} A_1 & \cdots & A_4 & C_1 & \cdots & C_8 \\ 0 & \cdots & 0 & U_{11} & \cdots & U_{18} \\ \vdots & \ddots & \vdots & \vdots & \ddots & \vdots \\ 0 & \cdots & 0 & U_{41} & \cdots & U_{48} \\ V_{11} & \cdots & V_{14} & 0 & \cdots & 0 \\ \vdots & \ddots & \vdots & \vdots & \ddots & \vdots \\ V_{81} & \cdots & V_{84} & 0 & \cdots & 0 \end{bmatrix} \tag{4.13}$$

After that, limit super matrix is obtained by raising the weighted super matrix to powers by multiplying the matrix itself (Table 4.8). The limit super matrix can be expressed as follows:

$$S_{\text{limited}} = \lim_{n \to \infty} S_{\text{weighted}} \tag{4.14}$$

Examples of weighted super matrix and limit super matrix are given to show the relations among the criteria and alternatives for one expert opinion (Tables 4.7 and 4.8). At the end, the weighted overlay approach was used for applying a weight priority of the criteria to generate a land suitability map for cassava production in the GIS environment.

GIS Analysis

Suitability assessment criteria were used as the reclassified raster data layers for land cover, slope angles, elevation levels, soil types, rainfall levels, distance from rivers, distance from roads, and the vegetation index. All of the reclassified raster data were combined with weighted overlay tools. This reclassification was used to simplify or

Table 4.7 The weighted super matrix for ANP analysis

		Alternatives				Criteria							
		N	S1	S2	S3	Elevation	LULC	NDVI	Rainfall	River	Road	Slope	Soil
Alternatives	N	0.000	0.000	0.000	0.000	0.055	0.055	0.055	0.055	0.055	0.055	0.055	0.055
	S1	0.000	0.000	0.000	0.000	0.565	0.565	0.565	0.565	0.565	0.565	0.565	0.565
	S2	0.000	0.000	0.000	0.000	0.262	0.262	0.262	0.262	0.262	0.262	0.262	0.262
	S3	0.000	0.000	0.000	0.000	0.118	0.118	0.118	0.118	0.118	0.118	0.118	0.118
Criteria	Elevation	0.089	0.090	0.089	0.089	0.000	0.000	0.000	0.000	0.000	0.000	0.000	0.000
	LULC	0.194	0.194	0.194	0.194	0.000	0.000	0.000	0.000	0.000	0.000	0.000	0.000
	NDVI	0.194	0.194	0.194	0.194	0.000	0.000	0.000	0.000	0.000	0.000	0.000	0.000
	Rainfall	0.040	0.035	0.040	0.040	0.000	0.000	0.000	0.000	0.000	0.000	0.000	0.000
	River	0.020	0.023	0.020	0.020	0.000	0.000	0.000	0.000	0.000	0.000	0.000	0.000
	Road	0.023	0.024	0.023	0.023	0.000	0.000	0.000	0.000	0.000	0.000	0.000	0.000
	Slope	0.078	0.079	0.078	0.078	0.000	0.000	0.000	0.000	0.000	0.000	0.000	0.000
	Soil	0.361	0.361	0.361	0.361	0.000	0.000	0.000	0.000	0.000	0.000	0.000	0.000

Table 4.8 The limited super matrix for ANP analysis

		Alternatives				Criteria							
		N	S1	S2	S3	Elevation	LULC	NDVI	Rainfall	River	Road	Slope	Soil
Alternatives	N	0.028	0.028	0.028	0.028	0.028	0.028	0.028	0.028	0.028	0.028	0.028	0.028
	S1	0.283	0.283	0.283	0.283	0.283	0.283	0.283	0.283	0.283	0.283	0.283	0.283
	S2	0.131	0.131	0.131	0.131	0.131	0.131	0.131	0.131	0.131	0.131	0.131	0.131
	S3	0.059	0.059	0.059	0.059	0.059	0.059	0.059	0.059	0.059	0.059	0.059	0.059
Criteria	Elevation	0.045	0.045	0.045	0.045	0.045	0.045	0.045	0.045	0.045	0.045	0.045	0.045
	LULC	0.097	0.097	0.097	0.097	0.097	0.097	0.097	0.097	0.097	0.097	0.097	0.097
	NDVI	0.097	0.097	0.097	0.097	0.097	0.097	0.097	0.097	0.097	0.097	0.097	0.097
	Rainfall	0.018	0.018	0.018	0.018	0.018	0.018	0.018	0.018	0.018	0.018	0.018	0.018
	River	0.011	0.011	0.011	0.011	0.011	0.011	0.011	0.011	0.011	0.011	0.011	0.011
	Road	0.012	0.012	0.012	0.012	0.012	0.012	0.012	0.012	0.012	0.012	0.012	0.012
	Slope	0.039	0.039	0.039	0.039	0.039	0.039	0.039	0.039	0.039	0.039	0.039	0.039
	Soil	0.181	0.181	0.181	0.181	0.181	0.181	0.181	0.181	0.181	0.181	0.181	0.181

change our interpretation of raster data by changing a single value to a new value or by grouping ranges of values into single values. Each criteria source map was reclassified into four classifications. The classification used the following suitability classes: highly suitable (S1), moderately suitable (S2), marginally suitable (S3), and not suitable (N). Spatial data were converted into raster layers and were then processed in ArcGIS® (ESRI, USA). They were then classified into four classes as integer rasters that represented different suitability levels based on the assigned threshold values (Tienwong et al. 2009). Weighted overlays are overlay analysis tools used to identify the best or most preferable locations for cassava production. The criteria included in the weighted overlay analysis were not equal in importance. The weights of key criteria were calculated using the AHP/ANP application. Using the reclassification and weighted overlay method, a spatial analysis was conducted, and a suitability map for cassava production was created (Eckert and Shetty 2011; Gatrell et al. 2011).

4.2.6 Ground Truth Information and Field Survey

Primary data were collected through questionnaires, interviews, and surveys. GPS data and field survey for cassava production locations were collected in November 2016. Ground references were collected to determine the locations of cassava fields located in the highly suitable areas of Serang to check the accuracy of the model.

4.2.7 Sustainability Evaluation

Several indicators and frameworks are commonly used for sustainability evaluation (Ahamed et al. 2015; Von Wiren-Lehr 2001). In this study, we focused on pillars of agroecological sustainability indicators that are related to ecological, social, and economic factors and are associated with several criteria, such as availability, accessibility, affordability, and profitability. The criteria were considered to evaluate the sustainability of cassava production between 2010 and 2015 (Fig. 4.6).

4.3 Results

In the GIS analysis, the reclassified rasters were used with AHP and ANP weights and ranked accordingly. The CR was the indicator of judgments to refer to the AHP weight, whether consistent or not. All the CR value was less than 10% which is acceptable for AHP analysis. Among the eight sub-criteria identified, the AHP application ranked soil type as the first priority (34%) followed by land cover (18%), the vegetation index (16%), rainfall (11%), elevation level (8%), slope
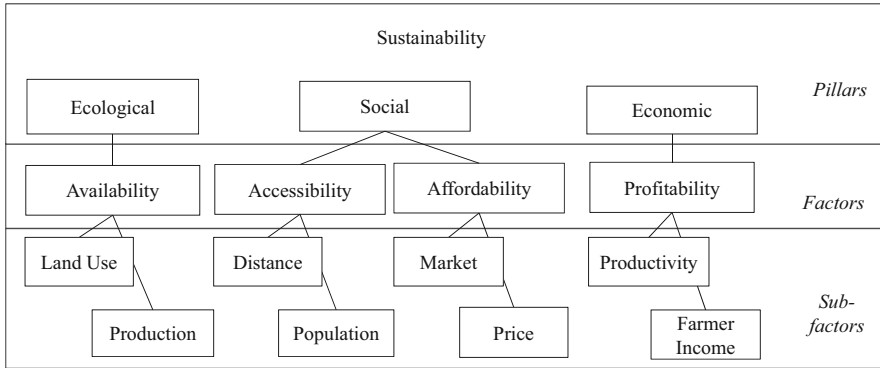
Fig. 4.6   Criteria of sustainability evaluation

(7%), distance from roads (3%), and distance from rivers (3%) when selecting suitable lands for cassava (Table 4.9). The ANP model also included a consistency test and observed 6.3%, which was also less than 10% to assess the degree of consistency of the experts. The ANP application ranked soil as the first priority (36%) followed by land cover (18%), the vegetation index (14%), rainfall (11%), elevation (8%), slope (6%), distance from rivers (4%), and distance from roads (3%) (Table 4.9).

The weighted overlay was used for applying a weight priority of the criteria to generate the land suitability map for cassava production. The reclassified raster data layers of land cover, slope angles, elevation levels, soil types, rainfall, distance from rivers, distance from roads, and the vegetation index were combined with weighted overlay tools and AHP/ANP weights to generate suitability map (Fig. 4.7). A suitability map for cassava production was created from a weighted overlay, and we found in the AHP analysis that 41.60% (11,094 ha) of the study area was highly suitable for cassava production, 30.87% (8233 ha) was moderately suitable, and 9.83% (2623 ha) was marginally suitable. Whereas the result of ANP analysis found that 44.62% (11,901 ha) of the study area was highly suitable for cassava production, 27.17% (7246 ha) was moderately suitable, and 10.51% (2803 ha) was marginally suitable. Additionally, the same result of AHP and ANP shows 17.69% (4718 ha) of the land area was found occupied by residences and settlements (Fig. 4.7 and Table 4.10). Highly suitable areas for cassava production covered 41.60% (11,094 ha) of the total area of Serang city. These areas were mainly dry lands with moderately well-drained soils. Soils in this group were loamy with topsoil that was leveled and bounded for paddy rice. There is high possibility to use this area for growing casava after draining to avoid waterlogging. The moderately suitable area covered 30.87% (8233 ha) of the total area of Serang. These areas were poorly drained and coarsely textured with alluvial terraces. Marginally suitable areas for cassava production cannot support cassava plantations. Only 9.83% (2623 ha) of the land area was categorized as marginally suitable. Deep and coarsely textured soils positioned on slopes of less than 20% of the mentioned areas. Soil fertility levels were moderately low. Upland crops and fruit trees are often found with low levels of
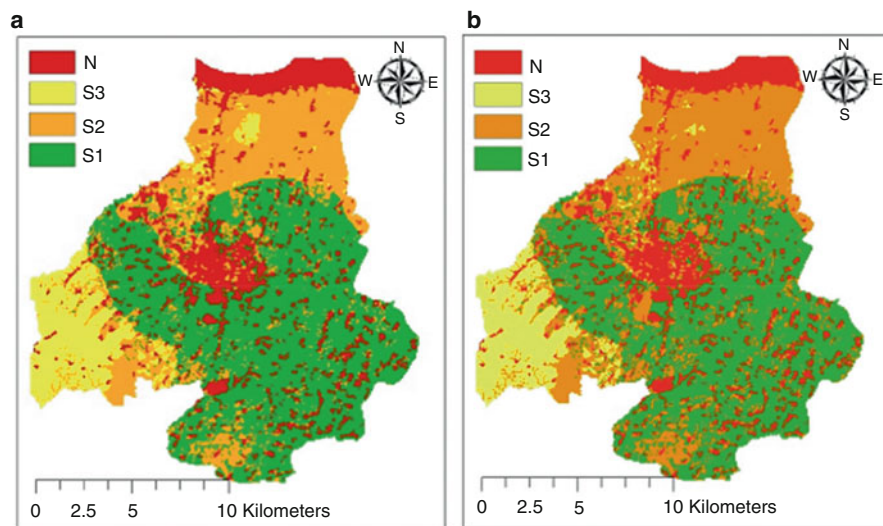
Table 4.9 Priority criteria weights according to expert's opinions for selecting land suitability in cassava production

	Weights of criterion											
	Experts initials											
	(Experience of experts, years)											
	Expert A		Expert B		Expert C		Expert D		Expert E		Mean	
	(11 years)		(10 years)		(20 years)		(21 years)		(15 years)			
Criterion names	AHP	ANP	AHP	ANP	AHP	ANP	AHP	ANP	AHP	ANP	AHP	ANP
Soil	0.356	0.387	0.408	0.436	0.339	0.345	0.355	0.361	0.244	0.246	0.340	0.355
LULC	0.214	0.223	0.181	0.175	0.198	0.198	0.194	0.194	0.102	0.100	0.178	0.178
NDVI	0.184	0.156	0.170	0.165	0.198	0.198	0.194	0.089	0.067	0.064	0.162	0.134
Elevation	0.109	0.100	0.085	0.069	0.099	0.096	0.091	0.089	0.034	0.032	0.083	0.077
Slope	0.074	0.059	0.072	0.037	0.080	0.080	0.079	0.079	0.038	0.039	0.069	0.059
Rainfall	0.031	0.036	0.042	0.022	0.043	0.040	0.042	0.037	0.398	0.407	0.111	0.108
Road	0.014	0.022	0.023	0.019	0.024	0.023	0.024	0.024	0.054	0.052	0.028	0.028
River	0.020	0.017	0.021	0.078	0.021	0.020	0.021	0.022	0.063	0.061	0.029	0.040
CR	0.080	0.080	0.058	0.065	0.033	0.039	0.043	0.040	0.091	0.091		

Fig. 4.7 (a, b) Land suitability distribution using weighted overlay

Table 4.10 Suitable area for cassava production

	AHP		ANP	
Suitability class	Area (%)	Area (ha)	Area (%)	Area (ha)
Highly suitable	41.60	11,094	44.62	11,901
Moderately suitable	30.87	8233	27.17	7246
Marginally suitable	9.83	2623	10.51	2803
Not suitable	17.69	4718	17.69	4718

fertility, a lack of water during dry seasons, soil erosion on steep slopes, and high levels of acidity in some areas.

The 4718-ha (17.69%) area of land that was classified as unsuitable for cassava production due to the presence of settlements and residences cannot be replaced with cassava fields. This area included the coastal area in the northern part of Serang and is characterized by sandy soils with high mineral contents. Although cassava can grow under high nitrogen (N), potassium (K), and organic matter (OM) application conditions, to obtain high-quality yields, appropriate management strategies must be applied to boost cassava production in coastal areas. The weighted overlay map used to locate suitable cassava production areas could serve as a reference map for predicting production methods that could support measures to increase local food production in the city of Serang. According to the GPS locations for cassava production recorded in November 2016, most cassava-growing areas were concentrated in the southern part of the region (Fig. 4.8).

In the sustainability evaluation, several sub-criteria (e.g., land use, production, population, distance, market, price, productivity, and income) were considered.
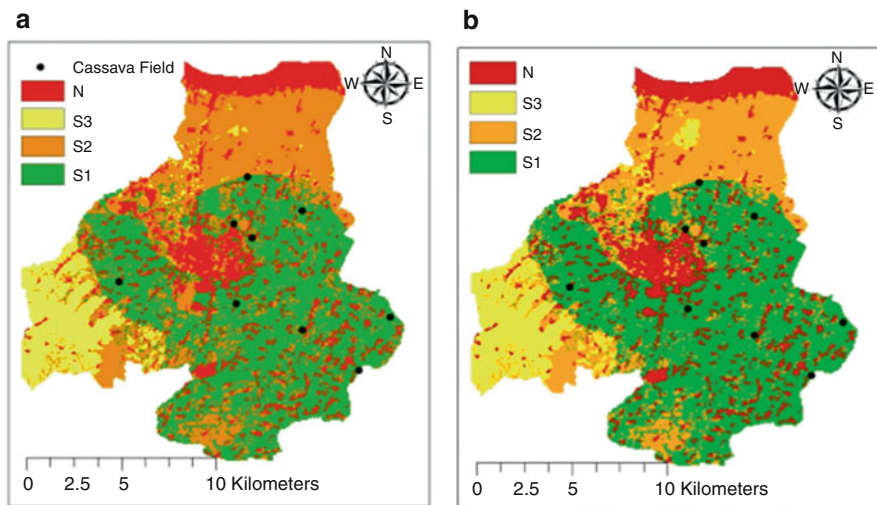
Fig. 4.8 (**a**, **b**) Validation of land suitability analysis using ground reference information

These data were collected from primary and secondary sources. Over the period examined, production and land use were unsustainable due to a shift from agricultural to settlement land use. Although cassava production has been located in the most suitable areas, we found that the land of cassava fields from 2010 to 2015 decreased 3.38% annually based on our collected data (Table 4.11). Furthermore, the NDVI images based on Landsat-4 TM and Landsat-8 OLI showed the vegetation conditions, which reflect the land use change and physical features that cover the Earth's surface (land cover) (Fig. 4.9). Most land in the city of Serang was cultivated land with plantation fields, irrigated paddy fields, and rain-fed areas. Additionally, protected areas were occupied by settlements.

4.4 Discussion

We found that most land areas suitable for cassava production were located in the southern part of Serang in the Banten Province because the soil steepness levels in this area are less than 15%, and this condition could affect soil formation. From the ground truth survey, cassava farmers with fields in this area grow cassava in rotation with other crops to prevent depletion of nutrients from soil. The production of cassava in new areas has faced several barriers, especially regarding labor and the conversion of peatland and forests in agricultural areas. Future yields can be maximized through the implementation of several management practices (e.g., minimum tillage, contour ridging, fertilization, strip cropping, and intercropping

Table 4.11 Agricultural data assessment from 2010 to 2015 (BPS 2017)

Factors	Sub-factors	2010	2011	2012	2013	2014	2015	Trend of change (%)	Annual rate of change (%)
Availability	Land use (ha)	321	253	327	391	211	62	−67.62	−3.38
	Production (ton)	4600	3289	4400	6374	3175	4162	−5.00	−0.24
Accessibility	Population (people)	577,785	598,407	611,897	618,802	631,101	643,205	5.35	0.26
	Road condition (%)	54.87	54.87	54.87	52.25	55.50	53.83	−0.95	−0.04
Affordability	Traditional market (unit)	6	6	6	6	6	6	0	0
	Cassava price (USD/kg)	0.075	0.075	0.075	0.09	0.12	0.12	23.07	1.15
Profitability	Productivity (ton/ha)	14.33	14.52	14.58	15.33	15.03	67.12	64.81	3.24
	Farmer income (USD/kg)	0.036	0.076	0.114	0.152	0.152	0.152	61.70	3.08
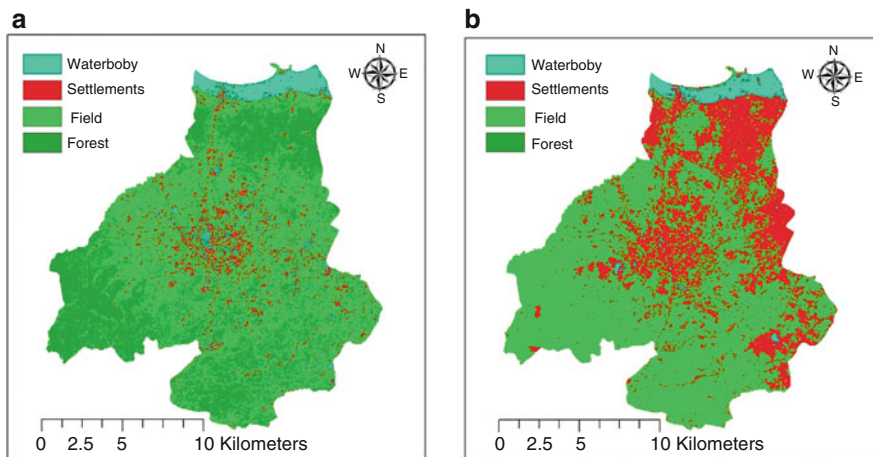
Fig. 4.9 (**a**, **b**) Land use changes in Serang city drawn from Landsat satellite information for 2010 and 2016

with government support and rural appraisals from experts). Our study results illustrate the effectiveness of spatial assessments for evaluating suitable land use for sustainable cassava production. Therefore, geospatial technologies that combine GIS, remote sensing, and AHP could be used to support land suitability assessments of cassava production. Geospatial modeling has limitations in obtaining highly accurate validation results due to a lack of ground reference information of previous years. As such, future studies should integrate several indicators based on high-resolution spatial and temporal remote sensing data.

Furthermore, this empirical method accepted key input from experts through AHP-based questionnaires and structured questionnaire surveys for cassava growers and agricultural officers in the study area, which significantly enhanced the decision-making capabilities of the land use plan. However, the AHP method has limitations in that it employs suitability determinations that can be subject to bias in both the scope and quality of outputs for the variation of weights. We thought of many ways to provide equal weights after fieldwork was conducted extensively in the city of Serang. Inequality usually varies for site-specific cases and crop selection (such as with cassava) in regional contexts. The judgment of pertinent criteria is complicated, and there are preferences of priority among the criteria. In such a case, AHP has the advantage of weighting the criteria based on experts' opinions. However, it is very difficult to judge the subjectivity of decision-making during the modeling stages. To overcome the limitation and influences of criteria, we have also employed ANP for further confirmation of weights. Additionally, consistency ratio was introduced for AHP and ANP to validate the judgment of experts. The consistency ratio indicates the degree of coincidence between the AHP or ANP models and experts' opinions for weighting the criteria in the model. The weights were given to identify the preferences of criteria to analyze in the GIS environment.

In the GIS analysis, weights from AHP and ANP were used to develop the weighted overlay using the criteria. The ground truth information validated the weighted overlay and confirmed the suitable locations of cassava fields in Serang city. Most of the fields were located in the highly suitable areas and some were in the marginally suitable areas. The validation was required to understand spatial variability of cassava production for regional perspective and identify the causes of decreasing production of cassava. Along with spatial variability, socio-economic factors should be included for increasing cassava production.

4.5 Conclusions

This study identified suitable areas to evaluate the sustainability of land use for cassava production using a multi-criteria model integrating with GIS, remote sensing, and AHP. The multi-criteria model for suitability assessment used eight criteria: LULC, rainfall, distance from rivers, slope angle, elevation level, soil type, distance from roads, and NDVI. From these criteria, we found that priority criteria, such as the soil type, LULC, and NDVI, influenced the sustainability of cassava production. All of the criteria were processed through a weighted overlay using AHP to calculate the weights of each criterion. To cut on the bias of AHP, the results also confirmed with the ANP. The land suitability assessment for cassava production indicated that 41.6 and 44.6% of the study area were highly suitable using AHP and ANP, respectively. Furthermore, the sustainability of cassava production was analyzed using several indicators classified into four categories: availability, accessibility, affordability, and profitability. The results show that the land use for cassava cultivation areas declined annually 3.38% between 2010 and 2015. The results obtained from this research are very significant in the decision-making processes to increase the production of cassava in suitable areas of Serang city. The production scenario is one of the most important points for the suitability understanding for increasing regional production of cassava in Indonesia. The model can be further expanded spatially by including a fuzzy approach with AHP and ANP to overcome the limitation of the multi-criteria model.

References

Ahamed T, Noguchi R, Takigawa T, Tian L (2013) Bioproduction engineering: a road map for sustainable agricultural practices. Nova, New York

Ahamed T, Noguchi R, Takigawa T (2015) Sustainability: integrating environment, agriculture and renewable energy for food security. Nova, New York, pp 10–11

Ahmed B (2015) Landslide susceptibility mapping using multi-criteria evaluation techniques in Chittagong metropolitan area, Bangladesh. Landslides 12(6):1077–1095

Akıncı H, Ozalp AY, Turgut B (2013) Agricultural land use suitability analysis using GIS and AHP technique. Comput Electron Agric 97:71–82. https://doi.org/10.1016/j.compag.2013.07.006

Ariningsih E (2018) Cluster-based cassava production improvement in West Java and South Sulawesi provinces. AKP 14(2):125–148

Azizi A, Malekmohammadi B, Jafari HR, Nasiri H, Parsa VA (2014) Land suitability assessment for wind power plant site selection using ANP-DEMATEL in a GIS environment: case study of Ardabil province, Iran. Environ Monit Assess 186(10):6695–6709

Badan Pusat Statistik (BPS) (2014) Statistics Indonesia. Statistics Indonesia, Jakarta. https://www.bps.go.id/publication/2015/11/02/f4bbb65bbc11ad61a75695b3/statistik-pemudaindonesia-2014.html

BPS (2017) Regional statistics Banten Province 2017 Badan Pusat Statistik (the central statistics Agency of Indonesia). BPS, Banten

Brandt P, Kvakic M, Butterbach-Bahl K, Rufifino MC (2015) How to target climate-smart agriculture? Concept and application of the consensus-driven decision support framework "targetCSA". Agr Syst 151:234–245. https://doi.org/10.1016/j.agsy.2015.12.011

Bunruamkaew K, Murayam Y (2011) Site suitability evaluation for ecotourism using GIS & AHP: a case study of Surat Thani province, Thailand. Procedia Soc Behav Sci 21:269–278. https://doi.org/10.1016/j.sbspro.2011.07.024

Campo BVH, Hyman G, Bellotti A (2011) Threats to cassava production: known and potential geographic distribution of four key biotic constraints. Food Secur 3(3):329. https://doi.org/10.1007/s12571-011-0141-4

Ceballos-Silva A, Lopez-Blanco J (2003) Delineation of suitable areas for crops using a multi-criteria evaluation approach and land use/cover mapping: a case study in Central Mexico. Agr Syst 77(2):117–136. https://doi.org/10.1016/S0308-521X(02)00103-8

Devendra C, Thomas D (2002) Smallholder farming systems in Asia. Agr Syst 71(1):17–25. https://doi.org/10.1016/S0308-521X(01)00033-6

Eckert J, Shetty S (2011) Food systems, planning and quantifying access: using GIS to plan for food retail. Appl Geogr 31(4):1216–1223. https://doi.org/10.1016/j.apgeog.2011.01.011

Elhag M (2014) Sensitivity analysis assessment of remotely based vegetation indices to improve water resources management. Environ Dev Sustain 16(6):1209–1222. https://doi.org/10.1007/s10668-014-9522-0

Elsheikh R, Shariff ARBM, Amiri F, Ahmad NB, Balasundram SK, Soom MAM (2013) Agriculture land suitability evaluator (ALSE): a decision and planning support tool for tropical and subtropical crops. Comput Electron Agric 93:98–110. https://doi.org/10.1016/j.compag.2013.02.003

FAO (1976) A framework for land evaluation, 1st edn. FAO, Rome

FAO (2000) Land resources information systems in Asia. World soil resource reports. FAO, Rome

FAO (2013) Save and grow: cassava a guide to sustainable production intensification. FAO, Rome

Feenstra GW (1997) Local food systems and sustainable communities. Am J Altern Agric 12(01):28–36. https://doi.org/10.1017/S0889189300007165

Feizizadeh B, Blaschke T (2014) An uncertainty and sensitivity analysis approach for GIS-based multicriteria landslide susceptibility mapping. Int J Geogr Inf Sci 28(3):610–638

Ferretti V, Pomarico S (2013) An integrated approach for studying the land suitability for ecological corridors through spatial multicriteria evaluations. Environ Dev Sustain 15(3):859–885. https://doi.org/10.1007/s10668-012-9400-6

Gatrell JD, Reid N, Ross P (2011) Local food systems, deserts, and maps: the spatial dynamics and policy implications of food geography. Appl Geogr 31(4):1195–1196. https://doi.org/10.1016/j.apgeog.2011.01.013

Heumann BW, Walsh SJ, McDaniel PM (2011) Assessing the application of a geographic presence-only model for land suitability mapping. Eco Inform 6(5):257–269. https://doi.org/10.1016/j.ecoinf.2011.04.004

Howeler RH (1991) Long-term effect of cassava cultivation on soil productivity. Field Crop Res 26(1):1–18. https://doi.org/10.1016/0378-4290(91)90053-X

Khumaida N, Ardie SW, Sopandie D (2016) Influence of agro-ecology on growth and performance of several potential mutants of cassava. Procedia Environ Sci 33:70–77

Kolawole PO, Agbetoye L, Ogunlowo SA (2010) Sustaining world food security with improved cassava processing technology: the Nigeria experience. Sustainability 2(12):3681–3694. https://doi.org/10.3390/su2123681

Lobell DB, Thau D, Seifert C, Engle E, Little B (2015) A scalable satellite-based crop yield mapper. Remote Sens Environ 164:324–333. https://doi.org/10.1016/j.rse.2015.04.021

Malczewski J (1999) GIS and multicriteria decision analysis. Wiley, New York

Malczewski J (2004) GIS-based land-use suitability analysis: a critical overview. Prog Plan 62(1):3–65

Malczewski J (2006) GIS-based multicriteria decision analysis: a survey of the literature. Int J Geogr Inf Sci 20(7):703–726. https://doi.org/10.1080/13658810600661508

Misra G, Cawkwell F, Wingler A (2020) Status of phenological research using Sentinel-2 data: a review. Remote Sens (Basel) 12(17):2760.10.3390/rs12172760

Noerwijati K, Budiono R (2015) Yield and yield components evaluation of cassava (Manihot esculenta Crantz) clones in different altitudes. Energy Procedia 65:155–161. https://doi.org/10.1016/j.egypro.2015.01.050

Pramanik MK (2016) Site suitability analysis for agricultural land use of Darjeeling district using AHP and GIS techniques. Model Earth Syst Environ 2(2):56

Purnamasari RA, Noguchi R, Ahamed T (2019) Land suitability assessments for yield prediction of cassava using geospatial fuzzy expert systems and remote sensing. Comput Electron Agric 166:105018. https://doi.org/10.1016/j.compag.2019.105018

Qureshi MRN, Singh RK, Hasan MA (2017) Decision support model to select crop pattern for sustainable agricultural practices using fuzzy MCDM. Environ Dev Sustain 20:641–659. https://doi.org/10.1007/s10668-016-9903-7

Rinner C, Voss S (2013) MCDA4ArcMap–an open-source multi-criteria decision analysis and geovisualization tool for ArcGIS 10. Cartouche Newslett Can Cartogr Assoc 86:12–13

Rouse JW, Haas RH, Schell JA, Deering DW (1973) Monitoring vegetation systems in the Great Plains with ERTS, third ERTS symposium, NASA SP-351 I, pp 309–317

Saaty TL (1989) Group decision making and the AHP. In: Golden BL, Wasil EA, Harker PT (eds) The analytic hierarchy process. Springer, Berlin, Heidelberg

Saaty TL (1990) Decision making for leaders: the analytic hierarchy process for decisions in a complex world. RWS Publications

Smyth AJ, Dumanski J (1993) FESLM: an international framework for evaluating sustainable land management. FAO, Rome, p 76

Sydorovych O, Wossink A (2008) The meaning of agricultural sustainability: evidence from a conjoint choice survey. Agr Syst 98(1):10–20. https://doi.org/10.1016/j.agsy.2008.03.001

Tienwong K, Dasananda S, Navanugraha C (2009) Integration of land evaluation and the analytical hierarchical process method for energy crops in Kanchanaburi, Thailand. ScienceAsia 35:170–177. https://doi.org/10.2306/scienceasia1513-1874.2009.35.170

Tiwari DN, Loof R, Paudyal GN (1991) Environmental–economic decision-making in lowland irrigated agriculture using multi-criteria analysis techniques. Agr Syst 60(2):99–112. https://doi.org/10.1016/S0308-521X(99)00021-9

Von Wiren-Lehr S (2001) Sustainability in agriculture—an evaluation of principal goal-oriented concepts to close the gap between theory and practice. Agric Ecosyst Environ 84(2):115–129. https://doi.org/10.1016/S0167-8809(00)00197-3

Vrieling A, de Beurs KM, Brown ME (2011) Variability of African farming systems from phenological analysis of NDVI time series. Clim Change 109(3–4):455–477. https://doi.org/10.1007/s10584-011-0049-1

Wargiono J, Sudaryanto B (2000) Cassava leaves and forage crops for ruminant feed in the establishment of sustainable cassava farming system in Indonesia. In: National workshop-seminar on sustainable livestock production on local feed resources, pp 496–503. http://ciat-library.ciat.cgiar.org/Articulos_Ciat/proceedings_workshop_02/496.pdf

Widiatmaka W (2016) Integrated use of GIS, AHP and remote sensing in land use planning for tropical high altitude vegetable crops. J Appl Hortic 18:87–99

Zabihi H, Ahmad A, Vogeler I, Said MN, Golmohammadi M, Golein B, Nilashi M (2015) Land suitability procedure for sustainable citrus planning using the application of the analytical network process approach and GIS. Comput Electron Agric 117:114–126. https://doi.org/10.1016/j.compag.2015.07.014

Zolekar RB, Bhagat VS (2015) Multi-criteria land suitability analysis for agriculture in hilly zone: remote sensing and GIS approach. Comput Electron Agric 118:300–321. https://doi.org/10.1016/j.compag.2015.09.016

Chapter 5
Drought Estimation from Vegetation Phenology Analysis of Maize in Indonesia Using Deep Learning Algorithm

Muhammad Iqbal Habibie, Ryozo Noguchi, and Tofael Ahamed

Abstract The goal of this research was to collect visual information at the crop production that can be used for drought estimation. The study was completed to create an automated detection system of drought with high accuracy, low computing cost, and a lightweight deep learning model. Considering the advantages of YOLOv3, it was proposed to detect and localize vegetation phenology analysis under conditions of season in Indonesia. The study was planned to analyze the vegetation phenology to forecast drought during maize production at the central East Java areas of Indonesia. In the study, the vegetation index was utilized to produce the normalized difference vegetation index (NDVI) and normalized difference water index (NDWI) derived from Sentinel-2 to estimate water stress due to drought. According to the NDVI trajectory, the maize planting season was in April 2018, and the harvest was concluded in late August 2018. This study presents a convolutional neural network (CNN)-based you only look once (YOLO) model for detecting drought at the maize growth phases. The drought estimation was validated from the vegetation phenology analysis based on the growing season. The accuracy assessment of the deep learning model reported Intersection of Union (IoU) 83.4%, precision 98%, recall 99%, F1-Score 98%, and mean average precision 96% for the drought-prone areas. The deep learning analysis suggested that the proposed YOLOv3 model can perform robust and accurate detection of drought estimation from vegetation phenology.

Keywords Vegetation phenology · Sentinel 2 · Maize · YOLO · Deep learning

M. I. Habibie
Center of Technology Region Resource Development (PTPSW), Research Organization for the Assessment and Application of Technology, National Research and Innovation Technology (ORPPT-BRIN), Jakarta, Indonesia

R. Noguchi · T. Ahamed (✉)
Faculty of Life and Environmental Sciences, University of Tsukuba, Tsukuba, Ibaraki, Japan
e-mail: tofael.ahamed.gp@u.tsukuba.ac.jp

5.1 Introduction

The future environment would depend on global warming caused by man-made pollution of the past and future and natural environment (IPCC 2015). Climate variability can cause severe dry precipitation and droughts in the affected areas, resulting in natural, economic, and social impacts. Several reports predict that drought is one of the most destructive natural hazards and is becoming more extreme and common due to climate change and variability. Precipitation is a major factor in the cycle of water and energy cycle, and is also an important factor (Gottschalck et al. 2005). Drought was defined for many months or even several years by subaverage rainfall (Dai 2011). Due to the limitations of ground observation with respect to spatial coverage, satellite precipitation data have been developed over the last two decades (Kidd et al. 2003; Joyce et al. 2004; Aonashi et al. 2009). The global satellite mapping of precipitation (GSMaP) was created in 2002 to produce global precipitation high-resolution and high-precision global precipitation products (Ushio et al. 2009). However, there are further uncertainties in the data with unrelated patterns over diverse regions due to the indirect nature of satellite measurements, influenced by inaccuracies in cloud top reflectance, thermal radiation, and infrequent satellite overpasses (AghaKouchak et al. 2009). Patterns of change in vegetation phenology can be defined through a multi-scale study of environmental drivers using two parameters, the first being basic environmental drivers that consistently drive vegetation dynamics from year to year in a given area and phenological used as landscape predictors of variability in vegetation response over time (Kariyeva and van Leeuwen 2011).

Drought and human activities contribute to environmental changes like desertification in semiarid and dry subhumid zones when soil quality deteriorates and bio-productive resources dwindle or disappear (Trenberth 2018). In Indonesia, for example, three harvests per year might be planned in both flooded and perfect rainfed conditions. Indonesia has two seasons: wet and dry, which are the country's irrigation water supplies and drought causes, respectively. Drought is a widespread absence of available or available water, resulting in a scarcity of surface and groundwater for crop production, notably maize. The Central East Java has one of the largest maize crops, which has also been affected by the drought. Drought is caused by a gradual decrease in the amount of rainfall over a long period of time, usually one season or more, but certain climate influences (such as extreme temperatures, strong winds, and comparatively low humidity) also apply to other parts of the world and can greatly exacerbate the extent of the phenomenon (Chang et al. 2018). Drought warnings for farms were issued in one of the examined regencies. There are six types of droughts: meteorological, climatological, atmospheric, agricultural, hydrologic, and water-management droughts (Wilhite and Glantz 1985). According to the weather monitoring system, Central East Java had the greatest impact on drought-prone areas. The vegetation phenology was used to monitor drought regions with Google Earth Engine (GEE) (Venkatappa et al. 2020).

The GEE carriers out remote sensing for the big data analysis and it is a cloud platform that allows the parallel processing of geospatial data at a global scale (Gorelick et al. 2017). The GEE includes climate, weather, and geophysical facilities and ready products like Enhanced Vegetation Index (EVI) and the Normalized Difference Vegetation Index (NDVI) (Tamiminia et al. 2020). GEE is a code editor that is available on the web for data exploration, visualization, and catalogue in Integrated Developed Environment (IDE) platform (Kumar and Mutanga 2018). Thus, the objective of this research was to conduct the drought estimation from vegetation phenology analysis of Maize in Central East Java Indonesia using Deep Learning algorithm. Therefore, the vegetation phenology was utilized and weather for drought periods was predicted during the maize growth season in Indonesia. Then, the vegetation phenology was validated with the assessment of the precipitation data. The validated location was used for the objective of this research.

5.2   Methodology

5.2.1   Study Area

The study was conducted in the Central East Java, which consists of 12 regencies, namely, Gresik, Lamongan, Malang, Mojokerto, Pasuruan, Sidoarjo, Tuban, Batu City, Malang City, Mojokerto City, Pasuruan City, and Surabaya City (Fig. 5.1). The important crops are rice, maize, cassava, and different types of vegetables. The potential markets on the Indonesian island of Java make maize a crop with a bright future. Lands in Indonesia are suitable for intercropping with soybean cultivars and maize production on dryland-upland in East Java, Indonesia (Harsono et al. 2020). Using secondary data, recent research on maize commodities has focused more on the expenses of agricultural income, demand, or supply of maize (Barokah et al.
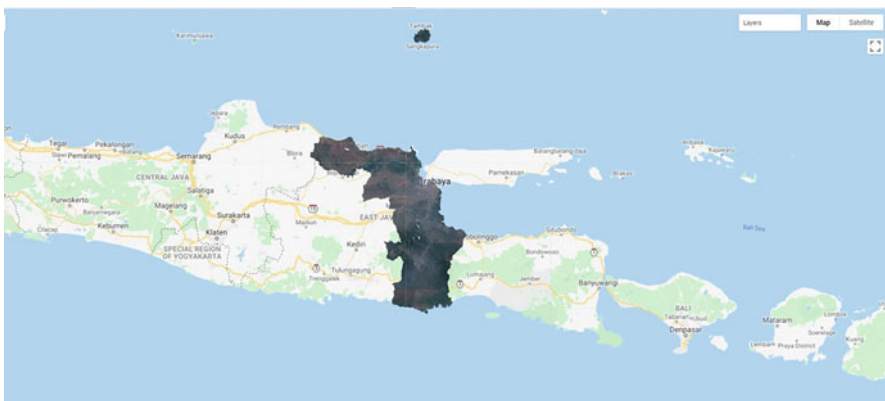
Fig. 5.1   True color view of the study area

2019). Given the importance of maize, considerable measures are required to secure its long-term availability. The supply of water for irrigation was supported from the flow of rivers, which flows from the northern part also traversed by the Surabaya River in the Southern region.

5.2.2 Methodology

The satellite imageries were collected from the Sentinel 2 satellite source and the vegetation phenology Normalized Difference Vegetation Index (NDVI), the Normalized Difference Water Index (NDWI), and land surface temperature (LST) was calculated from the related bands. It was processed with ArcGIS 10.4.1®. The images were evaluated and validated with precipitation datasets. We utilized precipitation datasets to validate for Global Rainfall map (GSMaP, JAXA) with the local rainfall station (Indonesia Meteorology and Climate Agency, BMKG). The drought was reported in 2018, statistics and precipitation datasets were utilized for further analysis of this year (Fig. 5.2).

5.2.3 Vegetation Phenology

Phenology is important to study the vegetative growth cycles. In addition, phenology refers the sensitiveness to climate variability and provides basic information for analyzing trends in ecological processes or climatology, which can detect the impact of climate at the multiple scales regionally. NDVI and NDWI of vegetation indices were separated into two seasons: dry and wet seasons. The wet seasons occur from January to April. On the other hand, the dry seasons occur from June to October 2021. Furthermore, the LST was used as the important factor that is susceptible to climatic fluctuation.
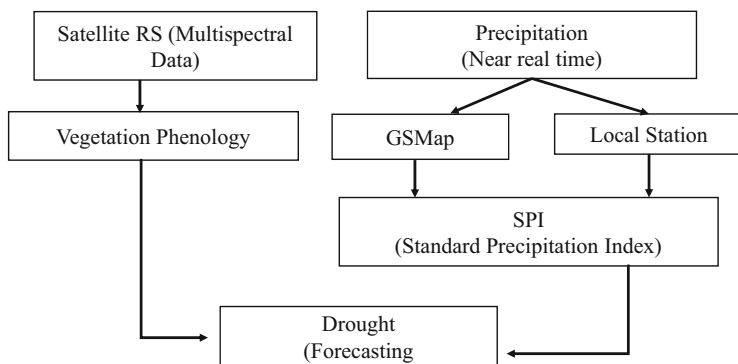
Fig. 5.2 Conceptual framework for forecasting the drought areas in Central East Java

Normalized Difference Vegetation Index (NDVI)

NDVI can be used to examine various aspects of vegetation, such as plant characteristics, production, and the impact of temperature on the plant, visualizing vertical spatial and temporal distributions and horizontal structures such as vegetative cultivation and vegetation biomass (Xue and Su 2017). Vegetation phenology was processed with high computing using Google Earth Engine (GEE). NDVI can be expressed as:

$$\mathrm{NDVI} = \frac{\mathrm{NIR - RED}}{\mathrm{NIR + RED}} \tag{5.1}$$

Because of the index's normalization technique, the range of NDVI values is between 0 and 1, with a sensitive responsiveness to green vegetation even in low vegetation covered locations.

Normalized Difference Water Index (NDWI)

NDWI are widely and effectively used in the detection and mapping of surface water bodies (Özelkan 2020; Sarp and Ozcelik 2017). The index uses remote sensing imagery from the green and Short Wave Infrared (SWIR) bands. It is susceptible to land construction and leads to overestimated water bodies. In combination with the NDVI, the NDVI served to determine the change in the NDWI. NDWI can be formulated as follows (Mcfeeters 2007):

$$\mathrm{NDWI} = \frac{\mathrm{Green - NIR}}{\mathrm{Green + NIR}} \tag{5.2}$$

Land Surface Temperature (LST)

Climate data produced from satellite imaging of land surface temperature (LST) is critical for monitoring and comprehending the consequences of climate change at both the small and big scales (Wongsai et al. 2017). Temperature variation may be explained by evaluating LST, which can be impacted by factors such as elevation, land cover, and the NDVI can be formulated as follows (De Jesus and Santana 2017).

$$\mathrm{LST} = \frac{\mathrm{BT}}{1 + \left(\frac{\lambda \mathrm{BT}^*}{\mathrm{PV}} \ \ln \mathrm{LSE}\right)} \tag{5.3}$$

where BT is the satellite brightness temperature (Celsius), λ is the Top of Atmosphere (ToA) spectral radiance at the sensor's aperture, PV is the proportion vegetation (PV), and LSE is the land surface emissivity.

5.2.4 Assessment of Precipitation Data

Two forms of precipitation data were used in this research: first Global Rainfall Map (GSMaP, JAXA) and second, local station precipitation data (Indonesia Meteorology and Climate Agency, BMKG).

Precipitation Datasets

GSMaP is a microwave radiometer technique that can be used with a precipitation radar algorithm to generate a detail precipitation map with high temporal and geographic precise location (Fig. 5.3).

Regional Precipitation Datasets

Precipitation observation data were collected from the Tuban Regency station. The datasets were accessible and received from the rain gauges to observe the rainfall information from 2016 for precipitation monitoring. In 2018, the Tuban Regency was reported as dry, with the lowest precipitation in May and the highest was in February. During the baseline period, the average trend of precipitation at the Tuban Regency was 13 mm/month. Precipitation in the study region tends to drop from April to September and rises from October to February. The local station rainfall was compared with the worldwide precipitation databases. To validate the data, we use
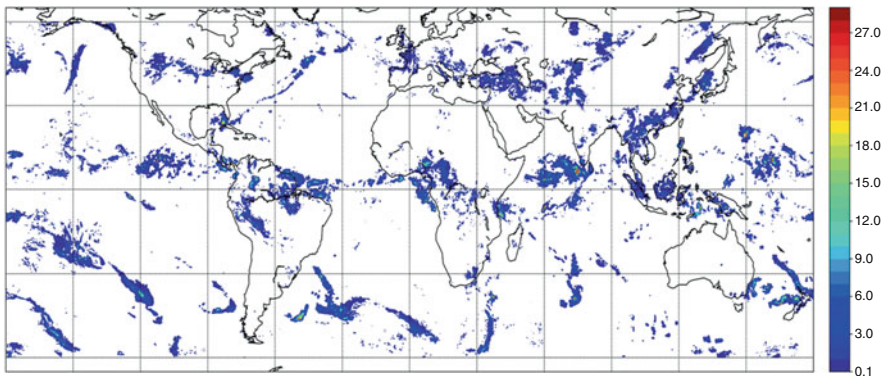
Fig. 5.3 Precipitation on May 2018 using GSMaP, JAXA, Japan

two precipitations data, GSMaP and local station. GSMaP was developed by the JAXA Japan and local station was obtained from the Indonesia Meteorological and Climate agency.

Both precipitations were computed using the Standard Precipitation Index (SPI). The SPI was expressed in the cumulative distribution using gamma function. The gamma distribution (McKee et al. 1993) may be expressed as:

$$G(x_i) = \int_0^{x_i} g(X_i) \mathrm{d}x_i = \frac{1}{\beta^\alpha \Gamma(\alpha)} \int_0^{x_i} t^{\alpha-1} e^{-x_i/\beta} \mathrm{d}x_i \tag{5.4}$$

The symbols α and β denote shape and scale parameters (Alam et al. 2013). Both factors have a value larger than zero, whereas x is the precipitation in millimeters during consecutive months i (selected time scale). The gamma function is denoted by $\Gamma(\alpha)$. If $x_i = 0$ and the cumulative probability encounters this condition, the cumulative gamma distribution is unknown. For each station, the SPI calculation additionally includes a matching density function of the gamma probability to the rainfall frequency distribution.

$$\alpha = \frac{1}{4A}\left(1 + \sqrt{1 + \frac{4A}{3}}\right) \tag{5.5}$$

$$\beta = \frac{x}{\alpha} \tag{5.6}$$

$$A = \ln(x) - \frac{\sum \ln(x)}{n} \tag{5.7}$$

Due to the undefined gamma function, when $x_i = 0$, the value of $G(x_i)$ is as follows:

$$H(x_i) = q + (1 - q) \cdot G(x_i) \tag{5.8}$$

where q represents the probability of zero. The SPI is then calculated by transforming the cumulative probability $H(x_i)$ into the standard normal distribution. To calculate the SPI, the cumulative probability distribution is converted into a normal distribution using the following approximation:

$$z = \mathrm{SPI} = -\left(t - \frac{c_0 + c_1 t + c_2 t^2}{1 + d_1 t + d_2 t^2 + d_3 t^3}\right), \quad t = \sqrt{\ln\left(\frac{1}{(H(x))^2}\right)} \tag{5.9}$$

when $0 < H(x) < 0.5$, the following is true:

$$z = \text{SPI} = + \left(t - \frac{c_0 + c_1 t + c_2 t^2}{1 + d_1 t + d_2 t^2 + d_3 t^3} \right), \quad t = \sqrt{\ln \left(\frac{1}{1 - (H(x))^2} \right)} \quad (5.10)$$

when $0.5 < H(x) < 1.0$ and $c_0 = 2.515517$, $c_1 = 0.802853$, $c_2 = 0.010328$, $d_1 = 1.432788$, $d_2 = 0.189269$, $d_3 = 0.001308$.

According to World Meteorological Organization (WMO), 3-month SPI is more effective in highlighting the humidity in agricultural areas (World Meteorological Organization 2012). SPI based on 3 months provides a comparison of precipitation in 3-month period with a total precipitation in 1 year including in long-term historical data. We utilized a 3-month SPI for this analysis to compare with the vegetation phenology for the drought-prone areas.

5.2.5 Deep Learning

The creation of artificial neural networks using machine learning was further extended in the sample areas sufficiently to apply the deep learning training, validation, and testing of sampling areas (Fig. 5.4).

Training Dataset with Labels

The availability of using high resolution imagery is an opportunity to characterize and identify the water objects used as indices of drought stress. Therefore, the NDWI indices were utilized as the training dataset. The training dataset due to the precision led to a need of new image analysis methods using region-based (or object-based) approaches. The training dataset were labeled using LabelImg®. It is developed in
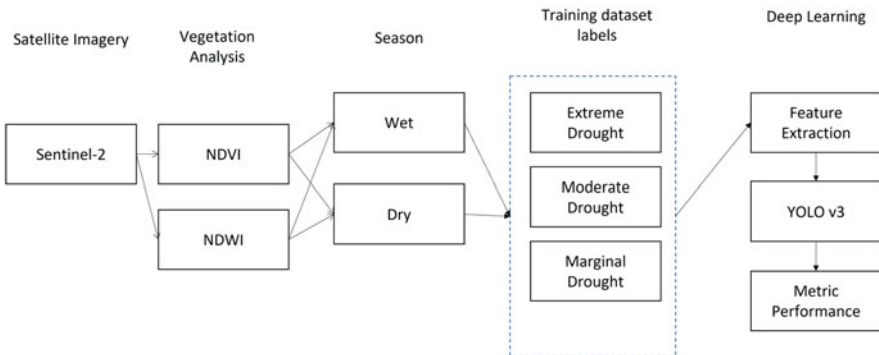
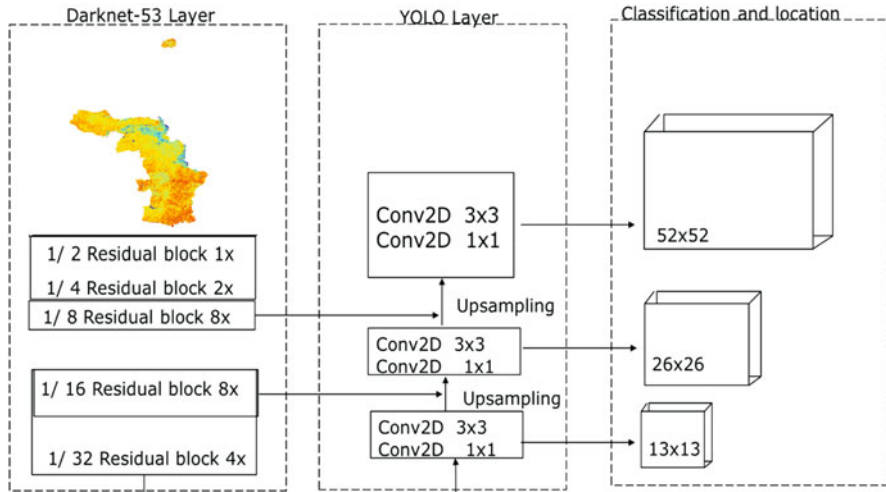**Fig. 5.4** Deep learning process to categorize drought severity using vegetation indices

Fig. 5.5 Schematic of YOLOv3 Network Architecture

Python and use Qt for its graphical user interface. ImageNet stores annotations in XML files in the Pascal VOC format, and it also supports the YOLO format in text files.

You Only Look Once (YOLO)

The YOLO series algorithms are originally target recognition methods based on regression proposed by Redmon and Farhadi (2017). By 2018, YOLO has evolved into its third version, YOLOv3, which has a fast speed detection and good detection precision for small and dense objects. YOLOv3 is now the state of the art for one stage object detection (Redmon and Farhadi 2018). On a standard computer with a graphics processing unit (GPU), YOLOv3 can effectively achieve real-time performance (Fig. 5.5).

5.3   Results and Discussion

5.3.1   Vegetation Phenology Analysis

The vegetation indices are referred to inform the status of maize during the growing seasons. For NDVI, the growing season was scheduled for April and late August 2018 (Figs. 5.6 and 5.7). Other indices, NDWI, discovered in April 2018, indicated that planting time for maize and growing season was dry (Fig. 5.8). As well, LST was high in the mid and southern part of the Central East Java, Indonesia (Fig. 5.9).
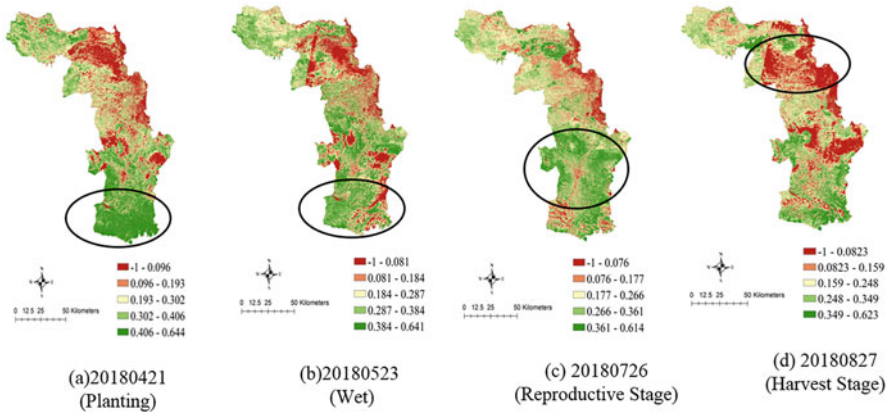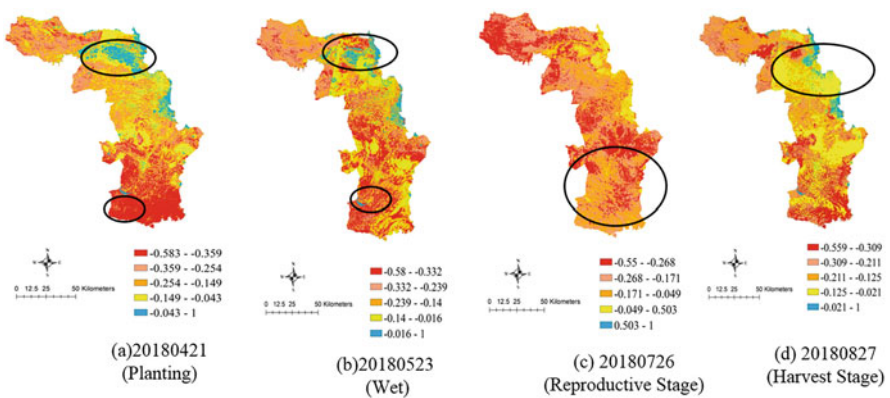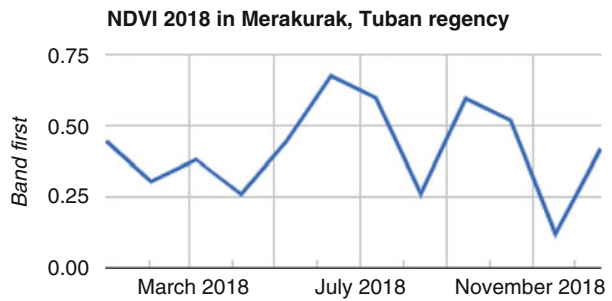
Fig. 5.6 NDVI during growing season in Central East Java, left to right (**a**) Planting, (**b**) Wet, (**c**) Reproductive stage, (**d**) Harvest stage

Fig. 5.7 Vegetation phenology NDVI

Fig. 5.8 NDWI during growing season in Central East Java, left to right (**a**) Planting, (**b**) Wet, (**c**) Reproductive stage, (**d**) Harvest stage
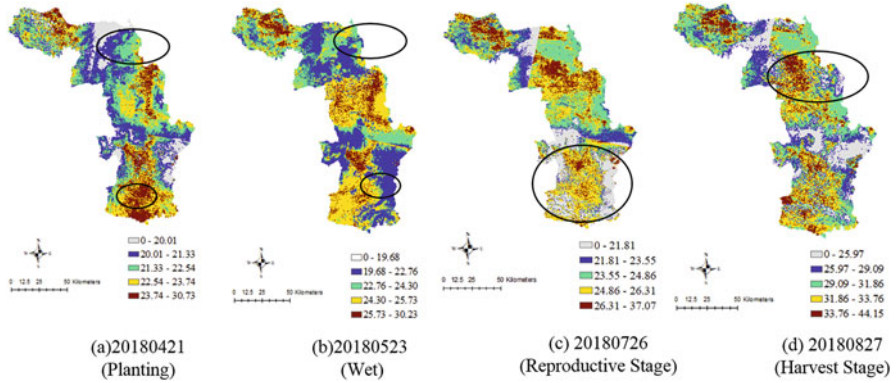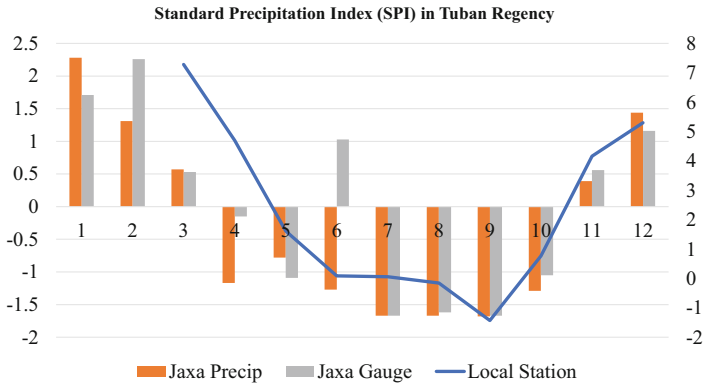
Fig. 5.9 LST during growing season in Central East Java, left to right (**a**) Planting, (**b**) Wet, (**c**) Reproductive stage, (**d**) Harvest stage

Fig. 5.10 One of the reference station in Tuban regency was compared using GSMaP, Jaxa, and local station (BMKG)

5.3.2 Validation Data

The drought indicator SPI was calculated from the precipitation information of the global rainfall map (GSMaP, JAXA) and local stations from the study area (Fig. 5.10). From the precipitation record of 2018, the SPI data was referred as SPI-1 for the short term to analyze drought information. The data from six local stations were analyzed to understand the drought indicators. Based on SPI results, drought occurred between April and October 2018. The value of SPI was between -1.21 and -1.34 during this period. The SPI index declined in September and expanded increase in October.

5.3.3 Deep Learning

Metric to Measure YOLO Performance

YOLOv3 were trained using the images of two datasets based on NDVI and NDWI. Extreme drought, moderate drought, and marginal drought were the three categories of satellite images. The information from the categorized classes was then recovered using feature extraction with Darknet 53 in convolutional layers and turned into YOLO for object detection (Table 5.1). Table 5.1 shows the performance metrics obtained with the YOLOv3 model, which trained using the two different datasets and both compared with each other. It can be noticed that the extreme drought was less than the other classes, and by the object detection, it shows that this region had moderate drought about 62%.

Perfomance Metrics in YOLO

The validation detection can represent an overfitting, such that a different collection of 160 annotated images were used for testing. The testing was processed in a high-performance and produced the performance metrics affirm that overfit was reduced at iteration 6000 (Table 5.2).

Precision and recall has a high value of 0.98 and 0.99, which means that the total positive detections are true positive detections and ground truth objects. The drought object detection may be obtained.

Table 5.1 Metric to Measure YOLO Performance NDWI

Class ID	Name	AP	TP	FP	Average IoU	mAP
0	Extreme drought	60.5%	59%	54%	50%	52%
1	Moderate drought	62%	58%	56%	51%	54%
2	Marginal drought	61.7%	58%	57%	53%	53%

Table 5.2 Testing from the trained network with iteration = 6000, network resolution of 416 × 416

Performance metrics	Values
Average IoU	83.40
Precision	0.98
Recall	0.99
F1-score	0.98
mAP @ 50	0.96

Detecting Objects Deep Learning

In the validation process, the object detection showed the drought areas of the whole images. The images show the drought classes: extreme drought, moderate drought, and marginal drought. The detection performance was defined by the color of NDVI and NDWI. The extreme drought shows a large amount and cumulative in red, the moderate drought shows few red and yellow, and marginal drought shows in yellow and blue. The object detection was able to define the growing stage of maize during 2018 from the planting stage until the post-harvest stage (Fig. 5.11). In Fig. 5.11. the
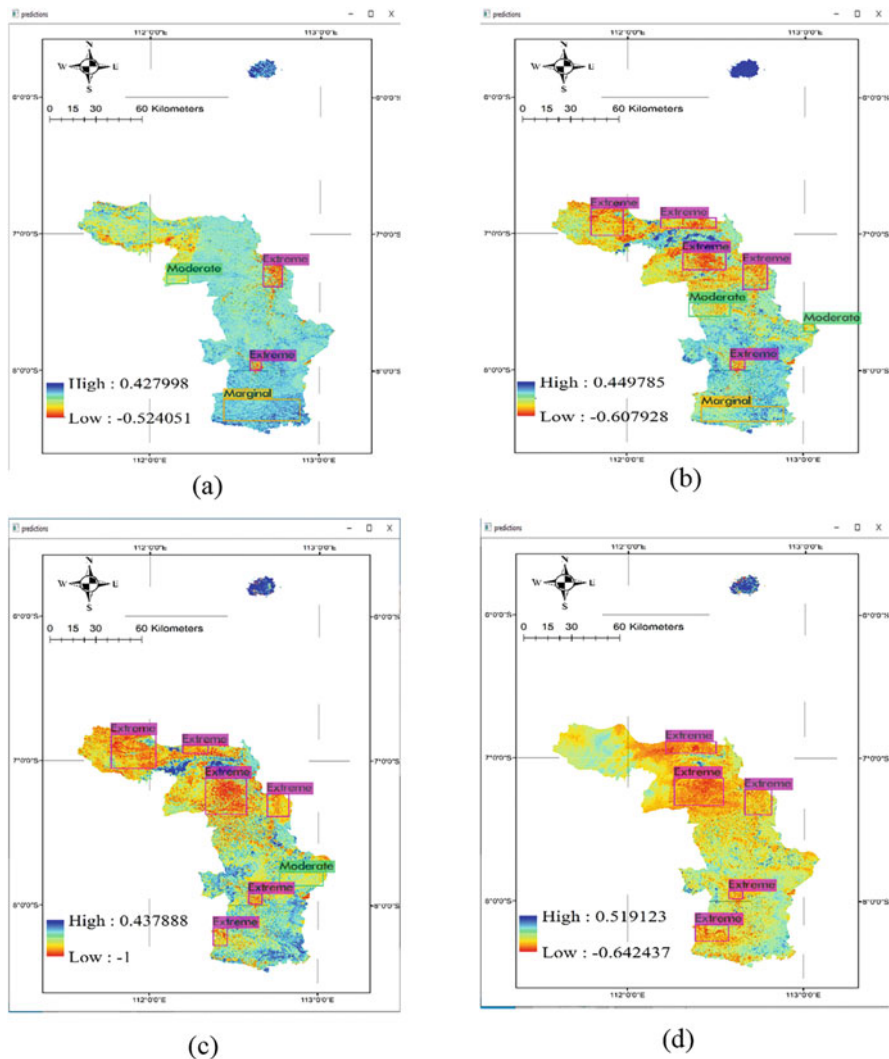
Fig. 5.11 (a) Planting; (b) Reproductive stage; (c) Harvest stage; (d) Post-harvest stage (Habibie et al. 2020)

top left image shows the planting stage has a few drought indicator; the top right image shows the reproductive stage until the post-harvest where the drought shows extreme drought in the central East Java, Indonesia.

5.4   Conclusion

We studied the performance of two approaches for detecting vegetation in this research. Two of these approaches were based on deep learning, while the third was computed utilizing high-performance NDVI, NDWI, and LST techniques with GEE. The experimental findings demonstrated that the YOLOv3 model, utilizing vegetation phenology, performed quite well. This research was done provincially to classify drought-prone areas based on vegetation phenology for maize production. The vegetation phenology was processed based on the vegetation indices. Among the vegetation indices, the NDVI was used the vegetation profile and to find the growing season for plants. For agricultural circumstances, NDWI was utilized to detect water scarcity in the region and was connected to temperature using LST. NDWI and LST were used for vegetation phenology and SPI for the severity index. The results showed that drought severity and vegetation phenology were compared at the same time and occurred during the maize growing season from April to October 2018. This study can be used to determine drought using the YOLOv3 and GEE works rapidly and is useful to define the location of drought-prone areas. To validate the yield model, a more in-depth examination of vegetation phenology will be used. Moreover, forecasting the severity of drought and vegetation phenology ensures that yield declines are avoided, and that regional food security can be verified.

NDVI and NDWI were utilized to identify drought-prone regions using a deep learning algorithm based on Sentinel 2 datasets. Deep learning identification accuracy was determined to be 83.4%, 98%, 99%, 98%, and 96% in drought-prone locations using IoU, precision, recall, F1-Score, and mean average precision (mAP), respectively.

The large-scale computing efficiency was required for the raster datasets. Further research will be conducted to increase the accuracy of dataset training and testing in drought-prone locations, as well as to offer improvements to other deep learning algorithms. Furthermore, this study, which is carried out in high computational and real-time monitoring by researchers who can foresee catastrophe management in a simple and shortest way, frequently assists farmers in protecting their land from the impact of disasters.

References

AghaKouchak A, Nasrollahi N, Habib E (2009) Accounting for uncertainties of the TRMM satellite estimates. Remote Sens (Basel) 1(3):606–619. https://doi.org/10.3390/rs1030606

Alam A, Rahman M, Saadat A, Huq M (2013) Gamma distribution and its application of spatially monitoring meteorological drought in Barind, Bangladesh. J Environ Sci Nat Resour 5(2): 287–293. https://doi.org/10.3329/jesnr.v5i2.14832

Aonashi K, Awaka J, Hirose M, Kozu T, Kubota T, Liu G et al (2009) Gsmap passive microwave precipitation retrieval algorithm: algorithm description and validation. J Meteorol Soc Japan 87A(May 2014):119–136. https://doi.org/10.2151/jmsj.87A.119

Barokah U, Fajarningsih RU, Rahayu W (2019) Sustainability of maize farming in Grobogan, Central Java, Indonesia. IOP Conf Ser Earth Environ Sci 347(1):012113. https://doi.org/10.1088/1755-1315/347/1/012113

Chang KY, Xu L, Starr G, Paw UKT (2018) A drought indicator reflecting ecosystem responses to water availability: the normalized ecosystem drought index. Agric For Meteorol 250–251(May 2017):102–117. https://doi.org/10.1016/j.agrformet.2017.12.001

Dai A (2011) Drought under global warming: a review. Wiley Interdiscip Rev Clim Chang 2(1): 45–65. https://doi.org/10.1002/wcc.81

De Jesus JB, Santana IDM (2017) Estimation of land surface temperature in caatinga area using Landsat 8 data. J Hyperspectral Remote Sens 77(3):150–157. www.periodicos.ufpe.br/revistas/jhrs

Gorelick N, Hancher M, Dixon M, Ilyushchenko S, Thau D, Moore R (2017) Google earth engine: planetary-scale geospatial analysis for everyone. Remote Sens Environ 202:18–27. https://doi.org/10.1016/j.rse.2017.06.031

Gottschalck J, Meng J, Rodell M, Houser P (2005) Analysis of multiple precipitation products and preliminary assessment of their impact on global land data assimilation system land surface states. J Hydrometeorol 6(5):573–598. https://doi.org/10.1175/JHM437.1

Habibie MI, Ahamed T, Noguchi R, Matsushita S (2020) Deep learning algorithms to determine drought prone areas using remote sensing and GIS. In: 2020 IEEE Asia-Pacific Conference on Geoscience, Electronics and Remote Sensing Technology (AGERS), pp 69–73. https://doi.org/10.1109/AGERS51788.2020.9452752

Harsono A, Elisabeth DAA, Muzaiyanah S, Rianto SA (2020) Soybean-maize intercropping feasibility under drought-prone area in East Java, Indonesia. Biodiversitas 21(8):3744–3754. https://doi.org/10.13057/biodiv/d210842

IPCC (2015) IPCC, 2014: climate change 2014: synthesis report. In: Contribution of Working Groups I, II and III to the Fifth Assessment Report of the Intergovernmental Panel on Climate Change. IPCC, Geneva. https://doi.org/10.1017/CBO9781139177245.003

Joyce RJ, Janowiak JE, Arkin PA, Xie P (2004) CMORPH: a method that produces global precipitation estimates from passive microwave and infrared data at high spatial and temporal resolution. J Hydrometeorol 5(3):487–503. https://doi.org/10.1175/1525-7541(2004)005<0487:CAMTPG>2.0.CO;2

Kariyeva J, van Leeuwen WJD (2011) Environmental drivers of NDVI-based vegetation phenology in Central Asia. Remote Sens (Basel) 3(2):203–246. https://doi.org/10.3390/rs3020203

Kidd C, Kniveton DR, Todd MC, Bellerby TJ (2003) Satellite rainfall estimation using combined passive microwave and infrared algorithms. J Hydrometeorol 4(6):1088–1104. https://doi.org/10.1175/1525-7541(2003)004<1088:SREUCP>2.0.CO;2

Kumar L, Mutanga O (2018) Google earth engine applications since inception: usage, trends, and potential. Remote Sens (Basel) 10(10):1–15. https://doi.org/10.3390/rs10101509

Mcfeeters SK (2007) The use of the normalized difference water index (NDWI) in the delineation of open water features. Int J Remote Sens 17(7):1425–1432. https://doi.org/10.1080/01431169608948714

McKee TB, Doesken NJ, Kleist J (1993) The relationship of drought frequency and duration to time scale. In: Eighth Conference on Applied Climatology, 17–22 January 1993, Anaheim, CAL, pp 179–184

Özelkan E (2020) Water body detection analysis using NDWI indices derived from landsat-8 OLI. Pol J Environ Stud 29(2):1759–1769. https://doi.org/10.15244/pjoes/110447

Redmon J, Farhadi A (2017) YOLO9000: better, faster, stronger. In: Proceedings—30th IEEE Conference on Computer Vision and Pattern Recognition, CVPR 2017, 2017-Janua, pp 6517–6525. https://doi.org/10.1109/CVPR.2017.690

Redmon J, Farhadi A (2018) YOLOv3: an incremental improvement. In: arxiv, v1(1804.02767). http://arxiv.org/abs/1804.02767

Sarp G, Ozcelik M (2017) Water body extraction and change detection using time series: a case study of Lake Burdur, Turkey. J Taibah Univ Sci 11(3):381–391. https://doi.org/10.1016/j.jtusci.2016.04.005

Tamiminia H, Salehi B, Mahdianpari M, Quackenbush L, Adeli S, Brisco B (2020) Google earth engine for geo-big data applications: a meta-analysis and systematic review. ISPRS J Photogramm Remote Sens 164(January):152–170. https://doi.org/10.1016/j.isprsjprs.2020.04.001

Trenberth KE (2018) Climate change caused by human activities is happening and it already has major consequences. J Energy Nat Resour Law 36(4):463–481. https://doi.org/10.1080/02646811.2018.1450895

Ushio T, Sasashige K, Kubota T, Shige S, Okamoto K, Aonashi K et al (2009) A kalman filter approach to the global satellite mapping of precipitation (GSMaP) from combined passive microwave and infrared radiometric data. J Meteorol Soc Japan 87A(June 2008):137–151. https://doi.org/10.2151/jmsj.87A.137

Venkatappa M, Sasaki N, Anantsuksomsri S, Smith B (2020) Applications of the google earth engine and phenology-based threshold classification method for mapping forest cover and carbon stock changes in Siem Reap province, Cambodia. Remote Sens (Basel) 12(18):3109. https://doi.org/10.3390/RS12183110

Wilhite DA, Glantz MH (1985) Understanding: the drought phenomenon: the role of definitions. Water Int 10(3):111–120. https://doi.org/10.1080/02508068508686328

Wongsai N, Wongsai S, Huete AR (2017) Annual seasonality extraction using the cubic spline function and decadal trend in temporal daytime MODIS LST data. Remote Sens (Basel) 9(12):1254. https://doi.org/10.3390/rs9121254

World Meteorological Organization (2012) Standardized Precipitation Index User Guide (WMO-No.1090). World Meteorological Organization, Geneva

Xue J, Su B (2017) Significant remote sensing vegetation indices: a review of developments and applications. J Sens 2017:1–17. https://doi.org/10.1155/2017/1353691

Chapter 6
Land Suitability Analysis for Grape (*Vitis vinifera* L.) Production Using Satellite Remote Sensing, GIS, and Analytical Hierarchy Process

Sara Tokhi Arab, Tariq Salari, Ryozo Noguchi, and Tofael Ahamed

Abstract Land suitability analysis is essential for a vineyard to increase its production and productivity under the dry conditions due to climate change. In this context, the purpose of this chapter is to determine the suitable locations for vineyards based on satellite remote sensing and GIS (geographical information system) to assess the suitability of land and least suitable land to support the vineyard growers for subsidy allocation. In this regard, the Landsat 8 operational land imager (OLI) and thermal infrared sensor (TIRS) and digital elevation (DM) shuttle radar topography mission (SRTM) images were processed to obtain the normalized difference vegetation index (NDVI), normalized difference moisture index (NDMI), land surface temperature (LST), and topographic maps (elevation, aspect, and slope). Moreover, JAXA rainfall information (mm per hour) and soil properties were used to incorporate climatic and soil conditions. Besides, socioeconomic information was collected through field surveys in Kabul Province in order to develop the vineyard suitability map. Finally, the suitable classes were determined using a weighted overly method based on the analytical hierarchy overlay process (AHP). The combined (physical and socioeconomic) suitability results indicated that highly suitable (12.9%), moderately suitable (25.5%), marginally suitable (28.5%), and not suitable lands (32.9%) were reported for grapes production in Kabul Province. The suitability models also indicated that 175.46 ha of vineyards out of 10599.96 ha of vineyards were located in marginal and not suitable areas. This research can support decision-makers, stakeholders, and growers with precise land assessments by identifying the main

S. T. Arab
Graduate School of Life and Environmental Sciences, University of Tsukuba, Tsukuba, Ibaraki, Japan

Agriculture Faculty of Kabul University, Jamal Mina, Kabul, Afghanistan

T. Salari
Agriculture Faculty of Kabul University, Jamal Mina, Kabul, Afghanistan

R. Noguchi · T. Ahamed (✉)
Faculty of Life and Environmental Science, University of Tsukuba, Tsukuba, Ibaraki, Japan
e-mail: tofael.ahamed.gp@u.tsukuba.ac.jp

limiting criterion for producing table grape management. Furthermore, GIS analysis determined the vineyard growers from marginal and not suitable areas for providing support of subsidy to improve their livelihoods.

Keywords Vineyards · Physical criteria · Socioeconomic · AHP · Land suitability

6.1   Introduction

Determining the best location for vineyard cultivation is essential for growers to increase table grape production and reduce the cost of production (Schmidt et al. 2014). Furthermore, it also depends on plant requirements, soil properties, and environmental criteria that refer to the use of land on a sustainable basis (Bramley et al. 2011). Land suitability comprises the qualitative and quantitative assessment of land. Criterion such as climate, hydrology, topography, vegetation, and soil properties are considered in the qualitative assessment of land. However, in the quantitative assessment of land criteria such as yield, motivation of farmers, cultivation patterns, capital, investment capacity, cost-benefits ratio, location of vineyards and other criterion are considered (Taghizadeh-Mehrjardi et al. 2020). The qualitative and quantitative land assessment classification based on the Food and Agriculture Organization (FAO 1976) refers to highly suitable (S1), moderately suitable (S2), marginally suitable (S3), and not suitable (N). Like other crops and fruits, climate change, pests, and diseases have a significant impact on grape production and quality of yield (Table 6.1).

Grapes (*Vitis vinifera* L.) have become an important crop in the world that has a significant role in the global economy. According to the US Department of Agriculture's Foreign Agricultural Service, global table grape production in the years 2020–2021 was estimated about 24.7 million metric tons (USDA 2021). China is the world's largest producer of grapes, followed by European countries (EU), Turkey, Uzbekistan, and the USA. These countries are also the top countries in terms of quantity of production. However, in the Asian countries, China has the first position in production of grapes with 24.28 million tons, India is second with 3.04 million

Table 6.1 Land suitability classes and descriptions based on FAO

| Suitability classes	Description
S_1 (highly suitable)	These types of land have no significant limitations for production
S_2 (moderately suitable)	These types of land have moderate limitations for production. It will reduce productivity; by increasing the input into a certain amount can change it to S_1
S_3 (marginally suitable)	These types of lands have marginal limitations. These limitations reduce the productivity; by increasing the input the expenditure of land will increase
N (not suitable)	These types of lands having severe limitations with the use of technique and technology cannot make it suitable
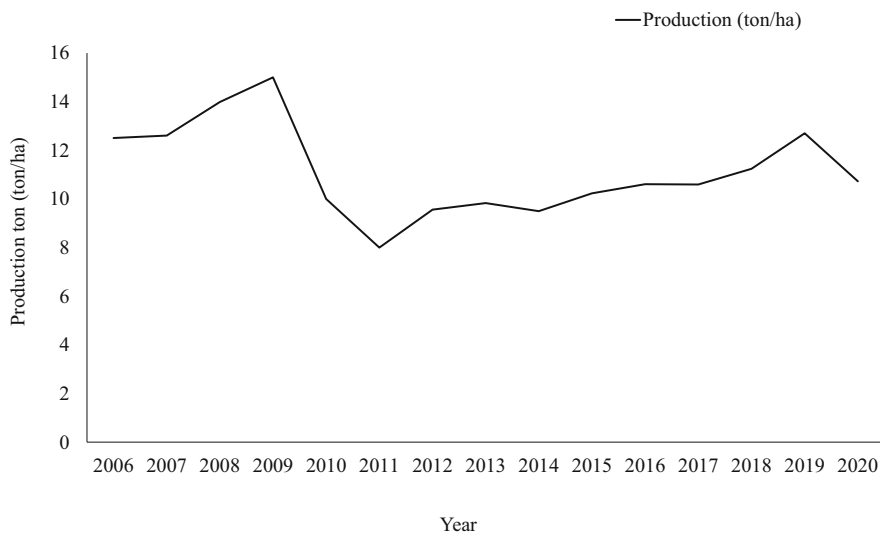
Fig. 6.1 Table grape production from 2006–2020 in Afghanistan

tons, and Afghanistan has the third position with production of 1.12 million tons in 2019 (FAO 2020).

In Afghanistan, table grapes are also one of the most economically important horticultural crops. Afghanistan has a history of grape production, and it is a major horticultural product and the main export agricultural product. The grape production was significantly higher in last 15 years (Fig. 6.1). The highest production was 15 tons/ha in 2009. The highest production indicated that climate change and internal war had a significant impact on grape production in Afghanistan. However, the productivity of table grapes is much lower in Afghanistan than in developed countries due to climate change and limited knowledge of production systems, soil quality, and postharvest losses. The postharvest losses are higher due to lack of storage facilities of table grapes. Furthermore, strict regulation of winery from grapes, makes more dependency of table grapes consumption and benefit to the farmers.

In 2020, the COVID-19 pandemic, in addition to climate variability, had an impact on grape production, and the global trader faced significant challenges such as labor shortages and transportation. Moreover, other criteria such as temperature, rainfall, elevation, slope, soil pH, and soil properties have a significant impact on grape yield. The small-scale farmers faced challenges in production, and income from grape production. Therefore, it is required to analyze the physical and socio-economic criteria that greatly influence grape production and bring support to the farmers. One of the potentials for analyzing the physical criteria is through geographical information systems (GIS) combined with satellite remote sensing datasets and multi-criteria decision analysis tools. The multi-criteria-based suitability analysis can help the growers in deciding the suitable production lands for increasing

production and alternate support system for marginals and not suitable lands. The main benefit of multi-criteria decision analysis as an analytical hierarchy process (AHP) can be incorporated with experts' opinions in land suitability analysis (Ridley and Devadoss 2021). This method was developed by Saaty. The criterion importance of two or more than two at a time was evaluated with pairwise comparisons in suitability analysis (Saaty 1980) (Table 6.1).

Very few studies have been done for vineyard land suitability analysis. Land suitability for vineyards was performed in China using five evaluation criteria such as agricultural land, climate conditions, water policies, irrigation status, and proximity to waste water treatment (Paul et al. 2020). Another study done in the USA used soil properties, soil pH, and elevation. Similarly in Italy, soil pH, soil properties, elevation, aspect, slope, and heat index have been considered in land suitability analysis, (Modica et al. 2014; Cardell et al. 2019). However, in Afghanistan, there has been no research regarding land suitability for vineyards using satellite remote sensing datasets and multi-criteria decision-making. In land suitability performance, we used several parameters such as climate, vegetation, topography, soil, and socioeconomic parameters to detect both less productive areas and potential growing zones for grape production. In this regard, temperature and rainfall are the main climatic parameters that affect the grape growth rate (Lorenzo et al. 2013; Hatfield and Prueger 2015). Land slope and aspect are topographic parameters that are essential for soil, water drainage, air movement, and total heat balance. Soil properties such as soil structure, soil pH, soil salinity, and soil organic matter influence on vine growth and grape quality (Gattullo et al. 2020). Socioeconomic parameters such as population density, benefit–cost ratio, distance from roads and markets are important for marketing purposes and access to inputs. These two criteria have a significant impact on grape production. Climate change effect on preharvest stages of production and postharvest losses of grapes are the main causes for reducing the production of grapes by farmers. Government incentives are required to support the growers to increase the most important agricultural commodities.

Most governments around the world have introduced a series of subsidies to encourage farmers to increase production and adopt sustainable production. As an instance, the Indian government provides farmers the input, price infrastructure, and export subsidies to support agricultural development (Fan et al. 2008). China's agricultural policy has undergone a fundamental transformation over the past 40 years (Lopez et al. 2017) and a series of agricultural subsidy policies have been introduced (Qian et al. 2015). In this regard, it is very important for government to know about the land suitability using physical and socioeconomic criteria to provide subsidies to farmers.

Therefore, the main objective of this chapter was to integrate geographical information systems (GIS) and satellite remote sensing methods for physical and socioeconomic criteria using AHP to assess the suitability of lands for increasing grape production. Furthermore, recommend a subsidy allocation system for the least suitable land for grape production.

6.2 Materials and Methods

6.2.1 Description of the Study Area

The study was carried out in a densely populated Province of Afghanistan, Kabul, located between latitudes 34.53330 N and Longitudes 69.16670E (Fig. 6.2). It consists of 14 districts and 689 villages with a total population of 5.26 million, which made up 16% of the total population in Afghanistan (ACSO 2020). This province is located at a very high elevation of about 4654 m above sea level including a dry, continental climate with four seasons and annual rainfall of 400 mm. The total arable land in the province comprises a mix of rainfed and a small area of irrigated land. Kabul Province is dominated by wheat, rice, maize, and different types of vegetables and fruits. Among them, fruit trees are 4000 ha and vines 10,600 ha, which makes up about 3.2% of arable land in 2020 (Walt 2018). Therefore, grape is one of the strategic fruits that can be produced up to 115,450 tons (ACSO 2020). Unfortunately, due to climate change and traditional cultivation patterns, the productivity of grapes is very low.

6.2.2 Data Collection and Criteria Selection for Table Grapes Land Suitability Analysis

The agricultural, metrological, soil, and socioeconomic data were collected from primary and secondary sources. The criteria for physical suitability were considered NDVI, NDMI, LST, JAXA rainfall, digital elevation model (DEM), slope, aspect, soil component, soil pH, soil organic matter, and soil salinity. Likewise, the socio-economic parameters such as distance from roads, distance from water bodies, and population density were collected from the secondary data sources. However, the distance from national and local markets and the benefit–cost ratio of each vineyard were developed from the primary dataset collected during the field survey conducted between November and December 2020 in Kabul Province (Fig. 6.3).

A geographic position system (GPS) Coordinate® was used to collect the geographical location for each of the vineyards. All the datasets and the sources were explained in Table 6.2 and the methods were followed in this research explained in the flowchart (Fig. 6.3).

Normalized Difference Vegetation Index (NDVI)

NDVI can be used for real-time plant growth monitoring and estimating the density of greenness (Li et al. 2019). In this study, Landsat 8 multispectral images were used to develop NDVI maps. To ensure an appropriate representation of vegetation evaluation in the study, the images were acquired corresponding to active growing
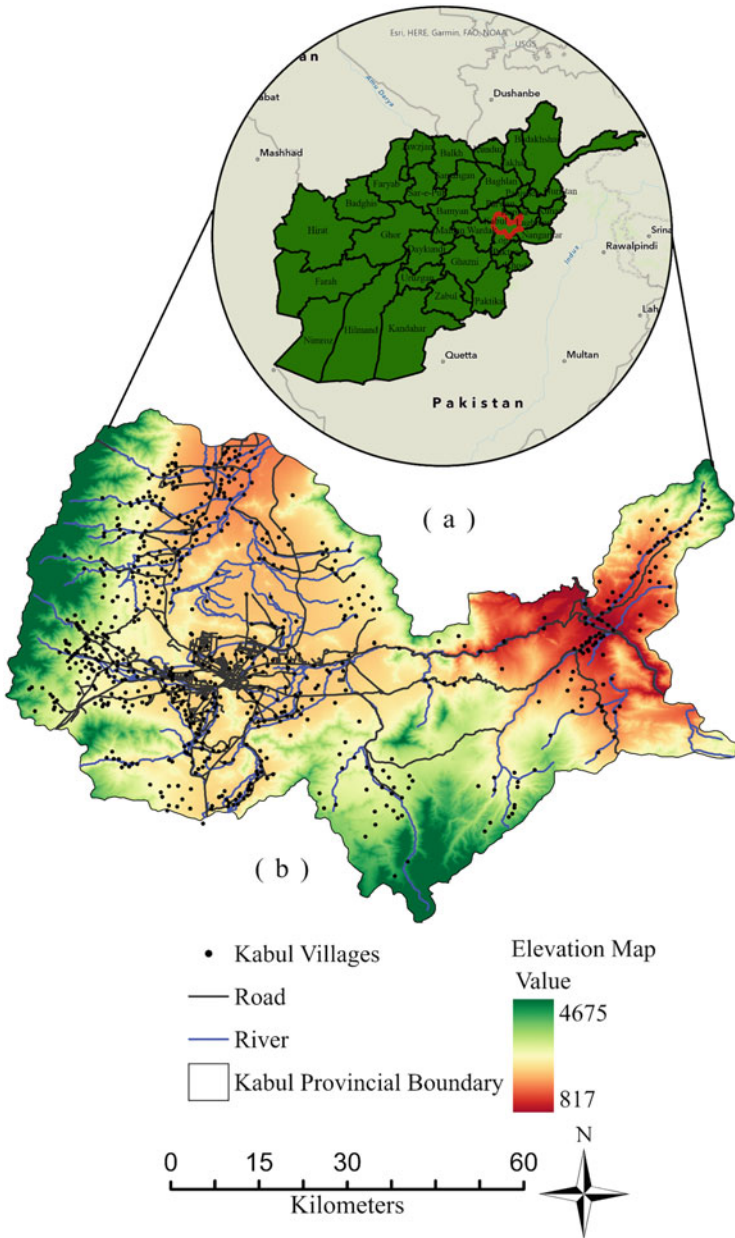
Fig. 6.2 Geographical location of the study area: (**a**) Afghanistan administrative map, and (**b**) Kabul Province elevation map
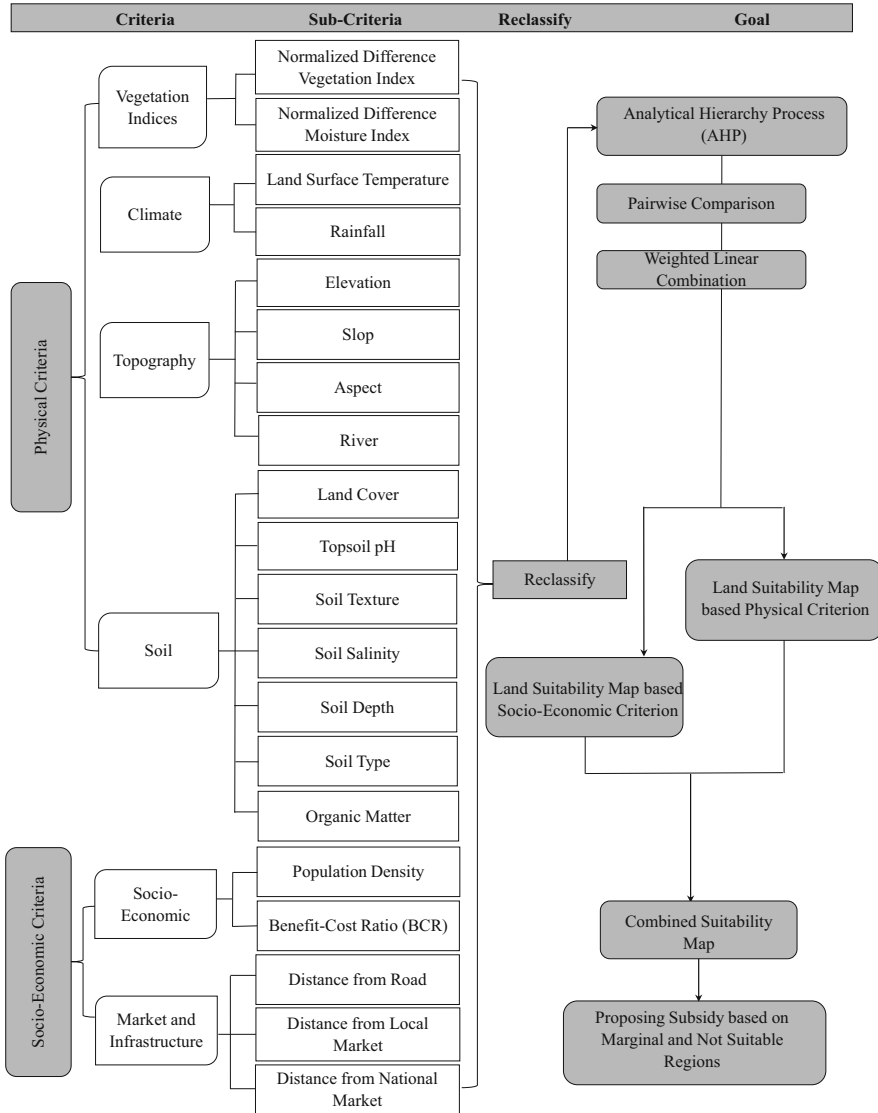
Fig. 6.3 Schematic chart shows the methodologies that are applied for land suitability analysis for vineyards under dry conditions in Afghanistan

stages of table grapes (April to October) (Anyamba and Tucker 2012; Hadri et al. 2021; Islam et al. 2021) from 2016 to 2020. NDVI can be expressed as:

$$\text{NDVI} = \frac{\text{NIR} - \text{Red}}{\text{NIR} + \text{Red}} \tag{6.1}$$

Table 6.2 List of data and source of datasets for table grapes land suitability analysis

No	Data	Description	Data source
1	Land use map	Derived from Spot (10 m color), Google Earth (2.5 m 1 m, /0.6 m color), and Arial Photographs (1 m color/0.5 m B and W)	FAO 2016
2	Slope map		DEM SRTM USGS 2014 & 2015
3	Elevation map		DEM SRTM USGS 2014 & 2015
4	Aspect map		DEM SRTM USGS 2014 & 2015
5	Rainfall map (SPI)	Resample to 30 m resolution	JAXA Rainfall GSMAP 2016–2020
6	Land surface temperature map	Derived from 30 m (band10 and band11)	Lansat 8 Scenes USGS 2016–2020
7	NDVI map	Derived from 30 m resolution (band 4 and band 5)	Lansat 8 USGS 2016–2020
8	NDMI		
9	Soil pH	Afghanistan soil atls, scale 1:50000	FAO 2020
10	Topsoil texture		FAO 2020
11	Topsoil types		FAO 2020
12	Topsoil depth		FAO 2020
13	Soil texture		FAO 2020
14	Soil organic matter (OM)		FAO 2020
15	Topsoil salinity		FAO 2020
16	Road map	1:250,000	AIMS, OSM, OCHA 2019
17	River map	Scale 1:50,000	AIMS OSM OCHA 2019
18	Population density	Spatial resolution 0.000833333 decimal degrees (approximate 100 m at the equator)	World Bank Group 2017
19	Distance from national market	GPS point	Field survey 2020
20	Distance from local market	GPS point	Field survey 2020
21	Vineyard's locations	Polygon	FAO 2016
22	Benefit–cost ratio	GPS points	Field survey2020

where NDVI is the normalized difference vegetation index and NIR is the near-infrared reflectance, ranging from 0.85 to 0.88 μm, and Red is the wavelength reflectance ranging from 0.64 to 0.67 μm in Landsat 8 OLI scenes.

Normalized Difference Moisture Index (NDMI)

This parameter is very important for vineyards because any variation in the moisture of plants can affect the mesophyll in plants, which interact with solar radiation (Bhattacharya et al. 2021). The NDMI was calculated from Landsat 8 OLI images over 5 years from April to October. The NDMI can be expressed as follows:

$$\text{NDMI} = \frac{\text{NIR} - \text{SWIR}}{\text{NIR} + \text{SWIR}} \tag{6.2}$$

where NDMI is the normalized difference moisture index and NIR is the near-infrared wavelength, SWIR is the shortwave infrared reflectance ranging from 1.57 to 1.65 μm in Landsat 8 OLI scenes.

Land Surface Temperature (LST)

LST is the temperature of the surface of the Earth using the Kelvin (K) scale and is an essential criterion for monitoring temperature for crop growth (USGS website and Karnieli et al. 2010). Temperature during the growing season directly impacts the production of sugar in grapes and this element also influences the type and quality of the grapes produced. The fluctuation of daily temperatures during midwinter is usually more harmful for grapevines than steady cool temperatures (Wolf and Boyer 2005). Grape vines can be injured or killed by winter cold. Temperatures greater than 30 °C can reduce the vine's ability to photosynthetically convert carbon dioxide into sugars and other carbohydrates. Nighttime temperatures greater than about 18 °C tend to increase the vine's respiration of this energy. In fact, respiration can consume up to 60% of the energy generated by photosynthesis (Iacono et al. 2000) decreasing the productivity of vines. The LST was calculated from Landsat 8 thermal bands with 30 m resolution in different steps from 2016 to 2020 (Shamsuzzoha et al. 2021). Landsat 8 Thermal Infra-Red Scanner (TIRS) has two bands in the TIR region (Band 10 and Band 11). These thermal bands have a 100 m native spatial resolution but are resampled with cubic convolution at 30 m before distribution by United States Geological Survey (USGS) (Loveland and Irons 2016; Gemitzi et al. 2021). The steps can be explained as following:

The first step of the LST calculation is the top of the atmosphere reflectance (TOA)

$$\text{TOA} = M_\text{L} \times Q_\text{cal} + A_\text{L} \tag{6.3}$$

where M_L represents the band-specific multiplicative rescaling criterion from the metadata, Q_cal corresponds to band 10 or 11 Landsat 8 thermal bands, and A_L is the band-specific additive rescaling criterion from the metadata.

The second step of this process is the conversion of radiance to sensor temperature. In this, the digital numbers (DNs) are converted to reflection. The TIRS band

data should be converted from spectral radiance to brightness temperature (BT). BT can be expressed as follows:

$$BT = \left(\frac{K_2}{\ln\left(\frac{K_1}{L} + 1\right)} \right) - 273.15 \tag{6.4}$$

where K_1 and K_2 are the band-specific thermal conversion constants from the metadata, and L is the top of atmospheric spectral radiance.

The third step is the calculation of the proportion of vegetation needed to calculate and P_v is required to calculate the emissivity. P_v is determined from NDVI. Therefore, the calculation of the proportion of vegetation is as follows:

$$P_v = \left(\frac{NDVI - NDVI_{min}}{NDVI_{max} - NDVI_{min}} \right)^2 \tag{6.5}$$

where P_v is the proportion of vegetation, NDVI is the normalized difference vegetation index and max and min is the minimum and maximum NDVI values. Emissivity can be expressed as follow:

$$\varepsilon = 0.004 + P_v \times 0.986 \tag{6.6}$$

where ε is the emissivity and P_v is the proposition vegetation.

The final step retrieving the LST is computed as follows:

$$T_s = \frac{BT}{1 + \left(\frac{\lambda \times BT}{P_v}\right) \times \ln \varepsilon} - 273.15 \tag{6.7}$$

where T_s is the land surface temperature in Celsius, BT is the brightness temperature at the sensor, λ is the average wavelength of band 10 or 11, and $\varepsilon\lambda$ is the emissivity.

The satellite datasets were downloaded from the USGS website. Following that, the NDVI, NDMI, and LST from 5 years of datasets (2016–2020) were calculated using ArcGIS pro®. Finally, an average of 5 years of datasets was used for the final suitability analysis.

Rainfall

Rainfall is one of the essential parameters for the production of grapes and lack of rainfall has a severe impact on table grapes productivity. The minimum level of recommended rainfall for vineyards is about 500 mm (Ted 2018). Therefore, the total water requirement is met through stored winter rainfall, irrigation, and in-season rainfall. Since the area is arid and semiarid, the historical average annual rainfall is about 473 mm. In this research, hourly rainfall dataset mm per hour from

the global rainfall map (GSMap, JAXA) for each month and districts for 5 years from 2016 to 2020 were downloaded. After processing the data, the sum of the cumulative rainfall was calculated for all districts and imported to GIS file. Then, the vector images were converted to raster, and resampling was done for 30 m spatial resolution. Finally, an average of 5 years was used for the final suitability analysis.

Elevation

According to previous research, high-elevation regions are more vulnerable to climate change than low-altitude regions (Xu et al. 2016). The highest elevation in Kabul Province is about 4654.4 m above sea level. Furthermore, elevation determined the micro-climate and air temperature variation in a particular area and had a direct influence on the phenology of a vine (Acharya and Yang 2015). Usually, lower elevations are good for high latitudes, and higher elevations are more desirable at lower latitudes. Increased water stress can reduce the vineyard yield and fruit composition.

Slope

The slope has an influence on practicability of agricultural activities, especially referring to the mechanization of vineyards. Vineyards with steep slopes hinder the practical use of machinery, while topography also affects the movement of air and particularly cold air drainage. Therefore, moderate slopes (5–15%) are regarded as optimum (Jones et al. 2009). Besides, the soil water holding capacity can change a slope (Casanova et al. 2000; Bonfante et al. 2015) and that up-slope vines are more prone to water stress, as soils there commonly have lower water holding capacity than down-slope soils (Basile et al. 2020). Kabul Province slopes ranges are from 0–75° and the range between 0–10° are optimal slope for vineyard cultivation.

Aspect

This criterion directly influences the amount of solar radiation to the soil surface during the growing season. Therefore, this criterion plays a crucial role for high sugar content (Modica et al. 2014). It will also affect the angle that sunlight hits the vineyard and thus its total heat balance. This criterion directly influences the amount of solar radiation to the soil surface during the growing season. Therefore, this criterion plays a crucial role for vineyards, which requires very high sugar content for its enological transformation (Wolf and Boyer 2005). *In the southern part of Afghanistan, the intensity of the sun's rays is high, and the heat may have a negative effect on the vine. Therefore, north south is the best location for the vineyard's direction* (Ghulam Rasoul Samadi. Interview. Conducted by Sara Tokhi Arab, 24 July 2021).

In this study, all topographical parameters such as elevation, slope and aspect were developed from the USGS EROS archive of digital elevation-shuttle radar topography mission (SRTM). The study area had two different paths therefore, two images were mosaicked using ArcGIS Pro®. Further mask operations were conducted to find the study area.

Distance from River

Different rivers and water channels flow in Kabul Province. Most of these rivers in all districts feed by snowmelt runoffs from the Paghman mountains in the west; the Qorugh Mountain in the southwest; the Shir Darvazeh, Asmayee, and Aliabad mountains in the center; the Safi Mountain in the northeast; and the southeastern Bagrami, Shina, Lathaband, and Tang Gharo dynasties (Serries or chain of mountain). The most popular river is the Kabul River that flows from the Paghman Mountain toward South Pass about 70 km west of Kabul. It flows in an easterly direction, past Kabul, and through Jalalabad city, and then on to Dakka where it enters Pakistan territory and finally runs into the Indus at the Attock region. The river distance was calculated from the polyline and then changed to raster. After changing to raster, the Euclidean distance was calculated from the nearest river to each vineyard (Purnamasari et al. 2019). This criterion is important for accessing water for irrigation purposes. According to the expert suggestion, proximity from river or water bodies more than 1 km is the ideal distance. The closer to the river, the more humidity will cause fungal disease for the vineyard (Ghulam Rasoul Samadi. Interview. Conducted by Sara Tokhi Arab, 24 July 2021).

Soil Components

Soil affects vine productivity and wine quality; soil, like the climate, comprises many components. Soil can be described in terms of its depth, parent rock origin, soil types, organic matter content, texture, chemical properties, hydrology, and in terms of its microbial and other invertebrate fauna density and diversity. All these variables may ultimately affect vine growth and grape quality, but precise relationships are not well characterized for all such variables (Stanchi et al. 2013). The soil datasets were collected from the FAO office branch in Kabul, Afghanistan, then resampled to 30 m resolution and reclassified based on references to four suitability classes (Appendix Table 6.10).

Soil pH

Soil pH values between 6.0 and 6.8 provide the optimum availability of nutrients in vineyard soils. Soil pH of less than 5.0 increases the aluminum solubility within the root zone and precipitates essential micronutrients such as iron out of the soil

solution. However, some grape cultivars prefer low soil pH, preferably pH value less than 5.5 (Kurtural 2007). When the soil alkaline increases, it causes shortage of micronutrients, such zinc, iron, and copper, and decreases yields and creates vine problem. Soil pH datasets were collected from the FAO office branch located in the Kabul Province of Afghanistan.

Soil Salinity

This parameter is very important for the vineyard assessment. Soil salinity is mostly caused by poor irrigation practices in most underdeveloping countries. Subsequently, the accumulation of the salt in the root zone of grapevines happens. Soil salinity can have drastic effects on their growth and yield. If the salt concentration is very high in the soil, it kills the vine. Afghanistan is a dry area; therefore, the soil salinity increases during the dry periods since the absence of flushing out salts from the soil causes the soil to become salinized (De Clercq et al. 2009; Aragüés et al. 2014). The soil salinity dataset was collected by the FAO office in Kabul, Afghanistan.

Soil Organic Matter

Organic matter improves soil structure, moisture retention, and fertility. Three percent organic matter is considered ideal for grapes. It also balances various chemical and biological processes and helps to maintain soil quality parameters at an ideal level in the vineyards (Goldammer 2018). The organic matter mostly influences soil aggregation and is related to pore space distribution and has the same effect as clay on water holding capacity (Saxton and Rawls 2006) (Table 6.2). The dataset was collected from the FAO office in Kabul.

Land Use Map

A land use map was used to identify the locations of all vineyards in Kabul Province. Land use map was obtained from FAO geospatial local office. The land use classes were aggregated into 11 generalized and self-explicative classes. Similar land use classes were merged to the same class based on ability of land to change to vineyards in the future. There were 11 classes reclassified to 4 categories based on suitability classes (Worqlul et al. 2017).

Distance from Road

This criterion is important to access the market to sell the product or buy inputs for vineyard management. Different types of roads exist in Kabul Province, such as

expressways, major roads, minor roads, and nonstandard roads, which include the urban and rural roads (Kabul Province master plan). Previous research proved that the proximity of vineyards to roads and industrial areas causes metal accumulation in the soil and causes soil pollution (Deluisa et al. 1996). *Therefore, suggestions from experts were considered to select more than 1000 m location of vineyards from main roads considered as suitable areas* (Ghulam Rasoul Samadi. Interview. Conducted by Sara Tokhi Arab, 24 July 2021). The road distance was calculated from the polyline and then changed to raster. After changing to raster, the Euclidean distance is used to calculate the proximity of the nearest paved road to each vineyard (Purnamasari et al. 2019).

Population Density

The number of people per unit area is called population density. When the population density increases in a region, there is a chance of land use conversion, from agricultural and forest areas to settlements and other services. Population density has a direct relationship with water scarcity and climate change. Several studies have found that density increases across the continent should lead to a significant increase in the extent of water-stressed zones, especially in overpopulated regions (Le Blanc and Perez 2008; Gong et al. 2012). The population density map was developed by the World Bank group to estimate the number of people per grid square with the national total adjusted to match the united nation (UN) population division estimation (Worqlul et al. 2017).

Benefit–Cost Ratio (BCR)

The benefit–cost ratio is a measure of efficiency that compares a vineyard's benefit to its cost. A higher benefit–cost ratio value means a grape grower can produce more benefit using fewer costs (Wali et al. 2016). The benefit and cost of all the vineyards were collected through field survey in December 2020. Subsequently, the BCR was calculated through the below expression:

$$\text{Benefit} - \text{Cost Ratio} = \frac{\text{Total benefit earned from vineyard}}{\text{Total cost of production required in vineyard}} \tag{6.8}$$

The benefit–cost ratio was added to a separate sheet in a tabular form for all 100 vineyards. After that, the waypoints (x, y coordinate) of benefit–cost ratio were generated. The higher benefit -cost ratio value showed the higher suitability, and the lower value showed the less suitable vineyards. More than 1.2 was considered as suitable and less than 1.2 was considered not suitable vineyards.

Distance from Market

Access to the market is a very important criterion for vineyard site selection specially for underdeveloping countries, which mostly does not have access to modern storage and packing systems. Since table grapes are very perishable therefore access to regional, national, and local markets is very essential. Access to the markets offers opportunities for higher returns to the growers. Vineyard distance to the market was collected through the field survey in December 2020. The tabular form of 100 vineyards was prepared in Microsoft Excel® then market distance was inserted to the location of each vineyard in ArcGIS Pro® (Worqlul et al. 2017).

All the further criteria descriptions and sources are described in Table 6.2 and the criteria classification thresholds are explained in Appendix Table 6.10.

6.2.3 Criteria Reclassification and Weighted Linear Combintion

Reclassification was done in ArcGIS Pro® in order to create a new single classified raster map from the main raster. The raster maps of each criterion were classified based on reference to four classes: highly suitable, moderately suitable, marginally suitable, and not suitable. Each class is explained on Appendix Table 6.10.

6.2.4 Analytical Hierarchy Process (AHP)

AHP was developed by Saaty (1985) to provide a framework for solving multi-criteria decision problems based on relative importance assigned to each criterion. In this research, the criteria were chosen based on their importance for physical and socioeconomic suitability for vineyards under the dry condition of Afghanistan. We selected a total of 20 sub-criteria from two main criteria. The AHP has three main steps as the development of pairwise comparison matrix, computation of weight criterion, and estimation of consistency ratio (CR) (Table 6.5). Therefore, as the first step, the pairwise comparison matrix development from the 14 criteria for physical and 6 criteria for socioeconomic were chosen. Subsequently, three questionnaires were developed to obtain the expert's opinions relative to the importance of each criterion. Two AHP questionnaires were designed to collect the expert's opinions regarding the physical and socioeconomic criterion of vineyards in Kabul Province. The thrid one was used to know the influence of each in total. The intensity of the importance of each criterion was scaled from 1 to 9. In the scale, 1 is showed equal to importance and 9 is referred to the extreme importance of the criteria. On the contraray, the opposite is 1/9, which means extremely less important. The

consistency index (CI) showed the level of deviation from consistency and was computed using the following expression (Saaty and Kearns 2014) (Tables 6.3 and 6.4):

$$CI = \frac{\lambda_{max} - n}{n - 1} \tag{6.9}$$

where λ_{max} is the maximum eigen value and n is the number of criteria or sub-criteria in the matrix of pairwise comparison (Tables 6.2 and 6.3).

CR is the ratio of CI to the average Random Consistency Index (RI) for the same order matrix and was computed using the following expression:

$$CR = \frac{CI}{RI} \tag{6.10}$$

where CI is the consistency index and RI is the Random Index (Table 6.5). When the CR value was less than 10% the matrices were consistent and AHP could be continued. If the CR is higher than 10%, the assesment required revision because the materix is not consistent.

$$S_i = \sum_{i=1}^{n} C_i \times W_n \tag{6.11}$$

where C_i is the criterion i that was reclassified and W_n is the number of criteria n that were wieghted.

The score (weight) of each criterion was calculated in excel from the AHP (Tables 6.2, 6.3, and 6.4). Finally, the ArcGIS Pro® was used to combine the spatial data with S_i in order to generate a land suitability map.

6.3   Results

6.3.1   Reclassification of Criteria

The raster and vector layers were reclassified based on suitability classes into highly suitable, moderately suitable, marginally suitable, and not suitable categories (Table 6.6). The reclassification of all the citeria were done based on references (Appendix Table 6.10). In the reclassification of criteria, vegetation indices, NDVI reported that 6.4% of lands (30,489 ha) were highly suitable. However, in climatic varibles, rainfall had the highest percentage for area coverage for the highly suitable areas during the study periods (Fig. 6.4a–c and Table 6.6).

Moreover, the reclassification of topographic criterion reported that 52.7% of land were located in the highly suitable category (Fig. 6.4d–g and Table 6.6). Again, soil texture covered 98% (6601.7 ha) and soil types 82.7% (381497.9 ha) located in

Table 6.3 Parirwise comparison matirx for grape based on physical criterion to evaluate in Kabul Province of Afghanistan

Criteria	Soil type	Soil pH	Soil depth	Soil texture	Soil organic matter	Soil salinity	Normalized difference vegetation index	Normalized difference moisture index	Rainfall	Slope	Elevation	Land surface temperature (LST)	Land cover	Aspect
Soil type	**1**	1/2	1/2	1	1	2	5	5	1	4	2	3	4	5
Soil pH	2	**1**	1	1	1	4	7	4	4	6	4	4	7	9
Soil depth	2	1	**1**	1	1	2	3	5	1	9	8	8	6	8
Soil texture	1	1	1	**1**	1	2	8	8	2	7	7	6	6	6
Soil organic matter	1	1	1	1	**1**	5	7	7	2	6	6	7	7	8
Soil salinity	1/2	1/4	1/2	1/2	1/5	**1**	5	6	1	9	7	3	8	9
Normalized difference vegetation index (NDVI)	1/5	1/7	1/3	1/8	1/7	1/5	**1**	1	1	2	2	2	9	9
Normalized difference moisture (NDMI)	1/5	1/4	1/5	1/8	1/7	1/6	1	**1**	1	1	2	2	7	9
Rainfall	1	1/4	1	1/2	1/2	1	1	1	**1**	9	9	5	9	9
Slope	1/4	1/6	1/9	1/7	1/6	1/9	1/2	1	1/9	**1**	2	2	3	3
Elevation	1/2	1/4	1/8	1/7	1/6	1/7	1/2	1/2	1/9	1/2	**1**	1	2	2
Land surface temperature (LST)	1/3	1/4	1/8	1/6	1/7	1/3	1/2	1/2	1/5	1/2	1	**1**	3	3

(continued)

Table 6.3 (continued)

Criteria	Soil type	Soil pH	Soil depth	Soil texture	Soil organic matter	Soil salinity	Normalized difference vegetation index	Normalized difference moisture index	Rainfall	Slope	Elevation	Land surface temperature (LST)	Land cover	Aspect
Land cover	1/4	1/7	1/6	1/6	1/7	1/8	1/9	1/7	1/9	1/3	1/2	1/3	**1**	1
Aspect	1/5	1/9	1/8	1/6	1/8	1/9	1/9	1/9	1/9	1/3	1/2	1/3	1	**1**
Sum	10.4	6.3	7.2	7	6.72	18.2	39.7	40.3	14.6	55.6	52	44.6	73	82

$CI = \frac{(\lambda_{max} - n)}{(n-1)}$

RI = 1.57

Maximum Eigen value = 15.82

n = 14

CR = 0.09

Table 6.4 Normalized matrix of the criteria for grapes based on socioeconomic criterion under the dry condition

Criteria	Distance from road	Distance from river	Population density	Benefit–cost ratio	Distance from local market	Distance from national market
Distance from road	1	2	1/2	3	8	8
Distance from river	1/2	1	1	1	6	2
Population density	2	1	1	6	9	6
Benefit–cost ratio	1/3	1	1/6	1	1	2
Distance from local market	1/8	1/6	1/9	1	1	1
Distance from national market	1/8	1/2	1/6	1/2	1	1
Sum	4.0833	5.6667	2.9444	12 1/2	26	20
$CI = \frac{(\lambda_{max} - n)}{(n-1)}$						
RI = 1.24						
Maximum Eigen value = 6.44						
$n = 6$						
CR = 0.071						

highly suitable category (Fig. 6.4i–o). However, in the case of the socioeconomic criterion, there were six parameters considered for reclassification. Among them, population density referred to the highest percentage (94.9%) of lands that belonged to highly suitable areas (Fig. 6.4p–t and Table 6.6). The results indicated that population density was the important criterion because the average population is important for proper agricultural intensification in vineyard operations.

6.3.2 Analytical Hierarchy Process Wieghts (AHP)

In this study, the suitable area was monitored in the vineyards of Kabul Province using the weighted overlay method. First, each parameter was reclassified referring to the perivous research, and then the AHP weight was assigned based on the expert's opinions (Tables 6.7 and 6.8). The AHP results for physical criterion were indicated that soil texture (13.2%) was the most influenced, followed by organic matter (11.9%), soil pH (11%), soil depth (10.6), soil salinity (8.2%), rainfall (7.6%), NDVI (5.6%), soil type (5.6%), LST (5.1%), NDMI (4.8%), aspect (4.8%), land cover (4.7%), elevation (3.4%) and with the least influenced by the slope (3.2%). Moreover, the AHP determined weight for the socioeconomic parameters

Table 6.5 Value of Random Consistency Index (RI) (Aguaron et al. 2003)

n	3	4	5	6	7	8	9	10	11	12	13	14	15
RI	0.525	0.882	1.115	1.252	1.341	1.404	1.452	1.484	1.513	1.535	1.555	1.570	1.583

Table 6.6 Reclassification of all physical and socioeconomic criteria for land suitability evaluation of vineyards

Criteria	S1 (highly suitable) Hectare	Percentage	S2 (moderately suitable) Hectare	Percentage	S3 (marginally suitable) Hectare	Percentage	N (not suitable) Hectare	Percentage
NDVI	30489.0	6.5	50573.1	10.9	0	0	384462.4	82.6
NDMI	7875.8	1.7	33855.8	7.3	28162.3	6.0	395630.6	85.0
LST	120249.5	25.8	228912.8	49.2	55044.8	11.8	61317.4	13.2
Rainfall	455461.7	100.0	0.0	0.0	0.0	0.0	0.0	0.0
Elevation	246017.8	52.7	131720.6	28.2	56679.5	12.1	32184.5	6.9
Slope	235639.7	51.2	147469.0	32.1	57799.4	12.6	19146.4	4.2
Aspect	258362.5	48.5	122650.3	23.0	115074.3	21.6	36355.7	6.8
River	1746.4	35.7	1097.3	22.4	745.1	15.2	1307.5	26.7
LC	81289.0	17.5	236768.9	50.9	9300.0	2.0	138168.0	29.7
pH	0.0	0.0	6703.2	100.0	0.0	0.0	0.0	0.0
Soil text	6601.7	98.5	0.0	0.0	77.2	1.2	23.7	0.4
Soil salinity	818.7	12.2	5875.9	87.7	0.0	0.0	8.6	0.1
Soil depth	149413.6	32.1	226194.4	48.6	37312.6	8.0	52580.7	11.3
Soil types	381497.9	82.7	22037.4	4.8	29374.2	6.4	28330.5	6.1
OM	378.7	5.6	2198.5	32.8	2484.7	37.1	1641.2	24.5
Population density	437732.6	94.9	16134.9	3.5	1090.3	0.2	6286.5	1.4
Benefit–cost	76.6	0.02	312.9	0.1	70099.7	15.4	384972.4	84.5
Road	2190.8	28.1	1371.0	17.6	952.2	12.2	3270.4	42.0
Local market	22431.9	4.9	34302.3	7.5	42439.6	9.3	356285.0	78.2
National Market	16032.5	38.9	9637.2	23.4	4763.7	11.6	10751.6	26.1
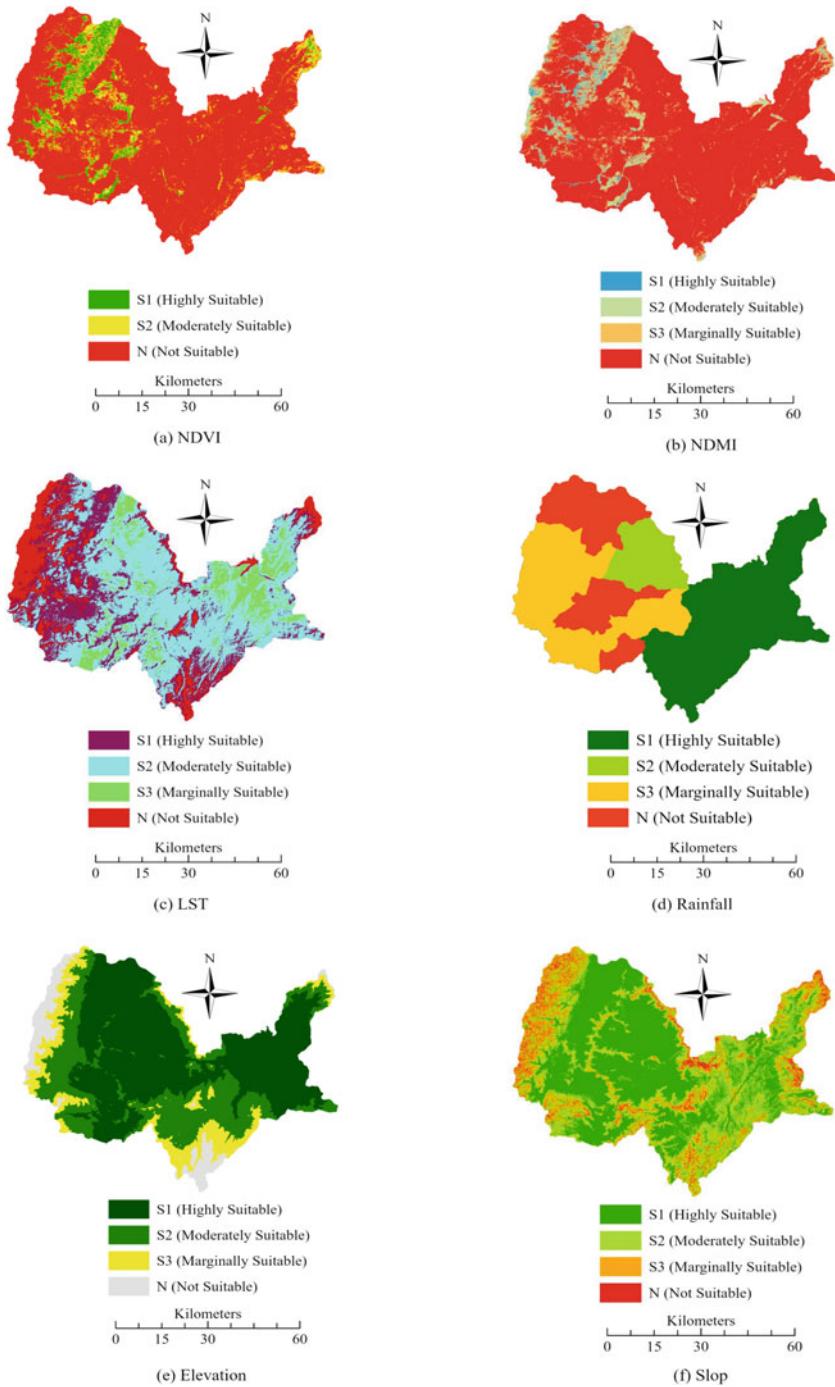
Fig. 6.4 Reclassification of criteria (**a–o**) for physical criterion and from (**p–t**) for socioeconomic criterion for vineyards suitability analysis
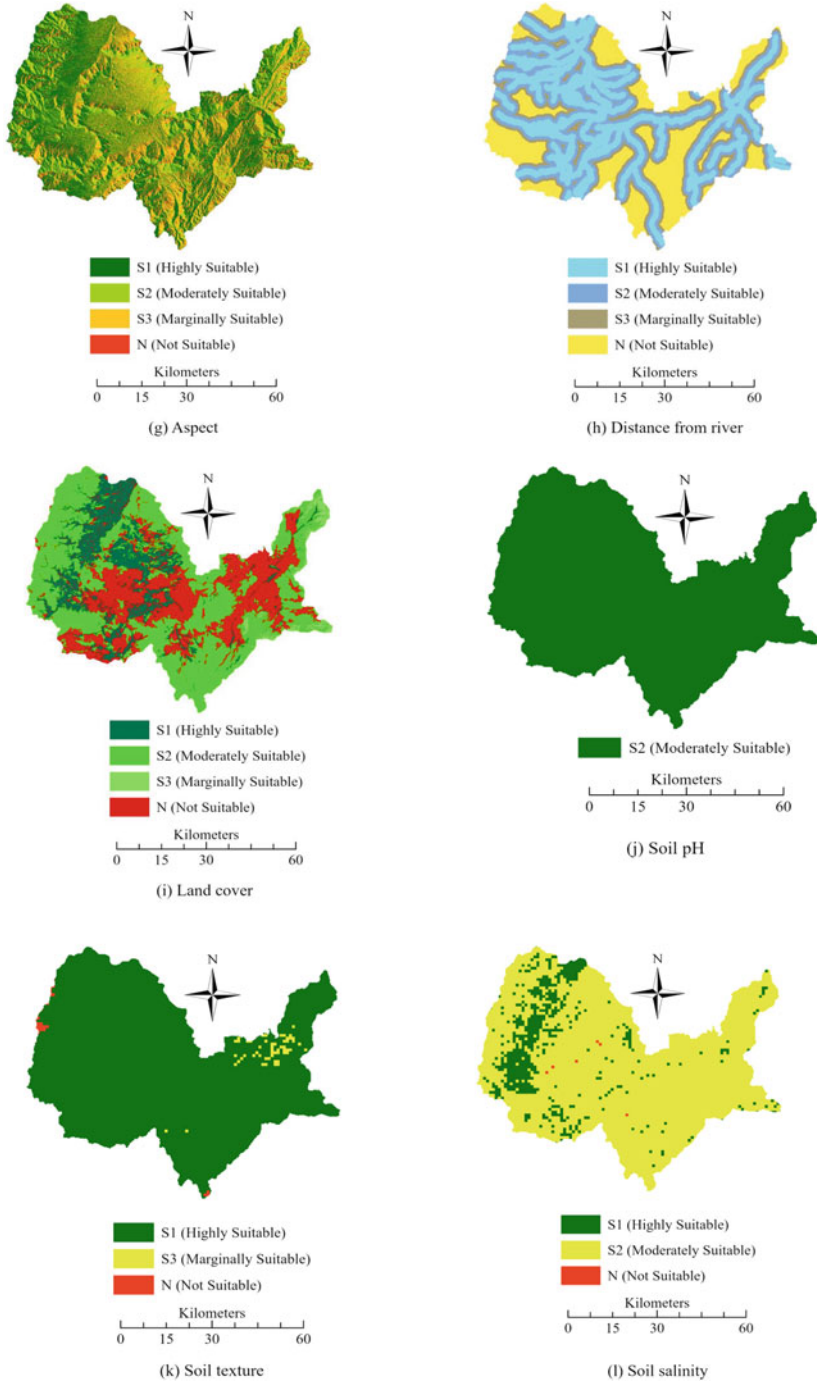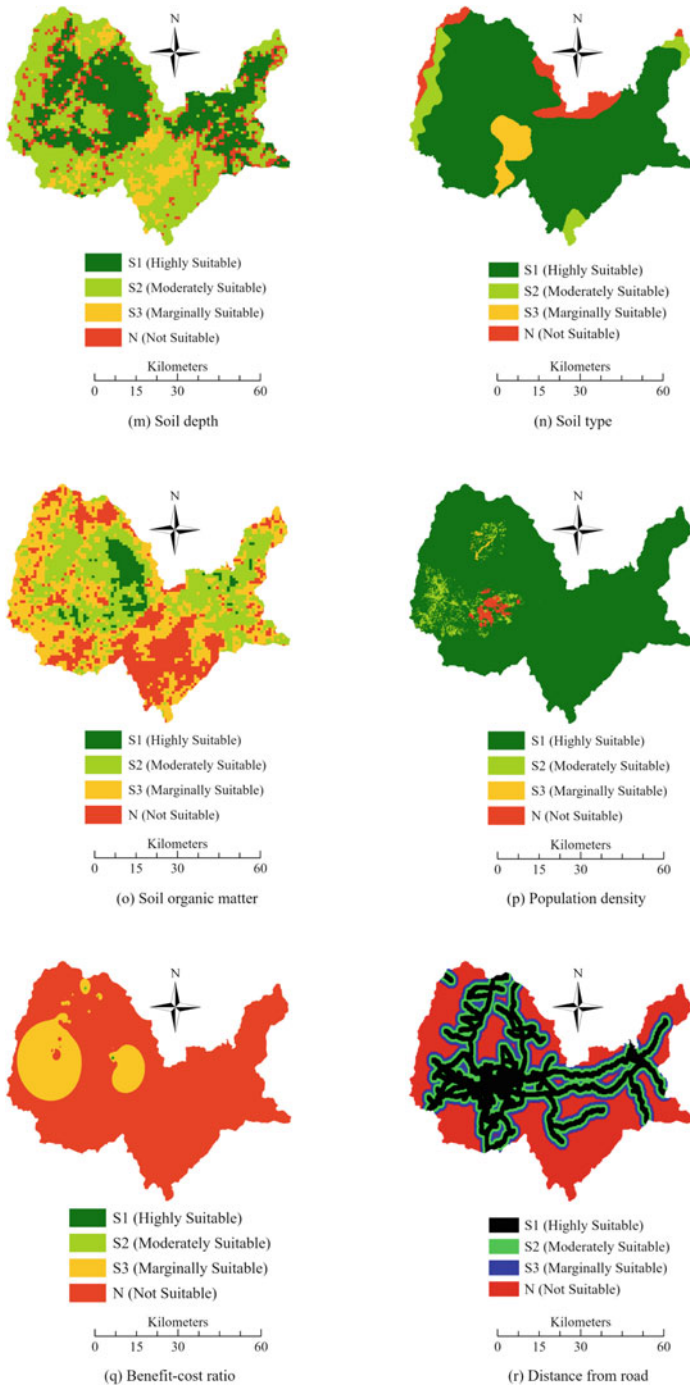
(g) Aspect

(h) Distance from river

(i) Land cover

(j) Soil pH

(k) Soil texture

(l) Soil salinity

Fig. 6.4 (continued)

(m) Soil depth

(n) Soil type

(o) Soil organic matter

(p) Population density

(q) Benefit-cost ratio

(r) Distance from road

Fig. 6.4 (continued)
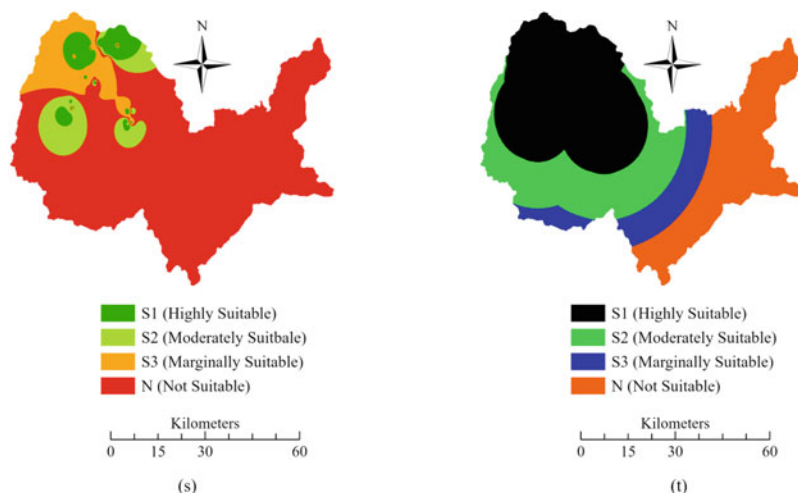
Fig. 6.4 (continued)

and the highest weight was observed for the distance from the road (22.4%), followed by distance from the national market (18.8%), distance from river (17.1%), population density (16.4%), the distance from local market (13.3%), and the benefit–cost ratio (12%). The integrated average weights were assigned from the expert's opinions and reported that the physical criterion had an influnce of 58%, and the socioeconomics criterion had 42% for table grape production (Tables 6.7 and 6.8).

6.3.3 Land Suitability Analysis

Suitable conditions were determined and reclassification was done for suitability analysis according to Appendix Table 6.10. First, the physical criterion map was developed using an AHP-based weighted overlay in the ArcGIS® environment. The results indicated that 11.1% of lands (739.17 ha) were highly, 24.8% (1654.5 ha) moderately, 35.7% (2376.4 ha) marginally, and 28.4% (1892.8 ha) lands were not suitable for grape production in the Kabul Province (Fig. 6.5). According to the physical criterion, the highly suitable lands were located in the north and east regions of Kabul Province. Furthermore, the socioeconomic criterion also considered AHP-based weights for developing the suitability map based on the socioeconomic criteria. The findings revealed that 15.7% (764.6 ha) of lands were highly suitable for grape production, 17.6% (861.7 ha) were moderately suitable, 28.4% (1385.3 ha) were marginally suitable, and 38.3% (1870.7 ha) were not suitable for grape production in Kabul Province (Fig. 6.6). The socioeconomic criterion is not directly

Table 6.7 AHP weights according the expert's opinions for physical criterion

No	Criteria	A (35)	B (16)	C (9)	D (8)	E (12)	Mean	Weight
1	Soil type	0.090	0.013	0.048	0.073	0.015	0.06	5.6
2	Soil pH	0.145	0.022	0.132	0.143	0.061	0.11	11.0
3	Soil depth	0.131	0.027	0.145	0.123	0.145	0.11	10.6
4	Soil texture	0.134	0.090	0.159	0.145	0.020	0.13	13.2
5	Soil organic matter	0.144	0.039	0.134	0.160	0.080	0.12	11.9
6	Soil salinity	0.088	0.014	0.126	0.101	0.172	0.08	8.2
7	Normalized difference vegetation index (NDVI)	0.043	0.081	0.065	0.040	0.161	0.06	5.7
8	Normalized difference water index in plant leaf (NDMI)	0.040	0.065	0.046	0.043	0.078	0.05	4.8
9	Rainfall	0.091	0.066	0.058	0.087	0.127	0.08	7.6
10	Slope	0.024	0.067	0.018	0.020	0.041	0.03	3.2
11	Elevation	0.021	0.080	0.015	0.019	0.026	0.03	3.4
12	Land surface temperature (LST)	0.023	0.132	0.031	0.020	0.019	0.05	5.1
13	Land cover	0.013	0.149	0.011	0.014	0.031	0.05	4.7
14	Aspect	0.012	0.155	0.011	0.013	0.023	0.05	4.8
Sum							1.00	100
Overall weight		0.8	0.6	0.6	0.5	0.4		0.58

[*]A–E indicated the expert numbers and number in parenthesis indicated the years of working experiences in the Agriculture sector for each of the experts, respectively
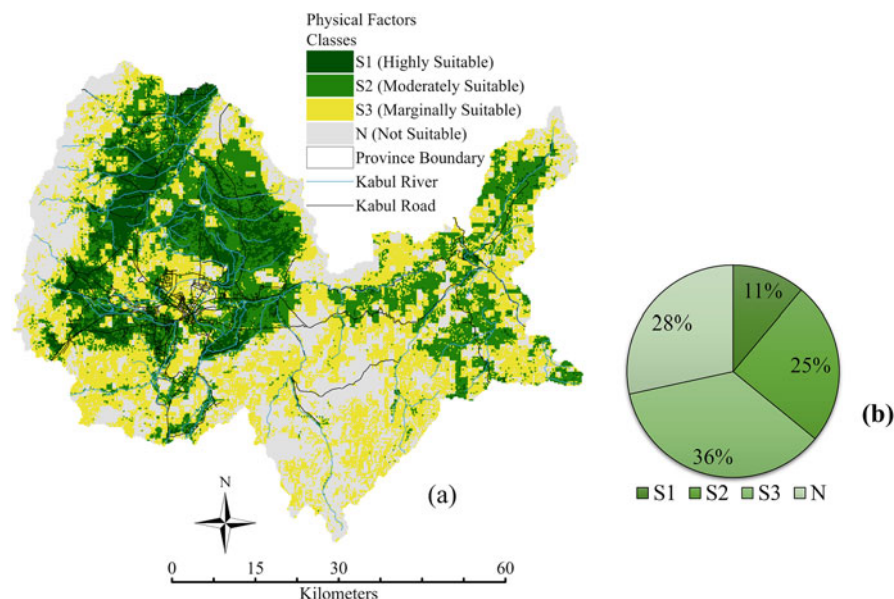
Table 6.8 AHP weights according the expert's opinions for socioeconomic criteria

No	Criteria	A (35)	B (16)	C (9)	D (8)	E (12)	Mean	Weight
1	Distance from road	0.286	0.386	0.227	0.087	0.133	0.22	22.4
2	Distance from river	0.175	0.283	0.330	0.026	0.040	0.17	17.1
3	Population density	0.355	0.063	0.329	0.037	0.037	0.16	16.4
4	Benefit–cost ratio	0.089	0.144	0.039	0.192	0.136	0.12	12.0
5	Distance from local market	0.044	0.074	0.038	0.131	0.380	0.13	13.3
6	Distance from national market	0.051	0.049	0.037	0.528	0.275	0.19	18.8
	Sum						1.00	100
	Overall weight	0.20	0.40	0.40	0.50	0.60		0.42

[*]A–E indicated the expert numbers and number in parenthesis indicated the years of working experiences in the Agricutlure sector for each of the experts, respectively

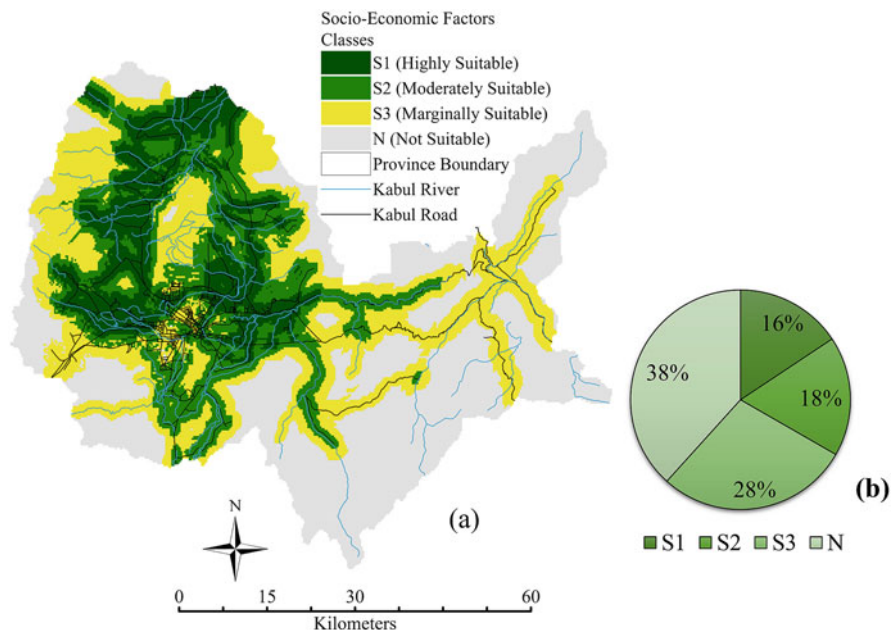**Fig. 6.5** (**a**) Land suitability analysis for grape production based on physical criterion in Kabul Province of Afghanistan and (**b**) pie chart showing the percentage of land for each of the four suitability classes

related to grape production, however, it has an important role in limiting table grape production.

Furthermore, the combined suitability map was developed from the physical and socioeconomic maps by considering average weights from the experts opionions. Both maps were overlaid based on the overall percentage of influence. According to the land suitability results, the most suitable areas were 12.9% (6993 ha) highly, 25.6% (1240.83 ha) moderately, 28.5% (1384.2 ha) marginally, and 32.9% (1600.9 ha) not suitable for grape production in the Kabul Province of Afghanistan (Fig. 6.7 and Table 6.9). Lastly, not suitable and marginal lands were identified from the combined land suitability map to support the growers by providing subsidies specially marginal and not suitable lands for production. According to the final suitability map, out of 1759 survey vineyards in the study area 1112 vineyards were located in highly suitable areas and 549 vineyards were located in moderately suitable areas. Therefore, the land suitabaility analysis based on phyiscal and socioeconomic criteria has a good scope to support the grapes growers to improve their livelihoods in the Kabul Province of Afghanistan.

Fig. 6.6 (**a**) Land suitability map for grape production based on socioeconomic criterion in Kabul Province of Afghanistan and (**b**) pie chart showing the percentage of land for each of the four suitability classes

6.4 Discussion

Synthesizing Landsat 8 OLI and TIRS scenes, metrological, topographic, soil, and socioeconomic datasets were used to develop a land suitability map for grape production in the Kabul Province of Afghanistan. The expert's judgment indicated that the soil texture and soil pH were the most important criteria for producing the grapes (13% and 11%). In the socioeconomic criteria, the distance from the road and distance from the national market were observed as the most essential criteria (22% and 18%). Previous studies also implied that the physical properties of vineyards, such as soil, are critically important for the grape's quality and productivity (Zdruli et al. 2014). These two socioeconomic indicators mentioned above were significant because of carrying the inputs to vineyards and transporting fresh grapes to the market in the study areas. On the other hand, field management practices, vineyard site selection based on topographic criterion, genotype, cultivar selection, soil texture, soil pH, fertilizer application, irrigation, and pest control play essential roles in determining quality, size, color, flavor, texture, and nutritional values of table grapes. Vineyards are in remote areas and it is difficult for farmers to carry fresh grapes to local and national markets. The infrastructure of a region is also most important for grape transportation. It causes the table grapes loses and waste due to
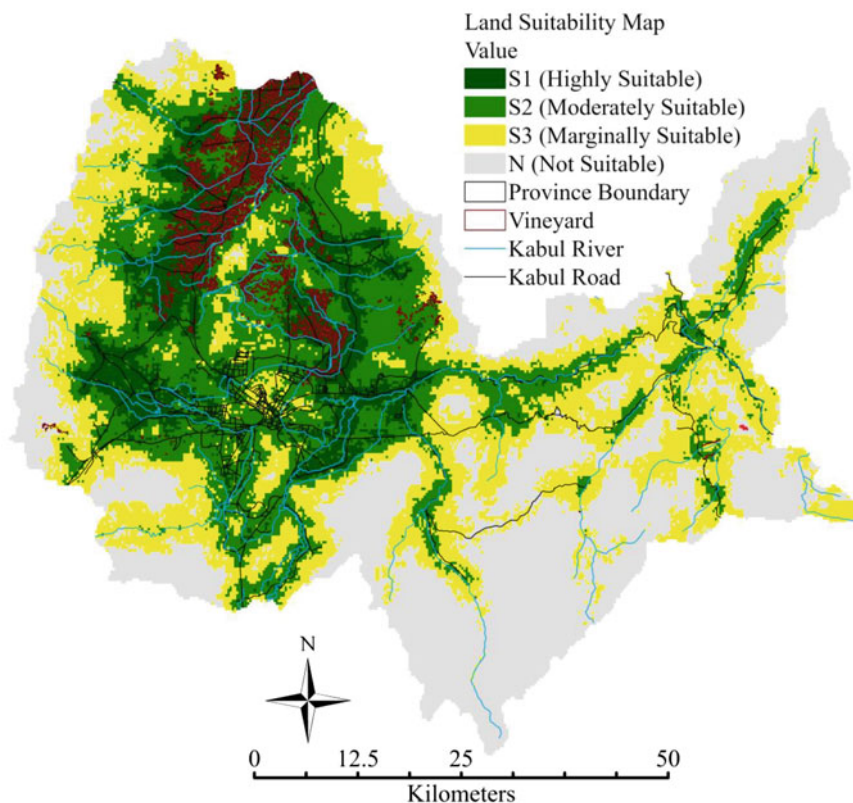
Fig. 6.7 Land suitability analysis combining physical and socioeconomic for grape production in Kabul Province

Table 6.9 Vineyards suitability classes based in Kabul Province of Afghanistan

Classes	Pixels	Area (ha)	Area%	Surveyed vineyards	Vineyards area (ha)
S1	6993	629.37	12.96248	1112	8223.90
S2	13,787	1240.83	25.55609	549	2200.59
S3	15,380	1384.2	28.50893	75	152.69
N	17,788	1600.92	32.97249	23	22.766
Total				1759	10599.96

lack of storage and poor transportation facilities. Therefore, a huge number of postharvest losses occur for fresh grapes each year in Afghanistan.

To promote grape production and improve grape grower household's income and livelihood, implementing a national subsidy program is very important for grape production based on land suitability and access to facilities and infrastructure. In

most countries, especially underdeveloped countries, the government has tried to reduce production costs, increase the welfare of farmers and their competitive power in global markets by providing a proper subsidy scheme to them. Currently, in Afghanistan, there is no specific subsidy scheme for grape growers, although agricultural subsidies are an essential aspect of agricultural production and play an important role in international trade. Therefore, a subsidy program can be introduced to increase grape production regionally by considering land suitability based on physical and socioeconomic criteria that influence production very much.

6.5   Conclusions

Appropriate selection of physical and socioeconomic criteria is important in land suitability analysis for increasing table grape production and productivity. The socioeconomic criteria significantly influence the livelihoods of vineyard growers and their decisions on whether to grow table grapes. Therefore, this study carried out the selection of multiple criteria to develop a land suitability model on a provincial scale to find out the suitable areas for table grape production. The multi-criteria decision analysis was performed for suitability assessment using 20 criteria, 14 focusing on the physical criterion and six for the socio-economic criterion. The physical criteria were elevation, slope, aspect, LST, rainfall vegetation indices (NDVI and NDMI), soil types, soil texture, soil structure, soil pH and soil organic matter. In the case of socioeconomic criteria, distance from road and river, distance from national market, distance from local market, population density, and benefit–cost ratio were taken into account in the suitability analysis. The suitability model used the FAO land use/land cover layer and masked the restricted zones for selecting the vineyard area. Through this research, we found that only 11% physically, 15% socioeconomically, and 13% of lands in a combination of both physical and socio-economic criteria were highly suitable for grape production in the Kabul Province of Afghanistan. This research has the potential to be applied toward determining the suitable areas on a regional scale with similar environmental conditions. Furthermore, inclusion of socioeconomic criteria in regional land suitability analysis can support the vineyard growers with the allocation of subsidies to increase the total production of table grapes and the livelihoods of growers.

Appendix

Table 6.10 Criteria classification for vineyard suitability analysis based on physical and socio-economics criterion

Criteria	Suitability classes	Threshold value	References
NDVI	S1	0.2–0.5	Hashim et al. (2019)
	S2	0.5–0.8	
	S3	0.8–0.9	
	N	>0.199	
NDMI	S1	0.6–0.8	Zhang et al. (2016)
	S2	0.4–0.6	
	S3	0.4–0.2	
	N	>0.2	
LST	S1	25–30 °C	Stanchi et al. (2013) and USAID (2016)
	S2	30–36	
	S3	36–43	
	N	<20	
Rainfall	S1	500 mm	Ted (2018)
	S2	–	
	S3	–	
	N	<800 mm	
Elevation	S1	800–2000 m	Stanchi et al. (2013)
	S2	2000–2500	
	S3	2500–3000	
	N	>3000	
Slope	S1	0–10°	Stanchi et al. (2013)
	S2	10–25°	
	S3	25–35°	
	N	35–44°	
Aspect	S1	North, Northeast, East	Modica et al. (2014)
	S2	South, Southeast, Southwest	
	S3	West, Northwest	
	N	North	
Soil PH	S1	5.5–6.5	Brown (2013)
	S2	4–8.5	
	S3	6.5–8.0	
	N	<5.0 and <8.0	
Topsoil texture	S1	Sandy loam, loam very fine sandy loam, loam very fine sand, coarse sandy loam	Badr et al. (2018)
	S2	Silt loam, loamy sand, loamy fine sand, loamy coarse sand	
	S3	Silt, silty clay loam, silty clay, clay loam, Sandy clay loam	
	N	Clay	

Criteria	Suitability classes	Threshold value	References
Topsoil types	S1	CMe (Eutric CAMBISOLS), CMg (Gleyic CAMBISOLS) CMu (Humic CAMBISOLS), CMx (Chromic CAMBISOLS), LVx (Chromic LUVISOLS).	Acharya and Yang (2015)
	S2	CMo (Ferralic CAMBISOLS),GLe (Eutric GLEYSOLS), PHc (Calcaric PHAEOZEMS), PHh (Haplic PHAEOZEMS RGd).	
	S3	RGd (Dystric REGOSOLS), RGi (Gelic REGOSOLS), FLc (Calcaric FLUVISOLS), LPi (Gelic LEPTOSOLS), RGe (Eutric REGOSOLS)	
	N	Rock outcrop Glacier, inland ice Lake, inland water	
Topsoil depth	S1	>50 cm	Rameshkumar et al. (2006)
	S2	20–50	
	S3	–	
	N	<20	
Soil organic matter (OM)	S1	Rich soil organic matter	Goldammer (2015)
	S2	–	
	S3	–	
	N	Poor soil organic matter	
Soil salinity	S1	Slight saline	Park et al. (2011)
	S2	Moderately saline	
	S3	N/A	
	N	Strongly saline	
Distance from road	S1	1000 m	Purnamasari et al. (2019)
	S2	1000–2000	
	S3	2000–3000	
Distance from river	N	>3000	
	S1	1000	
	S2	1000–15,000	
	S3	<500	
	N	>1000	
Population density	S1	Medium	Steiner et al. (2000)
	S2	Low	
	S3	–	
	N	High	
Distance from local market	S1	<2 km	Hossain and Das (2010)
	S2	2–4	
	S3	4–5	
	N	>5	

Criteria	Suitability classes	Threshold value	References
Distance from national market	S1	0–5 km	Nguyen et al. (2020)
	S2	5–10 km	
	S3	>10	
	N	–	
Benefit–cost ratio	S1	Above 1.2	Wali et al. (2016)
	S2	–	
	S3	–	
	N	Below 1.2	

References

Acharya TD, Yang IT (2015) Vineyard suitability analysis of Nepal. Int J Environ Sci 6(1):13. https://doi.org/10.6088/ijes.6002

Afghanistan Central Statistics Organization (ACSO) (2020) Central statistics organization of Afghanistan's statistical yearbook of 2018-2019. Islamic Republic of Afghanistan National Statistics and Information Authority, Kabul Afghanistan (42). April 2021. https://invest.gov.af/theme3/wp-content/uploads/2021/06/Afghanistan-Statistical-Yearbook-first-Version.pdf

Aguaron J, Escobar MT, Moreno-Jiménez JM (2003) Consistency stability intervals for a judgement in AHP decision support systems. Eur J Oper Res 145(2):382–393. https://doi.org/10.1016/S0377-2217(02)00544-1

Anyamba A, Tucker CJ (2012) Historical perspective of AVHRR NDVI and vegetation drought monitoring. In: Remote sensing of drought: innovative monitoring approaches, vol 23, p 20. https://digitalcommons.unl.edu/cgi/viewcontent.cgi?article=1217&context=nasapub

Aragüés R, Medina ET, Clavería I, Martínez-Cob A, Faci J (2014) Regulated deficit irrigation, soil salinization and soil sodification in a table grape vineyard drip-irrigated with moderately saline waters. Agric Water Manag 134:84–93. https://doi.org/10.1016/j.agwat.2013.11.019

Badr G, Hoogenboom G, Moyer M, Keller M, Rupp R, Davenport J (2018) Spatial suitability assessment for vineyard site selection based on fuzzy logic. Precis Agric 19(6):1027–1048. https://doi.org/10.1007/s11119-018-9572-7

Basile A, Albrizio R, Autovino D, Bonfante A, De Mascellis R, Terribile F, Giorio P (2020) A modelling approach to discriminate contributions of soil hydrological properties and slope gradient to water stress in Mediterranean vineyards. Agric Water Manag 241:106338. https://doi.org/10.1016/j.agwat.2020.106338

Bhattacharya S, Halder S, Nag S, Roy PK, Roy MB (2021) Assessment of drought using multi-parameter indices. In: Advances in water resources management for sustainable use, vol 131, p 243. https://www.usgs.gov/core-science-systems/nli/landsat/landsat-provisional-surface-temperature?qt-science_support_page_related_con=0#qt-science_support_page_related_con

Bonfante A, Agrillo A, Albrizio R, Basile A, Buonomo R, De Mascellis R, Terribile F et al (2015) Functional homogeneous zones (fHZs) in viticultural zoning procedure: an Italian case study on Aglianico vine. Soil 1(1):427–441. https://doi.org/10.5194/soil-1-427-2015

Bramley RGV, Ouzman J, Boss PK (2011) Variation in vine vigour, grape yield and vineyard soils and topography as indicators of variation in the chemical composition of grapes, wine and wine sensory attributes. Aust J Grape Wine Res 17(2):217–229. https://doi.org/10.1111/j.1755-0238.2011.00136.x

Brown D (2013) Soil sampling vineyards and guidelines for interpreting the soil test results. Michigan State Univ Ext 2(15):08. https://www.canr.msu.edu/news/soil_sampling_vineyards_and_guidelines_for_interpreting_the_soil_test_resul

Cardell MF, Amengual A, Romero R (2019) Future effects of climate change on the suitability of wine grape production across Europe. Reg Environ Chang 19(8):2299–2310. https://doi.org/10.1007/s10113-019-01502-x

Casanova M, Messing I, Joel A (2000) Influence of aspect and slope gradient on hydraulic conductivity measured by tension infiltrometer. Hydrol Process 14(1):155–164. https://doi.org/10.1002/(SICI)1099-1085(200001)14:1<155::AID-HYP917>3.0.CO;2-J

De Clercq WP, Van Meirvenne M, Fey MV (2009) Prediction of the soil-depth salinity-trend in a vineyard after sustained irrigation with saline water. Agric Water Manag 96(3):395–404. https://doi.org/10.1016/j.agwat.2008.09.002

Deluisa A, Giandon P, Aichner M, Bortolami P, Bruna L, Lupetti A, Stringari G et al (1996) Copper pollution in Italian vineyard soils. Commun Soil Sci Plant Anal 27(5–8):1537–1548. https://doi.org/10.1080/00103629609369651

Fan S, Gulati A, Thorat S (2008) Investment, subsidies, and pro-poor growth in rural India. Agric Econ 39(2):163–170. https://doi.org/10.1111/j.1574-0862.2008.00328.x

FAO (1976) Food and agriculture organization. A framework for land evaluation. FAO, Rome. http://www.fao.org/3/x5310e/x5310e00.htm. Accessed 25 Oct 2021

FAO (2020) Grape production in Asia Pacific in 2019, by country. Survived by FAO. https://www.statista.com/statistics/679330/asia-pacific-grape-production-by-country/#statisticContainer. Accessed 20 Oct 2021

Gattullo CE, Mezzapesa GN, Stellacci AM, Ferrara G, Occhiogrosso G, Petrelli G, Castellini M, Spagnuolo M (2020) Cover crop for a sustainable viticulture: effects on soil properties and table grape production. Agronomy 10(9):1334. https://doi.org/10.3390/agronomy10091334

Gemitzi A, Dalampakis P, Falalakis G (2021) Detecting geothermal anomalies using Landsat 8 thermal infrared remotely sensed data. Int J Appl Earth Obs Geoinf 96:102283. https://doi.org/10.1016/j.jag.2020.102283

Goldammer T (2015) Grape grower's handbook—a guide to viticulture for wine production, 2nd edn. APEX Publishers, Centreville, VA, p 484

Goldammer, T., (2018). Grape grower's handbook. A guide to viticulture for wine production. http://www.wine-grape-growing.com/

Gong J, Liu Y, Chen W (2012) Land suitability evaluation for development using a matter-element model: a case study in Zengcheng, Guangzhou, China. Land Use Policy 29(2):464–472. https://doi.org/10.1016/j.landusepol.2011.09.005

Hadri A, Saidi MEM, Boudhar A (2021) Multiscale drought monitoring and comparison using remote sensing in a Mediterranean arid region: a case study from west-Central Morocco. Arab J Geosci 14(2):1–18. https://doi.org/10.1007/s12517-021-06493-w

Hashim H, Abd Latif Z, Adnan NA (2019) Urban vegetation classification with NDVI thresold value method with very high resolution (VHR) PLEIADES imagery. Int Arch Photogramm Remote Sens Spat Inf Sci 2019:237–240. https://doi.org/10.5194/isprs-archives-XLII-4-W16-237-2019

Hatfield JL, Prueger JH (2015) Temperature extremes: effect on plant growth and development. Weather Clim Extrem 10:4–10. https://doi.org/10.1016/j.wace.2015.08.001

Hossain MS, Das NG (2010) GIS-based multi-criteria evaluation to land suitability modelling for giant prawn (Macrobrachium rosenbergii) farming in Companigonj Upazila of Noakhali, Bangladesh. Comput Electron Agric 70(1):172–186. https://doi.org/10.1016/j.compag.2009.10.003

Iacono MJ, Mlawer EJ, Clough SA, Morcrette JJ (2000) Impact of an improved longwave radiation model, RRTM, on the energy budget and thermodynamic properties of the NCAR community climate model, CCM3. J Geophys Res Atmos 105(D11):14873–14890. https://doi.org/10.1029/2000JD900091

Islam MM, Matsushita S, Noguchi R, Ahamed T (2021) Development of remote sensing-based yield prediction models at the maturity stage of boro rice using parametric and nonparametric approaches. Remote Sens Appl Soc Environ 22:100494. https://doi.org/10.1016/j.rsase.2021.100494

Jones BM, Kolden CA, Jandt R, Abatzoglou JT, Urban F, Arp CD (2009) Fire behavior, weather, and burn severity of the 2007 Anaktuvuk River tundra fire, north slope, Alaska. Arct Antarct Alp Res 41(3):309–316. https://doi.org/10.1657/1938-4246-41.3.309

Karnieli A, Agam N, Pinker RT, Anderson M, Imhoff ML, Gutman GG, Panov N, Goldberg A (2010) Use of NDVI and land surface temperature for drought assessment: merits and limitations. J Climate 23(3):618–633. https://doi.org/10.1175/2009JCLI2900.1

Kurtural SK (2007) Vineyard site selection. University of Kentucky Cooperative Extension Service. https://simpson.ca.uky.edu/files/vineyard_site_selection_in_ky_based_on_climate_and_soil_properties.pdf

Le Blanc D, Perez R (2008) The relationship between rainfall and human density and its implications for future water stress in sub-Saharan Africa. Ecol Econ 66(2–3):319–336. https://doi.org/10.1016/j.ecolecon.2007.09.009

Li C, Li H, Li J, Lei Y, Li C, Manevski K, Shen Y (2019) Using NDVI percentiles to monitor real-time crop growth. Comput Electron Agric 162:357–363. https://doi.org/10.1016/j.compag.2019.04.026

Lopez RA, He X, De Falcis E (2017) What drives China's new agricultural subsidies? World Dev 93:279–292. https://doi.org/10.1016/j.worlddev.2016.12.015

Lorenzo MN, Taboada JJ, Lorenzo JF, Ramos AM (2013) Influence of climate on grape production and wine quality in the Rías Baixas, North-Western Spain. Reg Environ Chang 13(4):887–896. https://doi.org/10.1007/s10113-012-0387-1

Loveland TR, Irons JR (2016) Landsat 8: the plans, the reality, and the legacy. Remote Sens Environ 185:1–6. https://doi.org/10.1016/j.rse.2016.07.033

Modica G, Laudari L, Barreca F, Fichera CR (2014) A GIS-MCDA based model for the suitability evaluation of traditional grape varieties: the case-study of 'Mantonico'Grape (Calabria, Italy). Int J Agric Environ Inf Syst 5(3):1–16. https://doi.org/10.4018/ijaeis.2014070101

Nguyen H, Nguyen T, Hoang N, Bui D, Vu H, Van T (2020) The application of LSE software: a new approach for land suitability evaluation in agriculture. Comput Electron Agric 173:105440. https://doi.org/10.1016/j.compag.2020.105440

Park S, Jeon S, Kim S, Choi C (2011) Prediction and comparison of urban growth by land suitability index mapping using GIS and RS in South Korea. Landsc Urban Plan 99(2):104–114. https://doi.org/10.1016/j.landurbplan.2010.09.001

Paul M, Negahban-Azar M, Shirmohammadi A, Montas H (2020) Assessment of agricultural land suitability for irrigation with reclaimed water using geospatial multi-criteria decision analysis. Agric Water Manag 231:105987. https://doi.org/10.1016/j.agwat.2019.105987

Purnamasari RA, Noguchi R, Ahamed T (2019) Land suitability assessments for yield prediction of cassava using geospatial fuzzy expert systems and remote sensing. Comput Electron Agric 166:105018. https://doi.org/10.1016/j.compag.2019.105018

Qian J, Ito S, Zhao Z, Mu Y, Hou L (2015) Impact of agricultural subsidy policies on grain prices in China. J Fac Agric Kyushu Univ 60(1):273–279

Rameshkumar S, Vadivelu S, Reddy R, Naidu L, Hegde R, Srinivas S (2006) Land suitability for grape cultivation and its economic evaluation in Rajanukunte watershed, Karnataka. http://isslup.in/wp-content/uploads/2018/09/Land-suitability-for-grape-cultivation-and-its.pdf

Ridley W, Devadoss S (2021) The effects of COVID-19 on fruit and vegetable production. Appl Econ Perspect Policy 43(1):329–340. https://doi.org/10.1002/aepp.13107

Saaty TL (1980) The analytic hierarchy process (AHP). J Oper Res Soc 41(11):1073–1076

Saaty TL (1985) Axiomatization of the analytic hierarchy process. In: Decision Making with multiple objectives. Springer, Berlin, Heidelberg, pp 91–108. https://doi.org/10.1007/978-3-642-46536-9_4

Saaty TL, Kearns KP (2014) Analytical planning: the organization of system, vol 7. Elsevier, Amsterdam

Saxton KE, Rawls WJ (2006) Soil water characteristic estimates by texture and organic matter for hydrologic solutions. Soil Sci Soc Am J 70(5):1569–1578. https://doi.org/10.2136/sssaj2005.0117

Schmidt HP, Kammann C, Niggli C, Evangelou MW, Mackie KA, Abiven S (2014) Biochar and biochar-compost as soil amendments to a vineyard soil: influences on plant growth, nutrient uptake, plant health and grape quality. Agric Ecosyst Environ 191:117–123. https://doi.org/10.1016/j.agee.2014.04.001

Shamsuzzoha M, Noguchi R, Ahamed T (2021) Damaged area assessment of cultivated agricultural lands affected by cyclone bulbul in coastal region of Bangladesh using Landsat 8 OLI and TIRS datasets. Remote Sens Appl Soc Environ 23:100523. https://doi.org/10.1016/j.rsase.2021.100523

Stanchi S, Godone D, Belmonte S, Freppaz M, Galliani C, Zanini E (2013) Land suitability map for mountain viticulture: a case study in Aosta Valley (NW Italy). J Maps 9(3):367–372. https://doi.org/10.1080/17445647.2013.785986

Steiner F, McSherry L, Cohen J (2000) Land suitability analysis for the upper Gila River watershed. Landsc Urban Plan 50(4):199–214. https://doi.org/10.1016/S0169-2046(00)00093-1

Taghizadeh-Mehrjardi R, Nabiollahi K, Rasoli L, Kerry R, Scholten T (2020) Land suitability assessment and agricultural production sustainability using machine learning models. Agronomy 10(4):573. https://doi.org/10.3390/agronomy10040573

Ted G (2018) The grape grower's handbook: a complete guide to viticulture for wine production, 3rd edn. Apex. https://www.amazon.com/Grape-Growers-Handbook-Viticulture-Production/dp/0967521254

United States Agency for International Development (USAID) (2016) Commercial Horticulture and Agricultural Marketing Program. Best Practices for GRAPE Production and Marketing in Afghanistan. https://static1.squarespace.com/static/5b69fa24506fbeb93ef780e2/t/5c65bc46e5e5f088ebcad662/1550171215318/Best+Practices+for+GRAPE+Production+and+Marketing+in+Afghanistan+Roots+of+Peace+ROP.pdf

United States Department of Agriculture (2021) Apples, grapes, and pears: world markets and trade. USDA, Washington, DC. https://apps.fas.usda.gov/psdonline/circulars/fruit.pdf

Wali E, Datta A, Shrestha RP, Shrestha S (2016) Development of a land suitability model for saffron (Crocus sativus L.) cultivation in Khost Province of Afghanistan using GIS and AHP techniques. Arch Agron Soil Sci 62(7):921–934. https://doi.org/10.1080/03650340.2015.1101519

Walt SM (2018) Land cover atlas. Foreign policy. https://ufdc.ufl.edu/AA00003612/00001/4j

Wolf TK, Boyer JD (2005) Vineyard site selection. https://vtechworks.lib.vt.edu/bitstream/handle/10919/50983/463-020_pdf.pdf

Worqlul AW, Jeong J, Dile YT, Osorio J, Schmitter P, Gerik T, Clark N et al (2017) Assessing potential land suitable for surface irrigation using groundwater in Ethiopia. Appl Geogr 85:1–13. https://doi.org/10.1016/j.apgeog.2017.05.010

Xu Y, Ramanathan V, Washington WM (2016) Observed high-altitude warming and snow cover retreat over Tibet and the Himalayas enhanced by black carbon aerosols. Atmos Chem Phys 16(3):1303–1315. https://doi.org/10.5194/acp-16-1303-2016

Zdruli P, Calabrese J, Ladisa G, Otekhile A (2014) Impacts of land cover change on soil quality of manmade soils cultivated with table grapes in the Apulia region of South-Eastern Italy. Catena 121:13–21. https://doi.org/10.1016/j.catena.2014.04.015

Chapter 7
GIS-Based MCA Modeling to Locate Suitable Industrial Sites in Suburb Areas of Bangladesh for Sustainability of Agricultural Lands

Nazia Muhsin, Ryozo Noguchi, and Tofael Ahamed

Abstract Land use changes significantly affect the sustainability of food security, ecological balance, and environmental protections in developing countries. Bangladesh is such a country that faces challenges from limited arable land resources, including the urbanization of agricultural lands and urban developments in suburban areas. Therefore, the aim of this chapter was to determine the land use changes over time in suburban areas that have potential for industrial growth. This chapter also assesses potential locations and the further growth of industries by land suitability analysis (LSA) to emphasize both agriculture and industries in terms of sustainable growth. A geographical information system (GIS)-based multi-criteria analysis (MCA) model was developed for the LSA to distinguish compact lands that were suitable for the economic zones of industries. Nine criteria, including seven constraints and 23 factors, are evaluated by the spatial analysis tools of ArcGIS®. An analytical hierarchy process (AHP) was applied to prioritize the criteria based on experts' opinions for the decision-making process of LSA. The study finds that densely located industrial areas have decreased agricultural lands by greater than 10% in the last two decades. Furthermore, the results of the LSA showed that only 4% of the lands were most suitable for industrial sites, whereas four compact lands had 16–10 ha of land, which was suitable for small industrial zones. Thus, the integrated GIS-MCA model could serve as a policy-planning tool to locate the economic zones of industries with sustaining agricultural lands and environmental protections.

Keywords Land suitability analysis · Geographic information system · Multi-criteria analysis · Analytical hierarchy process

N. Muhsin
Faculty of Engineering Studies, BGMEA University of Fashion and Technology, Dhaka, Bangladesh

R. Noguchi · T. Ahamed (✉)
Faculty of Life and Environmental Sciences, University of Tsukuba, Tsukuba, Ibaraki, Japan
e-mail: tofael.ahamed.gp@u.tsukuba.ac.jp

7.1 Introduction

Land use changes significantly affect the sustainability of food security, ecological balance, and environmental protection in developing countries. Bangladesh is the ninth most densely populated country in the world with 1265 people per sq. km of land area (World Bank 2020), faces similar challenges from limited arable land resources. Thus, agricultural land use has become an important domain for sustainable development to feed an increasing population. However, studies have noted that the agricultural lands of Bangladesh have decreased over time (Rahman et al. 2019; Islam et al. 2010). Aerial photographs and Landsat imageries were analyzed by Bangladesh's Soil Resource Development Institute (SRDI) to determine this land transformation (Hasan et al. 2013). Approximately, 0.13% of agricultural land was transformed to nonagricultural land per year from 1963 to 1983 (Rahman and Hasan 2003). The Rio + 20: National Report on Sustainable Development also mentioned that Bangladesh had been losing 1% of its agricultural land per annum to nonagricultural purposes during 1990–2010 (Bangladesh Ministry of Environment and Forests (BMEF) 2012). Further study reported that Bangladesh had lost 23,391 ha of agricultural land per year from 1976 to 2000 (Hasan et al. 2013). This annual loss of agricultural land increased drastically to 33,140 ha during the period of 2000–2010, resulting in a total of 8% of agricultural land losses from 1976 to 2010 (Hasan et al. 2013). Conversely, the settlement area had been rapidly increased, 1.1% in 2014 (Reddy et al. 2016).

The loss of agricultural land and increasing land area for urbanization and industrialization are causing unsustainable land use practices (Rahman et al. 2018; Mahfuza et al. 2019). Industries had been expanded from city areas to suburban areas and occupied agricultural lands, creating a major challenge for food production in the long run (Rezvi 2018). Thus, National Strategy for Accelerated Poverty Reduction II (NSAPR II) emphasized developing efficient land markets and modern economic zones to improve land use management and to achieve environmentally and socially compliant industrialization (Planning Commission 2009). Furthermore, referring to the Bangladesh Economic Zones Act (No. 42, 2010), Bangladesh Economic Zones Authority (BEZA) aims to establish economic zones in all potential areas of Bangladesh including backward and underdevelopment regions. In addition, according to this act, the government could notify the official gazette, to select any specific land area and could declare it as an economic zone. Since the economy is in the growing stage, there is a high possibility of land encroachment across the country to establish industrial and manufacturing sectors. However, priority should be given to protect existing agricultural lands and environmental issues while identifying any suitable land sites. In this regard, land suitability analysis (LSA) could be the most appropriate approach to evaluate and fulfill the required criteria for these facilities. Therefore, the hypothesis of this empirical research is that the suitable site location of the industry for economic growth could reduce the pressure of transformation of agricultural lands to scatted expansion of industries throughout the suburb areas.

The LSA tool is used to identify the most suitable places for a specific land use type (Collins et al. 2001). It has identified the most appropriate spatial patterns for future land uses according to specific requirements, preferences, or predictors of some activities (Malczewski 2004). In other words, LSA is a spatial decision-making process where a number of elements are evaluated to follow the requirements of stakeholders and environmental issues (Jankowski and Richard 1994).

Thus, this study uses multi-criteria decision analysis (MCDA) with spatial solutions in a geographic information system (GIS) to conduct LSA. Multi-criteria analysis with GIS has the advantages to support decision-making process by a systematic way and reflect a transparent decision by the use of thematic maps (Ferretti and Pomarico 2013). The GIS-based MCDA method is described as a procedure that accumulates and transforms spatial and nonspatial data (input) into a resultant decision (Malczewski 2004). The MCDA method builds a connection between the input map and output map by utilizing geographical data and the judgment values of decision makers according to the facts and correlates the specified decision rules (Malczewski 2004; Rahman et al. 2012). The MCDA methods can be used in a GIS environment, such as Boolean overlays, Weighted Linear Combinations (WLC), Ordered Weighted Averaging (OWA), the Analytical Hierarchy Process (AHP), and Multiple-objective land allocation (MOLA) (Rikalovic et al. 2014). The integration of multi-criteria methods for land suitability analysis with a GIS system has broadened the spatial proficiencies of GIS and explored this system's analytical power as a decision-support tool.

This multidisciplinary approach has diverse applications in spatial analysis such as it has been widely used for the land suitability analysis for different agricultural crops (Joshua et al. 2013; Bera et al. 2017; Habibie et al. 2021). Further, this approach used for evaluating land use and land cover change (Hassan and Nazem 2016), siting waste incinerator plant (Ferretti and Pomarico 2012), development of urban aquaculture (Hossain et al. 2009), ecotourism (Mansour et al. 2020), landfill site selection (Rahmat et al. 2017), locating wind and solar power plants (Anwarzai and Nagasaka 2017). A group of researchers (Chandio et al. 2013) had listed peer-reviewed papers published during 1980–2011 using MCA in various spatial analysis on his review paper. Researchers had stated the MCA approach as a powerful integrated method for land suitability analysis of complex land use scenario (Saleh et al. 2015). In spite of having feasible application of this spatial approach for selecting land sites for sustainable urbanization and industrialization, few attempts were made in the past and require developing a robust system to practice in different land use scenarios.

Past studies of industrial site selection process showed there is a scope to develop the technique. For example, a macro-level-based study for the industrial site selection used GIS based fuzzy inference systems (FIS) and AHP to establish the weights for the different criteria, and the final aggregation conducted in MCDA4ArcMap (Rikalovic et al. 2015). This system is useful only when the spatial analysis is done on vector-based GIS system, a system deal with point, lines and polygons which is not suitable for a mixed land use type. An attempt was done to use the GIS-based AHP approach for the industrial site selection where seven criteria were selected for

evaluation (Edrahim et al. 2015). Here, AHP was conducted taking one expertise's evaluation, which had the possibility of having a bias judgment. In addition, the scoring of the individual criterion was not explained properly. Furthermore, Eldin and Sui (2003) used Component Object Model (COM) for designing a decision support system for industrial site selection. The study suggested two phases, where first phase was used for site screening which was done by the expert system (ES) and the GIS. In the second phase, AHP was used to evaluate nonspatial criteria. However, a prototype approach was applied as it was unable to deal with complexities of GIS and can deal with a limited range of industrial facilities and criteria. In addition, the COM Technology was applied for integrating loose coupling and tight coupling for industrial site selection (Eldrandaly et al. 2005). The research was the initial attempt to provide a user-friendly approach where the only candidate sites were taken to evaluate the approach and among those sites four final sites where chosen by the AHP method. Considering the limitations of the past research, the present study has introduced a model of land suitability analysis for industrial site selection using GIS and AHP. The latitude of flexibility of LSA model must have the applicability from the local level to national level for industrial site selection.

Therefore, the objective of this study is to perform LSA to locate the most suitable economic zone of industries without affecting existing agricultural land uses. Furthermore, land use changes that exhibit greater influence on industrialization in suburban areas are considered for spatial analysis to determine sustainable uses of agricultural lands and the growth of industries. In search of the potential regions to complement Bangladesh Economic Zones Act 2010, the study selected Savar, an adjacent subdistrict of the capital city Dhaka as a case study. However, the research approach also focuses the application in the larger spatial scale, especially micro- to macro-level geographical extents.

7.2   Materials and Methods

7.2.1   Conceptual Framework

This research was conducted in two phases. During the first phase, an analysis was conducted to assess agricultural land use changes in terms of the effects of industrial growth on agricultural land use (Fig. 7.1). The study area was mostly reported rapid growth from urbanization and industrialization over the last three decades (Rashid 2003; Sharif and Esa 2014). Thus, statistical data of agricultural land use was collected from the local agricultural office named Office of the Upazila Agriculture Officer, Savar, Dhaka, Bangladesh. A map was prepared in ArcGIS 10.3® based on statistical agricultural land use data from 2002 to 2011. On the other hand, the geographical positions of 420 factories were collected with a Garmin eTrex 30® during the field surveys. The geographical positions of the factories were mapped over the study area and observed the industrial growth over the agricultural land use during 2002–2011.
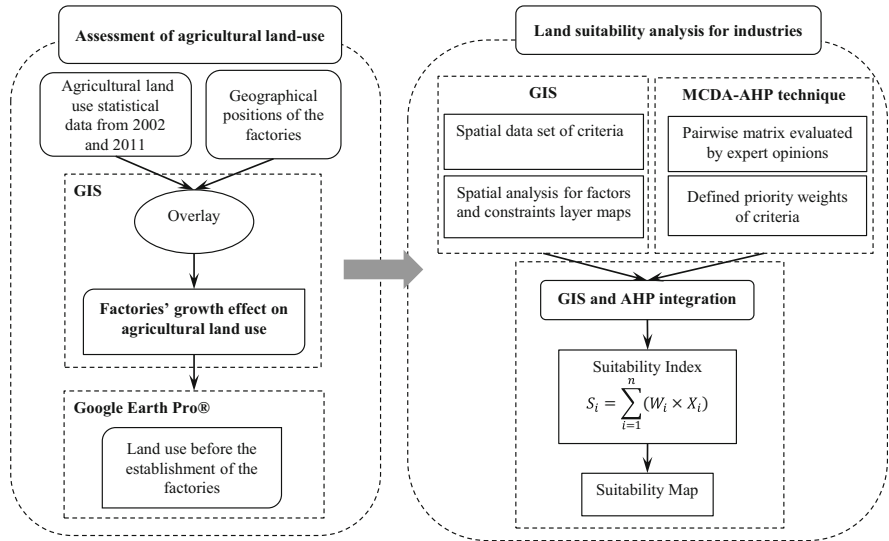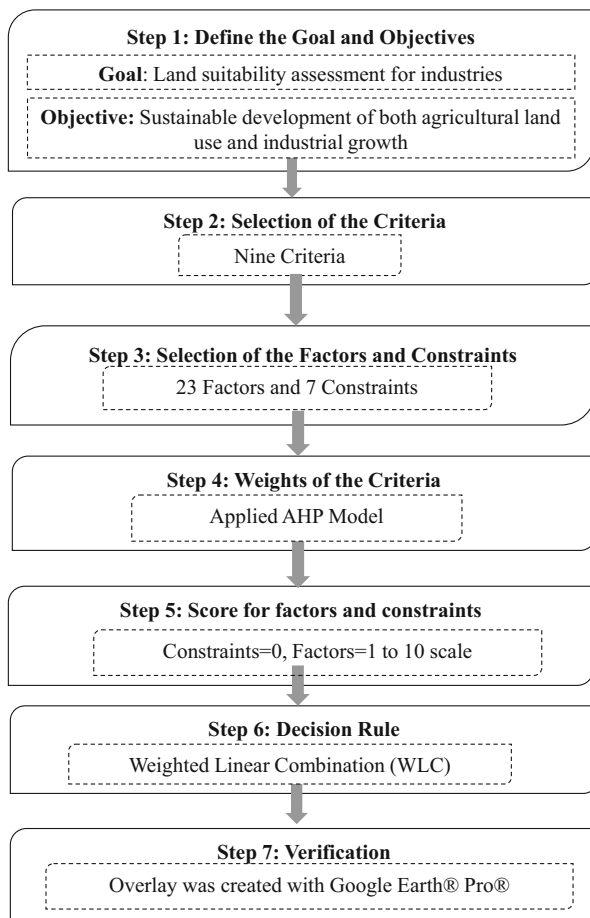
Fig. 7.1 Conceptual framework for the agricultural land use assessment and land suitability analysis

In the second phase, LSA was performed to locate suitable sites for expanding industries. Studies have mentioned that 80% of the data used by the decision makers and managers are related to geographical matters (Worall 1991). Thus, a widely used combination for spatial decisions, GIS and AHP as an MCA technique, was adopted for the LSA. The MCA was conducted with 23 factors and 7 constraints under 9 criteria, which were selected based on field surveys, previous research, and discussions with experts. The AHP approach was used to incorporate experts' preferences to prioritize the criteria's weights. On the other hand, GIS was applied to manage the thematic spatial data set of the criteria and to prepare the factors and constraint layer maps by spatial analysis tools. A decision rule was applied to integrate the GIS and AHP to extract a suitability map.

7.2.2   MCA Procedure for LSA

LSA is a difficult task since there are different domains such as socioeconomic situations, environmental aspects, topographic elements involved. In addition, it also relates to the local legislation and availability of lands. The complexity increases while dealing with mixed land use and densely populated areas (Morales and de Vries 2021). Hence, this study used MCA in seven steps in spatial environment (Fig. 7.2). The study selected nine criteria to conduct the MCA following the research goal and objectives. Beinat and Nijkamp (1998) defined criteria as a basis for decisions that could be measured and evaluated. While selecting criteria for

Fig. 7.2 Multi-criteria
analysis for land suitability

Step 1: Define the Goal and Objectives

Goal: Land suitability assessment for industries

Objective: Sustainable development of both agricultural land use and industrial growth

Step 2: Selection of the Criteria

Nine Criteria

Step 3: Selection of the Factors and Constraints

23 Factors and 7 Constraints

Step 4: Weights of the Criteria

Applied AHP Model

Step 5: Score for factors and constraints

Constraints=0, Factors=1 to 10 scale

Step 6: Decision Rule

Weighted Linear Combination (WLC)

Step 7: Verification

Overlay was created with Google Earth® Pro®

industries location, Eugene and Prasanta (2005) stated that environmental and social factors are the most important aspects for sustainable development of industries. Ensuring these factors for site selection helps in maintaining high level of productivity throughout the project's life. Thus, selected criteria for the current study mostly focused on the environmental and social aspects.

The criteria of this study were the proximity to major roads, proximity to local roads, distance from rivers, distance from water bodies, distance from settlements, flood flow zones, distance from agricultural lands, slope, and elevation. These criteria were further classified into factors and constraints for assessment. According to Beinat and Nijkamp (1998), a factor is a criterion that enhances or detracts from suitable alternatives for the activity under consideration, and a constraint serves to limit any alternatives. Furthermore, expert opinions were taken based on a questionnaire for the AHP technique to evaluate the priority weights of the criteria. A score was assigned to each factor on a scale of "1–10" and constraints stated as

"restrictions." To aggregate the weights of the criteria and the scores of corresponding factors and constraints under each criterion, a decision rule called weighted linear combinations (WLC) was applied to determine suitable locations for industries. The resulting map was further analyzed to distinguish compact lands that could be suggested for industrial zones. The result was then projected in Google Earth Pro® to evaluate the results.

7.2.3   Study Area

The study was conducted in Savar, 25 km from the capital city of Dhaka, a part of *Rajdhani Unnayan Kartripakkha* (RAJUK), the Capital Development Authority of the Government of Bangladesh. According to the Savar Agricultural Department data of 2011, Savar had 63.75% agricultural lands. The interface between rural and urban areas is significant in the northwestern and southeastern areas of Savar. The geographical position of Savar is located between 23°44′15.51″N and 24°1′29.19″N and between 90°11′22.78″E and 90°21′31.17″E (geographical coordinates in degrees-minutes-seconds, WGS84). The total area of Savar is 280.13 km^2 and the neighbor subdistricts are Kaliakair and Gazipur Sadar to the north; the Keraniganj to the south; Mirpur, Mohammadpur, Pallabi and Uttara Thanas of the Dhaka City Corporation to the east; and the Dhamrai and Singair subdistricts to the west (Fig. 7.3). The land height gradually increases from east to west, and the area is bounded by the Bangshi, Turag, Buriganga, and Karnatali rivers. The population density of Savar was 4948 per km^2 in 2011, an increase of 8.84% per year from the previous census in 2001. Around 78.6% of the population was distributed in rural areas and the rest in urban areas (Bangladesh Bureau of Statistics (BBS) 2011).

The study area has several land types, including highland, medium highland, medium high- to medium lowland, lowland and very lowland, based on their drainage, elevation, and pedological properties (Rashid 2003). The highlands are flood free and are mostly used for growing vegetables throughout the year. These lands are relatively less productive for rice. Highlands are the most suitable for permanent infrastructural development. The medium high to medium lowlands are used for single crops, such as High Yielding Variety (HYV) and Boro rice, because these areas are fertile lands. The lowlands and very lowlands are very suitable for agricultural purposes because these lands receive prolonged flood waters from the Dhaleshwari, Bansi, and Turag Rivers. As per the 2011–2012 data from the Savar Agricultural Office, Savar provides rice (Boro, T-aman, Aus), wheat, maize, mustard, nuts, pluses, vegetables, fruits, spices, etc. According to the employment status of the dwellers of Savar, 14.54% people were engaged in agriculture, 42.57% in industry, and rest 42.89% in Service sector (BBS 2011). The agricultural industries in Savar include combined fisheries, dairies, poultries, and hatcheries. On the other hand, Savar is mostly known as industrial hubs due to the number of manufacturing industries such as ceramics, beverages, garments, footwear, jute mills, textile mills,
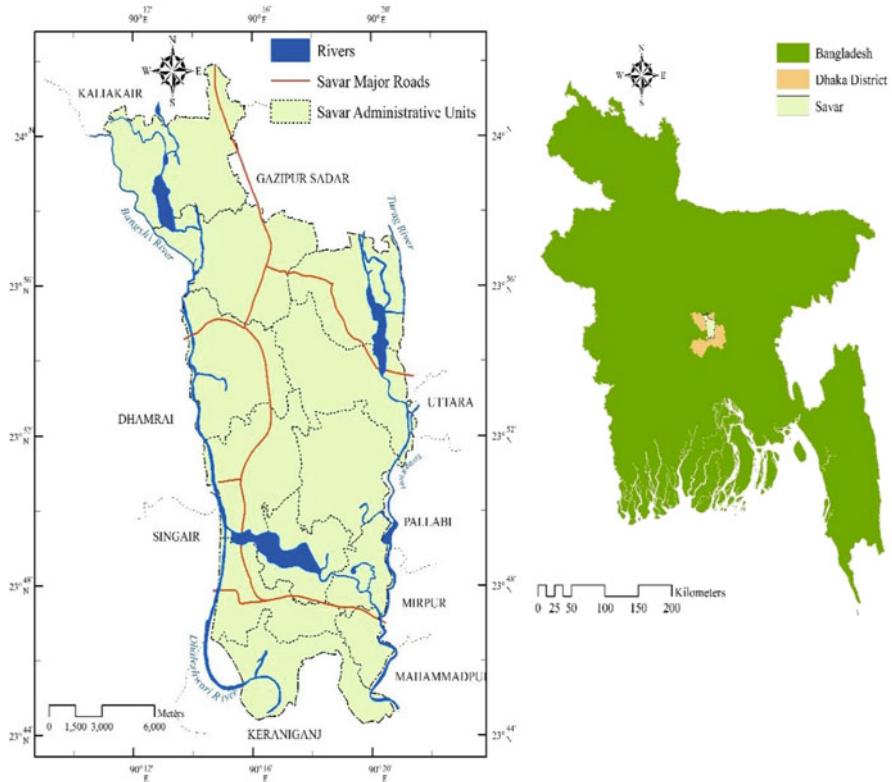
Fig. 7.3 Location map of the study area

automobiles, pharmaceuticals, brick fields, etc. The second largest export processing zone, Dhaka EPZ of Bangladesh was established in 1993 in Savar.

7.2.4 Field Survey

Statistical data of agricultural land in 2002 and 2011 were collected from the local agricultural office during a field survey in Savar. A list of cloth industries in Savar was received from the Bangladesh Garment Manufacturers and Exporters Association (BGMEA). A global positioning system (GPS) (GARMIN eTrex 30®) was used to collect the geographical positions of 420 factories. Nine criteria were selected based on field observations and discussions with stakeholders. A questionnaire based on the AHP method was used to record experts' opinions for the pairwise comparison of criteria. In addition, spatial maps of the criteria were received from different organizations for GIS analysis (Table 7.1).

Table 7.1 List of feature maps that were analyzed in GIS

No.	Maps	Source	Scale
1	Savar Administrative Boundary Map, 2010	LGED[a], Bangladesh	1:50,000
2	Savar Main Roads Map, 2013	LGED, Bangladesh	1:50,000
3	Savar Local roads Map, 2013	LGED, Bangladesh	1:50,000
4	Savar Settlement Boundary Map, 2010	LGED, Bangladesh	1:50,000
5	Savar Rivers Map, 2010	LGED, Bangladesh	1:50,000
6	Savar Water Bodies Map, 2010	LGED, Bangladesh	1:50,000
7	Savar Agricultural land Map, 2013	RAJUK[a], Bangladesh	1:50,000
8	Savar Flood Zone Map, 2013	RAJUK, Bangladesh	1:50,000
9	Digital Elevation Map (DEM)	Shuttle Radar Topography Mission (SRTM)	1 arc-second for global coverage (~30 m)

[a]*LGED* Local Government Engineering Department, *RAJUK Rajdhani Unnayan Kartripakkha* (Capital Development Authority)

7.2.5   Criteria, Factors, and Constraints

One of the major steps in locating suitable sites is to form a set of dominant factors that are applicable to site selection (Rikalovic et al. 2014). Thus, combined knowledge from local stakeholders, discussion with experts, field observations, and previous studies can be applied to select and score the factors and constraints of criteria (Table 7.2).

Proximity to Major Roads

Road communication media was the most important criterion when selecting a factory site. Import of the raw materials and exports of the final goods are conducted though the main port. National highways, regional highways, and district roads are the main routes to the Chittagong port, which is located in the southeastern part of the country, 308 km from Savar. Chittagong city is the second largest city in the country. The national highway N1 or Dhaka Chittagong National route connects the two largest cities of Bangladesh by 250 km road taking approximately 7–8 h travel time. Emphasizing on the efficiency of the road communication network, in 2016, the N1 national highway has developed with four lanes highway to reduce the travel time. Thus, assessing the distances of the factory locations to national highways is very important. A higher distance affects the transportation costs and production lead time. The closer the factory's location, the lower the transportation costs and

Table 7.2 Scores and suitability classifications of factors and constraints

No.	Name of the criteria	Factors/constraints	Classified	Score[a]	Suitability
1	Proximity to major roads	0–100 m	Constraints	0	Not suitable
		100–500 m	Factors	10	Most suitable
		500–1000 m	Factors	8	Moderately suitable
		1000–1500 m	Factors	6	Less suitable
		1500–2000 m	Factors	4	Least suitable
		>2000 m	Factors	2	Suitable but avoided
2	Proximity to local roads	0–50 m	Constraints	0	Not suitable
		50–200 m	Factors	10	Most suitable
		200–400 m	Factors	6	Less suitable
		>400 m	Factors	2	Suitable but avoided
3	Distance from rivers	0–500 m	Constraints	0	Not suitable
		500–750 m	Factors	4	Least suitable
		750–1000 m	Factors	8	Moderately suitable
		>1000 m	Factors	10	Most suitable
4	Distance from water bodies	0–100 m	Constraints	0	Not suitable
		>100	Factors	10	Most suitable
5	Distance from settlements	0–50 m	Constraints	0	Not suitable
		>50 m	Factors	10	Most suitable
6	Flood flow zones	Flood flow zone	Factors	2	Suitable but avoided
		Non-flood flow zone	Factors	10	Most suitable
7	Distance from agricultural lands	0–50 m	Factors	2	Suitable but avoided
		>50 m	Factors	10	Most suitable
8	Slope	0–5%	Factors	10	Most suitable
		6–10%	Factors	8	Moderately suitable
		11–15%	Factors	6	Less suitable
		>15%	Constraints	0	Not suitable
9	Elevation	0–5 m	Constraints	0	Not suitable
		6–10 m	Factors	6	Less suitable
		11–15 m	Factors	8	Moderately suitable
		>15 m	Factors	10	Most suitable

[a]Scores are given based on field observations, discussion with experts, and previous studies

production lead time. In addition, considering the existing distribution of factories, which are mostly located near the local and major roads, the buffer zones distances were taken. Distance beyond 100 m, namely, 100–500 m, were scored "10" for "most suitable"; 500–1000 m were scored "8" for "moderately suitable"; 1000–1500 m were scored "6" for "less suitable"; 1500–2000 m were scored "4" for "least suitable"; and greater than 2000 m were scored "2" for "suitable but avoided." However, 100 m buffer zones from major roads are not suitable for any industrial site to maintain a safe distance from major roads; thus, the 100 m buffer

area around major roads were considered as constraints of the criterion and scored "0," i.e., "not suitable" (Ohri et al. 2010).

Proximity to Local Roads

Most of the factories were connected to major roads via local roads. Therefore, 50–200 m buffer zones around the roads were scored "10" for "most suitable"; 200–400 m were scored "6" for "less suitable"; and greater than 400 m were scored "2" for "suitable but avoided." A 50 m buffer zone around the roads was taken as a constraint and scored "0," i.e., "not suitable," for any industrial operation to maintain a safe distance (Ohri et al. 2010).

Distance from Rivers

The study area is surrounded by rivers. During the last few decades, due to drain, the untreated industrial waste of the existing textile industries, the quality of the river water has degraded extensively (Arefin and Rahman 2016). The Department of Environment (DoE) of Bangladesh, in 2009, declared that Turag and Buriganga rivers of the study area are in ecologically critical state (River Quality Report 2015). Considering the environmental protections and hazard risks, the "most suitable" industrial sites were considered to be 1000 m from the rivers, which were scored "10." In addition, a 500-m buffer zone around the rivers was considered "not suitable" for any industrial site and thus was considered a constraint and scored "0." Beyond this constraint, a 500–750-m buffer zone was scored "4," i.e., "least suitable," and a 750–1000-m zone was scored "8," i.e., "moderately suitable."

Distance from Water Bodies

Water bodies are also a concern because of environmental hazard issues. Industrial wastewater and solid waste can affect water bodies and the agricultural lands. Thus, a 100-m buffer zone around water bodies was treated as a restriction, i.e., "not suitable", and scored "0". Areas beyond this restriction zone were considered "most suitable" and scored "10" (Ohri et al. 2010).

Distance from Settlements

Settlements were the most significant criteria. The rapid transformation of land use and the growth of urbanization and industrialization have a complex land cover of Savar. Industries are scattered from city areas to suburban areas and influence rural settlements. However, industrial sites must maintain a certain distance from the settlements to prevent environmental hazards. Eugene and Prasanta (2005)

suggested 100 m distance between residential area and limestone quarry operations for cement industry. However, the current study focused on searching suitable sites for compact zones, which will be separated from the other urban settlements. In addition, considering the vacant land crisis in Bangladesh, a 50 m buffer zone around the settlement area was chosen as restrictions, i.e., "not suitable," and scored "0." Other locations were considered "most suitable" and scored "10."

Flood Flow Zone

Flood flow zones are mostly located in the eastern and western areas of Savar. Floods occur mostly during the monsoon season (Jakobsen et al. 2005). Once flood water starts to decrease, the land become usable for agriculture. Thus, flood flow zones were scored "2" for "suitable but avoided", and non-flood zones were considered the "most suitable" places under this criterion and scored "10".

Distance from Agricultural Lands

Agricultural lands are located mostly in the middle of Savar. As mentioned above, the flood risk areas are also used for agricultural purposes when the water level decreases. In Bangladesh, the agricultural lands are mostly owned by the small-scale farmers and thus it is comparatively less expensive and easy to transform for nonagricultural purposes (Add reference). The study also stated that the land ownership and the nonagricultural occupation of household heads were the two prime reasons for agricultural land transformation, resulting in degradation of the agrarian income and productivity (Quasem 2011). On the other hand, there was lack of impact and implementation of the land-use policies reported in the 1950 State Acquisition and Tenancy Act and the 2001 National Land Use Policy of Bangladesh (Alam et al. 2016). Although these historical land policies emphasized on the conservation of the agricultural lands and confined transformation to nonfarming purposes, there was room for flexibility, which caused the policies ineffective (Quasem 2011). The most recent initiative from the ministry of land is the draft of "Agricultural Land Protection and Land Use Act 2015," which is in the pipeline to be finalized (Karim 2015). However, it is undoubtful by existing policies that agricultural lands should not be used for nonagricultural uses. Thus, a buffer zone of 50 m around the agricultural lands was considered as "suitable but avoided" and scored "2" and beyond 50 m was taken as "most suitable."

Slope

Higher slope increases the cost of the facility's construction and the inconvenience of the transportation of goods. The study area has no sloped areas, but the slope is considered a basic criterion for land suitability analysis. Thus, a 0–5% slope rise was

considered "most suitable" and scored "10," and 6–10%, 11–15%, and greater than 15% were considered "moderately suitable," "less suitable," and "not suitable" and scored "8," "6," and "0," respectively.

Elevation

Elevation is another important criterion for any industrial site. Highlands are always the first choice for infrastructures. The elevation of the central administrative area of Savar is 15 m. However, flood zones also exist in the eastern and western areas. Thus, greater than 15 m was considered "most suitable" and scored "10"; 11–15 m was scored "8," i.e., "moderately suitable"; 6–10 m was considered "less suitable" and scored "6"; and less than 5 m was taken as a constraint and scored "0."

7.2.6 AHP

The most difficult task in the land suitability analysis approach for a particular land use type is to assign the relative weights of individual criteria. AHP is a technique, which allows to calculate and evaluate the relative weights (Duc 2006). In addition, one of the most benefits of using AHP is that experts from different backgrounds can give their judgment to evaluate the diverse dimensions of the problem (Oguztimur 2011).

However, there were many studies on the validity of the AHP specially when Belton and Gear (Belton and Gear 1982) first introduced the phenomenon of rank reversal. Rank reversal is an occurrence when adding or removing an alternative for the AHP changes the relative rankings of the existing alternatives. To deal with this rank reversal problem, studies and discussions were conducted and new mathematical approaches were introduced (Shin et al. 2013; Wang and Elhag 2006). On the other hand, there were also debates on the legitimacy of rank reversal (Saaty and Vargas 1984; Saaty 1987a). In addition, researchers also proved that the rank reversal also appears in other multiple- criteria decision-making (MCDM) approaches like Borda-Kendall (BK), Technique for Order Preference by Similarity to Ideal Solution (TOPSIS), and the simple additive weighting (SAW) (Shin et al. 2013; Wang and Luo 2009). Nevertheless, researchers believe that AHP has reached beyond the academic boundary and the use of AHP in real world will be continued by the practitioners (Ishizaka and Labib 2011; Chandio et al. 2013).

Following the footsteps of the successful applications of AHP in LSA, this study applied the technique to prioritize the weights of the criteria. A questionnaire was designed according to the AHP model for a pairwise comparison of each criterion to another criterion based on a nine-point scale (Table 7.3). Saaty (1990) stated that the number of elements for the comparison must be less than or equal to nine to improve consistency and the corresponding accuracy of the measurement. Saaty (1987a, b) also mentioned that if the number of the elements is large then their relative priorities

Table 7.3 Nine-point scale (Saaty 1990)

Intensity of importance on an absolute scale	Definition	Explanation
1	Equal importance	Two activities contribute equally to the objective
3	Moderate importance of one over another	Experience and judgment slightly favor one activity over another
5	Essential or strong importance	Experience and judgment strongly favor one activity over another
7	Very strong importance	An activity is strongly favored, and its dominance is demonstrated in practice
9	Extreme importance	Evidence that favors one activity over another is of the highest possible order of affirmation
2, 4, 6, 8	Intermediate values between two adjacent judgments	When compromise is needed
Reciprocals	If activity i is assigned one of the above numbers compared to activity j, then j has the reciprocal value compared to i	
Rational	Ratios that arise from the scale	If consistency were to be forced by obtaining n numerical values to span the matrix

would be small, and error could affect the judgment. Thus, the study limited the criteria within nine most important aspects.

The judgments from the experts were used to prepare a pairwise matrix followed by normalization, i.e., each column in the matrix was summarized individually, and then each cell in the column was divided by the respective column's sum. The column sum of the resultant matrix was equal to 1. The pairwise matrix can be expressed as follows:

$$\begin{bmatrix} C_{11} & C_{12} & C_{13} \\ C_{21} & C_{22} & C_{23} \\ C_{31} & C_{32} & C_{33} \end{bmatrix} \qquad (7.1)$$

where C_{11} is the value of the row i (first row) and column j (first column) in the pairwise comparison matrix. The column sum of the pairwise matrix can be expressed as follows:

$$C_{ij} = \sum_{i=1}^{n} C_{ij} \qquad (7.2)$$

Therefore, the normalization for each column value can be expressed by the following equations:

$$X_{ij} = \frac{C_{ij}}{\sum\limits_{i=1}^{n} C_{ij}} = \begin{bmatrix} X_{11} & X_{12} & X_{13} \\ X_{21} & X_{22} & X_{23} \\ X_{31} & X_{32} & X_{33} \end{bmatrix} \qquad (7.3)$$

After normalization, the row sum in the new matrix was divided by the total number of criteria. The resultant matrix represents the weighted matrix and can be expressed as follows:

$$W_{ij} = \frac{\sum\limits_{j=1}^{n} X_{ij}}{n} = \begin{bmatrix} W_{11} \\ W_{12} \\ W_{13} \end{bmatrix} \qquad (7.4)$$

This weight matrix can only be used after calculating the consistency ratio as it evaluates the credibility of the judgments of individual respondents. Pairwise matrices are considered consistent when the CR is less than 0.1 (10%). These matrices are considered inconsistent, and the resultant weight matrix of the criteria is not acceptable when the CR is greater than 0.1 (Saaty 1980).

At first, a consistency vector was derived by multiplying the pairwise matrix by the weights vector:

$$\begin{bmatrix} C_{11} & C_{12} & C_{13} \\ C_{21} & C_{22} & C_{23} \\ C_{31} & C_{32} & C_{33} \end{bmatrix} * \begin{bmatrix} W_{11} \\ W_{12} \\ W_{13} \end{bmatrix} = \begin{bmatrix} C_{11}W_{11} + C_{12}W_{21} + C_{13}W_{31} \\ C_{21}W_{11} + C_{22}W_{21} + C_{23}W_{31} \\ C_{31}W_{11} + C_{32}W_{21} + C_{33}W_{31} \end{bmatrix} \qquad (7.5)$$

The principal eigenvector ($\lambda_{\max}$) was then calculated by averaging the value of the consistency vector:

$$\lambda_{\max} = \sum\limits_{i}^{n} CV_{ij} \qquad (7.6)$$

The consistency index (CI) was measured by

$$C = \frac{\lambda_{\max} - n}{n - 1} \qquad (7.7)$$

Here, n is the total number of criteria. The consistency ratio (CR) was calculated by

$$CR = \frac{CI}{RI} \qquad (7.8)$$

where RI is the random index from Table 7.4.

Table 7.4 Random inconsistency indices for $n = 10$ (Saaty 1987a, b)

n	1	2	3	4	5	6	7	8	9	10
Random inconsistency index (RI)	0	0	0.58	0.9	1.12	1.24	1.32	1.41	1.45	1.49

7.2.7 GIS Application for LSA

The GIS analysis was designed to conduct in ArcGIS 10.3® using vector and raster layers. Initially seven thematic vector layers, major roads, local roads, rivers, water bodies, settlements, flood flow zones, and agricultural lands were taken in a base geographical coordinate system, WGS 1984. These vector layers were projected in WGS 1984 UTM Zone 45N to obtain the same geographic extent. The thematic layers were then converted to raster layers to conduct the spatial analysis. Here, the polyline feature layers of major roads and local roads were converted to raster layers by using the conversion tool "Polyline to Raster." The polygon feature layers of rivers and water bodies were converted to raster layers by the "Polygon to Raster" conversion tool, and the three remaining polygon layers, which included settlements, flood flow zones, and agricultural lands, were converted by the "Feature to Raster" tool (Fig. 7.4).
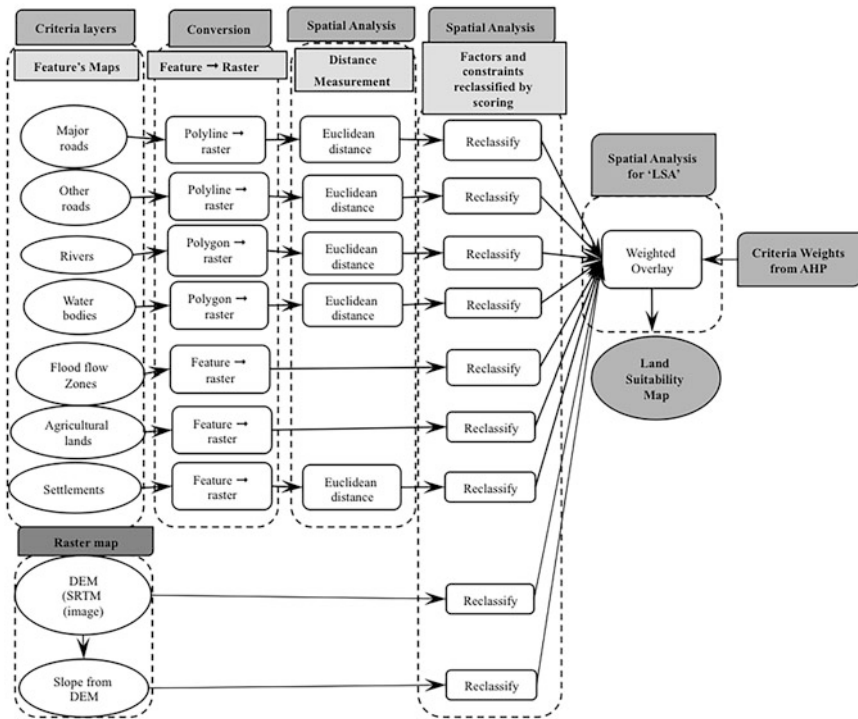
Fig. 7.4 Model diagram for land suitability analysis

The Digital Elevation Model (DEM) of the study place of 30 m resolution was extracted from the Shuttle Radar Topography Mission (SRTM) data set. However, before the extraction, spatial analysis tool "Mosaic" was used to get a seamless data from the two tiles of SRTM data for the study area. The slope layer was obtained from the DEM layer using the spatial analysis tool "Slope" in percent-rise unit and classified according to the factors and constraint intervals. The SRTM elevation map was also used as a reference layer to synchronize the raster layers in terms of cell size and processing extent. Thus, the vector thematic layers were generated in 30×30 m cell size while converting to raster layers.

The spatial analysis tool "Euclidean distance" was used for the proximity analysis of major roads and local roads and for the distance analysis of rivers, water bodies, and settlements. The Euclidean distance tool measured the distance from each cell to the closest source of features. Further, the range of distance was classified according to the factors and constraints of each criterion.

Further the "Reclassify" tool was used to reclassify the raster layers according to the score rankings of the factors and constraints. Here, the constraints were given the number "1" and the factors were assigned using numerical numbers from "2" according to the ranking order of their scores. The output raster layer of individual criterion was generated showing the suitability ranking in color gradient.

7.2.8   Land Suitability for Industry

To aggregate the factors and constraints with the weights of the criteria, spatial analysis tool "Weighted Overlay" was used. The tool worked as a decision rule to integrate the AHP and GIS for the land suitability analysis. The weighted–overlay procedure followed the principle of WLC, where the weights of the criteria was combined with the scores of the factors and constraints to produce a suitability index for each cell of the output map (Eastman et al. 1995). The following expression shows the suitability index:

$$S_i = \sum_{i=1}^{n} (W_i \times X_i) \tag{7.9}$$

Here "W_i" is the weight of each criterion "i," which is calculated from the AHP technique of the MCDA, and "X_i" is the score of each factor and constraint. The scale for the weighted overlay tool was set for 1–10. The constraints, which were given ranking as "1" in the reclassification stage, were stated as "restrictions" while applying weighted overlay function. The factors were assigned scores between 1 and 10 according to Table 7.2. The resultant map was a land suitability map for industries, where each cell of the raster layer was scored with a suitability index on a 0–10 scale, "0" was assigned for the "restriction" cells. The map was further

reclassified into four clusters, the rank "0" for "not suitable," "1–5" for "less suitable," "5–7" for "moderately suitable," and "8–10" for "most suitable."

7.2.9 Industrial Zone Selection

Once the LSA was done for the industrial sites, GIS was further utilized to select the compact areas for industrial zones. Spatial analysis tool "Set Null" was used to segregate the cells of "most suitable." The Structured Query Language (SQL) was set for values less than 8, i.e., cells with values between 8 and 10 would be the true values for the most suitable places. Further, the raster layer was converted from raster to feature by the conversion tool "raster to polygon." The raster cells for the "most suitable" areas were transformed into individual polygons, and the areas of each polygon were calculated. A spatial analysis tool for the feature class "select" was applied to distinguish polygons from the most suitable places with at least 10 ha of land to build industrial zones. The SQL was set to a value that was less than or equal to 100,000 m^2.

7.3 Results

7.3.1 Agricultural Land Use Changes Versus Industries Growth

The statistical data from the local agricultural office showed that Savar lost an average of 6% of its agricultural lands from 2002 to 2011 from each administrative unit. In total, 1064 ha of agricultural land was lost during 2002–2011. However, four administrative units in Savar, namely, "Yearpur," "Ashulia," "Tetuljhora," and "Dhamsona," exhibited higher losses of agricultural land, namely, 15%, 9%, 8%, and 7%, respectively (Fig. 7.5a).

The visual interpretation of the agricultural land use changes was reflected in GIS, where the color gradient shows the locations of the highest agricultural land losses (Fig. 7.5b). According to the BGMEA database of 2013, approximately 577 cloth factories are in Savar and were scattered in the urban, suburban, and rural areas. The study succeeded to collect 420 factories geographical locations during the field survey, and these were mapped through GIS. The map shows that the density of the factory locations was higher in areas where the agricultural land decreased the most from 2002 to 2011 (Fig. 7.5b).
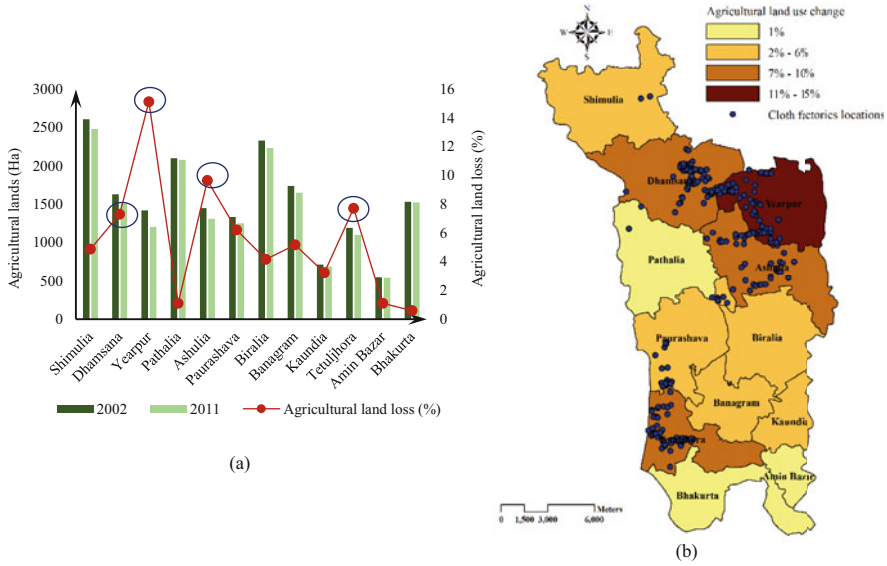
Fig. 7.5 (**a**) Statistical representation of agricultural land use changes in 2002 and 2011; (**b**) interpretation of the agricultural land use changes in GIS

7.3.2 Experts Judgment

An AHP-based pairwise matrix was developed from the experts' responses. After normalizing the matrix, the weights of each criterion were calculated for individual judgment, followed by the consistency measures, consistency indices, and consistency ratios. The CR of the five-expert's judgment was less than 0.1, i.e., the judgments for the pairwise comparison proved to be consistent. The average of each criteria weight of individual judgment was used for the LSA. Based on the judgments, the priority was given to proximity to major roads, which is 22%, followed by proximity to local roads (14%), elevation (14%), and distance from agricultural lands (13%) (Table 7.5).

7.3.3 GIS Spatial Analysis

The reclassify tool of ArcGIS categorized the study area based on the ranking order of the factors and constraints of each criterion. The first map (Fig. 7.6a) shows the proximity to major roads, where 13% of the area was found "most suitable," i.e., the lands were located between 100 m and 500 m from the major roads. Under this criterion, the moderate, less, and least suitable areas were found, 15%, 13%, and

Table 7.5 Experts' judgments when prioritizing the weights of the criteria (A: Author, B-E experts from different fields)

Criteria	A	B	C	D	E	Mean
Proximity to major roads	0.23	0.30	0.09	0.26	0.25	0.22
Proximity to local roads	0.18	0.19	0.08	0.18	0.06	0.14
Distance from rivers	0.07	0.02	0.09	0.07	0.10	0.07
Distance from water bodies	0.11	0.06	0.11	0.06	0.06	0.08
Distance from settlements	0.09	0.10	0.14	0.05	0.05	0.09
Distance from flood flow zones	0.05	0.06	0.15	0.05	0.06	0.08
Distance from agricultural lands	0.11	0.15	0.24	0.14	0.03	0.13
Slope	0.04	0.03	0.06	0.02	0.11	0.05
Elevation	0.13	0.09	0.06	0.17	0.28	0.14
CR	0.08	0.06	0.06	0.09	0.09	

12%, respectively. However, maximum area, i.e., 44%, was found in the zones of "suitable but avoided." The proximity to major roads was selected as the first priority for the LSA of industries by the Experts. Therefore, 13% of most suitable lands under the proximity to major roads limited the possibility to obtain considerable lands for the industries. The reclassification resultant map of the second priority criteria, proximity to local roads, found 15% of land under the factor "most suitable" followed by 19% "less suitable" and 6% "not suitable" and 60% of land was found under "suitable but avoided" (Fig. 7.6b).

Approximately 54% of land was found located beyond 1000 m away from rivers, i.e., "most suitable." Since most of the rivers are situated around the administrative boundary of the study place, only 29% land was found as "not suitable" (Fig. 7.6c). In addition, due to the few numbers of water bodies, 95% of the study area was found beyond 100 m, i.e., "most suitable" (Fig. 7.6d).

Settlement, which was an important criterion to find out the open spaces, showed 54% land was located 50 m away from the settlements, mentioned as "most suitable" (Fig. 7.6e). To evaluate only the hazard-free lands, 22% land was detected as flood zones and the rest 78% land was found as most suitable (Fig. 7.6f).

In addition, the spatial analysis found 69% of the land of the study was at 50 m from the agricultural lands, i.e., "most suitable." Whereas the rest, i.e., 31% land, was within 50 m of the agricultural lands (Fig. 7.6g). This result carried an important role on the final LSA output since the study aimed to secure the existing agricultural lands.

Furthermore, under the criteria of slope, 66% land was found "most suitable" and 29% "moderately suitable" (Fig. 7.6h). Whereas, considering elevation, 19% land was found on an elevation of more than 15 m height, i.e., "most suitable" (Fig. 7.6g). The details of the land suitability classification on individual criterion are given in Table 7.6.
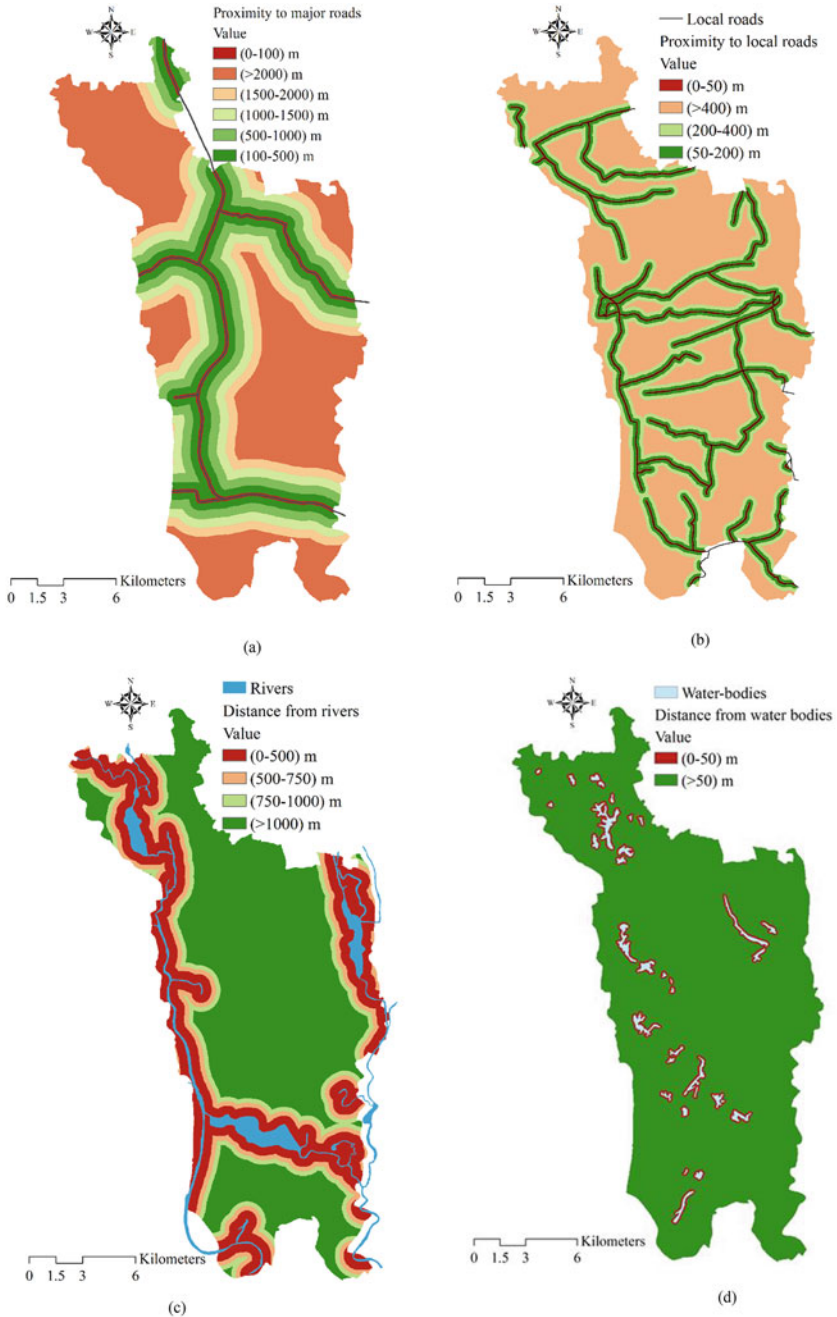
Fig. 7.6 Reclassification layers of criteria according to factors and constraints: (**a**) proximity to major; (**b**) Proximity to local roads; (**c**) Distance from rivers; (**d**) Distance from water bodies; (**e**) Distance from settlements; (**f**) Flood flow zone; (**g**) Distance from agricultural lands; (**h**) Slope; (**i**) Elevation
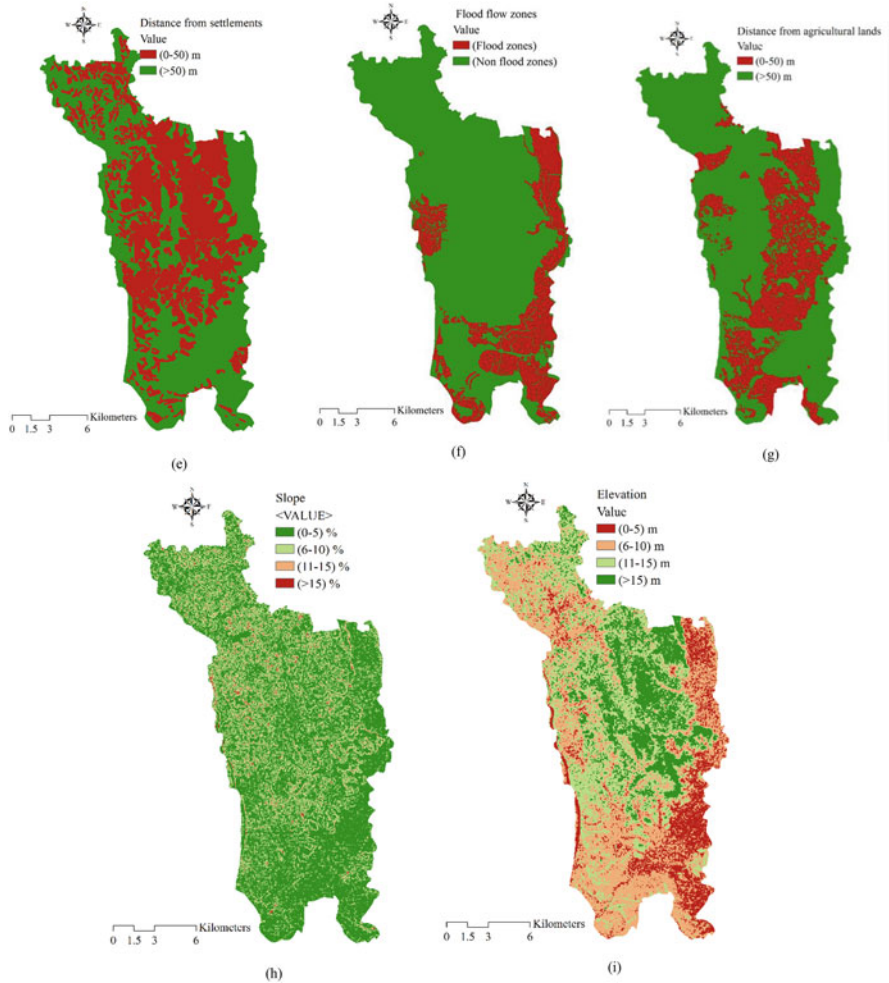
Fig. 7.6 (continued)

7.3.4 Industrial Zone Selection

The resultant map of the weighted overlay shows the land suitability raster layer, where the cells with identical score values of "0," "1–5," "6–7," and "8–10" were clustered into four groups: "not suitable," "less suitable," "moderately suitable," and "most suitable" (Fig. 7.7). Based on the calculated areas of the polygons, 93% of the land in the study area was found "not suitable" for industrial sites. On the other hand, only 4% of the land in the study area was "most suitable" (Table 7.7). The results showed that the spatial analysis worked based on the priority weights of the criteria that were incorporated into GIS by the multi-criteria analysis technique, AHP. The

Table 7.6 Scores and suitability classifications of factors and constraints

Name of the criteria	Factors/constraints	Classified	Suitability	Area in percentage (%)
Proximity to major roads	0–100 m	Constraints	Not suitable	4%
	100–500 m	Factors	Most suitable	13%
	500–1000 m	Factors	Moderately suitable	15%
	1000–1500 m	Factors	Less suitable	13%
	1500–2000 m	Factors	Least suitable	12%
	>2000 m	Factors	Suitable but avoided	44%
Proximity to local roads	0–50 m	Constraints	Not suitable	6%
	50–200 m	Factors	Most suitable	15%
	200–400 m	Factors	Less suitable	19%
	>400 m	Factors	Suitable but avoided	60%
Distance from rivers	0–500 m	Constraints	Not suitable	29%
	500–750 m	Factors	Least suitable	9%
	750–1000 m	Factors	Moderately suitable	8%
	>1000 m	Factors	Most suitable	54%
Distance from water bodies	0–100 m	Constraints	Not suitable	5%
	>100	Factors	Most suitable	95%
Distance from settlements	0–50 m	Constraints	Not suitable	46%
	>50 m	Factors	Most suitable	54%
Flood flow zones	Flood flow zone	Factors	Suitable but avoided	22%
	Non-flood flow zone	Factors	Most suitable	78%
Distance from agricultural lands	0–50 m	Factors	Suitable but avoided	31%
	>50 m	Factors	Most suitable	69%
Slope	0–5%	Factors	Most suitable	66%
	6–10%	Factors	Moderately suitable	29%
	11–15%	Factors	Less suitable	4%
	>15%	Constraints	Not suitable	1%
Elevation	0–5 m	Constraints	Not suitable	15%
	6–10 m	Factors	Less suitable	36%
	11–15 m	Factors	Moderately suitable	30%
	>15 m	Factors	Most suitable	19%

lands that were classified as "most suitable" for industries were converted from raster layers into vector polygons. According to the measured areas for each polygon, only four compact zones were found, which had minimum 10 ha of lands, marked in red in Fig. 7.7.

Fig. 7.7 Land suitability
analysis for industrial sites
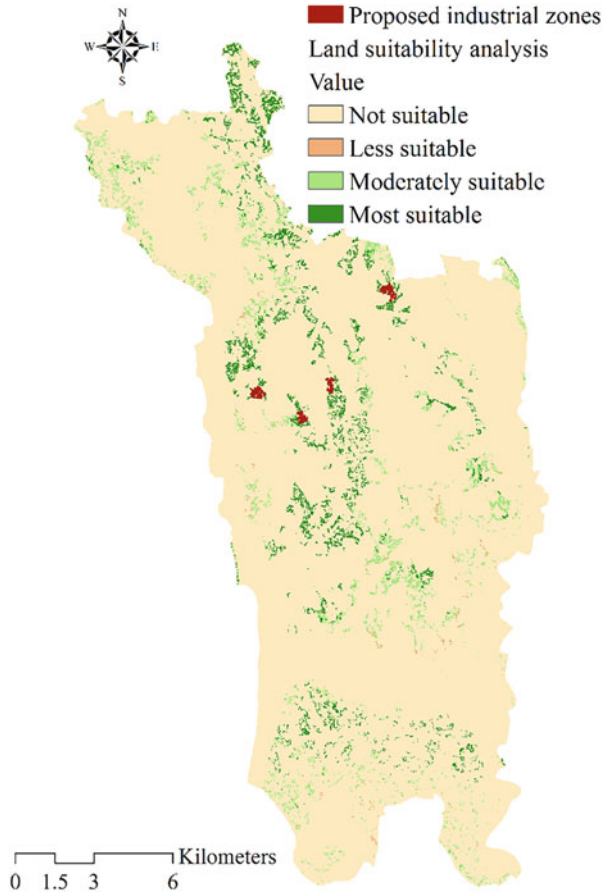
Table 7.7 Area under each classification of the land suitability map for industries

Ranking value	Recommendation	Hectares (ha)	Proportion (%)
0	Not suitable	26052.09	93%
1–5	Less suitable	0	0%
6–7	Moderately suitable	840.39	3%
8–10	Most suitable	1120.52	4%

7.3.5 Verification of the LSA

The feature map of the potential industrial zones of the study area was exported to the Google Earth Pro[®] to verify with the current satellite image. The four most suitable locations were recommended as potential sites for industrial zones. The individual locations contained of 15.17 ha, 10.28 ha, 10.11 ha, and 16.50 ha of lands
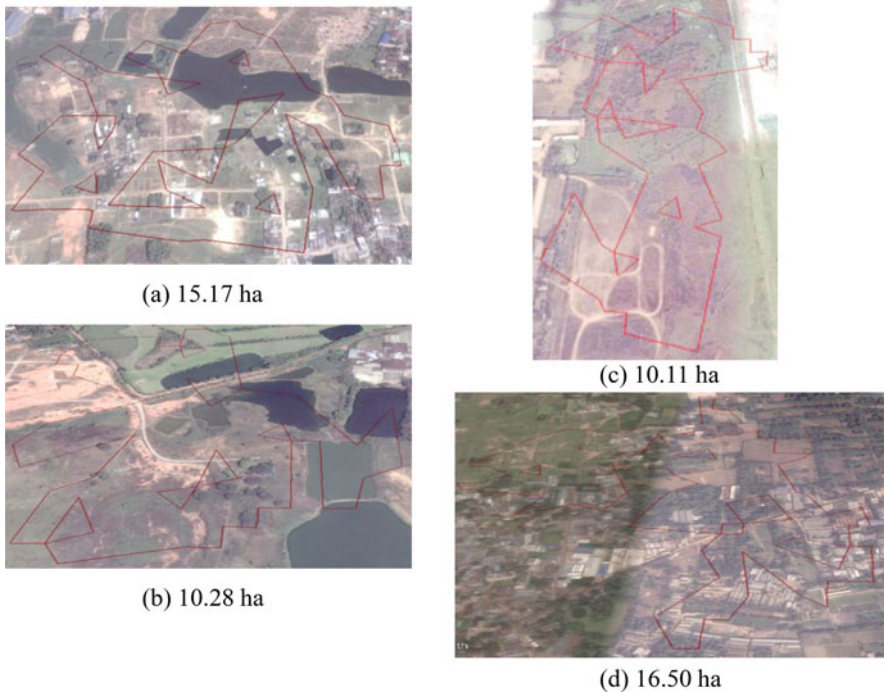
Fig. 7.8 Four most suitable areas: (**a**) 15.17 ha, (**b**) 10.28 ha, (**c**) 10.11 ha and (**d**) 16.50 ha (Google Earth Pro®, 2016/08/08)

(Fig. 7.8a–d). These lands were mostly vacant and situated adjacent to major and local roads but not in flood zones and agricultural lands. However, the images showing water bodies and settlements in the most suitable sites reflect some error in the accuracy of the result. The reason for such deviance is due to the base vector layers of the settlements and water bodies, which were not updated after 2010. During this course land use changed to settlements and water bodies.

7.4 Discussion

The study focused first on the statistical data of agricultural lands of Savar, which showed that Savar lost average 6% of land within 10 years. However, four administrative areas of Savar lost agricultural lands more than 6%, the highest was 10% in Yearpur. On the other hand, the geographical locations of 420 cloth factories, which were collected during the field survey, showed the growth of the industries was denser on those four areas. The industries were expanded in Savar for the last three decades, which were mostly cloth industries. In addition, according to the BGMEA

data, 77% of the cloth factories were established after 2000. Bangladesh is the second largest exporters of readymade cloth industries of the world and comprises about 84% of the export earnings of the country (ILO 2020). The economic growth of the nation through expanding manufacturing units influenced the transformation of agricultural lands of the suburban areas to industrialization. Therefore, industrialization had been an important domain for degrading agricultural lands in study area. Savar has always been very promising to establish industries as it is near the capital city, Dhaka, and is well connected with the Chittagong port area. In addition, the Dhaka Export Processing Zone is also located in Savar.

The novel approach of the study was to conduct the LSA for industries to find out whether there are any suitable lands exists for future industrial zones. The spatial analysis of GIS was proved the most efficient tool to find out suitable lands over the mixed land use of vast areas while evaluating multi-criteria for the industries. AHP, a widely used multi-criteria method, enable the study to evaluate the criteria on priority ranking and weighting. The result of the AHP showed that the proximity to major roads was the most preferred criteria for the industrial site selection, weighted 22% among the nine criteria followed by the proximity to local roads and elevation, each weighted 14%. The fourth highest preferred criterion was distance from the agricultural lands (13%). Since Bangladesh is an agricultural land, it is hard to avoid the agricultural lands for the infrastructure development. However, research succeeds to protect the core agricultural lands using spatial dataset in the GIS environment. Considering the agricultural lands as an individual criterion helped to protect the existing agricultural lands.

Finally, combing the factors and constraints by the decision rule, weighted overlay, the LSA found only 4% of land that could be used to expand for industries in the future. The result certainly showed the most significant aspect of the land use of Savar. It is evident that complying the designed LSA with referred criteria and factors, the study area would not be suitable for further expansion of industries. The area is already occupied with build-up areas without any proper land use management. In addition, the study also tried to find out compact zones for industrial areas, which could be more effective for practicing sustainable land use. The present research found only one economic zone with 16 ha of land.

However, LSA mostly depends on the spatial data set, which must be upgraded with recent changes. In particular, land use maps with settlements are the most important elements that could be changed frequently. Nevertheless, open-source satellite images have made land use management easier and more relevant for policy planners and researchers. The research approach has the potential to acquire credibility of practical implementation in Bangladesh. However, such research needs to have collaborations of Government organizations to draw the attention of policy makers and researchers. Furthermore, apart from searching new land areas for economic zones, abandoned property or old industries could be utilized to facilitate efficiency of land use management. One example could be mentioned here: *Adamjee* Jute Mill, which was established in 1951 in the Narayanganj district of Bangladesh and eventually became the largest jute mill in the world (World Bank 1980). However, in the 1970s the polypropylene products replaced the traditional jute

products and the mill faced heavy losses from the 1990s. Finally, in 2002 the mill was shut down and handed over to Bangladesh Export Processing Zones Authority (BEPZA) to transform it into an export-processing zone. The *Adamjee* Export Processing zone started in 2006. The process of transforming old or abandoned industrial sites into new industrial site is a long-term planning process, which need large investments to move out the industrial buildings and reform process. In that case, the economic and environmental assessments are also necessary. Thus, Bangladesh government encourages private sectors and foreign investors to transform old industries or abandon unproductive lands into economic zones. This micro research approach has the scope to consider several districts surrounding Dhaka where the new and abandoned properties or old export-processing zone can be included for analysis as an alternative of most suitable location of economic zones.

7.5 Conclusions

Unplanned growth of industries in the suburban areas has significant impacts on the land use changes, which eventually could affect the national food security. Thus, it is important for a nation to have a sustainable land use management balancing the food security, environmental protections, and economic development. In this regard, site suitability analysis for any urban development, especially for industrial growth, carries a significant domain of land use. The geographical position of the industrial sites needs to comply with the social, environmental, and economic legislations of the nation as well as the stakeholders and experts' involvement. GIS is the most useful tool to support the spatial decision-making process and AHP facilitate to involve experts' decision. The study focused to solve the most difficult crisis in Bangladesh. Unlike most developing countries, Bangladesh has huge population compared to land. In addition, due to lack of land use policy planning and proper monitoring of existing legislation, the land use management has become inactive. Under these circumstances, the presented GIS-based MCA model for industrial site selection would help the policy makers and government to practice better land use management.

References

Alam AA, Asad R, Kabir ME (2016) Rural settlements dynamics and the prospects of densification strategy in rural Bangladesh. SpringerPlus 5(1):254

Anwarzai MA, Nagasaka K (2017) Utility-scale implementable potential of wind and solar energies for Afghanistan using GIS multi-criteria decision analysis. Renew Sustain Energy Rev 71:150–160

Arefin MT, Rahman MM (2016) Heavy metal contamination in surface water used for irrigation: functional assessment of the Turag River in Bangladesh. J Appl Biol Chem 59(1):83–90

Bangladesh Bureau of Statistics (BBS) (2011) Population & housing census (Community Report 2011). Bangladesh Bureau of Statistics (BBS), Dhaka

Bangladesh Ministry of Environment and Forests (BMEF) (2012) Bangladesh Rio + 20: National Report on sustainable development, May 2012. https://policy.asiapacificenergy.org/sites/default/files/Rio%2B20_Bangladesh_reduced.pdf. Accessed 25 Oct 2021

Beinat E, Nijkamp P (eds) (1998) Multi-criteria analysis for land-use management, vol 9. Springer Science & Business Media, Berlin

Belton V, Gear T (1982) On a shortcomimg of Saaty's method of analytic hierarchies. Omega 11(3):226–230

Bera S, Ahmad M, Suman S (2017) Land suitability analysis for agricultural crop using remote sensing and GIS-A case study of Purulia District. Int J Sci Res Dev 5(06):999–1024

Chandio IA, Matori ANB, WanYusof KB, Talpur MAH, Balogun AL, Lawal DU (2013) GIS-based analytic hierarchy process as a multi-criteria decision analysis instrument: a review. Arab J Geosci 6(8):3059–3066

Collins MG, Steiner FR, Rushman MJ (2001) Land-use suitability analysis in the United States: historical development and promising technological achievements. Environ Manag 28(5):611–621

Duc TT (2006) Using GIS and AHP technique for land-use suitability analysis. In: International symposium on geoinformatics for spatial infrastructure development in earth and allied sciences, pp 1–6

Eastman JR, Jin W, Keym PAK, Toledano J (1995) Raster procedures for multi-criteria/multi-objective decisions. Photogramm Eng Remote Sens 61(5):539–547

Edrahim F, Mehdi A, Habib F, Ali MD (2015) Industrial state site selection using MCDM method and GIS in Germi, Ardabil, Iran. J Ind Intell Inform 3(4):324–329

Eldin N, Sui DA (2003) COM-based spatial decision support system for industrial site selection. J Geogr Inf Decis Anal 7(2):72–92

Eldrandaly KA, Eldin N, Sui DZ, Shouman MA, Nawara G (2005) Integrating GIS and MCDM using COM technology. Int Arab J Inf Technol 2(2):162–167

Eugene KR, Prasanta KD (2005) The role of environmental factors in industrial site selection activities: a case of limestone quarry expansion in Barbados, West Indies. Impact Assess Proj Apprais 23(2):147–154. https://doi.org/10.3152/147154605781765670

Ferretti V, Pomarico S (2012) Integrated sustainability assessments: a spatial multicriteria evaluation for siting a waste incinerator plant in the province of Torino (Italy). Environ Dev Sustain 14(5):843–867

Ferretti V, Pomarico S (2013) An integrated approach for studying the land suitability for ecological corridors through spatial multicriteria evaluations. Environ Dev Sustain 15(3):859–885

Habibie MI, Noguchi R, Shusuke M, Ahamed T (2021) Land suitability analysis for maize production in Indonesia using satellite remote sensing and GIS-based multicriteria decision support system. GeoJournal 86(2):777–807

Hasan MN, Hossain MS, Bari MA, Islam MR (2013) Agricultural land availability in Bangladesh. SRDI, Dhaka, p 42. http://www.srdi.gov.bd/wpcontent/uploads/2014/03/Agriculturalland-availability-in-Bangladesh-monograph-1.pdf. Accessed 5 Oct 2021

Hassan MM, Nazem MNI (2016) Examination of land use/land cover changes, urban growth dynamics, and environmental sustainability in Chittagong city, Bangladesh. Environ Dev Sustain 18(3):697–716

Hossain MS, Chowdhury SR, Das NG, Sharifuzzaman SM, Sultana A (2009) Integration of GIS and multicriteria decision analysis for urban aquaculture development in Bangladesh. Landsc Urban Plan 90(3):119–133

International Labour Organization (ILO) (2020) Recommendations for garment manufacturers on how to address the COVID-19 pandemic. https://www.ilo.org/wcmsp5/groups/public/%2D%2D-asia/%2D%2D-ro-bangkok/documents/briefingnote/wcms_741642.pdf. Accessed 14 Oct 2021

Ishizaka A, Labib A (2011) Review of the main developments in the analytic hierarchy process. Expert Syst Appl 38(11):14336–14345

Islam MR, Zhang W, Mao S, Eneji AE, Hu Y (2010) Status of land degradation and desertification in Bangladesh and the role of agro forestry in their control. J Agric Biotechnol Ecol 3:107–116

Jakobsen F, Hoque AZ, Paudyal GN, Bhuiyan S (2005) Evaluation of the short-term processes forcing the monsoon river floods in Bangladesh. Water Int 30(3):389–399

Jankowski P, Richard L (1994) Integration of GIS-based suitability analysis and multicriteria evaluation in a spatial decision support system for route selection. Environ Plann B Plann Des 21(3):323–340

Joshua JK, Anyanwu NC, Ahmed AJ (2013) Land suitability analysis for agricultural planning using GIS and multi criteria decision analysis approach in greater Karu urban area, Nasarawa state, Nigeria. Afr J Agric Sci Technol 1(1):14–23

Karim M (2015) Draft laws to protect agricultural land: tough actions proposed against violators. The Daily Observer. http://www.observerbd.com/2015/03/27/80268.php. Accessed 14 Oct 2021

Mahfuza S, Hossain MS, Islam M (2019) Impacts of urbanization on land cover pattern in Bangladesh: a downscaled approach for Chuadanga District. J Environ Sci Nat Resour 12(1–2):37–42

Malczewski J (2004) GIS-based land-use suitability analysis: a critical overview. Prog Plan 62(1): 3–65

Mansour S, Al-Awhadi T, Al-Hatrushi S (2020) Geospatial based multi-criteria analysis for ecotourism land suitability using GIS & AHP: a case study of Masirah Island, Oman. J Ecotour 19(2):148–167

Morales F, de Vries WT (2021) Establishment of land use suitability mapping criteria using analytic hierarchy process (AHP) with practitioners and beneficiaries. Landarzt 10(3):235

Oguztimur S (2011) Why fuzzy analytic hierarchy process approach for transport problems? European Regional Science Association, Louvain-la-Neuve, Belgium

Ohri A, Singh PK, Singh PK (2010) Spatial multi criteria analysis for siting industries. Int J Ind Eng Res Dev (IJIERD) 1(1):94–114

Planning Commission (2009) Steps towards change-National Strategy for accelerated poverty reduction II (revised). FY 2009–11. Government Peoples Republic of Bangladesh, Dhaka

Quasem M (2011) Conversion of agricultural land to non-agricultural uses in Bangladesh: extent and determinants. Bangladesh Dev Stud 34(1):59–85

Rahman MT, Hasan MN (2003) Assessment of shifting of agricultural land to non-agricultural land in Bangladesh. Soil Resource Development Institute (SRDI), Dhaka

Rahman MA, Rusteberg B, Gogu RC, Ferreira JL, Sauter M (2012) A new spatial multi-criteria decision support tool for site selection for implementation of managed aquifer recharge. J Environ Manage 99:61–75

Rahman MM, Hassan MS, Bahauddin K, Khondoker Ratul A, Hossain Bhuiyan MA (2018) Exploring the impact of rural–urban migration on urban land use and land cover: a case of Dhaka city. Bangladesh Migr Dev 7(2):222–239

Rahman MM, Mostafa G, Razia S, Shoaib JU (2019) Land degradation in Bangladesh. In: Response to land degradation. CRC, Boca Raton, FL, pp 117–129

Rahmat ZG, Niri MV, Alavi N, Goudarzi G, Babaei AA, Baboli Z, Hosseinzadeh M (2017) Landfill site selection using GIS and AHP: a case study: Behbahan, Iran. KSCE J Civil Eng 21(1):111–118

Rashid MS (2003) A study of land transformation in Savar Upazila, Bangladesh, 1915–2001: an integrated approach using remote sensing, census, map and field data. Durham Theses, Durham University

Reddy CS, Pasha SV, Jha CS, Diwakar PG, Dadhwal VK (2016) Development of national database on long-term deforestation (1930-2014) in Bangladesh. Global Planet Change 139:173–182

Rezvi MR (2018) The factors of declining agricultural growth in Bangladesh and its impact on food security. South Asian J Social Stud Econ 1:1–9

Rikalovic A, Cosic I, Lazarevic D (2014) GIS based multi-criteria analysis for industrial site selection. Procedia Eng 69:1054–1063

Rikalovic A, Cosic I, Labati RD, Piuri V (2015) A comprehensive method for industrial site selection: the macro-location analysis. IEEE Syst J 11(4):2971–2980

River Quality Report (2015) River Quality Report 2014. Department of Environment (DoE), Dhaka. https://doe.portal.gov.bd/sites/default/files/files/doe.portal.gov.bd/publications/53bdd241_6208_4848_95ff_4cca3e059033/Water%20Quality%20Report%202014%20(3).pdf. Accessed 14 Oct 2021

Saaty TL (1980) The analytic hierarchy process. McGraw-Hill, New York

Saaty RW (1987a) The analytic hierarchy process—what it is and how it is used. Math Model 9(3–5):161–176

Saaty TL (1987b) Decision making, new information, ranking and structure. Math Model 8:125–132

Saaty TL (1990) How to make a decision: the analytic hierarchy process. Eur J Oper Res 48(1):9–26

Saaty TL, Vargas LG (1984) The legitimacy of rank reversal. Omega 12(5):513–516

Saleh A, Biswajeet P, Shattri M, Mohamed AR, S. (2015) GIS-based modeling for the spatial measurement and evaluation of mixed land use development for a compact city. GISci Remote Sens 52(1):18–39

Sharif MS, Esa AJ (2014) Dynamics of land price and land use change: a case of Savar municipality. Bangladesh J South Asian Stud 2(1):83–89

Shin YB, Lee S, Chun SG, Chung D (2013) A critical review of popular multi-criteria decision making methodologies. Iss Inform Syst 14(1):358–365

The Bangladesh Economic Zones Act (Act No. 42) (2010). http://beza.gov.bd/wp-content/uploads/2015/06/BEZA-Act-English.pdf. Accessed 14 Oct 2021

Wang YM, Elhag TM (2006) An approach to avoiding rank reversal in AHP. Decis Support Syst 42(3):1474–1480

Wang YM, Luo Y (2009) On rank reversal in decision analysis. Math Comput Model 49(5):1221–1229

Worall L (1991) Spatial analysis and spatial policy using geographic information system. In: Spatial analysis and spatial policy using geographic information system. Belhaven Press, London

World Bank (1980) Jute Mill Rehabilitation Project. https://documents1.worldbank.org/curated/en/181151468013807784/pdf/multi-page.pdf. Accessed 14 Oct 2021

World Bank (2020). https://data.worldbank.org/indicator/EN.POP.DNST. Accessed 14 Oct 2021

Chapter 8
Change Detection and Land Suitability Analysis for Extension of Potential Forest Areas in Indonesia Using Satellite Remote Sensing and GIS

Nety Nurda, Ryozo Noguchi, and Tofael Ahamed

Abstract The objective of this research was to detect changes in forest areas and, subsequently, the potential forest area that can be extended in the South Sumatra province of Indonesia, according to the Indonesian forest resilience classification zones. At first, multispectral satellite remote sensing datasets from Landsat 7 ETM+ and Landsat 8 OLI were classified into four classes, namely, urban, vegetation, forest, and waterbody to develop Land Use/Land Cover (LULC) maps for the year 2003 and 2018. Secondly, criteria, namely, distance from rivers, distance from roads, elevation, LULC, and settlements were selected, and the reclassified maps were produced from each of the criteria for the land suitability analysis for forest extension. Thirdly, the Analytical Hierarchy Process (AHP) was incorporated to add expert opinions to prioritize the criteria referring to potential areas for forest extension. In the change detection analysis, Tourism Recreation Forest (TRF), Convertible Protection Forest (CPF), and Permanent Production Forest (PPF) forest zones had a decrease of 20%, 13%, and 40% in area, respectively, in the forest class from 2003 to 2018. The Limited Production Forest (LPF) zone had large changes and decreased by 72% according to the LULC map. In the AHP method, the influential criteria had higher weights and ranked as settlements, elevation, distance from roads, and distance from rivers. CPF, PPF, and LPF have an opportunity for extension in the highly suitable classification (30%) and moderately suitable classification (41%) areas, to increase coverage of production forests. Wildlife Reserve Forests (WRFs) have potential for expansion in the highly suitable classification (30%) and moderately suitable classification (52%) areas, to keep biodiversity and ecosystems for wildlife resources. Nature Reserve Forests (NRFs) have an opportunity for extension in the highly suitable classification (39%) and moderately suitable classification

N. Nurda
National Resilience Institute of the Republic of Indonesia (LEMHANNAS RI), Jakarta, Indonesia

R. Noguchi · T. Ahamed (✉)
Faculty of Life and Environmental Sciences, University of Tsukuba, Tsukuba, Ibaraki, Japan
e-mail: tofael.ahamed.gp@u.tsukuba.ac.jp

(48%) areas, to keep the forests for nature and biodiversity. In case of TRF, there is limited scope to propose a further extension and is required to be managed with collaboration between the government and the community.

Keywords Change detection · Land use/Land cover · Forest classification · Land suitability analysis · GIS · Remote sensing

8.1 Introduction

Indonesia has been losing up to two million hectares of land annually, mainly due to illegal cutting and land conversion (World Bank 2006). Due to a faster growing population, the land conversion takes place to support the infrastructure expansion investment in agriculture and the establishment of cash-crop plantations (United Nations 2017). Indonesia's urbanization and growth are covered for economic security through conversion of millions of hectares of forest to palm oil plantations (United Nations 2009). Deforestation rates have increased throughout Indonesia due to urbanization and palm oil plantations covering 5,418,413 ha (Ministry of Forestry 2015). In addition, forest fires, poor forest management practices and an increasing demand for forest products and agriculture contribute to the damage of forests, which are more severe in the South Sumatra province of Indonesia. Many forests in South Sumatra have recently experienced high rates of deforestation due to human migration and the expansion of agriculture or industry. Land-use planning has not taken place over time to align the changes in forest resources according to the Indonesian forest resilience classification. It is also necessary to increase the growth of the economy and, on the other hand, the sustainability of forests through improving the resilience of forest coverage. Forest coverage must be estimated periodically to detect these changes. The change detection analysis has the advantage to visualize the dynamics of changes in forest and deforestation processes. Though the forest is a gift of nature, to maintain the carbon cycle, stocking, and sequestration processes in vulnerable areas, further expansion of forest areas needs to be extended by locating such potential areas in time. Production and convertible type forests have the opportunity to expand into these potential areas, which can support the Indonesian forest management system through community support (Santika et al. 2017). In Indonesia, there are six types of forest classification zones, defined by the Indonesian forest resilience system: Tourism Recreation Forest (TRF), Convertible Protection Forest (CPF), Permanent Production Forest (PPF), Limited Production Forest (LPF), Wildlife Reserve Forest (WRF), and Nature Reserve Forest (NRF) (Ministry of Forestry 2016). A TRF is a forest used for tourism, research, education, and cultural activities. CPFs are spatially reserved for use in the development of transmigration, agricultural and plantation settlements. A PPF is a forest exploited for the treatment of selective logging or by clear-cutting. An LPF is allocated to produce wood on a small scale and is located in mountainous areas. A WRF is the natural reserve zone

for wild animals and other natural ecosystems. In turn, an NRF consists of natural forest and has the function of protecting the forest, controlling soil erosion, preventing seawater intrusion, and maintaining soil fertility. In each type of forest, change detection could help to project the changes in the ecosystem, carbon stocking, and sequestration.

The change detection analysis can be mapped using satellite remote sensing datasets for the coverage and changes in the spatial and time scales. Remote sensing techniques provide a source of data that updates land-cover information to monitor ecosystem changes over time (Houghton 1991; Potter et al. 2007; Yelwa 2005). The change detection analysis has the advantages of determining the nature, biodiversity, extent, and rate of land-cover changes, as well as aiding future planning and land management, such as plantation, urbanization, water management, and extending the land (Rogan and Miller 2006; Mancino et al. 2014; Rawat and Kumar 2015). Monitoring and analysis for change detection is the most adopted application of the satellite data (Mickelson et al. 1998; Yuan et al. 2005; Li et al. 2017). Among them, Landsat satellite datasets have been used for change detection analysis (Yuan et al. 2005; Brown et al. 2006; Mancino et al. 2014; Tarantino et al. 2015). Change detection analysis can enhance the land-use planning within a framework of laws and policies to guide forest zone allocation. The change detection assessment has become central to diverse facets of the natural environment (Foody 2002; Diallo et al. 2009; Hegazy and Kaloop 2015). The changed information is highly needed to encourage forest management and to inform appropriate expansion. It is thus important to detect when, where, and why change occurs, as well as study the patterns of the changes for the future (Brown et al. 2000).

In the change detection analysis, remote sensing and GIS help to drive and integrate the present land-use planning criteria, including important factors such as elevation, settlements, distance from roads, and distance from rivers. These factors govern the possibility of expansion. However, land encroachment for forest expansion is a critical problem in many countries. Land encroachment and conversion need the opinions of the government and local stakeholders (Sawathvong 2004). In the stakeholder opinion, the population and settlement factors are very much significant when considering the potential expansion of production forests. Both expert opinion and government policy maker participation are very important to enable successful forest expansion. Analytical Hierarchy Process (AHP) has the potential to include expert opinion into GIS and remote sensing datasets (Escobar and Moreno-Jiménez 2000; Huang 2002; Chen and Kocaoglu 2008). Expert opinion and stakeholder participation are required to minimize the adverse effect due to deforestation, and to confirm the change detection for the classified forest areas. Once the classified forest changes are largely identified, it is necessary to propose further extended areas that have the potential to extend new plantations as production forest. Therefore, the objective of this research is to perform a change detection analysis for the classified forest zones and a suitability analysis to locate potential areas for extension.

8.2 Materials and Methods

8.2.1 Geographical Extent and Forest Coverage in Study Area

The study area is located in South Sumatra covered with TRF, CPF, PPF, LPF, WRF, and NRF declared by the local government in the forest management system (Fig. 8.1). The six forest zones located in the four different locations were taken
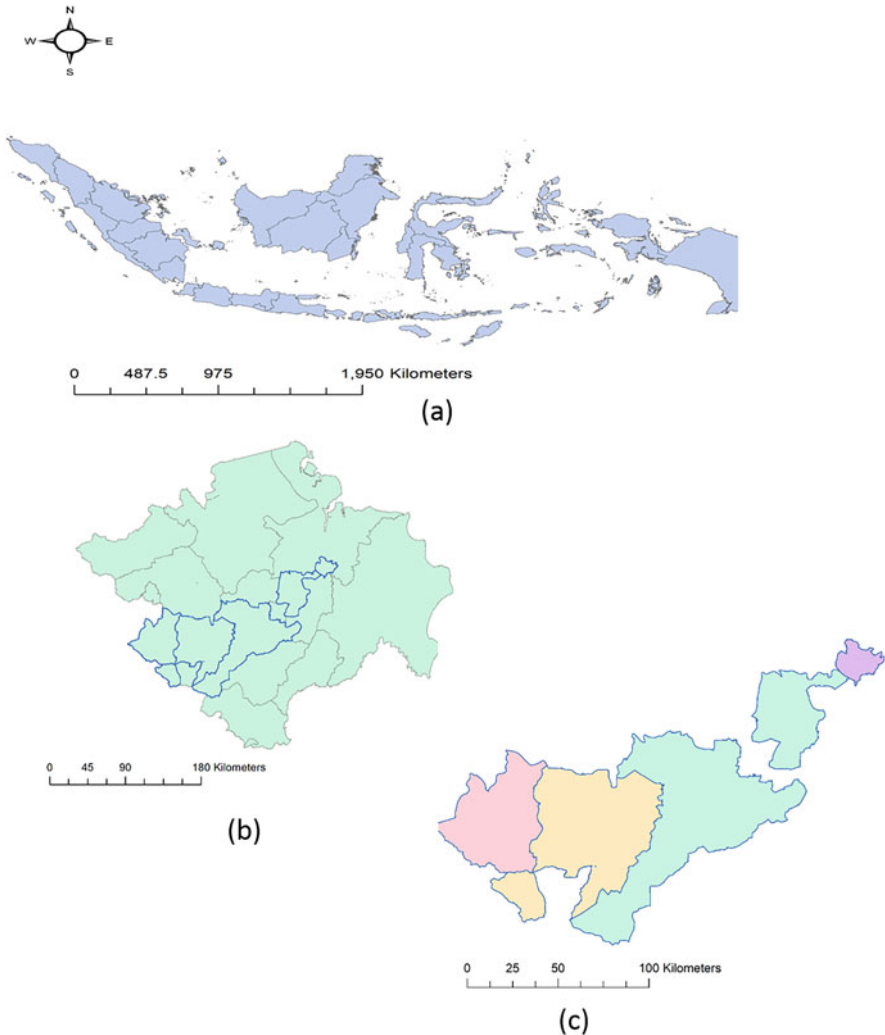

Fig. 8.1 Geographical extent and forest zones in the South Sumatra province of Indonesia. (**a**) Indonesia, (**b**) South Sumatra, and (**c**) the forest zones: Tourism Recreation Forest (TRF), Convertible Protection Forest (CPF), Permanent Production Forest (PPF), Limited Production Forest (LPF), Wildlife Reserve Forest (WRF), and Nature Reserve Forest (NRF)

spatially to analyze the changes in those zones. Three types of forest zones are located in the same area of South Sumatra (Fig. 8.1c). TRF is located in the Palembang city, the capital of the province of South Sumatra with an area of 40 ha, inside the city area of 3,585,500 ha. CPF, PPF, and LPF are located in the agricultural area covered with 81,581,400 ha in the middle of South Sumatra. CPF covers only 819.84 ha of land, which is used for the production of forest products and reserved for the development of transmigration, agriculture, and plantations. PPF has an area of 172.75 ha and can be used through selective logging or clear-cutting of wood products. LPF covers 312.33 ha of forest land that is allocated for the production of wood on a small scale. WRF covers 989 ha with a total area of 407,600 ha as a reserve zone for wild animals and other natural ecosystems. NRF covers 305 ha with a total area of 22,565,100 ha (Forest Area 2016). NRF has the function of protecting the forest, controlling soil erosion, preventing seawater intrusion, and maintaining soil fertility (Fig. 8.1).

8.2.2 Change Detection Analysis

Change detection of forest land is important to understand the trends of changes in the past, currently, and projections for the future. This study considered the time scale of 2003–2018 to assess the trend of changes over the last 15 years. The post-classification method was employed for change detection to provide the matrix table of "from–to" change for the two date images on the base pixel comparison (Badamasi and Yelwa 2010). The change area is the area of the target vegetation cover type at the beginning (2003) and the end (2018) of the study period, respectively. Since it is a large forest area, the continuing years of change may not have as much of a significant difference compared to the highly urbanized areas where land-use changes are very frequent and yearly reporting is very important.

Data Acquisition and Sources

The change detection analysis was conducted using 2-year series of multispectral datasets for South Sumatra, using Landsat 7 for 2003 and Landsat 8 OLI for 2018. Data were collected from the USGS satellite remote sensing datasets resources and Indonesia Geospatial Agency (BIG). Selected criteria were taken into account in the GIS analysis to map the potential areas for further extension of forests (Table 8.1).

Image Processing for Land Use/Land Cover (LULC)

Satellite datasets from Landsat 7 ETM+(2003) and Landsat 8 OLI (2018) were used to develop the LULCs. The imagery was visually interpreted to prepare the change detection maps using a knowledge-based supervised and maximum likelihood

Table 8.1 Satellite and GIS datasets for land suitability analysis for extension of potential forest areas

No	Data and map	Description	Source
1	LULC	Extracted from 30 m resolution	2018, Landsat 8 OLI, Landsat 7 ETM+
2	River	Scale 1:25,000	2005, Indonesia Geospatial Agency
3	Road	Scale 1:25,000	2005, Indonesia Geospatial Agency
4	Elevation	Extracted 90 m from Data Elevation Model National SRTM	2015, USGS
5	Settlements	Extracted from 30 m resolution	2018, Landsat 8

Table 8.2 Selected features for supervised classification in Land Use/Land Cover (LULC) analysis

Class name	Description
Urban	Areas designated as urban zone
Waterbodies	River, lakes, waterlogged, and swamp areas
Vegetation	Areas covered by trees, both agriculture and planted
Forest	Areas covered by forest

classification in the ArcMap environment. The maximum-likelihood classifier was adopted from a parametric classification algorithm (Stehman and Czaplewski 1998; Liu et al. 2002; Currit 2005; Bailly et al. 2007) and divided into four classes: urban, vegetation, forest, and waterbodies (Table 8.2). The classes that were involved in the selection of the training sites were used as a reference in the user-guided approach (Wright et al. 1980; Campbell 1987; Olmo and Abarca-Hernández 2000; Jensen 2007; Tarantino et al. 2015). For each of the predetermined change detection types, training samples were selected by delimiting the polygons in the study area. Spectral signatures from the satellite imagery were chosen by pixels. A satisfactory spectral signature was ensured for the land-cover map (Gao and Liu 2010) (Fig. 8.2a).

Accuracy Assessment

The accuracy assessment was conducted using reference data points from the base map used to validate the LULC. A stratified random sampling method was employed for selecting 200 points on the map with each class of 50 points (Fig. 8.2a). The accuracy was evaluated using the Producer's Accuracy (PA), User's Accuracy (UA), and Overall Accuracy (OA) (Thomlinson et al. 1999; Congalton 1991; Teodoro and Araújo 2016) for consideration of the nearest results to accept as true. PA is the map accuracy from the point of the mapmaker (the producer) to represent how well the reference pixels of the ground cover type are classified. The PA refers to the number of correctly classified pixels in each category (on the major diagonal) by the number of reference pixels "known" to be of that category (the column total), while the UA was computed by dividing the number of correctly classified pixels in each category by the total number of pixels that were classified in that category (the row total). The
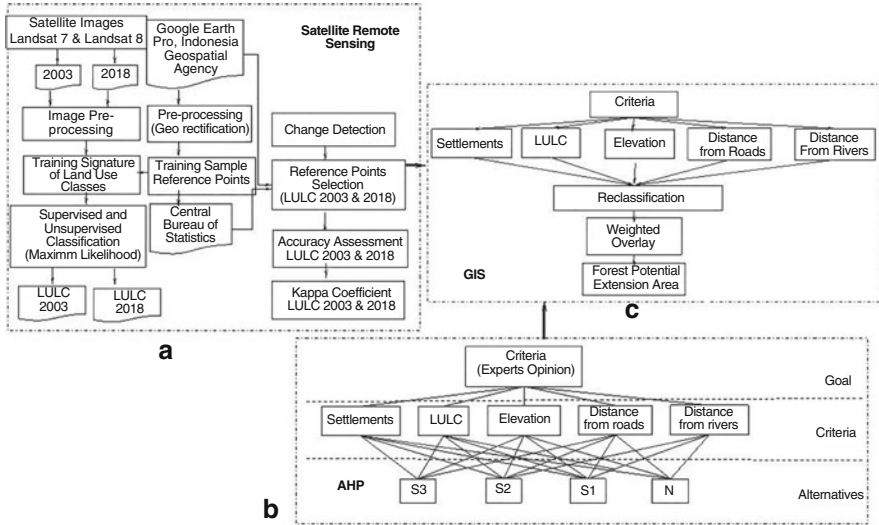
Fig. 8.2 Research framework for land suitability analysis to propose the extension of potential forest area. (**a**) Land use and land cover for change detection analysis from Landsat 7 and Landsat 8 OLI datasets; (**b**) Analytical Hierarchy Process (AHP) to integrate the expert opinion's weight in the suitability analysis; and (**c**) the land suitability analysis

UA represents the probability that a pixel classified into a given category actually represents that category on the ground, referred to as reliability. In addition, to measure the agreement, we used the Kappa coefficient (Fig. 8.2a). Kappa measures the percentage of data values in the main diagonal of the table and then adjusts these values for the amount of agreement that could be expected due to chance alone. The Kappa needs to calculate the observed level of agreement and then compares it to the value that is expected. The value of Kappa is defined as

$$\widehat{K} = \frac{N \sum_{i=1}^{r} X_{ii} - \sum_{i=1}^{r} \left(X_{ij} * X_{ji} \right)}{N^2 - \sum_{i=1}^{r} \left(X_{ij} * X_{ji} \right)} \tag{8.1}$$

where $\widehat{K}$ is the Kappa coefficient; r is the number of rows in error matrix; N is the total number of observations (pixels) in the matrix; X_{ii} is the number of observations in row i, column i; X_{ij} is the total number of observations in row I; and X_{ji} is the total number of observations in column I. To interpret the Kappa coefficient following the formula is more useful:

$$\widehat{K} = \frac{p_o - p_e}{1 - p_e} \tag{8.2}$$

where p_o is the accuracy of the observed agreement, $\frac{\sum X_{ij}}{N}$; and p_e is the estimate of chance agreement, $\sum \frac{\sum_{i=1}^{r} \left(X_{ij} * X_{ji} \right)}{N^2}$. The coefficient of agreement Kappa is $-1 \leq k \leq 1$. Interpretation of Kappa is referred to as a poor agreement if it is less than 0.20; a fair agreement is from 0.20 to 0.40; a moderate agreement ranges between 0.40 and 0.60; a good agreement ranges from 0.60 to 0.80; and a very good agreement ranges from 0.80 to 1.00. An accuracy assessment provides the information for estimating the uncertainty of map classes and the construction of confidence intervals. Accuracy assessment is performed by comparing the map created by remote sensing analysis to a reference map based on a different information source. Both of the maps were evaluated and registered geometrically to each other.

8.2.3 Suitability Analysis for Extension of Potential Forest Area

The suitable potential area refers to the lands that have the opportunity for conversion of forest with economic return over a period of time. In the forest extension planning process, it is important to understand the problem of finding suitable locations for the potential areas. The vegetation land was considered with the timeframe for coverage. Basic land-use change focuses on the land use covered by humans and their habitats (such as agriculture, settlements, industry, etc.), apart from natural disaster factors. The suitable areas for forest potential extension were computed using the weighted overlay procedure in ArcGIS® (ESRI, Redlands, NY, USA). In this research, five criteria were selected: settlements, LULC, elevation, rivers, and roads. The description of the criteria and reclassification are described in the following section.

Criteria for Suitability Analysis

The criteria for suitability analysis were settlements, LULC, elevation, distance from rivers, and distance from roads (Table 8.3 and Fig. 8.3).

Settlements

Settlements include buildings for residences or for industrial activity that has that land-use component (Strand 1993; Chaudhary et al. 2008). Settlements are areas of human habitation with buildings, civil facilities (hospitals, schools, places of worship, and sports areas). The forest loss corresponded with an increase in human settlement. Settlements are driven to overexploit natural resources in forest areas and accelerate land degradation (Nayak et al. 2014). A settlements map was produced

Table 8.3 Criteria of the land suitability analysis for the extension of forest areas

Criteria	Suitability class	Sub-criteria	Reference
Settlements	S1	<214	Strand (1993)
	S2	264–365	Strand (1993)
	S3	365–414	Strand (1993)
	N	>414	Strand (1993)
LULC	S1	Forest	Demissie et al. (2017)
	S2	Vegetation	Demissie et al. (2017)
	S3	Urban	Demissie et al. (2017)
	N	Waterbodies	Demissie et al. (2017)
Elevation	S1	<350 m	Li et al. (2017)
	S2	350–900 m	Li et al. (2017)
	S3	900–1600 m	Li et al. (2017)
	N	>1600 m	Li et al. (2017)
Distance from roads	S1	<10 m	Gigovic et al. (2019)
	S2	10–23 m	Gigovic et al. (2019)
	S3	23–45 m	Gigovic et al. (2019)
	N	>45 m	Gigovic et al. (2019)
Distance from rivers	S1	<6 m	Nigussie et al. (2019)
	S2	6–13 m	Nigussie et al. (2019)
	S3	13–21 m	Nigussie et al. (2019)
	N	>29 m	Nigussie et al. (2019)

from Landsat 8 OLI satellite images that were verified using Google Earth Pro and confirmed with an overlay process using Indonesian geospatial datasets (Fig. 8.3a).

LULC

LULC was built using satellite remote sensing from Landsat 7 ETM+ and Landsat 8 OLI. Landsat 7 was used to develop the classifier for the study area in 2003 and Landsat 8 OLI was used for the classifier in 2018. Both Landsat images were processed using supervised maximum likelihood classification. Land-cover classes were defined by a string of classifiers with the aim of achieving a logical and functional hierarchical arrangement of the classifiers; certain criteria were applied. The four categories urban, waterbody, vegetation, and forest were used in the LULC for 2018 (Fig. 8.3b).

Elevation

The study area is comprised of lowlands, although there were no peatlands in the forest zones. However, South Sumatra had deforestation due to plantation potential and agriculture. In addition, this area has a tropical rainforest heritage. Tropical
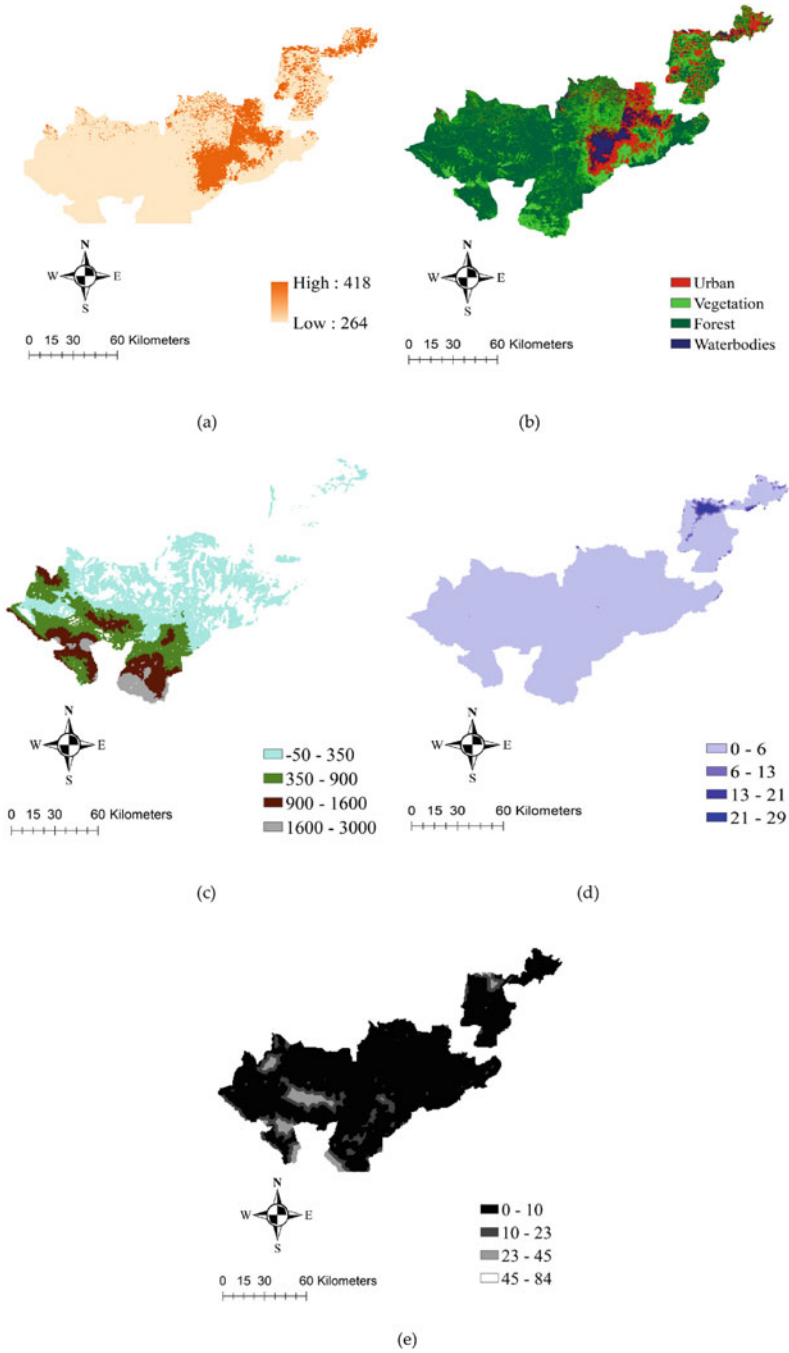
Fig. 8.3 Criteria for the land suitability analysis for extension of potential forest areas. (**a**) Settlements, (**b**) LULC, (**c**) elevation, (**d**) distance from rivers, and (**e**) distance from roads

elevation areas have high biodiversity and rich ecosystem services (Gradstein et al. 2010; Spracklen and Righelato 2014) (Fig. 8.3c).

Distance from Rivers

The unavailability of water strongly constrains the distribution of plants on the Earth's surface (Holdridge and Hubbert 1947; Major 1963), ecosystems, and forests (Churkina and Running 1998; Law et al. 2002; Schuur 2003; Berner and Law 2015). Therefore, rivers are a source of water to get potential area for extensions. The data for distance from rivers were collected from the Indonesian geospatial agency (Fig. 8.3d). It is worth mentioning that the rivers are important in supporting regional biodiversity and provides important services for people, such as food, fodder, shelter, construction materials, and medicine (Johnson and Omland 2004). The ecology in forests refers to the relationships that living organisms have with each other and with their environment. In that case, access to water sources (rivers) is required for new forestation. Consider supporting potential forest areas: The distance to a river has a direct impact on the importance of the relationship between forests and water; the location of the rivers needs to be close to the vegetation and the dependent animal life. To protect a variety of forest ecological processes, distance from rivers is one of the factors. There are several types of forest ecological processes that depend on dry areas (distance from rivers is far) or wet areas (distance from rivers is close) (Kirchmair 2017). The rivers have been highlighted as a priority for scientists, policymakers, and managers (Datry et al. 2014).

Distance from Roads

The availability of roads in forest areas was considered in order to increase the forest plantation area to facilitate the extension of some plantation forest. The potential extension might be difficult when the road is unavailable in forest zones (except, of course, the roads that were built for the plantation system) (Fig. 8.3e). Furthermore, the masking of areas in each forest type was done to understand the changes that occurred in each forest (Fig. 8.4).

Reclassification of Criteria

The selected criteria were reclassified to understand the importance of each of the criteria and their suitability assessment. The reclassification was performed using the criteria to classify the vector and raster data by replacing a new value in the four classifications based on FAO recommendations. The classification was suggested based on the following levels of suitability: highly suitable (S1), moderately suitable (S2), marginally suitable (S3), and not suitable (N). The classification of the spatial
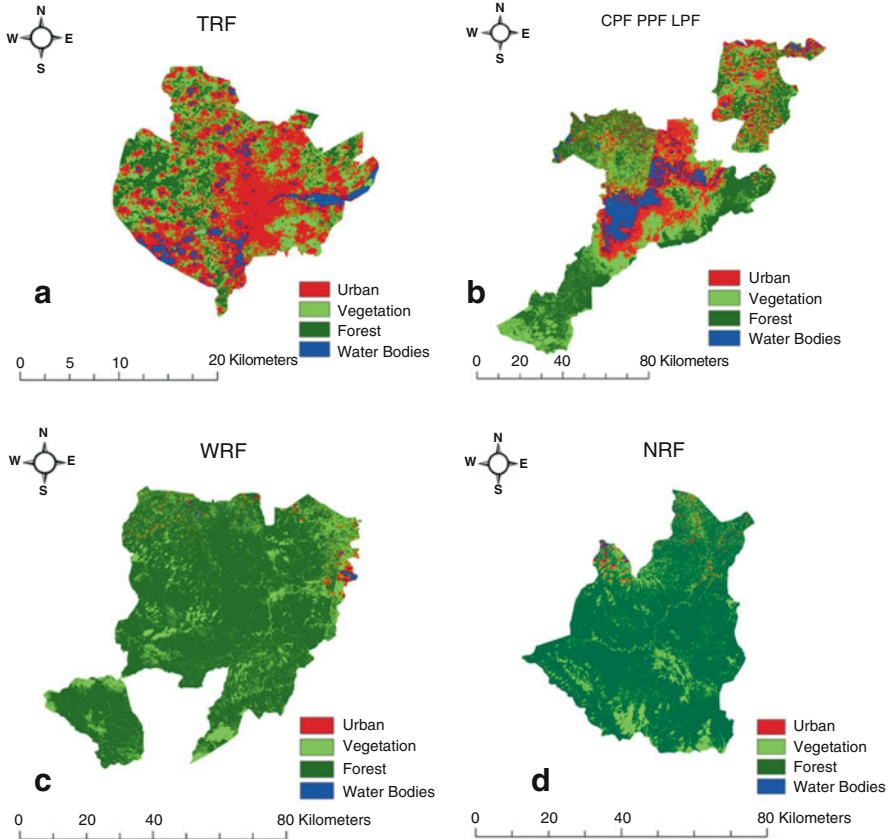
Fig. 8.4 LULC for each type of forest: (**a**) TRF; (**b**) CPF, PPF and LPF; (**c**) WRF; and (**d**) NRF

data, such as vector datasets, were translated into raster layers and were processed using ArcGIS® 10.4 (Table 8.4).

8.2.4 AHP

AHP is a mathematical method that uses several criteria to analyze complex decisions (Saaty 1980, 1990). This method has been successfully applied to forestry applications (Mendoza and Sprouse 1989; Saaty 1990; Kangas 1991, 1992; Schmoldt et al. 1994; Tarp and Helles 1995). In this AHP analysis, weighting of several criteria was used to conduct the pairwise comparison of two criteria at a time. Each weight was determined by experts to choose for the pairwise comparison matrix. In our research framework, the top class was to determine the potential

Table 8.4 Reclassification of the criteria of land suitability for forest extension areas

Criteria	Suitability class	Suitability range	Percentage area (%)	Area (ha)
Settlements	**S1**	<214	57.47	1310
	S2	264–365	23.48	535
	S3	365–414	13.72	313
	N	>414	5.33	121
LULC	**S1**	Forest	57.6	790,712
	S2	Vegetation	24.2	333,020
	S3	Urban	13.2	180,615
	N	Waterbodies	5	68,806
Elevation	**S1**	<350	53.28	495,989
	S2	350–900	25.56	237,940
	S3	900–1600	15.82	147,314
	N	>1600	5.34	49,681
Distance from roads	**S1**	<10	85.77	1,163,759
	S2	10–23	9.77	132,494
	S3	23–45	3.73	50,577
	N	>45	0.74	9985
Distance from rivers	**S1**	<6	97.96	1,339,701
	S2	6–13	1.38	18,856
	S3	13–21	0.44	6032
	N	>29	0.22	2994
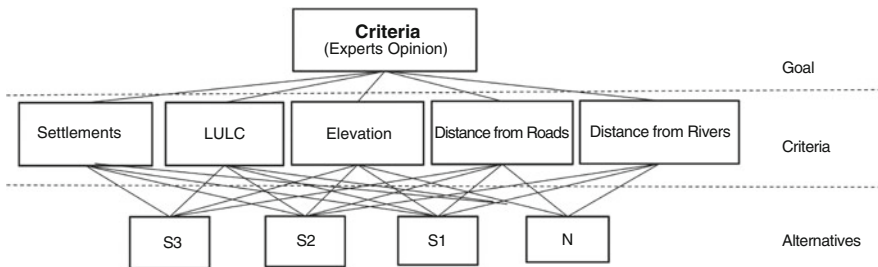
Fig. 8.5 The AHP framework to incorporate expert opinion into the land suitability analysis for extension of potential forest areas

forest extension areas (goal), the middle class being the criteria and bottom class the alternative. The middle class of the hierarchy was considered the rules or criteria of the goal. The bottom class was considered alternative decisions (Fig. 8.5). Questionnaires were used to gather expert opinions on the relative importance of the criteria and factors. Comparative results (for each factor pair) were described as integer values of 1 (equal value) to 9 (extremely different), where a higher number indicated that the chosen factor was more important than the other factors to which it was compared (Table 8.5). In the AHP analysis, first, five criteria were selected

Table 8.5 Saaty scale for pairwise comparison between the criteria in the AHP

Index	Definition	Index	Definition
1	Equally important	1/1	Equally important
2	Equally or slightly more important	1/2	Equally or slightly less important
3	Slightly more important	1/3	Slightly less important
4	Slightly to much more important	1/4	Slightly to way less important
5	Much more important	1/5	Way less important
6	Much too far more important	1/6	Way to far less important
7	Far more important	1/7	Far less important
8	Far more important to extremely more important	1/8	Far less important to extremely less important
9	Extremely more important	1/9	Extremely less important

Table 8.6 Random indices in the AHP

n	3	4	5	6	7		8	9	10
RI	0.58	0.9	1.12	1.24	1.32		1.41	1.45	1.49

based on a literature review and expert opinion. All scores were assembled in a pairwise comparison matrix, with diagonal and reciprocal scores located in the lower left-hand triangle. Reciprocal values (1/3, 1/5, 1/7, and 1/9) were used where the row criterion was found to be less important than the column criterion. Secondly, scoring was involved in the criteria via pairwise comparisons and scales of relative importance. The random indices of Saaty (1977) are listed for the observation from 3 to 9 (Table 8.6). Thirdly, the matrix was calculated and ensured the consistency of the pairwise comparison criteria. The pairwise matrix was calculated with the comparison results, creating a matrix form C with dimensions of $m \times n$ by the following expression:

$$\begin{bmatrix} C_{11} & C_{12} & C_{13} & \cdots & C_{1n} \\ C_{21} & C_{22} & C_{23} & \cdots & C_{2n} \\ \vdots & \vdots & \vdots & \cdots & \vdots \\ \vdots & \vdots & \vdots & \cdots & \vdots \\ C_{m1} & C_{m2} & C_{m3} & \cdots & C_{mn} \end{bmatrix} \tag{8.3}$$

The sum of each column of the pairwise matrix was denoted as follows:

$$C_{ij} = \sum_{i=1}^{n} C_{ij} \tag{8.4}$$

Then the element of the matrix was divided by its column total to generate a normalized pairwise matrix:

$$X_{ij} = \frac{C_{ij}}{\sum\limits_{i=1}^{n} C_{ij}} = \begin{bmatrix} X_{11} & X_{12} & X_{13} & \cdots & X_{1n} \\ X_{21} & X_{22} & X_{23} & \cdots & X_{2n} \\ \vdots & \vdots & \vdots & \cdots & \vdots \\ \vdots & \vdots & \vdots & \cdots & \vdots \\ X_{m1} & X_{m2} & X_{m3} & \cdots & X_{mn} \end{bmatrix} \tag{8.5}$$

The AHP generates a weight for each evaluation criterion according to the expert's pairwise comparisons of the criteria. The higher weight is more important than the corresponding criteria. Then the AHP combines the weights and the scores to determine the total score for each option and a consequent ranking was used (n) to generate the weighted matrix of the priority criteria (W):

$$W_{ij} = \frac{\sum\limits_{j=1}^{n} X_{ij}}{n} \begin{bmatrix} W_{11} \\ W_{12} \\ \vdots \\ W_{1n} \end{bmatrix} \tag{8.6}$$

To compute an estimate of the eigenvector for a pairwise comparison matrix, we multiplied the normalized matrix with the priorities vector (principal eigenvector of the matrix). Then we divided the elements in the resulting vector of priorities and took the average. The initial consistency vectors were derived by multiplying the pairwise matrix by the vector of weights:

$$\begin{bmatrix} C_{11} & C_{12} & C_{13} & \cdots & C_{1n} \\ C_{21} & C_{22} & C_{23} & \cdots & C_{2n} \\ \vdots & \vdots & \vdots & \cdots & \vdots \\ \vdots & \vdots & \vdots & \cdots & \vdots \\ C_{m1} & C_{m2} & C_{m3} & \cdots & C_{mn} \end{bmatrix} \times \begin{bmatrix} W_{11} \\ W_{12} \\ \vdots \\ W_{1n} \end{bmatrix}$$

$$= \begin{bmatrix} C_{11}W_{11} & C_{12}W_{12} & \cdots & C_{1n}W_{1n} \\ C_{21}W_{21} & C_{22}W_{22} & \cdots & C_{2n}W_{2n} \\ \vdots & \vdots & \vdots & \vdots \\ \vdots & \vdots & \vdots & \vdots \\ C_{m1}W_{m1} & C_{m2}W_{m2} & \cdots & C_{mn}W_{mn} \end{bmatrix} = \begin{bmatrix} V_{11} \\ V_{12} \\ \vdots \\ V_{1n} \end{bmatrix} \tag{8.7}$$

The number of objectives and alternatives should not exceed seven, respectively, to make the decision process manageable. The principal eigenvector (λ_{max}) was calculated by averaging the values of the consistency vector:

$$\lambda_{\max} = \sum_{i}^{n} CV_{ij} \tag{8.8}$$

Eigenvalues were calculated by averaging the rows of each matrix. Eigenvalues were also referred to as relative weights. The largest eigenvalue was equal to the number of criteria, and when $\lambda_{\max} = n$, judgments were consistent. Normalized eigenvalues were generated as the weights of the priority criteria. The consistency index (CI) was calculated following Saaty (1980), where the deviation $\lambda_{\max}$ from n is a measure of inconsistency:

$$CI = \frac{\lambda_{\max} - n}{n - 1} \tag{8.9}$$

The evaluation is considered acceptable if the consistency ratio (CR) < 0.1 (Saaty 1980). The evaluation is considered as moderately consistent and acceptable if $0.1 < CR < 0.2$ (Wedley 1993) or CR < 0.2 (Lakiãeviã and Srðeviã 2012). CR is calculated as follows:

$$CR = \frac{CI}{RI} \tag{8.10}$$

8.2.5   Land Suitability for Forest Extension Areas

The land suitability analysis for potential forest extension areas was carried out using various classification categories suggested by the FAO. The reclassified criteria were selected to perform the weighted overlay to develop the land suitability map for forest extension. In the weighted overlay, the AHP weights were used and can be expressed as

$$Weighted\ Overlay = \sum_{i=1}^{n} C_i * W_n \tag{8.11}$$

where C_i is the criteria (i) that was reclassified, and W_n is the amount of weighted data (n). The classes are noted as highly suitable (S1), moderately suitable (S2), marginally suitable (S3), or not suitable (N) within the FAO land assessment framework. Then these suitability classes can be subdivided further as needed. These three classes, S1, S2, and S3, were used to identify highly suitable, moderately suitable, and marginally suitable lands for potential forest extension areas. In the GIS environment, suitability analysis was conducted to find the potential areas for extension of forests.

8.3 Results

8.3.1 Change Detection Analysis

Based on the landscape of the study area, change detection analysis was done in four categories: urban, waterbody, vegetation, and forest for six types of forest zones (Fig. 8.6 and Table 8.7). A negative value is presented to show a decrease in change detection while a positive value indicates an increase in the change detection class. In the study area, TRF was observed as an increasing trend in the urban class by 37.03% (14.78 ha). A decreasing trend was observed in the vegetation and forest classes by 21.47% (8.61 ha) and 20.09% (8.06 ha), respectively. CPF, PPF, and LPF
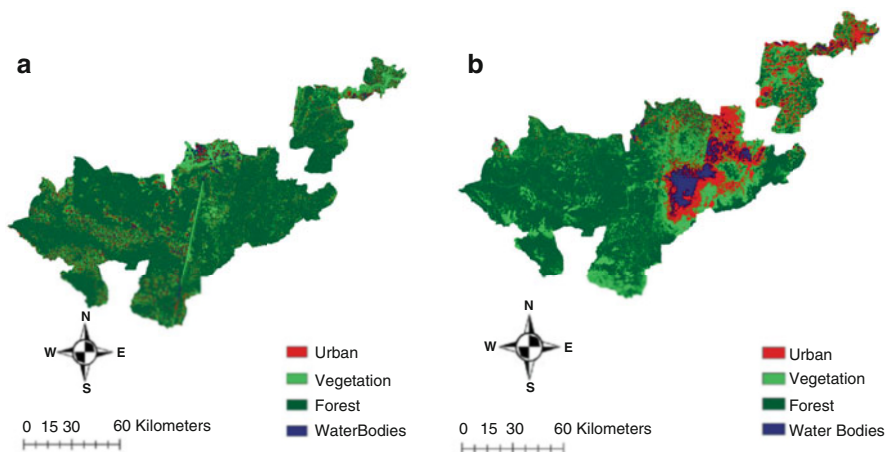
Fig. 8.6 Change detection in the LULC for classified forest areas in South Sumatra. (**a**) LULC, 2003; and (**b**) LULC, 2018

Table 8.7 Change detection of forest classes from 2003 until 2018

Forest zone	Changing area (urban class)		Changing area (vegetation class)		Changing area (forest class)		Changing area (waterbody class)	
	(%)	(ha)	(%)	(ha)	(%)	(ha)	(%)	(ha)
TRF	37.03	14.78	−21.47	−8.61	−20.09	−8.06	–	–
NRF	−19.78	−55.22	–	–	33.05	92.26	−0.99	−2.75
WRF	3	29.56	–	–	33.44	329.7	−6.2	−61.15
CPF	4.56	372.16	10.09	823.49	−13.56	−1105.72	−1.09	−88.66
PPF	9.52	163.72	31.16	535.7	−40.21	−691.12	–	–
LPF	48.75	1514.34	23.63	733.92	−72	−2236.62	−0.37	−11.65

had an increased rate in the urban land-use class. The highest percentage of increased area was observed in the LPF area of 48.75% (1514.34 ha). The CPF and PPF were 4.56% (372.16 ha) and 9.52% (163.72 ha). An increasing trend was observed in the vegetation class with the highest percentage in the PPF area of 31.16% (535.7 ha). In the case of the LPF and CPF, vegetation class was increased by 23.63% (733.92 ha) and 10.09% (823.49 ha), respectively. CPF, PPF, and LPF had a decreasing trend in the percentage of forest classes by 72% (2236.62 ha), 40.21% (691.12 ha), and 13.56% (1105.72 ha). Waterbodies were decreased by 1.09% (88.66 ha) for CPF and 0.37% (11.65 ha) for LPF. WRF was increased in urban and forest classes by 3% (29.56 ha) and 33.44% (329.7 ha). Waterbody classes were decreased by 6.2% (61.15 ha). NRF had an increasing trend in the forest class by 33.05% (92.26 ha). However, the declining trend was also observed in urban and waterbody classes by 19.78% (55.22 ha) and 0.99% (2.75 ha), respectively (Table 8.7).

8.3.2 Accuracy Assessment

The accuracy assessment was referred to by the producer's accuracy of 86% and 96% for the urban class in 2003 and 2018 in the six types of forest zones. The vegetation class had a producer's accuracy of 86% and 100% for both the years in 2003 and 2018. The forest class also had a producer's accuracy of 90% and 96% in 2003 and 2018. The waterbody class had a producer's accuracy of 80–96%. The Kappa coefficient of agreement was more than 0.60 (Table 8.8). The interpretation of Kappa showed a good agreement for all types of forests.

Table 8.8 Accuracy assessments for LULC in 2003 and 2018

Accuracy assessment	Class	TRF (%)		CPF, PPF, and LPF (%)		WRF (%)		NRF (%)	
		2003	2018	2003	2018	2003	2018	2003	2018
Producers accuracy	Urban	96	90	92	92	88	94	92	86
	Vegetation	90	96	88	100	94	96	86	86
	Forest	92	96	92	90	96	94	96	96
	Waterbody	92	80	88	84	96	96	96	90
User accuracy	Urban	96	82	92	85	100	98	90	86
	Vegetation	90	96	88	85	87	87	91	86
	Forest	92	100	92	100	89	96	96	96
	Waterbody	92	85	88	100	100	100	92	90
Overall accuracy		93	91	90	92	94	95	93	90
Kappa coefficient		0.84	0.79	0.80	0.82	0.86	0.89	0.83	0.78

8.3.3 Land Suitability Analysis for Extension of Potential Forest Area

Reclassification of Criteria

The reclassifications of criteria were categorized into four classifications, namely, highly suitable, moderately suitable, marginally suitable, and not suitable, according to a land suitability analysis (FAO 1979). The settlements criteria showed that 57.47% of the areas were highly suitable (1310 ha) and 23.48% of the areas were moderately suitable (535 ha). In the case of the LULC reclassification, 57.6% of the areas had forest and were highly suitable (790,712 ha). On the other hand, 24.2% of the areas were observed as vegetation and were reported as moderately suitable (333,020 ha). From the reclassification of elevation criteria, 53.28% of the areas were noted as highly suitable (495,989 ha) and 25.56% were moderately suitable (237,940 ha). The roads were measured using the Euclidean distance and a reclassification of this criteria showed that 85.77% of the areas were highly suitable (1,163,759 ha) and 9.77% were moderately suitable (132,494 ha). Evaluating the distance from rivers in a similar way, the reclassification referred that 97.96% of the areas were highly suitable (1,339,701 ha) and 1.38% were moderately suitable (18,856 ha) (Table 8.4, Fig. 8.7).

8.3.4 AHP

In the AHP, the expert's opinions were considered using a comparison of the scale matrix for each criterion, whose expert judgment for the ranking of the criteria affected the area of land suitability. A pairwise matrix was used in the AHP for the expert opinion using five criteria. The AHP weight results indicated that the settlements weight was scored first, LULC second, elevation third, distance from road fourth, and distance from a river fifth (Table 8.9). In ArcGIS®, the criteria were reclassified as raster-based data layers and integrated with a weighted overlay according to the weight rank given by the experts. The rank was given to prioritize the influence of the criteria for the extension of potential areas of forest in the land suitability analysis.

8.3.5 Land Suitability Analysis for Extension of Potential Forest Area

Change detection analysis was performed not only to detect changes that occurred in the forest but also to identify the potential areas for further extension of production forest. In the land suitability analysis, five criteria were used in the TRF, CPF, LPF,
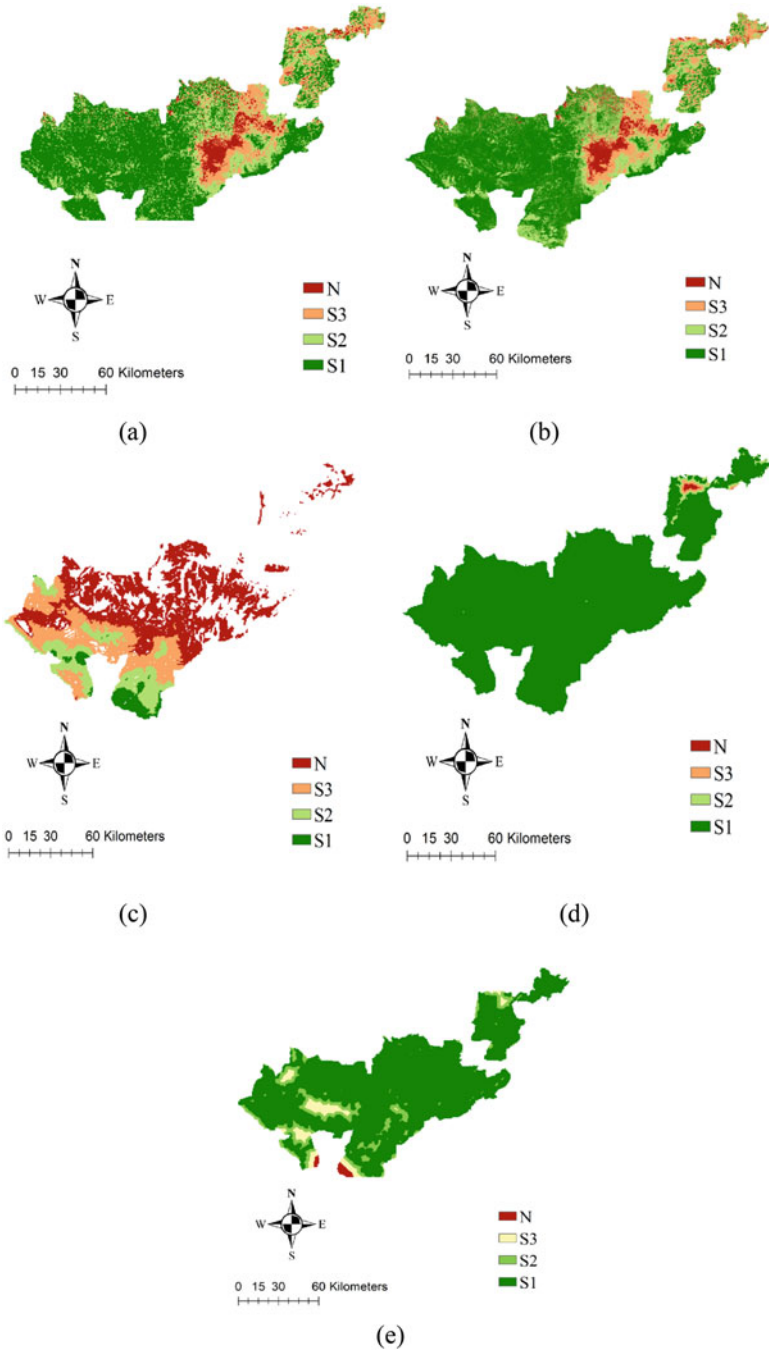
Fig. 8.7 Reclassification of the criteria for the land suitability analysis to propose extension of potential forest areas. (**a**) Settlements, (**b**) LULC, (**c**) elevation, (**d**) distance from rivers, and (**e**) distance from roads

Table 8.9 Expert opinion weights for prioritizing the criteria in AHP

Criteria	Expert A	Expert B	Expert C	Expert D	Expert E	Average weight	Weight (%)
Settlements	0.190	0.354	0.160	0.245	0.102	0.210	29
LULC	0.214	0.222	0.102	0.143	0.379	0.212	29
Elevation	0.086	0.066	0.379	0.119	0.160	0.162	23
Distance from roads	0.092	0.097	0.065	0.100	0.065	0.084	12
Distance from rivers	0.074	0.049	0.043	0.033	0.043	0.048	7

PPF, WRF, and NRF zones to find out the potential areas for forest extension (Fig. 8.8). In these types of forest zones, a highly suitable classification had the highest preferences followed by the moderately suitable classification. In the TRF, forest extension could be possible in 7% and 8% of the limited areas belonging to the highly suitable class and moderately suitable class (Table 8.10). There were highly and moderately suitable classes in the CPF, LPF, and PPF areas of 30% (81,663.91 ha) and 41% (112,191.20 ha), respectively. In the case of a WRF, there is the possibility of extension in 30% (98,133.18 ha) in highly suitable areas and 52% in areas (167,012.93 ha) in the moderately suitable class. The potential areas for an NRF forest zone were 39% (79,798.61 ha) in the highly suitable class and 48% of areas (99,498.03 ha) in the moderately suitable class (Table 8.10).

8.4   Discussion

South Sumatra is one of the most important provinces for conservation of biodiversity and forest resources in Indonesia. The stewardship and use of forest land must be managed for their biological diversity, productivity, regeneration capacity, vitality, and potential to fulfill the current and future needs relevant to ecological, economic, and social functions at the local, national, and global levels (FAO 2000). Potential forests area extension strategies can be targeted with creating sustainable forestry market opportunities, such as oil palm plantations and agricultural lands (Fitzherbert et al. 2008; Lawson 2014; Martin et al. 2016). In this research, CPF, PPF, and LPF are referred to as community forestry. Potential land can be set up for new forest generation to promote plantations that bring benefits to the environment and surrounding communities (Cossalter and Pye-Smith 2003; Kanowski et al. 2005; Weber 2005; Martin et al. 2016). Protecting and restoring forests could provide the best decision with the local communities to get the benefit and restore the environmental and economic functions of the forests (Sanchirico and Siikamaki 2007). The challenges in achieving sustainable forest management and forest conservation need to develop with collaborative solutions between stakeholders and communities (Sheil et al. 2002; Gunningham 2009). CPF, PPF, and LPF entail forest production, providing support and opportunities for enhancing the economic benefits through wood and palm oil. In the demographic shift, TRF can play an important role in
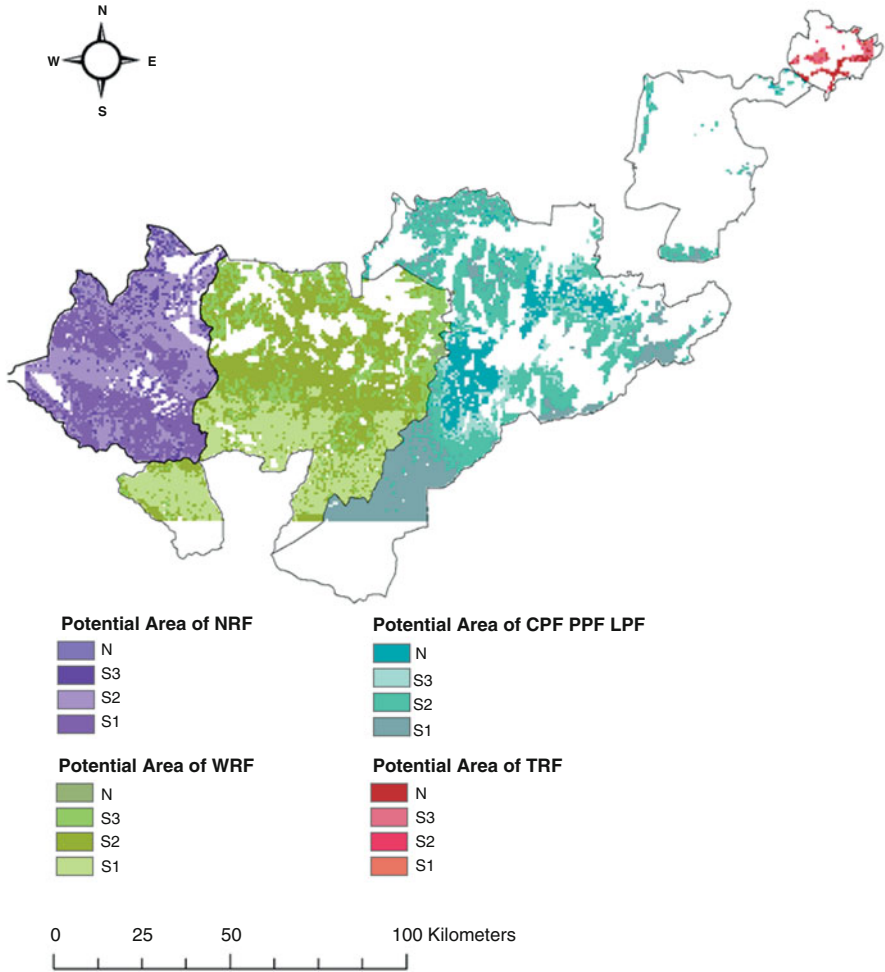
Fig. 8.8 Land suitability analysis for the extension of potential areas in NRF, CPF, LPF, PPF, WRF, and TRF forest zones

Table 8.10 Land suitability analysis for extension of potential forest areas in the forest zones

Land suitability classes	TRF		CPF, PPF, and LPF		WRF		NRF	
	(%)	(ha)	(%)	(ha)	(%)	(ha)	(%)	(ha)
N	45	3730.61	16	44,994.77	1	2638.72	2	4913.48
S3	40	3275.66	13	37,215.08	17	54,503.27	11	22,793.10
S2	8	682.43	41	112,191.20	52	167,012.93	48	99,498.03
S1	7	591.44	30	81,663.91	30	98,133.18	39	79,798.61
Total	100	8280.13	100	276,064.96	100	322,288.09	100	207,003.22

supporting efforts of urban forestry and urban landscapes to provide ecosystem and natural infrastructure (Costanza et al. 1997; Landell-Mills 2002) and NRF have an important role in maintaining and protecting the biodiversity of wildlife habitat and natural land (Sheil et al. 2002; Balmford et al. 2002). The proposed potential areas can be extended by forest classifications to balance the deforestation with production forests, such as plantations. Therefore, the change detection analysis and periodic determination of potential forest extension areas could help to create a new policy space for plantation forests and ecosystems to be present in designing national and subnational policies.

8.5 Conclusions

In this research, remotely sensed data were used to monitor the changes in the LULC and quantify the differences in the forest classes in the South Sumatra province of Indonesia from 2003 to 2018. In the LULC analysis, six types of forest zones: CPF, PPF, LPF, WRF, TRF, and NRF were focused upon to find out their changes and locate potential areas for extension of forest. In the change detection analysis, we have observed that the TRF, CPF, and PPF forest zones had a decrease of their forest class by 20%, 13%, and 40%, respectively, from 2003 to 2018. LPF regions had large changes and decreased by 72% in LULC for its forest class. Palm oil plantations had a significant impact on the LPF forest classification areas. For the extension of forest types that decreased over the time period, the AHP analysis incorporated selected criteria using weights from experts. The weights were used in the GIS analysis to propose the potential areas for extension. The influential criteria had higher weights and ranked as settlements, elevation, distance from roads and rivers. We found CPF, PPF, and LPF had an opportunity of extension in the highly suitable classification (30%) and moderately suitable classification (41%) areas, in order to increase coverage of production forests. WRF had a forest potential area in the highly suitable classification of 30% and moderately suitable classification of 52% to keep biodiversity ecosystems for wildlife resources. The potential areas for NRF were 39% (79,798.61 ha) in the highly suitable class and 48% of areas (99,498.03 ha) in the moderately suitable class, to keep the natural ecosystem. TRFs had a very limited scope to propose a further extension and are required to be managed with collaboration between the government and the community.

References

Badamasi MM, Yelwa SA (2010) Change detection and classification of land cover at Falgore game reserve: a preliminary assessment. BEST J 7:75–83

Bailly J-S, Arnaud M, Puech C (2007) Boosting: a classification method for remote sensing. Int J Remote Sens 28:1687–1710. https://doi.org/10.1080/01431160500469985

Balmford A, Bruner A, Cooper P, Costanza R, Farber S, Green RE, Jenkins M, Jefferiss P, Jessamy V, Madden J et al (2002) Ecology: economic reasons for conserving wild nature. Science 297:950–953

Berner LT, Law BE (2015) Water limitations on forest carbon cycling and conifer traits along a steep climatic gradient in the Cascade Mountains, Oregon. Biogeosciences 12:6617–6635. https://bg.copernicus.org/articles/12/6617/2015/

Brown D, Pijanowski B, Duh J (2000) Modeling the relationships between land use and land cover on private lands in the upper Midwest, USA. J Environ Manag 59:247–263. https://www.sciencedirect.com/science/article/pii/S0301479700903694?via%3Dihub

Brown ME, Pinzon J, Didan K, Morisette J, Tucker C (2006) Evaluation of the consistency of long-term NDVI time series derived from AVHRR, SPOT-vegetation, SeaWiFS, MODIS, and Landsat ETM+ sensors. IEEE Trans Geosci Remote Sens 44:1787–1793. https://ieeexplore.ieee.org/document/1645279

Campbell JB (1987) Introduction to remote sensing. Geocarto Int 2:64. https://doi.org/10.1080/10106048709354126

Chaudhary BS, Saroha GP, Yadav M (2008) Human induced land use land cover changes in northern part of Gurgaon District, Haryana, India: natural resources census concept. J Hum Ecol 23:243–252. https://doi.org/10.1080/09709274.2008.11906077

Chen H, Kocaoglu DF (2008) A sensitivity analysis algorithm for hierarchical decision models. Eur J Oper Res 185:266–288. https://doi.org/10.1016/j.ejor.2006.12.029

Churkina G, Running SW (1998) Contrasting climatic controls on the estimated productivity of global terrestrial biomes. Ecosystems 1:206–215. https://doi.org/10.1007/s100219900016

Congalton R (1991) A review of assessing the accuracy of classifications of remotely sensed data. Remote Sens Environ 37:35–46. https://doi.org/10.1016/0034-4257(91)90048-B

Cossalter C, Pye-Smith C (2003) Fast-wood forestry: myths and realities. CIFOR, Bogor, Indonesia

Costanza R, D'arge R, Groot RE, Stephen F, Grasso M, Hannon B, Limburg K, Naeem S, O'Neill RV, Paruelo J et al (1997) Natural capital. Nature 387:253–260. https://doi.org/10.1038/387253a0

Currit N (2005) Development of a remotely sensed, historical land-cover change database for rural Chihuahua, Mexico. Int J Appl Earth Obs Geoinform 7:232–247. https://doi.org/10.1016/j.jag.2005.05.001

Datry T, Larned ST, Tockner K (2014) Intermittent rivers: a challenge for freshwater ecology. BioScience 64:229–235. https://doi.org/10.1093/biosci/bit027

Demissie F, Yeshitila K, Kindu M, Schneider T (2017) Land use/land cover changes and their causes in Libokemkem District of south Gonder, Ethiopia. Remote Sens Appl Soc Environ 8: 224–230. https://doi.org/10.3390/ijgi8020079

Diallo Y, Hu G, Wen X (2009) Applications of remote sensing in land use/land cover change detection in Puer and Simao counties, Yunnan Province. J Am Sci 5:157–166

Escobar M, Moreno-Jiménez JM (2000) Reciprocal distributions in the analytic hierarchy process. Eur J Oper Res 123:154–174. https://doi.org/10.1016/S0377-2217(99)00086-7

FAO (1979) A framework for land evaluation, 1st edn. FAO, Rome. https://www.fao.org/3/x5310e/x5310e00.htm

FAO (2000) Asia-Pacific Forestry Commission: development of national-level criteria and indicators for the sustainable management of dry forests of Asia. In: Workshop Report, RAP Publication 2000/07. Food and Agriculture Organization, Rome. http://www.fao.org/3/x6896e/x6896e00.htm. Accessed 5 Feb 2019

Fitzherbert E, Struebig MJ, Morel A, Danielsen F, Brühl C, Donald P, Phalan B (2008) How will oil palm expansion affect biodiversity? Trends Ecol Evol 23:538–545. https://doi.org/10.1016/j. tree.2008.06.012

Foody GM (2002) Status of land cover classification accuracy assessment. Remote Sens Environ 80:185–201. https://doi.org/10.1016/S0034-4257(01)00295-4

Forest Area and Conservation Area of South Sumatra Province, Forestry Data South Sumatra (2016). http://data.dishut.sumselprov.go.id/layers/geonode:KawasanHutan_AR_2016_ SumateraSelatan_PPH_250_. Accessed 11 Feb 2019

Gao J, Liu Y-S (2010) Determination of land degradation causes in Tongyu County, Northeast China via land cover change detection. Int J Appl Earth Obs Geoinform 12:9–16. https://doi.org/ 10.1016/j.jag.2009.08.003

Gigovic L, Drobnjak S, Pamucˇar D (2019) The application of the hybrid GIS spatial multi-criteria decision analysis best–worst methodology for landslide susceptibility mapping. ISPRS Int J Geo-Inform 8:79. https://doi.org/10.3390/ijgi8020079

Gradstein RS, Homeier J, Gansert D (eds) (2010) Tropical Mountain Forest: patterns and processes in a biodiversity hotspot. University of Akron Press, Akron, OH, p 224

Gunningham N (2009) The new collaborative environmental governance: the localization of regulation. J Law Soc 36:145–166. https://doi.org/10.1111/j.1467-6478.2009.00461.x

Hegazy IR, Kaloop MR (2015) Monitoring urban growth and land use change detection with GIS and remote sensing techniques in Daqahlia governorate Egypt. Int J Sustain Built Environ 4: 117–124. https://doi.org/10.1016/j.ijsbe.2015.02.005

Holdridge LR, Hubbert MK (1947) Determination of world plant formations from simple climatic data. Science 105:367–368. https://doi.org/10.1126/science.105.2727.367

Houghton RA (1991) Releases of carbon to the atmosphere from degradation of forests in tropical Asia. Can J For Res 21:132–142. https://doi.org/10.1139/x91-017

Huang Y-F (2002) Enhancement on sensitivity analysis of priority in analytic hierarchy process. Int J Gen Syst 31:531–542. https://doi.org/10.1080/0308107021000042499

Jensen JR (2007) Remote sensing of the environment, 2nd edn. Pearson Prentice Hall, Upper Saddle River, NJ, p 17

Johnson JB, Omland KS (2004) Model selection in ecology and evolution. Trends Ecol Evol 19: 101–108. https://doi.org/10.1016/j.tree.2003.10.013

Kangas J (1991) A method for utility comparison of forest drainage alternatives. Suo 42:49–59

Kangas J (1992) Choosing the regeneration chain in a forest stand: a decision model based on multi-attribute utility theory. Univ Joensuu Publ Sci 24:1–230

Kanowski J, Catterall CP, Wardell-Johnson G (2005) Consequences of broadscale timber plantations for biodiversity in cleared rainforest landscapes of tropical and subtropical Australia. For Ecol Manage 208:359–372. https://doi.org/10.1016/j.foreco.2005.01.018

Kirchmair I (2017) Biogeography of west African gallery forests. PhD Thesis, Johann Wolfgang Goethe-Universität, Frankfurt, Germany. http://publikationen.ub.uni-frankfurt.de/frontdoor/ index/index/docId/44536. Accessed 22 Mar 2019

Lakiãeviã M, Srðeviã B (2012) AHP group decision-making in selecting tree species for urban wet sites. Contemp Agric 61:8–14

Landell-Mills N (2002) Developing markets for forest environmental services: an opportunity for promoting equity while securing efficiency? Philos Trans Ser 360:1817–1825. https://doi.org/ 10.1098/rsta.2002.1034

Law BE, Falge E, Gu L, Baldocchi DD, Bakwin P, Berbigier P, Davis K, Dolman H, Falk M, Fuentes J et al (2002) Environmental controls over carbon dioxide and water vapor exchange of terrestrial vegetation. Agric For Meteorol 113:97–120. https://doi.org/10.1016/S0168-1923(02) 00104-1

Lawson S (2014) Consumer goods and deforestation: an analysis of the extent and nature of illegality in forest conversion for agriculture and timber plantations. Forest Trends, Washington, DC, pp 1–158. http://www.forest-trends.org/documents/files/doc_4718.pdf. Accessed 11 Feb 2019

Li Q, Huang J, Wang C, Lin H, Zhang J, Jiang J, Wang B (2017) Land development suitability evaluation of Pingtan Island based on scenario analysis and landscape ecological quality evaluation. Sustainability 9:1292. https://doi.org/10.3390/su9071292

Liu X-H, Skidmore A, Van Oosten H (2002) Integration of classification methods for improvement of land-cover map accuracy. ISPRS J Photogramm Remote Sens 56:257–268. https://doi.org/10.1016/S0924-2716(02)00061-8

Major J (1963) A climatic index to vascular plant activity. Ecology 44:485–498. https://doi.org/10.2307/1932527

Mancino G, Nolè A, Ripullone F, Ferrara A (2014) Landsat TM imagery and NDVI differencing to detect vegetation change: assessing natural forest expansion in Basilicata, southern Italy. iForest Biogeosci For 7:75–84. https://doi.org/10.3832/ifor0909-007

Martin RM, Kneeland D, Brooks D, Matta R (2016) The state of the world's forests in brief. In: Forests and agriculture: land-use challenges and opportunities. FAO, Rome, p 46. ISBN 978-92-5-107292-9

Mendoza GA, Sprouse W (1989) Forest planning and decision making under fuzzy environments: an overview and illustrations. For Sci 35:481–502

Mickelson JG, Civco DL, Silander JA (1998) Delineating vegetation coverage canopy species in the northeastern United States using multi-temporal TM imagery. Photogramm Eng Remote Sens 64:891–904

Ministry of Forestry (2015) Forest Production Map for Use of Forest Utilization, Directorate General of Forestry Business Forestry Ministry of Forestry, 2015; Forest area and Conservation Area of South Sumatra Province, Forestry Data South Sumatra, 2015 (Peta Indikatif Arahan Pemanfaatan Hutan Pada Kawasan Hutan Produksi Yang Tidak Dibebani Izin Untuk Usaha Pemanfaatan Hasil Hutan Kayu. 2014. Lembar Peta, Sumatera Selatan, Indonesia. http://appgis.dephut.go.id/appgis/Arahan_Pemanfaatan_2015/Sumsel.pdf. Accessed 12 Jan 2019

Ministry of Forestry (2016) Forest area and Conservation Area of South Sumatra Province, Forestry Data South Sumatra. Available online http://data.dishut.sumselprov.go.id/layers/geonode:KawasanHutan_AR_2016_SumateraSelatan_PPH_250_. Accessed 11 Feb 2019

Nayak P, Oliveira LE, Berkes F (2014) Resource degradation, marginalization, and poverty in small-scale fisheries: threats to social-ecological resilience in India and Brazil. Ecol Soc 19:73. https://doi.org/10.5751/ES-06656-190273

Nigussie G, Moges MA, Moges MM, Steenhuis TS (2019) Assessment of suitable land for surface irrigation in ungauged catchments: Blue Nile Basin, Ethiopia. Water 11:1–17. https://doi.org/10.3390/w11071465

Olmo MC, Abarca-Hernández F (2000) Computing geostatistical image texture for remotely sensed data classification. Comput Geosci 26:373–383. https://doi.org/10.1016/S0098-3004(99)00118-1

Potter C, Genovese V, Gross P, Boriah S, Steinbach M, Kumar V (2007) Revealing land cover change in California with satellite data. Eos 88:269–274. https://doi.org/10.1029/2007EO260001

Rawat JS, Kumar M (2015) Monitoring land user/cover change using remote sensing and GIS techniques: a case study of Hawalbagh block, district ALmora, Uttarakhand, India. Egypt J Remote Sens Space Sci 18:77–84

Rogan J, Miller J (2006) Integrating GIS and remotely sensed data for mapping forest disturbance and change. In: Wulder MA, Franklin SE (eds) Understanding forest disturbance and spatial pattern. CRC, Boca Raton, FL, pp 133–171

Saaty T (1977) A scaling method for priorities in hierarchical structures. J Math Psychol 15:234–281. https://doi.org/10.1016/0022-2496(77)90033-5

Saaty TL (1980) The analytical hierarchy process. McGraw-Hill, New York, NY, p 350

Saaty TL (1990) How to make a decision. The analytic hierarchy process. Eur J Oper Res 48:9–26. https://doi.org/10.1016/0377-2217(90)90057-I

Sanchirico JN, Siikamaki J (2007) Natural resource economics and policy in the 21st century: conservation of ecosystem services. Resources 165:8–10

Santika T, Meijaard E, Budiharta S, Law EA, Kusworo A, Hutabarat JA, Indrawan TP, Struebig MJ, Raharjo S, Huda I et al (2017) Community forest management in Indonesia: avoided deforestation in the context of anthropogenic and climate complexities. Glob Environ Chang 46:60–71. https://doi.org/10.1016/j.gloenvcha.2017.08.002

Sawathvong S (2004) Experiences from developing an integrated land-use planning approach for protected areas in the Lao PDR. For Policy Econ 6:553–566. https://doi.org/10.1016/S1389-9341(03)00005-4

Schmoldt DL, Peterson DL, Silsbee DG (1994) Developing inventory and monitoring programs based on multiple objectives. Environ Manag 28:707–727. https://doi.org/10.1007/BF02394635

Schuur EA (2003) Productivity, and global climate revisited: the sensitivity of tropical forest growth to precipitation. Ecology 84:1165–1170. https://doi.org/10.1890/0012-9658(2003)084[1165:PAGCRT]2.0.CO;2

Sheil D, Puri R, Basuki I, Van Heist M, Wan M, Liswanti N, Rukmiyati, Sardjono MA, Samsoedin I, Sidiyasa K et al (2002) Exploring biological diversity, environment and local peoples perspectives in forest landscapes, 2nd edn. CIFOR, Bogor, Indonesia

Spracklen DV, Righelato R (2014) Tropical montane forests are a larger than expected global carbon store. Biogeosciences 11:2741–2754

Stehman SV, Czaplewski RL (1998) Design and analysis for thematic map accuracy assessment. Remote Sens Environ 64:331–344. https://doi.org/10.1016/S0034-4257(98)00010-8

Strand GH (1993) Settlement planning with GIS. A case study of Thmarpouk, Cambodia. Habitat Int J 17:75–85. https://doi.org/10.1016/0197-3975(93)90017-7

Tarantino E, Novelli A, Aquilino M, Figorito B, Fratino U (2015) Comparing the MLC and JavaNNS approaches in classifying multi-temporal LANDSAT satellite imagery over an Ephemeral River area. Int J Agric Environ Inf Syst 6:83–102. https://doi.org/10.4018/IJAEIS.2015100105

Tarp P, Helles F (1995) Multi-criteria decision making in forest management planning—an overview. J For Econ 1:273–306

Teodoro AC, Araújo R (2016) Comparison of performance of object-based image analysis techniques available in open-source software (spring and Orfeo toolbox/Monteverdi) considering very high spatial resolution data. J Appl Remote Sens 10:16011. https://doi.org/10.1117/1.JRS.10.016011

Thomlinson JR, Bolstad PV, Cohen WB (1999) Coordinating methodologies for scaling land cover classifications from site-specific to global: steps toward validating global map products. Remote Sens Environ 70:16–28. https://doi.org/10.1016/S0034-4257(99)00055-3

United Nations (2009) The state of food and agriculture. Choice Rev Online 3:1–180

United Nations (2017) Country factsheet on food and agriculture policy trends, vol 8. FAO, Jakarta, Indonesia, pp 1–6

Weber N (2005) Afforestation in Europe: lessons learned, challenges remaining. In: Restoration of boreal and temperate forests. CRC, Boca Raton, FL, pp 121–135

Wedley WC (1993) Consistency prediction for incomplete AHP matrices. Math Comput Model 17:151–161. https://doi.org/10.1016/0895-7177(93)90183-Y

World Bank (2006) Sustaining economic growth, rural livelihoods, and environmental benefit: strategic options for Forest assistance in Indonesia. World Bank Office, Jakarta, Indonesia

Wright J, Lillesand TM, Kiefer RW (1980) Remote sensing and image interpretation. Geogr J 146:448. https://doi.org/10.2307/634969

Yelwa SA (2005) Land cover changes across Nigeria as detected from high temporal resolution meteorological data. Maid J Arts Soc Sci 3:73–79

Yuan F, Sawaya KE, Loeffelholz BC, Bauer ME (2005) Land cover classification and change analysis of the twin cities (Minnesota) metropolitan area by multitemporal Landsat remote sensing. Remote Sens Environ 98:317–328. https://doi.org/10.1016/j.rse.2005.08.006

Chapter 9
Estimating Productivity and Carbon Stock Using Phonological Indices from Satellite Remote Sensing in Indonesia

Nety Nurda, Ryozo Noguchi, and Tofael Ahamed

Abstract Indonesia has the highest forest density in the world, and the productivity of its forests can potentially be maximized to minimize CO_2 emissions. However, due to anthropogenic activities, phenological properties are subject to risk to ensure productivity and carbon exchange in the different forest ecosystems in Indonesia. Early prediction of carbon values could indicate a declining trend of forest quality with reference to vegetation levels. Thus, the purpose of this research is to evaluate forest productivity and carbon stock using phonological properties for different forests. The vegetation phenology was used to assess the level of forest productivity with different classifications to estimate carbon stock in six types of forest in south Sumatra using gross primary productivity (GPP) approaches. The vegetation phonologies were analyzed to develop a system dynamics model under two scenarios: first, a changing trend of normalized difference vegetation index (NDVI), and second, a changing trend of area, considering either increasing or decreasing solar radiation in both scenarios. This system was run through the geographic information system (GIS) environment to develop a database and to simulate results for future predictions. Verification was performed to test the simulation model by comparing the results with the Intergovernmental Panel on Climate Change (IPCC) reference. NDVI showed good correlations with GPP using MODIS MOD13Q1 for convertible production forest (CPF $R^2 = 0.97$), permanent production forest, PPF ($R^2 = 0.99$), limited production forest (LPF, $R^2 = 0.98$), tourism recreation forest (TRF, $R^2 = 0.95$), and wildlife reserve forest (WRF, $R^2 = 0.95$), nature reserve forest (NRF, $R^2 = 0.99$). The explicit differential function was used to estimate net primary productivity (NPP), which was related to the changes in area and productivity over time. Productivity and carbon stock analysis was performed via the proposal of five levels referring to Indonesian forest policy planning, considering resilience classified

N. Nurda
National Resilience Institute of the Republic of Indonesia (LEMHANNAS RI), Jakarta, Indonesia

R. Noguchi · T. Ahamed (✉)
Faculty of Life and Environmental Sciences, University of Tsukuba, Tsukuba, Ibaraki, Japan
e-mail: tofael.ahamed.gp@u.tsukuba.ac.jp

as high forest productivity (V1), moderate forest productivity (V2), marginal forest productivity (V3), very low forest productivity (N1), and no forest productive (N2). TRF was found to fall below the IPCC levels from 2015 to 2017, and NRF fall below the IPCC standards from 2015 to 2018. Therefore, the satellite-based remote sensing, system dynamics model can be implemented in the Indonesian forest policy system for assessing forest productivity and carbon stocks.

Keywords Forest productivity · Carbon stock · Satellite remote sensing and GIS · System dynamics

9.1 Introduction

Forests play an important role as efficient carbon sinks in tropical areas (IPCC 1997). Concerning the carbon content of forest biomass, 50% of forest vegetation is composed of carbon elements (Brown 1997). The estimation of forest biomass is useful for assessing forest productivity (Návar 2009; Thiffault et al. 2011; Fleming et al. 2014). Accurate biomass information obtained using remote sensing is necessary (Ahamed et al. 2011; Romijn et al. 2015; Sung et al. 2016) to describe the conditions of deep forest ecosystems for sustainable forest resource management (Wang et al. 2005). Deforestation and degradation are reported along with carbon mapping and monitoring data, which are used to adapt policies for reducing emissions (Defries et al. 2002; Mollicone et al. 2007; Houghton 2005; Gibbs et al. 2007). The release of CO_2 in the air due to deforestation has led to global warming in Indonesia. By measuring the amount of carbon stored in a living plant, we can describe the amount of CO_2 in the atmosphere absorbed by plants. Therefore, the estimation of carbon is very important for understanding forest ecosystems, especially in Indonesia, where they play a significant role in absorbing CO_2 from the air.

In Indonesia, anthropogenic activities are mainly responsible for decreasing forest productivity due to illegal logging, the preparation of new land for oil palm plantations, and frequent forest fires. Efficient planning is required to address the problems of anthropogenic activities. It is not wise to stop these activities altogether; however, forest classification measures and policies can be proposed for Indonesia that match the government targets. In large-scale planning and adaptation, satellite remote sensing datasets for the assessment of forest vegetation phenology can provide an indication of changes (Ruimy et al. 1994). For vegetation phenology, indices developed from Satellite Pour l'Observation de la Terre (SPOT), Landsat, and Moderate Resolution Imaging Spectroradiometer (MODIS) satellite imagery are often evaluated over time series (Foody et al. 2003; Goward et al. 1985; Sonawane and Bhagat 2016; Turner et al. 2006; Rasib et al. 2007). Researchers developed gross primary productivity (GPP) data from the MODIS GPP/net primary productivity (NPP) (MOD17) product based on the radiation use efficiency of vegetation (Zhao et al. 2005, 2006; Zhang et al. 2008; Zhao and Running 2010; Tian et al. 2010). The normalized difference vegetation index (NDVI) is one of the indices that can be used to estimate forest productivity. In productivity estimations, GPP or NPP is

considered a performance indicator of forest health. GPP and NPP are fundamental indicators of ecosystem health and productivity (IPCC 2001). Furthermore, NPP reflects the amount of carbon stored by plants through photosynthesis and autotrophic respiration after assimilation (Clark et al. 2001). The productivity of a forest is vulnerable to anthropogenic activities (Zhang et al. 2009a, b) and perpetual developmental pressures. NPP is often correlated with NDVI in various geographical areas and ecosystems (Box et al. 1989; Burke et al. 1990; Hobbs 1995). In addition, NDVI serves as an alternate estimator of NPP (Schloss et al. 1999; Jobbágy et al. 2002; Wessels et al. 2008; Irisarri et al. 2012).

Furthermore, in large areas with different forest classifications, it is difficult to understand the changes in phenological properties due to geospatial variability in a forest. A GIS approach can help to visualize the dynamic changes in NPP over a period of time, which will support forest management in Indonesia. As carbon sequestration is a long process, datasets over consecutive years are needed for regular monitoring, which is essential for productivity and carbon inventory planning necessary for the government to propose forest strategies. The projection of productivity in a given time frame can be performed on the basis of system dynamics under different scenarios. Through system dynamic modeling, forecasting of productivity can be achieved as early as possible by increasing vegetation or expanding the area in accordance with the expected productivity values via a simulation process.

To the best of our knowledge, no research has previously been undertaken to outline the associations between vegetation phenology, system dynamics, and forest productivity assessments. However, satellites have the potential to measure forest productivity. Understanding the ability of forests to absorb carbon over a long period of time provides an opportunity for Indonesia to engage in emissions trading activities, which is a new paradigm in the forestry sector. A net positive carbon sink due to the growth of forests (trees) can be effectively utilized for cancelling CO_2 emissions from fossil fuels. In this context, depending on whether the forest is native or artificial, the product of the density and the area is important as well as scheduled tree trimming and wood utilization. In this regard, it is very important to determine the site-specific vegetation status of a forest. Mapping such productivity data will provide insight into the ecosystem and can be used to establish sites a carbon resource in the environment (Ulsig et al. 2017); then, legislation for countermeasures can be proposed to ensure sustainable forest conservation and utilization of forests with different classifications (Yu and Chen 2016). Therefore, the purpose of this research is to develop a decision support system to assess productivity approaches for different forest classifications in Indonesia. Furthermore, WebGIS is proposed to determine the current productivity value along with a system dynamics model to estimate productivity over a long period of time.

9.2   Methods

9.2.1   Study Areas and Classification of Forests

The research was conducted in South Sumatra of Indonesia (Fig. 9.1a), which is an area vulnerable to increased deforestation rates due to the development of oil palm plantations and land use planning. The classified forest areas cover 361,760 km^2 in the 13 districts of South Sumatra. The involvement of the government in establishing regulations governing the use of wood forest products is critical for forest sustainability. Forest utilization takes into account the needs of the surrounding people as well as the preservation of the forest. As a result, the government categorizes forest types based on their intended utilization. The forest areas are located in the Empat Lawang, Muara Enim, Lahat, and Palembang districts (Fig. 9.1b). The locations of the forest areas form four clusters. However, three of the clusters are located in the northeastern part of South Sumatra (Fig. 9.1c). The following section introduces the six types of classified forests and their locations in the study area. The forest classification was confirmed by the central government (Ministry of Forestry 2015) to conduct vegetation phenology analysis for productivity assessment.
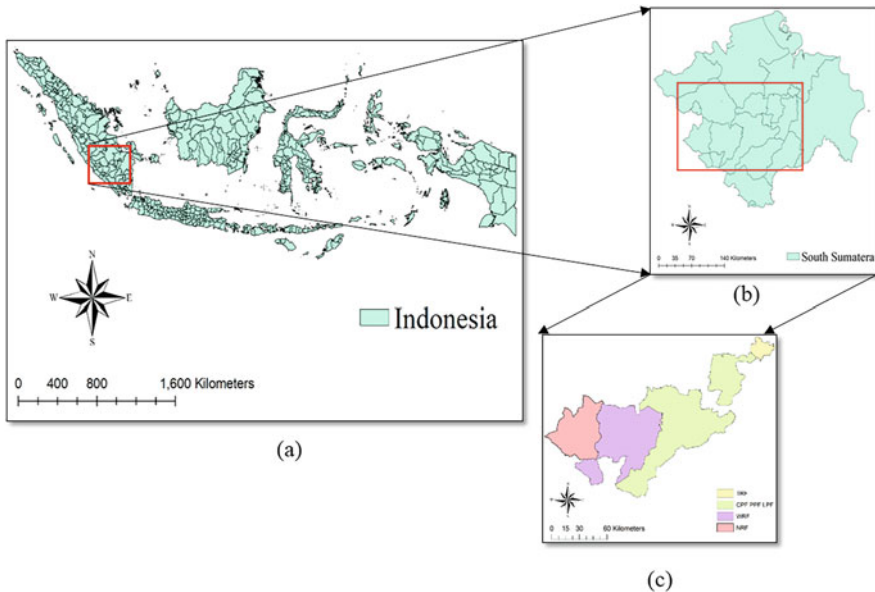
Fig. 9.1 Study area: (**a**) Indonesia, (**b**) South Sumatra, and (**c**) forest locations in South Sumatra of Indonesia

9.2.2 Convertible Production Forest (CPF)

It is a type of forest area that is spatially reserved for the development of transmigration, agricultural uses, and plantation settlements. Furthermore, CPF is reserved for developments other than forestry and can be converted to non-forestry management areas. CPF is also used to produce forest products to benefit the community consumption, industry, and exports. The CPF area is in northeastern South Sumatra and has an area of 819.84 ha (Fig. 9.2). CPF rain is growing increasingly popular in Indonesia as the country's population grows. Land is necessary for both shelter and
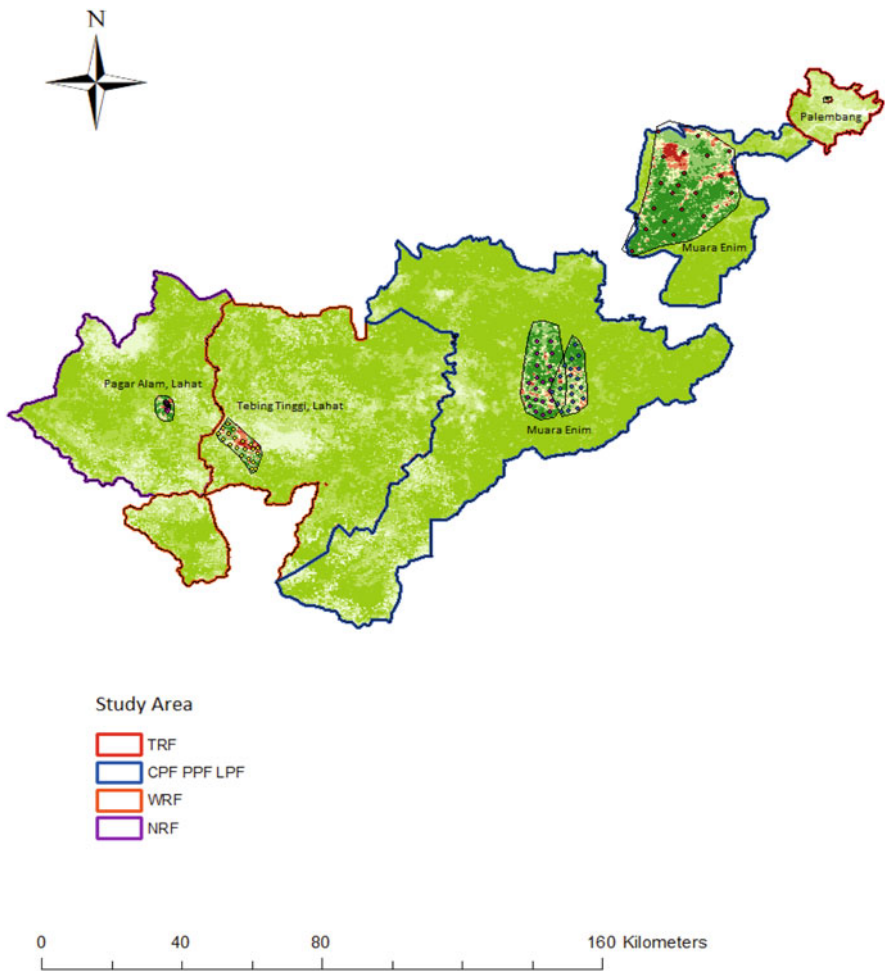
Fig. 9.2 Administrative boundaries of the locations of classified forests and reference points in each type of forest in South Sumatra (CPF, PPF, LPF, TRF, WRF, and NRF) to be carried out

increasing production of forest products. CPF forest types are most numerous in the Indonesian provinces of Sumatra, Kalimantan, and Sulawesi.

9.2.3   Permanent Production Forest (PPF)

It refers to forest that can be exploited through selective logging or clear-cutting. PPF areas are fully monitored by the government and the private sector that manages them and are used by the surrounding community as a source of employment. In permanent production forests, the cutting limit of trees with diameters of 50 cm is set by the forestry regulation. Forest products and commodities were rated second in terms of foreign exchange profits after oil and gas. The PPF areas are in South Sumatra, covering 172.75 ha (Fig. 9.2).

9.2.4   Limited Production Forest (LPF)

It is allocated to produce wood on a small scale. The LPF areas are in mountainous areas with steep slopes that do not allow large-scale timber production.

The LPF areas are fully monitored by the government and the private sector and provide employment to the surrounding communities. A limited production forest is designed for soil erosion mitigation as well as wood production. The LPF areas are also located in South Sumatra, covering 312.33 ha.

9.2.5   Tourism Recreation Forest (TRF)

The areas are designated for tourism and maintained for recreation research; education and cultural activities are also encouraged in TRF regions. Forest tourism is the most effective strategy to boost local revenue. Furthermore, tourist forest management can assist in offsetting the expenses of sustainable wood production while also promoting biodiversity conservation. Furthermore, there is a tourism forest in the heart of the city, which encourages the formation of healthy and pure air. TRF areas are in the central region of Palembang city with an area of 40 ha (Fig. 9.2).

9.2.6   Wildlife Reserve Forest (WRF)

It is the natural reserve zone with the primary function of a preservation area to ensure the diversity of ecosystems. As the rate of deforestation rises, it appears difficult to achieve zero deforestation. However, conservation of animals and

ecosystems, as well as reduction of greenhouse gas emissions, is still required. The WRF presents limited forest functions for wild animals and other natural ecosystems. The WRF is located in Lahat, with an area of 989 ha (Fig. 9.2).

9.2.7 Nature Reserve Forest (NRF)

It is administered by the government and has the function of protecting the forest, regulating water systems, preventing flooding, controlling soil erosion, preventing seawater intrusion, and maintaining soil fertility. The NRF is located in Empat Lawang, with an area of 305 ha (Fig. 9.2).

9.3 Phenological Properties

9.3.1 NDVI

Phenological properties were analyzed for the six different forest types. Among the vegetation indices, NDVI is an index that describes the greenness of a plant according to a combination of the red band and near-infrared (NIR) bands and can be expressed as follows (Rouse et al. 1973):

$$NDVI = \frac{NIR - Red}{NIR + Red} \tag{9.1}$$

Vegetation, as indicated by the NDVI, depends on solar radiation. Absorbed photosynthetically active radiation (fAPAR) is the fraction of photosynthetically active radiation (PAR) absorbed by vegetation over the growing season (Ochi and Shibasaki 1999a, b). PAR is assimilated during the process of photosynthesis in plants, which requires sunlight, and only half of the light is intercepted. The main factor in determining vegetation surface productivity is how much solar radiation is intercepted by biomass. NDVI and fAPAR have been shown to present a strong relationship in theoretical and experimental analyses (Myneni and Williams 1994; Hooda and Dye 1996; Inoue et al. 2008; Dadhwal et al. 2012) and can be used as spatial determinants of the variation in land cover. This formula is applied in Asian countries to estimate NPP-based agricultural production and is used to calculate the fAPAR for the six types of forests. fAPAR is often represented using a nonlinear or linear function of a vegetation index within satellite-based production efficiency models (Ruimy et al. 1996; Running et al. 2004).

The NDVI is the most commonly used remote sensing index and is considered a surrogate measure for primary production (Box et al. 1989). Many studies have indicated the positive relationship between NDVI and annual aboveground NPP for different geographical areas and ecosystems (Goward et al. 1985; Box et al. 1989;

Burke et al. 1991; Hobbs 1995; Paruelo et al. 1997). Such data-based approaches to remote sensing have provided useful insight into the dynamics of short-term vegetation, including changes in NPP and GPP (Tucker et al. 1981; Tucker and Sellers 1986; Fung et al. 1987). We acquired two sets of image data in each month (16 days intervals) from MOD13Q1 to present the solar radiation, and these data were used to calculate PAR. fAPAR and PAR can be expressed as follows:

$$fAPAR = -0.08 + 1.075 NDVI \tag{9.2}$$

$$PAR = 0.5 * \text{Incoming Solar Radiation} \tag{9.3}$$

Equation (9.2) is commonly used to measure the NPP, especially in forest areas in Asian countries, as first introduced by Ochi and Shibasaki (1999a, b) at the 20th Asian Conference on Remote Sensing. Other NPP researchers in Indonesia (Ochi et al. 2000; As-syakur et al. 2011; Supeni 2006, Setyono et al. 2020) and India (Mariappan 2010) then widely used this equation, and this method is presented in a book entitled Stability of Tropical Rainforest Margins: Linking Ecological, Economic, and Social Constraints of Land Use and Conservation (Tscharntke et al. 2007). PAR absorption by the plant canopy is an instantaneous process that changes during the day and periodically throughout the year. To determine exactly how much light is absorbed by a plant canopy over time, it appears required to continually measure instantaneous fAPAR. Many satellite sensors do not obtain information continuously over the same place; measurements from the same locations are taken every few (or more) days by the satellite.

The average daily fAPAR value may be estimated from a single instantaneous measurement by determining the systematic fluctuation of instantaneous fAPAR throughout the day for a certain canopy. A daily integration (sum) of the PAR incident at the canopy's top may be combined with an instantaneous fAPAR measurement to obtain an estimate of the amount of PAR absorbed (APAR) by the canopy on a daily basis. An estimate of the amount of PAR absorbed (APAR) by the canopy on a daily basis may be obtained by combining a daily integration (sum) of the PAR incident at the top of the canopy with a measurement of instantaneous fAPAR.

9.3.2   GPP

GPP is the amount of carbon converted during photosynthesis and is used to measure the global carbon cycle. Using remote sensing MODIS MOD13Q1, GPP is referred to as the light use efficiency (LUE) for estimating the changes in carbon between vegetation and the atmosphere in an ecosystem. Photosynthetic assimilation of vegetation is represented in all light use efficiency models as a function of the quantity of photosynthetically active radiation absorbed by plants (aPAR) (Monteith

1972; Running et al. 2000). All environmental and biophysical restrictions on photo energy conversion of plant biomass are summed up in the term light use efficiency in these models (LUE). GPP is defined as follows:

$$GPP = LUE * aPAR \qquad (9.4)$$

$$GPP = faPAR * PAR \qquad (9.5)$$

where faPAR is the percentage of photosynthetically active radiation absorbed, which requires little auxiliary data, these models are based on remote sensing products and meteorological fields (Hilker et al. 2008; McCallum et al. 2009). faPAR and incident PAR are calculated using various methods and might differ significantly (McCallum et al. 2010). The following formula would be used to calculate GPP:

$$GPP = LUE * fAPAR * PAR \qquad (9.6)$$

LUE is defined as the amount of carbon produced by absorbed photosynthetically active radiation (APAR) and GPP and is directly related to APAR through the LUE (Running et al. 2004; Tian et al. 2010; Obi Reddy and Singh 2018). The LUE approach links GPP to a linear combination of remotely sensed variables, such as NDVI and PAR. LUE influences how much vegetative biomass accumulates. The LUE model is seen to have the best chance of properly addressing the spatial and temporal GPP dynamics. LUE is a direct variable that correlates biological production with the amount of PAR absorbed by the plant canopy (APAR) (Xiao et al. 2005; Zhang et al. 2009a, b, 2017). LUE models refer to carbon exchange as a function of the amount of light energy absorbed by vegetation and the efficiency of light energy used to transform carbon.

These methods are one of the most frequently used for estimating GPP (Wu et al. 2009; Sjöström et al. 2011; Croft et al. 2015; Joiner et al. 2018). Vi's are applied to determine the leaf and canopy biophysical characteristics for the estimation of LUE and fAPAR (Xiao et al. 2004; Gitelson et al. 2005; Inoue et al. 2008; Wu et al. 2009). GPP estimations from LUE, fAPAR, and PAR may be affected by the uncertainty of the VIs or fAPAR relationship (Running et al. 2000; Gitelson et al. 2006). As a tropical country, Indonesia is covered by evergreen broadleaf forest (EBF) with tropical rainforest, tropical monsoon and tropical savanna climates. The monthly LUE of EBF is 1.82 ± 0.26 g C m^{-2} MJ^{-1} APAR on average (Wei et al. 2017).

9.3.3 NPP

The GPP calculation is basically the first step. Net primary production (NPP) is the output of stand growth models that are used to estimate forest productivity or calculate carbon balances. Global processes for NPP models based on the NDVI

have been developed for regional forest productivity analysis (Potter et al. 1993; Prince 1991; Ruimy et al. 1994; Running and Hunt 1993; Running et al. 1994). NPP is measured based on the NDVI values in different types of forests at different vegetation growth levels. The factor influencing NPP is solar radiation (Garbulsky et al. 2010; Zhao and Running 2010). The NPP/GPP ratio is relatively stable and independent of ecosystem type (Gifford 1995; Landsberg and Waring 1997; Dewar et al. 1998). NPP is determined using NDVI as a primary input, with the area and solar radiation as supporting inputs. A better understanding of NPP can help to develop and maintain plans for addressing human needs and managing climate change (Smith et al. 2012). The biological processes contributing to GPP are the sum of respiration and NPP. NPP can be expressed as follows:

$$NPP = GPP - Respiration \qquad (9.7)$$

In this regard, NPP is the difference between total vegetation photosynthesis and the total respiration of vegetation in an ecosystem where respiration is used for maintenance and growth. The findings of this research assume that the NPP/GPP ratio is consistent regardless of ecosystem type (Zhang et al. 2009a, b). Stand growth and maintenance respiration are both included in respiration. The uncertainty involved with respiration estimation makes using Eq. (9.7) as a foundation for calculating NPP in the field problematic. NPP was obtained from the percentage of the GPP lost through respiration, which was approximately 70% of the forest (Ruimy et al. 1996; Gunin et al. 1999; Schwarz et al. 2004; Luyssaert et al. 2007). NPP can be expressed in terms of GPP as follows:

$$NPP = 0.3 * GPP * Forest\ Area \qquad (9.8)$$

Through system dynamic modeling, forecasted forest resilience can be predicted as early as possible by increasing vegetation coverage or expanding the area in accordance with the expected productivity simulations. The simulation consists of designing a model of a real system and conducting experiments to understand the behavior of the system and/or evaluate various strategies for the operating system (Pedgen et al. 1995). Furthermore, simulation refers to the modeling process to mimic the response of an event in an actual system that takes place over time (Schriber 1987). As a consequence of increased market demands, the possible impact of climate change (IPCC 2007), and the growing concern for environmental preservation, forest productivity has lately become more essential (IPCC 2007). The Food and Agriculture Organization of the United Nations (FAO) published a report in 2016, as a result, an accurate estimate of forest productivity appears to be essential in determining long-term forest management decisions.

Some models have predicted that NPP respiration occurs faster under global warming during the overall photosynthesis process (Ryan 1991; Ciais et al. 2013; Huntingford et al. 2017). NPP may change over time due to changes in the area over time. The rate of the change in organic matter can be modeled by the explicit

differential function between forest area and NPP. The rate of change can be expressed as follows:

$$\frac{(\mathrm{d}Q)}{\mathrm{d}t} = A\,\frac{\mathrm{d}P}{\mathrm{d}t} + \frac{\mathrm{d}A}{\mathrm{d}t}\,(\mathrm{NPP}) \tag{9.9}$$

Q is the total organic matter produced in the forest, which is related to productivity; A is the forest area; and NPP represents productivity. This equation is used to predict the productivity for the following year based on this and the preceding year's productivity. The forest structure has a considerable impact on productivity and biomass. This is an essential factor to consider when estimating current carbon budgets or calculating climate change scenarios for the different amount of forest in south Sumatra. To identify forest areas, the minimum and maximum NDVI values were identified. The productivity level can be further subdivided into five levels based on the NDVI, which was proposed in line with Indonesian forest resilience planning (Fig. 9.3).

9.3.4   High Forest Productivity

Areas that exhibit a very high abundance of vegetation and potential for high productivity are referred to as showing high forest productivity (V1). V1 areas are overgrown with high density trees, so the function of this type of forest supports the ecosystem of the surrounding living organisms. These forest areas can support land use indefinitely and provide benefits to forest functioning.

9.3.5   Moderate Forest Productivity

Forest areas with limited vegetation and less productivity and a lower forest density than V1 are referred to as showing moderate forest productivity (V2). These forest areas are not pristine; however, the area presents the potential to exhibit high productivity.

9.3.6   Marginal Forest Productivity

In this type of forest productivity classification, forest areas show limitations in the aggregate and can be referred to as showing marginal forest productivity (V3). This type of forest area presents a lower forest density than V2.
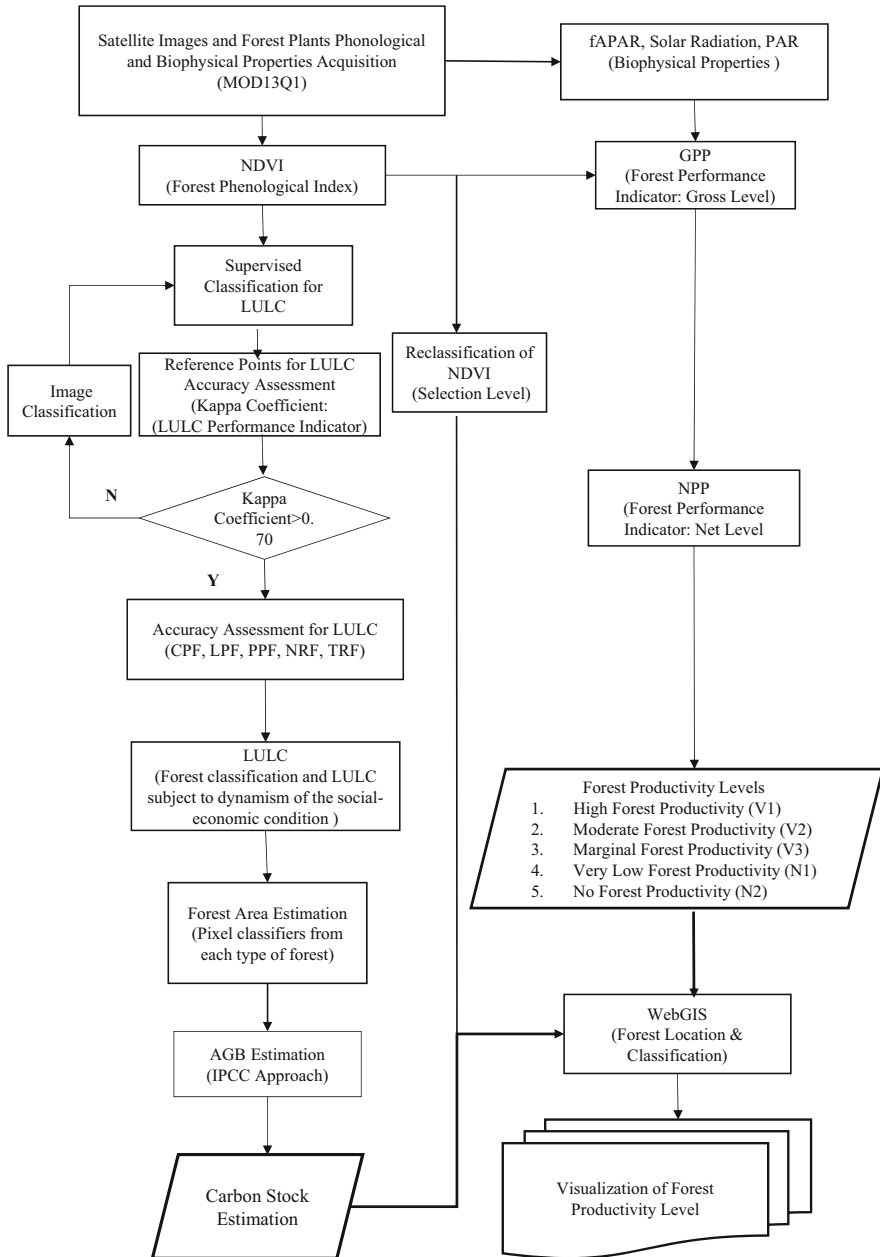
Fig. 9.3 Research flowchart for forest productivity assessment and carbon stock estimation

9.3.7   Very Low Forest Productivity

In the type of forest areas referred to as showing very low forest productivity (N1), the vegetated area is very limited, and productivity is lacking. The functions of these forests are poor, and the changes lead to their transformation into non-forest land (grass, small trees, and garden land). These forest areas are not expected to be able to support an increase in productivity.

9.3.8   No Forest Productivity

In this classification, the land is not forested. The land includes non-vegetated land, rocky land, bare soil, and almost no canopy cover and can be referred to as showing an absence of forest productivity (N2). This land requires further development for planting if possible.

9.3.9   WebGIS Application

In this research, MODIS MOD13Q1 satellite datasets were obtained to perform the analysis of phenological indices. The datasets were mapped using forest inventory classes based on the NDVI using 20 random points in each type of forest determined from Google Earth Pro® and MODIS raster datasets. In the 6 types of forest, 120 sampling points were selected to observe the changes in the vegetation phenology from 2015 to 2018. The maximum NDVI indicates dense vegetation, and the minimum represents limited vegetation or an absence of vegetation. The pixel values corresponding to the NDVI were calculated and broadly grouped into five classes. In the classification, we distinguished the highly vegetated, moderately vegetated, marginally vegetated, very low vegetated, and non-vegetated categories. The GIS analysis and WebGIS application were performed using ArcGIS®10.6 (ESRI Environment Science and Research Institute, California, USA) (Fig. 9.3).

The web application was designed to respond to user requests through a client application (web browser), and the results can be returned to the user. From the results, users can directly choose a forest location. The development of GIS-based web applications was carried out based on the research site. This web application references the database and reference information for each forest type to monitor forest productivity. The productivity data (NPP) were obtained using a client-to-server communication system, as data were provided through a web protocol such as hypertext transfer protocol (HTTP) using hypertext preprocessor (PHP). The web application could respond to every request made by the users through a client application (web browser). In the web applications, the pages that appear on the web browser screen were designed to be dynamic. This graphical interface was run

through ArcGIS web services to visualize the locations of the forests for monitoring productivity (Fig. 9.3).

9.4 System Dynamics Modeling for Simulation

System dynamics (SD) is a technique for assessing the interconnectivity, complexity, and change of a system through time. When utilizing system dynamics, a modeler must consider the system to be modeled as a collection of interacting feedback loops, stocks, and relevant flows that influence them. Long-term strategy models often employ system dynamics, which imply a high degree of object aggregation. Expressions, function calls, statements, classes, interfaces, inheritance, and polymorphism are not necessary in system dynamics, as they are in software development. When changes in the stock impact the inflow or outflow of the stock, a feedback loop is established. There are two sorts of feedback loops: the first is balancing feedback loops, which seeks to keep the stock at a specific level or range. Second, when a system element has the potential to replicate itself or expand at a constant percentage of its original size, it amplifies the feedback loop.

In this research, a system dynamics model was developed for productivity analysis (Fig. 9.4), in which NDVI, area and solar radiation were used as inputs to the simulation to quantitatively investigate indicators such as NDVI, forest areas, and trends in solar radiation. Causal loops were generated to identify related values using Powersim Studio 10® (Powersim Software AS, Norway). The causal loop for the problem of productivity was included in a positive causal loop (Richardson 1997), where two nodes changed in the same direction and presented exponential values. NPP was affected by NDVI because when NDVI increased, the overall value increased. Regarding the area, the changes in productivity were dependent on the extent of forest or loss of forest. To increase productivity, a scenario was developed by changing the NDVI and areas. Logically, the productivity increases if the NDVI increases and when the forest area increases. However, it is necessary to estimate the quantified value over a period of time using the system dynamic approach. The results were optimized using two input scenarios: Scenario I: NDVI input and Scenario II: forest area input (Fig. 9.5). This system can be used to calculate the values for six types of forest that exist in the study areas. In both scenarios, the solar radiation trend was considered to increase and decrease.

9.5 Land Use Land Cover (LULC) Analysis

The LULC change in a forest is important to help track changes in aboveground biomass (AGB) to calculate carbon estimations using the IPCC approach. Changes in land use and management affect the amount of carbon in plant biomass and soils. The impacts of future land use on terrestrial biosphere–atmosphere exchanges have
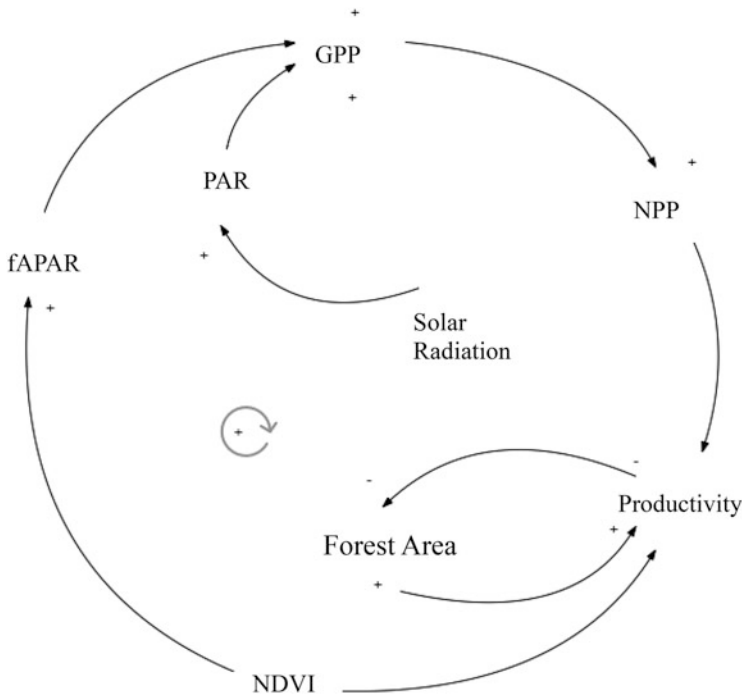
Fig. 9.4 The causal loop for productivity analysis in system dynamics modeling

the potential to modify atmospheric CO_2 concentrations on this timescale (IPCC 2018). Forest carbon accounting is required to establish the extent of the accounting area, both spatially and temporally, offering details for land use planning with low carbon impacts (Watson 2009). The MOD13Q1 satellite products were visually interpreted to prepare the change detection maps using a knowledge-based supervised and maximum likelihood classification (Fig. 9.3). The classification algorithms were divided into four classes: urban, vegetation, forest, and water bodies in the GIS environment. Each of the classes was chosen by pixels with spectral signatures and ensured for the land cover map (Fig. 9.12a–d).

The accuracy assessment was carried out using reference data points from the base map used to validate the LULC. An uncertainty matrix (or error matrix) was used as the quantitative method for characterizing the accuracy in the classification of images. A stratified random sampling approach was used to select 400 points on the map with 100 points from each class. The accuracy assessment was performed using the producer's accuracy (PA), user's accuracy (UA) and overall accuracy (OA) to consider the closest results to be accepted as true (Congalton 1991; Thomlinson et al. 1999). PA is the accuracy of the map from the map maker's point of view. PA considers how many actual features on the ground are correctly observed on the classified map. UA is the accuracy from a map user's point of view,
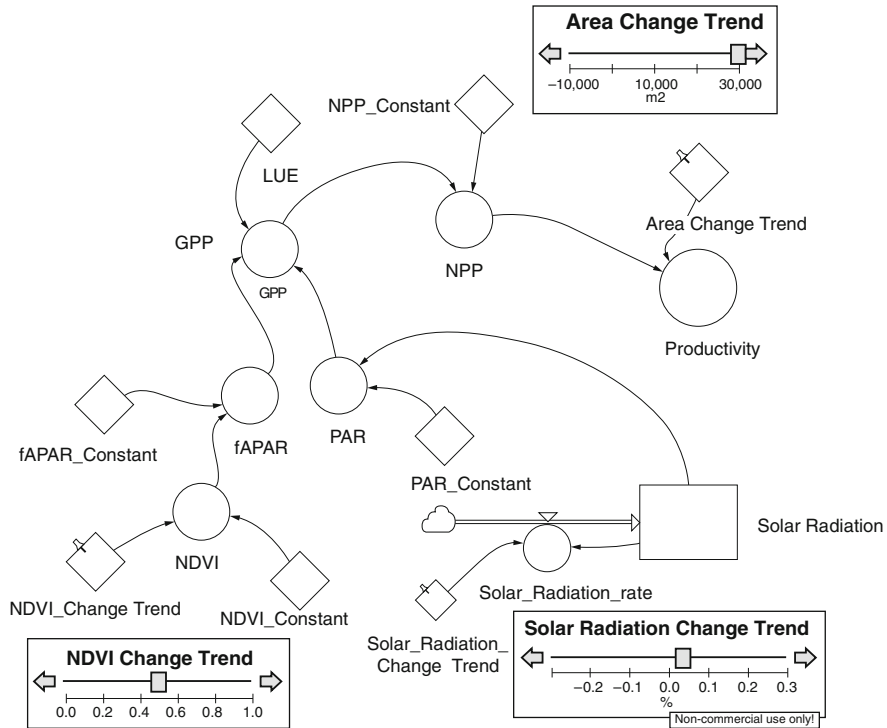
Fig. 9.5 System dynamics simulation process for each classified forest type with three variable parameters: NDVI, forest area, and solar radiation

not the map's maker. The accuracy of the user effectively informs how much of the ground that is actually covered by each class on the map (reliability). OA is generally measured as a percentage, with 100% accuracy being a flawless measurement in which all reference sources have been correctly categorized. OA basically informs what proportion was correctly mapped out of all the reference locations. In this regard, Cohen's Kappa is used to compensate for the possibility of some variance. Kappa essentially tests how well the classification worked compared to simply allocating random values. To assess the accuracy of classification, the kappa coefficient was calculated from a statistical test. The Kappa coefficient is computed as follows:

$$K = \frac{N\sum_{i=1}^{n} m_{ii} - \sum_{i=1}^{n}(A_i B_i)}{N^2 - \sum_{i=1}^{n}(A_i B_i)} \tag{9.10}$$

A Kappa of 1 indicates complete agreement. With a Kappa of -1, there is less agreement than you would anticipate by chance (very rare). Ordinal or nominal categories can be used. Where K is the kappa coefficient; i is the class number; N is

the total number of classified values compared to true values; m_{ii} is the number of values belonging to the true class i that have also been classified as class i; B_i is the total number of predicted values belonging to class i; and A_i is the total number of true values belonging to class i.

By definition, kappa values are considered a weak agreement if they are less than 0.20; fair agreement ranges between 0.20 and 0.40; moderate agreement ranges from 0.40 to 0.60; good agreement ranges from 0.60 to 0.80, and very good agreement ranges from 0.80 to 1.00.

9.6 Carbon Estimation

The IPCC approach was used to estimate the carbon stock for various forest classes with a hierarchy of tiers (IPCC 2006). The IPCC has established a three-tier carbon accounting system based on the available data and capacity. Tier 1: No new data have been collected. Default emission factor values from the IPCC database are used. Activity data are usually a rough estimate and are considered "the global defaults." Tier 2: No new data have been collected. Defined emission factors for each country are used. High-resolution activity data are used, and the "local defaults" are used for specific regions and land use categories. Finally, Tier 3: Models, inventory management systems, and high-resolution data customized to reflect national features are used including national and subnational inventories of carbon and repeated measurements in areas with land use changes. The models are tested by field measurements and optimized. The assurance is very high, but the method is expensive, and a high degree of technical competence is needed. IPCC refereed data were used under the available conditions using Tier 1. The area belonging to each forest class in South Sumatra was referred for the AGB, and carbon fraction values were used to estimate the carbon stock referring to the global defaults from the IPCC. The emission factors from deforestation were calculated based on the AGB and an estimated carbon density of 47%. The carbon value in terms of forest area and AGB can be expressed as follows:

$$\text{Carbon}_{\text{tC/ha}} = \text{Forest area} * 47\% * \text{AGB} \tag{9.11}$$

At the global level, 19% of the carbon in the Earth's biosphere is stored in plants, and 81% is stored in the soil. In all forests, tropical, temperate and boreal together, approximately 31% of the carbon is stored in the biomass and 69% is stored in the soil. In tropical forests, approximately 50% of the carbon is stored in the biomass and 50% is stored in the soil. Carbon accounts for approximately 47% of all biomasses of living vegetation, both woody and herbaceous, above the soil, including stems, stumps, branches, bark, seeds, and foliage (IPCC 2007). Several studies have reported on results for woodland vegetation (Abetu and Bekele 2019), tropical lowland dipterocarp forestland, arid and semiarid forestland (Bastin et al. 2017),

mangrove species (Rodrigues et al. 2015), Bornean logged-over dipterocarp forests (Mbaabu 2012), tropical regions in Latin America (Saatchi et al. 2011), the Miombo woodland, and other parts of the tropical rainforest mesocosm in Australia (Lin et al. 1998).

9.7 Results

9.7.1 Forest Phenological Properties

The NDVI maps show the result of the variability and explain the moving average of pixel values from 2015 to 2018 (Fig. 9.6a–d). After NDVI was determined, fAPAR and GPP were obtained. GPP provided a projection of the vegetation status and was strongly influenced by NDVI. The correlation between NDVI and GPP presented a strong association, indicating that increases in NDVI mean that the GPP value also increases (Fig. 9.7).

The NDVI maps show the result of the variability and explain the moving average of pixel values from 2015 to 2018 (Fig. 9.6a–d). After NDVI was determined, fAPAR and GPP were obtained. GPP provided a projection of the vegetation status and was strongly influenced by NDVI. The correlation between NDVI and GPP presented a strong association, indicating that increases in NDVI mean that the GPP value also increases (Fig. 9.7). The NDVI is an activity of photosynthesis (Myneni et al. 1995) and is related to the composition of evergreen and deciduous vegetation (DeFries et al. 1995). In our research, TRF is a type of forest that presents less vegetation than the other forest types (Fig. 9.8). The length of the NDVI growing season was related to phenological changes (Tucker 1979) and NPP changes (Fig. 9.9). Thus, annual changes in NDVI presented recent changes to refer the level of productivity for different forest classes.

9.7.2 Forest Productivity Analysis

In the assessment process, CPF exhibited an increasing trend (0.20%) for all levels of forest productivity. The changes in the different forest productivity classes in PPF increased as follows: high forest productivity (0.22%) and moderate forest productivity (0.20%); decreased marginal forest productivity and very low forest productivity (0.19%); and no forest productivity (0.18%). The forest productivity in the LPF was predicted, and all forest productivity levels showed a decreasing trend. The following results were obtained for the different productivity levels: decreasing high forest productivity (0.22%); moderate forest productivity (0.25%); marginal forest productivity (0.19%); very low forest productivity (0.16%); and no forest productivity (0.18%). The productivity of TRF was predicted, and an increasing trend was observed: high forest productivity (0.20%); moderate forest productivity (0.21%);
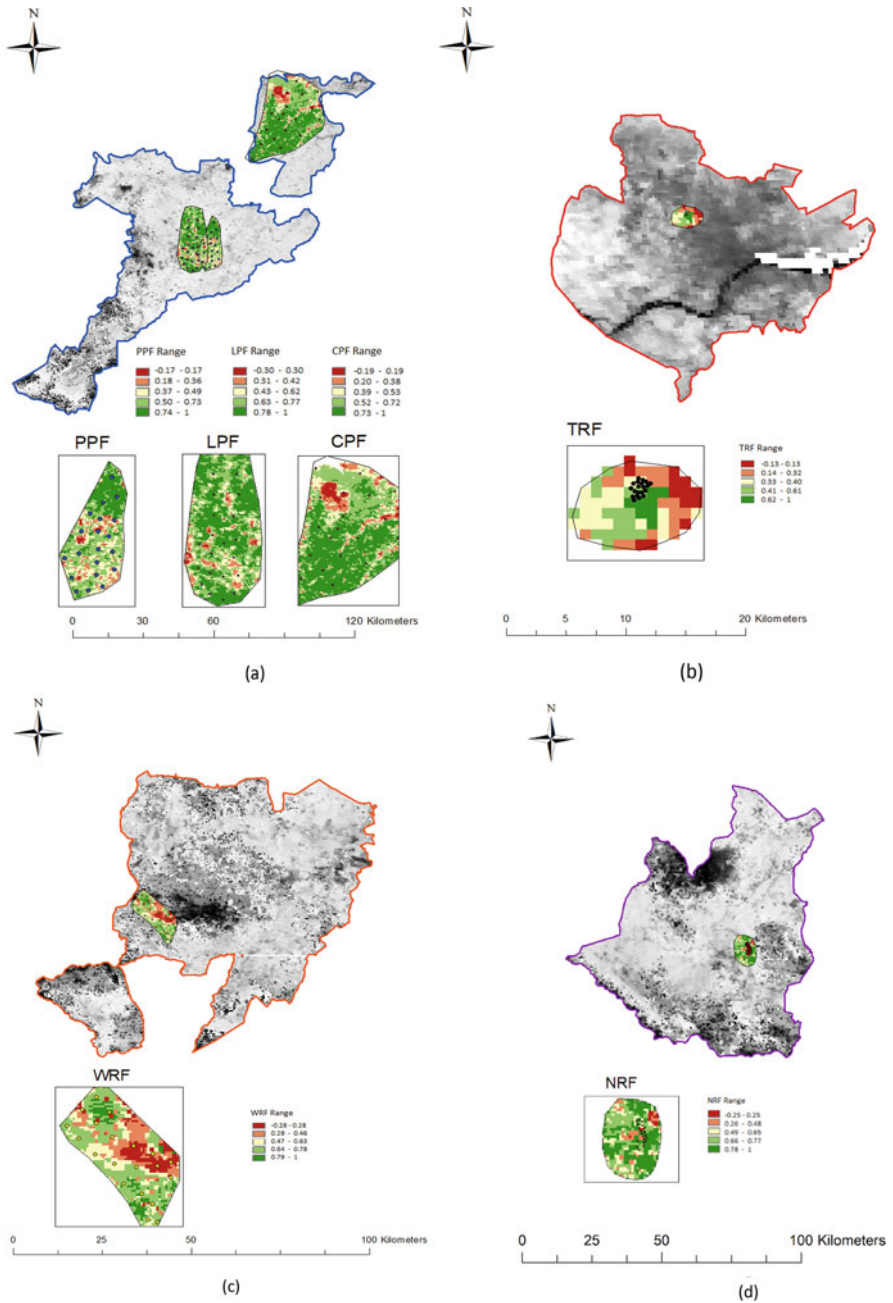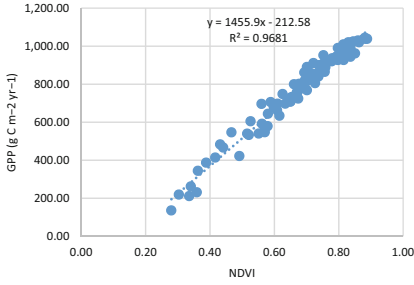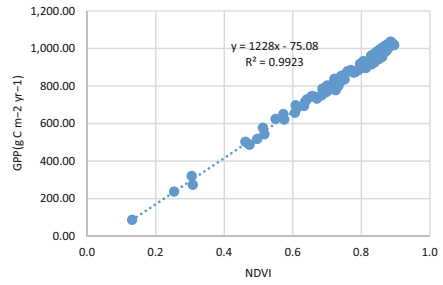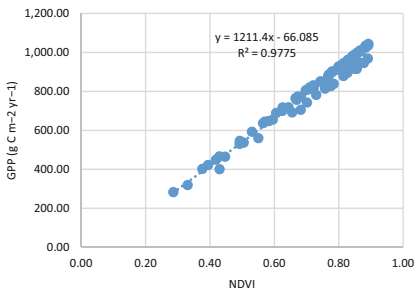
Fig. 9.6 NDVI distribution for (**a**) CPF, PPF, and LPF, (**b**) TRF, (**c**) WRF, and (**d**) NRF (moving average of pixel values from 2015 to 2018)
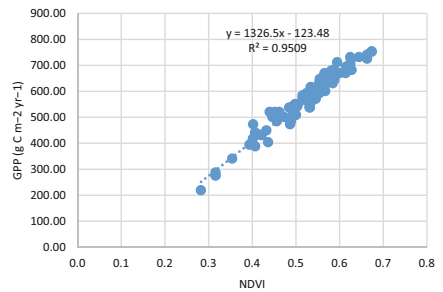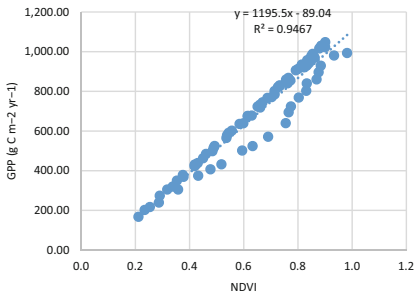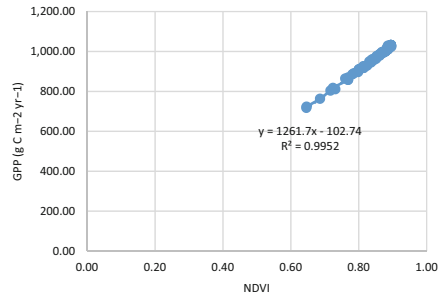
Fig. 9.7 Correlation between the NDVI and GPP (**a**) CPF, (**b**) PPF, (**c**) LPF, (**d**) TRF, (**e**) WRF, and (**f**) NR

marginal forest productivity and very low forest productivity (0.20%); and no forest productivity increased (0.19%). The productivity assessment of WRF showed a decreasing trend, with high and moderate forest productivity (0.20%), marginal forest productivity (0.21%), very low forest productivity (0.20%), and no forest
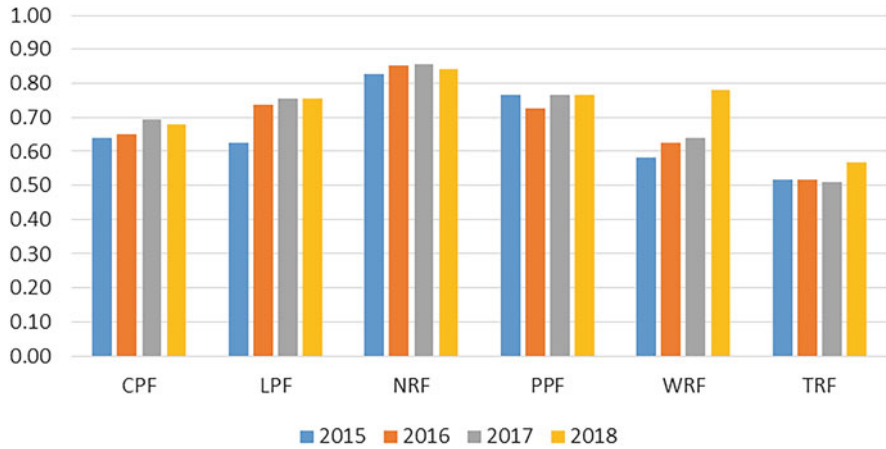
Fig. 9.8 Annual changes in NDVI for the different forest classifications from 2015 to 2018
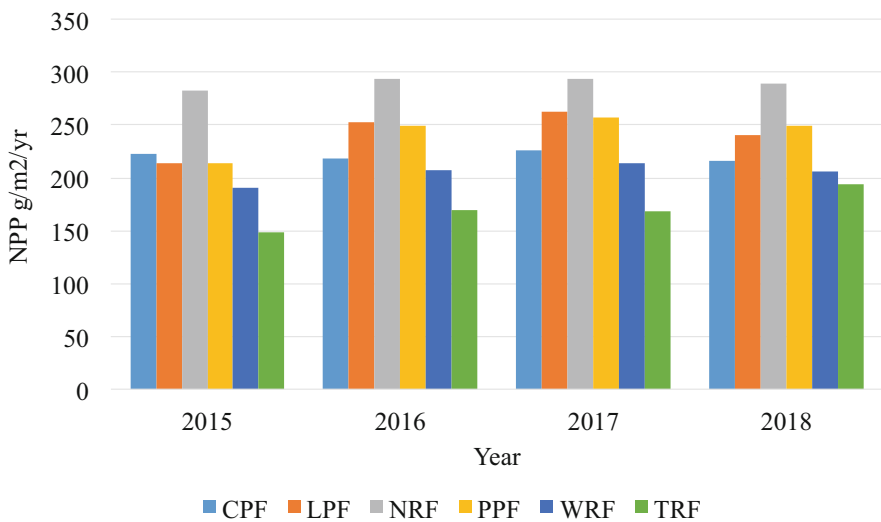
Fig. 9.9 Annual changes in NPP for the different forest classifications from 2015 to 2018

productivity (0.19%). NRF also experienced decreasing productivity: high forest productivity (0.27%); moderate forest productivity (0.35%); marginal forest productivity (0.29%); very low forest productivity (0.06%); and no forest productivity (0.03%) (Appendix).

9.7.3   GIS Application

GIS was used to add NDVI values to estimate GPP and NPP in each forest type. The results for the average NDVI for each type of forest indicated a different level of vegetation. Through inputting NDVI values and selecting forest types in GIS, estimation of GPP and NPP values can be shown. From the results of the NDVI range, we concluded that TRF presented the lowest vegetation cover compared to the other forest types, while the highest vegetation cover was observed in NRF. The result was visualized for the current estimation and did not indicate an increase or decrease in forest vegetation from the previous stage. For this reason, the system approach was used to estimate productivity under different scenarios.

9.7.4   Simulation Model for Scenario Assessment

The simulation model was developed to determine forest changes using vegetation phenological parameters. The scenario was divided into two phases: Scenario I involved a moving average of NDVI considering a solar radiation increase (SR+) or decrease (SR−). This model was valid if the basic structure and pattern were accurate. In Scenario I, the NDVI changed with increasing or decreasing solar radiation (Fig. 9.10). On the other hand, Scenario II was simulated based on the changes in forest area. Scenario II was calculated for the changes in area where an increasing or decreasing trend was associated with solar radiation changes (Fig. 9.11). According to the State of the World's Forest's 2018, the world forest areas decreased by 30.6% between 1990 and 2015. It is assumed that there was a
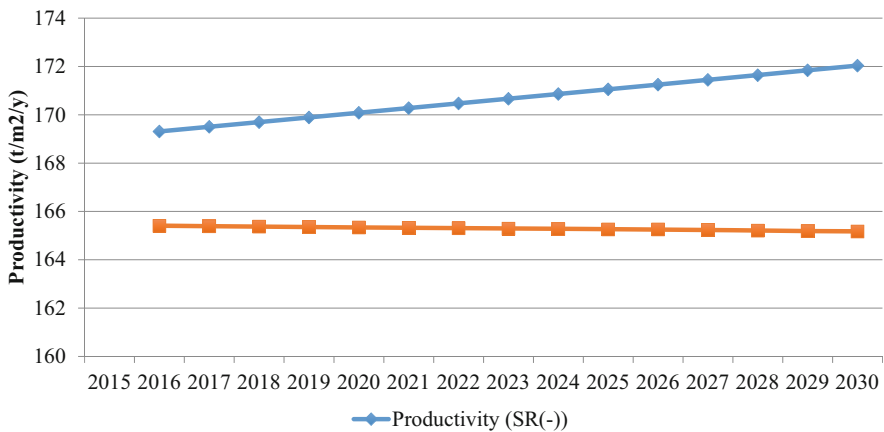

Fig. 9.10 Presence of productivity based on the NDVI with the changing trend of solar radiation

Fig. 9.11 Productivity assessment based on the changes in forest areas with the changing trend of solar radiation

decrease in the forest area of approximately 1.23% every year (FAO 2018). When the trend of solar radiation was positive, the productivity exhibited an increasing trend every year; however, when solar radiation decreased overall, the productivity also showed a decreasing trend every year.

9.7.5 Land Use Change Analysis for Forest Class

The LULC map was developed to identify only forest classes consisting of all types of forests for carbon estimation (Fig. 9.12a–d). An accuracy assessment for LULC was conducted to ensure the performance according to the PA, UA, and OA. The average accuracy was more than 80% for the 6 types of forests. The kappa coefficient was greater than 0.80 (Table 9.1). The interpretation of Kappa showed very good agreement for all types of forests. The results of the carbon estimation were obtained using the IPCC standard. In the LULC analysis, PPF was found to be 135.23 ha, LPF 253.02 ha, CPF 599.99 ha, TRF 12.81 ha, WRF 661.11 ha, and NRF 254.36 ha with tropical rainforest or tropical dry forest covered by plantation or natural vegetation (Table 9.2).

9.7.6 Carbon Stock Estimation Based on the Biomass

The IPCC standard was used for carbon stock estimations according to the area of the forest based on the AGB. Tropical rainforest and tropical dry forest were determined based on the types of vegetation formation (Faber-langendoen et al.
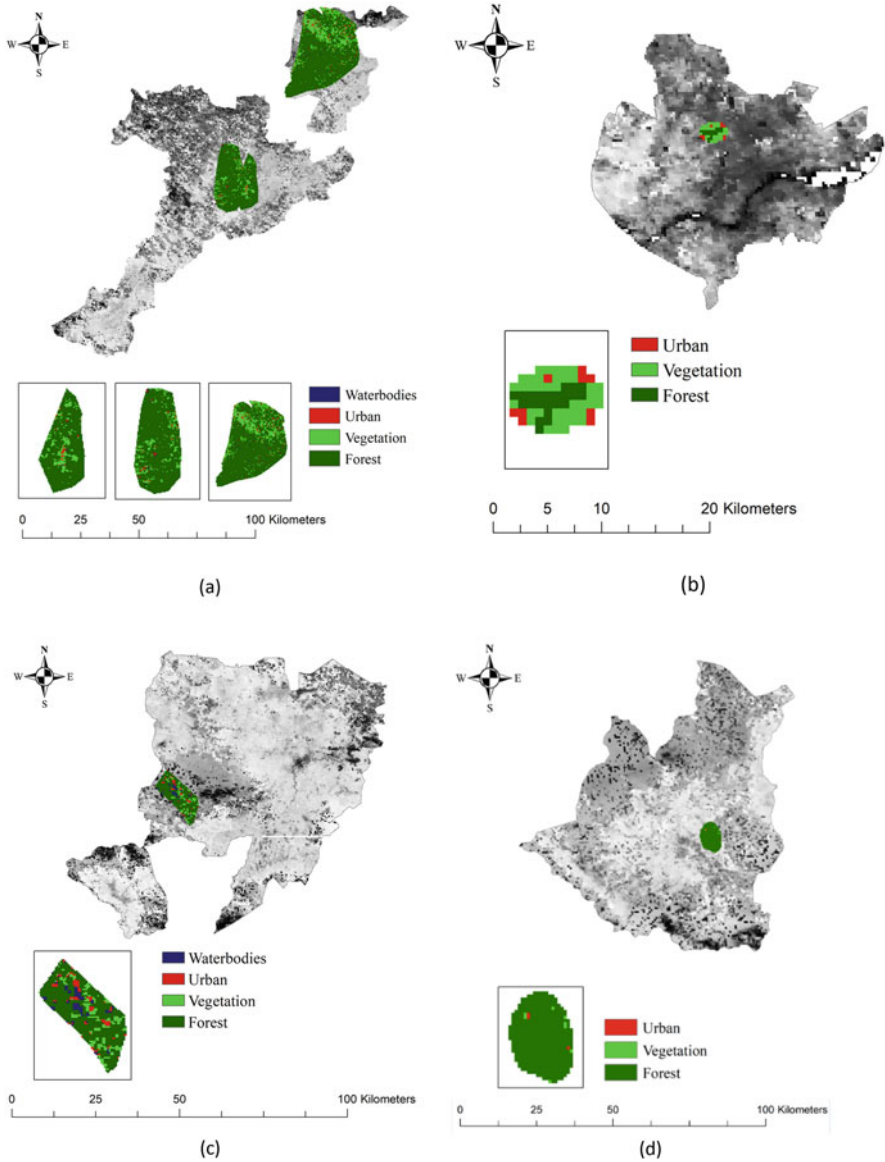
Fig. 9.12 LULC for the forest class (**a**) CPF, PPF, and LPF; (**b**) TRF; (**c**) WRF; and (**d**) NRF

2016). Planting forests and natural forests were determined based on their respective forest types. AGB was taken as 130 t/ha for tropical dry forest, while it was naturally referenced for WRF. TRF, CPF, PPF, and LPF had an average AGB of 150 t/ha for tropical rainforests and plantations (Table 9.2, IPCC 2006). In the case of NRF, the

Table 9.1 Accuracy assessments for the LULC for the six types of forests

Accuracy assessment	Class	CPF (%)	PPF (%)	LPF (%)	TRF (%)	WRF (%)	NRF (%)
Producer's accuracy	Urban	89	90	99	88	100	89
	Vegetation	88	90	99	88	94	99
	Forest	88	87	81	90	79	78
	Water body	88	100	100	100	100	100
User's accuracy	Urban	89	90	88	88	100	77
	Vegetation	89	90	88	89	99	84
	Forest	88	87	99	89	94	100
	Water body	88	87	100	100	77	100
Overall accuracy		89	89	94	92	93	90
Kappa		0.86	0.86	0.93	0.90	0.91	0.88

Table 9.2 Carbon stock estimation based on the IPCC standard for the six types of forest

Forest type	AGB type (t/ha)	AGB (ha) (t/ha)	LULC on forest (ha) 2019	Carbon fraction	Carbon tC/ha
WRF	Tropical dry forest (natural)	130	661.11	0.47	40,393.82
TRF	Tropical rainforest (plantation)	150	12.81	0.47	903.11
CPF	Tropical rainforest (plantation)	150	599.99	0.47	42,299.30
PPF	Tropical rainforest (plantation)	150	135.23	0.47	9533.72
LPF	Tropical rainforest (plantation)	150	253.02	0.47	17,837.91
NRF	Tropical rainforest (natural)	300	254.36	0.47	35,864.76

AGB was 300 t/ha with a natural distribution. WRF and CPF had larger forest areas than the others and had an average carbon stock of 40,000 tC/ha. NRF had a carbon stock of 35,000 tC/ha, and LPF and PPF had average carbon stocks of 17,000 and 9000 tC/ha, respectively. TRF had a very small carbon stock of 900 tC/ha (Table 9.2).

9.8 Discussion

This study describes how to composite MODIS data to track vegetation variability and productivity considering the classified resilience of a forest, and productivity is estimated using a system dynamics model, which can be used for future predictions. Mapping such productivity data provides insight into the ecosystem and can be used to establish sites as carbon resources in the environment (Ulsig et al. 2017). The results of this study also pointed to the need for more robust calculations of the solar

radiation effects on climate change in the GIS environment using a system dynamics approach. The MODIS-based models developed in this study can serve as a baseline to take advantage of satellite-based models of NDVI of the six types of forest. Therefore, the investigation of NDVI dynamics and its influencing factors is the foundation to ensure forest ecosystem health. Empirical relations between NPP and remotely sensed data have been extensively investigated (Cheng and Zhao 1990; Jiang et al. 1999; Zheng et al. 2003). The results of this study showed a strong statistical relationship between the NDVI and GPP, which were positively correlated (Huang et al. 2019; Cai et al. 2017; Ulsig et al. 2017) in the six types of forest.

Given the accuracy of these estimates, the developed system dynamics models successfully estimated the future GPP for different forest types. Moreover, the factors affecting the reflectance of this area should be studied more in the future, including the effect of the aboveground and belowground vegetation, forest age, disturbance, site quality, soil type, tree height, and canopy type. This study does not allow for the comparison of the strength of the relationship between other factors, such as forest age, disturbance, site quality, soil type, and ecosystem type, because regression techniques are sensitive to restricted variations. The challenge of the vegetation productivity level is to move toward a more accurate method for gathering vegetation data and reliably linking these observations to direct observation data in the field. Therefore, a system dynamics model was developed to understand the sensitivity and dynamic changes to predict productivity using two scenarios. First, Scenario I included a moving average of NDVI from 2015 to 2018 to show the productive changes when solar radiation presented either an increasing trend or decreasing trend. Second, Scenario II was used to describe the increasing or decreasing forest areas when solar radiation presented either increasing or decreasing trends. This satellite-based cost-effective approach would be very advantageous for countries with large forest areas for quick assessment of forest productivity.

According to a vegetation index, the forest can be recognized as healthy or unhealthy, and forest productivity levels can be estimated. This classification of forests based on the average range of vegetation yields refers to a forest index of 1–5 following the range of forests established by the Indonesian government. Thus, the government requires long-term forest policy planning when there are changes in forest functions, forest fires, indiscriminate logging or massive exploitation of forests without planning for industrial development, settlement, or encroachment. To achieve the carbon target indicated by the IPCC, we propose to increase the forest area. Furthermore, GIS can be utilized to refer to the forest NDVI and projected NPP levels for forest productivity over a long period of time. From this point of view, other vegetation phenology research needs to extend further to understand the effects of LULC changes in forest ecosystems in the six forest classifications. A more detailed study in this line can lead to improved environmental management of forests in the future.

9.9   Conclusion

In this research, the NDVI was used to investigate vegetation responses to estimate productivity in South Sumatra, Indonesia. Vegetation phenology-based methods were employed to assess productivity according to the categories defined by forest classes. The results indicated that the customized NDVI approach achieved superior performance for determining the productivity level and that the government can use the analysis for the management of forests. The government can use WebGIS to quickly determine the value of productivity and performance indicator for different types of forests. Therefore, decisions about forest conditions can be made immediately. This application is based on a database of NPP calculations from 2015 to 2018. This application will allow sufficient input for further extension of NDVI, GPP, and NPP for monitoring forest productivity. The forest vegetation mapping and carbon assessment under different forest classifications can be further adapted. The system dynamics approach predicted that solar radiation is an important parameter for increasing productivity when the area does not change or when the area increases with the same value of solar radiation. The current status and optimum options for land resource use and management approaches could be based on the satellite remote sensing spatial scales to project the LULC changes from the forest zones of PPF, LPF, CPF and WRF, TRF, and NRF. Furthermore, information on the productivity of different types of forests provides justification for the protection and management of forests on different timescales.

Appendix (Table 9.3)

Table 9.3 Productivity (NPP) estimation for the six classified forests

Forest type (Total area, ha)	Vegetation level	2017		2018		(P) Productivity (g/m²) Change of productivity (2017–2018) (t/m²)	Change of area (m²) (2017–2018)	Productivity (t/m²) next year	Percentage of changing (%) (increase/decrease)
		Area (ha)	NPP range (t/m²)	Area (ha)	NPP range (t/m²)				
CPF (819.84)	No forest vegetation (N2)	87.13	−14 to 71.64	8.69	79.77–175.58	221 10.57	−871,291	10.34	0.20 (Increase)
	Very low forest vegetation (N1)	116.05	71.65–143.24	52.84	175.59–210.13		−1,160,447	10.26	0.20 (Increase)
	Marginal forest vegetation (V3)	190.32	143.25–203.61	88.93	210.14–236.83		−1,903,111	10.06	0.20 (Increase)
	Moderate forest vegetation (V2)	257.53	203.62–251.34	249.38	236.84–254.89		−2,575,051	9.88	0.20 (Increase)
	High forest vegetation (V1)	168.81	251.35–344.00	420	254.90–280.02		−1,687,680	10.12	0.20 (Increase)
PPF (172.75)	No forest vegetation (N2)	3.84	6.59–106.90	0	126.42–193.37	253.12 −7.51	−38,400	−7.57	0.18 (Decrease)
	Very low forest vegetation (N1)	7.86	106.91–181.82	3.97	193.38–216.89		−78,596	−7.63	0.19 (Decrease)
	Marginal forest vegetation (V3)	17.68	181.83–237.70	30.11	216.90–236.80		−176,770	−7.77	0.19 (Decrease)
	Moderate forest vegetation (V2)	50.22	237.71–273.25	67.46	236.81–254.89		−502,133	−8.25	0.20 (Decrease)
	High forest vegetation (V1)	93.15	273.26–330.39	71.21	254.90–280.23		−931,429	−8.87	0.22 (Decrease)
LPF (312.33)	No forest vegetation (N2)	9.3	−4.05 to 94.19	4.37	99.52–177.11	251.51 −74.34	−92,996	−74.41	0.18 (Decrease)
	Very low forest vegetation (N1)	18.51	94.20–169.24	1.85	177.12–215.54		−185,098	−74.49	0.16 (Decrease)
	Marginal forest	41.85	169.25–	35.1	215.55–		−418,465	−74.68	0.19

(continued)

Table 9.3 (continued)

	vegetation								
	vegetation (V3)		223.82	5	237.61				(Decrease)
	Moderate forest vegetation (V2)	86.83	223.83–263.39	129.81	237.62–255.40		−868,170	−75.04	0.25 (Decrease)
	High forest vegetation (V1)	155.84	263.40–343.90	141.15	255.41–281.03		−1,558,259	−75.59	0.22 (Decrease)
TRF (40)	No forest vegetation (N2)	3	−197.70 to 36.09	3.02	−107.96 to 32.23	181.13 25.15	20	25.15	0.19 (Increase)
	Very low forest vegetation (N1)	4.72	36.10–68.36	4.75	32.24–111.28		30	25.15	0.20 (Increase)
	Marginal forest vegetation (V3)	10.47	68.37–131.43	10.57	111.29–157.51		100	25.15	0.20 (Increase)
	Moderate forest vegetation (V2)	10.83	131.44–188.58	10.86	157.52–203.74		30	25.15	0.21 (Increase)
	High forest vegetation (V1)	10.76	188.59–304.86	10.8	203.75–272.35		40	25.15	0.20 (Increase)
WRF (989)	No forest vegetation (N2)	5.76	−29.9 to-111.68	8.05	−54.98–91.92	209.98 −8.32	22,900	−8.27	0.19 (Decrease)
	Very low forest vegetation (N1)	25.51	111.69–192.98	15.48	91.93–171.62		−100,300	−8.53	0.20 (Decrease)
	Marginal forest vegetation (V3)	37.02	192.99–243.45	54.12	171.63–229.44		171,000	−7.96	0.20 (Decrease)
	Moderate forest vegetation (V2)	242.39	243.45–270.08	240.65	229.44–268.51		−17,400	−8.36	0.21 (Decrease)
	High forest vegetation (V1)	678.32	270.09–327.55	670.7	268.52–343.52		−76,200	−8.48	0.20 (Decrease)
NRF (305)	No forest vegetation (N2)	5.12	−3.72 to 179.2	4.15	10.73–171.29	291.63 −4.71	−51,195.85	−9.68	0.03 (Decrease)
	Very low forest vegetation (N1)	12.51	179.21–212.46	9.89	171.30–209.74		−125,090.11	−16.85	0.06 (Decrease)
	Marginal forest vegetation (V3)	92.12	212.47–238.59	106.45	209.75–239.14		−921,093.55	−94.10	0.29 (Decrease)
	Moderate forest vegetation (V2)	111.13	238.60–261.16	109.13	239.15–262.89		−1,111,190.87	−112.54	0.35 (Decrease)
	High forest vegetation (V1)	84.12	261.17–299.17	75.38	262.90–299.07		−841,124.62	−86.33	0.27 (Decrease)

References

Abetu D, Bekele T (2019) Carbon stock in the Dirki woodland vegetation of Central Ethiopia: a case study in Ilu Gelan District, West Shewa Zone, Oromia Regional state. Trop Plant Res 6: 438–451. https://doi.org/10.22271/tpr.2019.v6.i3.054

Ahamed T, Tian L, Zhang Y, Ting KC (2011) A review of remote sensing methods for biomass feedstock production. Biomasss Bioenergy 35(7):2455–2469. https://doi.org/10.1016/j.biombioe.2011.02.028

As-syakur AR, Osawa T, Adnyana IS (2011) Estimation of gross primary production using satellite data and Gis in urban area, Denpasar. Int J Remote Sens Earth Sci 7:84–95. https://doi.org/10.30536/j.ijreses.2010.v7.a1544

Bastin J, Berrahmouni N, Grainger A, Maniatis D, Mollicone D, Moore R, Patriarca C, Picard N, Sparrow B, Abraham EM, Aloui K, Atesoglu A, Attore F, Bassüllü Ç, Bey A, Garzuglia M, GarcíaMontero LG, Groot N, Guerin G, Laestadius L, Lowe AJ, Mamane B, Marchi G, Patterson P, Rezende M, Ricci S, Salcedo I, Sanchez-Paus Diaz A, Stolle F, Surappaeva V, Castro R (2017) The extent of forest in dryland biomass. Science 356(6338):635–638

Box EO, Holben BN, Kalb V (1989) Accuracy of the AVHRR vegetation index as a predictor of biomass, primary productivity and net CO2 flux. Vegetatio 80:71–89. https://doi.org/10.1007/BF00048034

Brown S (1997) Estimating biomass and biomass change of tropical forests: a primer. FAO forestry paper (ISBN: 92-5-103955-0)

Burke IC, Schimel DS, Yonker CM, Parton WJ, Joyce LA, Lauenroth WK (1990) Regional modeling of grassland biogeochemistry using GIS. Landsc Ecol 4:45–54. https://doi.org/10.1007/BF02573950

Burke IC, Kittel TGF, Lauenroth WK, Snook P, Yonker CM, Parton WJ (1991) Regional analysis of the Central Great Plains. Bioscience 41:685–692

Cai Z, Jönsson P, Jin H, Eklundh L (2017) Performance of smoothing methods for reconstructing NDVI time-series and estimating vegetation phenology from MODIS Data. Remote Sens 9: 1271. https://doi.org/10.3390/rs9121271

Cheng S, Zhao Y (1990) Remote sensing and geosciences analysis. Measurement Press, Beijing, p 220

Ciais P, Sabine C, Bala G, Bopp L, Brovkin V, Canadell J, Chhabra A, DeFries R, Galloway J, Heimann M, Jones C, Le Quéré C, Myneni RB, Piao S, Thornton P (2013) Carbon and other biogeochem. Cy in: climate change 2013: the physical science basis. In: Stocker TF, Qin D, Plattner G-K, Tignor M, Allen SK, Boschung J, Nauels A, Xia Y, Bex V, Midgley PM (eds) Contribution of working group I to the fifth assessment report of the intergovernmental panel on climate change. Cambridge University Press, Cambridge

Clark DA, Brown S, Kicklighter DW, Chambers JQ, Thomlinson JR, Ni J, Holland EA (2001) Net primary production in tropical forests: an evaluation and synthesis of existing field data. Ecol Appl 11:371–384. https://doi.org/10.1890/1051-0761(2001)011[0371:NPPITF]2.0.CO;2

Congalton R (1991) A review of assessing the accuracy of classifications of remotely sensed data. Remote Sens Environ 37:35–46

Croft H, Che JM, Froelich NJ, Chen B, Staebler RM (2015) Seasonal controls of canopy chlorophyll content on forest carbon uptake: implications for GPP modeling. J Geophys Res 120(8): 1576–1586. https://doi.org/10.1002/2015JG002980

Dadhwal VK, Kushwaha SPS, Singh S, Patel NR, Nayak RK, Patil P, Dutt CBS, Murthy MSR, Jha CS, Rajsekhar G, Pujar GS, Trivedi S, Sharma N, Ali MM (2012) Recent results from EO studies on Indian carbon cycle assessment. Arch Photogram Remote Sens Spat Inf Sci ISPRS Int. https://doi.org/10.5194/isprsarchives-xxxviii-8-w20-3-201

DeFries RS, Field CB, Fung I, Justice CO, Los S, Matson PA, Matthews E, Mooney HA, Potter CS, Prentice K, Sellers PJ, Townshend JRG, Tucker CJ, Ustin SL, Vitousek PM (1995) Mapping the land surface for global atmosphere-biosphere models: toward continuous distributions of vegetation's functional properties. J Geophys Res 100:20867–20882. https://doi.org/10.1029/95JD01536

DeFries RS, Houghton RA, Hansen MC, Field CB, Skole D, Townshend J (2002) Carbon emissions from tropical deforestation and regrowth based on satellite observations for the 1980s and 1990s. Proc Natl Acad Sci U S A 99(22):14256–14261

Dewar RC, Medlyn BE, McMurtrie RE (1998) A mechanistic analysis of light and carbon use efficiencies. Plant Cell Environ 21:573–588

Faber-langendoen D, Keeler-Wolf T, Meidinger D, Josse C, Weakley A, Tart D, Navarro G, Hoagland B, Ponomarenko S, Fults G, Helmer E (2016) Classification and description of world formation types. United States Department of Agriculture, Fort Collins, p 222

FAO (2018) The state of the world's forests

Fleming RL, Leblanc JD, Hazlett PW, Weldon T, Irwin R, Mossa DS (2014) Effects of biomass harvest intensity and soil disturbance on jack pine stand productivity: 15-year results. Can J For Res 44:1566–1574. https://doi.org/10.1139/cjfr-2014-0008

Foody GM, Boyd DS, Cutler MEJ (2003) Predictive relations of tropical forest biomass from Landset TM data and their transferability between regions. Remote Sens Environ 85:463–474

Fung IY, Tucker CJ, Prentice KC (1987) On the variability of atmosphere-biosphere exchange of CO2. Adv Space Res 7(11):175–180. https://doi.org/10.1016/0273-1177(87)90309-7

Garbulsky MF, Peñuelas J, Papale D, Ardö J, Goulden ML, Kiely G, Richardson AD, Rotenberg E, Veenendaal EM, Filella I (2010) Patterns and controls of the variability of radiation use efficiency and primary productivity across terrestrial ecosystems. Glob Ecol Biogeogr 19: 253–267. https://doi.org/10.1111/j.1466-8238.2009.00504.x

Gibbs HK, Brown S, Niles JO, Foley JA (2007) Monitoring and estimating tropical forest carbon stocks: making REDD a reality. Environ Res Lett 2:1–13. https://stacks.iop.org/1748-9326/2/045022

Gifford RM (1995) Whole plant respiration and photosynthesis of wheat under increased CO2 concentration and temperature: long-term vs. short-term distinctions for modeling. Glob Change Biol 1:385–396

Gitelson AA, Viña A, Ciganda V, Rundquist DC, Arkebauer TJ (2005) Remote estimation of canopy chlorophyll content in crops. Geophys Res Lett 32:L08403

Gitelson AA, Keydan GP, Merzlyak MN (2006) Three-band model for noninvasive estimation of chlorophyll, carotenoids, and anthocyanin contents in higher plant leaves. Geophys Res Lett 33: L11402. https://doi.org/10.1029/2006GL026457

Goward SN, Tucker CJ, Dye DG (1985) North American vegetation patterns observed with the NOAA-7 advanced very high-resolution radiometer. Vegetatio 64:3–14. https://doi.org/10.1007/BF00033449

Gunin PD, Vostokova EA, Dorofeyuk NI, Tarasov PE, Black CC (1999) Vegetation dynamics of Mongolia. Springer, New York, p 240

Hilker T, Coops NC, Black TA, Wulder MA, Guy RD (2008) The use of remote sensing in light use efficiency based models of gross primary production: a review of current status and future requirements. Sci Total Environ 404:411–423. https://doi.org/10.1016/j.scitotenv.2007.11.007

Hobbs TJ (1995) The use of NOAA-AVHRR NDVI data to assess herbage production in the arid rangelands of Central Australia. Int J Remote Sens 16(7):1289–1302

Hooda RS, Dye DG (1996) Estimating carbon-fixation in India based on remote sensing data. In: Proceedings of ACRS, Colombo, Sri Lanka

Houghton RA (2005) Aboveground forest biomass and the global carbon balance. Glob Change Biol 11:945–958. https://doi.org/10.3390/rs11151823

Huang X, Xiao J, Ma M (2019) Evaluating the performance of satellite-derived vegetation indices for estimating gross primary productivity using FLUXNET observations across the globe. Remote Sens 11:1823. https://doi.org/10.3390/rs11151823

Huntingford C, Atkin OK, Martinez-de la Torre A, Mercado LM, Heskel MA, Harper AB, Bloomfield KJ, O'Sullivan OS, Reich PB, Wythers KR, Butler EE, Chen M, Griffin KL, Meir P, Tjoelker MG, Turnbull MH, Sitch S, Wiltshire A, Malhi Y (2017) Implications of improved representations of plant respiration in a changing climate. Nat Commun 8:1602

Inoue Y, Peñuelas J, Miyata A, Mano M (2008) Normalized difference spectral indices for estimating photosynthetic efficiency and capacity at a canopy scale derived from hyperspectral and CO2 flux measurements in rice. Remote Sens Environ 112:156–172. https://doi.org/10.1016/j.rse.2007.04.011

IPCC (1997) Climate change 1995: the science of climate change. Contribution of working group I to the second assessment report of the intergovernmental panel on climate change

IPCC (2001) Climate change 2001: the scientific basis. Contribution of working group I to the third assessment report of the IPCC

IPCC (2006) Guidelines for national greenhouse gas inventories. https://www.ipcc-nggip.iges.or.jp/public/2006gl/

IPCC (2007) Summary for policymakers. Climate change: the physical science basis. Contribution of working group i to the fourth assessment report of the intergovernmental panel on climate change

IPCC (2018) The carbon cycle and atmospheric carbon dioxide. https://www.ipcc.ch/site/assets/uploads/2018/02/TAR-03.pdf

Irisarri JGN, Oesterheld M, Paruelo JM, Texeira MA (2012) Patterns and controls of above-ground net primary production in meadows of Patagonia. A remote sensing approach. J Veg Sci 23:114–126. https://doi.org/10.1111/j.1654-1103.2011.01326.x

Jiang H, Apps MJ, Zhang Y, Peng C, Woodward PM (1999) Modelling the spatial pattern of net primary productivity in Chinese forests. Ecol Model 122:275–288

Jobbágy EG, Sala OE, Paruelo JM (2002) Patterns and controls of primary production in the Patagonian steppe: a remote sensing approach. Ecology 83(2):307–319

Joiner J, Yoshida Y, Zhang Y, Duveiller G, Jung M, Lyapustin A, Yujie W, Tucker CJ (2018) Estimation of terrestrial global gross primary production (GPP) with satellite data-driven models and eddy covariance flux data. Remote Sens 10(9):1346. https://doi.org/10.3390/rs10091346

Landsberg JJ, Waring RH (1997) A generalized model of forest productivity using simplified concepts of radiation-use efficiency, carbon balance, and partitioning. For Ecol Manag 95:209–228

Lin G, Marino BDV, Wei Y, Adams J, Tubiello E, Berry JA (1998) An experimental and modeling study of responses in ecosystems carbon exchanges to increasing CO2 concentrations using a tropical rainforest mesocosm. Aust J Plant Physiol 25:547–556

Luyssaert et al (2007) CO2 balance of boreal, temperate, and tropical forests derived from a global database. Glob Change Biol 13:2509–2537. https://doi.org/10.1111/j.1365-2486.2007.01439.x

Mariappan N (2010) Net primary productivity estimation of eastern Ghats using multispectral MODIS data. Int Geomatics Geosci 1:406–413

Mbaabu P (2012) AGB/prediction of lidar-derived data using optical imagery for improved pine plantation structure quantification 98

McCallum I, Wagner W, Schmullius C, Shvidenko A, Obersteiner M, Fritz S, Nilsson S (2009) Satellite-based terrestrial production efficiency modeling. Carbon Balance Manag 4:8. https://doi.org/10.1186/1750-0680-4-8. http://www.cbmjournal.com/content/4/1/8

McCallum I, Wagner W, Schmullius C, Shvidenko A, Obersteiner M, Fritz S, Nilsson S (2010) Comparison of four global FAPAR datasets over northern Eurasia for the year 2000. Remote Sens Environ 114:941–949. https://doi.org/10.1016/j.rse.2009.12.009

Ministry of Forestry (2015) Forest production map for use of forest utilization, directorate general of forestry business forestry ministry of forestry, 2015; Forest area and conservation area of South Sumatra Province, forestry data South Sumatra, 2015 (Peta Indikatif Arahan Pemanfaatan Hutan Pada Kawasan Hutan Produksi Yang Tidak Dibebani Izin Untuk Usaha Pemanfaatan Hasil Hutan Kayu. 2014. Lembar Peta, Sumatera Selatan, Indonesia). https://appgis.dephut.go.id/appgis/Araha n_Pemanfaatan_2015/Sumsel.pdf. Accessed 12 Jan 2019

Mollicone D, Freibauer A, Schulze ED, Braatz S, Grassi G, Federici S (2007) Elements for the expected mechanisms on 'reduced emissions from deforestation and degradation, REDD' under the UNFCCC. Environ Res Lett 2:045024. https://stacks.iop.org/1748-9326/2/045024

Monteith JL (1972) Solar radiation and productivity in tropical ecosystems. J Appl Ecol 9:747. https://doi.org/10.2307/2401901

Myneni RB, Williams DL (1994) On the relationship between FAPAR and NDVI. Remote Sens Environ 49:200–211. https://doi.org/10.1016/0034-4257(94)90016-7

Myneni RB, Hall FG, Sellers PJ, Marshak AL (1995) The meaning of spectral vegetation indices. IEEE Trans Geosci Remote Sens 33:481–486

Návar J (2009) Allometric equations for tree species and carbon stocks for forests of northwestern Mexico. For Ecol Manag 257:427–434. https://doi.org/10.1016/j.foreco.2008.09.028

Obi Reddy GP, Singh SK (2018) Geospatial technologies in land resources mapping, monitoring and management. Springer, Berlin, p 395

Ochi S, Shibasaki R (1999a) Algorithm for generating drainage direction matrix using DEM (GTOPO30) and DCW. J Jpn Soc Photogram Remote Sens 38(3):60–68

Ochi S, Shibasaki R (1999b) Estimation of NPP based agricultural production for Asian countries using remote sensing data and GIS. In: Proceeding of the 20th Asian conference on remote sensing

Ochi S, Shibasaki R, Murai S (2000) Assessment of primary productivity for food production in major basins of Asia using R. S., and GIS. Int Arch Photogramm Remote Sens XXXIII:1051–1057

Paruelo JM et al (1997) ANPP estimates from NDVI for the central grassland region of the United States. Ecology 78(3):953958. https://doi.org/10.1890/00129658(1997)078[0953:AEFNFT]2.0.CO;2

Pedgen C, Sadowski R, Shannon R (1995) Introduction to simulation using SIMAN, 2nd edn. McGraw-Hill, Singapore

Potter CS, Randerson JT, Field CB, Matson PA, Vitousek PM, Mooney HA et al (1993) Terrestrial ecosystem production: a process model based on global satellite and surface data. Global Biogeochem Cycles 7:811–841

Prince SD (1991) A model of regional primary production for use with coarse resolution satellite data. Int J Remote Sens 12:1313–1330

Rasib AW, Ibrahim AL, Cracknell AP, Fandi MA, Kadir WHW (2007) Mapping net primary production in tropical rain forest using MODIS satellite data. In: 28th Asian conference on remote sensing 2007, ACRS 2007, vol 1, pp 322–327

Richardson GP (1997) Problems in causal loop diagrams revisited. Syst Dyn Rev 13:247–252. https://doi.org/10.1002/(SICI)1099-1727(199723)13:3<247:AID-SDR128>3.0.CO;2-9

Rodrigues DP, Hamacher C, Estrada GCD, Soares MLG (2015) Variability of carbon content in mangrove species: effect of species, compartments and tidal frequency. Aquat Bot 120:346–351. https://doi.org/10.1016/j.aquabot.2014.10.004

Romijn E, Lantican CB, Herold M, Lindquist E, Ochieng R, Wijaya A, Murdiyarso D, Verchot L (2015) Assessing change in national forest monitoring capacities of 99 tropical countries. For Ecol Manag 352:109–123. https://doi.org/10.1016/j.foreco.2015.06.003

Rouse JW, Hass RH, Schell JA, Deering DW (1973) Monitoring vegetation systems in the great plains with ERTS. In: Third Earth Resour Technol Satell Symp, vol 1, pp 309–317. https://www.citeulike-article-id:12009708

Ruimy A, Saugier B, Dedieu G (1994) Methodology for the estimation of terrestrial net primary production from remotely sensed data. J Geophys Res 99:5263–5283

Ruimy A, Dedieu G, Saugier B (1996) TURC: a diagnostic model of continental gross primary productivity and net primary productivity. Global Biogeochem Cycles 10(2):269–285. https://doi.org/10.1029/96GB00349

Running SW, Hunt ER (1993) Generalization of a forest ecosystem process model for other biomes, BIOME-BGC, and an application for global-scale models. In: Ehleringer JR, Field CB (eds) Scaling physiological processes: leaf to globe. Academic, San Diego, pp 141–158

Running SW, Justice CO, Salomonson V, Hall D, Barker J, Kaufman YJ et al (1994) Terrestrial remote sensing science and algorithms planned for EOS/MODIS. Int J Remote Sens 15:3587–3620

Running SW, Thornton PE, Nemani RR, Glassy JM (2000) Global terrestrial gross and net primary productivity from the Earth Observing System. In: Sala O, Jackson R, Mooney H (eds) Methods in ecosystem science. Springer, New York, pp 44–57

Running SW, Ramakrisha R, Nemani FAH, Zhao M, Reeves M, Hashimoto H (2004) A continuous satellite-derived measure of global terrestrial primary production. Bioscience 54(6):547–560

Ryan MG (1991) Effects of climate change on plant respiration. Ecol Appl 1(2):157–167

Saatchi SS, Harris NL, Brown S, Lefsky M, Mitchard ETA, Salas W, Zutta BR, Buermann W, Lewis SL, Hagen S, Petrova S, White L, Silman M, Morel A (2011) Benchmark map of forest carbon stocks in tropical regions across three continents. Proc Natl Acad Sci U S A 108:9899–9904. https://doi.org/10.1073/pnas.1019576108

Schloss AL et al (1999) Comparing global models of terrestrial net primary productivity (NPP): comparison of NPP to climate and the Normalized Difference Vegetation Index (NDVI). Glob Change Biol 5(1):25–34. https://doi.org/10.1046/j.1365-2486.1999.00004.x

Schriber TJ (1987) The nature and role of simulation in the design of manufacturing systems. In: Retti J, Wichmann KE (eds) Simulation in CIM and artificial intelligence techniques. Society of Computer Simulation, pp 5–18

Schwarz PA, Law BE, Williams M, Irvine J, Kurpius M, Moore D (2004) Climatic versus biotic constraints on carbon and water fluxes in seasonally drought-affected ponderosa pine ecosystems. Global Biogeochem Cycles 18(4):GB4007. https://doi.org/10.1029/2004GB002234

Setyono P, Himawan W, Sari CP, Gunawan T, Murti SH (2020) Greenhouse gas pollution based on energy use and its mitigation potential in the city of Surakarta, Indonesia

Sjöström M, Ardö J, Arneth A, Boulain N, Cappelaere B, Eklundh L, de Grandcourt A, Kutsch WL, Merbold L, Nouvellon Y, Scholes RJ, Schubert P (2011) Exploring the potential of MODIS EVI for modelling gross primary production across African ecosystem. Remote Sens Environ 115(4):1081–1089

Smith P, Davies CA, Ogle S, Zanchi G, Bellarby J, Bird N, Boddey RM, McNamara NP, Powlson D, Cowie A, van Noordwijk M, Davis SC, Richter DDB, Kryzanowski L, van Wijk MT, Stuart J, Kirton A, Eggar D, Newton-Cross G, Adhya TK, Braimoh AK (2012) Towards an integrated global framework to assess the impacts of land use and management change on soil carbon: current capability and future vision. Glob Chang Biol 18:2089–2101. https://doi.org/10.1111/j.1365-2486.2012.02689.x

Sonawane K, Bhagat V (2016) Improved change detection of forests using landsat TM and ETM data. Remote Sens Land 1:18–40. https://doi.org/10.21523/gcj1.17010102

Sung S, Nicklas F, Georg K, Lee DK (2016) Estimating net primary productivity under climate change by application of global forest model (G4M). J Korean Soc People Plants Environ 19:549–558. https://doi.org/10.11628/ksppe.2016.19.6.549

Supeni A (2006) Estimation of net primary production using the netpro 1.0 model (case study: Cidanau watershed) Ania Supeni Faculty of Math and Natural Sciences

Thiffault E, Hannam KD, Paré D, Titus BD, Hazlett PW, Maynard DG, Brais S (2011) Effects of forest biomass harvesting on soil productivity in boreal and temperate forests—a review. Environ Rev 19:278–309. https://doi.org/10.1139/a11-009

Thomlinson JR, Bolstad PV, Cohen WB (1999) Coordinating methodologies for scaling land cover classifications from site-specific to global: steps toward validating global map products. Remote Sens Environ 70:16–28

Tian H, Chen G, Liu M, Zhang C, Sun G, Lu C, Xu X, Ren W, Pan S, Chapelka A (2010) Model estimates of net primary productivity, evapotranspiration, and water use efficiency in the terrestrial ecosystems of the southern United States during 1895–2005. For Ecol Manag 259(7):1311–1327

Tscharntke T, Leuschner C, Zeller M, Guhardja E, Bidin A (2007) Stability of tropical rainforest margins: linking ecological, economic, and social constraints of land use and conservation (environmental science and engineering) (English edition) 2007th edition, kindle edition. ISBN 978-3-540-30290-2

Tucker CJ (1979) Red and photographic infrared linear combinations for monitoring vegetation. Remote Sens Environ 8:127–150

Tucker CJ, Sellers PJ (1986) Satellite remote sensing of primary production. Int J Remote Sens 7:1395–1416. https://doi.org/10.1080/01431168608948944

Tucker CJ, Holben BN, Elgin JH, McMurtrey JE (1981) Remote sensing of total dry-matter accumulation in winter wheat. Remote Sens Environ 11:171–189

Turner DP, Ritts WD, Zhao M, Kurc SA, Dunn AL, Wofsy SC, Small EE, Running SW (2006) Assessing interannual variation in MODIS-based estimates of gross primary production. IEEE Trans Geosci Remote Sens 44:1899–1907. https://doi.org/10.1109/TGRS.2006.876027

Ulsig L, Nichol CJ, Karl FH, David RL, Elizabeth MM, Alexei IL, Lyapustin IM, Janne L, Albert PC (2017) Detecting inter-annual variations in the phenology of evergreen conifers using long-term MODIS vegetation index time series. Remote Sens 9:49. https://doi.org/10.3390/rs9010049

Wang Q, Ni J, Tenhunen J (2005) Application of a geographically-weighted regression analysis to estimate net primary production of Chinese forest ecosystems. Glob Ecol Biogeogr 14:379–393. https://doi.org/10.1111/j.1466-822X.2005.00153.x

Watson C (2009) Forest carbon accounting: overview and principles. UNDP: CDM Capacity Development in Eastern and Southern Africa

Wei S, Yi C, Fang W, Hendrey G (2017) A global study of GPP focusing on light-use efficiency in a random forest regression model. Ecosphere 8(5):e01724. https://doi.org/10.1002/ecs2.1724

Wessels KJ, Prince SD, Reshef I (2008) Mapping land degradation by comparison of vegetation production to spatially derived estimates of potential production. J Arid Environ 72(10):1940–1949

Wu C, Niu Z, Gao S (2009) Gross primary production estimation from MODIS data with vegetation index and photosynthetically active radiation in maize. J Geophys Res 115:D12127. https://doi.org/10.1029/2009JD013023

Xiao XM, Hollinger D, Aber J, Goltz M, Davidson EA, Zhang QY, Moore B III (2004) Satellite-based modeling of gross primary production in an evergreen needleleaf forest. Remote Sens Environ 89:519–534. https://doi.org/10.1016/j.rse.2003.11.008

Xiao X, Zhang Q, Hollinger D, Aber J, Moore B (2005) Modeling gross primary production of an evergreen needleleaf forest using modis and climate data. Ecol Appl 15(3):954–969. https://doi.org/10.1890/04-0470

Yu B, Chen F (2016) The global impact factors of net primary production in different land cover types from 2005 to 2011. Springerplus 5(1):1235. https://doi.org/10.1186/s40064-016-2910-1

Zhang YQ, Yu Q, Jiang J, Tang YH (2008) Calibration of Terra/MODIS gross primary production over an irrigated cropland on the North China Plain and an alpine meadow on the Tibetan Plateau. Glob Chang Biol 14(4):757–767. https://doi.org/10.1111/j.1365-2486.2008.01538.x

Zhang Y, Ming X, Hua C, Jonathan A (2009a) Global pattern of NPP to GPP ratio derived from MODIS data: effects of ecosystem type, geographical location, and climate. Glob Ecol Biogeogr 18(3):280–290. https://doi.org/10.1111/j.1466-8238.2008.00442.x

Zhang Q, Middleton EM, Margolis HA, Drolet GG, Barr AA, Black TA (2009b) Can a satellite-derived estimate of the fraction of PAR absorbed by chlorophyll (FAPARchl) improve predictions of light-use efficiency and ecosystem photosynthesis for a boreal aspen forest? Remote Sens Environ 113:880–888

Zhang Y, Xiao X, Wu X, Zhou S, Zhang G, Qin Y, Dong J (2017) A global moderate resolution dataset of gross primary production of vegetation for 2000–2016. Sci Data 4:170165

Zhao M, Running SW (2010) Drought-induced reduction in global. Science 329:940–943. https://doi.org/10.1126/science.1192666

Zhao M, Heinsch FA, Nemani RR, Running SW (2005) Improvements of the MODIS terrestrial gross and net primary production global data set. Remote Sens Environ 95:164–176. https://doi.org/10.1016/j.rse.2004.12.011

Zhao M, Running SW, Nemani RR (2006) Sensitivity of moderate resolution imaging Spectroradiometer (MODIS) terrestrial primary production to the accuracy of meteorological reanalyses. J Geophys Res 111:G01002. https://doi.org/10.1029/2004JG000004

Zheng D, Prince S, Wright R (2003) Terrestrial net primary production estimates for 0.5° grid cells from field observationsa contribution to global biogeochemical modelling. Glob Change Biol 9:46–64

Chapter 10
GEE-Based Spatiotemporal Evolution of Deforestation Monitoring in Malaysia and Its Drivers

Ling Hu, Abdul Rashid Bin Mohamed Shariff, Hamdan Omar, Dan-Xia Song, and Hao Wu

Abstract Despite recognizing the importance of tropical forest systems, deforestation in Malaysia has increased rapidly over the past 15 years. Since the first civilian earth observation satellite launched in 1972, remote sensing techniques and image processing analysis have been extensively used for long-term and continuous forest monitoring. This chapter selected the Google Earth Engine (GEE) platform to monitor deforestation in Malaysia from 2000 to 2020. GEE is a cloud-based platform that works with substantial geospatial datasets using high-performance computing resources. This chapter quantified trends of deforestation in Malaysia through the statistical approach based on GEE and used the quantitative data as a basis for analyzing the drivers of deforestation. The deforestation statistics for Malaysia from 2000 to 2020 was 86,893 km^2, with the highest deforestation in

L. Hu
Department of Biological and Agricultural Engineering, Faculty of Engineering, Universiti Putra Malaysia, Serdang, Malaysia
e-mail: gs63140@student.upm.edu.my

A. R. B. M. Shariff (✉)
Department of Biological and Agricultural Engineering, Faculty of Engineering, Universiti Putra Malaysia, Serdang, Malaysia

SMART Farming Technology Research Center, Faculty of Engineering, Universiti Putra Malaysia, Serdang, Malaysia

Laboratory of Plantation System Technology and Mechanization (PSTM), Institute of Plantation Studies (IKP), Universiti Putra Malaysia, Serdang, Malaysia
e-mail: rashidpls@upm.edu.my

H. Omar
Geoinformation Programme, Division of Forestry & Environment, Forest Research Institute Malaysia (FRIM), Kepong, Selangor, Malaysia
e-mail: hamdanomar@frim.gov.my

D.-X. Song · H. Wu
College of Urban and Environmental Sciences, Central China Normal University, Wuhan, People's Republic of China
e-mail: dxsong@mail.ccnu.edu.cn; haowu@mail.ccnu.edu.cn

2014. Overall, the statistical results demonstrated a high level of accuracy, and the GEE platform was confirmed to be suitable for forest monitoring on a national scale. Based on the statistical data of states in Malaysia, we further elaborated on the main drivers of deforestation. There is no single driver of tropical deforestation in Malaysia; the palm oil industry, forest fires, and illegal logging are attributed to the loss. The GEE monitoring tool was found appropriate for monitoring deforestation and has potential in guiding Malaysia's management and conservation of forest resources.

Keywords Tropical forest systems · Remote sensing · Google Earth Engine · Statistical approach · Drivers of deforestation

10.1 Introduction

Tropical forest ecosystems provide essential ecosystem services, primarily climate regulation and stabilization, carbon sequestration for global warming mitigation, biodiversity, and water supply, and 25% of terrestrial biosphere carbon comes from tropical forests (Bonan 2008). Tropical forests can absorb large amounts of greenhouse gases and counteract rising carbon dioxide levels. It is one of the most effective defenses against the greenhouse effect (Pennisi 2020). It absorbs 95% of the carbon dioxide from trees worldwide, and more than 50% of the biomass in tropical trees has a carbon sequestration effect. Therefore, tropical forests have a significant role in mitigating global warming and the occurrence of climate extremes (Mackey et al. 2020). At the same time, tropical forests provide an excellent living environment for wildlife. Tropical forests account for 72% of biodiversity hotspots in the world (Myers et al. 2000). Tropical forests cover only 7% of the land area but contain more than 65% of the world's biodiversity (Giam 2017).

However, by the early twentieth century, the world had lost 50% of its tropical forest area (FAO 2000), and it equals losing one big football field in the forest every 6 years (Mikaela Weisse 2020). Tropical forests dominate three essential regions: North America, West and Central Africa, Southeast Asia and Oceania. In developing countries, higher rates of deforestation turn forests into agricultural and pastoral lands (FAO 2015). In the 1990s, nearly 46 billion tons of carbon dioxide were extracted, compared to 25 billion tons in the 2010s (Gov 2009). Overall, tropical forests in the 1990s decreased 17% of human-made CO_2, compared to just 6% in the 2010s (Hubau et al. 2020). In addition to the surge in global CO_2 emissions, the most important reason is the 19% reduction in the area of intact tropical forests (Hubau et al. 2020). Concurrent anthropogenic impacts threaten tropical forests, including primary deforestation, overexploitation, ecological damage, and species invasions that are synergistic. For example, deforestation and climate change both exacerbate fires, thus threatening tropical forests (Barlow and Peres 2008). Since the first satellite launch in 1972, remote sensing data processing analysis has been widely needed in monitoring large forest areas consistently and repeatedly (Song et al. 2015). The forest research and operations agencies use several remote sensing data

types, including aerial photography, optical multispectral images, synthetic aperture radar (SAR), light detection and ranging (LiDAR), and video imaging data, to track, locate, classify, analyze, and quantify different types of forest cover and their changes. Various forest features can be observed, marked, categorized, evaluated, and measured by remote sensing techniques (Hussin and Bijker 2000).

Malaysia is one of the 12 megadiversity countries, but in the meantime is among the top 50 countries in the world in terms of deforestation rates (Kadir et al. 2019). Oil palm plantations expansion is responsible for 50% of this deforestation. Deforestation in Malaysia has shown a rising trend over the past 15 years, especially after 2009 (Butler 2013). The monitoring of forest areas in Malaysia is one of the important activities for managing forest resources to ensure that the forests provide goods and services sustainably and for the conservation of biodiversity in Malaysia.

However, deforestation in the tropics is a complex and long-term process that requires repeated measurements of time, space, and reversibility (Lambin 1999). Deforestation monitoring is a huge challenge, especially for larger forests (Reis et al. 2019; Omar et al. 2020) processed a total of 580 Landsat imagery and measured Malaysian forests at 5-year intervals. GEE is a cloud-based platform that makes working with huge geospatial datasets using high-performance computing resources possible (Amani et al. 2020). GEE can perform in a few days what would take a computer 15 years to compute and identify changes in forest cover with high resolution and short intervals (Dacosta et al. 2019). To this effect, the GEE platform used in this study can easily monitor deforestation in Malaysia and benefit from its capabilities.

In this study, we examined the status of forest cover and its changes in Malaysia with the GEE. We demonstrated how the GEE could be used to monitor large areas of deforestation. The specific objectives are: (a) to monitor the spatial and temporal evolution of deforestation in Malaysia on the GEE platform for 2000–2020; (b) to evaluate the feasibility of GEEs in analyzing the land cover change at a national scale; (c) to quantify the deforestation in Malaysia and across states over the past 20 years to analyze the drivers of deforestation.

10.2 Materials and Methods

10.2.1 Study Area

Malaysia is a Southeast Asian country located between 1° and 7° North latitude, with a typical tropical rainforest climate (Fig. 10.1). The country has a total land area of 330,524 km^2, divided into Peninsular Malaysia and East Malaysia, which straddles the South China Sea. Malaysia has a vibrant tropical ecosystem, with tropical rainforests covering 59% of the country's land area and 7616 km^2 of mangrove forests (Kanniah et al. 2015). Malaysia's lowlands are covered with 2.76 million hectares of peatland, an environmentally sensitive area (ESA) under the National Physical Plan (NPA). As a result, Malaysia has a unique tropical peatland forest, a
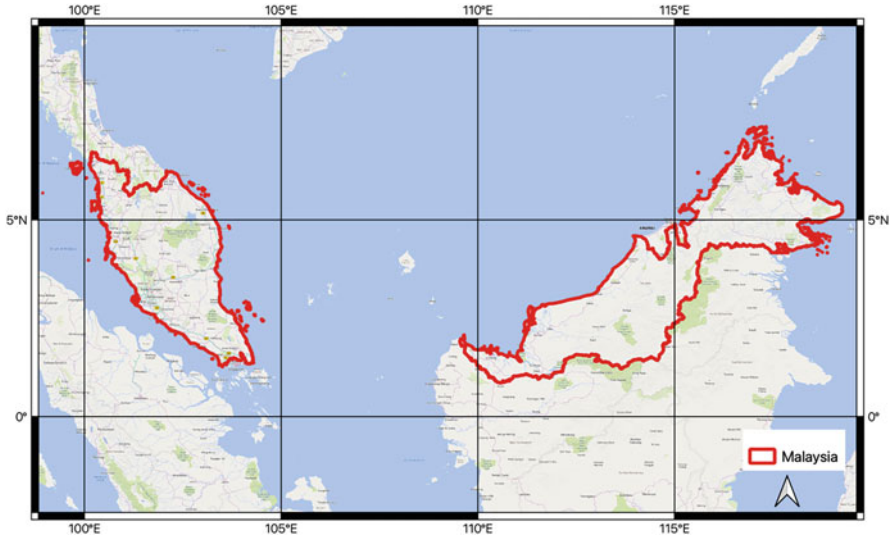
Fig. 10.1 Study area (Please note this map is not an authority on boundaries)

dual ecosystem of tropical rainforest and peatland (Melling 2015). Countries in tropical regions such as Malaysia lack optical imagery data because high cloud coverage limits valuable observations (Othman et al. 2018). Various noises such as clouds, atmospheric clarity (water vapor, dust, chemical, etc.), satellite location, and other noise can interrupt the data applications, decrease the values, and increase application complexity (Menzel 2012). The study repeated monitoring over a vast region of land and followed a set monitoring cycle. GEE appears to be the best contender for meeting these requirements, and it's a cloud-based platform for working with large geographic datasets and high-performance computing resources.

Malaysia's administrative boundary was obtained from the Large-Scale International Boundary (LSIB) dataset. This dataset was provided by the United States Office of the Geographer. It is split into two parts: line vector data from the LSIB and world vector coastline data from the National Geospatial-Intelligence Agency. The code for LSIB's boundary vector data collection and the interactive development environment on the GEE platform in this study are shown in Fig. 10.2. The border vector data for the states of Malaysia on the GEE platform in this study were obtained from the Humanitarian Data Exchange (HDX) tool.

10.2.2 Datasets Description

This study is based on satellite forest cover data—the Hansen et al. (2013) Global Forest Change dataset, developed by Hansen et al. in 2013 based on Landsat satellite data to map global forest cover, deforestation, and forest gain from 2000 to 2012. Since then, annual increases have been made. For the selection of underlying data,

Fig. 10.2 The Large-Scale International Boundary (LSIB) dataset on GEE

Landsat data is the best choice for global analysis. A global analysis of Landsat data was already done, which converts the digital number (DN) to the top of the atmospheric radiation values. However, the atmospheric radiance values do not accurately reflect the surface conditions due to the influence of the atmosphere. Therefore, Hansen et al. (2013) eventually performed atmospheric corrections to produce surface reflection images. After generating the surface reflection images, orthorectification techniques are applied to the data processing to reduce the effect of topography on the global forest cover images. A key reason for the appearance of false information about the land cover is the variation in solar zenith and azimuth angles in rugged terrain. The following Eq. (10.1) normalizes the illumination factor (IL), which can be calculated as the actual amount of solar radiation incident at any slope:

$$IL = \cos Z * \cos S + \sin Z * \sin Z * \cos (\Phi_z - \Phi_s) \qquad (10.1)$$

where Z is the solar zenith angle, S is the inclination angle, Φ_z is the solar azimuth angle, and Φ_s is the longitudinal and transverse angle of the inclined plane.

10.2.3 Methodology

In this study, four main steps were undertaken: (a) data processing; (b) implementation of statistical methods; (c) charting yearly deforestation; and (d) data validation. The processing is based on Google Earth Engine with JavaScript
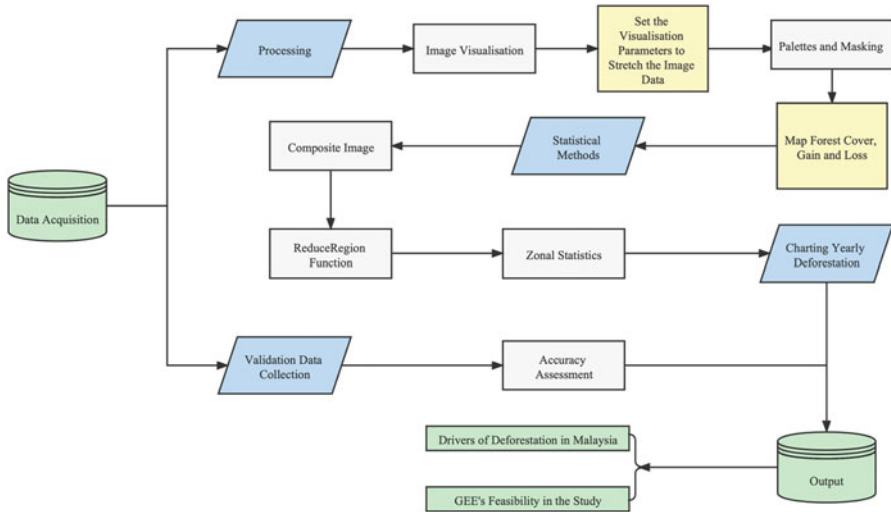
Fig. 10.3 The flowchart of methodology

API, and all processing was done based on GEE to assess its applicability further. JavaScript is a ready-to-compile programming language for web development. CamelCase is used in JavaScript, and Google has published its own authoritative JavaScript style as Google's source code standard. Data in this study had already been trained by Hansen et al. (2013), and validation data was from the Global Forest Watch (GFW) real-time data under the World Resources Institute (WRI) initiative. The study's goal is to use the GEE platform to monitor deforestation's spatial and temporal dynamics in Malaysia. In addition to the national scale, the study looks at deforestation in 13 states and 3 federal territories in Malaysia. The disparities in deforestation by the state were analyzed based on the geographical and temporal evolution data for further research of the drivers of deforestation and verification of the Google Earth platform's capability.

The methodology used in this study is illustrated in the methodological flowchart shown in Fig. 10.3, which illustrates the general methodological procedures for accomplishing the study's objectives. GEE allows coverage of huge areas, enabling regional surveys on various themes and identification of extensive features. Forests are generally over a relatively large area, so GEE can save the cost of field surveys when detecting forest changes. Landsat data makes it possible to evaluate ecosystems that can evaluate the health and integrity of ecosystems with the help of spectral indices. The parameterization of the annual curve of spectral vegetation indices allows deriving indices or attributes of three factors key to the functioning of ecosystems (productivity, seasonality, and phenology) to establish the reference conditions and evaluate the changes that occur. Therefore, through the analysis of a long-term series, it is possible to identify directional change trends which are useful in global change.

10.2.4 *Image Processing*

To better quantify the area of deforestation in Malaysia and for further analysis, the Global Forest Change dataset is processed on the GEE platform in this study. The processing is divided into two steps: (a) image visualization; (b) palettes and masking.

Image Visualization

The global forest change dataset shows the extent of forests in 2000 and forest increase and decrease after 2000. However, as shown in Fig. 10.4, for the dataset provided by Hansen et al. (2013), the loss and gain bands are not clearly visible on the image. Therefore, the first step in processing is to set the visualization parameters to stretch the image data. The forest cover for 2020 was displayed as an RGB (red, green, and blue) composite image, and bands 5, 4, and 3 (False Color) were selected. The visual parameter "max" was used to set the stretching range for each band.

Palettes and Masking

Cascading Style Sheets (CSS) is a syntax used in web programming, with multiple keywords to specify styles' names. In this study, the CSS color under the palette function defines the forest overlay layer as "00FF00" green, the loss layer as "FF0000" red, and the gain layer as "0000FF" blue. Areas that had no forest cover and areas outside the territory of Malaysia were masked off.
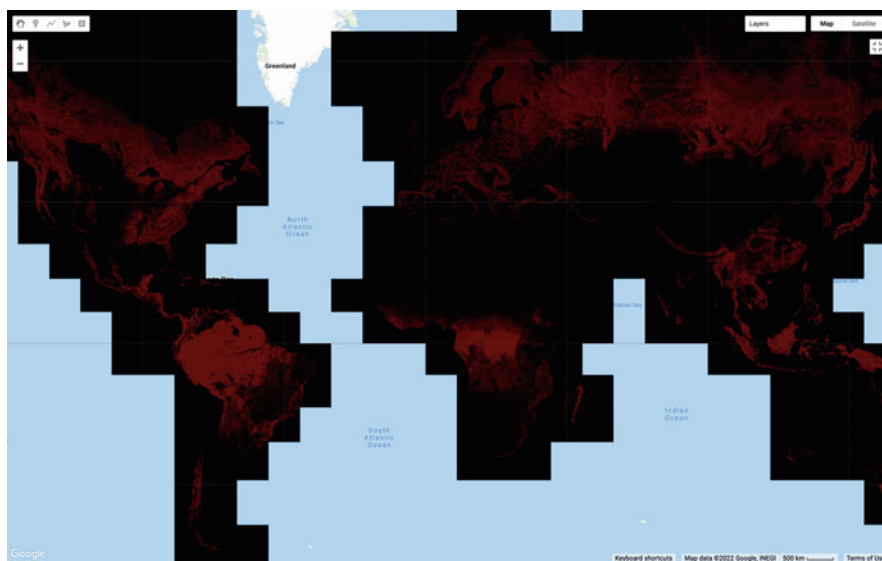

Fig. 10.4 Image visualization based on the dataset of Hansen et al. (2013) on GEE

10.2.5   Statistical Methods

Reducers in Earth Engine are methods/functions for aggregating data in time, space, bands, arrays, and other data structures. There are some reducer functions in GEE, as shown in Table 10.1. Statistical Methods in GEE to calculate annual deforestation in Malaysia.

The Reduce Region Grouped Reductions (Zonal Statistics) reducer methods were used to calculate the pixel area of the study area: (a) the Reduce Region method was used to calculate the total forest area lost in Malaysia and each state. All pixels in the study region are reduced to a statistic or a histogram representation of the pixel data in the area to provide a statistic of the pixel values of a region in Malaysia. Figure 10.5 shows how the region is represented as geometry, and the output is a statistic obtained from the pixels in the area.

(b) The ultimate goal of this study is to calculate annual losses. Therefore, once the pixel area of the target area had been calculated, using the "zonal statistics" method, the study area was designated as a grouping zone. Zonal statistics is one of the primary spatial analysis methods. The pixel values determine the results in the input value raster that fall into the specified input area data set. In zonal statistics, the role of the value raster is to evaluate the values of the specified area (Singla and Eldawy 2018). Deforestation was grouped by year. As shown in Fig. 10.6, the Zone layer shows the input raster data in the target area, such as shape, value, position, etc. The Value layer defines the statistics of the target area.

In this study, integer pixel values are used to identify the input values for the target region. The loss year band is added to the image, with values between 0 and 20 in each pixel in the band, indicating the years from 2000 to 2020 when

Table 10.1 The functions of reducer on GEE

Reducers	Example	Mode of Operation
Simple	Count, distinct, first, etc.	Context-dependent
Mathematical	Min, max, sum, product, etc.	
Logical	Logical, etc.	
Statistical	Mode, percentile, mean, median, etc.	
Correlation	Kendall, Spearman, etc.	
Regression	Linear regression, etc.	

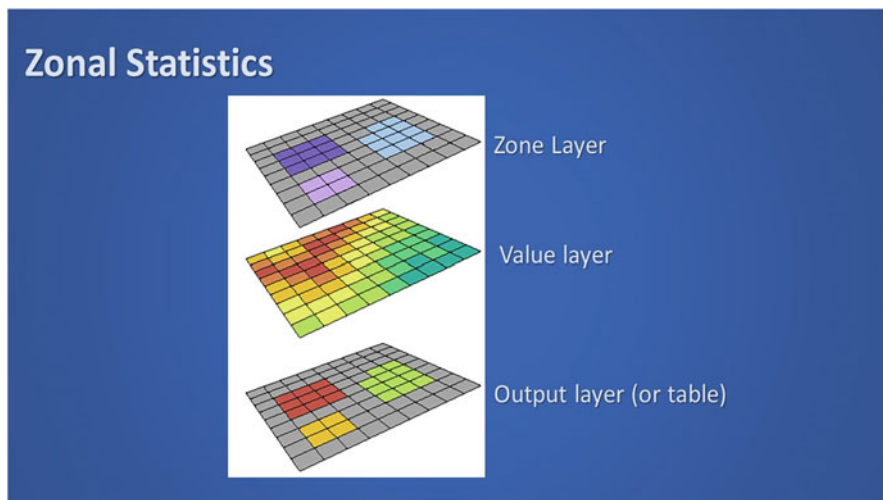**Fig. 10.5** Reduce region function on GEE
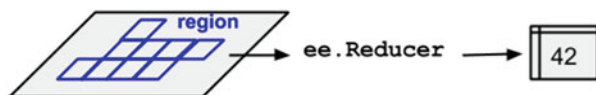
Fig. 10.6 Zonal statistics

Fig. 10.7 Examples of
chart types on GEE

```
'ScatterChart'
'LineChart'
'ColumnChart'
'BarChart'
'PieShart'
'AreaChart'
```

deforestation occurred. Using a grouped reducer (Fig. 10.6), the grouped band 1 was specified as the band index to find the pixel area sum of the target area. After counting the pixels by zonal statistics, the format conversion can be made in GEE.

10.2.6   Charting Yearly Deforestation

GEE can create scatter, line, bar, pie, and bar charts, among other chart styles. Google Visualization is a JavaScript-based framework for creating various interactive charts on websites. Set the chart type with the ui.Chart.setChartType() method, the chart type as shown in Fig. 10.7. The ui.Chart.array.values() method was used in this study to chart the yearly deforestation of Malaysia and its states.

10.2.7 Drivers of Deforestation Elaborating

Curbing forest loss is very difficult for a rapidly developing economy like Malaysia. In general, commodity crops are the main driver of forest loss in Malaysia, with the oil palm industry being the main cause (Shevade and Loboda 2019). Remote sensing has a wide variety of forest change applications, including cover measurements, plant composition, chemistry, and moisture of vegetation, biodiversity, and soil properties (Lechner et al. 2020). These variables produce forest inventories to measure the number of trees per acre, base area, and timber value. This study completed data collection, image processing, application of statistical methods, and output of statistical results. Based on the statistical results and other works on deforestation, an analysis of the tropical forest drive in Malaysia was conducted.

10.2.8 Data Validation

The validation data for this study comes from Global Forest Watch (GFW), a platform that has expanded from providing assessments on the state of forests in a few nations to offering global data on forests (Fig. 10.8). As for the validation data, the overall accuracy of the DFW dataset was higher than other remote sensing products (Zhang et al. 2020), and the study of Tyukavina et al. (2015) showed that DFW data performed well in assessing forest loss in tropical areas.
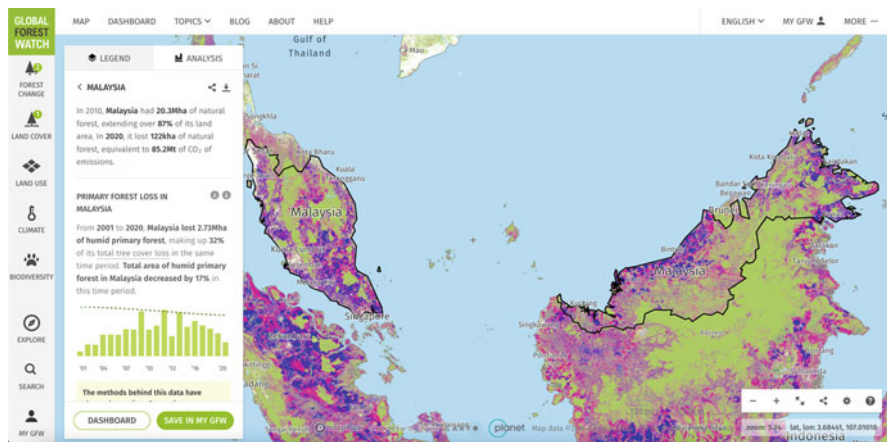

Fig. 10.8 Validation through GFW

10.3 Results

The experimental results of the GEE platform are presented, analyzed, and further discussed in the following four subsections: (a) processing output; (b) results of the numerical study; (c) drivers of deforestation in Malaysia, and (d) results of the validation. The quantitative data on deforestation in Malaysia and its states is explored. The quantitative data summarizes further the drivers of deforestation and the feasibility of the GEE platform.

10.3.1 Processing Output

The main goal of image processing was to collect, synthesize, and visualize the images. After collecting images of global forest change from 2000 to 2020, the RGB composite image was created as shown in Figs. 10.9 and 10.10 shows the land outside the forest being masked. Subsequently the setting up of a color palette, designing parameters to stretch the images, and cropping the administrative boundaries of Malaysia was done (Fig. 10.11). The processing results are shown in Fig. 10.11 for Malaysia's 2000 forest cover, 2020 deforestation, and 2020 forest gain. The green legend shows forest cover in 2000, red shows deforestation from 2000 to 2020, and blue shows forest gain from 2000 to 2020.

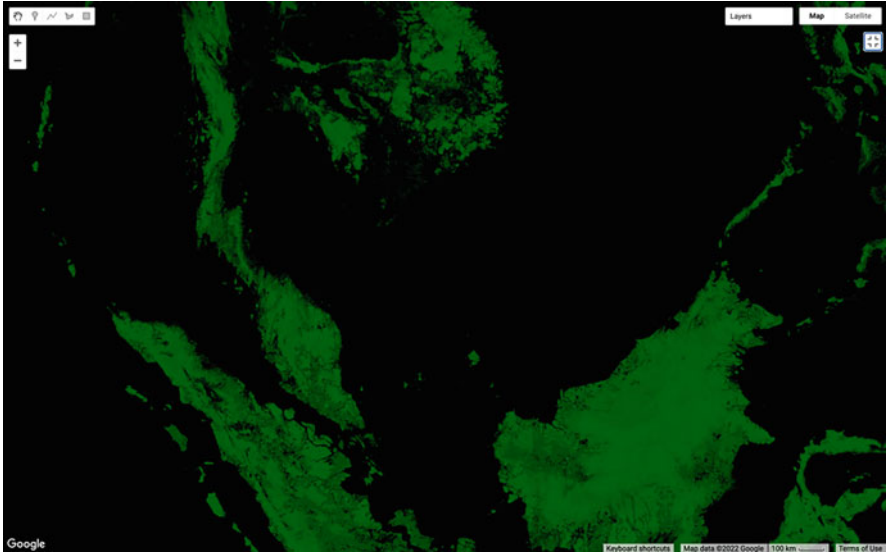**Fig. 10.9** RGB composite image (False color) with bands 5, 4, and 3

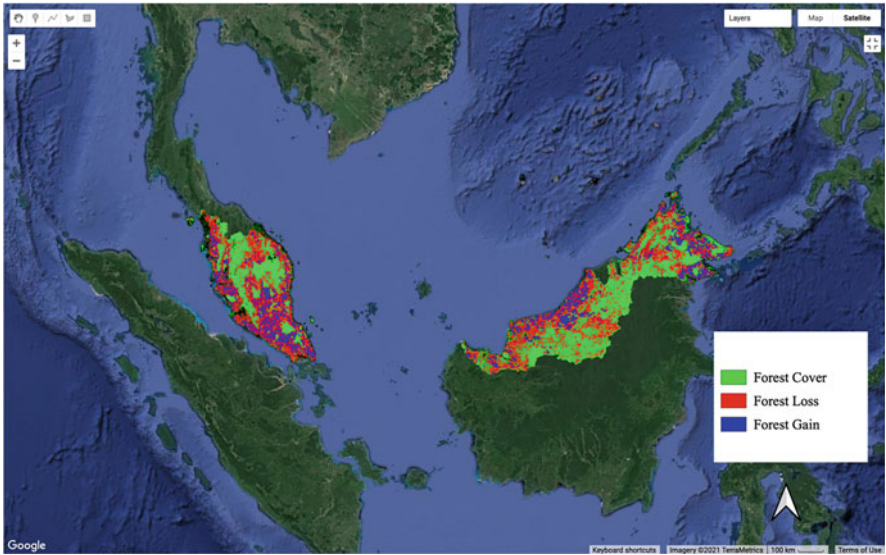**Fig. 10.10** Masking the land outside the forest

Fig. 10.11 Forest cover, loss, and gain map created after processing dataset

10.3.2   Results of Numerical Study

This study defines forest coverage as vegetation above 5 m in height, so it does not distinguish between artificial forests and natural forests. Forest cover was visualized on GEE in layers based on the Hansen et al. (2013) Global Forest Change dataset. With a land area of 330,524 km^2, Malaysia has lost approximately 86,893 km^2 of forest in the last 20 years, with deforestation accounting for 26% of the total area. The largest deforestation was in 2014, at 6804.67 km^2, or 2.06% of the total area. Malaysia had the lowest deforestation in 2003 with 1855.71 km^2 of deforestation or 0.56% of the total area (Figs. 10.12 and 10.13). There are many factors that influence deforestation, whether it is plantation expansion, logging, or urban sprawl, all of which are tied to human activity (Didenko et al. 2017). In 2002, the Malaysian government promulgated the Environmental Impact Assessment (EIA) Guidelines
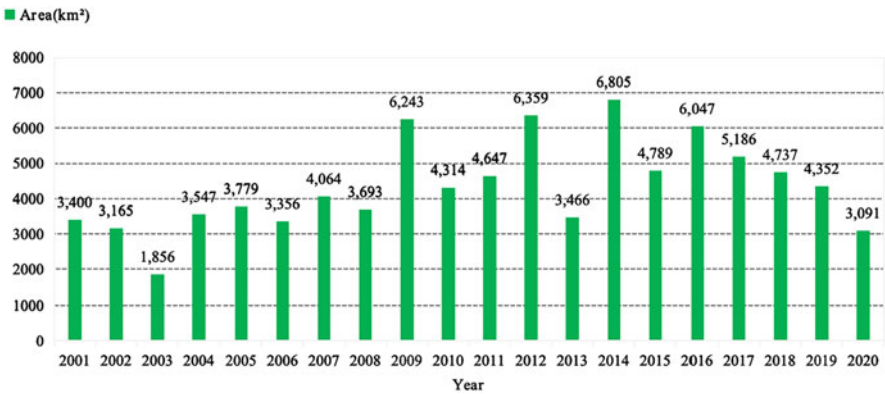

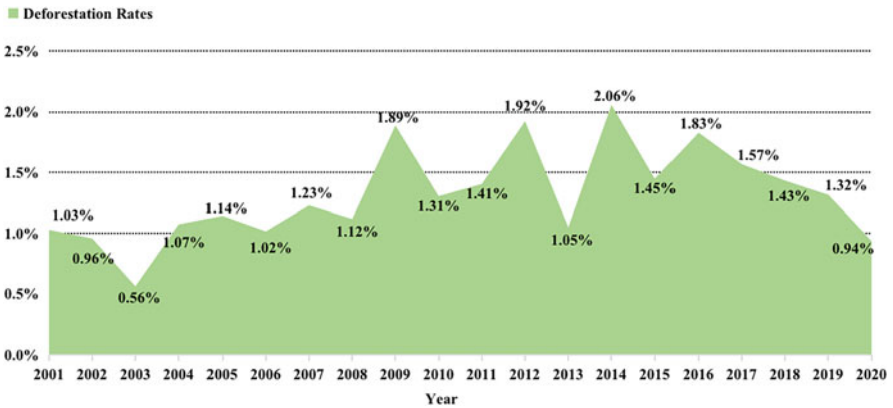**Fig. 10.12** Yearly deforestation in Malaysia

Fig. 10.13 Yearly rate of deforestation in Malaysia

for Logging and Forest Clearance Activities (Foo and Yusoff 2002). In the year following the promulgation of the guidelines, deforestation was at its lowest. Compared to 2014, the year with the highest deforestation, the amount of deforestation in 2003 was about 1/4 of the former. The largest deforestation of 6046.66 km^2 was in 2016. After 2016 the deforestation decreased every year until 2020 when the deforestation was 3090.67 km^2. As a percentage of the total area, deforestation also decreases from 1.83% to 0.94% (Figs. 10.12 and 10.13). And the deforestation decrease is also closely related to the 2015 Malaysian Sustainable Palm Oil Certification Program (Yap et al. 2021).

Overall, Sarawak has the largest area of deforestation, about 36% of Malaysia's deforestation over the past 20 years, ranking first among the 13 states and 3 federal territories. This was followed by Sabah and Pahang, which accounted for 20% and 14% of the total area of lost forestry in Malaysia (Fig. 10.14). The land in these three states is covered by large areas of tropical rainforest with a great variety of life. At the same time, the agricultural sector accounts for a large share of GDP in these three states, at 13.5%, 19.1%, and 23.4%, respectively (Department of Statistics Malaysia Official Portal 2018). Negeri Sembilan, Johor, and Malacca had the highest rates of deforestation (ratio of the area of forest lost to land area), with Negeri Sembilan losing 41% of its forest, Johor 39%, and Malacca 38% (Fig. 10.15). The relatively low rate of deforestation in Labuan, Penang, Perlis, and Kuala Lumpur is related to their land areas and their primary industries (Ngu et al. 2020). Tourism, services and
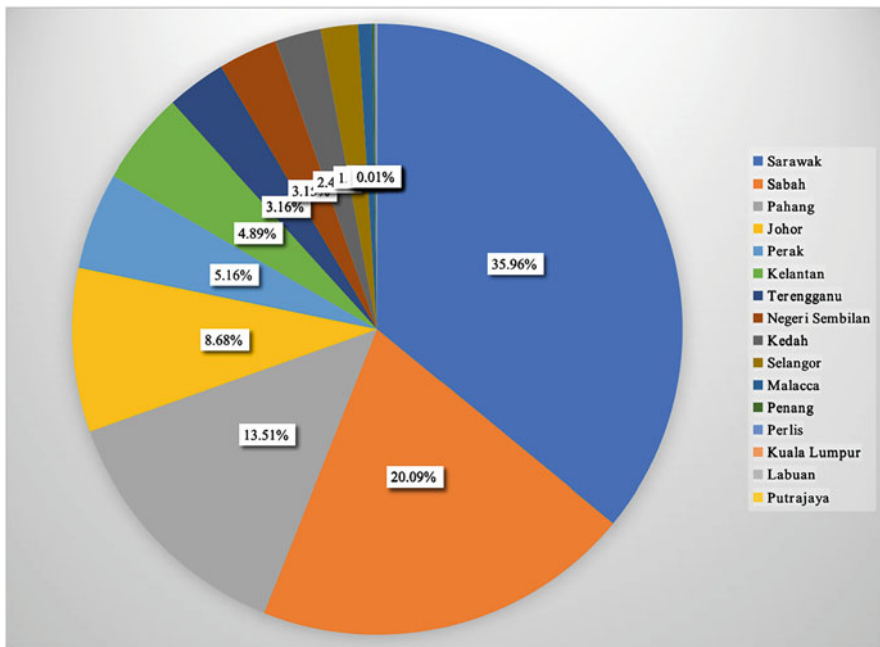

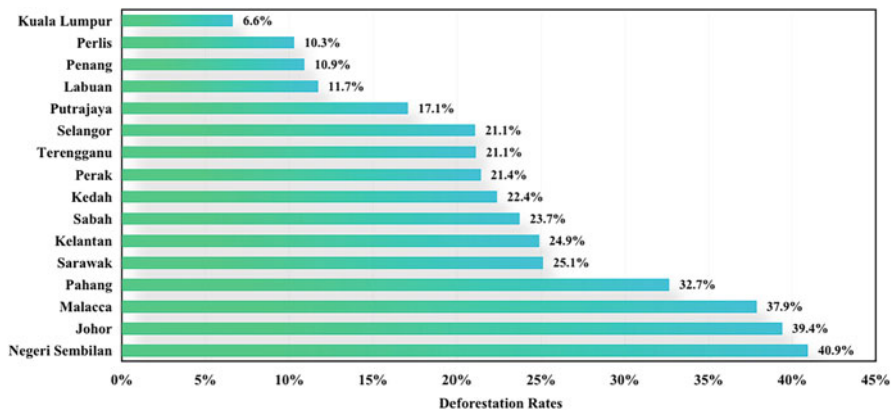**Fig. 10.14** Contribution of deforestation by state

Fig. 10.15 Deforestation rates of Malaysia's states

manufacturing are their main pillar industries and contribute a high share of GDP (Kuala Lumpur Travel | All Malaysia 2009).

10.3.3 Drivers of Deforestation in Malaysia

Except for Kedah, Perlis, and Penang, most states in Malaysia have essentially returned to the lower deforestation levels of 2000 (Figs. 10.13, 10.14 and 10.15). For continuous changes in deforestation at national scales and states, it is valuable to quantify deforestation at high resolution over a short interval. After outputting the quantified forest results for 2000–2020 in this study, the drivers of deforestation in Malaysia are defined based on data characteristics, graphical trends, and human activity correlations.

Palm Oil Industry

Malaysia is the world's second largest exporter of palm oil (Malaysia - Agricultural Sector 2021). Seventeen million metric tons of palm oil was exported from Malaysia in 2020, accounting for 34% of global palm oil exports. The study shows that the area under oil palm cultivation in Malaysia has increased significantly with a growth rate of 83.5% during 2000–2018 (Malaysian Palm Oil Industry – MPOC 2020). By 2020, Malaysia has 42,000 km^2 of oil palm plantations, accounting for 12.7% of its land area. Table 10.2 (Danylo et al. 2021) provides the area of oil palm expansion in Malaysia in 2017 and the share of oil palm cultivation in three different periods (pre-2000, 2000–2009, and 2010–2017). As shown in Malaysia's annual deforestation in Fig. 10.16, the red dividing line positioned at the year 2016 shows

Table 10.2 Extent of oil palm plantations in Malaysia (Danylo et al. 2021)

Region	Extent in 2017 (million ha)	Planted before 2000 (%)	Planted 2000–2009 (%)	Planted 2010–2017 (%)
Peninsular Malaysia	2.41	17.31	39.04	43.66
Sabah and Sarawak states	1.72	22.34	31.35	46.30

deforestation in Malaysia has decreased significantly after 2016. The greater practice of sustainability in oil palm cultivation could be a contributing factor. According to the Malaysian Palm Oil Board (MPOB), the Malaysian Sustainable Palm Oil Certification Scheme (MSPO) is the Malaysian government's certification scheme for palm cultivation and palm oil processing, which started in 2015 and aimed to improve palm oil sustainability (Yap et al. 2021). As shown in Fig. 10.17, the oil palm expansion in Malaysia began to moderate significantly in 2015, particularly in Sarawak. Moreover, the oil palm expansion became negative, which means that no new oil palm area was opened but existing oil palm area decreased. The slowdown in the expansion of oil palm could be one of the factors to explain the trend in deforestation in Malaysia while the approach of not opening up new lands but focusing on replanting shows positive results.

Wildfire

From 2000 to 2020, the cumulative area burned is $8771 km^2$ in Malaysia (Fig. 10.18). Malaysia has a vibrant tropical ecosystem, with tropical rainforests covering 59% of the country's land area and $7616 km^2$ of mangrove forests (Kanniah et al. 2015). Malaysia's lowlands are covered with 2.76 million hectares of peatland, an ESA under the NPA. As a result, Malaysia has a unique tropical peatland forest, a dual ecosystem of tropical rainforest and peatland (Melling 2015). The threat of forest fires to biodiversity is enormous. In tropical humid rainforests, organisms lack targeted adaptation to forest fires. Thus, forest fires are a greater threat to tropical ecosystems, with more than 90% of the tropics under threat from forest fires. Tropical rainforest ecosystems in Southeast Asia are typically fire-sensitive systems, with most organisms lacking the ability to recover rapidly after burning (WWF Deutschland 2017).

Illegal Logging

In 2019, the export share of timber and its products from Malaysia was USD 5369 million (WWF Deutschland 2017). In the 1990s, 30% of Malaysia's log exports were illegal. Illegal logging accounted for more than 20% of Malaysia's timber exports before 2003 (Hashiramoto et al. 2003). Although the rate of illegal logging
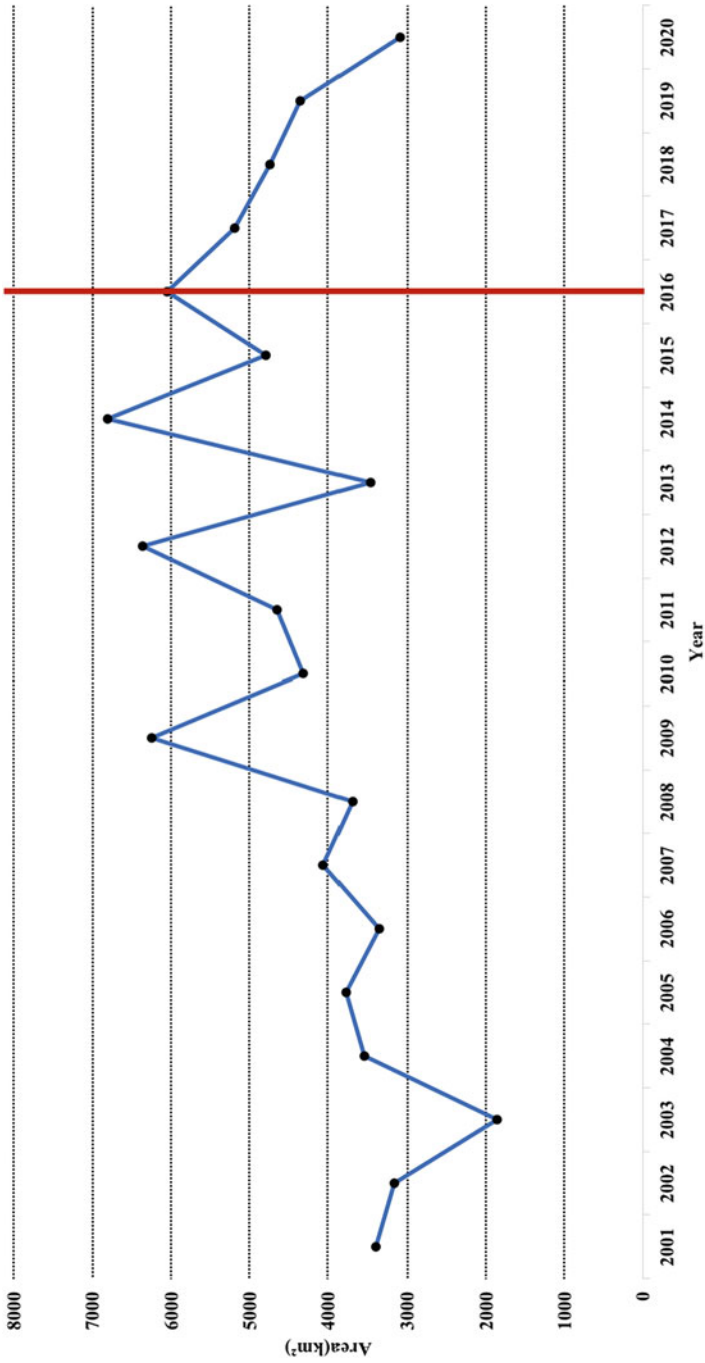
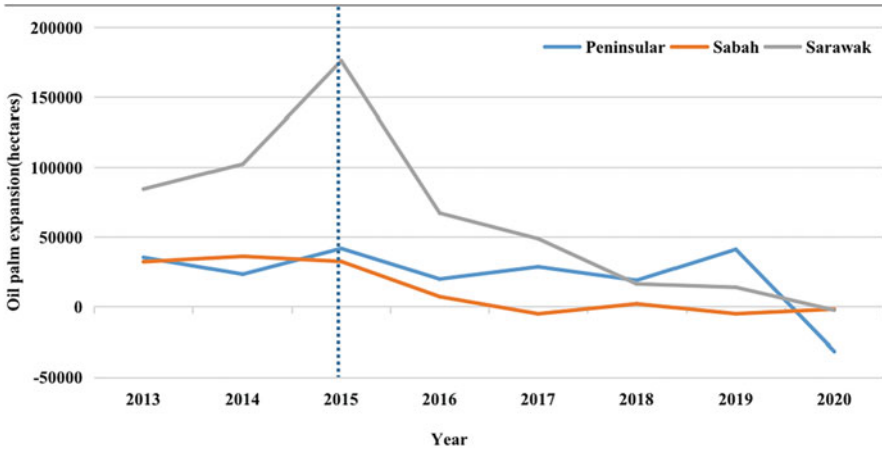**Fig. 10.16** Yearly deforestation in Malaysia

Fig. 10.17 Oil palm expansion in Malaysia (hectares). (Source: Malaysian Palm Oil Board)
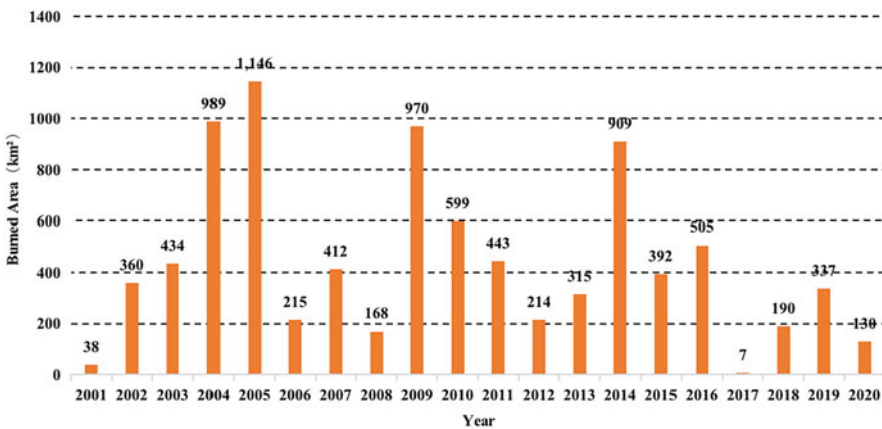
Fig. 10.18 Burned area in Malaysia. (Source: Global Forest Watch)

has declined after 2003, it remains one of Malaysia's challenges. Malaysia is ranked in the middle of Transparency International's 2013 Corruption Perceptions Index, with forestry being the sector most affected by corruption. As Malaysia's 13 states and 3 federal municipalities have the power to set their land and forest use, there needs to be greater coordination in the implementation of the relevant policies. This may help to lower the rate of illegal logging in the Malaysian states on Borneo Island.

As shown in Fig. 10.14, Sarawak and Sabah states in the Malaysian Borneo have contributed 36% and 20%, respectively, of the total deforestation over the last 20 years, ranking first and second out of 13 states and 3 federal territories. Sarawak

is rich in natural resources, and the state has a single industry heavily dependent on primary industries. Agriculture and mining account for 34.7% of GDP, and Sarawak is one of the largest exporters, accounting for 65% of Malaysia's log exports in 2000 according to UN statistics for 2001. Likewise, Sabah's industry is based on the export of primary products, and there is a massive demand for raw materials such as timber and oil. Illegal logging is more significant in Sabah, with more than 30,000 m^3 logged illegally per year (Hoare 2015). Although there are fines and arrest warrants for illegal logging, the market value of the timber seized is much higher than the fine, and it is often impossible to identify the illegal logger. However, the reported illegal logging activities have been reduced since the year 2005 after a few revisions of forest policies, strengthening of enforcement at the fields, and improvement of forest management structure. Forestry Department Peninsular Malaysia (FDPM), States Forestry Departments, Forest Department Sarawak (FDS), and Sabah Forestry Department (SFD) have always been putting the greatest efforts to ensure our forest resources are managed sustainably for both production and protection purposes within the remaining forests.

10.3.4 Results of Validation

This study validates the results with data from the GFW platform and thus evaluates the feasibility of the GEE for analyzing forest areas at a national scale.

The validation results in Table 10.3 show that the results of this study based on the GEE showed high accuracy, which is closely related to the deforestation data and the study method. The Hansen et al. (2013) global forest change dataset defined trees as vegetation above 5 m. As a result, some planted forests, agricultural land, and smallholder economic land were incorrectly classified as forests when classifying the land use data. In addition, the zonal statistics in this study counted and calculated the discrete pixels, which do not precisely represent forests in real life. As a result, these data can overestimate forest cover to some extent. Although the results based on the GEE and data result in some overestimation, the data results in this study still maintain a high level of accuracy. In some years, the accuracy of the results was above 99%. The average accuracy reached 96.43%. The high accuracy performance demonstrates the high feasibility of GEE for large-scale land monitoring.

10.4 Discussion

Over the past 20 years, Malaysia has lost 86,893 km^2 of forests, accounting for 26% of the total land area. The rate of deforestation declined for the fourth consecutive year since 2016. In 2020, most states in Malaysia had essentially returned to the lower deforestation levels of 2000. However, the area of deforestation in Malaysia in 2020 was 3090 km^2. Sarawak lost the most forest area, contributing 36% of

Table 10.3 Results of validation

Yearly	Results of deforestation computed in this study (km^2)	Validation data from GFW (km^2)	Accuracy (%)
2001	3399.94	3324.97	97.75
2002	3164.64	3125.54	98.75
2003	1855.71	1839.11	99.10
2004	3546.55	3518.02	99.19
2005	3778.59	3754.20	99.35
2006	3356.2	3339.01	99.49
2007	4063.81	4051.59	99.70
2008	3692.71	3679.72	99.65
2009	6243.22	6227.80	99.75
2010	4313.75	4306.07	99.82
2011	4646.91	4630.78	99.65
2012	6358.66	6281.71	98.78
2013	3465.97	3332.21	95.99
2014	6804.67	6457.79	94.63
2015	4789.08	4543.45	94.59
2016	6046.66	5652.49	93.03
2017	5185.88	4834.16	92.72
2018	4737.19	4379.85	91.84
2019	4352.03	3953.67	89.92
2020	3090.67	2687.21	84.99
Average value	4344.64	4195.97	96.43

Malaysia's total deforestation. This was followed by Sabah and Pahang, which contributed 20% and 14% of Malaysia's total deforestation, respectively. Negeri Sembilan, Johor, and Malacca had the highest deforestation rates. In contrast, the lowest deforestation rates were in Labuan, Penang, Perlis, and Kuala Lumpur, which have much less land, with the land use in Penang and Kuala Lumpur being mostly commercial, residential, and industrial.

This study uses data from the GFW platform to validate the results and thus assess the feasibility of the GEE for quantitative analysis of forests at the national scale. The validation results based on the graph above reveal that the study's GEE results are often higher than the validation data related to the deforestation statistics and the study's methodology. Trees were considered vegetation if their height was over 5 m in the Hansen et al. (2013) global forest change dataset. As a result, while classifying land use data, some planted forests, agricultural land, and smallholder economic land were wrongly classified as forests. Furthermore, marginalized pixels are considered in this study's zonal statistics-based pixel computation and categorization. As a result, these data may overestimate forest cover. The accuracy of the results was above 99% in several years of data, with the average accuracy being 96.43%. This high level of accuracy illustrates GEE's suitability for large-scale land monitoring.

Curbing deforestation is very difficult for a rapidly developing economy like Malaysia. In general, commodity crops are the main driver of deforestation in Malaysia, with the oil palm industry being the main cause. The palm oil industry is significant in Malaysia, with palm oil constituting 1/3 of Malaysia's agricultural output. Compared to other drivers of deforestation, deforestation from commodity crops is permanent and irreversible. In addition, wildfires and illegal logging also constitute drivers of deforestation in Malaysia. In the last decade, Sarawak and Sabah are the states that contributed to the highest rates of illegal logging. However, the policies have continued to improve, and enforcements have been strengthened. Most states in Malaysia rely heavily on agriculture for economic development, which has resulted in deforestation due to the over-representation of agriculture commodities such as oil palm. The states that have contributed the most to total deforestation over the last 20 years are Sarawak, Sabah, and Pahang, where the agricultural sector accounts for a substantial share of GDP at 13.5%, 19.1%, and 23.4%, respectively. For states with lower rates of deforestation, such as Labuan, Penang, and Kuala Lumpur, tourism and services are undoubtedly the mainstays of their industries while these are already well built-up areas. There are some limitations in this study, especially in terms of data to be further improved. In the Hansen et al. (2013) global forest change dataset, tree cover was defined as vegetation with a height above 5 m, so there would be neglect for young canopy forest cover. In addition, the adhesion of the relationship between the forest gain, drivers analyzing deforestation and the effects of other human activities was not high enough, and the network of relationships between variables should be strengthened and explored in future studies.

10.5 Conclusions

This study's objective was to model the spatial and temporal evolution of deforestation in Malaysia based on the GEE platform. In addition to the national scale, the study analyzed deforestation in Malaysia covering the 13 states and 3 federal territories. Based on the spatial and temporal evolution results, the differences in deforestation by states were compared for further analysis of the drivers of deforestation and verification of the feasibility of the Google Earth platform. Overall, the statistical results in this study still maintain a high level of accuracy and demonstrate the suitability of the GEE platform for national-scale forest monitoring. Based on the statistical results, this study elaborates on the main drivers of deforestation in Malaysia. The palm oil industry, forest fires, and illegal logging all contribute to deforestation in Malaysia. Quantifying Malaysia's past deforestation can effectively engage in forest management, climate protection, ecological resource conservation, and sustainable ecosystem services.

References

Amani M, Member S, Ghorbanian A, Ahmadi SA, Kakooei M, Moghimi A, Mirmazloumi SM, Member S, Hamed S, Moghaddam A, Mahdavi S, Ghahremanloo M, Parsian S (2020) Google Earth Engine cloud computing platform for remote sensing big data applications: a comprehensive review. IEEE J Select Top Appl Earth Observ Remote Sens 13:5326–5350

Barlow J, Peres CA (2008) Fire-mediated dieback and compositional cascade in an Amazonian forest. Philos Trans R Soc B Biol Sci 363(1498):1787–1794. https://doi.org/10.1098/rstb.2007.0013

Bonan GB (2008) Forests and climate change: forcings, feedbacks, and the climate benefits of forests. Science 320(5882):1444–1449. https://doi.org/10.1126/science.1155121

Butler RA (2013) Malaysia has the world's highest deforestation rate, reveals Google forest map. https://news.mongabay.com/2013/11/malaysia-has-the-worlds-highest-deforestation-rate-reveals-google-forest-map/

Dacosta OJ, Matthew E, Jnr O (2019) Long term monitoring of Ghana's forest reserves using Google Earth Engine Salamatu Shaibu View project research on lunar regolith thermal parameters based on passive and active remote sensing techniques and their geological significance view project. https://doi.org/10.20944/preprints201909.0016.v1

Danylo O, Pirker J, Lemoine G, Ceccherini G, See L, McCallum I, Hadi, Kraxner F, Achard F, Fritz S (2021) A map of the extent and year of detection of oil palm plantations in Indonesia, Malaysia and Thailand. Sci Data 8(1):96. https://doi.org/10.1038/s41597-021-00867-1

Department of Statistics Malaysia Official Portal (2018). https://web.archive.org/web/201808040 81413/https://www.dosm.gov.my/v1/index.php?r=column%2FcthemeByCat&cat=102&bul_ id=VS9Gckp1UUpKQUFWS1JHUnJZS2xzdz09&menu_id=TE5CRUZCblh4 ZTZMODZIbmk2aWRRQT09. Accessed 16 Nov 2021

Didenko N, Popkova AA, Skripnuk D, Mirolyubova O (2017) Deforestation and human activity: a global perspective. https://doi.org/10.5593/sgem2017/53

FAO (2000) Global Forest Resources Assessment 2000. http://www.fao.org/forestry/fra/86626/en/. Accessed 14 Dec 2020

FAO (2015) FRA 2015 | Global Forest Resources Assessments | Food and Agriculture Organization of the United Nations. http://www.fao.org/forest-resources-assessment/past-assessments/fra-2015/en/. Accessed 14 Dec 2020

Foo SM, Yusoff MR (2002) Environmental impact assessment - Malaysia perspectives. In: International conference on health, safety and environment in oil and gas exploration and production, pp 749–758. https://doi.org/10.2118/73983-MS

Giam X (2017) Global biodiversity loss from tropical deforestation. Proc Natl Acad Sci 114(23): 5775–5777. https://doi.org/10.1073/pnas.1706264114

Gov WE (2009) Emissions of greenhouse gases in the United States 2009, DOE/EIA-0573(2009). www.eia.gov

Hansen MC, Potapov PV, Moore R, Hancher M, Turubanova SA, Tyukavina A, Thau D, Stehman SV, Goetz SJ, Loveland TR, Kommareddy A, Egorov A, Chini L, Justice CO, Townshend JRG (2013) High-resolution global maps of 21st-century forest cover change. Science 342 (6160):850–853. https://doi.org/10.1126/science.1244693

Hashiramoto O, Castano J, Johnson S (2003) Changing global picture of trade in wood products. https://www.fao.org/3/y5918e/y5918e05.htm

Hoare A (2015) Illegal logging and related trade the response in Malaysia. Chatham House, London

Hubau W, Lewis SL, Phillips OL, Affum-Baffoe K, Beeckman H, Cuní-Sanchez A, Daniels AK, Ewango CEN, Fauset S, Mukinzi JM, Sheil D, Sonké B, Sullivan MJP, Sunderland TCH, Taedoumg H, Thomas SC, White LJT, Abernethy KA, Adu-Bredu S et al (2020) Asynchronous carbon sink saturation in African and Amazonian tropical forests. Nature 579(7797):80–87. https://doi.org/10.1038/S41586-020-2035-0

Hussin YA, Bijker W (2000) International archives of photogrammetry and remote sensing

Kadir G, Parveez A, Lip K, Charles Hill T, Arn TY, Kushairi A (2019) Sustainable oil palm cultivation in Malaysia—are peatlands a suitable choice? J Oil Palm Environ Health 10:13–18. https://doi.org/10.5366/jope.2019.03

Kanniah K, Sheikhi A, Cracknell A, Goh HC, Tan K, Ho C, Rasli FN (2015) Satellite images for monitoring mangrove cover changes in a fast growing economic region in southern peninsular Malaysia. Remote Sens 7:14360–14385. https://doi.org/10.3390/rs71114360

Kuala Lumpur Travel | All Malaysia (2009). https://web.archive.org/web/20090827185613/http://all.talkmalaysia.com/kuala-lumpur/kuala-lumpur-travel/. Accessed 16 Nov 2021

Lambin EF (1999) Monitoring forest degradation in tropical regions by remote sensing: some methodological issues. Glob Ecol Biogeogr 8(3–4):191–198. https://doi.org/10.1046/J.1365-2699.1999.00123.X

Lechner AM, Foody GM, Boyd DS (2020) Applications in remote sensing to forest ecology and management. One Earth 2(5):405–412. https://doi.org/10.1016/J.ONEEAR.2020.05.001

Mackey B, Kormos CF, Keith H, Moomaw WR, Houghton RA, Mittermeier RA, Hole D, Hugh S (2020) Understanding the importance of primary tropical forest protection as a mitigation strategy. Mitig Adapt Strateg Glob Chang 25(5):763–787. https://doi.org/10.1007/s11027-019-09891-4

Malaysia - Agricultural Sector (2021). https://www.trade.gov/country-commercial-guides/malaysia-agricultural-sector. Accessed 16 Nov 2021

Malaysian Palm Oil Industry – MPOC (2020). http://mpoc.org.my/malaysian-palm-oil-industry/. Accessed 8 Jul 2021

Melling L (2015) Peatland in Malaysia. In: Tropical peatland ecosystems. Springer Japan, Tokyo, pp 59–73. https://doi.org/10.1007/978-4-431-55681-7_4

Menzel WP (2012) Remote sensing applications with meteorological satellites. Adv Space Res 7(3):49–57

Mikaela Weisse EDG (2020) How much forest did the world lose in 2019? World Resources Institute, Washington, DC. https://www.wri.org/blog/2020/06/global-tree-cover-loss-data-2019

Myers N, Mittermeier RA, Mittermeier CG, da Fonseca GAB, Kent J (2000) Biodiversity hotspots for conservation priorities. Nature 403(6772):853–858. https://doi.org/10.1038/35002501

Ngu HJ, Lee MD, bin Osman MS (2020) Review on current challenges and future opportunities in Malaysia sustainable manufacturing: remanufacturing industries. J Clean Prod 273:123071. https://doi.org/10.1016/J.JCLEPRO.2020.123071

Omar H, Rao Narayanamoorthy T, Mohd Johan Chuah N, Atikah Abu Bakar N, Afizzul Misman M (2020) Utilization of remote sensing technology for carbon offset identification in Malaysian forests. In: Remote Sensing. IntechOpen, London. www.intechopen.com

Othman MA, Ash'Aari ZH, Aris AZ, Ramli MF (2018) Tropical deforestation monitoring using NDVI from MODIS satellite: a case study in Pahang, Malaysia. IOP Conf Ser Earth Environ Sci 169(1):012047. https://doi.org/10.1088/1755-1315/169/1/012047

Pennisi E (2020) Tropical forests soak up huge amounts of greenhouse gas. Climate change could end that | Science | AAAS. https://www.sciencemag.org/news/2020/05/tropical-forests-soak-huge-amounts-greenhouse-gas-climate-change-could-end

Reis BP, Martins SV, Fernandes Filho EI, Sarcinelli TS, Gleriani JM, Leite HG, Halassy M (2019) Forest restoration monitoring through digital processing of high resolution images. Ecol Eng 127:178–186. https://doi.org/10.1016/J.ECOLENG.2018.11.022

Shevade VS, Loboda T (2019) Oil palm plantations in Peninsular Malaysia: determinants and constraints on expansion. PLoS One 14(2):e0210628. https://doi.org/10.1371/JOURNAL.PONE.0210628

Singla S, Eldawy A (2018) Distributed zonal statistics of big raster and vector data. In: GIS: proceedings of the ACM international symposium on advances in geographic information systems, pp 536–539. https://doi.org/10.1145/3274895.3274985

Song DX, Huang C, Sexton JO, Channan S, Feng M, Townshend JR (2015) Use of landsat and corona data for mapping forest cover change from the mid-1960s to 2000s: case studies from the eastern United States and Central Brazil. ISPRS J Photogramm Remote Sens 103:81–92. https://doi.org/10.1016/j.isprsjprs.2014.09.005

Tyukavina A, Baccini A, Hansen MC, Potapov P, Stehman SV, Houghton RA, Krylov AM, Turubanova S, Goetz SJ (2015) Aboveground carbon loss in natural and managed tropical forests from 2000 to 2012. Environ Res Lett 10(7):074002. https://doi.org/10.1088/1748-9326/10/7/074002

WWF Deutschland (2017) Forests

Yap P, Rosdin R, Abdul-Rahman AAA, Omar AT, Mohamed MN, Rahami MS (2021) Malaysian sustainable palm oil (MSPO) certification progress for independent smallholders in Malaysia. IOP Conf Ser Earth Environ Sci 736(1):012071. https://doi.org/10.1088/1755-1315/736/1/012071

Zhang D, Wang H, Wang X, Lü Z (2020) Accuracy assessment of the global forest watch tree cover 2000 in China. Int J Appl Earth Obs Geoinf 87:102033. https://doi.org/10.1016/J.JAG.2019.102033

Chapter 11
Climate-Resilient Agriculture Assessment, Targeting and Prioritization for the Adaptation, and Mitigation Initiative in Agriculture (AMIA) in the Cordillera Administrative Region, Philippines

Elizabeth E. Supangco, Janet P. Pablo, Roscinto Ian C. Lumbres, Charis Mae Tolentino-Neric, Levi Ezekiel O. Daipan, Gillian Katherine Inciong, and Ralphael Gonzales

Abstract The research project, "Climate-Resilient Agri-fisheries (CRA) Assessment, Targeting & Prioritization for the Adaptation and Mitigation Initiative in Agriculture (AMIA)" in Cordillera Administrative Region (CAR) contributes to the national government's agenda of addressing climate change threats in the country's agriculture sector. The major outputs include the Climate-Resilient Agri-fisheries (CRA) for the assessment of traditional and CRA cropping practices used by the farmers through cost-benefit analysis (CBA); and climate risk vulnerability assessment (CRVA) to determine the sensitivity and vulnerability assessment of crops of the province of Benguet. The CRVA assessment result showed that most of the municipalities in Benguet were classified as high to very high in terms of vulnerability to climate change based on their adaptive capacity, sensitivity of crops to the different climatic variables (temperature and precipitation) and hazards. Technologies identified for adaptation includes improving rainwater harvesting practice of the farmers to increase the yield and income of farmers especially during periods of drought and irregular rainfall. The use of blight-resistant variety Igorota (PO_3) can result in higher yield, cash returns, total returns, returns above cash costs, and returns above total costs. By planting PO_3, farmers significantly reduced their operational costs by about 50%. Effort is also thus needed to integrate the use of PO_3 with the water-saving practices to determine any synergies that could benefit the farmers in the vulnerable sites.

Keywords Adaptation · Climate Resilient Agri-fisheries · Climate Risk Vulnerability Assessment · Mitigation

E. E. Supangco · C. M. Tolentino-Neric · G. K. Inciong · R. Gonzales
University of the Philippines Los Baños, Los Baños, Laguna, Philippines

J. P. Pablo (✉) · R. I. C. Lumbres · L. E. O. Daipan
Benguet State University, La Trinidad, Benguet, Philippines
e-mail: j.pablo@bsu.edu.ph

11.1 Introduction

The Adaptation and Mitigation Initiative in Agriculture (AMIA) is the Department of Agriculture's (DA) chief integrated effort to contribute to the national government's agenda of addressing climate change threats in the country's agriculture sector. It seeks to enable the Department of Agriculture (DA) to plan and implement strategies to support local communities in managing climate risks—from extreme weather events to long-term climatic shifts. Under the leadership of the DA System-wide Climate Change Office (SWCCO), this project titled "Climate-Resilient Agri-fisheries (CRA) Assessment, Targeting & Prioritization for the Adaptation and Mitigation Initiative in Agriculture (AMIA) in CAR" supports the AMIA 2 in assessment, targeting, and prioritization of climate resilient agri-fisheries technologies and practices in CAR. The major outputs include the Climate-Resilient Agri-fisheries (CRA)—an assessment of traditional and CRA cropping practices used by the farmers through Cost-Benefit Analysis (CBA); and Climate Risk Vulnerability Assessment (CRVA)—sensitivity and vulnerability assessment of crops of the region as well as adaptive capacity of the provinces' agricultural sector in the effects of climate change in the Philippines.

The Cordillera Administrative Region or CAR is composed of six provinces, namely, Abra, Apayao, Benguet, Kalinga, Ifugao, Mountain Province, and two cities, Baguio City and the City of Tabuk. It is bounded by Ilocos Norte and Cagayan in the North, Pangasinan and Nueva Ecija in the south, Cagayan Valley in the east, and the Ilocos Region in the west. Located at the northern part of Luzon, CAR boasts a mountainous topography and rugged terrain, which significantly contributes to the low climate temperature in the region. Having said that, this region experiences Type II and III climate conditions. CAR has abundant natural resources and contributes highly in terms of agriculture and mining in the Philippines. It has an agricultural land area of 177,839 ha which is largely shared by crop lands. Among its major crops are palay, corn, potato, and cabbage. In 2013, the region was the top cabbage producer in the country.

The Cordillera Administration Region, however, also faces the threats of climate change. According to UNDP (2012), CAR is one of the areas in the country that are most vulnerable to climate change. The natural disasters have been continuously affecting the agriculture sector of the region. Recurring intense calamities often result to frequent erosions, landslides, and even crop susceptibility to diseases, which pose a huge impact on the crop production in CAR. Benguet experiences problems on vulnerability to landslides, soil nutrient depletion, and crop failure due to extreme temperatures. Realizing the impact of climate change in the Cordillera region's agriculture sector, climate change adaptation (CCA) measures in agriculture were developed in the provinces of Benguet and Ifugao using the participatory action research approach. The local stakeholders were capacitated to identify and enhance their own sustainable agricultural practices and combine these with knowledge-based technologies that are adaptive to climate change. Expanding and mainstreaming these CCA agricultural measures would help improve the capacity

of the country's farmers in facing the threats of climate change (Sandoval and Baas 2014).

This chapter describes the climate risks vulnerabilities of the agricultural areas and priority crops in Benguet Province as well as the economic benefits of the identified technologies used by the farmers to adapt to the climatic hazards.

11.2 Methodology

11.2.1 Description of the Study Site

This study covers the 13 municipalities of the province of Benguet (Fig. 11.1). Benguet is characterized by mountainous terrains, ridge, and canyons with a temperate and generally pleasant climate. Climate hazards such as persistent strong heavy rains, typhoons, flooding, and frost are experienced by farmers in this municipality. Records of the Philippine Atmospheric, Geophysical and Astronomical Services Administration (PAGASA) Agro-meteorological Station in La Trinidad from 1976 to 2009, show higher temperatures, warmer middays and colder afternoons, longer drought periods, and irregular rainfall (Calora et al. 2011).
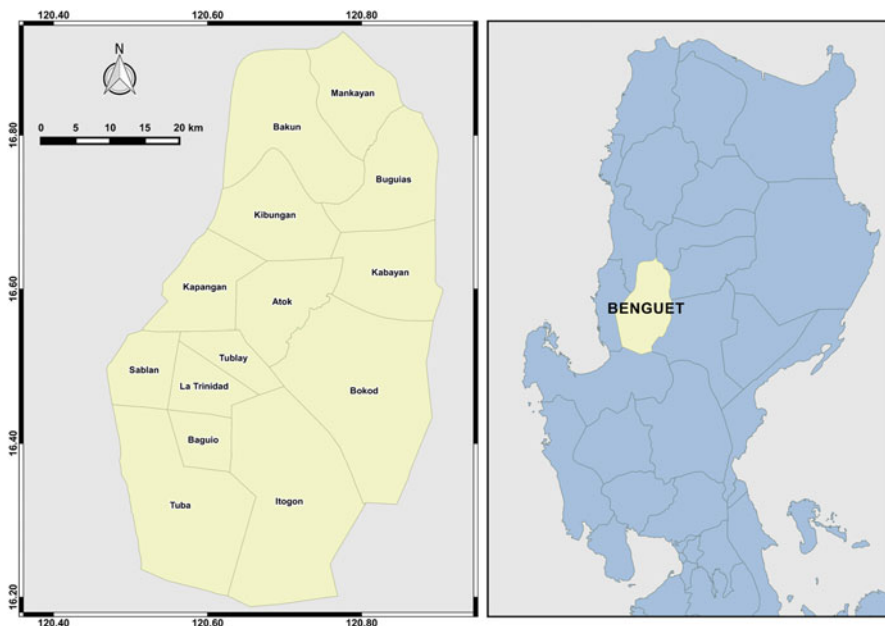

Fig. 11.1 Geographical Location Map of Benguet

11.2.2 Climate Risk Vulnerability Assessment of the Five Major Agricultural Crops in Benguet

The International Center for Tropical Agriculture (CIAT) created a framework in conducting CRVA for different crops in the various provinces of the Philippines as shown in Fig. 11.2. In this framework, three key dimensions are needed to assess the overall vulnerability of a specific crop for the different municipalities, and these are: sensitivity, exposure, and adaptive capacity. The IPCC (2014) definitions for these three concepts are used in this study.
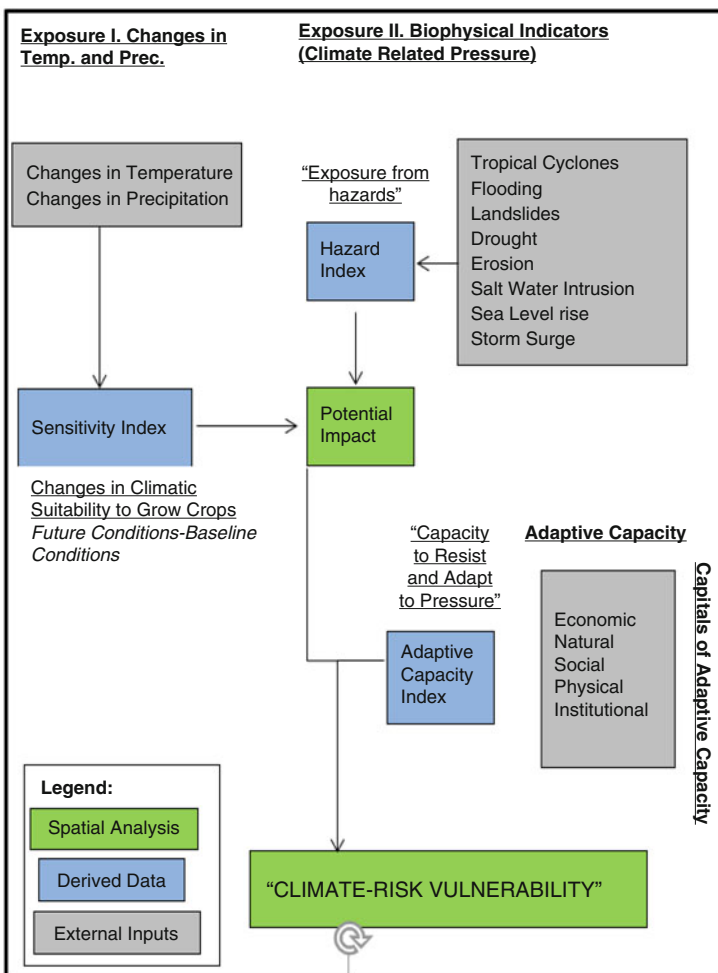

Fig. 11.2 Climate risk vulnerability framework. (Source: Jurgilevich et al. 2017)

All maps were developed by CIAT using the values for hazard, sensitivity, and adaptive capacity provided by the research team. The values for each hazard were normalized to give uniform weights and classifications. This was also done for the sensitivity and adaptive capacity values.

Hazard Assessment

Based on a consultation with relevant stakeholders, Palao et al. (2017) identified eight climate-related hazards that affect crop production in the Philippines, namely, tropical cyclone, flood, drought, erosion, landslide, storm surge, saltwater intrusion, and sea level rise. For Benguet however, representatives of the DA CAR Regional Field Office (RFO) stressed that frost must be included as one of the hazards. Because each hazard varies in degree, intensity, and frequency, the potential damage also varies, especially across the three main islands of the Philippines (Luzon, Visayas, and Mindanao). Thus, each hazard was weighted differently for each island group based on occurrence and impact.

New hazard weights for Benguet were developed with the inclusion of frost as shown on Table 11.1. CIAT provided the hazard maps in raster format and the hazard for each municipality was summarized using the zonal statistics of QGIS (Fig. 11.3). These values were normalized for each hazard using the equation shown below:

$$\text{hazidx\_norm} = \frac{x - x_{\min}}{x_{\max} - x_{\min}} \tag{11.1}$$

where: hazidx_norm is the normalized value of the hazard index and x is the value of a particular hazard, min is minimum value and max is maximum value.

To determine the overall hazard index for each municipality, the normalized value of each hazard for each municipality was multiplied with the corresponding hazard weight and were summed up.

Table 11.1 Hazard scores in the island groups and in Benguet province based on experts' consensus

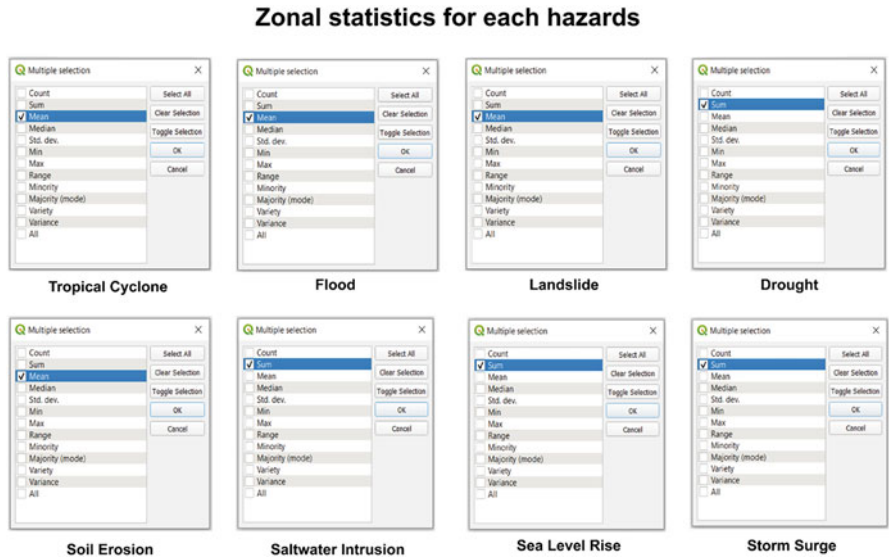| Hazards	Benguet	Island group		
		Luzon (%)	Visayas (%)	Mindanao (%)
Typhoon	19.38	20.00	18.21	16.95
Flood	16.00	19.05	16.40	15.25
Drought	12.92	14.25	16.17	16.95
Erosion	12.92	11.43	12.57	12.71
Landslide	13.37	8.57	10.72	14.41
Storm surge	4.46	9.52	10.39	8.47
Sea level rise	4.46	5.71	8.33	5.08
Saltwater intrusion	4.46	11.43	7.21	10.17
Frost	12.03	–	–	–

Zonal statistics for each hazards

Fig. 11.3 Zonal statistics for the different hazards

Analysis of Adaptive Capacity

CIAT invited various participants to a workshop to identify the different capitals for the determination of adaptive capacity. Participants came from the Department of Agriculture (DA) agencies, National Economic Development Authority (NEDA), United Nations Food and Agriculture Organization (UN-FAO), Non-Government Organizations (NGOs), and the academe. The capitals include economic, natural, human, physical, anticipatory, and institutional. Data were collected from the different agencies such as LGUs, Philippine Statistics Authority (PSA), and others (Table 11.2).

Each indicator for the capitals was normalized and the normalized values were summed up for each capital. Furthermore, the normalized values for each capital of the different municipalities were integrated in the Benguet shapefile that contains municipal boundaries. Five equal breaks were used to classify the adaptive capacity of each municipality: 0–0.20 (Very Low), 0.20–0.40 (Low), 0.40–0.60 (Moderate), 0.60–0.80 (High), and 0.80–1.00 (Very High).

Sensitivity Analysis

The Regional Field Office of the Department of Agriculture in CAR identifies five major crops in Benguet province and these were cabbage, carrot, snap bean, sweet potato, and white potato. Using participatory mapping, the researchers and the representatives from the Municipal Agriculture Office (MAO) of the

Table 11.2 List of capitals with their indicators

Capital	Indicator	Source
Economic	Income level	Benguet-LGU
	– Municipality class	
	Access to credit	Cities and Municipalities Competitive Index (CMCI) (2015)
	– Total number of financial institutions	
	– Number of finance cooperatives	
	Commodity price fluctuation	CMCI (2015)
	– Average inflation rate	
	Agriculture minimum wage (plantation/nonplantation)	CMCI (2015)
	Agriculture minimum wage (finance institutions)	Benguet-LGU
	Number of Micro Finance Institutions	CMCI (2015)
	Total Number of Banks and Finance Institutions	CMCI (2015)
	Average Diesel Price	CMCI (2015)
Natural	Supporting ecosystems and their health (e.g., mangroves, forests, lakes, coral reefs)	CMCI (2015)
	– Forest cover	
Human	– Number of Public Transport Vehicles	Benguet LGU
	– Ratio of schoolteachers to students	CMCI (2015)
	– Number of private secondary schools	CMCI (2015)
	– Number of secondary schools	CMCI (2015)
	– Number of public tertiary schools	CMCI (2015)
	– Number of public technical vocational schools	CMCI (2015)
	– Public health services	CMCI (2015)
	– Private doctors	CMCI (2015)
	– Private health service	CMCI (2015)
	– Health services manpower	CMCI (2015)
	– Public doctors	CMCI (2015)
	– Local citizen with Phil Health	CMCI (2015)
	– Total Public Health Facilities	CMCI (2015)
Physical	Access to irrigation infrastructure (total irrigated area in hectares)	CMCI (2015)
	– % of crops irrigated	
	Percent of Households (HH) with water services	CMCI (2015)
	Percent of HH with electricity services	CMCI (2015)
	Electricity Firms and customers (average)	CMCI (2015)
	Total Road Network	CMCI (2015)
	Road Density	CMCI (2015)
	Infra investment	CMCI (2015)
	Percent Infra to LGU Budget	CMCI (2015)
Anticipatory	Telephone companies and mobile services	CMCI (2015)
	Presence of DRRMO	CMCI (2015)
	Presence of Early Warning Systems	CMCI (2015)
	DRRM Budget Allocation	CMCI (2015)

(continued)

Table 11.2 (continued)

Capital	Indicator	Source
Institutional	Presence of Office Implementing CLUP	CMCI (2015)
	Presence of Executive Order and Ordinance	CMCI (2015)
	Presence of DRRMP	CMCI (2015)

13 municipalities of Benguet located the production areas of the 5 major crops. The mapping workshop enabled the rapid location of the production areas. Each participant worked with a 1 km by 1 km grid map, barangay boundary map, Google earth satellite image, and digital elevation model map. The participants then pointed out if a particular crop occurs in a specific grid.

In order to determine the sensitivity of a crop to climate change, Maximum entropy (MaxEnt) were used. MaxEnt model is a crop distribution model commonly used to estimate most suitable areas for a species or crop based on probability in geographic areas where the distribution of crops is scarce (Elith and Burgman 2002). This model makes use of the climatic conditions that meet the crop's environmental requirements and predicts the relative suitability of location (Davis et al. 2012). These requirements are represented by bioclimatic variables, which are combined to determine areas most suitable for the crop.

Using the MaxEnt program, researchers were able to determine the best location for the 5 major crops using 19 bioclimatic variables to assess the suitability of the selected crops in Benguet province (Table 11.3). For current conditions, datasets (available at WorldClim.org) were used. The described bioclimatic factors are relevant to understand species responses to climate change (O'Donell and Ignizio 2012). Eleven of the bioclimatic variables are temperature related and the eight are precipitation related.

Furthermore, this program also determined the best location of the five major crops based on future climatic projections. Representative concentration pathway (RCP) 8.5 scenario was used to project future climatic variables in the year 2050. RCP 8.5 is the worst-case scenario among the four scenarios (RCP 2.6, RCP 4.5, RCP 6, and RCP 8.5) developed by the IPCC. These scenarios are based on the projected amount of carbon dioxide (CO_2) emission.

To determine the sensitivity of each crop for the different municipalities, the equation suggested by CIAT was used in this study and this is shown below (Palao et al. 2017):

$$\frac{\text{Projected Conditions} - \text{Current Conditions}}{\text{Current conditions}} \times 100 \qquad (11.2)$$

An index was developed from −1.0 to 1.0 for the CRVA where the range from 0.25 to 1.0 indicates a loss in suitability, while −0.25 to −1.0 indicates a gain in suitability to climate change (Table 11.4).

Table 11.3 Bioclimatic variables used in sensitivity modeling

Parameters	Description
Bio 1—Annual mean temperature	Annual mean temperature derived from the average monthly temperature
Bio 2—Mean diurnal range	The mean of the monthly temperature ranges (monthly maximum minus monthly minimum)
Bio 3—Isothermality	Oscillation in day-to-night temperatures
Bio 4—Temperature seasonality	The amount of temperature variation over a given year based on standard deviation of monthly temperature averages
Bio 5—Maximum temperature of warmest month	The maximum monthly temperature occurrence over a given year (time-series) or averaged span of years (normal)
Bio 6—Minimum temperature of coldest month	The minimum monthly temperature occurrence over a given year (time-series) or averaged span of years (normal). Variation over a given period
Bio 7—Temperature annual range	A measure of temperature
Bio 8—Mean temperature of wettest quarter	This quarterly index approximates mean temperatures that prevail during the wettest season
Bio 9—Mean temperature of driest quarter	This quarterly index approximates mean temperatures that prevail during the driest quarter
Bio 10—Mean temperature of warmest quarter	This quarterly index approximates mean temperatures that prevail during the warmest quarter
Bio 11—Mean temperature of coldest quarter	This quarterly index approximates mean temperatures that prevail during the coldest quarter
Bio 12—Annual precipitation	This is the sum of all total monthly precipitation values
Bio 13—Precipitation of wettest month	This index identifies the total precipitation that prevails during the wettest month
Bio 14—Precipitation of driest month	This index identifies the total precipitation that prevails during the driest month
Bio 15—Precipitation seasonality	This is a measure of the variation in monthly precipitation totals over the course of the year. This index is the ratio of the standard deviation of the monthly total precipitation to the mean monthly total precipitation and is expressed as percentage
Bio 16—Precipitation of the wettest quarter	This quarterly index approximates total precipitation that prevails during the wettest quarter
Bio 17—Precipitation of driest quarter	This quarterly index approximates total precipitation that prevails during the driest quarter
Bio 18—Precipitation of warmest quarter	This quarterly index approximates total precipitation that prevails during the warmest quarter
Bio 19—Precipitation of coldest quarter	This quarterly index approximates total precipitation that prevails during the coldest quarter

Source: http://www.WorldClim.org

Climate Risk Vulnerability Assessment (CRVA)

To determine the vulnerability of each crop for the different municipalities, hazard, sensitivity, and adaptive capacity were summed up based on their weights. For the Adaptive capacity, it was 70% while it was 15% for hazard and sensitivity. Different

Table 11.4 Sensitivity index based on percent change in crop suitability from baseline to future condition

Percent change in suitability (range in %)	Index	Description
≤−50 (Very high loss)	1.0	Loss
>−50 and ≤−25 (High loss)	0.5	
>−25 and ≤−5 (Moderate loss)	0.25	
>−5 and ≤5 (No change)	0	No change
>5 and ≤25 (Moderate gain)	−0.25	Gain
>25 and ≤50 (High gain)	−0.5	
>50 (Very high gain)	−1.0	

Source: Palao et al. (2017)

Table 11.5 Scenarios with different weights for adaptive capacity, sensitivity, and hazard

Scenario	Adaptive capacity (%)	Sensitivity (%)	Hazards (%)
1 (reference)	70	15	15
RCP 2.6	33	33	33
RCP 4.5	50	25	25
RCP 6	60	20	20
RCP 8.5	40	30	30

scenarios were also created using different weights for adaptive capacity, hazard, and sensitivity (Table 11.5).

The equation used is shown below:

$$f(\text{Haz}, \text{Sens}, \text{AC}) = \sum_{n=i}^{n}\left(\left(\text{Haz}_{(w_h)} + \text{Sens}_{(w_s)}\right) + 1 - \text{AC}_{w_a}\right) \quad (11.3)$$

where: Haz = hazard index, Sens = sensitivity index ($_i$ = crop), and AC = adaptive capacity index. w_h = weight given for hazard, w_s = weight given for sensitivity, and w_a = weight given for adaptive capacity.

11.2.3 Climate-Resilient Agri-fisheries (CRA) Assessment, Targeting and Prioritization

To assess the CRA, researchers had a series of meetings with the Municipal Agricultural Office and the Department of Agriculture-Regional Field Unit to gather preliminary data and information regarding the identification of study sites and the adaptation strategies employed by farmers. A community meeting in Atok, Benguet and focus group discussion in Buguias, Benguet enabled the identification of climate hazard exposure and technological adaptation or CRA. Structured questionnaires were used to gather data from CRA and non-CRA practitioners in both

municipalities. Profitability of engaging in CRA was determined using cost and return analysis. The online Cost-Benefit Analysis tool (CBA) was used to determine the NPV, IRR, and payback period of the technologies used. Comparison of means using *t*-test was done in order to separate the CRA and non-CRA users.

The crops chosen for the study were those identified as priority crops by the Department of Agriculture—Regional Field Office of the Cordillera Region based on the volume and area of production. During the inception meeting, potato, cabbage, rice, and *camote* (sweet potato) were identified as the priority crops; however, potato and cabbage were prioritized for the CRA identification. Cabbage and white potato are popular vegetable cash crops grown in Benguet by small-, medium-, and large-scale farmers because they produce a very lucrative return on investment. The CRA practices of the farmers for both crops were validated during the FGD with the farmer stakeholders and the Municipal Agriculture Office Staff.

11.3   Results and Discussion

11.3.1   Climate Risk Vulnerability Assessment of the Five Major Agricultural Crops in Benguet

Hazard Assessment

This section describes the results of the VA based on six hazards to come up with the hazard index. These include tropical cyclone, flood, drought, erosion, landslide, and frost. Storm surge, saltwater intrusion, and sea level rise were not included in the analysis because Benguet is a landlocked province and therefore does not experience these hazards. Each hazard map was provided by CIAT. The values for each hazard were normalized to give uniform weights and classifications. Table 11.6 summarizes the hazard indices of the six hazards measured for sites in Benguet. The sites are listed in the table based on their location in the province from north to south. This was done in an attempt to determine if there is a pattern to the hazards measured based on geography. There is a pattern that can be seen but as there were no statistics involved, the pattern is only indicative.

Half of the sites are vulnerable to tropical cyclones, although flooding (which may result from the cyclones) is of importance in only two of the southern sites, La Trinidad and Itogon, which are generally of lower elevation than the rest. Drought is not a major concern except in Tuba. On the other hand, the dangers from frost are high to very high in the northern sites, especially Bakun, Buguias, Kabayan, and Bokod. There is also a clustering evident for the northern sites involving higher vulnerability to erosion, landslide, and frost. On the other hand, the southern sites of Tuba, Baguio City, and Itogon show medium to very high vulnerability for both erosion and landslide but not to frost.

Table 11.6 Summary of hazard indices of the six hazards measured for sites in Benguet Province, Philippines

SITE	Tropical Cyclone	Flood	Drought	Erosion	Landslide	Frost
Mankayan				Very High		Low
Bakun		Low		High	Moderate	Very High
Buguias	Moderate				High	Very High
Kibungan				Moderate	Very High	Moderate
Kabayan	Moderate				Very High	High
Kapangan				Low	Low	
Atok	Low				Very High	Low
Bokod	Very High	Low		Moderate	Moderate	Very High
Sablan	Low		Low		Very High	
Tublay	High					
La Trinidad	High	Very High			Low	
Tuba			High	Very High	Moderate	Low
Baguio City	Moderate			High	Moderate	
Itogon	Moderate	Very High	Moderate	Moderate	Very High	

| LEGEND | Very High | High | Moderate | Low | Very Low | |

Tropical Cyclone

An average of 20 tropical cyclones enters the Philippine Area of Responsibility (PAR) from January to November (PAGASA 2009). Thus, has the highest weight among all hazards and it is most prominent in Northern Luzon (Palao et al. 2017). Tropical cyclones are classified as tropical depressions, tropical storms, and typhoons. Typically, within a year, there are about four (4) to six (6) tropical depressions, three (3) to five (5) tropical storms, and six (6) to nine (9) typhoons that develop within the PAR. Results (Fig. 11.4) show that Benguet is divided lengthwise, i.e., north to south, when it comes to exposure to tropical cyclones. The eastern municipalities of Tuba, Bakun, Kapangan, Mankayan, Kibungan, Sablan, and Atok have the least exposure (low to very low) to tropical cyclones. On the west side, Baguio City, and the municipalities of Buguias, Kabayan, and Itogon have moderate exposures while the municipalities of La Trinidad, Tublay, and Bokod have the highest exposures.

Flood

Flood is one of the major problems in the country, primarily during the monsoon season, and it is caused by either typhoons or enhanced southwest monsoons. An
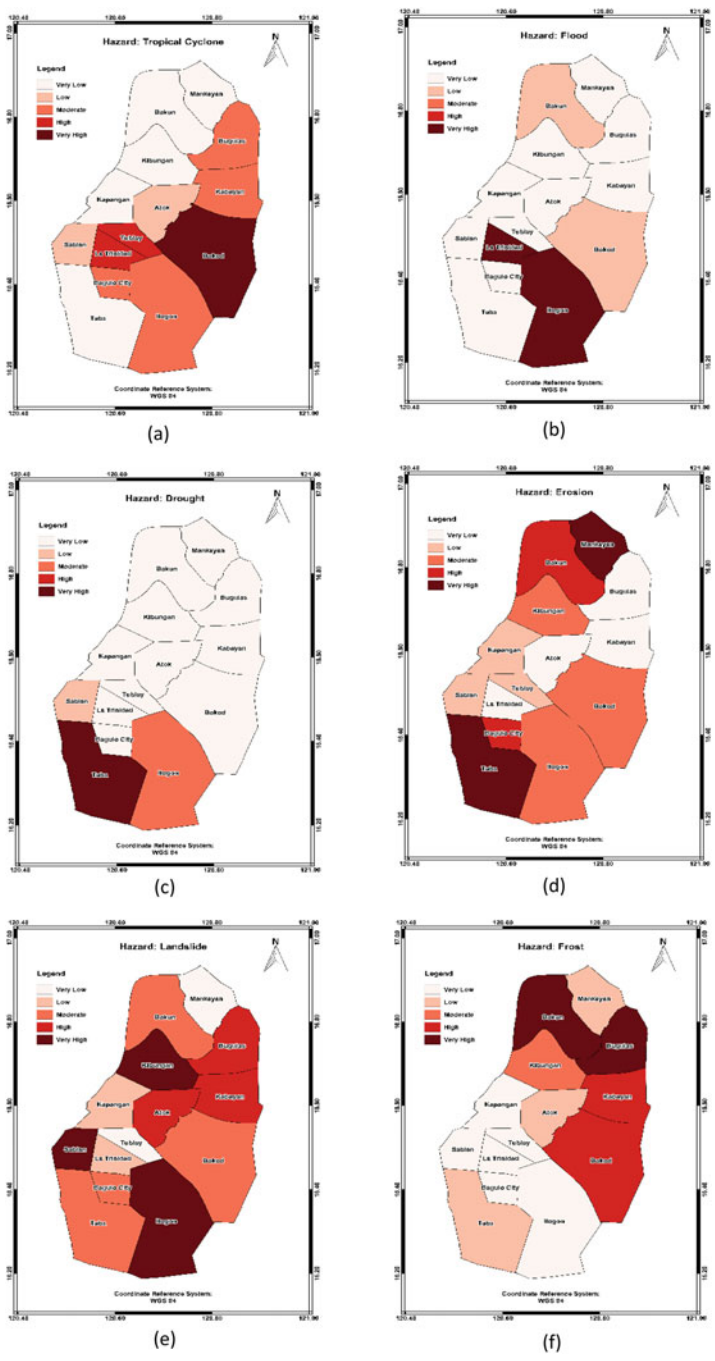
Fig. 11.4 Normalized (**a**) tropical cyclone, (**b**) flood, (**c**) drought, (**d**) erosion, (**e**) landslide, (**f**) frost index of the different municipalities in Benguet

enhanced southwest monsoon is a weather system where a typhoon or low pressure area located outside the PAR enhances the southwest monsoon winds that brings heavy rainfall in Luzon and parts of the Visayas. Flood dataset was acquired from the multihazard AMIA dataset in raster format (Palao et al. 2017). Figure 11.4 shows that La Trinidad and Itogon are the most prone to flooding. The municipalities of Bakun have low exposure, while Mankayan, Buguias, Sablan, Kapangan, Tublay, Kabayan, Atok, Kibungan, and Tuba have very low exposure.

Drought

Drought is one of the most challenging hazards to monitor because of the slow onset of its effects, and it is also difficult to observe and forecast quite well. Based on the results, the municipality of Tuba has the highest exposure to drought, followed by the municipality of Itogon (moderate), and Kapangan (low). All other municipalities, have the least exposure to drought as shown in Fig. 11.4. Knowledge of the possibility that drought can occur in a site will enable the farmer to act accordingly. They can choose either to avoid planting during those times that drought is likely to occur in the site or to choose varieties of crops with high tolerance to drought (Tad-awan and Shagol 2016).

Erosion

Erosion is a natural occurring process attributed to different factors such as soil properties, ground slope, vegetation/land cover, and the amount and intensity of rainfall (Montgomery 2007). It is usually a slow and gradual process, which involves movement of rocks and loosened soil on the Earth's surface from one place to another. In the coming years, the soil erosion rate is expected to increase due to higher amount of rainfall and more frequent extreme events brought by climate change. An increase in erosion rate may lead to poor soil productivity and accelerated siltation of waterways and reservoirs (Lal 2010). Based on the results, Mankayan and Tuba are the municipalities that are most prone to soil erosion. These were followed by the municipality of Bakun. Kibungan, Itogon, and Bokod are considered moderate. La Trinidad along with the six other municipalities have the least exposure to soil erosion. Half of the sites are prone to erosion. This reflects the reported vulnerability of Benguet (Benguet PENRO 2019) to erosion, as 81.03% of its lands are classified as severe.

Landslides

Landslides, also known as landslip, is a geological phenomenon, which includes a wide range of ground movements, such as rockfalls, deep failure of slopes, and shallow debris flows, which can occur in offshore, coastal, and onshore

environments. Landslides are caused when the force of gravity pulls rocks, debris, or soil down a slope. Fundamentally, they are one of the forms of erosion called mass wasting, defined as erosion involving gravity as the agent causing movement. Gravity constantly acts on a slope. Consequently, landslides only occur when the downslope weight or the driving force of the slide mass exceeds the strength of the soil or the resisting force along a slip surface. This happens when the water from rain sinks through the earth on top of a slope, seeps through cracks and pore spaces in underlying sandstone, and encounters a layer of slippery material, such as shale or clay, inclined toward the valley (Cruden and Arnes 1996).

In Benguet, the municipalities of Itogon, Kibungan, and Sablan are most exposed to landslides. Kabayan, Atok, and Buguias are also highly exposed to landslides. Furthermore, the municipalities of Bokod, Bakun, and Tuba are moderately exposed and the municipalities of Kapangan, La Trinidad, Tublay, and Mankayan have the least exposure to landslides. These results are not surprising as at least 60.16% of Benguet has a very steep slope (>50%) (Benguet PENRO 2019). On the whole, 80% of Benguet is steep to very steep and the remaining portion is distributed to level to nearly level, rolling, and rolling to moderately steep. The areas with least exposure represent less than 1% (0.99%) of the total land area of Benguet with slopes greater than 50%.

Frost

Frost usually forms in low lying areas, like Buguias and Bakun. Frost is a hazard that is unique to Benguet province. The municipalities of Buguias and Bakun were classified as very high in terms of exposure to frost. Kabayan and Bokod were classified as high while Kibungan had a moderate classification in frost hazard. As cool air sinks usually at night, it collects in the valleys and forms frost. Thus, it is in the higher altitude valleys that it is most experienced. When the frost melts in the daytime, it also destroys the vegetables on which it formed.

Hazard Index

The nine hazards were combined for the different municipalities using the assigned weights (Fig. 11.5). In Benguet, tropical cyclone, soil erosion, and landslide are consistently rated high across the 13 municipalities and are considered the major driving factors of high hazard exposure at the same time high hazard index. Based on the results, the municipality of Itogon has a very high exposure to hazards and it was followed by the Bokod municipality. While the municipalites of La Trinidad, Tuba, Buguias, and Bakun were classified as moderately hazardous. On the other hand, Mankayan, Kapangan, and Tublay municipalities are considered very low in hazard exposure as compared to other municipalites in Benguet province.

**Fig. 11.5** Overall hazard index map of Benguet
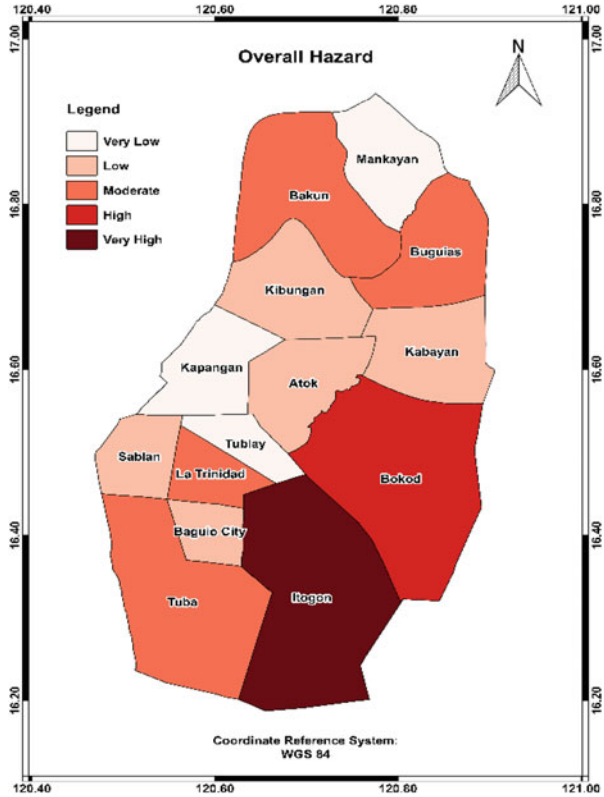
Adaptive Capacity Assessment

The adaptive capacity was based on a set of capitals including economic, natural, social, human, physical, anticipatory, and institutional. Each capital has indicators that were used as basis for each municipality's adaptive capacity. These factors have been previously defined as the factors that hold the key to adaptability and change (Ellis 2000). The concept of adaptive capacity depends on the level of strength and weakness and the balance between the capitals (Leonard 2010).

Anticipatory Capital

There are four (4) indicators used for the anticipatory capital: (a) presence of Disaster Risk Reduction Management Office (DRRMO), (b) presence of early warning systems, (c) number of telephone companies and mobile service providers, and (d) DRRM budget. Based on the results (Fig. 11.6), the municipality of La Trinidad has the highest adaptive capacity (very high) in terms of the anticipatory capital, followed by Tuba (moderate). The municipalities of Tublay and Sablan have low

Fig. 11.6 Normalized (**a**)
anticipatory, (**b**) economic,
(**c**) human, (**d**) natural, (**e**)
institutional, (**f**) physical,
and (**g**) social capital map of
Benguet
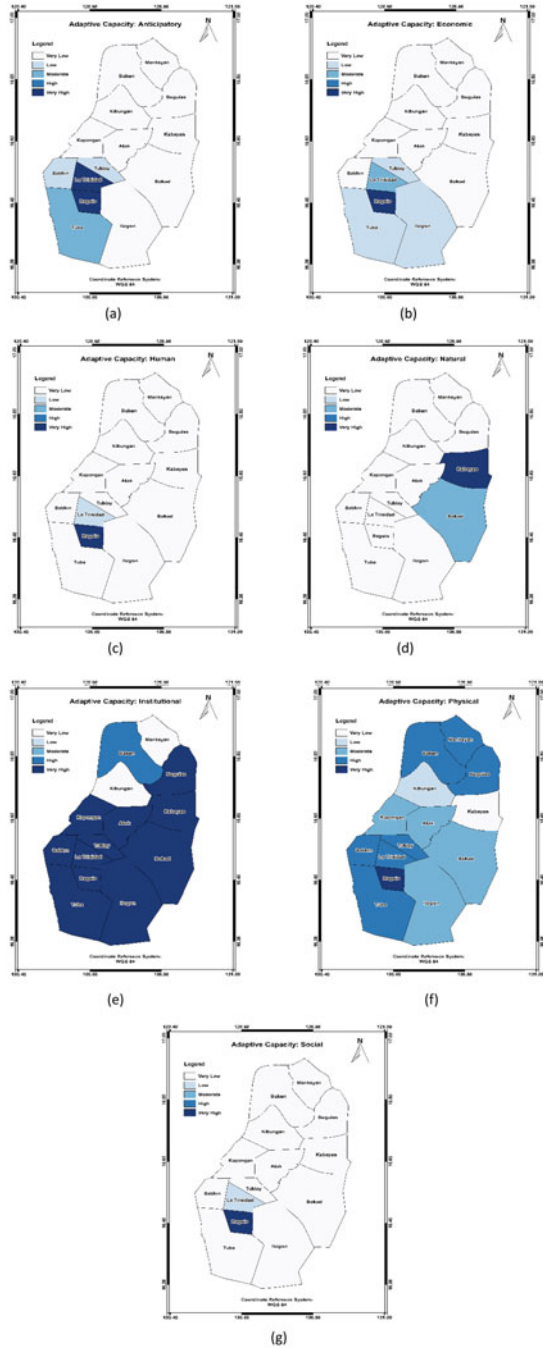
adaptive capacity. All other municipalities including Kibungan, Kapangan, Kabayan, Itogon, Buguias, Bokod, and Atok, have low adaptive capacity and the municipalities of Mankayan and Bakun as well.

Economic Capital

The economic capital includes municipality class, total number of finance institution, number of finance cooperatives, average inflation rate, agriculture minimum wage, number of microfinance institutions, and average diesel price. These indicators reflect the level, variability, and diversity of income sources, and access to other financial resources such as credit and savings For this capital, the municipality of La Trinidad has the highest adaptive capacity (moderate) as compared to all other municipalities (Fig. 11.6). On the other hand, the municipality of Itogon, Tuba, and Tublay have low economic adaptive capacity. All other municipalities have very low economical adaptive capacity. La Trinidad is the capital town of Benguet. As such, most of the financial institutions are located there. Thus, its residents have much better access to financial institutions and most likely will also have relatively higher wages than the other sites, except for the City of Baguio.

Human Capital

Capital has the highest number of indicators including the ratio of schoolteachers to students, number of private secondary schools, number of secondary schools, number of public tertiary schools, number of public technical vocational schools, public health services, private doctors, private health service, health services manpower, public doctors, local citizens with Phil Health, total public health facilities, and total private health facilities. For the human capital, all municipalities have low to very low adaptive capacity in terms of human capital including the capital town of La Trinidad.

Institutional Capital

There are three indicators for the institutional capital: (a) presence of offices implementing Comprehensive Land Use Plan (CLUP), (b) Presence of Executive Orders and Ordinances, and (c) presence of Disaster Risk Reduction Management Plan (DRRMP). The results show that almost all municipalities have high adaptive capacity in terms of this capital except for the municipalities of Kibungan and Mankayan, both with values of 0. The municipality of Bakun with a value of 0.67 has high institutional adaptive capacity and all other municipalities including Tublay, Tuba, Sablan, La Trinidad, Kapangan, Kabayan, Itogon, Buguias, Bokod, and Atok have very high institutional adaptive capacity, all with values of 1.

Natural Capital

Forest cover is the only indicator for the natural capital. Among all other municipalities, Kibungan has the highest (very high) natural adaptive capacity in terms of this capital followed by Bokod (moderate). The municipality of Itogon, and all other municipalities, have very low adaptive capacity. Figure 11.6 shows the adaptive capacity map of Benguet in terms of natural capital. This may reflect the fact that Benguet has the smallest area of natural closed forest in the Region (PSA CAR 2020).

Physical Capital

Physical capital refers to the infrastructure, equipment, and improvements in genetic resources such as for crops and livestock (Leonard 2010). For this capital, the indicators include percent of crops irrigated, percent of households (HH) with water services, percent of HH with electricity services, average number of electricity firms and customers, total road network, road density, infrastructure investment, and percent infrastructure to LGU Budget. Based on the map (Fig. 11.6), the municipalities of Kibungan and Kabayan have the least physical adaptive capacity. This can be explained by their relative distance from the capital or business center, as well as the relative difficulty in reaching some of the communities in these places. The municipalities of Bokod, Kapangan, Itogon, and Atok have moderate physical adaptive capacity. On the other hand, the municipalities including Bakun, Tuba, Mankayan, La Trinidad, Sablan, and Buguias, have high physical adaptive capacity.

Social Capital

The number of public transport vehicles is the only indicator that contributes for the social capital. The result (Fig. 11.6) shows that all of the 13 municipalities have low to very low adaptive capacity in terms of public transportation. With values ranging from 0 to 0.20, the municipalities of Bokod, Kibungan, Bakun, Atok, Kabayan, Tuba, Kapangan, Tublay, Sablan, Mankayan, Buguias, and Itogon have very low social adaptive capacity. On the other hand, the municipality of La Trinidad, with a value of 0.22, has low social adaptive capacity.

Adaptive Capacity Index

The adaptive capacity inherent in a system represents the set of resources available for adaptation, as well as the ability or capacity of that system to use these resources effectively in the pursuit of adaptation. Such resources may be natural, financial, institutional, or human, and might include access to ecosystems, information, expertise, and social networks. There are many indicators that could form a strong

Fig. 11.7 Normalized
adaptive capacity map of the
different municipalities of
Benguet province
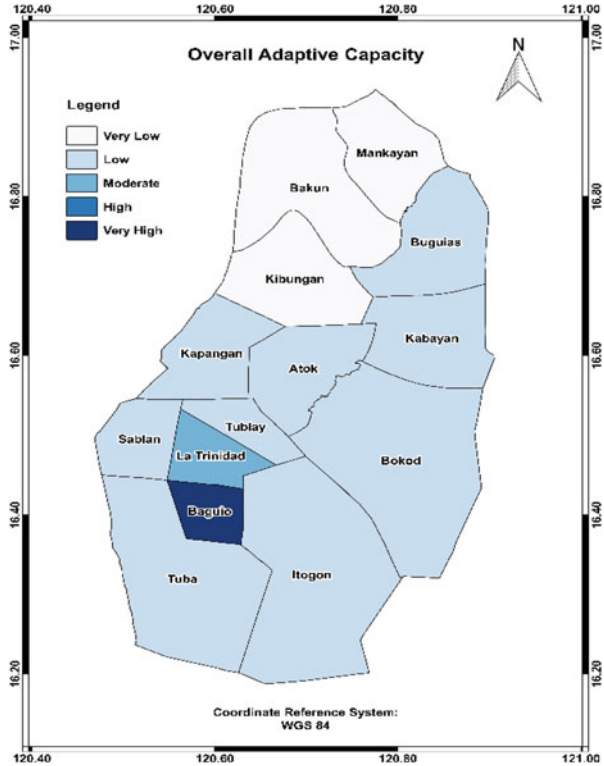
adaptive capacity index, but data availability was a driving factor in establishing the
final index for the province of Benguet. The following presents the spatial analysis of
all seven capitals as well as the aggregated overall adaptive capacity index
(Fig. 11.7). It can be seen that almost all of the municialities have low adaptive
capacity with La Trinidad having moderate adaptive capacity.

Sensitivity Analysis

The municipalities of Buguias, Kabayan, and Tuba are expected to be the most
sensitive for cabbage, carrot, and white potato production using the Maxent program
and based on the different bioclimatic variables used in this study. Results also
showed that snap bean production will be more sensitive in La Trinidad and Tuba.
For the sweet potato, it is projected that the municipality of Tuba will have the
highest loss as compared to other municipalities (Table 11.7). On the other hand,
Bokod, Kibungan, and Kapangan are expected to gain production for the cabbage
(Fig. 11.8). For the carrot production, Atok, Bokod, Itogon, Kibungan, and
Kapangan are expected to have future gains. For snap bean, municipalities of
Atok, Bakun, Bokod, Kibungan, Kapangan, and Sablan are projected to have

Table 11.7 Sensitivity of the major crops in the different municipalities in Benguet province

Crop	Loss	No change	Gain
Cabbage	Buguias, Kabayan, Tuba	Atok, Bakun, Itogon, La Trinidad, Mankayan, Sablan, Tublay	Bokod, Kibungan, Kapangan
Carrot	Buguias, Kabayan, Sablan, Tuba	Bakun, La Trinidad, Mankayan, Tublay	Atok, Bokod, Itogon, Kibungan, Kapangan
Snap bean	La Trinidad, Tuba	Buguias, Itogon, Kabayan, Mankayan, Tublay	Atok, Bakun, Bokod, Kibungan, Kapangan, Sablan
Sweet potato	Tuba	Buguias, Kabayan, Kapangan, La Trinidad, Mankayan, Sablan	Atok, Bakun, Bokod, Itogon, Kibungan, Tublay
White potato	Buguias, Kabayan, Tuba	Bakun, La Trinidad, Mankayan, Sablan, Tublay	Atok, Bokod, Itogon, Kibungan, Kapangan

gains in the production based on the bioclimatic variables. The municipalities of Atok, Bakun, Bokod, Itogon, Kibungan, and Tublay are projected to have gains for sweet potato while the municipalities of Atok, Bokod, Itogon, Kibungan, Kapangan for the white potato production.

Overall CRVA Assessment

The three key dimensions which are hazard (15%), adaptive capacity (70%), and sensitivity (15%) were combined to determine the overall vulnerability of the different municipalities in Benguet province for the various major crops (Fig. 11.9). Furthermore, this assessment focused on the agricultural sector and therefore Baguio City was excluded from the CRVA. For cabbage, snap bean, and white potato, the municipalities of Bakun, Itogon, Kibungan, and Mankayan have the highest vulnerability. Bakun, Kibungan, and Mankayan are classified as very highly vulnerable for carrot and sweet potato production.

11.3.2 Climate-Resilient Agri-fisheries (CRA) Assessment, Targeting and Prioritization

Climate Risk and Mitigation and Adaptation Strategies for Cabbage Production

Assessment of Exposure and Sensitivity to Climatic Hazards

Farmers and local officials who participated in the focus group discussion identified the occurrence of landslide, drought, hailstorm, frost, and strong winds as the major climatic hazards. Landslide occurs due to continuous monsoon rain, heavy rain, and
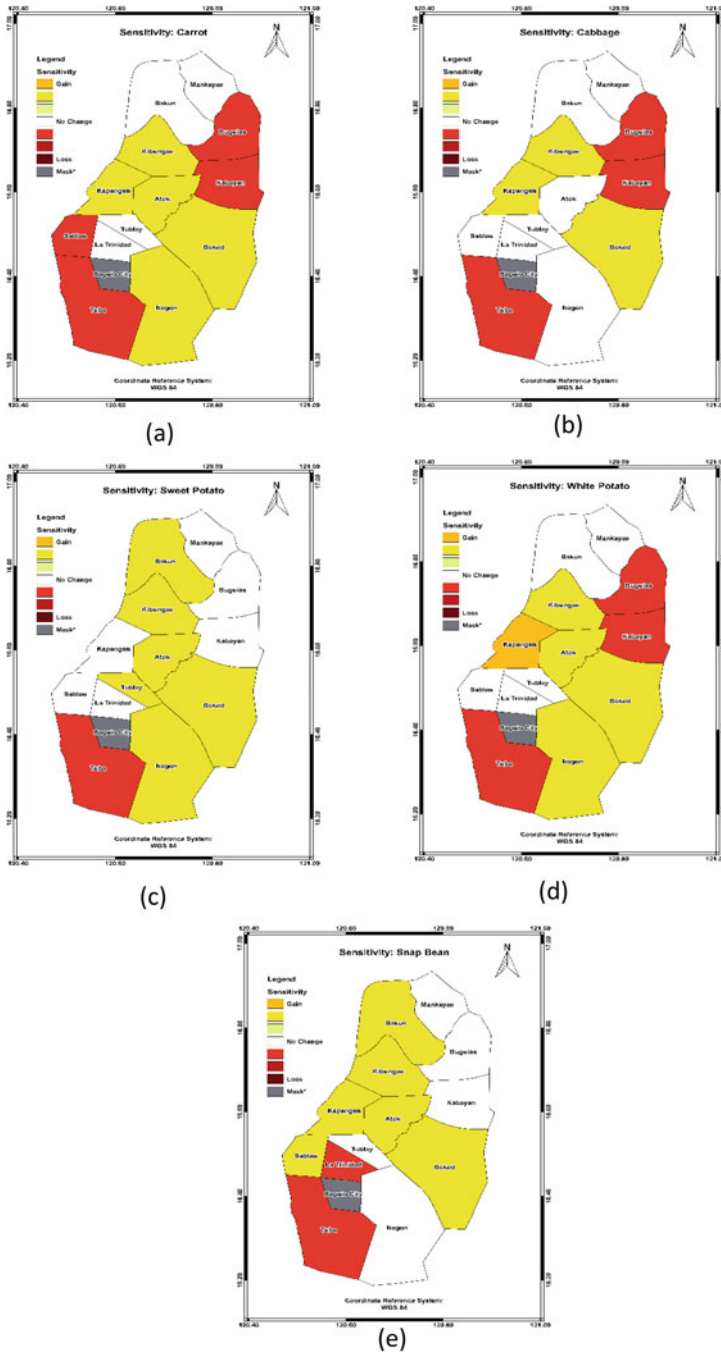
Fig. 11.8 Sensitivity map of (**a**) carrot, (**b**) cabbage, (**c**) sweet potato, (**d**) white potato, and (**e**) snap bean in the different municipalities of Benguet province
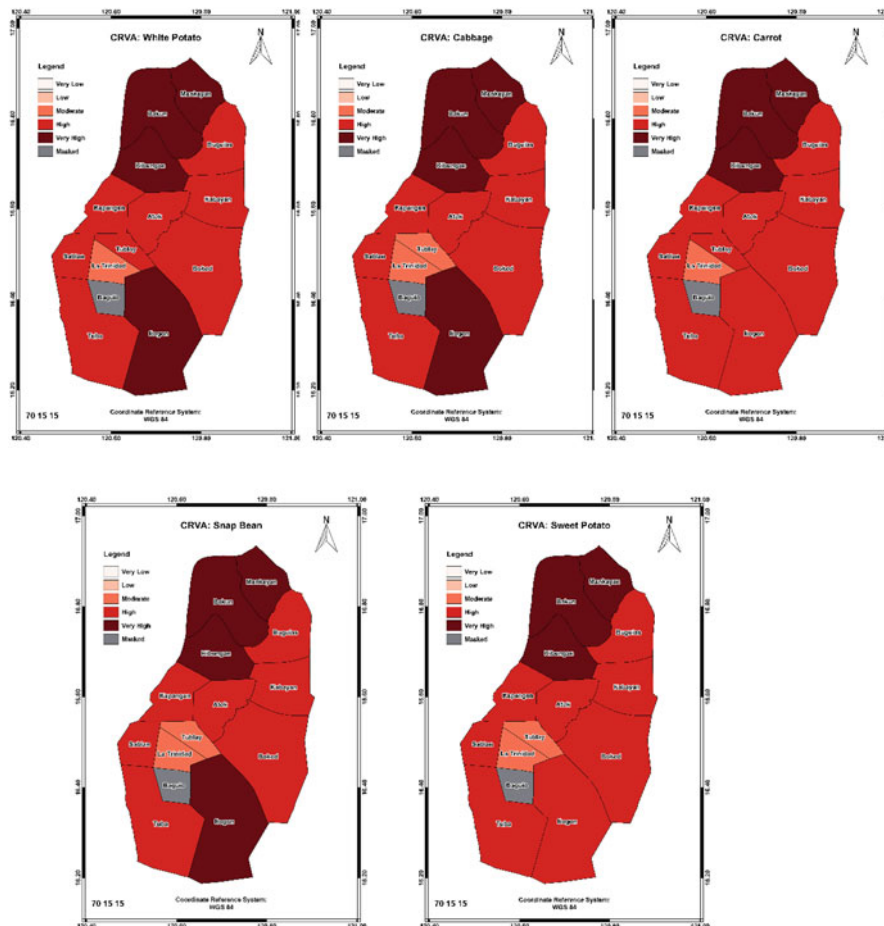
Fig. 11.9 Climate risk vulnerability map of the five crops in the different municipalities of Benguet province

typhoon. This reduces the planting areas, especially if the area is sloping. Road closures are also frequent during landslides due to the blocking of farm-to-market roads. Undelivered harvest is a common problem faced by the farmers. During the community meeting and FGD, the farmers estimated an average of 50% reduction in the volume of leafy vegetables based on experience. This reduction is eventually converted into losses in income. When the supply available in the market is affected, prices of the commodities in the market are also affected.

Drought and a change in the usual pattern of dry and wet season are now experienced in Atok. The dry season normally occurs in the month of April; however, drought is now also experienced even in October, which used to be in the wet season. Since vegetable cultivation is rainfed-dependent, production is limited by the absence of rainfall. Farmers thus can cultivate a limited area only

depending on the water harvested or available irrigation water in the locality. Others would plant crops that require less water or crops that are tolerant to drought such as camote (sweet potato), gabi (taro), and radish. Another hazard experienced is the occurrence of hailstorm especially in the three barangays of Atok: Paoay, Abiang, and Cattubo. Hailstorms normally occur in the locality from February to March but in the last 2 years, farmers observed that hailstorms now occur in September, which is the onset of rainy season. The magnitude of damage of hailstorm during the initial heading stage of cabbage is about 90%. Cabbage does not head after having been hit by a hailstorm.

Moreover, frost occurs for about 3 months from December to February in the same barangays. The farmers also identified strong winds occurring during the months from October to December to be damaging to crops. Two weeks of strong winds is the most detrimental to plants and affects three barangays, which are major growers of cabbage. Farmers report that frost occurrence reduces cabbage production by about 5–30%, especially when around 1 mm of ice covers the leaves. The effect is worse if the frost persists for about 3 days. Generally, plants are sensitive to strong winds, which causes breakage in plants. Some are even uprooted especially with continuous strong winds. Strong winds occurring during the vegetative stage of the cabbage plants results in about 95% damage and if the occurrence is during the heading stage, only about 80% of the plants can be salvaged.

All of the above climate-related hazards were claimed to be damaging to crop production; however, farmers rated the absence of rain or prolonged drought as the most damaging. Because the farmers rely on rainfall for their irrigation, planting can be delayed or may not happen at all for that cropping season. The overall CRVA showed that cabbage production is exposed to higher hazards in the Itogon Municipality while lower in the other municipalities. Sensitivity of cabbage production is higher in Tuba, Buguias, and Kabayan municipalities, while higher adaptive capacity is noted in Mankayan and Kibungan municipalities. For potato production, higher exposure to climate hazards is recorded in Itogon and greater sensitivity in the municipalities of Tuba, Buguias, and Kabayan. Similarly, the municipalities of Mankayan Bakun, and Kibungan have more adaptive capacities (Fig. 11.10).

Assessment of Mitigation and Technological Adaptive Capacity

Benguet farmers employ several adaptation strategies in response to the adverse effects of climate change. They establish drainage canals to direct water and prevent soil erosion. For hailstorm and frost, the farmers' most common adaptation is to irrigate or spray the plants with water before the sun rises to thaw the ice deposits on the leaves. The cabbage seedlings are protected from hailstorm by using black net as cover. However, farmers mentioned that there is no adaptation strategy yet for strong winds. The government's intervention such as provision of few greenhouses for common use is limited to seedling and nursery use, and only for cut flower production.
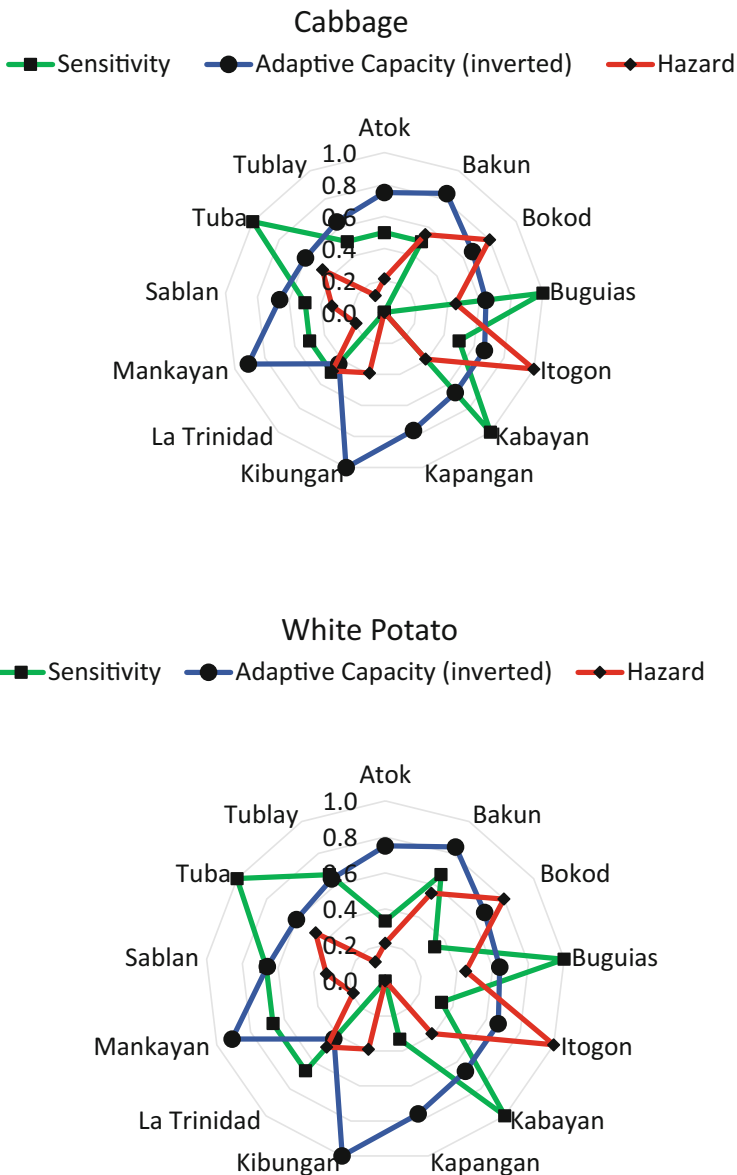
Fig. 11.10 Overall CRVA of cabbage and white potato considering the weights for 15% for hazard, 15% sensitivity, and 70% adaptive capacity

During the dry season, the farmers use an improvised rainwater harvester, called "kwelo." During the rainy season, farmers improvise catchment basins by digging large pits lined with large plastic sheets or use tarpaulins for rainwater harvesting.

Those who can afford it build concrete water tanks. Depending on the amount of rainwater harvested, farmers are able to cultivate a limited area for vegetable production. Improving the rainwater harvester to be the farmers' source of irrigation is expected to increase farmers' yield and income even during longer drought periods and irregular rainfall. Irrigation water is also needed not only during drought but also when frost occurs, as mentioned earlier. The availability of the facility enhances the resilience of the vegetable farmers as it was claimed to be an effective strategy to cope with climate change in vegetable-producing areas.

Climate Risk and Mitigation and Adaptation Strategies for Potato Production

Assessment of Exposure and Sensitivity to Climatic Hazards

One of the climate-related hazards identified by the respondents in Buguias municipality was the occurrence of strong typhoons, which is usually experienced during November. For the last 3 years, however, strong typhoons are now observed to occur at any month of the year in the municipality. The rains and wind brought about by strong typhoons cause significant damage to crop. The resultant flooding leads to rotting of standing crops. Although prolonged dry season was identified as the most damaging climate hazard experienced by the farmers, increased incidence of pests and diseases was also observed during the dry season, further aggravating the loss in production. Higher population of leaf miner, thrips, aphids, and scab are affecting the potato plants. Hence, farmers resort to increasing the frequency of pesticide application, which further increases the input expenses of the farmers in both upland and lowland areas of the municipality.

Assessment of Mitigating and Technological Adaptive Capacity

Several adaptation options were identified by the farmers in Buguias such as organic farming, mixed farming, mulching, use of sacks or net screens for wind break, and the use of resistant varieties. Farmers in the higher elevation areas of Buguias adapted the use of resistant varieties to pest and diseases. Late blight is the most devastating potato disease, where fungicide spraying is necessary especially during the wet season cropping. Frequency of application is almost twice a week that adds up to about 50% of the total cost of production. The Northern Philippine Rootcrops Research and Training Center (NPRCRTC) of Benguet State University recommended the use of late blight resistant potato varieties like BSU PO$_3$ or "Igorota." Igorota is a locally bred potato variety, which is moderately resistant to late blight and leaf miner. The farmers commonly call this variety LBR, which stands for late blight resistant. This variety has a high dry matter content suited for both table use and processing, matures in 110 days and has a potential yield of 25–35 tons per hectare. However, the variety is planted only in the higher elevation areas of

the municipality, as farmers claim that the variety easily rots during transport, which leads to higher postharvest losses.

Aside from Igorota, Solibao (PO$_4$) is a variety that exhibits high levels of resistance to late blight, showing a negligible infection of 1% as compared to other potato varieties. The variety has a maturity of 90–120 days, with an actual yield of 18–40 tons per hectare and a potential yield of 40 tons per hectare.

11.3.3 Cost Benefit Analysis of Cabbage Production Using Rainwater Harvester

To determine the profitability of the CRA practice compared to the non-CRA practice, cost and return analysis was performed. Further, comparison of means using *t* test was done to analyze if significant differences between the CRA practice and the non-CRA practice exist. Table 11.8 shows the comparison of the costs and returns of cabbage production on a per hectare basis by type of practice in Atok, Benguet. It also shows the mean difference, standard error, and whether the mean difference is significantly different between traditional (without rainwater harvester) and CRA practice (with rainwater harvester), for each cost and return item.

It is noticeable that for both CRA and non-CRA adapters, food is the major cash cost item of the farmer-respondents. Food cost comprised 45% of the total cash costs of farmers who do not use rainwater harvester, and 43% of the total cash costs of those who use rainwater harvester. This means that these farmer-respondents exert extra care and money for their laborers and are willing to spend money on their food. Fertilizer expense comes in as the second biggest cash cost item, taking up 29% of the total cash costs of non-CRA adopters, and 27% of the total cash costs of the CRA users. The fertilizer expense of those who use rainwater harvester was significantly higher than those who do not use rainwater harvester, with a mean difference of Php 7509.70. These two cost items together comprise about 70% of the total cash costs of the farmer-respondents.

Among the labor cost items, the two groups of farmers spent the most on harvesting, fertilizer application, and irrigation and drainage. Land rental and transportation cost are the third and fourth largest cash cost items as reported by the farmer-respondents. Meanwhile, the total cash costs incurred by the CRA users are also significantly higher than the non-CRA users, with a mean difference of Php 7443.15. This means that those who use rainwater harvester spend more in producing cabbage than those who do not use rainwater harvester.

Field monitoring is the major non-cash cost item for both farmer-respondents who practice rainwater harvesting and for those who do not, taking up 63% of the total non-cash costs for the non-CRA users and 58% of the total non-cash costs for the CRA users. Field monitoring, though commonly performed by the farmers themselves almost on a day-to-day basis, is one of the most underestimated labor

Table 11.8 Costs and returns of cabbage production by type of practice, Atok, Benguet

Item	Traditional ($n = 15$)	CRA ($n = 22$)	Mean difference	Standard error
COSTS				
CASH COSTS				
Seeds	5018.00	5680.76	662.07	1752.69
Fertilizer**	19,048.33	26,558.03	7509.70	3404.05
Pesticide	2665.39	2398.20	−267.19	1212.31
Labor				
Land preparation	444.44	468.18	23.74	291.85
Seedbed preparation	340.00	431.82	91.82	295.53
Seed sowing	220.00	140.91	−79.09	172.95
Seedling care and maintenance*	0.00	479.55	479.55	273.75
Irrigation	906.67	1163.64	256.97	1204.11
Fertilizer application	1088.52	967.05	−121.47	493.85
Pesticide application	403.33	272.73	−130.61	276.62
Weeding	0.00	281.82	281.82	199.09
Field monitoring	0.00	27.27	27.27	24.25
Harvesting	1544.44	2806.82	1262.37	1008.08
Other costs				
Land rental	16,111.11	15,555.56	−555.56	8906.23
Food cost	29,423.61	31,029.41	1605.80	7775.71
Fuel cost	1952.78	2410.42	457.64	846.20
Transportation cost	14,333.33	25,666.67	11,333.33	8459.99
Total cash costs*	65,215.06	72,658.20	7443.15	12,040.23
NON-CASH COSTS				
Labor				
Land preparation	2434.07	2146.21	−287.86	719.84
Seedbed preparation**	250.37	592.61	342.24	134.04
Seed sowing	186.30	270.83	84.54	98.06
Seedling care and maintenance	1635.56	1667.05	31.49	451.61
Irrigation**	722.96	2506.06	1783.10	864.78
Fertilizer application	2346.67	2010.23	−336.44	693.24
Pesticide application	2368.15	3303.03	934.88	1107.73
Weeding	280.00	903.03	623.03	394.34
Field monitoring	18,264.44	19,881.06	1616.62	6979.02
Harvesting	593.33	1197.92	604.58	430.45
Total non-cash costs	29,081.85	34,478.03	5396.18	9279.01
TOTAL COSTS	94,296.91	107,136.20	12,839.32	13,661.05
RETURNS				
CASH RETURNS				
Yield (kg)**	11,287.04	16,421.21	5134.18	2573.02
Price	16.00	14.86	−1.14	2.56

(continued)

Table 11.8 (continued)

Item	Traditional (n = 15)	CRA (n = 22)	Mean difference	Standard error
Cash returns*	172,816.70	229,179.50	56,362.88	44,999.18
NON-CASH RETURNS				
Home consumption (Php)	122.83	87.31	−35.52	35.42
Given away (Php)	96.10	91.73	−4.37	35.54
Total non-cash returns	218.93	179.04	−39.89	63.19
TOTAL RETURNS*	157,035.60	229,358.60	72,322.99	41,549.25
RETURNS ABOVE CASH COSTS	**91,820.54**	**156,700.40**	**64,879.84**	**41,012.41**

Note: * significant at 10%, ** significant at 5%, *** significant at 1%

activities performed by the farmers. Farmers do not usually value this activity, but if compared with the other expense items, it also costs a lot.

Similar to the cash costs, the total non-cash costs of the CRA users are also higher than the total non-cash costs incurred by the non-CRA users. In terms of yield, those who use rainwater harvester have significantly higher harvest compared to those who do not use it; the mean difference is about 5132.18 kg. The cash returns of the CRA users are also significantly higher than that of the non-CRA users, with an average mean difference of Php 56,362.88. The total returns, returns above cash costs, and returns above total costs of those who use rainwater harvester are also higher than the returns of those who do not practice rainwater harvesting.

The cost benefit analysis shows the NPV, IRR, and payback period of investing in rainwater harvester for cabbage production. The NPV (7596.32) means that the project is profitable. Since it is greater than zero, it means that the additional benefits of investing in rainwater harvesting are greater than the additional costs. The IRR of 80.84% indicates that investing in rainwater harvester is more profitable than leaving money in the bank. It will take 3 years to be able to pay back the initial investment for the rainwater harvester.

Cost Benefit Analysis of the Use of Blight-Resistant Variety for Potato Production

The comparison of the costs and returns of cabbage production on a per hectare basis by type of practice in Buguias, Benguet is presented in Table 11.9. It also shows the mean difference, standard error, and whether the mean difference is significantly different between traditional and CRA practice, for each cost and return item. The CRA practice considered in this analysis is the use of blight-resistant potato variety, while the traditional users are those who do not use this variety. Seeds take up the bulk of the cash costs incurred by both CRA and traditional users. Around Php 67,700 or half of the cash costs paid by the CRA users can be accounted for by seeds while around Php 80,235 or 41% of the total cash costs are incurred by the traditional

Table 11.9 Costs and returns of potato production by type of practice, Buguias, Benguet

ITEM	Traditional (n = 20)	CRA (n = 13)	Mean difference	Standard error
COSTS				
CASH COSTS				
Seeds	80,235.00	67,700.00	−12,535.00	17,672.11
Fertilizer	28,484.00	19,981.54	−8502.46	5957.34
Pesticide	7515.93	9005.46	1489.53	2410.18
Labor				
Land preparation	1264.38	850.96	−413.41	562.67
Planting	1040.00	1535.90	495.90	383.49
Irrigation*	0.00	355.13	355.13	195.84
Fertilizer application***	0.00	210.98	210.98	75.79
Pesticide application	1076.66	1207.69	131.03	856.14
Weeding	895.00	328.21	−566.79	513.94
Harvesting	3769.02	4232.05	463.03	1290.57
Other costs				
Land rental	20,000.00	0.00	−20,000.00	24,946.59
Food cost	17,700.00	21,666.67	3966.67	4287.51
Fuel cost	2732.50	0.00	−2732.50	1713.33
Transportation cost	10,700.00	13,333.20	2634.00	9793.16
Total cash costs	196,058.80	134,005.40	−62,053.36	42,010.75
NON-CASH COSTS				
Labor				
Land preparation**	1188.75	2256.41	1067.66	395.54
Planting	1280.00	1538.46	258.46	402.67
Fertilizer application	1308.75	1611.54	302.79	435.39
Pesticide application	1385.00	2015.39	630.38	535.05
Irrigation***	0.00	4405.13	4405.13	874.48
Weeding	1015.00	574.36	−440.64	527.65
Field monitoring**	6727.50	16,984.62	10,257.12	4046.80
Harvesting	944.75	361.54	−583.21	360.99
Total non-cash costs**	13,849.75	25,342.31	11,492.56	4825.06
TOTAL COSTS	209,908.50	159,347.70	−50,560.80	41,964.21
RETURNS				
CASH RETURNS				
Quantity sold (kg)	16,335.00	18,897.44	2562.44	6033.87
Price	32.00	29.76	−2.24	1.68
Cash returns	517,350.00	576,733.30	59,383.33	184,989.50
NON-CASH RETURNS (PhP)				
Home consumption	705.56	372.15	−333.41	247.85
Given away	716.13	1481.16	765.03	785.20
Total non-cash returns	1421.69	1853.30	431.62	866.04

(continued)

Table 11.9 (continued)

ITEM	Traditional (n = 20)	CRA (n = 13)	Mean difference	Standard error
TOTAL RETURNS	518,771.70	578,586.60	59,814.95	184,854.90
RETURNS ABOVE CASH COSTS	321,291.20	442,727.90	121,436.70	176,244.20

Note: * significant at 10%, ** significant at 5%, *** significant at 1%

users for seeds alone. In potato production, the quality of seeds is very important as it is linked to increased harvest. Wang (n.d.) noted that the use of good quality seeds can increase yield by 30–50%, as compared to using farmers' seeds.

For those who do not use blight-resistant variety in potato production, fertilizers, land rental, and food cost are the next three biggest cash cost items contributing 14.5%, 10.2%, and 9.03%, respectively, to the total cash costs incurred by the traditional users. On the other hand, the next three biggest cash cost items for CRA users are food cost (16.2%), fertilizers (14.9%), and transportation cost (9.9%).

Among the labor costs paid for by the farmer-respondents, payment for harvesting is the biggest cash cost item, accounting for almost half of the total labor cash costs paid for by both CRA and traditional users. It can also be seen from Table 11.9 that there exists a significant difference in the irrigation labor expense of traditional and CRA users. This is mainly because traditional users rely on rain, while CRA users have more access to small-scale irrigation systems, hence the need to hire labor to irrigate their farms.

In terms of the total cash costs, those who do not use blight-resistant potato variety spend more compared to the CRA users. The traditional users spend around Php 196,058.8 as compared to the CRA users, who spend an average of Php 134,005.4.

Field monitoring is the biggest non-cash cost item for both traditional and CRA users. This activity took up 49% of the total non-cash costs for the traditional users and about two-thirds of the total non-cash costs for the CRA users. The mean difference between the traditional and CRA users for this activity is Php 10,257.12, and it is significant at 5%. This can be explained by the fact that CRA users spend more time monitoring their field compared to the traditional users because extra care is needed by the blight-resistant variety. While the total cash costs of the traditional users are higher than that of the CRA users, the case for the total non-cash costs is the opposite. CRA users have higher total non-cash costs (Php 25,342.31) compared to the traditional users (Php 13,849.75), and this difference is significant at 5%.

It is also observable that the cash returns of traditional users (Php 517,350) are less than that of CRA users (Php 576,733.3). In terms of home consumption, traditional users save more for their homes as compared to the CRA users, while for the quantity of harvest given away, CRA users have more compared to the traditional users. Finally, CRA users have a higher total return, returns above cash costs, and returns above total costs than the traditional users, although the differences

in these three items, is not statistically significant. Cost benefit analysis of investing in blight-resistant potato variety showed that NPV of US$30,195.52 means that the project is profitable. Since NPV is greater than zero, it means that the additional benefits of investing in blight-resistant potato variety are higher than the additional costs.

11.4 Conclusions and Policy Recommendations

Benguet province is very important in the food security of the Philippines. This province is one of the highest producers of temperate and high valued crops. However, climate change threatens this productivity and must be addressed. The CRVA tool was essential for the prioritization of the various municipalities of Benguet province for future climate change and agriculture-related projects such as the "AMIA village." Overall, most of the municipalities in Benguet were classified as very high and high in terms of vulnerability to climate change based on their adaptive capacity, sensitivity of crops to the different climatic variables (temperature and precipitation) and hazard. Improving rainwater harvesting practice of the farmers would increase the yield and income of farmers especially during periods of drought and irregular rainfall. Because those who use the *kwelo* have significantly higher yield and returns than those who do not, efforts thus must be taken to this practice and innovate on it to ensure that water is not lost unduly or that it is used more efficiently especially in the dry season. Based on the cost and return analysis, farmers in Buguias who use the blight-resistant variety Igorota (PO_3) had higher yield, cash returns, total returns, returns above cash costs, and returns above total costs. By planting PO_3, farmers significantly reduced their operational costs by about 50%. Effort is also thus needed to integrate the use of PO_3 with the water-saving practices to determine any synergies that could benefit the farmers in the vulnerable sites.

Five major crops in Benguet province were selected for the CRVA that has three key dimensions, which are adaptive capacity, sensitivity, and hazard. For cabbage and carrots, the municipalities of Atok and Buguias must be prioritized in terms of improving their resiliency in cabbage and carrots production. Although Atok and Buguias were classified as highly vulnerable as compared to other municipalities with very high classification, these two municipalities have the highest production (yield per ha) of cabbage and carrots in the province of Benguet, thus these two were recommended. For snap beans, Tuba and Buguias municipalities were recommended for prioritization as they have high production (yield per ha) of snap bean and were classified as highly vulnerable. Furthermore, Tuba was also selected for the sweet potato while Atok, Buguias, and Kibungan for white potato due to their vulnerability to climate change and high production for these crops. Overall, Atok and Buguias were recommended based on their vulnerability, crop productions, and

discussions during the consultation meeting with the Regional Field Office of the Department of Agriculture—Cordillera Administrative Region. Another recommendation is that the "AMIA village" must be conducted in the Benguet province to improve its resiliency to climate change.

For the improvement of future CRVA studies, it is recommended that different agencies from the national government and local government units develop an enhanced database related to adaptive capacity of each municipality that can be easily viewed and accessed. Mapping of the different high-valued crops for the various municipalities must be also done. The use of water harvesting technology is recommended in all vegetable production areas regardless of crops planted, especially in areas where water is a constraint for productivity as well as in areas where there is frost occurrence. The government through its line agencies and SUCs should expand the project on the distribution of small farm reservoirs or water tanks in drought- and frost-prone areas in the different vegetable and other priority crop production areas such as rice and corn. Aside from the use of rainwater harvesting technology to collect water, other technologies such as fog harvesting is recommended in Atok municipality since the relative humidity is high in some areas. The use of blight tolerant potato variety is recommended in high elevation areas especially during wet or rainy season planting time. Other potato varieties should be evaluated for resistance to other pest and diseases aside from late blight and determine yield potential during the wet season planting, where pest and diseases are prevalent.

11.5 Challenges

Data availability is one of the major challenges in this study. Secondary data was difficult to collect—some data can be accessed easily but some were not available or not collected. The unavailability of the other Agricultural Technologists for the participatory mapping due to their busy schedule was one of the challenges encountered. Thus, some workshops were cancelled. However, they accommodated our request for them to participate the best they can especially in the mapping of the vegetable crops.

References

Benguet PENRO (2019) General information. https://car.denr.gov.ph/images/R-CAR/2019_FILES/P_Benguet/penro-benguet.pdf

Calora FG Jr et al (2011) Biophysical characterization and socio-economic profiling in Benguet, Philippines (vulnerability and adaptation capacity assessment synthesis report). https://issuu.com/mdgf1656/docs/bsu_synthesis_report_final

Cities and Municipalities Competitive Index (2015) https://cmci.dti.gov.ph/data-portal.php?fbclid=IwAR1ormhg3lkvDljo1LdupgVQhgqG5XH-nGyyNwezEhiJvwujbiy2lyaIoVI

Cruden DM, Arnes DJ (1996) Landslide types and processes. In: Turner AK, Schuster RL (eds) Landslides investigation and mitigation

Davis A, Gole T, Baena S, Moat J (2012) The impact of climate change on indigenous Arabica coffee (Coffea arabica): predicting future trends and identifying priorities. PLoS One 7(11): e47981

Ellis F (2000) Rural livelihoods and diversity in developing countries. Oxford University Press

Elith J, Burgman M (2002) Predictions and their validation: rare plants in the Central Highlands, Victoria, Australia. Predicting species occurrences: issues of accuracy and scale. Island Press, Washington, DC, pp 303–313

Intergovernmental Panel on Climate Change (2014) Climate Change 2014: Synthesis Report Contribution of Working Groups I, II and III to the Fifth Assessment Report of the Intergovernmental Panel on Climate Change. In: Core Writing Team, Pachauri RK, Meyer LA (eds). IPCC, Geneva, Switzerland, 151 pp. https://www.ipcc.ch/site/assets/uploads/2018/05/SYR_AR5_FINAL_full_wcover.pdf

Jurgilevich A, Räsänen A, Groundstroem F, Juhola S (2017) A systematic review of dynamics in climate risk and vulnerability assessments. Environ Res Lett 12(1):013002

Lal R (2010) Soil erosion impact on agronomic productivity and environment quality [abstract]. Crit Rev Plant Sci 17(4):319–464

Leonard E (2010) A capital concept of adaptive capacity. In: Ground Cover Magazine (Supplement Issue). Grains Research and Development Corporation (GRDC), Australia. https://grdc.com.au/resources-and-publications/groundcover/ground-cover-supplements/ground-cover-issue-87-climate-supplement

Montgomery DR (2007) Soil erosion and agricultural sustainability. Proc Natl Acad Sci U S A 104: 13268–13272

O'Donell MS, Ignizio DA (2012) Bioclimatic predictors for supporting ecological applications in the conterminous United States. U.S. Geological Survey Data Series 691, 10 p

Palao LK, Guerten N, Martinez A, Parker L, Balanza JG, Leyte J, Dikitan R, Burra D (2017) A climate risk vulnerability assessment for the adaptation and mitigation initiative in agriculture program in the Philippines

Philippine Atmospheric Geophysical and Astronomical Service Administration (2009) 2009 Annual Report; Countering the Threat of Changing Global Climate. https://pubfiles.pagasa.dost.gov.ph/pagasaweb/files/hmd/tramsparency/Annex55.pdf

Philippine Statistics Authority Cordillera Administrative Region (2020) Regional compendium of environmental statistics: component 1—environmental conditions and quality land cover, ecosystem and biodiversity. http://rssocar.psa.gov.ph/sites/default/files/CAR-SR-2020-25-Land%20Cover%2C%20Ecosystem%20and%20Biodiversity.pdf

Sandoval R Jr, Baas S (2014) Adapting to climate change: the cordillera experience. Agric Dev Note 3(2). e-ISSN 2599-3860. https://www.searca.org/pubs/briefs-notes?pid=241

Tad-awan BA, Shagol CC (2016) Varietal response of cabbage to drought conditions in La Trinidad, Benguet, Philippines. BSU Res J 76:45–52

United Nations Development Programme (2012) Annual Report 2011/2012. https://www.undp.org/publications/undp-annual-report-2012

Chapter 12
A Review on Innovation of Remote Sensing Technology Based on Unmanned Aerial Vehicle for Sugarcane Production in Tropical Region

Khwantri Saengprachatanarug, Chanreaksa Chea, Jetsada Posom, and Kanda Saikaew

Abstract Sugarcane production data prior harvest are key information for optimizing harvest schedule and supply chain management, which contribute directly to the increase of profitability for both growers and sugar factories. Due to its flexibility, availability, and accessibility, unmanned aerial vehicle (UAV) imagery have been using to canopy detection, disease detection, sugar content estimation, and yield predictions of sugarcane. Vegetation index and machine learning technique were used to process images from multispectral camera and RGB camera and transformed into GIS data and validated with ground sampling data. Sugarcane canopy detection using linear discriminant analysis (LDA) obtained the highest accuracy of 97%. Normalized difference red edge index (NDREI) and green normalized difference vegetation index (GNDVI) yielded the highest potential for white-leaf disease detection for sugarcane. Chlorophyll Index-Red edge (ClRE) indicated good correlation with Brix of sugarcane around 0.90. Excess green (ExG) value was used to predict sugarcane yield with ordinary least square regression (OLSR) and obtained higher accuracy ($R^2 = 0.75$).

K. Saengprachatanarug (✉) · C. Chea · J. Posom
Department of Agricultural Engineering, Faculty of Engineering, Khon Kaen University, Khon Kaen, Thailand
e-mail: khwantri@kku.ac.th

K. Saikaew
Department of Computer Engineering, Faculty of Engineering, Khon Kaen University, Khon Kaen, Thailand

337

12.1 Introduction

To make crop management be efficient, timing of harvest schedule is crucial. So, getting information regarding crop's conditions at early stage of damages will help to increase the efficiency of applied solutions resulting in reduction of yield loss. The observation of crop's condition can be done in many forms such as using manual labor, and sensors attached on remote sensing platforms. Manual observation is only appropriate for small farm area, but it is tedious, has accessible difficulties, and high labor-cost when operating in large-scale farm area. So, the utilizations of sensors attached on remote sensing platforms have been used to develop several applications for facilitating activities in crop management and precision agriculture through provided spectral reflectance from a variety of sensors attached on three main platforms which are satellite, unmanned aerial vehicle or UAV-based platform, and ground-based machines. Recently, various research studies have focused more and more on using UAV-based platform to acquire data for calibrating many agricultural applications due to many reasons.

Firstly, aerial platform or unmanned aerial vehicle (UAV) is the most flexible among the three platforms for resolution adjustment as users can adjust flight attitude to get their required spatial resolutions. Secondly, UAV-based platform has more availability than satellite platform does because it can still operate the images capturing mission even during season, which has cloudy sky while satellite can only capture images in clear cloudless sky condition. Thirdly, if comparing with field machine platform, UAV platform has more accessibility due to its smaller size, lighter weight, and aerial operation. Thus, UAV platform can be operated in fields at any stage of crop development, which crop height cannot be barrier for its access while field machines have difficulties to access or cannot enter to operate in fields due to higher crop's height. Lastly, the technologies in UAV and camera sensors have been continuously innovated, which improved the performance of UAV-based platform by increasing the amount of covered area per single flight, for example, eBee Ag drone (senseFly Ltd., Cheseaux-Lausanne, Switzerland) can fly at altitude up to 900 m above ground and cover large area about 12 km^2 with spatial resolution 0.10 m in a single flight mission. Therefore, remote sensing applications based on UAV-based platform have potential to be adopted into commercial application for real practices.

So far, various remote sensing applications based on UAV for sugarcane production management have been developed such as detection of green canopy (Patrignani and Ochsner 2015), crop's skip mapping (Luna and Lobo 2016; Souza et al. 2017), diseases (Sanseechan et al. 2019), biomass and leaf nitrogen (Shendryk et al. 2020), and yield estimation (Sanches et al. 2018; Cholula et al. 2020; Xu et al. 2020; Yu et al. 2020; Sumesh et al. 2021; Tanut et al. 2021). The analytical methods for detections and estimation varies from effortless methods, which use values of single reflectance or vegetation indices to complicated methods, which involve machine learning or deep learning and image segmentation, for example, object-based image analysis (OBIA) approach.

Therefore, the objectives of this chapter are to review and summarize these advanced research and limitations to provide technical information for further development of remote sensing application based on UAV platform for sugarcane production, and to discuss the potential to be adopted into commercial services of the current remote sensing application based on UAV for precision agriculture.

12.2 Sugarcane's Canopy Detection

Remote sensing techniques mainly use spectral reflectance received from crop's canopies to calculate as various vegetation indices, for instance, normalized difference vegetation index, to make correlation with crop's physiological parameters such as nitrogen assessment (Lebourgeois et al. 2012), disease detections (Sanseechan et al. 2019), yield estimation, and emergence rate of sugarcane (Luna and Lobo 2016; Souza et al. 2017). Currently, there are many studies that have developed the method to extract crop's canopy, the simplest method being the use of vegetation indices thresholding value, and the common known vegetation indices for canopy detection are normalized difference vegetation index (NDVI) (Rouse et al. 1974) and Excess Green index (ExG) (Woebbecke et al. 1995). For NDVI, rock, sand, and snow have NDVI value below 0.1, while grassland and shrubs have NDVI value in range of 0.2–0.3, and the NDVI value from 0.5 to nearly 1.0 represent abundant crops and tropical forests (Heege 2013). Figure 12.1 shows NDVI map of sugarcane field, the canopy of which can be easily identified by color level.

However, in real-world practices, using vegetation indices thresholding value to detect or extract canopy area can be complicated and limited because the NDVI value of canopy can be varied by crop species and at different age, so the thresholding value might also require adjustment, for example, NDVI value of sugarcane canopy can range from 0.2 to 0.6 (Rahman et al. 2004), and according to (Chea et al. 2019) thresholding NDVI value at 0.3 and 0.4 can detect sugarcane canopy at age about 3 months old with quality percentage about 70%. Therefore, it demonstrates that it is necessary to do assessment studies to determine the suitable NDVI value for thresholding to detect canopy of the targeted crops. Meanwhile, the results of sugarcane canopy classification using thresholding ExG value $\geq$43.50 and $\geq$41.50 for KK3 variety and UT12 variety provided classification accuracy 88% and 84%, respectively (Som-ard et al. 2018).

These study results clearly demonstrate the requirements to determine the suitable values of selected vegetation indices (NDVI and ExG) as thresholding values for sugarcane canopy classification. Additionally, to detect canopy is not only about differentiating the green vegetation from soil background, but also to extract all canopy cover even some parts that are not green anymore. The causes are mentioned in some studies to track the change in greenness of canopy (Chea et al. 2020), for example, the changes of vegetation indices value and chlorophyll index related to
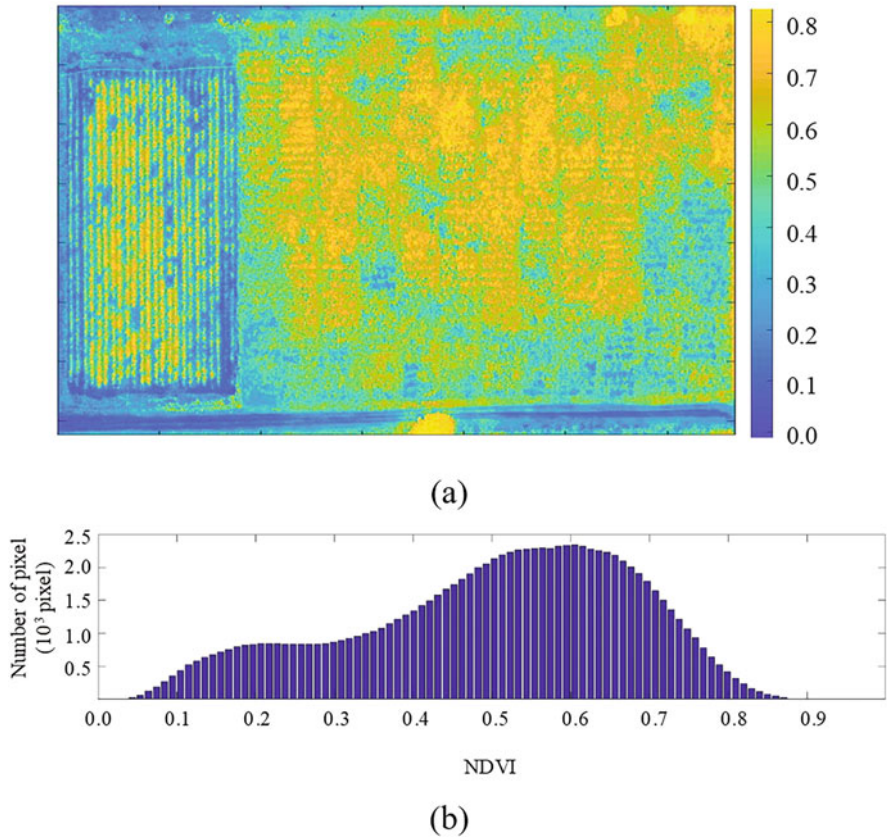
Fig. 12.1 (a) NDVI map of experiment sugarcane field in Khon Kaen, Thailand, (b) the NDVI distribution of the field

red edge (CRE) acquired from sugarcane canopy to interpret the Brix (R^2 0.91), Pol (R^2 0.77), and CCS (R^2 0.68) in sugarcane fields.

In addition, there was a study (Chea et al. 2019) that used principal component analysis (PCA) to divide soil pixels from sugarcane canopy pixels using combination spectral reflectance in five bands: Blue, Green, Red, NIR, and Red edge band (Fig. 12.2). This calibrated model received quite high accuracy with quality percentage about 78% (Fig. 12.3). Despite good accuracy of classification, this method essentially needs samples that cover the prediction scopes.

Machine learning algorithms are also used in sugarcane canopy classification studies, for example, linear discriminant analysis (LDA) (Luna and Lobo 2016) and K-nearest neighbor (Tanut and Riyamongkol 2020). Both studies randomly selected hundreds of point sites in studied plots and labeled those points sites as sugarcane, weed, and soil. Then, the samples were split into train and test dataset to train in
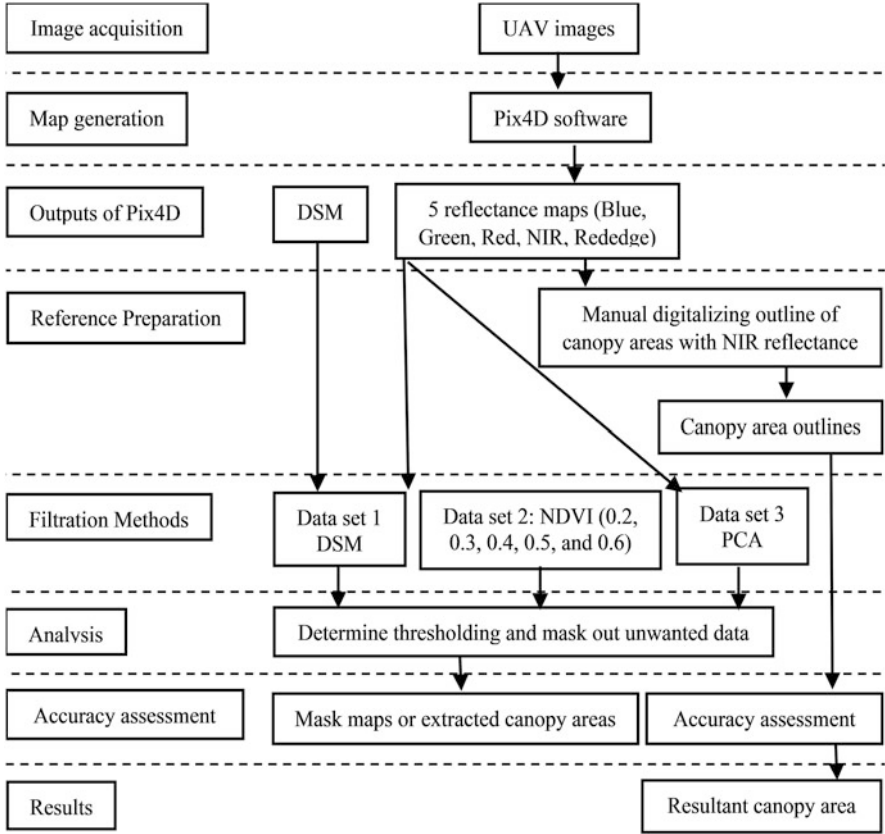
Fig. 12.2 Flowchart of sugarcane canopy detection experiment (Chea et al. 2019)

chosen machine learning algorithms. The sugarcane canopy classification using LDA obtained model accuracy of 97% and cross-validation accuracy of 92.9%, while using *K*-nearest neighbor algorithm provided model accuracy of 96.75% and cross-validation of 95.01%.

Additionally, those methods and results are used to develop a ready-to-use software, for instance, Canopeo (Patrignani and Ochsner 2015) is a free software which uses the thresholding value of color value in the red-green-blue (RGB) system to detect green cover and follows the criteria as shown below:

$$R/G < P1 \quad \text{and} \quad B/G < P2 \quad \text{and} \quad 2G - R - B > P3 \qquad (12.1)$$
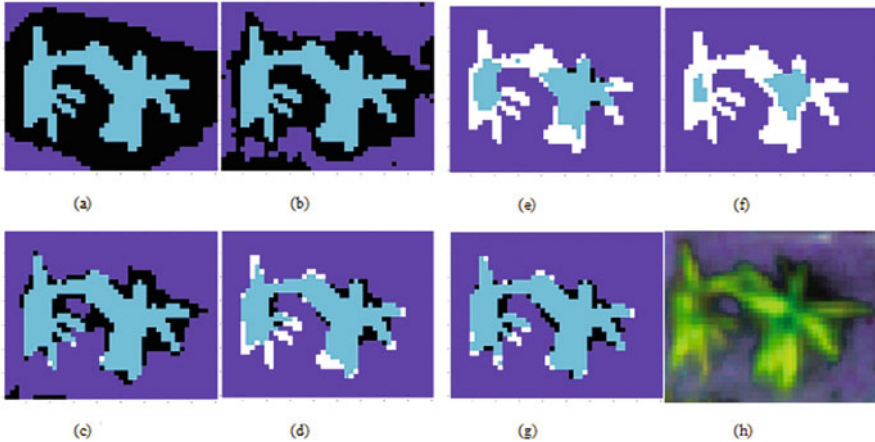
where $P1 = 0.95$, $P2 = 0.95$, and $P3 = 20$.

Fig. 12.3 The extracted canopies of sample n08 overlaid on reference canopy using method thresholding by DSM (**a**), NDVI level 0.2, 0.3, 0.4, 0.5, 0.6 (**b–f**), thresholding by PCA (**g**), and image in RGB (**h**). Light blue: TP, Black: FN, White: FP

12.3 Disease Detection

Disease management plays an important role to ensure crop vigor and high yield, so being able to detect disease symptoms as early as possible can significantly improve the efficiency of disease control measurements. The changes in the color of leaves of crops, for example, white or yellow rust, is one of the forms that crops respond to the damages caused by diseases that make disease detection using UAV platform a popular topic for research. The key predictors for developing the disease detection models are vegetation indices and spectral reflectance acquired from crop's canopy. For instance, Sanseechan et al. (2019) used flight altitude at 117 m above ground in their experiment to detect white leaf disease in sugarcane fields. This study calculated the percent difference of vegetation indices values between green leaves (healthy stalk) and white leaves (infected stalk) to identify the most sensitive vegetation indices to white leaves (Fig. 12.4).

The study results showed that normalized difference red edge index (NDREI) and green normalized difference vegetation index (GNDVI) yielded the highest difference percentage of green and infected leaf about 45%. According to high percentage difference of NDRE and GNDVI values between green leaves and white leaves, these two promising vegetation indices can be used as an input for further model developments using machine learning algorithm for classification such as Random Forest classification. As this experiment was conducted at high altitude and achieved high percent of difference between green leaves and white leaves, the results from further studies have the potential to be adopted into commercial services for large-scale farm areas. Table 12.1 shows the percent difference between green leaves and white leaves of all vegetation indices studied by Sanseechan et al. (2019). Figure 12.5 shows the example of the detection map.
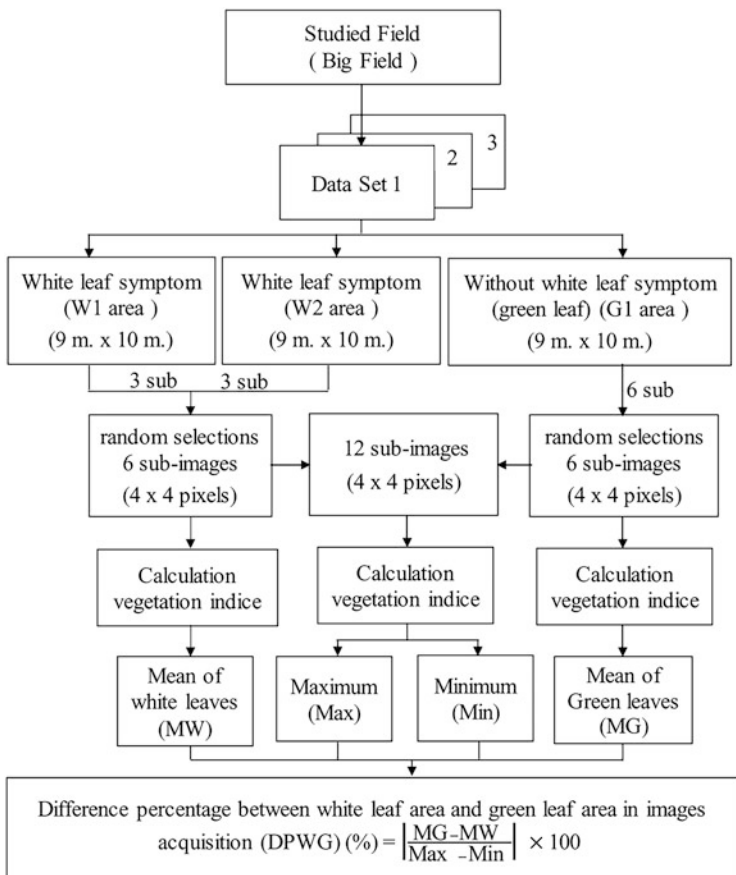
Fig. 12.4 Calculation of difference percentage between white leaf area and green leaf area in image acquired (DPWG) (Sanseechan et al. 2019)

12.4 Sugar Content Estimation in Sugarcane Fields

Brix information has played a key role in providing the data about sugar content in sugarcane fields to help with planning concerning harvest scheduling, production processes, price, and marketing strategies. Recently, remote sensing technologies using UAV has been adopted in many studies to estimate Brix content in sugarcane fields, for instance, Chea et al. (2018) has used simple linear regression between vegetation indices: GNDVI, CIG, ClRE, NDVI, and RVI, which are closely correlated to the changes of canopy's greenness to predict Brix content in sugarcane fields at age 10 months and the model calibrated with GNDVI gave the highest accuracy R^2 0.86.

Table 12.1 Detail information on the percent difference between green leaves and white leaves by vegetation indices

Name	Abbreviation	Formula	Percent difference
Vegetation indices calculated using NIR band			
Normalized difference red edge index	NDREI	$(N - \text{RE})/(N + \text{RE})$	45.10
Green normalized difference vegetation index	GNDVI	$(N - G)/(N + G)$	44.05
Ratio vegetation index	RVI	*N/R*	41.45
Simplified canopy ChlorophyII content index	SCCCI	NDRE/NDVI	37.61
Normalized difference vegetation index	NDVI	$(N - R)/(N + R)$	37.55
Optimized soil adjusted vegetation index	OSAVI	$1.16(N - R)/(N + R + 0.16)$	36.30
Triangular vegetation index	TVI	$0.5[120(N - G) - 200(N - G)]$	36.04
Soil adjusted vegetation index	SAVI	$1.5(N - R)/(N + R + 0.5)$	34.80
Enhanced vegetation index	EVI	$2.5(N - R)/(N + 6R - 7.5B + 1)$	33.31
Anthocyanin reflectance index	ARI	$(1/G)/(1/\text{RE})$	25.21
Transformed ChlorophyII ARI	TCARI	$3[(\text{RE} - R) - 0.2 * (\text{RE} - G)(\text{RE}/R)]$	19.70
ChlorophyII vegetation index	CVI	$(N * R)/(G)^2$	18.69
ChlorophyII index-green	CIG	$N/(G - 1)$	16.88
ChlorophyII index-red edge	ClRE	$N/(\text{RE} - 1)$	14.66
Vegetation indices calculated using visible band			
Greenness index	GI	*G/R*	26.04
Nitrogen reflectance index	NRI	$(G - R)/(G + R)$	24.04
Green leaf index	GLI	$(2G - R - B)/(2G + R + B)$	20.66
Triangular greenness index	TGI	$-0.5 * 190 * (R - G) - (120) * (R - B)$	14.96

Additionally, the continuous study (Chea et al. 2020) with extension range of age of sugarcane fields from 8 to 12 months old also indicated good accuracy around 0.90 with model using ClRE calibrated by simple linear regression (SLR). However, both the above studies have warned about the effect of variety because the change condition of canopy's greenness during sugar accumulation can be different by
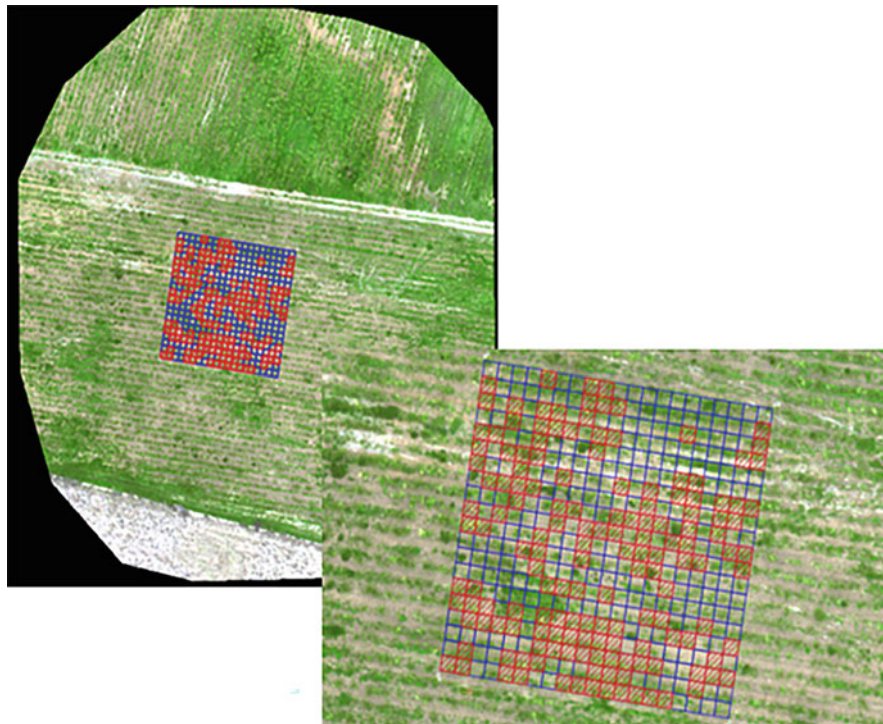
Fig. 12.5 The grids in red indicate the area that show white leaf disease symptom while blue grids have only green leaves

varieties, for example, flood-tolerant variety (UT84-12) have more concentration of chlorophyll in canopies than drought-tolerant variety (K88-92 and Khon Kaen 3) even during sugar accumulation period because this variety is normally grown in irrigated areas, while Khon Kaen3 and K88-92 are planted in rain-fed area and during their sugar accumulation stage, there are less or no rain which simulate senescence of canopy (Fig.12.6).

To be acceptable to apply in real world as commercial application, a project known as "Robotics platform and unmanned vehicle for precision agriculture to create a virtual mega farm," funded by Office of National Higher Education Science Research and Innovation Policy Council, has continued to improve the accuracy and practicability of Brix prediction models by collecting more data from sugarcane fields grown under different crop management, soil types, and seasons. In addition, the Brix models were developed using various machine learning regression such as Bayesian Ridge, Decision tree, Lasso, Random Forest, Ridge, and support vector machine (SVM) regression, and images captured from higher altitude about 117 m above ground resulting in resolution of 0.08 cm per pixel. The results of the project in the first year still showed the promising accuracy of Brix prediction models with low RMSEP 1.54 $^{\circ}$Bx for drought-tolerant variety (Khon Kaen 3) and RMSEP 1.44
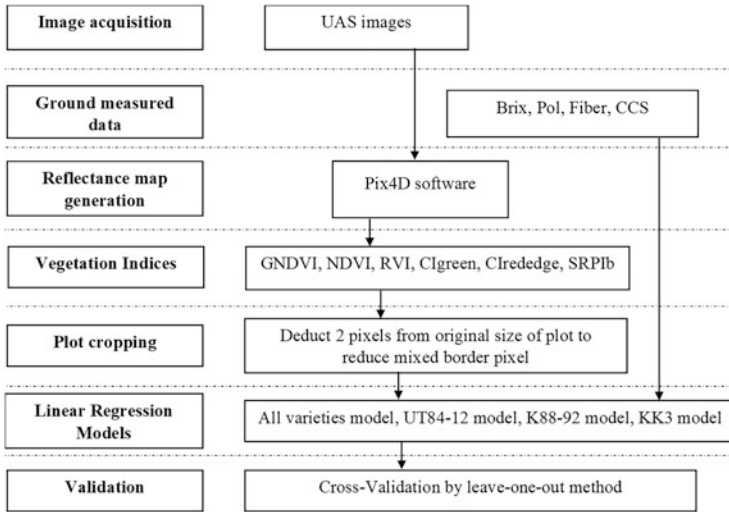
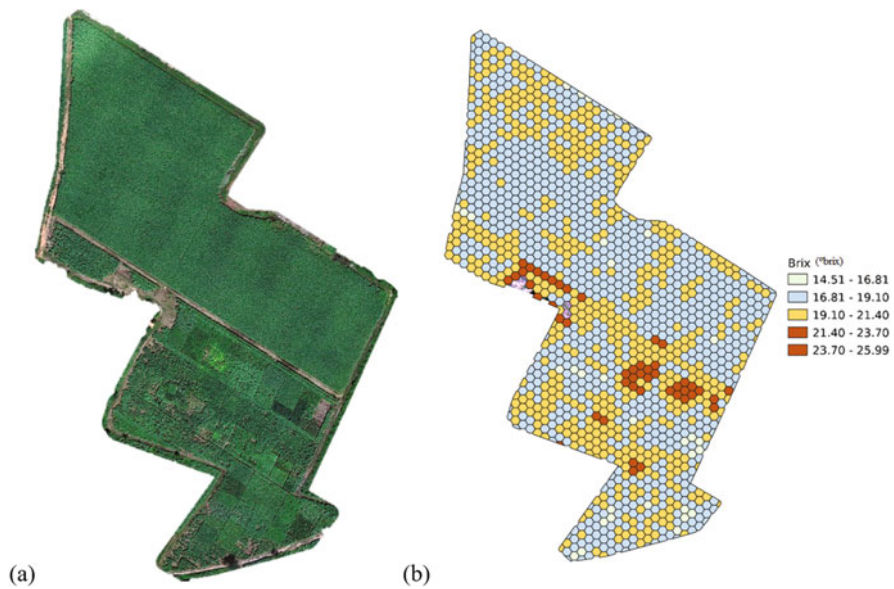**Fig. 12.6** Flowchart of sugar content estimation experiment (Chea et al. 2020)

Fig. 12.7 Sample of RGB map (**a**) and Brix prediction map in sugarcane field (**b**)

°Bx for flood-tolerant variety (UT84-12). Figure 12.7 shows the sample of Brix prediction map in sugarcane fields using developed Brix prediction model from project "Robotics platform and unmanned vehicle for precision agriculture to create a virtual mega farm."

12.5   Yield Predictions

Estimated yield data is an essential input for developing optimized harvest schedule (Jiao et al. 2005; Piewthongngam et al. 2009; Thuankaewsing et al. 2015) to ensure the steadiness of raw material supply throughout the harvest season, particularly sugarcane, which is an annually harvested crop and harvest window lasts only a few months. Thus, the earlier and frequent estimation of sugarcane yield is crucial for planning effective harvest schedule, production chain, and market prices. There are several studies about using UAV-based platform in developing sugarcane yield prediction models using single vegetation indices and fusion of vegetation indices with other parameters such as percent sugarcane canopy, height, planting distant, etc.

For using vegetation indices as predictor, Nodthaisong et al. (2019) used NDVI and ClRE, and volume of sugarcane fields, which acquired by multiplying sugarcane area with estimated height acquired from digital surface model or DSM to estimate yield in sugarcane fields. The results of this study show that NDVI and ClRE obtained accuracy R^2 0.59 and 0.61, respectively, which are quite low accuracy if compared with accuracy of model calibrated with volume of sugarcane fields, R^2 0.87 and root mean square error of cross-validation (RMSECV) 16.31 tons/ha. This high accuracy indicated that yield of sugarcane is strongly related to canopy area and height. Another study by Sanches et al. (2018) used Green-Red Vegetation Index (GRVI) and LAI from two period of sugarcane age, which are 230 days after planting (DAP) and 271 DAP as predictors for estimating sugarcane yield. The study results showed that GRVI and LAI value extracted from 271 DAP provided the highest correlation with yield and using only GRVI, LAI in simple linear regression provided the accuracy R^2 0.69 and 0.34, respectively, while the fusion of GRVI and LAI in multiple linear regression increase R^2 to 0.79 (Fig. 12.8).

To increase the accuracy of yield model, more potential predictors and machine learning algorithms are added in to model development process. Cholula et al. (2020) employed the combination of NDVI, ExG, percent canopy, and height of sugarcane from four periods: 273, 210, 153, and 118 DAP, to estimate yield of
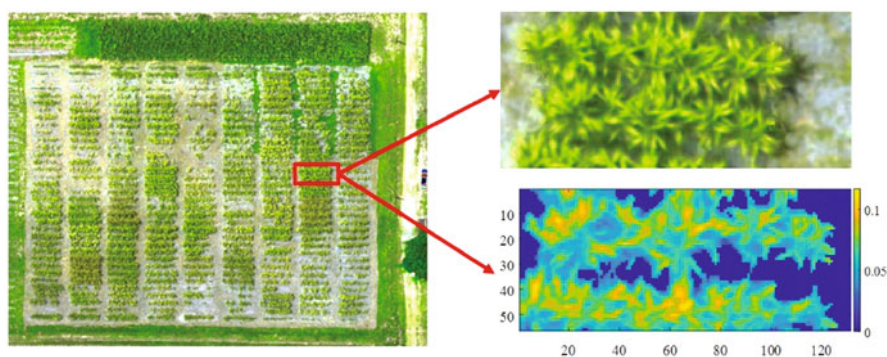

Fig. 12.8   Photo of 4-month-old sugarcane and extracted sugarcane parts by ExG value

energy sugarcane. The results of this study showed that the combination of percent canopy, height, and ExG value extracted at 273 DAP using stepwise regression provided the highest accuracy R^2 0.88 while using only NDVI as predictor, the NDVI value should be extracted at 153 DAP and the model gave R^2 0.71. Besides using vegetation indices values directly into the model, some studies used vegetation indices to estimate other parameters, for instance, sugarcane density or number of stalks per plot. The study by Sumesh et al. (2021) used ExG value to correlate with density of sugarcane in plot using ordinary least square regression (OLSR) and obtained accuracy R^2 0.75. Then, estimated yield was calculated by multiplying the density of sugarcane in plots with estimated weight of estimate millable stalk height (MSH). This study provided good accuracy, which the estimated yield, 200.66 tons, was close to the actual harvest yield, 192.1 tons. However, more experiment should be done to confirm its reproducibility because this study used data from selected small plots in only one field to make prediction models for density and weight of millable stalk, and then, those models were applied to predict the total yield of those same fields.

In conclusion, the best time to extract data for sugarcane yield prediction is at 9 months and above. Besides vegetation indices, sugarcane canopy area, percent of sugarcane canopy, and height of sugarcane are promising predictors for further improving yield model development.

12.6   Conclusion

Vegetation index and machine learning technique have shown high potential in predicting in-field sugarcane production data. However, to achieve the goal of adopting UAV-based technology into commercial services, accuracy is not only a factor for consideration, but reproducibility of developed models and less resources consumption are also important factors that encourage users to accept and utilize this platform. Regarding reproducibility of models, more data from various possible conditions should be collected and trained in models to update prediction models, so that those models can still provide good accuracy, even encounter samples from various conditions that can occur in real-world practices such as weather conditions (rainfall and temperature), soil types, and crop management practices (planting techniques, fertilizer application, weed management, and irrigation types).

References

Chea C, Saengprachathanarug K, Wongphati M, Posom J, Nodthaisong C, Taira E (2018) Feasibiltiy study of evaluation brix of sugarcane using multispectral camera mounted on unmanned aerial vehicle. In: The 11th Thai Society of Agricultural Engineering International Conference 2018, pp 148–159

Chea C, Saengprachatanarug K, Posom J, Wongphati M, Taira E (2019) Sugarcane canopy detection using high spatial resolution UAS images and digital surface model. Eng Appl Sci Res 46:312–317. https://doi.org/10.14456/easr.2019.35

Chea C, Saengprachatanarug K, Posom J, Wongphati M, Taira E (2020) Sugar yield parameters and fiber prediction in sugarcane fields using a multispectral camera mounted on a small unmanned aerial system (UAS). Sugar Tech 22:605–621. https://doi.org/10.1007/s12355-020-00802-5

Cholula U, da Silva JA, Thiago Marconi J, Thomasson A, Solorzano J, Enciso J (2020) Forecasting yield and lignocellulosic composition of energy cane using unmanned aerial systems. Agronomy 10:1–14. https://doi.org/10.3390/agronomy10050718

Heege HJ (2013) Precision in crop farming: site specific concepts and sensing methods: applications and results. Springer, Dordrecht. https://doi.org/10.1007/978-94-007-6760-7

Jiao Z, Higgins AJ, Prestwidge DB (2005) An integrated statistical and optimisation approach to increasing sugar production within a mill region. Comput Electron Agric 48(2):170–181. https://doi.org/10.1016/j.compag.2005.03.004

Lebourgeois V, Bégué A, Labbé S, Houlès M, Martiné JF (2012) A light-weight multi-spectral aerial imaging system for nitrogen crop monitoring. Precis Agric 13:525–541. https://doi.org/10.1007/s11119-012-9262-9

Luna I, Lobo A (2016) Mapping crop planting quality in sugarcane from UAV imagery: a pilot study in Nicaragua. Remote Sens 8:1–18. https://doi.org/10.3390/rs8060500

Nodthaisong C, Saengprachathanarug K, Chea C, Posom J, Wongpichet S, Konyai S, Wongphati M (2019) Feasibility study of sugarcane yield prediction using NDVI, CI rededge indices associated with volume of digital surface model (DSM). Khon Kaen Agric J 47(4):679–694. https://doi.org/10.14456/kaj.2019.65

Patrignani A, Ochsner TE (2015) Canopeo: a powerful new tool for measuring fractional green canopy cover. Agron J 107:2312–2320. https://doi.org/10.2134/agronj15.0150

Piewthongngam K, Pathumnakul S, Setthanan K (2009) Application of crop growth simulation and mathematical modeling to supply chain management in the Thai sugar industry. Agric Syst 102:58–66. https://doi.org/10.1016/j.agsy.2009.07.002

Rahman MR, Islam A, Rahman MA (2004) NDVI derived sugarcane area identification and crop condition assessment. Plan Plus 1(2)

Rouse W, Haas RH, Deering DW (1974) Monitoring vegetation systems in the Great Plains with ERTS, NASA SP-351. In: Third ERTS-1 symposium, vol 1, pp 301–317

Sanches GM, Duft DG, Kölln OT, dos Santos Luciano AC, De Castro SGQ, Okuno FM, Franco HCJ (2018) The potential for RGB images obtained using unmanned aerial vehicle to assess and predict yield in sugarcane fields. Int J Remote Sens 39:5402–5414. https://doi.org/10.1080/01431161.2018.1448484

Sanseechan P, Saengprachathanarug K, Posom J, Wongpichet S, Chea C, Wongphati M (2019) Use of vegetation indices in monitoring sugarcane white leaf disease symptoms in sugarcane field using multispectral UAV aerial imagery. In: IOP conference series: earth and environmental science, vol 301. https://doi.org/10.1088/1755-1315/301/1/012025

Shendryk Y, Sofonia J, Garrard R, Rist Y, Skocaj D, Thorburn P (2020) Fine-scale prediction of biomass and leaf nitrogen content in sugarcane using UAV LiDAR and multispectral imaging. Int J Appl Earth Observ Geoinform 92:102177. https://doi.org/10.1016/j.jag.2020.102177

Som-ard J, Hossain MD, Ninsawat S, Veerachitt V (2018) Pre-harvest sugarcane yield estimation using UAV-based RGB images and ground observation. Sugar Tech 20:645–657. https://doi.org/10.1007/s12355-018-0601-7

Souza CHW, Lamparelli RAC, Rocha JV, Magalhães PSG (2017) Mapping skips in sugarcane fields using object-based analysis of unmanned aerial vehicle (UAV) images. Comput Electron Agric 143:49–56. https://doi.org/10.1016/j.compag.2017.10.006

Sumesh KC, Ninsawat S, Som-ard J (2021) Integration of RGB-based vegetation index, crop surface model and object-based image analysis approach for sugarcane yield estimation using unmanned aerial vehicle. Comput Electron Agric 180:105903. https://doi.org/10.1016/j.compag.2020.105903

Tanut B, Riyamongkol P (2020) The development of a defect detection model from the high-resolution images of a sugarcane plantation using an unmanned aerial vehicle. Information 11: 1–19. https://doi.org/10.3390/info11030136

Tanut B, Waranusast R, Riyamongkol P (2021) High accuracy pre-harvest sugarcane yield forecasting model utilizing drone image analysis, data mining, and reverse design method. Agriculture 11(7):682. https://doi.org/10.3390/agriculture11070682

Thuankaewsing S, Khamjan S, Piewthongngam K, Pathumnakul S (2015) Harvest scheduling algorithm to equalize supplier benefits: a case study from the Thai sugar cane industry. Comput Electron Agric 110:42–55. https://doi.org/10.1016/j.compag.2014.10.005

Woebbecke DM, Meyer GE, Von Bargen K, Mortensen DA (1995) Color indices for weed identification under various soil, residue, and lighting conditions. Trans Am Soc Agric Eng 38:259–269. https://doi.org/10.13031/2013.27838

Xu J-X, Ma J, Tang Y-N, Wei-Xiong W, Shao J-H, Wan-Ben W, Wei S-Y, Liu Y-F, Wang Y-C, Guo H-Q (2020) Estimation of sugarcane yield using a machine learning approach based on UAV-LiDAR data. Remote Sens 12:2823. https://doi.org/10.3390/rs12172823

Yu D, Zha Y, Shi L, Jin X, Hu S, Yang Q, Huang K, Zeng W (2020) Improvement of sugarcane yield estimation by assimilating UAV-derived plant height observations. Eur J Agron 121: 126159. https://doi.org/10.1016/j.eja.2020.126159

Chapter 13
Big Data Scheme from Remote Sensing Applications: Concluding Notes for Agriculture and Forestry Applications

Tofael Ahamed

Abstract This chapter discusses the application of remote sensing perspective and how to develop the big data analytical platform for diversified land-use planning towards food and nutrition security, crop growth monitoring, yield forecasting, land suitability analysis, forest productivity and drought assessment for crops, vegetables, and fruits. The geospatial, mathematical, and logical modeling including multicriteria evaluation systems were conducted to determine the key outcomes of each chapter in this book have been lucidly discussed. Remote sensing and GIS-based systematic analysis are reported to indicate the biophysical and socio-economic factors that bring sustainability in regional policy planning. The big data scheme for regional planning requires the high-density levels of data that ensures trustworthiness, authenticity, availability, and accountability of datasets. Furthermore, geospatial planning has the advantages of trustworthiness and authenticity in the intervention process to support the livelihoods of farmers during damages due to drought and flash floods. In regard to carbon stock analysis and forest loss assessment, ecological resource conservation is discussed referring to vegetation signatures derived from satellite imageries. Additionally, forest productivity assessment is explained based on carbon stock analysis to establish resilience in forest ecosystems.

Keywords Big data scheme · Land-use planning · Yield forecasting · Drought assessments · Forest productivity

13.1 Introduction

Remote sensing technology and GIS applications for monitoring crop and forest conditions have been extensively studied during the past several decades, providing a timely assessment of changes in the growth and development of crops and forests. This chapter describes the summary notes from all the chapters and how this

---

T. Ahamed (✉)
Faculty of Life and Environmental Sciences, University of Tsukuba, Tsukuba, Ibaraki, Japan
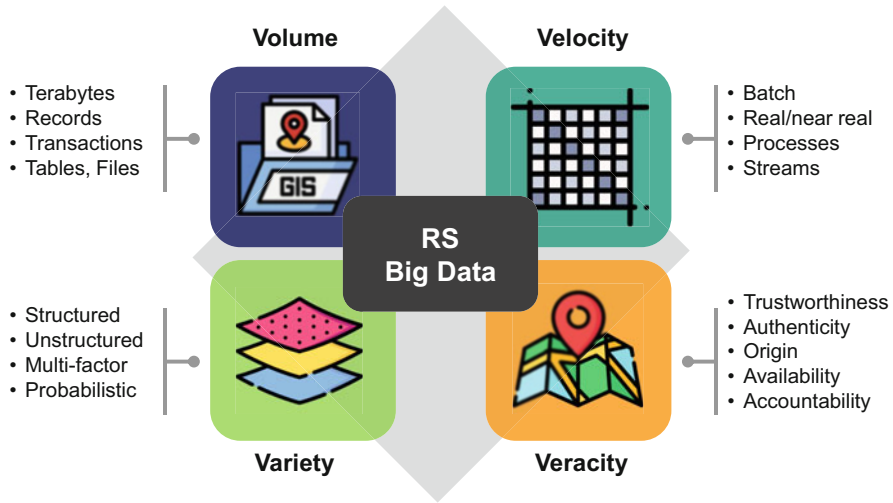e-mail: tofael.ahamed.gp@u.tsukuba.ac.jp

Fig. 13.1 Big Data and Remote Sensing (RS): geospatial data analytics in a GIS environment

application contributes to the big data scheme in policy planning. As a spatiotemporal tool, remote sensing and GIS have been used to conduct spatial and temporal analyses related to land suitability, change detection, plant phenology, economic features, forest phenological changes, natural hazards, and land-use planning and management. These applications are important and suggest that remote sensing technology is suitable for monitoring agricultural and forest activities. This book discusses remote sensing applications at various resolutions (from low to high) through satellite image-based vegetation indices as a part of big data analysis. Big data refers to large-scale datasets that have volume, veracity, and variety such that the volume of data is connected to each other for decision-making and analysis. The sustainable development goals (SDGs) are a framework for attaining a "better and more sustainable future for all" according to the united nations (UN). The internet of things (IoT), open data platforms, crowdsourced spatial data, and the advent of big data technology have all contributed to an enormously vast quantity of data becoming available that can assist countries in accomplishing the UN's SDGs. With the application of big data schemes in the fields of agriculture and forestry, relevant researchers can process high volumes of low-density, unstructured, structured, multifactor, and probabilistic datasets with high efficacy levels (Fig. 13.1).

In addition, this book highlights the applications of satellite remote sensing for the suitability assessments of different crops (rice, maize, cassava, grapes) along with climate adaptation and mitigation strategies for land-use planning in different South Asian countries. For example, at regional scales of land suitability assessment, satellite remote sensing allows phenological information about vegetation and can help in the decision-making process. The data sizes, multifactors, near real-time information, authenticity, and availability are discussed in light of the chapters presented in this book.

13.2 Diversified Land-Use Planning for Food and Nutrition Security

A seasonal land-use planning model was discussed in this book that has diverse crops for regional self-sufficiency of foods based on land suitability and calorie demand. Using GIS and fuzzy membership functions, a multicriteria decision-making analysis was conducted, and a set of multicrop land planning maps was created. Land suitability maps for the Kharif-1, Kharif-2, and Rabi seasons were developed using high-resolution vector and satellite remote sensing datasets that accounted for the geographical expanse. Furthermore, a GIS platform was applied to create seasonal land suitability maps with a balanced food demand ratio. The spatial distributions of different crops were clearly exposed using remote sensing data to evaluate biophysical soil factors. In the context of GIS, topographic data can be helpful for crop management decisions such as intensification or diversification of agricultural practices within a region. The integrated model provided herein could manage land allocation for diverse crop production, providing policymakers with additional decision-making information to ensure regional food security in the target area and other South Asian countries.

13.3 Land Suitability Analysis and Yield Forecasting for Rice

Satellite remote sensing technologies have high potential in applications for evaluating land conditions and can facilitate to optimize planning for agricultural sectors. However, misinformed land selection decisions limit crop yields and increase production-related costs to farmers. In Chap. 3, the land suitability assessment and yield forecasting model were discussed from satellite remote sensing-derived soil-vegetation indicators. A multicriteria decision analysis was conducted by integrating weighted linear combinations and fuzzy multicriteria analyses in a GIS platform for suitability assessment using the following eight criteria: elevation, slope, and the LST vegetation indices (SAVI, ARVI, SARVI, MSAVI, and OSAVI). In addition, a yield estimation method was developed using indices representing influential factors. The yield estimation using SAVI ($R^2 = 0.773$), ARVI ($R^2 = 0.689$), SARVI ($R^2 = 0.711$), MSAVI ($R^2 = 0.745$), and OSAVI ($R^2 = 0.812$) showed good accuracy. Also, every combination of these five indices represented the best accuracy ($R^2 = 0.839$), which was used to develop the yield maps for the corresponding years (2017–2020). The relative priorities of the indicators were identified using a fuzzy expert system. Furthermore, the results of the land suitability assessment were evaluated by ground truth yield data. In addition, a yield estimation method was developed using indices representing influential factors. The results of the land suitability evaluation for field crops will be very useful in the decision-making process to increase production as well as for the sustainable management of

agricultural lands. Thus, the influence of vegetation index evaluations, suitable condition assessments, and yield prediction models are essential for understanding future land use and production trends in the agricultural crop sector in Bangladesh, as well as in other applications.

13.4   Land Suitability Analysis for Cassava Production

In Chap. 4, a spatial model was developed to assess the suitability of land for supporting sustainable cassava production using a multicriteria model integrated with GIS, remote sensing, and AHP. The multicriteria model for suitability assessment used eight criteria: LULC, rainfall, distance from rivers, slope angle, elevation level, soil type, distance from roads, and NDVI. From these criteria, the study found that soil type, LULC, and NDVI influenced the sustainability of cassava production much more than the other factors did. All the criteria were processed through a weighted overlay using AHP to calculate the weights of each criterion. The results of AHP were also confirmed and validated with the ANP approach. The land suitability assessment for cassava production indicated that 41.6% and 44.6% of the study area was highly suitable using AHP and ANP, respectively. Furthermore, the sustainability of cassava production was analyzed using several indicators classified into four categories: availability, accessibility, affordability, and profitability. The results show that the land use for cassava cultivation areas declined annually by 3.38% between 2010 and 2015. The results obtained from this research are very significant in the decision-making processes to increase cassava production in suitable areas of Serang city, Indonesia. The production scenario is one of the essential points for understanding suitability to increase the regional production of cassava in Indonesia. The model can be further expanded spatially by including a fuzzy approach with AHP and ANP to overcome the limitation of the multicriteria model.

13.5   Drought Assessment Areas for Maize

Climate has affected primary crops on a global scale. Indonesia is a developing nation that facing a great challenge for climate change. Therefore, the study in Chap. 5 analyzed the vegetation phenology of maize to forecast the drought situation in the Central East Java areas of Indonesia. Two potential vegetation indices were used to determine the water stress level in the maize field through the NDVI and NDWI derived from Sentinel 2 images. According to the NDVI trajectory, the maize planting season was in April 2018, and the harvesting happened in late August. This study presents a CNN-based YOLO model for detecting drought conditions at different stages of maize production. Drought identification based on the growing season was discovered, and validation was performed by IoU, precision, recall, F1-score, and mean average precision (mAP) metrics that yielded 83.4%, 98%,

99%, 98%, 96%, respectively, in drought-prone areas in Indonesia. The concept enables the combination of remote sensing technologies to identify objects in real time with acceptable precision. This study can be used by stakeholders and farmers to identify drought-prone areas and can introduce interventions to support affected farmers. A more in-depth analysis and vegetation phenology will be applied to verify the yield model. Moreover, forecasting the severity of drought and vegetation phenology ensures that yield declines are avoided and that regional food security can be verified.

13.6   Land Suitability Analysis for Grapes

Appropriate land selection is a significant parameter for table grape production and productivity. Therefore, selecting improper land not only can reduce table grape quality and quantity but also increases production costs. In this regard, Chap. 6 is carried out to develop a land suitability model on the regional scale to find the most suitable areas for table grape production based on physical and socioeconomic criteria in Kabul Province of Afghanistan. The multicriteria decision analysis was performed for suitability assessment using 20 criteria, 14 for the physical factors and 6 for socioeconomic factors. The criteria considered for the physical factors were elevation, slope, aspect, LST, rainfall vegetation indices (NDVI and NDMI), soil types, soil texture, soil structure, soil pH, and soil organic matter. On the other hand, socioeconomic and demographic criteria included distance from roads and rivers, distance from national markets, distance from local markets, population density, and revenue cost ratio. An FAO land use/land cover layer was also used to mask restricted zones, and only the vineyard area was considered to derive a more accurate result. Finally, the suitable classes were determined using a weighted overlay based on a reclassification of each criterion based on AHP weights. The results showed that only 11%, 15%, and 13%, respectively, are physically, socioeconomically, and highly suitable for grape production in the study area. This research has the potential to be applied to determine suitable areas in all of Afghanistan.

13.7   Land-Use Planning of Suburb Areas for Agriculture and Industry

The unplanned growth of industries in suburban areas has significant impacts on land-use changes, which eventually could affect national food security. Thus, a nation needs to have a sustainable land-use management balancing food security, environmental protection, and economic development. However, land-use changes significantly affect food security, ecological balance, and environmental protections in developing countries. Bangladesh is one such country that faces challenges from

limited arable land resources, including the urbanization of agricultural lands and urban developments in suburban areas. Therefore, Chap. 7 determined the land-use changes over time in suburban areas with the potential for industrial growth. This study also assessed potential locations and the further development of industries by land suitability analysis to emphasize agriculture and sustainable growth. A GIS-based multicriteria analysis model was developed for the LSA to distinguish compact lands suitable for industries' economic zones. Nine criteria, including seven constraints and 23 factors, were evaluated by the spatial analysis tools of ArcGIS®. An AHP was applied to prioritize the criteria based on experts' opinions for the decision-making process of LSA. This study found that dense industrial areas have decreased agricultural lands by greater than 10% in the last two decades. Further-more, the LSA results show that only 4% of the land was the most suitable for industrial sites, whereas 4 compact lands have 16–10 ha of land, which is ideal for small industrial zones. Thus, the integrated GIS-MCA model can serve as a policy-planning tool to locate the economic zones of industries with sustained agricultural lands and environmental protection.

13.8   Forest Classification for Change Detection

Due to a faster-growing population, land conversion supports infrastructure expansion investment in agriculture and cash-crop plantations. In addition, forest fires, poor forest management practices, and increasing demand for forest products and agriculture contribute to the damage of forests. Many forests around the globe have recently experienced high deforestation rates due to human migration and the expansion of agriculture or industry. Proper forestland-use planning has not taken place over time to align the changes in forest resources. In this relation, Chap. 8 explained how change detection occurred over the last 15 years and identified the potential forest area that can be extended in the South Sumatra province of Indonesia. Remotely sensed data were used to monitor the changes in the LULC and quantify the differences in the forest classes in the South Sumatra province of Indonesia from 2003 to 2018. In the LULC analysis, six types of forest zones, CPF, PPF, LPF, WRF, TRF, and NRF, were focused upon to determine their changes and locate potential areas for extension of the forest. In the change detection analysis, the study observed that the TRF, CPF, and PPF forest zones decreased by 20%, 13%, and 40%, respectively, from 2003 to 2018. LPF regions had significant changes and decreased by 72% in LULC for its forest class. Palm oil plantations had a substantial impact on the LPF forest classification areas. For the extension of forest types that decreased over time, the AHP analysis incorporated with selected criteria using weights from experts. Forest classifications can extend the proposed potential areas to balance deforestation with production forests, such as plantations. Therefore, the change detection analysis and periodic determination of potential forest extension areas could help to create new policy space for plantation forests and ecosystems in designing national and subnational policies.

13.9   Forest Productivity and Carbon Stock Analysis

Indonesia has the highest forest density globally, and the productivity of its forests can potentially be maximized to minimize CO_2 emissions. However, due to anthropogenic activities, phenological properties are subject to risk to ensure productivity and carbon exchange in the different forest ecosystems in Indonesia. Early prediction of carbon values could indicate a declining trend of forest quality regarding vegetation levels. Thus, the purpose of Chap. 9 was to evaluate forest productivity and carbon stock using phenological properties for different forests. The results indicated that the customized NDVI approach achieved superior performance for determining the productivity level and that the government can use the analysis to manage forests. The government can use the developed WebGIS to quickly assess the level of productivity and performance indicators for different forests. Therefore, decisions about forest conditions can be made immediately. This application is based on a database of NPP calculations from 2015 to 2018. This application will allow sufficient input for further extension of NDVI, GPP, and NPP for monitoring forest productivity. Forest vegetation mapping and carbon assessment can be performed in the future. The system dynamics approach predicts solar radiation as an essential parameter for increasing productivity when the area does not change or increase with the same solar radiation value. The status and optimum options for land resource use and management approaches could be based on satellite remote sensing spatial scales to project the LULC changes from the forest zones of PPF, LPF, CPF, WRF, TRF, and NRF. Furthermore, information on the productivity of different types of forests justifies the protection and management of forests on different time scales. Therefore, the satellite-based remote sensing system dynamics model can be implemented in forest policy systems to assess forest productivity and carbon stocks globally.

13.10   Forest Loss Assessment for Ecological Resource Conservation

Despite recognizing the importance of tropical forest systems, deforestation in Malaysia has increased rapidly over the past 15 years. Since the first Earth observation satellite was launched in 1972, remote sensing techniques and image processing analysis have been extensively used for long term and continuous forest monitoring worldwide. Chapter 10 selects the Google Earth Engine (GEE) platform to monitor deforestation in Malaysia over the past 20 years. GEE is a cloud-based platform that works with substantial geospatial datasets using high-performance computing resources. The study quantified trends of deforestation in Malaysia through a statistical approach based on GEE and used quantitative data to analyze the drivers of deforestation. Overall, the statistical results demonstrated a high level of accuracy, and the GEE platform is suitable for forest monitoring on a national scale. According

to the statistical outcomes, we further elaborated on the main drivers of deforestation in Malaysia. There is no single driver of tropical deforestation in Malaysia; the palm oil industry, forest fires, and illegal logging are attributed to the destruction of forest areas in Malaysia. The GEE monitoring tool was found to be appropriate for observing deforestation and guiding Malaysia's management and conservation of forest resources. Quantifying Malaysia's past deforestation can effectively engage in forest management, climate protection, ecological resource conservation, and sustainable ecosystem services.

13.11   Climate-Resilient Agriculture for Adaptation and Profitability

Chapter 11 describes the climate risk vulnerabilities of the agricultural areas and priority crops in Benguet Province of the Philippines and the economic benefits of the identified technologies used by the farmers to adapt to climatic hazards. The Adaptation and Mitigation Initiative in Agriculture (AMIA) is the Department of Agriculture's (DA) chief integrated effort to contribute to the national government's agenda of addressing climate change threats in the agriculture sector of the Philippines. This project seeks to identify the vulnerable crops and areas in Benguet Province and potential adaptation technologies that will improve the resilience of the farming communities. Overall, most of the municipalities in Benguet were classified as very high and high in terms of vulnerability to climate change based on their adaptive capacity, the sensitivity of crops to the different climatic variables (temperature and precipitation), and hazards. Improving the rainwater harvesting practice of farmers would increase the yield and income of farmers, especially during periods of drought and irregular rainfall. Because those who use the rainwater harvester named as *kwelo* have significantly higher yields and returns than those who do not, thus, efforts must be made to address this practice and provide innovations to ensure that water is not lost unduly or used more efficiently, especially in the dry season. Based on the cost and return analysis, farmers in Buguias who use the blight-resistant variety Igorota (PO_3) had higher yields, cash returns, total returns, returns above cash costs, and returns above total costs. By planting PO_3, farmers significantly reduced their operational costs by approximately 50%. Efforts are thus needed to integrate the use of PO_3 with water-saving practices to determine any synergies that could benefit farmers at vulnerable sites. To improve future CRVA studies, it is recommended that different agencies from the national government and local government units develop an enhanced database related to the adaptive capacity of each municipality that can be easily viewed and accessed.

13.12 Farm Area Assessment and Monitoring for Harvest Scheduling

Remote sensing technology has provided spectral information on crop canopies for building on numerous agricultural applications for precision farming. Unmanned aerial vehicle (UAV) platforms have developed many agricultural applications among the three main remote sensing platforms due to their flexibility, availability, and accessibility. This review article highlights the applications of different remote sensing technologies based on UAV platforms to implement tropical crop management from planting to harvesting. Given the diverse applications of UAV-based remote sensing for precision agriculture, it is promising for UAV-based platforms to evolve into commercial applications that provide low-cost operations but high-accuracy results. These applications also help users or farmers reduce hazardous contact with chemical substances in pesticides, herbicides, and fertilizers. In the final chapter, a review on the innovation of remote sensing technology based on UAVs for sugarcane production in tropical regions was discussed. Sugarcane production data before harvest are essential information for optimizing harvest schedules and supply chain management, which contribute directly to the increase in profitability for growers and sugar factories. Due to its flexibility, availability, and accessibility, UAV imagery has been used to develop sugarcane canopy detection, disease detection, sugar content estimation, and yield predictions. The vegetation index and machine learning technique were utilized to process images from the multispectral camera and RGB camera and transformed into GIS data and validated with ground sampling data. Sugarcane canopy detection using LDA obtained the highest accuracy of 97%. NDREI and GNDVI yielded the highest potential for white-leaf disease detection for sugarcane. The CIRE indicated a good correlation with the Bix of sugarcane, approximately 0.90. The ExG value was used to predict sugarcane yield with OLSR and obtained accuracy ($R^2 = 0.75$).

13.13 Big Data Scheme for Remote Application in Agriculture and Forestry

Agriculture and forestry meet the most basic human and animal requirements, such as food, fiber, and shelter. However, rising food demand, a growing population, and rising income levels are all projected to place further pressure on natural resources. With a growing awareness of agriculture's and forestry's negative environmental implications, new techniques and approaches should be able to meet future food demands while maintaining or lowering agriculture's and forestry's environmental footprint. Innovative technologies such as geospatial technologies, big data analysis, and artificial intelligence (AI) can be used to make informed management decisions and aimed for increasing crop yields through suitability analysis, drought stress
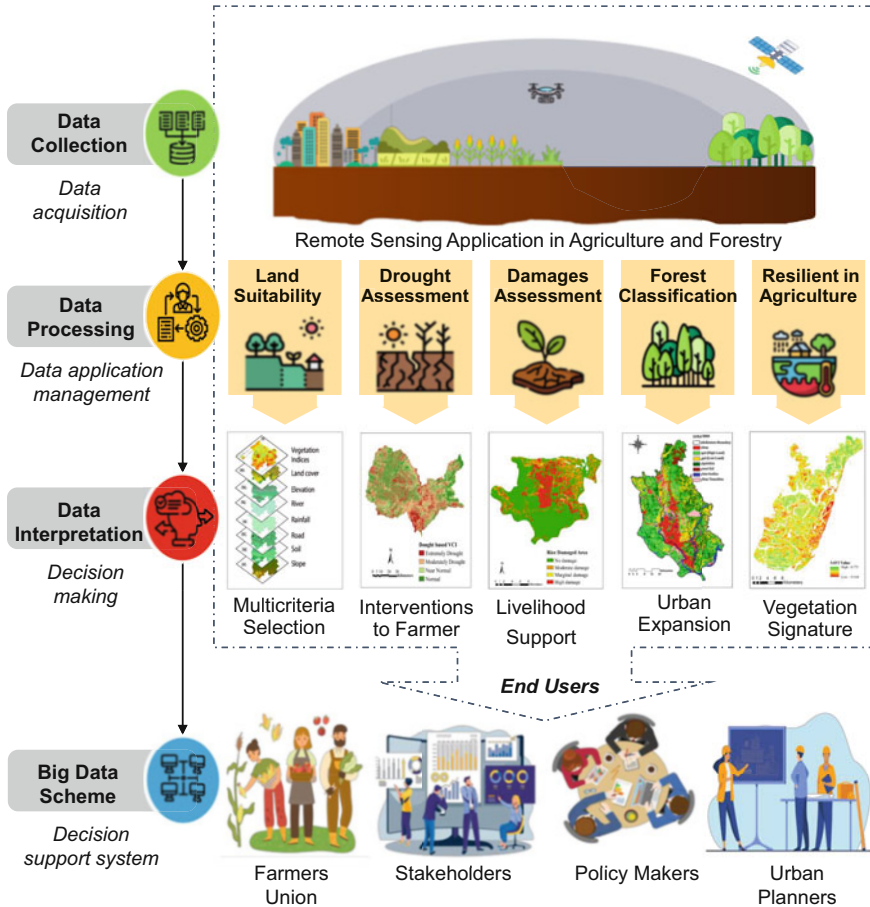
Fig. 13.2 Big data scheme from a remote application to connect with farmer unions, stakeholders, policy makers and urban planners

assessment, forest change detection, land-use planning, UAV applications, and yield predictions, among other things (Fig. 13.2).

13.14   Conclusions

During the last few decades, the use of remote sensing technologies for agriculture and forest research has brought a number of challenges and opportunities together. Crop monitoring, change detection, disease and pest management, yield prediction, forest management, land-use planning, and precision agriculture (PA) applications have benefited from the unprecedented availability of coarse- to high-resolution

(spatial, spectral, and temporal) satellite images combined with UAVs. In this regard, this book presented geospatial, mathematical, and logical modeling for a multicriteria evaluation system using biophysical and socioeconomic factors. These integrated models incorporate a large number of Earth observations, spaceborne and airborne sensors from different sources, which fosters the leading position of data-driven and interdisciplinary remote sensing applications in big data schemes related to decision support systems for farmer unions, stakeholders, policy-makers, and urban planners from regional perspectives.